FACULTY OF SCIENCE

AARHUS UNIVERSITY

Amyloid Fibrils and Oligomers

PhD thesis

Nikolai Lorenzen

Interdisciplinary Nanoscience Center, 2013

Aarhus University
iNANO and Department of Molecular Biology and Genetics
Gustav Wieds Vej 14
DK - 8000 Aarhus C

Thesis Title
Amyloid Fibrils and Oligomers

Author
Nikolai Lorenzen

Thesis Period
September 2009 to November 2013
(Including a 3 months leave)

Supervisor
Professor Daniel E. Otzen

PhD School
Graduate School of Science and Technology

PhD programme
iNANOschool

TABLE OF CONTENTS

Resumé (danish summary)

Misfoldning af peptider og proteiner til amyloide fibriller og fibrillerings relaterede oligomerer er associeret til sygdomsmekanismerne bag neurodegenerative sygdomme som Parkinsons, Alzheimers og Huntingtons syge. Der er en enorm interesse i at udvikle medicin målrettet mod helbredelse af disse sygdomme. Planlægning af rationelle strategier for udvikling af lægemiddel er dog vanskeligt, så længe at de bagvedliggende molekylære mekanismer i patogenesen ikke er beskrevet. I denne afhandling er neurodegenerative sygdomme og protein misfoldning blevet adresseret fra forskellige vinkler. Vi har prøvet at forstå, hvordan amyloide fibriller dannes, og hvordan denne proces kan inhiberes. Derudover, så har vi analyseret α-synuclein oligomerers struktur og cytotoksiske mekanisme.

Til at analysere fibrillerings kinetik har vi anvendt det ribosomale protein S6 som modelsystem. Baseret på kinetik og matematisk modellering lykkedes det os at adskille bidrag fra forskellige mekanismer under fibrillerings processen. Særligt interessant var vores opdagelse af, at den eksponentielle vækst fase i fibrillering, kunne tilskrives sekundære processer frem for primær nukleering. Generelt forventes det at rate konstanterne for fibril elongering og primær nukleering øges, når protein koncentration stiger. Mod forventning, har vi vist hvordan, fibrillering af S6 bliver inhiberet ved høje protein koncentrationer pga. dannelse af oligomerer, som ikke er en del af fibrillerings processen.

Det primære fokus i denne afhandling har været at belyse strukturen og de toksiske egenskaber af oligomerer dannet af det præsynaptiske protein α-synuclein (αSN), som er kædet sammen med Parkinson syge. Analyser med småvinkelspredning af røntgen (SAXS) stemmer overens med en struktur model for αSN oligomeren hvor formen er en langstrakt ellipse med en fast kerne og en diffus ydre skal. Dimensionerne af strukturmodellen, bestemt ved SAXS, stemmer overens med andre biofysiske teknikker. Fourier transform infrarød spektroskopi (FTIR) og cirkulær dikroisme viser at den sekundære struktur af kernen er domineret af båndformede strukturer (på engelsk β-sheets), imens FTIR og kernemagnetisk resonans (NMR) spektroskopi bekræfter tilstedeværelsen af ustrukturerede regioner i skallen. Med NMR har vi bestemt hvilken del af αSN sekvensen der indgår i kernen of hvilken del der udgør det diffuse ydre lag.

Oligomerer anses ofte for at være direkte associeret med fibrillerings processen. Med kinetik forsøg og modellering heraf, har vi illusteret hvordan αSN oligomerer ikke er nødvendige intermediater i fibrillerings processen, men i stedet tilhører en anden aggregerings proces.

Et af de helt store spørgsmål i amyloid feltet er hvordan oligomerer kan dræbe nerveceller, og hvorvidt dette er relevant. Den mest udbredte hypotese er at oligomerers cytotoksiske egenskaber er forbundet med deres evne til at permeabilisere cellemembraner. Det er anerkendt at αSN oligomerer interagerer favorabelt med negativt ladede vesikler, og vi har demonstreret, hvorledes de første 12 N-terminale aminosyrer er essentielle for denne interaktion. Baseret på den nuværende litteratur kombineret med vores oligomer-membran interaktions forsøg, spekulerer vi, at interaktionen er drevet af en kombination af elektrostatiske og hydrofobiske interaktioner. Endvidere, har vi vist

hvordan småmolekylet epigallocatechin gallate (EGCG) inhiberer oligomer cytotoksitet ved at interferere med oligomer-membran interaktioner.

Alt I alt, så præsenterer vi ny indsigt i de forskellige processer, som er involveret i fibrillerings processen og giver eksempler på mangfoldigheden i energi landskabet for protein foldning og aggregering. Yderligere, så præsenterer vi ny viden indenfor α-synuclein oligomerer, særligt om deres struktur, rolle i fibrillerings processen og deres cytotoksiske egenskaber.

Summary

The misfolding of a range of peptides and proteins into amyloid fibrils and pre- or non-fibrillar oligomers has been linked to the pathogenesis of neurodegenerative diseases, such as Parkinson's Disease (PD), Alzheimer's Disease and Huntington's Disease. There is an immense interest in the discovery of medicine targeted towards these diseases. The development of rationally designed drug discovery strategies is challenged by the lack of knowledge of the behind lying molecular mechanisms. In this thesis we have addressed neurodegenerative diseases and protein misfolding from different angles. On one side looking at the assembly process of amyloid fibrils, and inhibition hereof, and on the other side looking at the structure and toxicity of oligomers.

In our study of fibril formation we have used the ribosomal protein S6 as a model system. From systematic kinetic experiments of seeded fibril formation combined with kinetic modeling, we have been able to separate the contributions from different mechanisms in the assembly process. Of particular interest was the finding that the exponential phase in the growth phase of fibril formation is the consequence of secondary processes rather than primary nucleation. Generally, the rate constants of primary nucleation and fibril elongation are expected to increase together with increasing protein concentration. S6 is the unusual exception and we found that fibril formation was inhibited at high protein concentrations due to the formation of oligomers that were off-pathway to fibril formation.

The primary focus of this thesis has been to elucidate the structure and toxic function of oligomers formed by the presynaptic protein α-synuclein (αSN), which is linked to PD. Building on previous studies we have established a new low-resolution structural model of αSN oligomers. Small Angle X-ray Scattering (SAXS) data is consistent with a prolate ellipsoid, where the oligomers is build up by a solid core surrounded by a disordered shell. The oligomer dimensions as determined with SAXS are confirmed with other biophysical techniques. Fourier transform infrared spectroscopy (FTIR) and circular dichroism assign the secondary structure of the core to be built up by β-sheets and FTIR and Nuclear Magnetic Resonance (NMR) spectroscopy confirm the appearance of disordered polypeptide. With NMR we have assigned the residues that are located in the core and which are in the shell.

Oligomers are often considered to be on-pathway in fibril formation. By kinetic experiments and kinetic modeling, we have illustrated that αSN oligomers are not obligate intermediates in the process of fibril formation but instead likely to be off-pathway.

One of the key questions in the amyloid field is how oligomers can induce neuronal damage and whether this is relevant. One popular hypothesis is that oligomers can permeabilize cell membranes and thereby lead to cell death. αSN oligomers are known to interact strongly with anionic vesicles and we have demonstrated how the first 12 residues of the N-terminus are crucial for this interaction. Based on the current literature combined with our oligomer-membrane interaction studies we speculate that the interaction is driven by a combination of electrostatic and hydrophobic interactions. Furthermore, we present a case study on the potential of small molecules to inhibit oligomer cytotoxicity by interfering with oligomer-membrane interactions.

In conclusion, we present new insight on the different processes involved in fibril formation and on the multitude of the energy landscape of protein folding and aggregation. Moreover, we present novel data on the structure of αSN oligomers, their role in the fibrillation pathway and on their cytotoxic properties.

Acknowledgements

First I have to thank Daniel Otzen my scientific mentor for almost 5 years for many hours of scientific discussions and +500 e-mails. I cannot imagine a more dedicated supervisor, whenever I presented new data for Daniel he was like a little child on Christmas Eve. I hope, and am almost certain, that we will be collaborating on future projects.

As for protein folding the energy landscape of a PhD project might be smooth in theory but in practice it has its bumps on the way. Being part of the protein biophysics group made these bumps much smoother. I have laughed for many hrs in the laboratory, hallway and offices and have had a great time in the Otzen lab. During my time in the lab, +50 people have been associated with the lab and I am grateful to many of them. In particular, I would like to thank Brian Vad and Søren Nielsen who have been with me throughout my thesis and I am thankful for all our scientific and non-scientific discussions over the years.

I have had a lot of successful collaborations, where especially Gunna Christiansen who have taken ~500 electron microscopy pictures of my protein aggregates and Jørn Kaspersen and Jan Skov Pedersen who have analyzed the oligomers with SAXS, have been involved in several of my projects. Also, I would like to thank the rest of my many collaborators from Aarhus University, Cambridge University, UK and Pfizer Ltd for their many contributions.

Finally, I want to thank Lisbeth, Gustav, my family and friends for all the non-scientific quality time!

List of articles

I. Lise Giehm, Nikolai Lorenzen, Daniel E. Otzen
Assays for α-synuclein aggregation
Methods (2011), **53**, 3,295-305.

II. Nikolai Lorenzen, Daniel E. Otzen
α-synuclein oligomers: Picking the culprit in the line-up
In revision, Essays in Biochemistry "Amyloids in Health & Disease", Invited review

III. Nikolai Lorenzen, Erich E. Wanker, Daniel E. Otzen
Inhibitors of amyloid and oligomer formation
Amyloid Fibrils and Prefibrillar Aggregates.: Molecular and Biological Properties (2013)
Book chapter. ISBN 978-3-527-33200-7

IV. Nikolai Lorenzen, Samuel I. A. Cohen, Søren B. Nielsen, Teresa W. Herling, Gunna Christiansen, Christopher M. Dobson, Tuomas P. J. Knowles, Daniel E. Otzen
Role of Elongation and Secondary Pathways in S6 Amyloid Fibril Growth
Biophysical Journal (2012), **102**, 9, 2167-2175.

V. Taru Deva, Nikolai Lorenzen, Brian S. Vad, Steen V. Petersen, Ida Thøgersen, Jan J. Enghild, Torsten Kristensen, Daniel E. Otzen
Off-pathway aggregation can inhibit fibrillation at high protein concentrations
B B A - Proteins and Proteomics (2013), **1834**, 3, 677-687

VI. Michael Helwig, Akino Hoshino, Casey Berridge, Sang-Nam Lee, Nikolai Lorenzen, Daniel E. Otzen, Jason L. Eriksen, Iris Lindberg
The neuroendocrine protein 7B2 suppresses the aggregation of neurodegenerative disease-related proteins
Journal of Biological Chemistry (2013), **288**, 2, 1114

VII. Paula Lopes, Hans Dyrnesli, Nikolai Lorenzen, Daniel Erik Otzen, Elena E. Ferapontova
Electrochemical Analysis of the Fibrillation of Parkinson's Disease α-synuclein
Analyst. 2013, DOI: 10.1039/C3AN01616A

VIII. Nikolai Lorenzen, Søren B. Nielsen, Alexander K. Buell, Jørn D. Kaspersen, Paolo Arosio, Brian S. Vad, Wojciech Paslawski, Gunna Christiansen, Zuzana Valnickova-Hansen, Maria Andreasen, Jan J. Enghild, Jan S. Pedersen, Christopher M. Dobson, Tuomas P. J. Knowles, Daniel E. Otzen
The role of stable α-synuclein oligomers in the molecular events underlying amyloid formation
(*In revision, Journal of the American Chemical Society)*

IX. Nikolai Lorenzen, Lasse Lemminger, Jannik Pedersen, Søren B. Nielsen, Daniel E. Otzen
The N-terminus of α-synuclein is essential for both monomeric and oligomeric interactions with membranes
(In revision, FEBS letters)

X. Nikolai Lorenzen, Søren B. Nielsen, Cristine Betzer, Yuichi Yushimora, Brian S. Vad, Jørn D. Kaspersen, Jan S. Pedersen, Poul H. Jensen, Frans A. Mulder, Daniel E. Otzen
Epigallocatechin gallate (EGCG) inhibits α-synuclein oligomer toxicity
(Manuscript)

XI. Wojciech Paslawski, Maria Andreasen, Søren B. Nielsen, Nikolai Lorenzen, Karen Thomsen, Jørn D. Kaspersen, Jan S. Pedersen, Daniel E. Otzen
Cytotoxic α-synuclein oligomers are remarkably stable against dissociation
(Manuscript)

Abbreviations

AFM	Atomic force microscopy
ANS	8-Anilino-1-naphthalenesulfonic acid
αSN	α-synuclein
CD	Circular dichroism
DLS	Dynamic light scattering
DMPG	Dimyristoyl phosphatidylglycerol
DOPG	Dioleoyl phosphatidylcholine
DSC	Differential scanning calorimetry
FTIR	Fourier transform infrared spectroscopy
IDP	Intrinsically disordered protein
LB	Lewy Bodies
MALLS	Multi angle laser light scattering
NMR	Nuclear magnetic resonance
PBS	Phosphate buffer saline
SAXS	Small Angle X-ray Scattering
SDS	Sodium dodecyl sulphate
TEM	Transmission electron microscopy
ThT	Thioflavin T
wt	Wild-type

INTRODUCTION PART

1. PARKINSON'S DISEASE

The second most common neurodegenerative disease (after Alzheimer's Disease) is Parkinson's Disease (PD) and in Western Europe the prevalence is 0.16 %, increasing with age to 2.7 % for men and 2.0 % for women above 84 years (1). Together with the ageing population of the Western world the prevalence of PD is expected to increase. Common symptoms are motor symptoms as bradykinesis, shaking and rigidity, and non-motor symptoms as dementia, sleep difficulties, depression and behavioral problems as apathy and impulsivities (2). As of today there is no cure towards PD, but it is possible to treat symptoms to a certain degree (3). There are two pathological hallmarks of PD **(1)** degeneration of dopaminergic neurons in the substantia nigra (50-70 %), however not only restricted to substantia nigra, neurodegeneration is also observed in other brain regions (4). **(2)** the second hallmark is the accumulation in survival cells of Lewy bodies (LB), primarily consisting of insoluble amyloid material (**see chapter III**) which is able to spread form cell to cell in a prion-like fashion (5,6).

The presynaptic protein α-synuclein (αSN), which is widely expressed in the brain (7), was found to be the main constituent of LB (8,9). Many subsequent studies have suggested a direct link between LB formation and cell death (10-14). Today, the attention has shifted from insoluble fibrils towards soluble oligomers (see **Article II)**.

Another argument for the link between PD and αSN arose from genetic studies where point mutations in the gene coding for αSN (SNCA) were found to be connected with familial PD (15-17). Most instances of PD occur sporadically but approx 10 % originates from gene modifications e.g. by triplication of the αSN locus (18).

ALPHA-SYNUCLEIN

αSN is a 140 amino acid protein lacking both cystein and tryptophan residues. It is an intrinsically disordered protein (IDP), lacking persistent structure under physiological conditions (19). The association of αSN with membranes (20,21) is believed to be important for both the physiological role and in the pathogenesis of PD. Even though the physiological role of αSN is still under debate, it is reported to interact *in vivo* with proteins such as Synphilin-1 (22), the chaperones Hsp70 and Hsp40 (23), CSPα and SNARE proteins (24) in the membrane interface of synaptic vesicles, where it may play a role in the regulation of synaptic plasticity, vesicle recycling and neurotransmitter release (25). This is consistent with the finding that ca. 15 % of αSN is associated with membranes in neurons (26).

The N-terminal region (residues 1-60) is important for membrane interaction (Fig. 1) where especially the initial 12 residues have been found to be essential (see **Article IX**) (27,28). The N-terminal region consist of 5 imperfect 11 residue repeats and is highly positively charged with a theoretical pI of 9.5, remarkably high when considering that the theoretical pI of the full protein is 4.7.

MDVFMKGLSK AKEGVVAAAE KTKQGVAEAA GKTKEGVLYV GSKTKEGVVH GVATVAEKTK

N-terminal; residues 1-60; pI = 9.5

EQVTNVGGAVVTGVTAVAQKTVEGAGSIAAATGFV

NAC; residues 61-95; pI = 4.5

KKDQL GKNEEGAPQE GILEDMPVDPDNEAYEMPSE EGYQDYEPEA

C-terminal; residues 96-140; pI = 3.8

Fig 1. In the top is the structure of α-synuclein bound to SDS micelles, with the N-terminal marked in black (rest is grey). From (29). At the bottom, is the amino acid sequence of αSN. Acidic residues are marked red and basic residues are marked blue. pI is theoretical and calculated with ExPASy.

The NAC (non-A beta component) region was initially discovered in amyloid material found in Alzheimer's disease (30). It is hydrophobic with only few charged residues and it is believed to build up the core of the amyloid fibril (31) and oligomer (32,33) structures. Also, the NAC region and N-terminal forms an α-helical structure upon interaction with membranes (20,34).

The C-terminal (residue 96-140) (Fig. 1) is highly acidic with a theoretical pI at 3.8, rich in proline and posses no structural propensity. The C-terminal sequence is typical of an IDP; high overall charge resulting in strong electrostatic repulsion and low overall hydrophobicity reducing the driving force for protein folding (see chapter II) (35).

2. PROTEIN FOLDING AND STABILITY

PROTEIN FOLDING

A native protein is a polypeptide in its predominantly biologically relevant state e.g. an enzyme in its active conformation. For globular proteins the native state is the 3 dimensional organization of the polypeptide chain in α-helices, β-sheets and loops. The process in which the disordered polypeptide arranges into the ordered native state is called protein folding. Depending on the protein in question, the disordered state, typically called the unfolded or denatured state, is typically considered to be an ensemble of structures ranging from fully disordered to relative well-defined conformations (36,37). Whereas the denatured state is difficult to characterize due to its lack of global structure, the native state is in the simple case a well-defined conformation that can be determined at high resolution by e,g. NMR and X-ray crystallography.

In 1968, Cyrus Levinthal used a simple thought experiment to illustrate that protein folding on biologically relevant timescales cannot be achieved by a random sampling of all possible conformations of the polypeptide chain (38). Assuming the gross simplification that each peptide bond has only three allowed combinations of so-called ϕ and ψ torsion angles (39), a 101 residue protein, with 100 peptide bonds, could potentially sample 3^{100} different conformations before finding the correct fold. Assuming a fast sampling rate at the nano- or picoseconds scale, then the protein could be sampling conformations at a time scale longer than the age of the universe, before arriving at the native conformation. Since most small proteins fold within milli- or microseconds, the folding pathway must be biased possibly directed by folding intermediates. This is today known as Levinthal's paradox.

There exist different models of protein folding. The *nucleation-condensation model*, where secondary and tertiary structure forms simultaneously (40) is one of the most recognized models as it include features from existing models as the *hydrophobic collapse theory*. Polypeptide chains consist of alternating hydrophilic residues, which can hydrogen bond to water molecules in aqueous solutions, and hydrophobic residues which are nonpolar and poorly soluble in water. Folded proteins often have a central core which is primarily build up by hydrophobic residues. On the protein surface, *i.e.* the protein-water interface, there are primarily hydrophilic residues. The hydrophobic-collapse model explains how formation of contacts between hydrophobic side chains assist the folding process (41). Another recognized model is the *diffusion-collision model* where the formation (sometimes transient) of micro domains in the denatured state helps to guide the folding process (42).

Christian B. Anfinsen received the Nobel Prize in chemistry in 1972 for his work on ribonuclease. He demonstrated that the folding of ribonuclease *in vitro* can be a reversible process (43). He also established how protein folding could be a reversible process (44) which led to the thermodynamic description of protein folding where the native state is a free energy minimum. Today, protein folding is generally perceived as being possible by means of the funnel-shaped energy landscape of the reaction (45,46) which have been optimized through evolution (47) (Fig. 2).

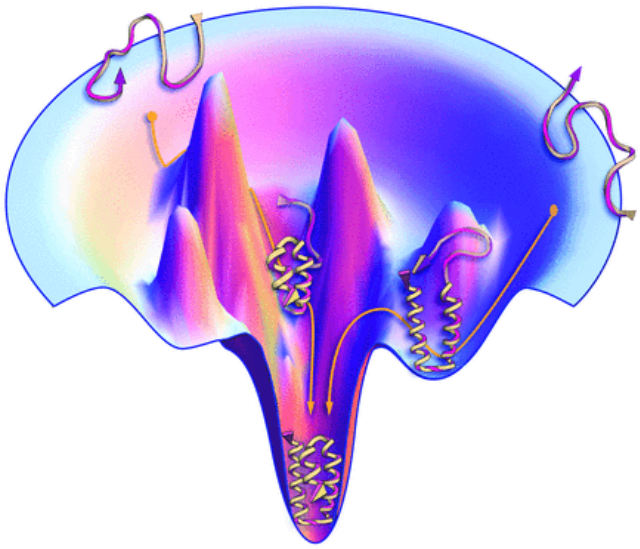

Figure 2. The funnel-shaped energy landscape of protein folding. Examples of protein conformations are shown. From (48).

The width of the folding funnel is the configurational entropy (*S*) and the depth reflects the internal energy of the configuration (*E*). As a protein proceeds down the funnel, *S* decreases whereas the enthalpy (*H*) increases. The entropy decrease is due to restrictions in the degree of freedom, the number of accessible conformations, of the polypeptide chain, and is counteracted by the release of water. The increase in *H* is the consequence of the formation of non-covalent interactions formed in the folding process. *E* decreases as we go down the funnel as the protein becomes more stable.

PROTEIN STABILITY

The analysis of protein stability is an important task in the pharmaceutical industry when developing protein-based pharmaceuticals. It can be a tremendous challenge to formulate a protein which is expected to remain stable in solution at room temperature for several years (49). In the following section I will discuss the thermodynamic stability of proteins. Another essential factor in protein science, that often is prerequisite for the analysis of proteins, is the protein's chemical stability. Examples of concerns are the cleavage of peptide bonds, oxidation of methionine residues at high temperature and elimination or interchange of disulfide bridges. An example of a classical chemical stability problem is the hydrolysis of the peptide bond of aspartic acid at low pH. We encountered this problem with the ribosomal protein S6 when incubated at low pH for several days (**Article II**). This was circumvented by substitution of the aspartic acid with an alanine (D55A), thereby preventing hydrolysis and yielding a native state that remained similar to that of the wild-type protein.

As proposed by the nucleation-condensation model, protein folding is considered as a cooperative process where the secondary and tertiary structure (un)fold simultaneously. This all or none, two-state, behavior where only the denatured state (D) and native state (N) are populated, is valid for small globular proteins, whereas the folding of larger proteins might be the sum of the folding of

several individually two-state folding domains (50,51). When the process is cooperative then protein folding can be described as a unimolecular reaction where D and N exist in equilibrium:

$$\mathrm{D} \leftrightarrows \mathrm{N}$$

$$K_{\mathrm{D-N}} = \frac{\mathrm{D}}{\mathrm{N}} \qquad (1)$$

Where $K_{\mathrm{D\text{-}N}}$ is the equilibrium constant. In a thermodynamically reversible system where temperature (T) and pressure are constant the thermodynamic parameters (discussed above) are related as follows:

$$\Delta G = \Delta H - T\Delta S \qquad (2)$$

The protein stability is defined as the difference in free energy ($\Delta G_{\mathrm{D\text{-}N}}$) between the free energy of Na (G_{N}) and D (G_{D}), and at any condition in the folding reaction the conformation with the lowest free energy will be the most stable, hence most populated state. Proteins are only marginally stable, and $\Delta G_{\mathrm{D\text{-}N}}$ is normally in the range of 5-10 kcal/mol (52). Thus $\Delta G_{\mathrm{D\text{-}N}}$ is the delicate balance of ΔS versus ΔH. Since ΔS and ΔH are difficult to determine experimentally, $\Delta G_{\mathrm{D\text{-}N}}$ is generally determined by estimation of the equilibrium using the following relationship

$$\Delta G_{\mathrm{D-N}} = -RT\ln(K_{\mathrm{D-N}}) \qquad (3)$$

Where R is the gas constant.

HOW TO DETECT CONFORMATIONAL CHANGES IN PROTEINS

When analyzing protein folding, misfolding (see chapter 3) and protein stability it is crucial to be able to experimentally distinguish the denatured state from the native state and any possible intermediates. Below I discuss only methods of relevance for the research part and have therefore excluded some important methods such as differential scanning calorimetry (53), which is one of the standard methods to probe conformational changes in proteins.

CIRCULAR DICHROISM

Circular dichroism (CD) is a unique method to analyze the structure and stability of proteins. When circularly polarized light travels through a CD active sample, then chiral molecules can lead to a difference in absorbance of left and right circulary polarized light. This difference leads to a CD signal. In the Far-UV region (180-250 nm) CD stems from the absorption of peptide bonds which leads to different spectra for different secondary structures as depicted in Figs. 3 and 4. Thus, CD provides an average measurement of the secondary structure content of the protein sample and based on the basis spectra (Fig. 3) it is possible to determine the content of different secondary structure elements by linear combination or deconvolution (54).

In the near-UV region (260-300 nm) it is the aromatic side chains (Trp, Tyr and Phe), cysteine bridges and prosthetic groups which lead to absorption (55). The CD signal is sensitive towards environmental changes in the vicinity of these residues, consequently providing a measure of the tertiary structure.

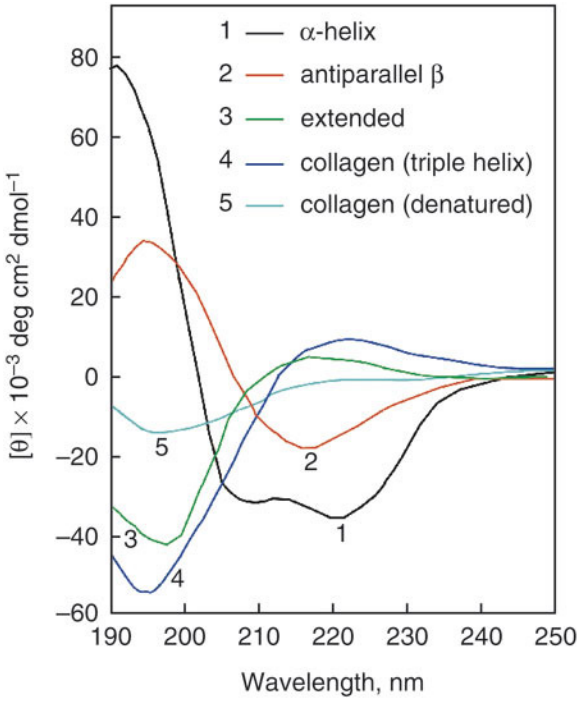

Figure 3. Far-UV circular dichroism. Poly-L-lysine in α-helical (1), antiparallel β-sheet (2) and extended (3) conformations. Also, collagen is shown in its native triple-helical state (4) and its denatured state (5). From (56)

FLUORESCENCE SPECTROSCOPY

The phenomenon of fluorescence is based on the excitation of electrons to an excited state by light. When the electrons return to the ground state the energy is emitted as light at a longer wavelength than that of the light that excited the electron (57). Fluorescence spectroscopy is a strong technique in protein science due to the sensitivity of the method and the occurrence of intrinsic fluorophores in proteins; the aromatic residues tryptophan (Trp), tyrosine and phenylalanine. Especially Trp is an important probe, as it has the highest quantum yield of the aromatic residues, which is defined as the ratio of photons emitted and the photons absorbed (57). Trp is normally excited at 280-295 nm and emits light at 330-360 nm. The emission spectrum of Trp is highly sensitive to the polarity in its vicinity. Since Trp is a hydrophobic amino acid it is often found buried in the hydrophobic core of folded globular proteins. When in the hydrophobic core, of the native protein, the emission spectra will have a different intensity and λ_{max} compared to when Trp is positioned in a hydrophilic local environment. Consequently Trp fluorescence is an efficient probe of changes in the tertiary structure (Fig. 4).

Another useful way to probe different conformational states of proteins with fluorescence spectroscopy is by extrinsic fluorescent probes. Especially probes that change their fluorescence properties upon binding to hydrophobic regions, e,g. Sypro Orange and ANS (58), are very useful in protein folding studies. Also, in **Article I** and Fig. 9A, are examples on how the fluorophore

Thioflavin T (ThT) can be used to monitor protein aggregation, due by recognition of a specific structural motif.

MEASURING THE HYDRODYNAMIC DIMENSIONS OF PROTEINS

As discussed above, a protein in its native state will have a more compact and well-defined structure than in its denatured state. Therefore the hydrodynamic volume of a native protein will appear smaller than of the denatured protein. The difference in hydrodynamic volume can readily be measured with light scattering methods as dynamic light scattering (DLS) where the diffusion rate of proteins can be translated into the corresponding hydrodynamic radius. DLS can reliably differentiate between the denatured and native state of proteins (59).

Standard size-separation methods such as native gel electrophoresis and size-exclusion chromatography (SEC) can also be used to distinguish between different conformational states, based on differences in their hydrodynamic dimensions. The denatured protein has the shortest elution time as it will have a shorter way through the column compared to the corresponding native protein.

PROTEIN DENATURATION

To understand how proteins denature, *i.e.* how the equilibrium in equation 1 becomes shifted towards D, is important when determining the protein stability and when aggregation should be prevented. Protein denaturation is often induced by high temperature, low or high pH and with chemical denaturants.

SOLVENT DENATURATION

Changes in solvent conditions can be used to alter the ratio of D to N. This is normally achieved by addition of chemical denaturants as urea, guanidinium hydrochloride and guanidinium thiocyanate, which at high concentrations will favour D. These denaturants are chaotropes as defined by the Hofmeister series (60) and lead to protein denaturation by increasing S of the system. Chaotropes interact with the polypeptide chain thereby solubilizing the protein, making non-covalent interactions less favorable (61). Chemical denaturants are routinely used to determine protein stability in equilibrium unfolding studies. For an apparent two-state folding protein, the fraction of folded protein as a function of the denaturant concentration is described by a sigmoidal transition as shown in Fig. 4 for the equilibrium unfolding of FK506-binding protein. This is an example of cooperative folding where the transition regions of the secondary structure and tertiary structure, as probed with Far-UV CD and Trp fluorescence, respectively, coincide. The protein stability in water, $\Delta G_{\mathrm{D-N}}^{\mathrm{H_2O}}$, can be determined with equation 3 and by determining $K_{\mathrm{D\text{-}N}}$ at several denaturant concentrations and extrapolating the stability using the following relationship

$$\Delta G_{\mathrm{D-N}} = \Delta G_{\mathrm{D-N}}^{\mathrm{H_2O}} + m_{\mathrm{D-N}} \cdot [\mathrm{Denaturant}] \qquad (4)$$

Where $m_{\mathrm{D\text{-}N}}$ is the proportionality constant between denaturant concentration and $\Delta G_{\mathrm{D\text{-}N}}$, and is correlated to the difference in solvent-accessible surface area between D and N (62)

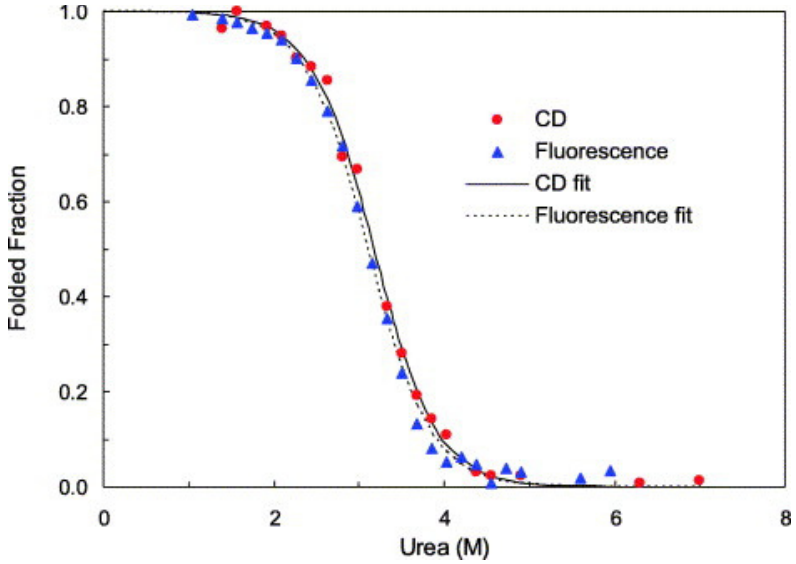

Figure 4. Fraction of folded FK506-binding protein estimated with Far-UV CD at 222 nm and Trp fluorescence at 356 nm with best fits shown. From (63).

3. AMYLOID FIBRILS, OLIGOMERS AND INHIBITION

AMYLOID FIBRILS

In 1984, Rudolph Virchow introduced the term "amyloid" based on his observation that amyloid material could be stained by iodine, in similar fashion as starch which in Latin is "amylum" (64). Going from a rare phenomenon, only observed in uncommon diseases, amyloid fibrils is today acknowledged as an important subject within fields as protein science, medicine, chemistry, nanoscience and microbiology. Amyloid fibrils are normally observed as long filaments, having a diameter of 3-10 nm (65) and of indefinite length (Fig. 5).

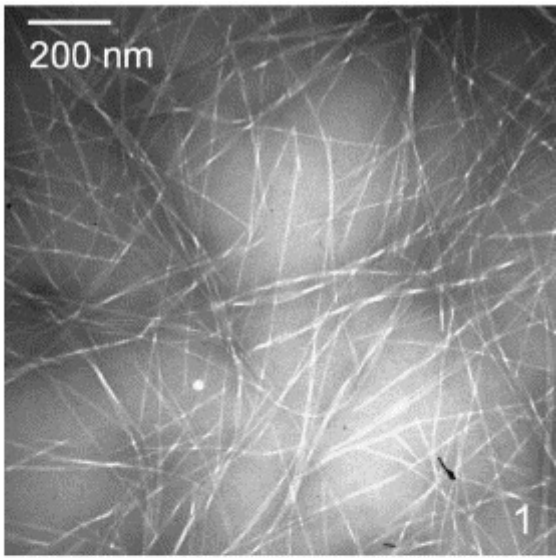

Figure 5. Transmission electron microscopy picture of glucagon amyloid fibrils, from (66).

More than 30 links between diseases and the formation of amyloid fibrils is known, including neurodegenerative diseases as Parkinson's Disease (see chapter 1) and Alzheimer's Disease, systemic amyloidosis as AL and AA amyloidosis and localized diseases as Type II diabetes (67).

In recent time a new class of amyloid fibrils, the "functional amyloids", has emerged and it is now evident that amyloid fibrils are not only related to disease. The best characterized example of functional amyloid is the use of amyloid fibrils by bacteria. They take advantage of the stability of amyloid fibrils in respect to dissociation and protease digestion and use them in the build-up and stabilization of biofilms. The responsible proteins have been characterized for several bacterias including Streptococcus mutans (68), Escherichia Coli (69), Bacillus subtilis (70) and different Pseudomonas species (71) and their conversion into fibrils have been correlated with biofilm formation. Two other remarkable examples of functional amyloids is the case of fibrils as the natural storage of peptide hormones in secretory granules (72) and the example of seemen-derived fibrils which enhance HIV infection (73).

PROTEIN MISFOLDING

Today numerous proteins have been identified to be able to form amyloid fibrils and whereas controversial when proposed (1999), it is now generally believed that fibril formation is a generic property of the polypeptide chain (74). Instead of discussing separate cases the amyloid community now discusses the amylome (75). The unambiguous existence of amyloid fibrils as an accessible conformational state have challenged the conventional view on the energy landscape of protein folding, as funnel-like for smaller proteins with the native state as a free energy minimum (see chapter 2).

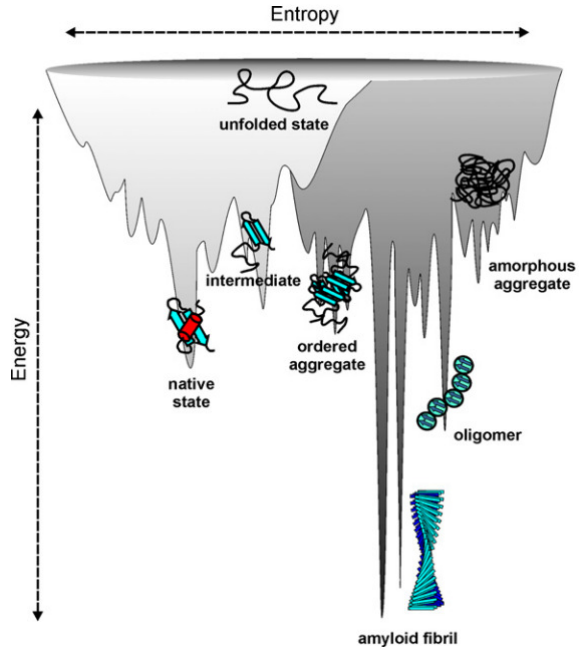

Figure 6. Illustration of the energy landscape of protein folding (light grey) and aggregation (dark gray).Possible protein conformational states is depicted on the figure. From (76).

The energy landscape of protein folding is now often seen extended to a protein folding and aggregation energy landscape (Fig. 6). Folding is not always smooth and especially larger proteins can have rough energy landscapes where partially folded structures, either as intermediates in the folding process or off-pathway, can be populated (77). It is often speculated that these folding intermediates are involved in the onset of fibril formation. Intriguingly, amyloid fibrils appear to have a deeper free energy minimum than the native state, thus thermodynamically more stable (Fig. 6). This have been confirmed experimentally by estimation of the thermodynamic stability of the fibril state of different peptides and proteins using chemical denaturation (see chapter 2) (78). The reversible nature of amyloid fibrils has been confirmed with pressure induced dissociation experiments supporting the view that the native and fibril state exist in equilibrium (79). This lead to an interesting question; if the fibril state is the thermodynamically most stable, then why do we not see more cases of fibril formation within the human body than what is already the case? One important reason is the house keeping system of the cell where evolution have fine tuned chaperones and turnover mechanisms to maintain proteins in their native state. Secondly, even

though the fibril state might be thermodynamically more stable, the energy barrier which a protein has to climb to initiate fibril formation might be astronomic under physiological conditions. Consequently, the native state is perhaps the most populated state due to its kinetic stability.

A remarkable correlation between the rate of fibril formation *in vitro* and the proteins expression level *in vivo* has been established based on a range of proteins (Fig. 7). This suggest that proteins have been optimized through evolution to have a solubility which match their concentration level in the cell (80). That this might indeed be a delicate balance is supported by the finding that triplication of the gene coding for αSN (SNCA), which leads to an increased expression of αSN, causes familial PD (18).

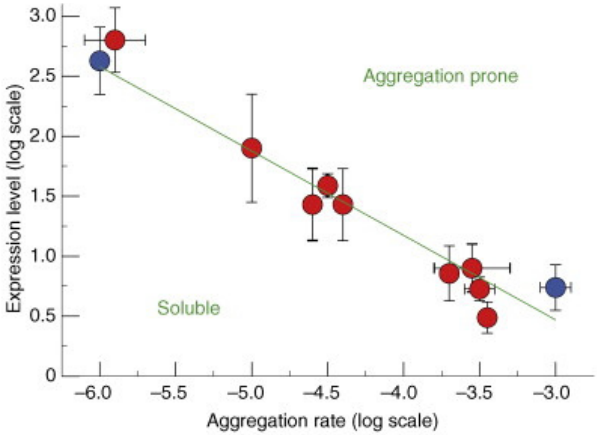

Figure 7. The in vivo expression level plotted as a function of the in vitro aggregation rate. From (80).

It is still an open question whether amyloid fibrils lead directly to cell death in neurodegenerative diseases. Today it is widely believed that none- or pre-fibrillar oligomers might be the toxic agents in neurodegenerative diseases. There are however still reports which correlate the formation of amyloid fibrils and *in vitro* toxicity (81). One speculative hypothesis suggest that everything which is misfolded in a cell might interact inappropriately with proteins or other cellular entities, leading to a disturbance of cellular processes (82).

AMYLOID FIBRILS SHARE A COMMON STRUCTURAL MOTIF

The cross-β ultra structure is the common structural motif of amyloid fibrils. Proteins are arranged in β-sheets perpendicular to the fibril axis (Fig. 8) (83,84). The structural model in Fig. 8 is of one single fibril which is often termed protofibril (or protofilament) and some fibrils are formed by the alignment of several protofibrils forming the mature fibril. Whereas the ultra structure of fibrils is defined it is still limited with high-resolution descriptions of fibril structures.

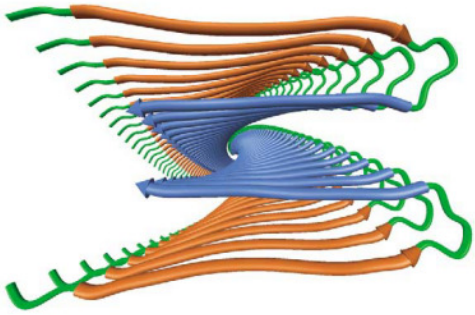

Figure 8. A: Ribbon diagram of the Amyloid-β_{1-40} protofibril showing the cross-β motif based on solid-state NMR data and fits constraints from EM, x-ray scattering, EPR and biochemical techniques, from (85).

However techniques as X-ray diffraction of microcrystals (86) solid-state nuclear magnetic resonance spectroscopy (NMR) and cryo-electron microscopy (85,87-90) have provided high-resolution structures of short peptide sequences. Based on current high-resolution structures it is seen that the cross-β structure is tightly packed and sheets are highly complementary by elaborate hydrogen bonding and strong adhesive forces, which is termed steric zippers (86,91).

Despite the shared cross-β motif of fibrils there are many different types of fibrils. It can even be possible for a single protein to form different types of fibrils and this phenomenon is called polymorphism (14,66,90,92,93). This is also depicted in the energy landscape of protein folding and aggregation in Fig. 6. Polymorphism is often a practical problem in structural determination and kinetic analysis of fibrils.

THE PROCESS OF FIBRIL FORMATION

It is generally agreed that fibril formation is a nucleation dependent process (94,95). This is one of the reasons for the sigmoidal profile often observed for fibril formation. On Fig. 9A, three phases are marked (1) the nucleation phase (2) the growth phase and (3) the saturation phase. In the nucleation phase, monomers come together to form the nuclei (Fig. 9B) *i.e.* the early pre-fibrillar oligomer. This is the primary nucleation which is the rate limiting step in fibril formation. When the fibril nucleus is formed the subsequent elongation *i.e.* association of monomers (Fig. 9B) is a favorable process (95). In the growth phase, primary nucleation and fibril elongation occur together with secondary processes which lead to the formation of additional growing ends capable of elongation, and it seems that the secondary processes dominate the growth phase compared with primary nucleation (96,97). Several types of secondary processes are known but the best described is the breaking of fibrils which lead to a doubling of growing ends, as illustrated in Fig. 9B (97,98) (see **Article IV**).

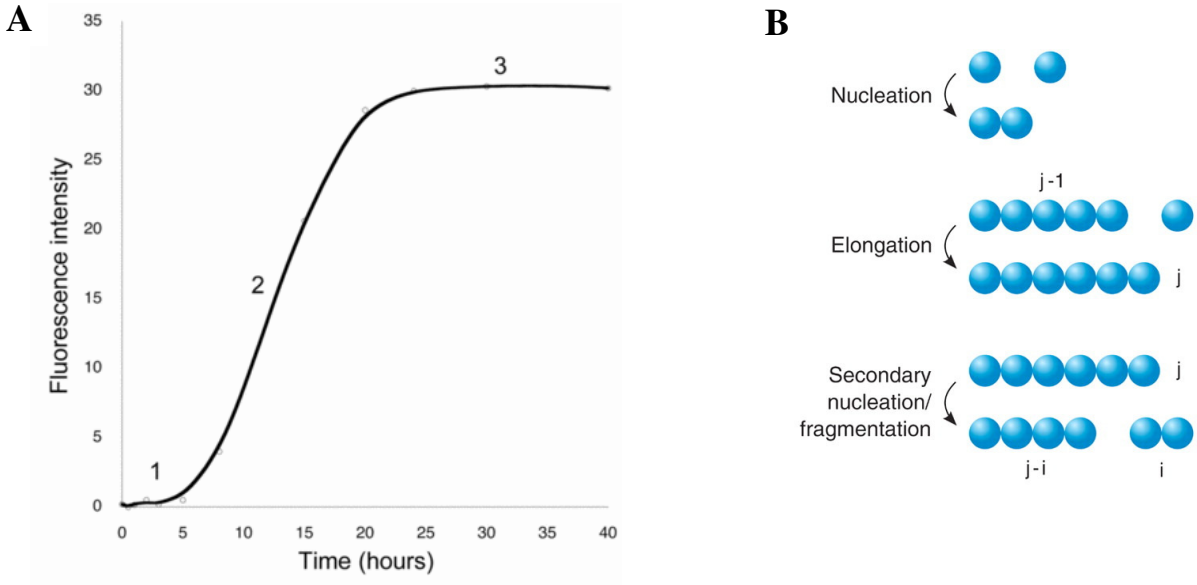

Figure 9. A: Fibril formation measured with ThT fluorescence, from (99). *B: schematic representation of fibril nucleation, elongation and secondary nucleation, from (97).*

The saturation phase is the situation where free monomer and monomer incorporated into fibrils is in equilibrium, meaning that the rate of monomer elongation is equal to the rate of monomer dissociation. Thus the sigmoidal profile of fibril formation is the product of a combination of different microscopic processes, which have recently been described mathematically (97,100-103)

In the above description of the fibril formation process I have confined myself with the model of nucleation polymerization combined with secondary processes (100-102) as this is the basis of the kinetic modeling included in **Articles IV & VIII**. Thus I have neglected the description of other models e.g. the Nucleation Conformational Convertion theory (104,105) Also, I have assumed that the elongating species is monomers rather than oligomers, which will be discussed in **Articles IV & VIII**.

REVIEWS

In the following three reviews we have discussed several important subjects relevant for the research part. In **Article I**, we have discussed purification of αSN, methods to detect fibril formation and how to set up robust fibrillation assay. This review is practical and highly relevant for all articles in the research part. In **Article II**, we zoom in on αSN oligomers, discussing their structure and their role in the process of fibril formation. Furthermore, we discuss their ability to interact with membranes and how this relates to toxicity. With **Article** III, we complete the introduction part, with a discussion of different strategies and examples on how to inhibit the formation and toxicity of amyloid fibrils and oligomers.

Article I

Methods 53 (2011) 295–305

Contents lists available at ScienceDirect

Methods

journal homepage: www.elsevier.com/locate/ymeth

Assays for α-synuclein aggregation

Lise Giehm [a,b], Nikolai Lorenzen [a], Daniel E. Otzen [a,*]

[a] Interdisciplinary Nanoscience Center (iNANO), Department of Molecular Biology, Gustav Wieds Vej 10C, DK - 8000 Aarhus C, Denmark
[b] Department of Pharmaceutics and Analytical Chemistry, Universitetsparken 2, DK – 2100 Copenhagen, Denmark

ARTICLE INFO

Article history:
Available online 14 December 2010

Keywords:
Amyloid
Plate reader assay
Thioflavin T
Shared micelles
SDS
Trifluoroethanol
Natively disordered proteins
Alpha-synuclein

ABSTRACT

This review describes different ways to achieve and monitor reproducible aggregation of α-synuclein, a key protein in the development of Parkinson's disease. For most globular proteins, aggregation is promoted by partially denaturing conditions which compromise the native state without destabilizing the intermolecular contacts required for accumulation of regular amyloid structure. As a natively disordered protein, α-synuclein can fibrillate under physiological conditions and this process is actually stimulated by conditions that promote structure formation, such as low pH, ions, polyamines, anionic surfactants, fluorinated alcohols and agitation. Reproducibility is a critical issue since α-synuclein shows erratic fibrillation behavior on its own. Agitation in combination with glass beads significantly reduces the variability of aggregation time curves, but the most reproducible aggregation is achieved by sub-micellar concentrations of SDS, which promote the rapid formation of small clusters of α-synuclein around shared micelles. Although the fibrils produced this way have a different appearance and secondary structure, they are rich in cross-β structure and are amenable to high-throughput screening assays. Although such assays at best provide a very simplistic recapitulation of physiological conditions, they allow the investigator to focus on well-defined molecular events and may provide the opportunity to identify, *e.g.* small molecule inhibitors of aggregation that affect these steps. Subsequent experiments in more complex cellular and whole-organism environments can then validate whether there is any relation between these molecular interactions and the broader biological context.

1. Protein aggregates/fibrils/amyloids: friends or enemies?

Over the last few decades, protein aggregation gone from being an irritating side product in the test tube to becoming a subject of great interest. This has been stimulated by the realization that a large and growing number of diseases are associated with the formation and accumulation of protein aggregates [1]. The ability to form amyloid structures has also been exploited by living systems, where proteins forming fibrils during the normal life-cycle have functional rather than disease associated properties [2–5]. Thus, understanding the structural features of fibrils, as well as the processes leading to their formation is important for designing new drugs as well as in development of new nano-biomaterials such as nano-tubes, wires, and scaffolds [6]. Understanding the process of amyloid formation requires an ability to reproduce this aggregation under controlled circumstances, in other words the development of robust aggregation assays. The following review focuses on ways in which this has been developed for α-synuclein (αSN), a key player in the development of Parkinson's disease. We focus specifically on the formation of the amyloid end product, rather than ways to optimize accumulation of the presumably cytotoxic prefibrillar aggregate, whose properties are deserving of a separate article.

2. How to obtain high yields of pure αSN: boiling or periplasmic purification

A prerequisite for characterizing the fibrillation process of αSN is high amounts of highly pure protein. This makes it desirable to have a simple and high yielding protocol of αSN expression and purification. Recombinant αSN is easily expressed in *Escherichia coli* [7] and the purification has mainly exploited acid precipitation or boiling of cell lysate [8]. We initially purified αSN by boiling cell lysate released by sonication of the cells. Such a step precipitates most of the natively folded cytoplasmic proteins through unfolding to a "sticky" thermally denatured state. By its very nature, this transformation is not possible for αSN, allowing it to remain in solution. The boiling step is followed by two successive chromatographic steps of ion-exchange and size-exclusion [9,10] resulting in a high purity of αSN estimated by SDS–PAGE and a yield of 50–60 mg/mL αSN per liter culture [9,10]. However, when we apply such a purification protocol, SDS–PAGE

Abbreviations: cac, critical aggregation concentration; scc, super-critical concentration.

* Corresponding author. Fax: +45 86 12 31 78.
E-mail address: dao@inano.au.dk (D.E. Otzen).

1046-2023/$ - see front matter © 2010 Elsevier Inc. All rights reserved.
doi:10.1016/j.ymeth.2010.12.008

reveals two bands (Fig. 1A insert). The expected full-length αSN in band A has the expected 14.46 kDa weight by full-length MS (Fig. 1A) but migrates at 18 kDa, probably due to poor binding of SDS to the acidic tail of αSN [8]. The much fainter band B shows a mass of approximately 12.1 kDa (Fig. 1B) but an intact N-terminal, corresponding to a C-terminal truncated αSN of 120 amino acids. Later, αSN expressed by *E. coli* was observed to be localized in the periplasm [8]. This led to a new two step method for purifying αSN [8] of (1) an osmotic shock releasing αSN from the periplasm and (2) ion-exchange chromatography to remove other periplasmic proteins. We have used this approach in combination with an additional size exclusion step to obtain approximately 60–65 mg/mL αSN per liter culture. In our experience this leads to a very pure αSN preparation without degradation bands (Fig. 1C lane 0 min). In contrast, degradation bands accumulate upon exposure to 100° C already after 10 min (Fig. 1C). Thus we recommend to use either the method developed by Huang and co-workers [8] or an initial sonication releasing cytosolic and periplasmic protein followed by acid precipitation with HCl[59] at pH 3.5 in 20 min. This precipitates the majority of the contaminating proteins, leaving 80–90% pure αSN is in the soluble fraction. We do not observe any degradation products caused by acid hydrolysis. A subsequent ion-exchange chromatography step is sufficient to obtain pure αSN.

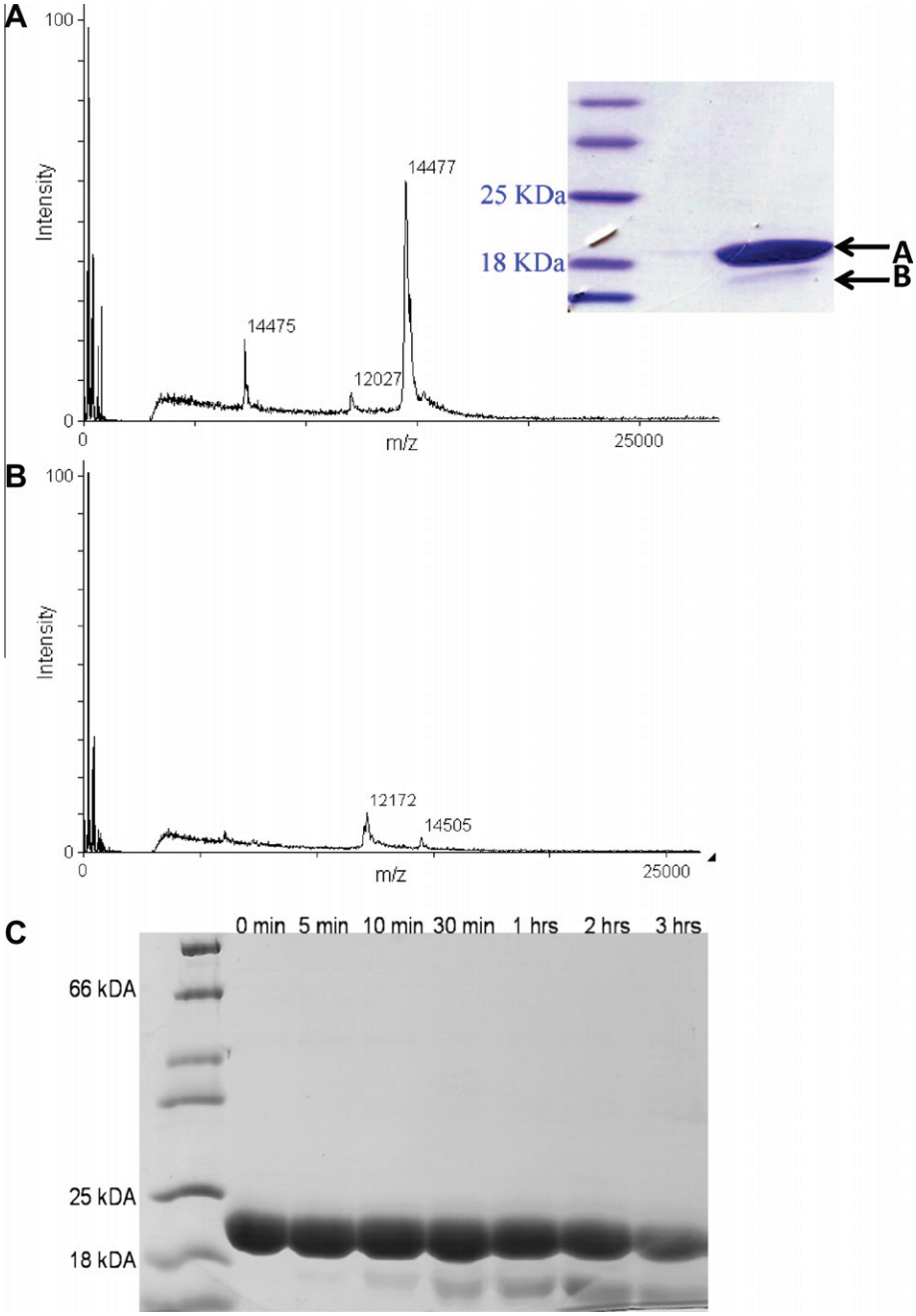

Fig. 1. Purification of αSN. (A) Mass spectrometric profile of the major band A migrating at 18 kDa in the SDS–PAGE gel insert. Notice the major peak of 14,477 kDa corresponding to full-length αSN (exact molecular weight: 14,460 Da). (B) Mass spectrometric profile of band B. The peak at 12,172 Da has an intact N-terminus, indicating that it is a C-terminal truncation cleaving after either Pro120 (molecular weight: 12,111 Da) or Asp121 (molecular weight: 12,226 Da). (C) SDS–PAGE of purified αSN incubated in PBS buffer at 100° C for the indicated lengths of time. The lower band corresponds to band B in panels A and B.

3. How to transform a soluble protein to an aggregate: finding the right window of destabilization

Amyloid fibrils normally form in a process where soluble protein is converted to insoluble proteinaceous aggregates of an essentially uniform, highly ordered, β-sheet rich structure (though soluble amyloid fibrils have also been detected [11]). The conversion typically involves dramatic structural rearrangements and is not restricted to proteins of specific structural classes. Proteins which in their native state are as diverse as β-sheets [12,13], β-barrels [14,15], β-sandwiches [16], α-helices [17,18], α/β mixtures [19,20] or even natively unfolded proteins [21] have been observed to fibrillate. Fibrillation of such globular proteins generally requires a population of fibrillation-competent partially unfolded conformations. Consequently fibrillation is promoted by conditions that destabilize the native fold, such as mutations, changes in pH, addition of denaturants and detergent and/or elevated temperature [22]. Such conditions typically expose otherwise buried hydrophobic regions in the protein, promoting intermolecular interactions with identical regions in other proteins and the formation of higher order species. These phenomena have been documented for several globular proteins including β_2-microglobulin [23,24], S6 [25], human lysozyme [26] and insulin [27] and this mechanism probably accounts for the conversion of many globular proteins into amyloid fibrils. However, fibril formation under conditions where the native state is the most stable species has been reported for *Drosophila melanogaster* acylphosphatase [28], which is suggested to aggregate directly from its native-like structure followed by a conversion into amyloid-like fibrils [28–30]. A similar model has been proposed for insulin incubated at low pH, where insulin oligomers/aggregates have almost the same α-helical content as the native structure and the conversion into β-sheet rich fibrils occurs later in the process [30]. Such models propose two distinct pathways for protein unfolding and misfolding, highlighting that multiple pathways for protein aggregation exists.

It is important to keep in mind that the chosen destabilizing conditions should not be so harsh as to completely destabilize intermolecular interactions. To force a very stable globular protein to fibrillate, one strategy would be to combine low concentrations denaturant/detergent with elevated pH and/or elevated temperature, thus avoiding high denaturant and detergent concentrations [25]. In addition, inorganic anions and cations that shield electrostatic repulsions between charged amino acids in the polypeptide chain (especially important at extreme pH) promote fibrillation [25,31]. Additional stress can be provided by agitation. Thus, as a rule of thumb when setting up a primary fibrillation assay of globular proteins, knowledge about the stability of a given protein should be combined with appropriate salts/metal ions and agitation. Having succeeded in establishing conditions in which the globular protein of interest fibrillates, one can start to fine-tune the setup to conditions most relevant for the issue in question, as well as fine-tuning the reproducibility.

In contrast, some proteins have a high degree of structural disorder in their native state and are characterized as natively unfolded [32]. They lack significant intra-chain interactions, existing in a very dynamic ensemble of different "unstructured" states. These proteins actually have to gain structure in order to form fibrils [33]. Refolding may be mediated by ligands, other proteins, membranes or changes in pH and ionic strength. In the absence of such conformational constraints these proteins would be expected to be less conformationally restricted and be expected to polymerize into fibrils much more readily than tightly packed globular proteins [33]. In addition to the "stars of the show", Aβ and tau (Alzheimer's) and α-synuclein (Parkinson's disease), other examples of natively unfolded proteins involved in amyloidegenic diseases include islet amyloid polypeptide IAPP (type II diabetes) [34,35]. Furthermore, the peptides ABri and ADan (which arise from abnormally elongated translation of the Bri gene and lead to Familial British and Danish Dementia, respectively) assume no regular folded structure in solution as monomers [36]. It is probably no coincidence that the protein CsgA, which forms the main component in naturally occurring *E. coli* curli fibrils, has no persistent structure in solution as a monomer but is optimized to aggregate directly to the amyloid state without any folded monomeric intermediate [37].

Nearly all of the natively unfolded proteins (apart from those arising from abnormal cleavage products) have a high net charge and low overall hydrophobicity compared to folded proteins [38]. These properties lead to high solubility and may in fact decrease their aggregation propensity under normal physiological conditions, although their extended structure potentially allows a multitude of intermolecular interactions [32,38,39]. Interestingly, αSN falls outside this classification, given that its N- and C-terminal ends have opposite charges and the hydrophobicity of αSN is in the same order of magnitude as that of a folded protein [38]. The most hydrophobic part of αSN is the NAC (non-amyloid β component) region, composed of residues 62–95. This region is believed to constitute the fibrillation core of αSN fibrils [40,41]. The C-terminal tail may shield the NAC-region by long-range interactions between the C-terminal and N-termini [42–44]. This means that the flexible structure of αSN is required to retain the monomeric state.

4. How to promote alpha synuclein fibrillation?

The exact molecular mechanism underlying αSN fibrillation is not yet clear and it is most likely determined by the experimental conditions used in the aggregation assay. However, conditions leading to enhanced fibril propensity have been associated with the occurrence of a partially folded structure of αSN. Fink, Uversky and co-workers have shown that protonation at low pH (pH 3) induces formation of a collapsed state with increased fibrillation propensity. This collapsed state has increased secondary structure contents (FTIR and Far-UV CD), a slightly more compact structure (SAXS), increased affinity towards the fluorophore 8-anilino-1-naphthalene-sulfonic acid (which binds to partially unfolded structures) [45] and a stiffened C-terminal tail which is engaged in more contacts with the NAC region (based on a combination of solution NMR and computations) [46]. Elevation of the incubation temperature induces similar overall structure and is also associated with increased fibrillation propensity [45]. Consequently, such a partially folded species is predicted to be essential not only in the formation of fibrils, but also in determining the fibrillation route, given that different pathways gives rise to different morphologies of the αSN aggregates [47–49].

Since aggregation in many cases involves self-assembly steps into higher-order structures from a fibrillation nucleus, the likelihood of such events to occur will increase with protein concentration until a certain concentration, termed the supercritical concentration (scc), is reached [50]. Above the scc, nucleation is no longer rate-limiting and the lag phase of fibrillation does not decrease significantly with increasing concentration. The phenomenon is well known for αSN, where increased protein concentration decreases the lag-phase of fibrillation [21] and for αSN the scc is, in our laboratory, estimated to be ~8.2 mg/mL (~574 μM) (data not shown). The scc will most like depend upon the given conditions in which αSN is fibrillated, (*e.g.* temperature, degree/type of agitation, pH etc.). This phenomenon should not be confused with the critical aggregation concentration (cac), which is

the minimum αSN concentration required to allow fibrillation to occur on the experimentally accessible time scale. This has been estimated to be around 15 μM [51], and can be taken as an indication of the thermodynamic stability of the fibrils. After the completion of the fibrillation process, there will typically be a reservoir of monomer left (at the concentration given by the cac) in equilibrium with the fibrils.

Other factors that have been demonstrated to accelerate αSN fibrillation *in vitro* include anions [52], polyanions [53,54], polycations [55,56], salts [52], pesticides and herbicides [57–59], heavy metals [60], negatively charged detergents [47], molecular crowding [61–63], low pH [45] and acidic phospholipids [64]. For polyanions, salts, pesticides, herbicides, heavy metals and negatively charged detergents, the proposed mechanism by which these very different molecules, with respect to charge, hydrophobicity and size, can accelerate the fibrillation of αSN is believed to be quite similar, namely the stabilization of a partially folded fibrillogenic conformation of αSN. Such a conformation has mainly been correlated to altered secondary structure estimated by Far-UV CD [45,47,52,54,57,58,60,64] and FTIR [45,57]. Structural changes in αSN has also been detected by increased ANS–fluorescence [45,60], changes in tyrosine fluorescence [58,60] (αSN has no Trp residues) and acrylamide quenching [60]. Polycations such as the very basic histone proteins do not induce any change in secondary structure elements [55,56], although SAXS indicate formation of a 2 αSN:1 histone complex [56]. Thus polycations may promote a fibrillation pathway that does not require a detectable change in the secondary structure content. The action and the molecular mechanisms by which a given molecule binds to αSN are most likely very different, given the wide range of different biochemical properties of the compounds and the fluctuating structure of αSN. The obvious interaction would include negatively charged molecules interacting with the N-terminus (net positive charge), positively charged molecules interacting with the C-terminus (net negatively charged) and hydrophobic molecules interacting with the NAC region and perhaps helping bridge to the NAC regions of other αSN molecules [65]. Such interactions could reduce the conformational flexibility of αSN, thereby preventing the C-terminal tail from shielding the NAC-region through long-range interactions with the N-terminus, and perhaps even bridging C/C- or N/N-terminal alignments in the αSN fibril. Additionally, such interactions could mask putative intramolecular repulsions between charged areas and the NAC-region, resulting in a collapsed αSN with regards to the NAC-region and N/C-terminus. Nevertheless, the known fibrillation inducers do not induce dramatic structural changes in the secondary structure [65]. Thus ligand-complexed αSN remains relatively unstructured though more compact than in the uncomplexed form.

Another important way to induce αSN fibrillation is by agitation. While the exact mechanism of agitation induced fibrillation is unknown, agitation is expected to increase the number of amyloid fibril ends through fragmentation or by increasing the collision of monomeric and oligomeric species [66] interacting with fibril ends. In addition, agitation is believed to increase the air–water interface, which in turn acts in a similar way as a hydrophobic surface to promote formation of partially stabilized structures [21,67].

5. Detecting and characterizing αSN fibrils

When setting up a fibrillation assay of αSN, a good detection method is needed, which is experimentally simple, does not perturb the fibrillation process, gives an unequivocal read-out and is robust towards changing solvent conditions. An overview of these methods is provided in Table 1. A widely used approach is to use the dye Thioflavin T (ThT) which is often used to verify the presence of fibrils as well as examine fibrillation kinetics *in situ* [68]. Here detection is based on the fluorescence characteristic of ThT. Free ThT has a very low fluorescence signal, but binding to amyloid increases the fluorescence of ThT by several orders of magnitude [69,70]. While the characteristic fluorescence of ThT is relatively specific towards fibrils [70,71], we have seen that amorphous aggregates of different proteins can in fact increase ThT fluorescence for different proteins, albeit to a much smaller extent on a per-mg level [72]. As demonstrated in Fig. 2 for αSN, low ThT intensities in a 384 well plate combined with linearly increasing ThT-emission over long time scales (in contrast to the traditional sigmoidal curve normally experienced in fibrillating systems) indicate amorphous aggregates in our experience. In contrast, high ThT-intensities and sigmoidal curves correlated to rod-like structures.

ThT fluorescence intensity *per se* cannot be used as an absolute measure for the amount of fibrils, and the intensity can vary considerably among different proteins that form fibrils [71]. Both Aβ and glucagon fibrils with different overall morphology have different intensities in emitted ThT fluorescence [73,74]. However, provided these issues are taken into account, ThT is an easy, cheap and rather specific fibril-detecting tool which furthermore does not interfere with the kinetics of αSN fibrillation [45].

Other probes that can be used for detection of amyloid structure are congo red (CR) and N-arylaminonaphthalene sulfonate (NAS) and derivatives. NAS and NAS-derivatives have been reported to be more sensitive and versatile probes for αSN aggregation than ThT and especially bis-NAS should be able to detect oligomeric as well as fibrillar species [75]. This is probably related to these probes' affinity for hydrophobic regions rather than the actual fibrillar repeat pattern. Fluorescent probes can be used both in plate readers (96 and 384 well plates are the most practical range) as well as in single-solution cuvettes in fluorometers, though the latter set-up obviously limits the amount of data-output. Earlier stages in the aggregation pathway may be probed by fluorescence polarization [76], which detects the decrease in mobility caused by higher-order structures and is particularly sensitive to transitions from monomers to oligomeric structures, or by FRET [77], which can detect contacts between two differently labelled molecules. In all cases it is necessary to investigate to what extent these probes could interfere with the aggregation process, *e.g.* by carrying out the assay at different probe concentrations. The stronger binding of NAS probes to hydrophobic regions could conceivably affect the stabilities of different aggregated species for simple mass-action reasons. Furthermore, labelling of αSN could also interfere with aggregation properties unless the labelled αSN is employed as a minor fraction of the whole population.

ThT-binding is not considered final proof of fibril formation. The ultimate gold standard is X-ray fiber diffraction, preferably using aligned samples to allow the equatorial reflection at 4.8 Å, corresponding to the distance between β-strands, to be distinguished from the meridional reflection around 10–12 Å which stems from the distance between laterally associated β-sheets [78,79]. The ultra structural level can be checked by transmission electron microscopy (TEM), small angle X-ray scattering (SAXS) and/or atomic force microscopy (AFM), whereas the secondary structure level can be investigated using Far-UV CD or FTIR.

In general, αSN can follow many different fibrillation pathways leading to different fibril morphologies [47,80]. A multitude of fibrillation pathways can arise by branching out from different species formed at different stages of the fibrillation pathway, αSN can populate different types of fibrillogenic partially folded monomeric conformations, different types of oligomers or different early- or late-stage fibrils. In view of αSN's flexible conformation as a monomer and the existence of many different kinds of oligomers [81] and fibrils [49], it is difficult to rule out branching at any given

Table 1
Overview of different common techniques used in the characterization of protein amyloid and their pitfalls.

Technique	Information provided	Pitfalls
Fluorescent amyloid-binding Probes	Simple way to monitor formation of fibrils in combination with the effect of changing solvent conditions or screening for fibril inhibitors. Can be scaled up to plate reader assays.	• Can affect the kinetics of the fibrillation process, though Thioflavin T (ThT) is generally non-invasive. • Possible competitive binding between the fluorescent probe and other additives such as small molecule inhibitors. Must be tested on individual basis, *e.g.* by adding inhibitor to mature fibril in presence of ThT to see if drop in ThT fluorescence is immediate (indicating quenching/displacement), slow (indicating fibril dissolution) or non-existent (indicating no affinity for fibrils). • Amyloid structures that do not bind the fluorescent probe (rather uncommon, but observed for Aβ [107]) • Dead time for loading a 96-well plate is ~15 min when the protein is loaded in the last step in individual wells. It is best only to measure one plate at a time since the plate reader also provides the necessary shaking. • Long-term shaking is detrimental to plate readers with monochromators, so filters are recommended instead.
Light scattering (absorbance 320–350 nm)	General (not amyloid-specific) aggregation	• A glass bead (which for αSN in agitation induced systems is crucial for increased reproducibility) may disturb the data output. • Low sensitivity.
Dynamic light scattering (DLS)	Size distribution of aggregated particles	• High sensitivity to dust particles sets high demands on sample preparation • Currently DLS experiments are most often run in batch mode which gives low data output.
Small angle X-ray scattering (SAXS)	Structure of aggregated species. Can provide information on several different co-existing species.	• *Ab initio* modelling of complicated systems such as fibrillating proteins requires high level of expertise and can take weeks to months. • Currently low throughput.
Transmission electron microscopy (TEM) atomic force microscopy (AFM)	Ultrastructure of aggregates.	• Low throughput. • Surface interactions which can interfere with the equilibrium of species involved in the fibrillation process. • Low binding of fibrils or intermediate to the surfaces used (mica (AFM) or grid (TEM)). • May require optimization of type of mica and grids in different protein formulations. • Unintended selection for species that have affinity for the AFM/TEM surfaces.
Far-UV circular dichroism (Far UV-CD)	Secondary structure of aggregates in solution	• Low throughput. • Spectra of fibrils do not necessarily give traditional β-sheet spectrum (*e.g.* minimum at 218 nm) [[74]]. • Light scattering artifacts (and noisy data) by aggregated material (this can in many cases be overcome by sonication of the fibril-sample).
Fourier transform infrared spectroscopy (FTIR)	Secondary structure of aggregates in dry state.	• Low throughput. • Solution FTIR requires high protein concentration. • Drying of sample can induce structural changes in the protein.
Fiber X-ray diffraction	Verification of amyloid structure	• Best results obtained with aligned samples, but this is often experimentally challenging. • Difficult to assign reflections apart from the canonical distances between strands (~4.8 Å) and between sheets (~10–12 Å).

stage. We have observed very different ThT-positive fibril structures made by αSN, depending on the conditions in which αSN was fibrillated. In the case of non-agitated SDS-induced fibrils, we obtain worm-like fibrils (imaged by TEM in Fig. 3A), which according to higher-resolution SAXS analysis are composed of beads on a string (see below). In contrast, agitation-induced fibrils of αSN have a simple and straight rod-like structure (Fig. 3B) [47].

6. Other techniques to follow αSN aggregation

Fibrillation may also be detected by light scattering, which simply monitors an increase in size and is not specific for amyloid structure as such. The absorbance spectrum at 320–350 nm (which should be a flat baseline for non-colloidal protein solution) is an easy way to detect the scattering from larger particles. However, such measurements in a plate reader are confounded by the presence of glass beads, which can be used to dramatically increase the reproducibility of fibrillation onset, elongation and ThT level at end fibrillation, probably by ensuring homogeneous agitation [82]. ThT fluorescence, on the other hand, is not affected by glass beads.

Dynamic light scattering (DLS) is a very sensitive method to detect formation of aggregates (including non-ThT binding structures such as oligomers), and less than 0.01% (w/w) aggregates can be detected under favourable conditions. Conversely, this means that DLS requires high purity of the samples, since low amounts of dust, etc. can lead to misinterpretations of the data. DLS is traditionally a single-cuvette method, but more recently high throughput 96- or 384-well plate reader formats have become available [83].

Small angle X-ray scattering (SAXS) has traditionally been used merely to follow the increase in size (radius of gyration and molecular weight) during the fibrillation process. Recent progress has also made it possible to obtain much more detailed (though still low-resolution) structural information by *ab initio* modeling. Vestergaard and co-workers [84] characterized the structural features of all the species involved in insulin fibrillation and in 2009 Oliveira et al. [85] confirmed the use of time resolved SAXS solution by analyzing the fibrillation of glucagon. Experimentally SAXS is

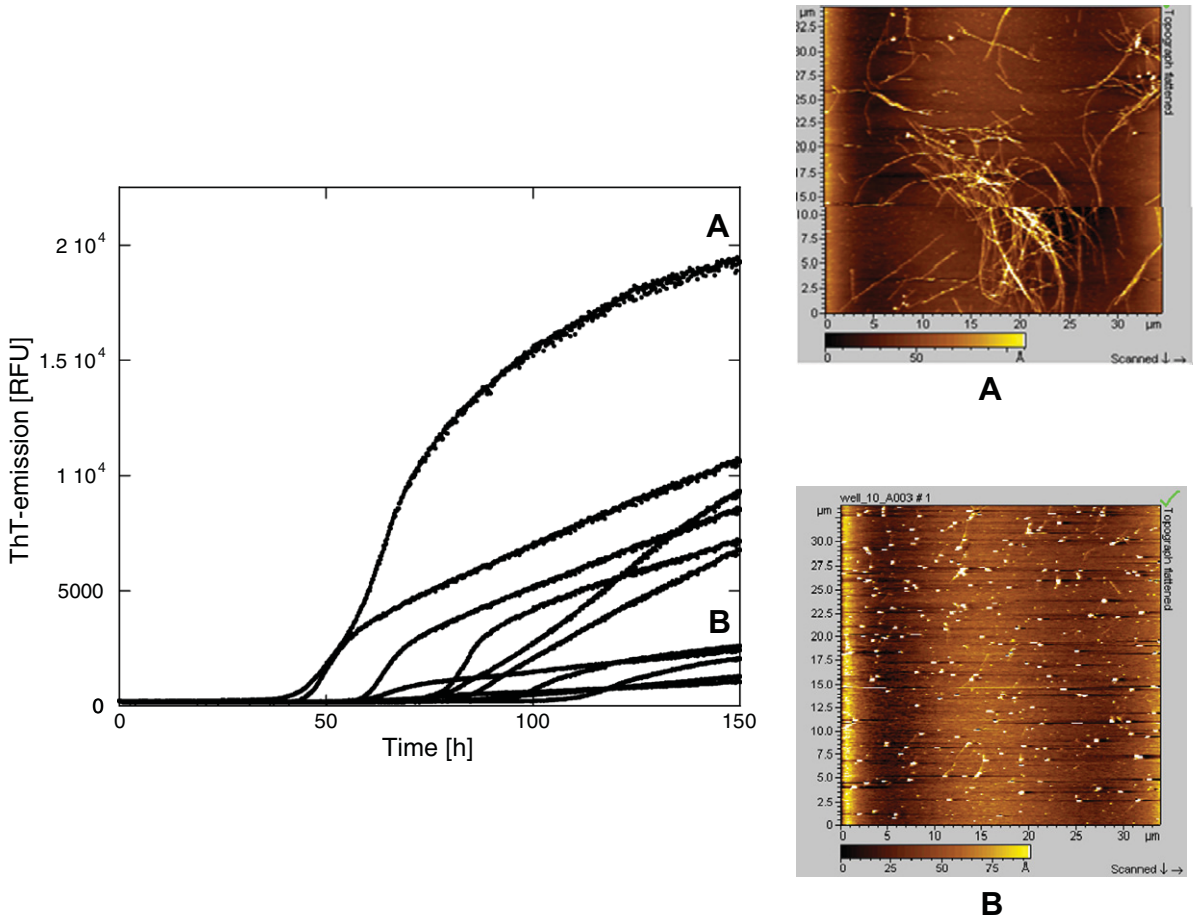

Fig. 2. Left: time profile for the increase in the Thioflavin T (ThT) fluorescence during aggregation of αSN by shaking at 37° C in PBS buffer. Notice the diversity of time profiles even though all samples are identical in composition, incubated in the same plate and subjected to the same degree of agitation. Right: atomic force microscopy images of samples giving rise to (A) high and (B) low ThT fluorescence. High ThT fluorescence is associated with formation of *bona fide* fibrils while low ThT fluorescence indicates small granular aggregates.

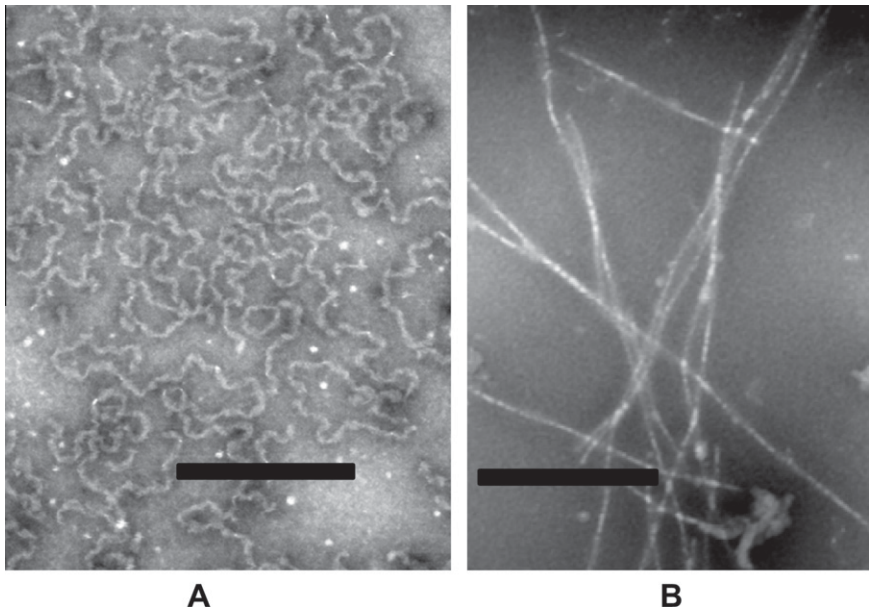

Fig. 3. Transmission electron microscopy of αSN aggregated (A) by incubating in 0.5 mM SDS and PBS buffer without shaking and (B) by shaking at 37° C in PBS buffer. The scale bar indicates 200 nm. Panel B adapted from [47].

very straightforward. Concentrations well below 1 mg/ml can yield good data provided large enough species are formed and the reaction proceeds sufficiently slowly to allow long exposure times. Overall dimensions and molecular weights can rapidly be calculated. For more high-resolution structures, the *ab initio* modelling process is computationally intensive and typically requires weeks to months of analysis and modelling. Nevertheless, SAXS is undergoing a methodological revolution these years, where modelling processes are continuously being improved and new programs and methods will in the near future undoubtedly accelerate the process tremendously [86]. We expect SAXS to become a mainstay of detailed fibrillation studies as the use of this technique becomes more wide-spread.

We have characterized the fibrillation process of αSN in physiological buffer (without SDS) by SAXS and identified a wreath-shaped oligomeric species of ~16 αSN molecules with overall dimensions corresponding to the approximate thickness of a lipid bilayer. Consistent with this, membrane disruptive activity is associated with this oligomeric species. In addition, the kinetic traces of the different species formed during the fibril formation suggest that the oligomer is the building block of fibrils, and the fibrils can in fact be reconstructed by stacking of the oligomers (L.G., D.I. Svergun, D.E.O and B. Vestergaard, data submitted).

7. Obtaining reproducible conditions for α-synuclein fibrillation

In general the degree of reproducibility needed in a given assay depends on the nature of the measurement. Thus detection of small variations in the nucleation and elongation rate will demand a higher reproducibility than a fibrillation assay which simply ascertains to what extent fibrils are formed after a given time period. Here high reproducibility in the fibrillation onset or elongation rate is not essential.

We have examined the reproducibility of αSN fibrillation in plate reader assays [82], and the general conclusion is that increased reproducibility is correlated to decreased lag-times. The nucleation process is a stochastic event and the activation barrier is proportional to the nucleation, thus the lower the activation barrier, the lower variance in the stochastic event of nucleation. Known fibrillation stimuli such as polyamines [80,87], metal-ions [21] and heparin [53] did not increase reproducibility in our plate reader assays [82]. Inspired by Fink and co-workers, we systematically tested the use of small glass beads in combination with agitation and empirically determined that the use of one glass bead (3–4 mm in diameter) in each well in a 96 well plate (rounded wells) in combination with orbital agitation was crucial to obtain good reproducibility [82]. Under these conditions, the dominant nucleation mechanism can be shown to be fragmentation of the initially formed fibrils [88] (S.I.A. Cohen, L.G., D.E.O. and T. Knowles, unpublished observations). Note that this optimization has to be repeated whenever fibrillation conditions change. Thus, to achieve the same degree of reproducibility in a 384 well plate (squared wells) we needed to incorporate two glass beads of 1.2–1.4 mm (diameter) in combination with orbital agitation. It is possible that the reproducibility of αSN fibrillation may be increased even further by combining known fibrillation stimuli as heparin, metal-ions etc. and the glass bead induced agitation.

8. Controlling the time frame and reproducibility of the fibrillation assay by structure-inducing solvent additives: SDS and TFE

Time is often of the essence in the development of good fibrillation assays. A prohibitively slow aggregation assay can severely hamper systematic studies and lead to problems with slow competing processes, such as evaporation, chemical modifications and photobleaching. Agitation decreases the time of αSN fibrillation dramatically from many weeks/months [89] to hours/days in *in vitro* systems and consequently makes it feasible to decrease the timeframe of the experiment. However, if one wishes to avoid agitation and still obtain data within days/weeks, SDS has proven to stimulate αSN fibrillation in a highly reproducible manner within a very narrow concentration window [47,82]. The proposed mechanism is very different from agitation induced fibrillation of αSN. Based on very detailed SAXS studies, we have proposed a model of stepwise growth of SDS-decorated αSN fibrils, which occurs by a process of continuous accretion rather than the rate-limiting accumulation of a distinct nucleus. In this process, ~4 αSN molecules are recruited to stabilize a shared micelle by forming a shell around the micellar core, presumably leaving part of the protein outside the micelle available for forming intermolecular contacts to other αSN molecules similarly engaged. Consistent with this, the process is not dependent on monomer concentration, since the rate limiting step is the bridging of the individual clusters which are formed very rapidly at the beginning of the process. This process is optimal at relatively low SDS:αSN ratios (~12:1), while higher SDS concentrations lead to the formation of complexes of 2 or fewer αSN molecules per micelle. As well as effectively short-circuiting the nucleation process, the shared micelle mechanism results in a flexible worm-like appearance which we refer to as a beads-on-a-string model [47].

It is very important to note that this SDS-induced stimulation of aggregation only occurs within a rather short window of opportunity; at lower SDS:αSN ratios, there is not enough SDS to allow shared micelles to form and at higher SDS:αSN ratios, there is not enough αSN to provide enough αSN molecules per micelle to allow "loose ends" of αSN to hang out and form bridge heads to other clusters (summarized in Fig. 4). Furthermore, the question inevitably arises whether aggregation under these conditions are representative of the more physiologically relevant SDS-free conditions found in the cell. Our own results suggest that SDS-induced aggregation is reasonably representative of other kinds of fibrillation, given that the potent aggregation inhibitor baicalein [90,91] also prevents SDS-induced αSN aggregation (L.G. and D.E.O., unpublished observations). Nevertheless, one cannot expect identical rankings of different compounds in SDS- versus SDS-free assays.

In addition to SDS, we have explored the possibility of using other structure-inducing solvents to obtain reproducible fibrillation of αSN. 2,2,2-trifluoroethanol (TFE) is widely used in peptide and protein chemistry to stabilize β-sheet and α-helix conformations of proteins. The dielectric constant is significantly decreased when TFE is added to water, resulting in a weakening of protein–protein hydrophobic interactions and a strengthening of inter- and intramolecular hydrogen binding. For a thorough discussion of the effect of TFE on proteins and the delicate interplay between polar and hydrophobic forces see [92]. TFE also induces secondary structure in αSN and phase diagrams obtained by circular dichroism reveal the following structural transitions: natively unfolded intermediate partially → folded intermediate (0–10% TFE); partially folded intermediate → β-structure-enriched (10–15% TFE), transformations within the β-structure species (15–25% TFE), (IV) β-structure-enriched → α-helical (25–35% TFE), and rearrangements within the α-helical species (35–60% TFE) [93]. From light scattering data αSN is monomeric at 7.5%, oligomeric at 15% and monomeric at 40% TFE [93]. However, a more recent study on the effect of TFE on monomeric αSN proposes a more refined model, simply that partly helical intermediate conformations of αSN exist in equilibrium with the natively disordered state at low TFE concentrations, leading to a highly α-helical conformation at high TFE concentrations [94].

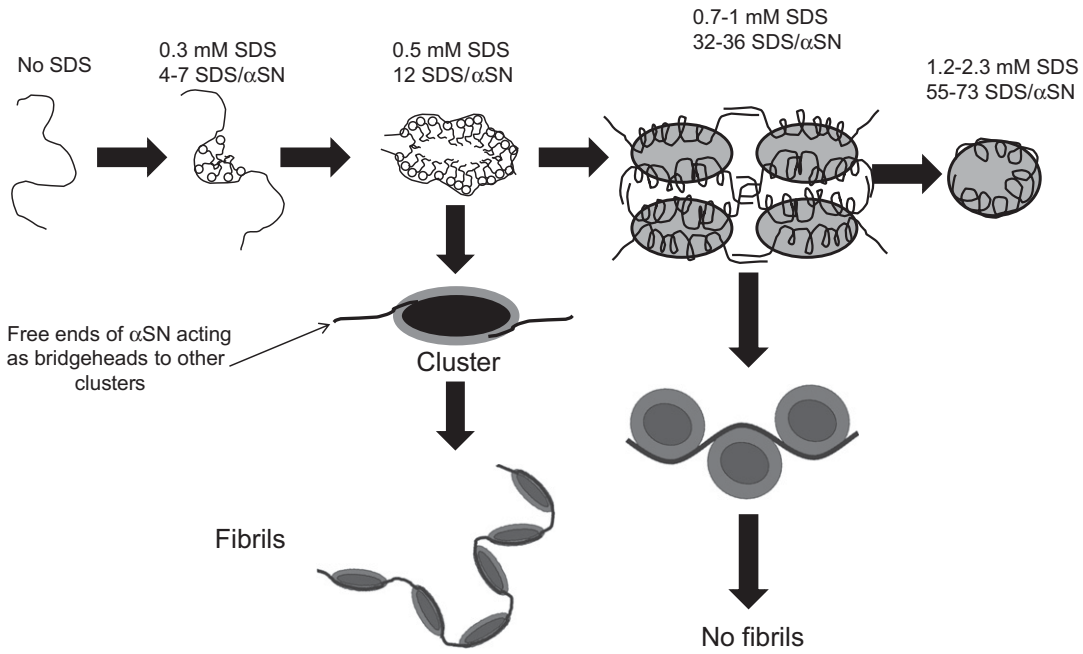

Fig. 4. Scheme depicting how different SDS:αSN ratios lead to formation of different types of αSN:SDS complexes with different aggregation propensities. At a ratio of around 12 SDS per αSN, shared micelles form in which ~4 αSN molecules associate around one micelle, leaving loose ends hanging out for bridging to other clusters. Low ratios provide insufficent SDS to form micelles, while there is not enough αSN per micelle at high ratios to allow loose ends to hang out and bridge to other clusters. Adapted from [47].

TFE is known as a potent inducer of the fibrillation of a wide array of proteins and peptides, including αSN [93,95–99]. We have investigated the kinetics and reproducibility of TFE induced αSN fibrillation following ThT-fluorescence. However, we find that although TFE is an effective inducer of αSN fibrillation and efficiently shortens the nucleation phase, the mechanism of the fibrillation seems extraordinarily complex and the time profiles of fibrillation vary dramatically with TFE concentration. This makes it much less suitable as a model system of fibrillation compared to the SDS-induced fibrillation assay. At low (8–12%) TFE concentrations, fibrillation initiates readily, but kinetics profiles are very sensitive to changes in TFE concentration and αSN concentration displaying several multiphasic time profiles including overshoots and decays to initial fluorescence values (data not published, N.L and D.E.O). The complexity of the system in this region is presumably the result of a borderline region of TFE-induced transitions of αSN as described above. Around 14–26% TFE, the kinetic profiles are less sensitive to TFE concentration. The extent of fibrillation follows a bell-shape form with a maximum at 16% TFE, consistent with recent observations for both αSN [94] and numerous other proteins [92]. TFE-induced fibrillation is therefore probably associated with a partly helical intermediate [94], just as seen for the SDS-induced fibrils; similar to these fibrils, the TFE-induced fibrils are curvilinear rather than straight [94]. At high (30–50%) TFE concentrations, we observe a relatively low degree of fibrillation, consistent with the stabilization of monomeric helical conformations.

9. Levels of data output: low, medium or high throughput?

Plate reader based assays in a 96 or 384 well format (typically monitored by fluorescent probes, absorbance measurements, DLS and SLS) increase the level of data output significantly compared to individual cuvettes. In plate reader assays we seal the plate with tape to avoid any evaporation and consequently changes in the sample volume in a given well of the plate. We have experienced that not only is a glass bead important for increased reproducibility in agitation induced fibrillation of αSN but indeed also a certain volume of sample in each well [82]. Other advantages of plate readers are the low sample volume, homogeneous shaking and automatic measurements over long time scales. If additional experiments are needed to provide information about, *e.g.* secondary structure contents (Far-UV CD and FTIR), the ultra structural level (AFM, TEM, X-ray fiber diffraction), the size distribution at a given time point (size exclusion (SEC) and/or field flow fractionation [100] (FFF)), vesicle permeabilization [101] and biological assays, the scientist needs to consider how much sample is needed to complete additional experiments. Here a batch mode investigation using eppendorf tubes or cuvettes typically requires ~0.5–1.5 mL sample compared to a well in plate readers of 80–200 μL. However, highly reproducible assays allow the contents of different wells to be pooled to obtain higher sample volumes for batch mode analyses.

10. Conclusion: how many ways to skin a cat?

There is no perfect way to induce αSN fibrillation, if by perfect we mean "physiologically representative yet experimentally approachable" – simply because αSN fibrillation is typically a long and stochastic process that is highly dependent on the precise cellular conditions found in the neuronal environment, including both small molecules such as the highly reactive dopamine, the presence of quality control pathways such as the ubiquitin–proteasome system [102,103] or the lysosome [104] and the surface of organelles such as mitochondria or the plasma membrane. Inevitably the inclusion of more components in the assay mixture leads to greater sources of error and more leeway for less predictable events. It is important to accept that all *in vitro* based fibrillation assays will be simplistic and reductionist. The very fact that αSN can be persuaded to fibrillate in so many different ways and with so many different kinds of stimuli truly illustrates that these fibrils can be made in many different ways. The weak point in the analysis lies in linking all this structural information to the state

of α-synuclein aggregation *in vivo*. Here information is much scarcer. Although αSN inclusions in the brain have been shown to be in the fibrillar form [105], nobody has to the best of our knowledge as yet reported the existence of different kinds of structures in the observed *in vivo* aggregates, though the conjugated luminescent polymers developed by Peter Nilsson at Linköping University hold much promise in this regard [106]. Nevertheless, *in vitro* assays have their virtues. Provided the assays can be optimized for high reproducibility, they allow the investigator to focus on well-defined molecular events and may provide the opportunity to identify, *e.g.* small molecule inhibitors of aggregation that affect these steps. Subsequent experiments in more complex cellular and whole-organism environments can then validate whether there is any relation between these molecular interactions and the broader biological context. The access to a broad array of such compounds can undoubtedly increase the chances of finding a few promising leads which may ultimately lead to ways to prevent unwanted levels of αSN aggregation – always assuming that this aggregation is indeed the main causative agent in Parkinson's disease.

Acknowledgments

We would like to thank the following wonderful collaborators: Jan Skov Pedersen, Cristiano Oliveira and Bente Vestergaard for fantastic SAXS work on αSN aggregation, Poul Henning Jensen for insightful and uncompromising discussions on the biochemical aspects of αSN aggregation, Jan Enghild, Peter Lüttge Jensen and Steen Vang Petersen for mass spectrometric analyses, Bjørn Holst from Bioneer A/S for the αSN expression vector used for these studies, and Sam Cohen and Tuomas Knowles for valuable discussions on the mechanism of αSN aggregation. This work is supported by the Danish Ministry of Science, Technology and Innovation (through the innovation consortium CureND) and a Rapid Response Award from the Michael J. Fox Foundation for Parkinson's Research.

References

[1] F. Chiti, C.M. Dobson, Protein misfolding functional amyloid, and human disease, Annu. Rev. Biochem. 75 (2006) 333–366.
[2] M.R. Chapman, L.S. Robinson, J.S. Pinkner, R. Roth, J. Heuser, M. Hammar, S. Normark, S.J. Hultgren, Role of *Escherichia coli* curli operons in directing amyloid fiber formation, Science 295 (2002) 851–855.
[3] J.M. Kenney, D. Knight, M.J. Wise, F. Vollrath, Amyloidogenic nature of spider silk, Eur. J. Biochem. 269 (2002) 4159–4163.
[4] J.F. Berson, A.C. Theos, D.C. Harper, D. Tenza, G. Raposo, M.S. Marks, Proprotein convertase cleavage liberates a fibrillogenic fragment of a resident glycoprotein to initiate melanosome biogenesis, J. Cell. Biol. 161 (2003) 521–533.
[5] M.P. Badtke, N.D. Hammer, M.R. Chapman, Functional amyloids signal their arrival, Sci. Signal 2 (2009) 43.
[6] I. Cherny, E. Gazit, Amyloids: not only pathological agents but also ordered nanomaterials, Angew. Chem. Int. Ed. Engl. 47 (2008) 4062–4069.
[7] R. Jakes, M.G. Spillantini, M. Goedert, Identification of two distinct synucleins from human brain, FEBS Lett. 345 (1994) 27–32.
[8] C. Huang, G. Ren, H. Zhou, C.C. Wang, A new method for purification of recombinant human alpha-synuclein in *Escherichia coli*, Protein Expr. Purif. 42 (2005) 173–177.
[9] P.H. Weinreb, W. Zhen, A.W. Poon, K.A. Conway, P.T. Lansbury Jr., NACP, a protein implicated in Alzheimer's disease and learning, is natively unfolded, Biochemistry 35 (1996) 13709–13715.
[10] L. Narhi, S.J. Wood, S. Steavenson, Y. Jiang, G.M. Wu, D. Anafi, S.A. Kaufman, F. Martin, K. Sitney, P. Denis, J.C. Louis, J. Wypych, A.L. Biere, M. Citron, Both familial Parkinson's disease mutations accelerate alpha-synuclein aggregation, J. Biol. Chem. 274 (1999) 9843–9846.
[11] T.S. Burkoth, T.L.S. Benzinger, D.N.M. Jones, K. Hallenga, S.C. Meredith, D.G. Lynn, C-terminal PEG blocks the irreversible step in [beta]-amyloid (10–35) fibrillogenesis, J. Am. Chem. Soc 120 (1998) 7655–7656.
[12] D. Hamada, C.M. Dobson, A kinetic study of beta-lactoglobulin amyloid fibril formation promoted by urea, Protein Sci. 11 (2002) 2417–2426.
[13] M.R.H. Krebs, D.K. Wilkins, E.W. Chung, M.C. Pitkeathly, A.K. Chamberlain, J. Zurdo, C.V. Robinson, C.M. Dobson, Formation and seeding of amyloid fibrils from wild-type hen lysozyme and a peptide fragment from the -domain, J. Mol. Biol. 300 (2000) 541–549.
[14] S. Srisailam, T.K.S. Kumar, D. Rajalingam, K.M. Kathir, H.S. Sheu, F.J. Jan, P.C. Chao, C. Yu, Amyloid-like fibril formation in an all beta-barrel protein partially structured intermediate state (s) is a precursor for fibril formation, J. Biol. Chem. 278 (2003) 17701.
[15] A.T. Alexandrescu, K. Rathgeb-Szabo, An NMR investigation of solution aggregation reactions preceding the misassembly of acid-denatured cold shock protein A into fibrils, J. Mol. Biol. 291 (1999) 1191–1206.
[16] A. Lim, M.J. Saderholm, A.M. Makhov, M. Kroll, Y. Yan, L. Perera, J.D. Griffith, B.W. Erickson, Engineering of betabellin-15D: a 64 residue beta sheet protein that forms long narrow multimeric fibrils, Protein Sci. 7 (1998) 1545–1554.
[17] M. Fändrich, M.A. Fletcher, C.M. Dobson, Amyloid fibrils from muscle myoglobin: even an ordinary globular protein can assume a rogue guise if conditions are right, Nature 410 (2001) 165–166 (London).
[18] T.A. Pertinhez, M. Bouchard, E.J. Tomlinson, R. Wain, S.J. Ferguson, C.M. Dobson, L.J. Smith, Amyloid fibril formation by a helical cytochrome, FEBS Lett. 495 (2001) 184–186.
[19] F. Chiti, M. Bucciantini, C. Capanni, N. Taddei, C.M. Dobson, M. Stefani, Solution conditions can promote formation of either amyloid protofilaments or mature fibrils from the HypF N-terminal domain, Protein Science: A Publication of the Protein Society 10 (2001) 2541.
[20] G. Damaschun, H. Damaschun, H. Fabian, K. Gast, R. Kröber, M. Wieske, D. Zirwer, Conversion of yeast phosphoglycerate kinase into amyloid-like structure, Proteins: Struct., Funct., Bioinf. 39 (2000) 204–211.
[21] Fink, A. (2007) In: Misbehaving Proteins, pp. 265-85, Springer, New York
[22] J.C. Rochet, P.T. Lansbury Jr., Amyloid fibrillogenesis: themes and variations, Curr. Opin. Struct. Biol. 10 (2000) 60–68.
[23] N.H. Heegaard, T.J. Jorgensen, L. Cheng, C. Schou, M.H. Nissen, O. Trapp, Interconverting conformations of variants of the human amyloidogenic protein beta2-microglobulin quantitatively characterized by dynamic capillary electrophoresis and computer simulation, Anal. Chem. 78 (2006) 3667–3673.
[24] T.R. Jahn, M.J. Parker, S.W. Homans, S.E. Radford, Amyloid formation under physiological conditions proceeds via a native-like folding intermediate, Nat. Struct. Mol. Biol. 13 (2006) 195–201.
[25] J.S. Pedersen, G. Christensen, D.E. Otzen, Modulation of S6 fibrillation by unfolding rates and gatekeeper residues, J. Mol. Biol. 341 (2004) 575–588.
[26] D.R. Booth, M. Sunde, V. Bellotti, C.V. Robinson, W.L. Hutchinson, P.E. Fraser, P.N. Hawkins, C.M. Dobson, S.E. Radford, C.C. Blake, M.B. Pepys, Instability, unfolding and aggregation of human lysozyme variants underlying amyloid fibrillogenesis, Nature 385 (1997) 787–793.
[27] J. Brange, L. Andersen, E.D. Laursen, G. Meyn, E. Rasmussen, Toward understanding insulin fibrillation, J. Pharm. Sci. 86 (1997) 517–525.
[28] G. Soldi, F. Bemporad, S. Torrassa, A. Relini, M. Ramazzotti, N. Taddei, F. Chiti, Amyloid formation of a protein in the absence of initial unfolding and destabilization of the native state, Biophys. J. 89 (2005) 4234–4244.
[29] M.K. Chow, A.M. Ellisdon, L.D. Cabrita, S.P. Bottomley, Polyglutamine expansion in ataxin-3 does not affect protein stability: implications for misfolding and disease, J. Biol. Chem. 279 (2004) 47643–47651.
[30] M. Bouchard, J. Zurdo, E.J. Nettleton, C.M. Dobson, C.V. Robinson, Formation of insulin amyloid fibrils followed by FTIR simultaneously with CD and electron microscopy, Protein Sci. 9 (2000) 1960–1967.
[31] J.S. Pedersen, J.M. Flink, D. Dikov, D.E. Otzen, Sulfates dramatically stabilize a salt-dependent type of glucagon fibrils, Biophys. J. 90 (2006) 4181–4194.
[32] V.N. Uversky, What does it mean to be natively unfolded?, Eur J. Biochem. 269 (2002) 2–12.
[33] V.N. Uversky, A.L. Fink, Conformational constraints for amyloid fibrillation: the importance of being unfolded, Biochim. Biophys. Acta 1698 (2004) 131–153.
[34] R. Kayed, Y. Sokolov, B. Edmonds, T.M. McIntire, S.C. Milton, J.E. Hall, C.G. Glabe, Permeabilization of lipid bilayers is a common conformation-dependent activity of soluble amyloid oligomers in protein misfolding diseases, J. Biol. Chem. 279 (2004) 46363–46366.
[35] C.E. Higham, E.T. Jaikaran, P.E. Fraser, M. Gross, A. Clark, Preparation of synthetic human islet amyloid polypeptide (IAPP) in a stable conformation to enable study of conversion to amyloid-like fibrils, FEBS Lett. 470 (2000) 55–60.
[36] L. Nesgaard, B. Vad, G. Christiansen, D.E. Otzen, Kinetic partitioning between aggregation and vesicle permeabilization by modified ADan, Biochim. Biophys. Acta 1794 (2009) 84–93.
[37] X. Wang, D.R. Smith, J.W. Jones, M.R. Chapman, *In vitro* polymerization of a functional *Escherichia coli* amyloid protein, J. Biol. Chem. 282 (2007) 3713–3719.
[38] V.N. Uversky, J.R. Gillespie, A.L. Fink, Why are natively unfolded proteins unstructured under physiologic conditions?, Proteins 41 (2000) 415–427
[39] V.N. Uversky, Natively unfolded proteins: a point where biology waits for physics, Protein Sci. 11 (2002) 739–756.
[40] B.I. Giasson, I.V. Murray, J.Q. Trojanowski, V.M. Lee, A hydrophobic stretch of 12 amino acid residues in the middle of alpha-synuclein is essential for filament assembly, J. Biol. Chem. 276 (2001) 2380–2386.
[41] H.N. Du, L. Tang, X.Y. Luo, H.T. Li, J. Hu, J.W. Zhou, H.Y. Hu, A peptide motif consisting of glycine, alanine, and valine is required for the fibrillization and cytotoxicity of human alpha-synuclein, Biochemistry 42 (2003) 8870–8878.
[42] M.M. Dedmon, K. Lindorff-Larsen, J. Christodoulou, M. Vendruscolo, C.M. Dobson, Mapping long-range interactions in [alpha]-synuclein using spin-label NMR and ensemble molecular dynamics simulations, J. Am. Chem. Soc 127 (2005) 476–477.

[43] C.W. Bertoncini, Y.S. Jung, C.O. Fernandez, W. Hoyer, C. Griesinger, T.M. Jovin, M. Zweckstetter, Release of long-range tertiary interactions potentiates aggregation of natively unstructured alpha-synuclein, Proc. Natl. Acad. Sci. USA 102 (2005) 1430–1435.
[44] Y. Sung, D. Eliezer, Residual structure backbone dynamics, and interactions within the synuclein family, J. Mol. Biol. 372 (2007) 689–707.
[45] V.N. Uversky, J. Li, A.L. Fink, Evidence for a partially folded intermediate in alpha-synuclein fibril formation, J. Biol. Chem. 276 (2001) 10737–10744.
[46] M.K. Cho, G. Nodet, H.Y. Kim, M.R. Jensen, P. Bernado, C.O. Fernandez, S. Becker, M. Blackledge, M. Zweckstetter, Structural characterization of alpha-synuclein in an aggregation prone state, Protein Sci. 18 (2009) 1840–1846.
[47] L. Giehm, C. L. Oliveira,G. Christiansen, J. S. Pedersen, D. E. Otzen, SDS-induced fibrillation of alpha-synuclein: an alternative fibrillation pathway, J. Mol. Biol. (2010).
[48] G. Bhak, Y.J. Choe, S.R. Paik, Mechanism of amyloidogenesis: nucleation-dependent fibrillation versus double-concerted fibrillation, BMB Rep. 42 (2009) 541–551.
[49] W. Hoyer, T. Antony, D. Cherny, G. Heim, T.M. Jovin, V. Subramaniam, Dependence of alpha-synuclein aggregate morphology on solution conditions, J. Mol. Biol. 322 (2002) 383–393.
[50] E.T. Powers, D.L. Powers, The kinetics of nucleated polymerizations at high concentrations: amyloid fibril formation near, above the supercritical concentration, Biophys. J. 91 (2006) 122–132.
[51] M.E. van Raaij, J. van Gestel, I.M.J. Segers-Nolten, S.W. de Leeuw, V. Subramaniam, Concentration dependence of a-synuclein fibril length assessed by quantitative atomic force microscopy and statistical-mechanical theory, Biophys. J. 107 (2008) (Epub).
[52] L.A. Munishkina, A.L. Fink, V.N. Uversky, Accelerated fibrillation of alpha-synuclein induced by the combined action of macromolecular crowding and factors inducing partial folding, Curr. Alzheimer Res. 6 (2009) 252–260.
[53] J.A. Cohlberg, J. Li, V.N. Uversky, A.L. Fink, Heparin and other glycosaminoglycans stimulate the formation of amyloid fibrils from alpha-synuclein in vitro, Biochemistry 41 (2002) 1502–1511.
[54] I.H. Liu, V.N. Uversky, L.A. Munishkina, A.L. Fink, W. Halfter, G.J. Cole, Agrin binds alpha-synuclein and modulates alpha-synuclein fibrillation, Glycobiology 15 (2005) 1320–1331.
[55] J. Goers, V.N. Uversky, A.L. Fink, Polycation-induced oligomerization and accelerated fibrillation of human alpha-synuclein in vitro, Protein Sci. 12 (2003) 702–707.
[56] J. Goers, A.B. Manning-Bog, A.L. McCormack, I.S. Millett, S. Doniach, D.A. Di Monte, V.N. Uversky, A.L. Fink, Nuclear localization of alpha-synuclein and its interaction with histones, Biochemistry 42 (2003) 8465–8471.
[57] V.N. Uversky, J. Li, A.L. Fink, Pesticides directly accelerate the rate of alpha-synuclein fibril formation: a possible factor in Parkinson's disease, FEBS Lett. 500 (2001) 105–108.
[58] V.N. Uversky, J. Li, K. Bower, A.L. Fink, Synergistic effects of pesticides and metals on the fibrillation of alpha-synuclein: implications for Parkinson's disease, Neurotoxicology 23 (2002) 527–536.
[59] A.B. Manning-Bog, A.L. McCormack, J. Li, V.N. Uversky, A.L. Fink, D.A. Di Monte, The herbicide paraquat causes up-regulation and aggregation of alpha-synuclein in mice. paraquat and alpha-synuclein, J. Biol. Chem. 277 (2002) 1641–1644.
[60] V.N. Uversky, J. Li, A.L. Fink, Metal-triggered structural transformations aggregation, and fibrillation of human alpha-synuclein. A possible molecular NK between Parkinson's disease and heavy metal exposure, J. Biol. Chem. 276 (2001) 44284–44296.
[61] V.N. Uversky, M.C. E., K.S. Bower, J. Li, A.L. Fink, Accelerated alpha-synuclein fibrillation in crowded milieu, FEBS Lett. 515 (2002) 99–103.
[62] L.A. Munishkina, A.L. Fink, V.N. Uversky, Concerted action of metals and macromolecular crowding on the fibrillation of alpha-synuclein, Protein Pept. Lett. 15 (2008) 1079–1085.
[63] M.D. Shtilerman, T.T. Ding, P.T. Lansbury Jr., Molecular crowding accelerates fibrillization of alpha-synuclein: could an increase in the cytoplasmic protein concentration induce Parkinson's disease?, Biochemistry 41 (2002) 3855–3860
[64] M. Zhu, A.L. Fink, Lipid binding inhibits alpha-synuclein fibril formation, J. Biol. Chem. 278 (2003) 16873–16877.
[65] V. N. Uversky, D. Eliezer, Biophysics of Parkinson's disease: structure and aggregation of alpha-synuclein, Curr. Protein Pept. Sci. (2009).
[66] T.R. Serio, A.G. Cashikar, A.S. Kowal, G.J. Sawicki, J.J. Moslehi, L. Serpell, M.F. Arnsdorf, S.L. Lindquist, Nucleated conformational conversion and the replication of conformational information by a prion determinant, Science 289 (2000) 1317–1321.
[67] V. Sluzky, J.A. Tamada, A.M. Klibanov, R. Langer, Kinetics of insulin aggregation in aqueous solutions upon agitation in the presence of hydrophobic surfaces, Proc. Natl Acad. Sci. USA 88 (1991) 9377–9381.
[68] L. Nielsen, R. Khurana, A. Coats, S. Frokjaer, J. Brange, S. Vyas, V.N. Uversky, A.L. Fink, Effect of environmental factors on the kinetics of insulin fibril formation: elucidation of the molecular mechanism, Biochemistry 40 (2001) 6036–6046.
[69] H. LeVine, Thioflavine T interaction with synthetic Alzheimer's disease beta-amyloid peptides: detection of amyloid aggregation in solution, Protein Sci. 2 (1993) 404–410.
[70] H. Naiki, K. Higuchi, M. Hosokawa, T. Takeda, Fluorometric determination of amyloid fibrils in vitro using the fluorescent dye, thioflavin T1, Anal. Biochem. 177 (1989) 244–249.
[71] H. LeVine, Quantification of beta-sheet amyloid fibril structures with thioflavin T, Methods Enzymol. 309 (1999) 274–284.
[72] D.E. Otzen, B.R. Knudsen, F.L. Aachmann, K.L. Larsen, R. Wimmer, Structural basis for cyclodextrins' suppression of human growth hormone aggregation, Protein Sci. 11 (2002) 1779–1787.
[73] S.J. Wood, B. Maleeff, T. Hart, R. Wetzel, Physical, morphological and functional differences between ph 5.8 and 7.4 aggregates of the Alzheimer's amyloid peptide Abeta, J. Mol. Biol. 256 (1996) 870–877.
[74] J.S. Pedersen, D. Dikov, J.L. Flink, H.A. Hjuler, G. Christiansen, D.E. Otzen, The changing face of glucagon fibrillation: structural polymorphism and conformational imprinting, J. Mol. Biol. 355 (2006) 501–523.
[75] M.S. Celej, E.A. Jares-Erijman, T.M. Jovin, Fluorescent N-arylaminonaphthalene sulfonate probes for amyloid aggregation of alpha-synuclein, Biophys. J. 94 (2008) 4867–4879.
[76] K.C. Luk, E.G. Hyde, J.Q. Trojanowski, V.M. Lee, Sensitive fluorescence polarization technique for rapid screening of alpha-synuclein oligomerization/fibrillization inhibitors, Biochemistry 46 (2007) 12522–12529.
[77] J. Kaylor, N. Bodner, S. Edridge, G. Yamin, D.P. Hong, A.L. Fink, Characterization of oligomeric intermediates in alpha-synuclein fibrillation: FRET studies of Y125W/Y133F/Y136F alpha-synuclein, J. Mol. Biol. 353 (2005) 357–372.
[78] M. Sunde, L.C. Serpell, M. Bartlam, P.E. Fraser, M.B. Pepys, C.C.F. Blake, Common core structure of amyloid fibrils by synchrotron X-ray diffraction, J. Mol. Biol. 273 (1997) 729–739.
[79] O.S. Makin, L.C. Serpell, X-ray diffraction studies of amyloid structure, Meth. Mol. Biol. 299 (2005) 67–80.
[80] T. Antony, W. Hoyer, D. Cherny, G. Heim, T.M. Jovin, V. Subramaniam, Cellular polyamines promote the aggregation of alpha-synuclein, J. Biol. Chem. 278 (2003) 3235–3240.
[81] K.M. Danzer, D. Haasen, A.R. Karow, S. Moussaud, M. Habeck, A. Giese, H.A. Kretzschmar, B. Hengerer, M. Kostka, Different species of a-synuclein oligomers induce calcium influx and seeding, J. Neurosci. 27 (2007) 9220–9232.
[82] L. Giehm, D.E. Otzen, Strategies to increase the reproducibility of protein fibrillization in plate reader assays, Anal. Biochem. 400 (2010) 270–281.
[83] G.A. Senisterra, E. Markin, K. Yamazaki, R. Hui, M. Vedadi, D.E. Awrey, Screening for ligands using a generic and highthroughput light-scattering-based assay, J. Biomol. Screening 11 (2006) 940–948.
[84] B. Vestergaard, M. Groenning, M. Roessle, J.S. Kastrup, M. Van de Weert, J.M. Flink, S. Frokjaer, M. Gajhede, D.I. Svergun, A helical structural nucleus is the primary elongating unit of insulin amyloid fibrils, PLoS Biol. 5 (2007) e134.
[85] C.L. Oliveira, M.A. Behrens, J.S. Pedersen, K. Erlacher, D. Otzen, J.S. Pedersen, A SAXS study of glucagon fibrillation, J. Mol. Biol. 387 (2009) 147–161.
[86] D. Franke, D.I. Svergun, DAMMIF, a program for rapid ab-initio shape determination in small-angle scattering, J. Appl. Crystallogr. 42 (2009) 342–346.
[87] C.O. Fernandez, W. Hoyer, M. Zweckstetter, E.A. Jares-Erijman, V. Subramaniam, C. Griesinger, T.M. Jovin, NMR of alpha-synuclein-polyamine complexes elucidates the mechanism and kinetics of induced aggregation, Embo. J. 23 (2004) 2039–2046.
[88] T.P.J. Knowles, C.A. Waudby, G.L. Devlin, S.I. Cohen, A. Aguzzi, M. Vendruscolo, E.M. Terentjev, M.E. Welland, C.M. Dobson, An analytical solution to the kinetics of breakable filament assembly, Science 326 (2009) 1533–1537.
[89] K.A. Conway, J.D. Harper, P.T. Lansbury, Accelerated in vitro fibril formation by a mutant alpha-synuclein linked to early-onset Parkinson disease, Nat. Med. 4 (1998) 1318–1320.
[90] M. Zhu, S. Rajamani, J. Kaylor, S. Han, F. Zhou, A.L. Fink, The flavonoid baicalein inhibits fibrillation of a-synuclein and disaggregates existing fibrils, J. Biol. Chem. 279 (2004) 26846–26857.
[91] D.-P. Hong, A.L. Fink, V.N. Uversky, Structural characteristics of alpha-synuclein oligomers stabilized by the flavonoid baicalein, J. Mol. Biol. 383 (2008) 214–223.
[92] D.E. Otzen, Amyloid formation in surfactants and alcohols: membrane mimetics or structural switchers?, Curr Protein Pept. Sci. 11 (2010) 355–371.
[93] L.A. Munishkina, C. Phelan, V.N. Uversky, A.L. Fink, Conformational behavior and aggregation of alpha-synuclein in organic solvents: modeling the effects of membranes, Biochemistry 42 (2003) 2720–2730.
[94] V. L. Anderson, T. F. Ramlall, C. C. Rospigliosi, W. W. Webb, D. Eliezer, Identification of a helical intermediate in trifluoroethanol-induced alpha-synuclein aggregation, Proc. Natl. Acad. Sci. USA. Oct 14 (2010) (Epub).
[95] I. Pallares, J. Vendrell, F.X. Aviles, S. Ventura, Amyloid fibril formation by a partially structured intermediate state of alpha-chymotrypsin, J. Mol. Biol. 342 (2004) 321–331.
[96] E. Zerovnik, M. Skarabot, K. Skerget, S. Giannini, V. Stoka, S. Jenko-Kokalj, R.A. Staniforth, Amyloid fibril formation by human stefin B: influence of pH and TFE on fibril growth and morphology, Amyloid 14 (2007) 237–247.
[97] M. Calamai, F. Chiti, C.M. Dobson, Amyloid fibril formation can proceed from different conformations of a partially unfolded protein, Biophys. J. 89 (2005) 4201–4210.
[98] K. Yamaguchi, H. Naiki, Y. Goto, Mechanism by which the amyloid-like fibrils of a beta 2-microglobulin fragment are induced by fluorine-substituted alcohols, J. Mol. Biol. 363 (2006) 279–288.
[99] G. Yamin, L.A. Munishkina, M.A. Karymov, Y.L. Lyubchenko, V.N. Uversky, A.L. Fink, Forcing nonamyloidogenic beta-synuclein to fibrillate, Biochemistry 44 (2005) 9096–9107.

[100] C.C. Hoppe, L.T. Nguyen, L.E. Kirsch, J.M. Wiencek, Characterization of seed nuclei in glucagon aggregation using light scattering methods and field-flow fractionation, J Biol Eng 2 (2008) 10.
[101] L. Nesgaard, B. Vad, G. Christiansen, D. Otzen, Kinetic partitioning between aggregation and vesicle permeabilization by modified ADan, Biochim. Biophys. Acta 1794 (2009) 84–93.
[102] K. Sneppen, L. Lizana, M.H. Jensen, S. Pigolotti, D.E. Otzen, Proteasome-fibrillation antagonism in a dynamic model for Parkinson's disease, Phys. Biol. 6 (2009) 36005.
[103] K.S. McNaught, P. Jenner, Proteasomal function is impaired in substantia nigra in Parkinson's disease, Neurosci. Lett. 297 (2001) 191–194.
[104] L. Stefanis, K.E. Larsen, H.J. Rideout, D. Sulzer, L.A. Greene, Expression of A53T mutant but not wild-type alpha-synuclein in PC12 cells induces alterations of the ubiquitin-dependent degradation system, loss of dopamine release, and autophagic cell death, J. Neurosci. 21 (2001) 9549–9560.
[105] W.P. Gai, D.L. Pountney, J.H.T. Power, Q.X. Li, J.G. Culvenor, C.A. McLean, P.H. Jensen, P.C. Blumbergs, A-Synuclein fibrils constitute the central core of oligodendroglial inclusion filaments in multiple system atrophy, Exp. Neurol. 181 (2003) 68–78.
[106] P. Hammarström, R. Simon, S. Nyström, P. Konradsson, A. Aslund, K.P.R. Nilsson, A fluorescent pentameric thiophene derivative detects *in vitro*-formed prefibrillar protein aggregates, Biochemistry 49 (2010) 6838–6845.
[107] C.S. Goldsbury, S. Wirtz, S.A. Müller, S. Sunderji, P. Wicki, U. Aebi, P. Frey, Studies on the in vitro assembly of A 1–40: implications for the search for a fibril formation inhibitors, J. Struct. Biol. 130 (2000) 217–231.

Article II

Oligomers of alpha-synuclein: picking the culprit in the line-up

Nikolai Lorenzen & Daniel Erik Otzen[1]

Interdisciplinary Nanoscience Center (iNANO), Department of Molecular Biology, Center for Insoluble Protein Structures (inSPIN), Aarhus University, Gustav Wieds Vej 14, 8000 Aarhus C, Denmark
[1]To whom correspondence should be addressed (email dao@inano.au.dk)

Abstract

In this chapter we will discuss the key findings on α-synuclein (αSN) oligomers from a biophysical point of view. Current structural methods cannot provide a high-resolution structure of αSN oligomers, due to their size, heterogeneity and tendency to aggregate. However, a low-resolution structure of a stable αSN oligomer population is emerging based on compelling data from different research groups. αSN oligomers are normally observed during the formation of amyloid fibrils and we will discuss how they are connected to this process. Another important topic is the interaction of αSN oligomers and membranes, and we will discuss the evidence which suggests that this interaction might be essential in the pathogenesis of PD and other neurodegenerative disorders. Finally we will present a remarkable example of how small molecules are able to stabilize non-amyloid oligomers and how this might be a potential strategy to inhibit the inherent toxicity of αSN oligomers.

Introduction: the role of α-synuclein in Parkinson's Disease

The interest in protein misfolding has increased spectacularly after it was established that the conversion of a range of soluble proteins into insoluble amyloid fibrils is linked to several diseases (see Chapter 1). This link is direct in systemic amyloidosis, where excessive accumulation of amyloid fibrils in joints or organs leads to pathology. However, in neurodegenerative disorders such as Parkinson's disease (PD), the link is more indirect. In PD, amyloid fibrils consisting of the protein α-synuclein (αSN) form intracellular deposits called Lewy bodies (LB), which appear to accompany the loss of dopaminergic neurons mainly in the part of the brain called *Substantia Nigra*. Analogous observations have been made for Alzheimer's Disease. Such observations initially led to the hypothesis that amyloid fibrils were responsible for the pathogenesis of PD and other neurodegenerative disorders. However, new observations have made a compelling case that pre-fibrillar oligomers, typically formed in the early stages of the fibril formation process, are the actual pathogenic culprits. This shift from amyloid fibrils to amyloid oligomers was inspired by the emergence of a similar oligomer hypothesis in Alzheimer's disease, where the peptide Aβ was shown to form a range of oligomeric structures with cytotoxic properties (*1*). Subsequently, Lansbury (*2-4*), Fink (*5*) and co-workers demonstrated that αSN oligomers, and not mature amyloid fibrils, have membrane-

permeabilizing properties. Their toxicity has been demonstrated *in vivo* (*6*), and elevated levels of αSN oligomers have been found in CSF from PD patients (*7*) and in post-mortem brain extracts from patients with LB dementia. Consequently αSN oligomers are now one of the primary targets in PD drug development. αSN oligomers are included in a clinical trial as potential biomarkers for the neurodegenerative disorder Multiple System Atrophy, known as a *Parkinson plus* syndrome (ClinicalTrials.gov, NCT01485549) while Aβ oligomers have been targeted by the compound scyllo-inositol (ClinicalTrials.gov, NCT00934050).

αSN consists of 140 residues and is intrinsically disordered, *i.e.* it lacks persistent secondary and tertiary structure (*8*). However, upon interaction with negatively charged membranes, residues 1-100 undergo a coil-helix conformational change (*9*). This ability of αSN to fold into membranes is believed to be essential for its physiological role. The basic N-terminal part (residues 1-60) initiates the interaction with membranes and leads to the subsequent folding of the NAC region (residues 61-95). The NAC region is hydrophobic and is known to constitute the core of amyloid fibrils (*10*). The C-terminal is highly acidic and unstructured. Apart from possible electrostatic interactions between the YEMPS region (residue 125-129) and other regions of the polypeptide, the C-terminal is disordered in both the free monomer, the membrane-bound monomer, the oligomer and the fibril structure (*10*). It has recently been suggested that αSN could form a tetramer *in vivo* (*11*) but this remains a minority position, contradicted by a vast literature on the properties of natively unfolded αSN as well as direct rebuttals which show αSN to naturally form a disordered monomer (*8*).

Lashuel *et al.* used electron microscopy (EM) to show that both αSN and Aβ oligomers form annular ring shaped oligomers (**Fig. 1**). Combined with the observation that the oligomers were able to permeabilize synthetic membranes (*3*), this suggested that pore formation in cell membranes led to oligomer toxicity (*4*). This pioneering finding has later been supported for amyloid oligomers formed by other peptides and proteins (ABri, ADan, serum amyloid A, amylin) which are ring formed and permeabilize membranes (*12*).

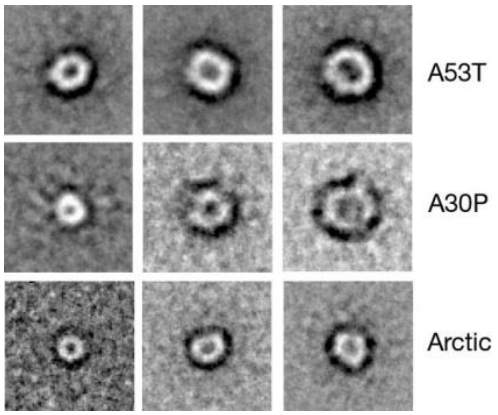

Figure 1. Amyloid oligomers of two disease promoting mutations of αSN (A30P and A53T) as well as the Arctic mutant of Aβ. The images are reconstructed from 5,000-6,000 individual particles, using the lowest molecular weight fraction of oligomer purified by size exclusion chromatography. Each picture has an area of 30.5 x 30.5 nm. Reproduced with permission from (4).

A low-resolution structure of αSN oligomers: compact core with diffuse shell

In this section we will discuss the structure of a type of αSN oligomers which has been studied thoroughly by the Subramaniam group (*10, 13, 14*), and which is highly similar (if not identical) to the oligomers that are studied in our research group. The Subramaniam group form stable αSN oligomers by incubating αSN at a concentration of 1 mM for 18 hrs at room temperature under vigorous shaking, followed by 2 hr incubation at 37 °C without shaking. Subsequently, oligomers are purified by size exclusion chromatography (SEC), similar to other established protocols (*4, 15*). Subramaniam and co-workers elegantly used a combination of sub-stoichiometric labeling and single-molecule photobleaching to count the number of monomers per oligomer, arriving at a number of ~31 and at the same time showing the oligomer population to be monodisperse (*i.e.* only one type of oligomer) (*13*). By labeling individual positions with the fluorescent residue Tryptophan, they were able to conclude that the N-terminal and NAC region are part of the oligomer core, whereas the C-terminal remains disordered (*10*).

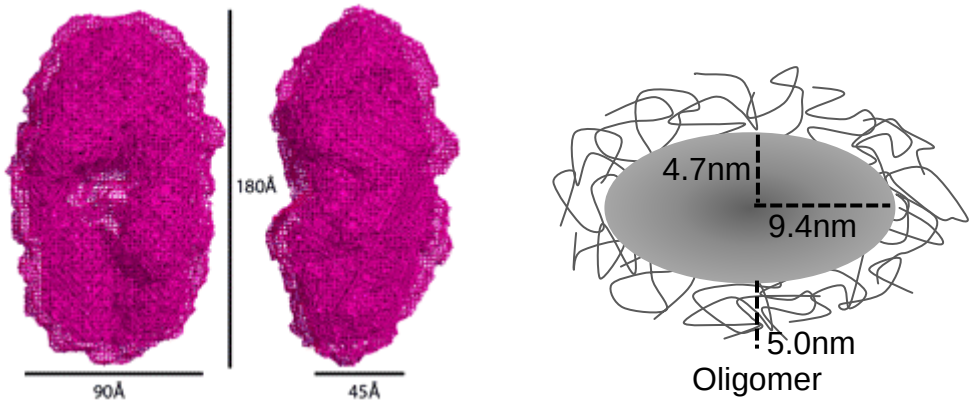

Figure 2. A: SAXS based model of a αSN oligomer which is populated during fibril formation. Reproduced with permission from (15). B: Schematic model of the structure of αSN oligomers having a β-sheet core build up by the N-terminal and NAC region and a disordered brush shell outer layer consisting of the C-terminal (J. D. Kaspersen, N.L., J. S. Pedersen and D.E.O., unpublished data).

In 2010 we used small angle X-ray scattering (SAXS) to resolve the structure of αSN oligomers that accumulate during fibril formation (*15*). We could resolve monomer, dimer, oligomers and fibrils in the fibril formation process and by *ab initio* modeling we determined the shape of the oligomers to

be an ellipsoid with dimensions given in **Fig. 2A**. More recently, we have gone a step further. We purified the oligomers from samples with fibril formation, by incubating 840 µM αSN for 5 hrs at 37 °C with vigorous shaking and subsequent purification with SEC, similar to the approach of other groups (*4, 13, 15*). This reasonably pure oligomer solution (< 10% monomers) has provided a more detailed structural model. The oligomers consist of a rigid core with the same dimensions as our first SAXS model, but this core is covered by a 5 nm thick outer layer consisting of disordered polypeptides (**Fig. 2B**) (J.D. Kaspersen, N.L., J.S. Pedersen and D.E.O., unpublished results). The SAXS analysis together with a complementary SEC-MALLS (multi angle laser light scattering) analysis estimate that the average oligomer is build up of ~29 monomers (N.L. and D.E.O., unpublished work), in excellent agreement with the Subramaniam group (*13*). All these size-estimation methods are independent of the shape and conformation of the molecules, giving more reliable data on the oligomer structure than SEC, DLS, EM and atomic force microscopy which either report on hydrodynamic radius (SEC, DLS) or are sensitive to drying artefacts (EM and AFM). Our revised structure of αSN oligomers is in good agreement with the proposed micellar structure by the Subramaniam group where the less charged and more hydrophobic N-terminal and NAC regions forms the compact core, whereas the highly charged C-terminal forms a brush-like shell (*16*). This compact organization might explain the monodispersity and the remarkable stability of the αSN oligomers.

The oligomer core is most likely organized in β-sheets (*5, 17*). Fourier Transform Infrared Spectroscopy suggests that both Aβ and αSN oligomers contain β-sheet structure. While mature amyloid of Aβ and αSN fibrils consist of parallel β-strands, oligomers appear to contain anti-parallel β-strands (*17*). This difference could arise in two ways. Either oligomers and fibrils belong to different aggregation pathways; alternatively, oligomers have to undergo structural rearrangements before they can become incorporated into fibril structures.

Note that there is not just *one* oligomer of αSN. Different oligomers have been reported, containing different types of secondary structure, ranging from mainly α-helical to disordered, and of varying sizes, *e.g.* coexisting oligomers of 10 and 15 monomers (*18*) (see below). Oligomers may also be induced by metal ions, lipids, alcohols and small molecules (*19, 20*). A tremendously important challenge is to determine which oligomer structures are relevant *in vivo*, and how they can be purified and stabilized for thorough analysis.

What is the role of α-synuclein oligomers in the process of fibril formation?

The amyloid fibril structure is a thermodynamic favorable state which has been suggested to be generic for all proteins. However, the mechanism of amyloid formation is not generic but varies between proteins and is also highly dependent on solution conditions. A key question in this regard is whether oligomers, which are often observed during fibril formation, are compulsory precursors for fibrils (on-pathway intermediates) or rather dead-end species that are not incorporated into the fibrils. There is no simple answer to this; on-and off-pathway oligomers may co-exist and conflicting observations may also reflect different assembly processes under different conditions. However, it is generally believed that monomers are the elongating species in αSN fibril formation (**Fig. 3**). On-pathway oligomers are formed at an early stage. They cover the whole range of species between monomers and fibrils and are also commonly known as fibril nuclei, pre-fibrillar oligomers and protofibrils. Off-pathway oligomers can also be observed under fibril forming conditions, but they belong to a separate aggregation pathway.

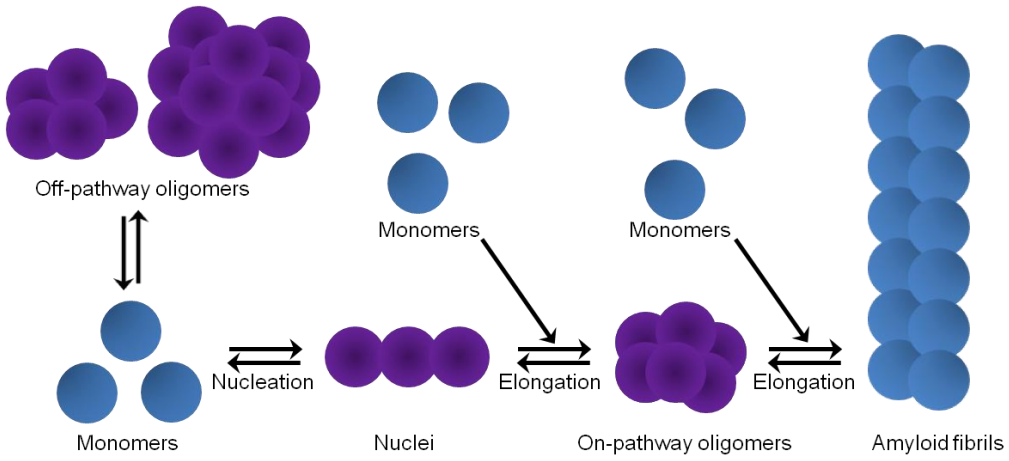

Figure 3. Schematic representation of the role of on- and off-pathway oligomers in the process of fibril formation. Oligomer structures are highlighted with purple color.

On-pathway αSN oligomers: Cremades *et al.* have combined single-molecule techniques with kinetic analysis to monitor the development of different αSN oligomers in the initial phases of the fibrillation process (*18*). A key tool was the level of FRET (Förster Resonance Energy Transfer) between different monomers in the oligomer. They observed four different oligomer distributions, denoted as A_{small}, A_{med}, B_{med} and B_{large}, (small ~2-5mers, medium ~5-15mers, large ~15-150mers). A and B refer to mid- and high-FRET values, respectively. The difference in FRET values of A and B oligomers suggest that they are of different structure. As shown in **Fig. 4**, A oligomers are just as sensitive to protease degradation as the monomer, indicating a highly flexible structure; B oligomers were much more protease resistant, suggesting compact β-sheet structure while mature fibril were

the most resistant. A_{small} and A_{med} formed at similar rates and with hardly any lag time, while B_{med} and B_{large} showed a longer lag time. Thus B oligomers are likely formed from the A oligomers; A oligomers accumulate because they are formed more quickly from monomers (by nucleation) than they decay to B (*18*). In this model, αSN follows *nucleated conformational conversion* (NCC) where non-amyloid oligomers are readily formed and accumulate, until they undergo structural re-arrangement to amyloid oligomers competent of being elongated into mature fibrils. This has also been proposed as a nucleation mechanism for Aβ (*21*).

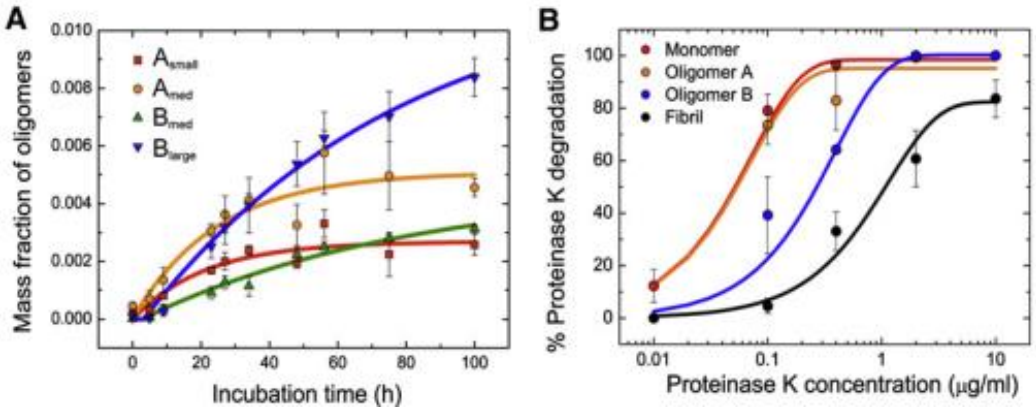

Figure 4. A: The time dependence of the mass fraction of the four oligomeric distributions A_{small} (red squares), A_{medium} (orange circles), B_{medium} (green triangles), and B_{large} (blue triangles). B: Proteinase K degradation curves of the different protein species (monomer in red, type A oligomer in orange, type B oligomer in blue, and fibrils in black). Reproduced with permission from (18).

Off-pathway αSN oligomers: We have found that oligomers depicted in Fig. 2B actually inhibit fibril formation and are unable to elongate mature amyloid fibrils (N. L. & D. E. O., unpublished data). Thus, although these oligomers accumulate during the fibril formation process, they appear to be unproductive in this process. These oligomers can aggregate further into non-fibrillar aggregates suggesting that they belong to an aggregation process distinct from fibril formation. However, it cannot be ruled out that these oligomers might also be connected to fibril formation by processes similar to NCC. Off-pathway oligomers have also been observed when stabilized by *e.g.* small molecules, where an example is given in the final section.

The variety of oligomers is the natural consequence of a process which has not undergone biological evolution to optimize formation of the end product (*5*). One current challenge is to understand to what extent off-pathway oligomers under different conditions might be able to undergo structural rearrangement and proceed in the process of fibril formation.

Oligomer-membrane interactions: the cause of toxicity?

Intriguingly, some conformational antibodies can recognize a range of different amyloid oligomers without recognizing the monomer or mature fibril form. This suggests that these oligomers have a common structure (*22*) which may be the basis for their cytotoxicity (*23*). Several oligomers have exposed hydrophobic regions and bind the hydrophobic probe ANS (*24*). A common fold exposing "sticky" surfaces may promote oligomer-membrane interactions and perturb the membrane (*3, 12, 14, 25, 26*). It is possible that oligomer structural flexibility, leading to hydrophobic exposure and structural rearrangements upon membrane interaction, is essential for toxicity.

The ability of αSN oligomers to permeabilize membranes has been investigated intensely. An example of the permeabilization of synthetic membranes, composed of the anionic POPG lipid, by αSN oligomers is shown in **Fig. 5**. The degree of permeabilization is monitored by the fluorophore/quencher pair HPTS/DPX and the kinetics reveals that complete permeabilization (efflux/influx) is obtained within 5 s. Staining of the membrane show that the form and size of the vesicles remains intact upon oligomer binding and permeabilization. The Subramaniam group has used single-tryptophan mutants to demonstrate that the N-terminal is involved in oligomer-membrane interactions, as is also the case for the monomer (*10*). The αSN oligomer selectively binds to anionic lipids and preferentially to liquid disordered phase regions of the membranes (*14*) where the lipid bilayer is loosely packed and the hydrophobic membrane interior is more accessible (*27*). Thus interaction of αSN oligomers with membranes seems to be governed by electrostatic interactions of the N-terminal with the membrane combined with hydrophobic interactions of accessible hydrophobic patches in the αSN oligomer structure with the membrane interior.

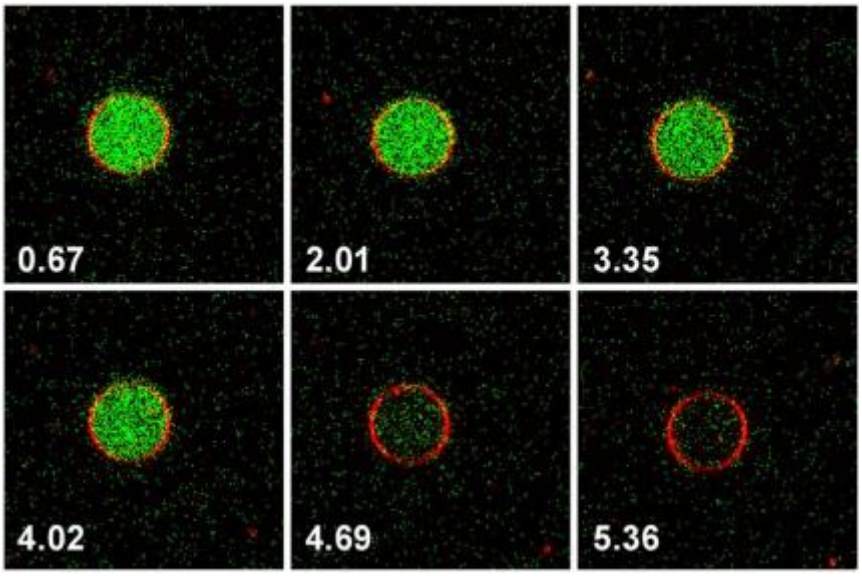

Figure 5.Confocal microscopy image of POPG giant unilamellar vesicles. The fluorophore HPTS (green) is entrapped inside the vesicle and the paired quencher, DPX, is present outside the vesicle. The membrane is stained with DOPE -Rhodamine (red). Time points are given in seconds. Reproduced with permission from (25).

Small molecules and α-synuclein oligomers: Structure inducing and potential drugs?

It is a tremendous challenge to develop drugs for neurodegenerative disorders due to the complex blood brain barrier (BBB). The difficulties in delivering macromolecules as antibodies and RNA aptamers, has put focus on identifying small molecules which are able to cross the BBB and interact specifically with αSN. Numerous small molecules with mono-, di-, and tri-hydroxyphenyl groups inhibit protein aggregation while promoting oligomer formation. Examples include the neurotransmitter dopamine (*19*), the flavonoid baicalein obtained from herbal medicine (*28*) and the catechin epigallocatechin gallate (EGCG) from green tea (*20*). The effect of EGCG on αSN oligomerization and fibril formation is a remarkable example of how small molecules can redirect aggregation pathways.

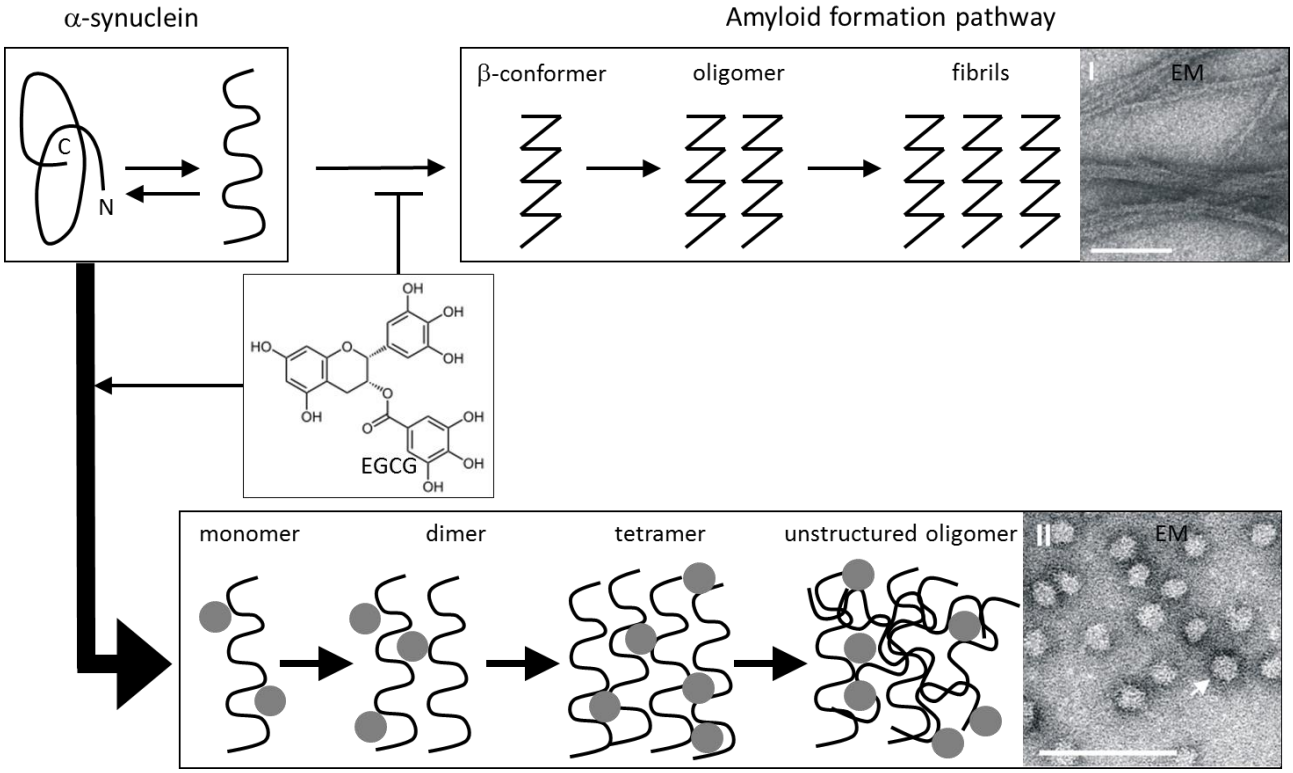

Figure 6. Schematic representation of the fibril formation pathway and the EGCG directed aggregation pathway. αSN monomers exist in equilibrium between disordered and partially folded conformations. Fibril formation occurs through the development of on-pathway oligomers by nucleation events and subsequent addition of monomers leads to mature fibrils. EGCG binds αSN monomers and leads to stepwise aggregation into disordered non-toxic and off-pathway oligomers. Reproduced with permission from (29).

EGCG binds preferentially to disordered polypeptides, but also to structured regions at high concentrations. Wanker and coworkers have proposed a model where EGCG binds the αSN monomer and redirects the protein from the process of fibril formation and into sequential aggregation, leading to stable, non-toxic oligomers (*20*) (**Fig. 6**). These off-pathway oligomers are amorphous and show no β-sheet content. Moreover, EGCG is able to reorganize mature amyloid fibrils of αSN and Aβ into amorphous and non-toxic oligomers (*20*).

The effect of EGCG on the aggregation of αSN and Aβ is only one of many possible strategies to prevent the formation of toxic amyloid oligomers. Another strategy is to use small molecules to stabilize the protein in the monomeric form; at the other extreme pro-aggregators can shift the equilibrium towards the amyloid fibrils, which is believed to be less toxic (*30*).

Conclusion

To clarify the role of αSN oligomers in the amyloid fibril formation process and their potential role in the pathogenesis of PD will be important for the understanding and treatment of not only PD but also other related neurodegenerative disorders such as Alzheimer's disease and Huntington disease. The major hurdle here is to define the cytotoxic species. Current research point towards oligomers as the prime suspects. Therefore it is crucial to establish which oligomers are relevant in the amyloid process *in vivo*, and whether it is a defined oligomer or rather a whole spectrum of different pre-fibrillar oligomers that are cytotoxic. Until then, it will be difficult to rationally design drug discovery programs towards oligomers. For now an alternative strategy might be the development of small molecules or nanoparticles which are specific towards αSN, and which stabilize the monomer form in such a way that amyloid formation is completely inhibited without compromising the protein's underlying biological function. This on the other hand will not be trivial to accomplish.

Summary

- *α-synuclein oligomers are likely the cytotoxic species in the pathogenesis of Parkinson's disease*

- *A low resolution structure is emerging for stable α-synuclein oligomers*
- *α-synuclein oligomers are observed both as on- and off-pathway in the fibril formation process*
- *Oligomers interact strongly with membranes and this is possibly the cause of neuronal damage in Parkinson's disease and other neudegenerative disorders*
- *Small molecules, such as epigallocatechin gallate (EGCG), redirect the aggregation pathway of α-synuclein*

Key words

α-synuclein, amyloid, amyloid pore, membrane permeabilization, oligomer, oligomer formation, oligomer membrane interaction, oligomer structure, small molecule, toxicity, EGCG

Acknowledgements

We apologize to the many authors whose work we could not include because of limitations in the number of references. We thank Jørn Døvling Kaspersen and Jan Skov Pedersen for very fruitful collaborations on SAXS analysis of the αSN oligomers.

Funding

We are supported by the Michael J. Fox Foundation and the Danish Research Foundation (inSPIN).

References

1. **Walsh, D. M., and Selkoe, D. J. (2007) A beta oligomers - a decade of discovery, *J Neurochem 101*, 1172-1184.**
2. **Conway, K. A., Lee, S. J., Rochet, J. C., Ding, T. T., Williamson, R. E., and Lansbury, P. T., Jr. (2000) Acceleration of oligomerization, not fibrillization, is a shared property of both alpha-synuclein mutations linked to early-onset Parkinson's disease: implications for pathogenesis and therapy, *Proc Natl Acad Sci U S A 97*, 571-576.**
3. **Volles, M. J., Lee, S. J., Rochet, J. C., Shtilerman, M. D., Ding, T. T., Kessler, J. C., and Lansbury, P. T., Jr. (2001) Vesicle permeabilization by protofibrillar alpha-synuclein: implications for the pathogenesis and treatment of Parkinson's disease, *Biochemistry 40*, 7812-7819.**
4. **Lashuel, H. A., Hartley, D., Petre, B. M., Walz, T., and Lansbury, P. T., Jr. (2002) Neurodegenerative disease: amyloid pores from pathogenic mutations, *Nature 418*, 291.**
5. **Kaylor, J., Bodner, N., Edridge, S., Yamin, G., Hong, D. P., and Fink, A. L. (2005) Characterization of oligomeric intermediates in alpha-synuclein fibrillation: FRET studies of Y125W/Y133F/Y136F alpha-synuclein, *J Mol Biol 353*, 357-372.**
6. **Winner, B., Jappelli, R., Maji, S. K., Desplats, P. A., Boyer, L., Aigner, S., Hetzer, C., Loher, T., Vilar, M., Campioni, S., Tzitzilonis, C., Soragni, A., Jessberger, S., Mira, H., Consiglio, A., Pham, E., Masliah, E., Gage, F. H., and Riek, R. (2011) In vivo demonstration that alpha-synuclein oligomers are toxic, *Proceedings of the National Academy of Sciences of the United States of America 108*, 4194-4199.**

7. Tokuda, T., Qureshi, M. M., Ardah, M. T., Varghese, S., Shehab, S. A., Kasai, T., Ishigami, N., Tamaoka, A., Nakagawa, M., and El-Agnaf, O. M. (2010) Detection of elevated levels of alpha-synuclein oligomers in CSF from patients with Parkinson disease, *Neurology 75*, 1766-1772.
8. Fauvet, B., Mbefo, M. K., Fares, M. B., Desobry, C., Michael, S., Ardah, M. T., Tsika, E., Coune, P., Prudent, M., Lion, N., Eliezer, D., Moore, D. J., Schneider, B., Aebischer, P., El-Agnaf, O. M., Masliah, E., and Lashuel, H. A. (2012) alpha-Synuclein in central nervous system and from erythrocytes, mammalian cells, and Escherichia coli exists predominantly as disordered monomer, *J Biol Chem 287*, 15345-15364.
9. Ulmer, T. S., Bax, A., Cole, N. B., and Nussbaum, R. L. (2005) Structure and dynamics of micelle-bound human alpha-synuclein, *J Biol Chem 280*, 9595-9603.
10. van Rooijen, B. D., van Leijenhorst-Groener, K. A., Claessens, M. M., and Subramaniam, V. (2009) Tryptophan fluorescence reveals structural features of alpha-synuclein oligomers, *J Mol Biol 394*, 826-833.
11. Bartels, T., Choi, J. G., and Selkoe, D. J. (2011) alpha-Synuclein occurs physiologically as a helically folded tetramer that resists aggregation, *Nature 477*, 107-110.
12. Quist, A., Doudevski, I., Lin, H., Azimova, R., Ng, D., Frangione, B., Kagan, B., Ghiso, J., and Lal, R. (2005) Amyloid ion channels: a common structural link for protein-misfolding disease, *Proc Natl Acad Sci U S A 102*, 10427-10432.
13. Zijlstra, N., Blum, C., Segers-Nolten, I. M., Claessens, M. M., and Subramaniam, V. (2012) Molecular composition of sub-stoichiometrically labeled alpha-synuclein oligomers determined by single-molecule photobleaching, *Angew Chem Int Ed Engl 51*, 8821-8824.
14. van Rooijen, B. D., Claessens, M. M., and Subramaniam, V. (2008) Membrane binding of oligomeric alpha-synuclein depends on bilayer charge and packing, *FEBS Lett 582*, 3788-3792.
15. Giehm L, S. D., Otzen DE, Vestergaard B. (2011) Low-resolution structure of a vesicle disrupting α-synuclein oligomer that accumulates during fibrillation., *Proc Natl Acad Sci U S A 108(8)*, 3246-3251.
16. Stockl, M. T., Zijlstra, N., and Subramaniam, V. (2013) Alpha-synuclein oligomers: an amyloid pore? Insights into mechanisms of alpha-synuclein oligomer-lipid interactions, *Mol Neurobiol 47*, 613-621.
17. Celej, M. S., Sarroukh, R., Goormaghtigh, E., Fidelio, G. D., Ruysschaert, J. M., and Raussens, V. (2012) Toxic prefibrillar alpha-synuclein amyloid oligomers adopt a distinctive antiparallel beta-sheet structure, *Biochem J 443*, 719-726.
18. Cremades, N., Cohen, S. I., Deas, E., Abramov, A. Y., Chen, A. Y., Orte, A., Sandal, M., Clarke, R. W., Dunne, P., Aprile, F. A., Bertoncini, C. W., Wood, N. W., Knowles, T. P., Dobson, C. M., and Klenerman, D. (2012) Direct observation of the interconversion of normal and toxic forms of alpha-synuclein, *Cell 149*, 1048-1059.
19. Conway, K. A., Rochet, J. C., Bieganski, R. M., and Lansbury, P. T., Jr. (2001) Kinetic stabilization of the alpha-synuclein protofibril by a dopamine-alpha-synuclein adduct, *Science 294*, 1346-1349.
20. Bieschke, J., Russ, J., Friedrich, R. P., Ehrnhoefer, D. E., Wobst, H., Neugebauer, K., and Wanker, E. E. (2010) EGCG remodels mature alpha-synuclein and amyloid-beta fibrils and reduces cellular toxicity, *Proc Natl Acad Sci U S A 107*, 7710-7715.
21. Lee, J., Culyba, E. K., Powers, E. T., and Kelly, J. W. (2011) Amyloid-beta forms fibrils by nucleated conformational conversion of oligomers, *Nature chemical biology 7*, 602-609.
22. Kayed, R., Head, E., Thompson, J. L., McIntire, T. M., Milton, S. C., Cotman, C. W., and Glabe, C. G. (2003) Common structure of soluble amyloid oligomers implies common mechanism of pathogenesis, *Science 300*, 486-489.
23. Bucciantini, M., Giannoni, E., Chiti, F., Baroni, F., Formigli, L., Zurdo, J., Taddei, N., Ramponi, G., Dobson, C. M., and Stefani, M. (2002) Inherent toxicity of aggregates implies a common mechanism for protein misfolding diseases, *Nature 416*, 507-511.

24. **Bolognesi, B., Kumita, J. R., Barros, T. P., Esbjorner, E. K., Luheshi, L. M., Crowther, D. C., Wilson, M. R., Dobson, C. M., Favrin, G., and Yerbury, J. J. (2010) ANS binding reveals common features of cytotoxic amyloid species, *ACS Chem Biol 5*, 735-740.**

25. **van Rooijen BD, C. M., Subramaniam V. (2010) Membrane Permeabilization by Oligomeric α-Synuclein: In Search of the Mechanism., *PLoS One 5*.**

26. **Campioni, S., Mannini, B., Zampagni, M., Pensalfini, A., Parrini, C., Evangelisti, E., Relini, A., Stefani, M., Dobson, C. M., Cecchi, C., and Chiti, F. (2010) A causative link between the structure of aberrant protein oligomers and their toxicity, *Nat Chem Biol 6*, 140-147.**

27. **van Rooijen, B. D., Claessens, M. M., and Subramaniam, V. (2009) Lipid bilayer disruption by oligomeric alpha-synuclein depends on bilayer charge and accessibility of the hydrophobic core, *Biochim Biophys Acta 1788*, 1271-1278.**

28. **Hong, D. P., Fink, A. L., and Uversky, V. N. (2008) Structural characteristics of alpha-synuclein oligomers stabilized by the flavonoid baicalein, *J Mol Biol 383*, 214-223.**

29. **Lorenzen, N., Wanker, E., and Otzen, D. E. (2013) Inhibitors of Amyloid and Oligomer Formation, In *Amyloid Fibrils and Prefibrillar Aggregates* (Otzen, D. E., Ed.), pp 345-372, Wiley-VCH Verlag GmbH.**

30. **Bieschke, J., Herbst, M., Wiglenda, T., Friedrich, R. P., Boeddrich, A., Schiele, F., Kleckers, D., Lopez Del Amo, J. M., Gruning, B. A., Wang, Q., Schmidt, M. R., Lurz, R., Anwyl, R., Schnoegl, S., Fandrich, M., Frank, R. F., Reif, B., Gunther, S., Walsh, D. M., and Wanker, E. E. (2011) Small-molecule conversion of toxic oligomers to nontoxic beta-sheet-rich amyloid fibrils, *Nat Chem Biol 8*, 93-101.**

Article III

16
Inhibitors of Amyloid and Oligomer Formation

Nikolai Lorenzen, Erich E. Wanker, and Daniel Otzen

16.1
Introduction: Amyloidoses versus Neurodegenerative Diseases

Amyloid-related diseases can be split into two groups which require different drug development strategies. The first group consists of non-neuropathic amyloidoses, either localized or systemic, where deposition of amyloid is a direct cause of disease by overloading of, for example, joint or organs. Examples include senile systemic amyloidosis, familial amyloidotic polyneuropathy, and corneal dystrophies [1]. Although pre-fibrillar aggregates have been suggested to play a role in the pathology of some amyloidoses such as dialysis-associated amyloidosis [2] and the fibrils themselves may sequester vital cellular proteins and thus derail essential cellular functions [3], the sheer accumulation of amyloid is considered to be the main problem and the challenge is simply to remove these fibrils from the system and/or prevent their accumulation. Approaches against amyloidosis diseases are discussed in Chapter 17, exemplified by tetrameric transthyretin (TTR) whose dissociation and partial unfolding are prerequisites for amyloid formation. Consequently, stabilization of the TTR tetramer is a straightforward strategy to reduce the accumulation of insoluble amyloid deposits. This approach specifically targets TTR-related amyloidosis. A promising general strategy has been developed recently to clear existing deposits [4]. Most amyloid deposits contain the non-amyloid serum amyloid P component (SAP), which was shown to protect amyloid aggregates against macrophage clearance [5]. However, removal of SAP from the plasma by the compound CPHPC, in combination with anti-SAP antibodies directed against SAP in amyloid deposits, allowed macrophages to clear deposits within a month [4]. This approach was initially used for deposits of serum amyloid A but is likely to be generic and, consequently, holds much promise for general treatment of amyloidoses [6].

The second group of amyloid-related diseases includes neurodegenerative diseases such as Alzheimer's, Parkinson's, and Huntington's diseases. In these disorders it is believed that toxicity is not caused by mature amyloid fibrils *per se* but rather by smaller pre-fibrillar aggregates, such as oligomers. Thus, the disease cause most likely is more complex than for the first group of amyloid diseases.

Amyloid Fibrils and Prefibrillar Aggregates: Molecular and Biological Properties,
First Edition. Edited by Daniel Erik Otzen.

First, for amyloid-related diseases the mechanism of cytotoxicity is currently under intense investigation but is still not clarified in molecular detail. It is likely to vary from one protein oligomer to the next (see Chapters 6 and 7), indicating that the nature of the disease-causing target is not settled. Secondly, the blood–brain barrier (BBB) presents a formidable obstacle to drug delivery and imposes strong restrictions on the candidate molecules that can be used for the treatment of brain diseases. This effectively rules out conventional protein ligands, such as antibodies and DNA/RNA aptamers, because they are too large and cannot efficiently enter the brain. Thus, for the treatment of brain diseases a major focus is on the development of small-molecule compounds that can cross the BBB. Nevertheless, the challenge remains formidable, even by some accounts intractable [7]. Specific blockage of protein–protein interactions has always been considered a major challenge for drug development [8]. This is particularly the case for the development of compounds that directly target protein aggregates, where the interacting surfaces are often much larger than the small molecules. Moreover, the protein surfaces are relatively featureless, lack specific binding hotspots and are often plastic in response to changing environments [9]. As a consequence, there are still no approved small-molecule aggregation inhibitors in use against neurodegenerative diseases. Current efforts are spearheaded by immunotherapeutic approaches. Consequently, we will discuss different strategies of antibody immunotherapy in neurodegenerative diseases before we turn to small molecule compounds. An overview of currently ongoing studies with therapeutic molecules targeting amyloid aggregates involved in neurodegenerative diseases is provided in Table 16.1.

16.1.1 Antibody-Mediated Immunotherapy

Antibodies are high affinity ligands for proteins which makes them potential inhibitors of protein–protein interactions. In passive immunotherapy, exogenously prepared antibodies are employed directly as drugs, whereas active immunization therapies introduce appropriate aggregate-mimicking epitopes to the patient to stimulate the immune system to make its own antibodies against endogenously produced aggregates, typically aided by microglial activation [15, 22]. Both approaches have been used against neurodegenerative diseases, mainly Alzheimer's disease (AD), and while no products have yet been approved, there are numerous candidates in clinical trials.

16.1.1.1 Active Immunization

Solomon and coworkers demonstrated in the mid 1990s that monoclonal antibodies raised against Aβ epitopes from early fibrillation stages are able to inhibit fibril formation of Aβ *in vitro* and to disaggregate preformed fibrils [23]. In 1999 Schenk *et al.* succeeded in vaccinating transgenic mice with AD-like neuropathologies using preparations of the amyloid precursor peptide Aβ which had been incubated overnight at 37 °C and, consequently, presumably had a fibrillar morphology [15]. In collaboration with Schenk, the pharmaceutical companies Elan and Wyeth

Table 16.1 Various therapeutic strategies against neurodegenerative diseases involve targeting of protein aggregation.

Approach and rationale	Example
Active immunization against Aβ aggregates	AN1792 Elan/Wyeth trial 2000–2006 using Aβ1–42 aggregates; terminated because of 6% incidence of acute meningoencephalitis (T-cell inflammatory response: dangers of active immunization) [10, 11]. A subgroup of antibodies that specifically bind residues 4–10 prevent Aβ toxicity without inflammatory response [12]. Beneficial effects on neurite morphology and tau pathology in hippocampal sections from human patients [13].
Passive immunization against Aβ aggregates	Reduction in Aβ plaques protects morphology and survival of adult-born neurons in transgenic mice [14]. Single-chain variable fragment (scFv) antibodies inhibit aggregation *in vitro* and reduce Aβ plaques *in vivo* . scFv can enter the brain after intranasal application.
Deplete soluble precursors	Immunization with soluble Aβ1–42 peptides prevents plaque formation and neuropathology in young and older mice [15].
Target cytotoxic oligomer immunologically; avoids indiscriminate clearance of all forms	Antibodies against the Aβ oligomer prevent cognitive decline in transgenic mice (passive immunization) [16, 17].
Active immunization against the phospho-tau peptide	Intracellular tau aggregates reduced [18]. Unknown mechanism. Treatment may reduce ''infectivity'' of tau aggregates exported from affected cells, just as extracellular tau aggregates can be internalized.
Active immunization against human α-synuclein	Reduction in α-synuclein deposits in neuronal cell bodies and neuronal membranes.
Inhibition of p53 activity reduces cell death	p53 inhibitors prevent Aβ-mediated apoptotic activation in neurons [19].
Preventing aggregation by sequestering necessary co-factors	Metal chelators such as PBT2 and clioquinol prevent aggregation-promoting Aβ-metal contacts.
Maintaining amyloid-β in the soluble state to inhibit amyloid-β formation and deposition	The compound Tramiprosate or Alzhemed™ (3-amino-1-propanesulfonic acid; 3APS) reduces amyloid-β aggregation and toxicity in AD transgenic mice but failed to demonstrate efficacy in phase 3 clinical trials in the U.S. This may be related to the fact that tramiprosate also promotes abnormal tau aggregation [20].
Targeting the formation of toxic amyloid-β oligomers	Scyllo-inositol (ELND005) reduces memory impairment and the level of amyloid-β oligomers in brains of AD transgenic mice [21]. Recently, a phase II clinical trial with a high dose of ELND005 was discontinued due to severe side effects.

launched the first human trial vaccinating AD patients with synthetic Aβ (AN1792) and QS-21 adjuvant. Following a successful phase I study, AN1792/QS-21 failed the subsequent Phase II trial in 2001 because 6% (18/300) of the patients developed meningoencephalitis [10, 24, 25]. This was a setback for antibody-mediated immunotherapy, however, further studies showed that AN1792 has positive effects in the brain, causing a reduction in amyloid plaques similar to observations in AD transgenic mice [10, 24, 26, 27]. Consequently, it is believed that Aβ immunotherapy still has a big potential as a future treatment of AD. Currently, AN1792 is again being applied for the treatment of patients in clinical trials using a new formulation for the peptide [10]. In a similar approach, Janus *et al*. injected β-sheet-rich aggregates of Aβ into mice, thereby inducing the production of antibodies that specifically bind to Aβ peptides [28]. This immunization reduced cerebral plaque deposition by 50% in an AD mouse model and alleviated cognitive dysfunction [28]. The total level of Aβ in the brain of vaccine-treated and control mice was similar, suggesting that soluble Aβ peptides were not depleted from the brain. However, vaccination may have modulated the activity or concentration of, for example, toxic Aβ oligomers [28]. Based on this study, several immunization strategies are currently being tested in clinical trials, including dendrimeric display of Aβ [29].

16.1.1.2 **Passive Immunotherapy**

The failed AN1792 trial raised safety concerns about the stimulation of prominent inflammatory responses induced by active immunization. A big question in the field is whether passive immunization would be less prone to induce unwanted side effects than active immunization. In particular, the side effects might be reduced if specific epitopes in Aβ peptides are targeted by antibodies. A few passive immunization strategies are currently under investigation in human trials. For example, the humanized monoclonal antibodies Solanezumab [30] and Bapineuzumab are currently in phase III clinical trials for AD. After successful completion of phase II trials, both antibodies are believed to have minimal safety issues. However, the phase II trial with Bapineuzumab did not reveal any significant effect on the AD disease phenotype [31]. A very interesting aspect of Solanezumab and Bapineuzumab is that they target different epitopes in the Aβ peptide, the N-terminal $A\beta_{1-5}$, and the C-terminal $A\beta_{33-40}$ epitopes, respectively [30, 32]. It has been proposed that the N-terminal amino acids in Aβ are the pharmacologically relevant epitope. This will be now evaluated *in vivo* in the ongoing phase III clinical trials with AD patients. Evidence was presented that Solanezumab targets only soluble Aβ peptides without recognizing an insoluble β-sheet conformation [33]. Potentially the phase III trials will help to resolve this highly relevant dilemma in Aβ drug discovery, that is, whether the soluble or the insoluble state of Aβ causes neuronal dysfunction or toxicity.

Antibodies are not the only binding proteins that can be used against Aβ. Affibodies displayed on phages have been developed to bind with high affinity to monomeric Aβ, and this inhibits Aβ aggregation *in vitro* [34] and rescues transgenic *Drosophila* flies [35], though the direct application as therapy remains a challenge.

16.1.1.3 The Blood Brain Barrier

The BBB is the bottleneck for the development of antibodies and drugs for the central nervous system (CNS). 95–98% of all small-molecule drugs do not cross the BBB [36, 37]. Small molecules (100–400 Da) have a high probability to enter the brain, while larger molecules do not cross the BBB very well [36]. This raises the question whether antibodies have the potential to cross the BBB at pharmaceutically relevant concentrations as efficiently as small molecules and nanoparticles (NPs)? The potential is there: peripheral administration of antibodies reduces AD pathology *in vivo* [22, 33]. Small amounts of antibodies have been shown to cross the BBB, corresponding to 0.1% of serum levels in mice and human cerebrospinal fluid [38]. Whether these concentrations are sufficient for pharmacological effects is still unknown. Furthermore, it has been proposed that it is not necessary for antibodies to cross the BBB. Instead they can sequester Aβ in the plasma where it can be degraded. This is described as the *peripheral sink hypothesis* where the binding of Aβ to antibodies in the plasma by mass action drains free Aβ from the brain and central nervous system (CNS) [33]. This can lead to a dramatic shift in the distribution of Aβ. A 1000-fold increase in total Aβ plasma levels (both free and bound) upon peripheral administration of an antibody has been observed [33, 39].

BBB penetration is inversely proportional to the propensity of a drug to form hydrogen bonds with water [36]. Thus, higher lipid solubility favors BBB crossing. The BBB may be overcome through craniotomy, where drugs are delivered to the brain through a hole in the skull. However, this method only results in a local distribution of the drug in the brain [40]. Nevertheless, the BBB is currently the most promising access route for the delivery of drugs to the brain, particularly for neurodegenerative diseases since the vascular system is connected to every single neuron in the brain, allowing a wide drug distribution. Thus, for drug delivery to the brain the most validated strategy is the formulation of small-molecules that are able to cross the BBB [36].

16.1.2 Nucleic Acid-Based Agents against Protein Aggregates

Aptamers, that is, oligonucleic acid molecules that specifically bind target molecules are common ligands for proteins. They show both high selectivity and specificity toward protein targets. Although it has been difficult to find aptamers that target intrinsically disordered proteins, very recently a DNA aptamer has been identified that binds to both monomers and oligomers of the natively unfolded protein α-synuclein [41]. However, aptamers have a relatively large size of 6–40 kDa [42], which makes it difficult for these molecules to cross the BBB. Thus, aptamers are most likely unsuitable as drugs for the treatment of neurodegenerative diseases such as Parkinson's disease (PD). They rather have a high potential use for diagnostic purposes to image amyloid plaques [41], showing up to a 15-fold higher sensitivity for amyloid aggregates than Thioflavin T [43]. However, their relatively

high RNA-sequence-independent affinity for the amyloid fold [43] makes it difficult to target the oligomeric state of proteins with these molecules [43].

16.1.3 Inhibition of Amyloid Formation by Small Molecules

Amyloid formation is a sequence of many steps, starting from the native state and typically going through an amyloidogenic precursor state, an oligomeric nucleus, protofilaments, and different levels of fibril assembly, as described in Chapters 7, 8 and 14. Consequently amyloid formation can be inhibited by interfering with any of these steps. Targeting the native state will be specific for the protein in question, while compounds that bind to oligomers and fibrils tend to bind to numerous different proteins.

16.1.3.1 Stabilizing the Native State

Few of the major amyloid-associated diseases involve proteins which adopt a well-defined globular structure, and thus present a clear drug target, under physiological conditions. AD involves a ''schizophrenic'' peptide cleaved from a membrane-bound precursor, while α-synuclein in PD is natively unfolded (see, however, [44, 45] for evidence that it can form a helical tetramer which presents an obvious drug target), and the polyQ tracts involved in Huntington's do not form stable globular structures. In contrast, there is a whole family of systemic or localized amyloidoses which are highly prevalent and involve the tetrameric protein transthyretin. Successful strategies to stabilize transthyretin, leading to an approved drug, are described in detail in Chapter 17. A rare mutation in human lysozyme (D67H) leads to hereditary systemic amyloidosis, and camelid antibodies designed to bind the native state of this protein show promise in inhibiting amyloid formation [46]. Small molecules stabilizing superoxide dismutase, implicated in amyotrophic lateral sclerosis, have been shown to prevent its aggregation *in vitro* [47]. All these approaches represent viable strategies provided their binding does not interfere with the biological functions of the target protein.

16.1.3.2 Structural Properties of Fibrillation Inhibitors

Identifying compounds that can bind to the dynamic and fluctuating species that occur during the aggregation process is a major challenge. However, chemical space is vast [48], and it is likely that small molecules exist or can be synthesized that bind to any given structure, effectively promoting the assembly of certain aggregate species or suppressing others [49]. From a mechanistic point of view, an advantage of having a large selection of different small molecule modulators of fibrillation is that one can manipulate aggregation pathways at will. How this modulation occurs has not been resolved at atomic detail for any present compound; in fact, even the details of binding of established compounds such as Thioflavin T and Congo Red to amyloid structures are not completely resolved, though recent structures indicate that Thioflavin T intercalates between β-sheets at right angles to the β-strands (Figure 16.1) [50]. Simulations may provide some provisional insights

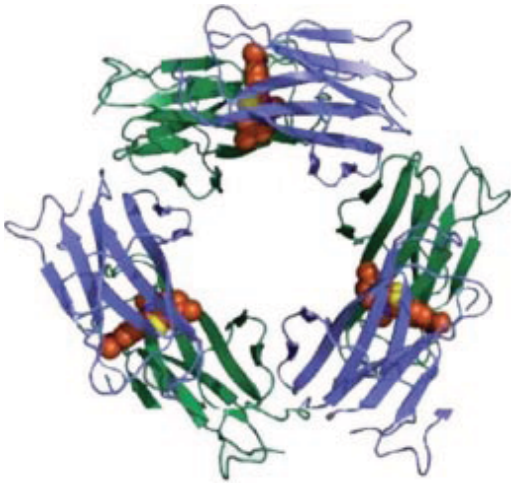

Figure 16.1 Binding of Thioflavin T to a β_2-microglobulin hexamer mimicking a fibrillar environment. The ThT molecules (orange) intercalate at right angles to the strands of the intersheet interfaces. (Reproduced with permission from Ref. [50].)

into the molecular mechanisms by which small molecules associate with amyloid aggregates. For example, some compounds have been suggested to promote a helical structure in the hydrophobic core of Aβ peptides, thus preventing this region from engaging in fibril formation [51].

The identification of small molecules as novel inhibitors of protein aggregation often involves high throughput screenings of comprehensive compound libraries. A list of examples is provided in Table 16.2. Clearly many different compounds inhibit aggregation of amyloidogenic proteins and peptides. Congo Red rescues hippocampal neurons against toxicity of Aβ and IAPP fibrils [52] and inhibits polyQ-mediated protein aggregation in cell-free and cell-based assays [53]. Its derivatives BSB ((trans, trans),-1-bromo-2,5-bis-(3-hydroxycarbonyl-4-hydroxy)styrylbenzene) and FSB ((*E,E*)-1-fluoro-2,5-bis(3-hydroxycarbonyl-4-hydroxy)styrylbenzene) [54] (Figure 16.2) are potent diagnostic tools for detecting brain plaques *in organo*. The amyloid binding ligands Chrysamine G (which inhibits toxicity and aggregation in cell assays, Figure 16.2 [55]) and Thioflavin S cannot cross the BBB, but derivatives have been synthesized that can enter the brain, while retaining their fibril-inhibiting properties *in vitro* and also inhibiting fibrillization in cells [56]. Curcumin (found in the Indian spice turmeric) is structurally similar to the amyloid fibrillization modulators Congo Red, Chrysamine G, and RS-0406 [57]. It is also able to block oligomer and plaque formation *in vitro* and *in vivo* at sub-micromolar concentrations and crosses the BBB in mice [58]. Interestingly, all these molecules contain two aromatic groups that are separated by a backbone of the appropriate length. The two terminal groups may be critical for the high affinity interaction of the compounds with Aβ peptides, while the linker facilitates binding of inhibitors to specific subregions of aggregates [9]. Successful targeting of compounds to aggregates may, therefore, require more extensive coupling of different binding groups to provide avidity as well as specificity [9].

Table 16.2 Overview of screening campaigns with small molecules against protein aggregation processes.

Target molecule	Assay	Library	Outcome
Tau	Aggregation of tau protein fragments at pH 7 with heparin followed by Thioflavin S fluorescence assays	Merck (200 000)	Several hydroxyanthraquinones with IC_{50} values of 1–5 μM able to dissolve paired helical filaments and to rescue toxicity in neuroblastoma cells identified [60]. Also series of phenylthiohydrazones [61] with cell-protective properties and ~10 μM IC_{50} values detected. Smaller screening also identifies porphyrins [62]. General work summarized in [63].
Tau	Aggregation leads to protease resistance.	Paired helical filament ligands from a previous study. About 10 in all.	Derivatives of methylene blue inhibit tau aggregation at nanomolar levels and facilitate degradation of tau [64].
Insulin	Fibrillation at pH 2 60 °C	Small selection of aromatic compounds related to the three-ring compound phenol-sulfonphthalein.	In most cases compounds require two groups for activity. One group is needed to bind aggregates and one to inhibit polymerization by steric hindrance. However, several monocyclic compounds identified [65]. In a screening of 144 flavonoids using the cyanine dye 7519, several candidates found [66].
polyQ	Filter retardation assay	184 000 compounds	In the primary screen ~300 compounds identified, 25 of which are benzothiazoles, one inhibits aggregation *in vivo* [67].
polyQ	Membrane-permeable yeast strain rescued from polyQ toxicity (GFP expression).	16 000 compounds from Chembridge	Of the nine best hits in yeast, four rescue mammalian cells. One polyaromatic derivative hereof rescues neurons and *Drosophila* against polyQ aggregate toxicity [68]

Table 16.2 *(Continued)*

Target molecule	Assay	Library	Outcome
Prion protein	Scanning for intensely fluorescent targets (antibody-aggregate complex)	10 000 compounds (DiverSet1, Chembridge)	Inhibitors disrupt complex and reduce prion signal. Four of the six hits share an *N*'-benzylidene-benzohydrazide core structure [69]. This compound class is also active against polyQ repeats and α-synuclein [70].
α-synuclein	PBS 37 °C with agitation assayed by ThT	169 compounds from 3,4-dihydroxyphenylacetic acid (LOPAC) library	Catecholamines similar to dopamine [71] stabilize covalent α-synuclein adducts against aggregation.
α-synuclein	PBS 37 °C with shaking	7-mer peptides covering α-synuclein	Residues in 64–86 region inhibit aggregation and oligomer formation [72].
Aβ	Small-molecule microarrays (SMMs) to identify Aβ ligands.	17 905 immobilized compounds (natural, commercial, and diversity-synthesized)	Of the 79 ligands identified, one of the two best hits rescues cells against Aβ cytotoxicity and promotes fibrillation presumable at the expense of oligomer formation [73].
Aβ	Small-molecule compounds promoting elongation of Aβ fibrils using biotin-Aβ detected by Eu^{3+}	640 members of LOPAC library (Sigma)	Calmidazolium chloride stimulates Aβ aggregation to stable protofibrillar clusters [74]. Methylene Blue also bypasses oligomeric species and promotes fibrillation of Aβ [75].
Aβ	Different aggregate species monitored by specific antibodies.	∼50 commercial compounds shown previously to inhibit aggregation	Different modes of action: compounds inhibit oligomers, fibrils, or both, showing oligomers are not compulsory fibril precursors [49].
Aβ	Aβ-GFP fusions aggregate and do not develop fluorescence.	∼1 000 triazole compounds.	Hits inhibit Aβ fibrillation in a dose-dependent manner [76]. Assay may miss compounds that cannot cross *E. coli* membrane and oligomer-inducing compounds may be false positives.

(continued overleaf)

Table 16.2 *(Continued)*

Target molecule	Assay	Library	Outcome
Aβ	Signal peptide-Aβ-lactamase fusion aggregates and lactamase is not exported, leading to antibiotic sensitivity.	~1 000 triazole compounds.	Four best hits inhibit Thioflavin T-monitored Aβ aggregation [77].
Aβ	Thioflavin T fibrillation assay	113 000 compounds	RS-0406 (*N,N′*-bis(3-hydroxyphenyl) pyridazine-3,6-diamine) inhibits fibrillation >10 μM and rescues toxicity in neurons at ~1 μM [57].
Aβ	Toxic Aβ aggregates depolarize PC12 cells, monitored by specific dye.	3 000 biologically active compounds	Best compound 4,5-dianilinophthalimide (DAPH) blocks fibrillation and dissociates fibrils, leading to small amorphous non-toxic aggregates that do not lead to Ca^{2+} efflux [78].
Aβ	Aβ-release factor fusion inhibits release factor activity in yeast and subsequent growth.	12 800 compounds (Diver, Chembridge)	Two compounds reduce Aβ fibrillation and oligomer formation [79].
β_2-micro-globulin	Affinity capillary electrophoresis to stabilize non-amyloidogenic form.	200 model sulfonated compounds.	Identify compounds by ACE, study affinity by MS and test *in silico* with docking experiments [80].
Modified κ-casein	ThT fluorescence in aggregation assay at neutral pH 37 °C	Known inhibitors of aggregation	Robust and inexpensive (but not very sensitive) assay of fibril inhibition potency based on naturally occurring amyloid process.

Typically, compounds with highly conjugated cyclic groups, such as anthracyclines, naphthaquinones, or benzofurans reduce Aβ aggregation and toxicity in cell model systems. *N*-benzylidenebenzohydrazide derivatives, for example, inhibit aggregation of prions [69], polyQ proteins, and α-synuclein [70]. Porphyrins and phthalocyanins inhibit initial stages of PrP conversion [81]. Polyphenols are also potent modulators of amyloid polymerization. They inhibit aggregation by a combination of structural rigidity (characteristic of polycyclic rings) and aromatic

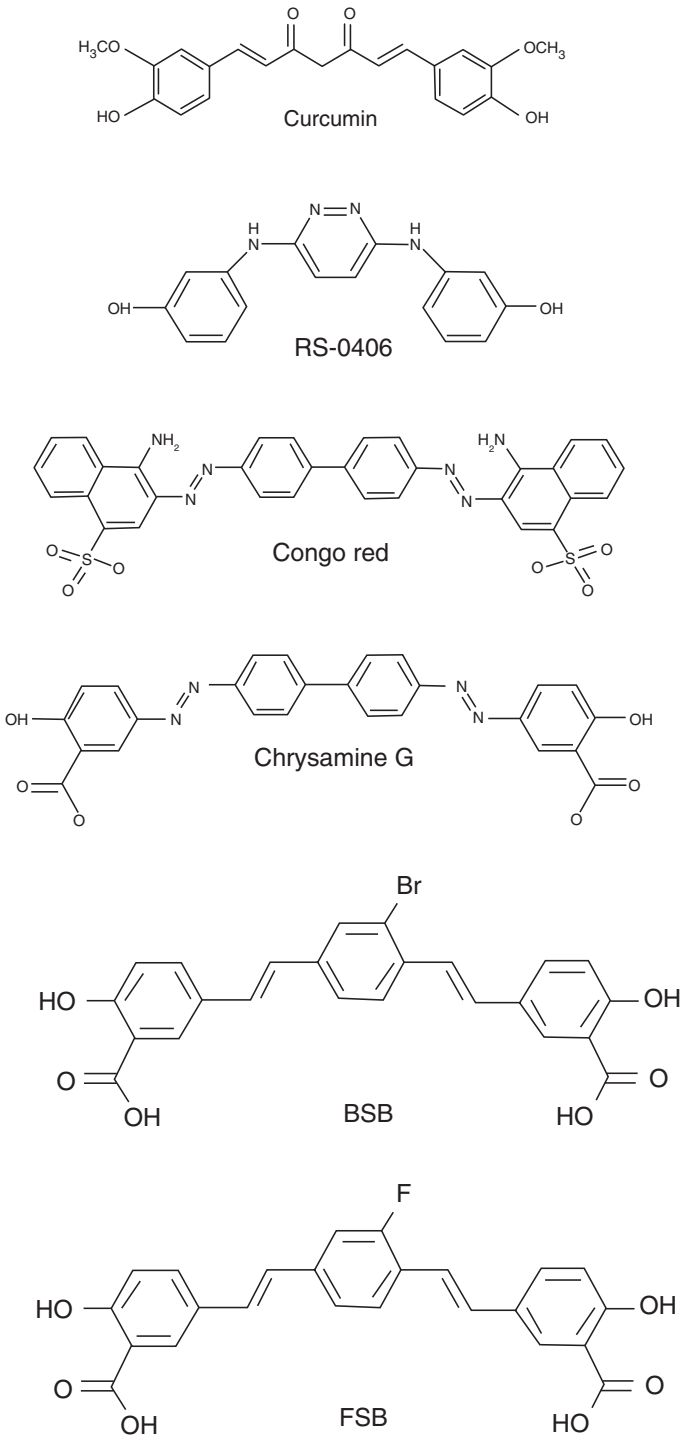

Figure 16.2 Structures of Aβ-inhibiting compounds [54, 58, 59].

stacking [82]. It is important to note that many polyphenols show antioxidant properties [83], but the degree of redox activity does not correlate with their anti-aggregative properties [82]. This is also supported by observations indicating that polyphenols do not inhibit cell death by hydrogen peroxide capturing or other oxidative stress factors [84]. Based on a thorough comparison of 25 known amyloid inhibitors, the best polyphenol candidates are suggested to contain at

least two phenolic rings with two to six atom linkers, and a minimum number of three OH groups on the aromatic rings [82, 85]. These properties are needed to target the growing cross-β amyloid structure through spatially correct aromatic–aromatic contacts and to interfere with continued amyloid growth. This agrees well with independent observations on the inhibition of α-synuclein aggregation, where the key features were identified as (i) aromatic elements for binding of compounds to the α-synuclein monomers or oligomers and (ii) vicinal hydroxy groups present on a single phenyl ring [86]. Aromatic (and to a lesser extent other nonpolar and polar) interactions have also been identified as the main driving force for binding amyloid structures in MD simulations [87]. However, specific binding at one site rather than ''smeared interactions'' over a larger part of the fibril may require electrostatic interactions, for example, with Lys side-chains [88].

Aggregation-prone polypeptides involved in AD remain the primary targets for therapeutic effects against neurodegenerative diseases. Yet, despite enormous efforts, no small-molecule inhibitors of Aβ aggregation are available for patients as drugs. Several small molecules are currently in clinical trials [9]. These include the hydroxyanaline derivative SEN1269 (Senexis), and the metal chelator PBT2 (Prana Biotechnology), while trials with scyllo-inositol (Transition Therapeutics and Elan) were recently stopped. A major challenge is to identify compounds that specifically target small toxic aggregate species *in vivo* , and so far little convincing evidence has been provided that such structures can be detoxified with small molecules.

16.1.3.2.1 Unspecific Effects by Colloidal Agents

Interestingly, many small-molecule aggregate inhibitors behave as colloids or chemical aggregators which undergo self-association [89]. Several of these compounds, including Congo Red, were shown to inhibit the activity of the detergent sensitive enzyme β-lactamase, indicating that they unspecifically target cellular proteins [89]. Supporting this, the activity of chemical aggregators on the amyloid formation processes is inhibited by detergent-sequestering proteins, such as BSA, which binds many small molecules in an unspecific way [89]. This is perhaps not surprising in view of the relatively generic interactions small molecules have to engage in to prevent aggregation. In fact, the mode of binding of these compound aggregates may be similar to detergents that bind to proteins in a cooperative fashion, unraveling the native structure in a series of steps [90]. Potentially, such promiscuous interactions may reduce the specificity required for therapeutic efficacy. Thus, any serious drug candidate should be screened at an early stage to investigate its ability to unspecifically bind to various human proteins. However, specific compound aggregation can occur. The small molecule scyllo-inositol forms stable micelles with Aβ oligomers and inhibits their cytotoxicity [91]. Furthermore, it has been suggested that Congo Red may promote non-toxic Aβ fibrillation at concentrations below its critical micelle concentration in a fashion similar to anionic detergents [92]. Micellar assemblies of Congo Red or lacmoid may also interact with specific regions of the unfolded α-synuclein [93].

16.1.3.3 Polyphenols: a Potent Class of Amyloid Inhibitors

Flavonoids are a very large group of amyloid modulators that are well-known for their antioxidative properties. They contain a benzene ring with vicinal dihydroxy-groups (Figure 16.4) and are commonly found in plants, where they are responsible for their different colors. Moreover, flavonoids are known to function as a defense system, which protects plants against other organisms. Flavonoids found in green tea confer numerous human health benefits. The Ohsaki National Health Insurance Cohort Study involving 40 530 Japanese adults has demonstrated that the consumption of green tea significantly reduces the mortality of people, especially with respect to cardiovascular diseases.

The pioneering work by Lansbury and coworkers [71] in 2001 highlighted flavonoids, such as dopamine, as inhibitors of α-synuclein fibrillation, and stimulated a broad interest in these compound structures. Subsequent reports on the *in vitro* effects of dopamine, its metabolic product DOPAC [94] and the related compound baicalein [95] revealed that fibrillation inhibition and disaggregation of mature fibrils occur through stabilization of small oligomers [96–99] (Figure 16.3). A comprehensive mutational study revealed that the region ^{125}YEMPS^{129} in α-synuclein is critical for the inhibition of fibril formation [97]. This region appears to be modified with an oxidation product of dopamine, dopaminochrome, and the interaction is reversible, that is, non-covalent [97]. A molecular dynamic and mutational study confirmed the role of ^{125}YEMPS^{129} and suggested that Glu83 stabilizes compound binding by long-range electrostatic interactions [96]. This residue was also considered to function as a fibrillation gatekeeper, preventing the spontaneous aggregation of α-synuclein molecules [100].

16.1.3.3.1 Epigallocatechin Gallate: the Universal Amyloid-Inhibitor?

Among the flavonoids, epigallocatechin gallate (EGCG) has been studied most intensively. EGCG is very abundant in green tea leaves and appears to have multiple

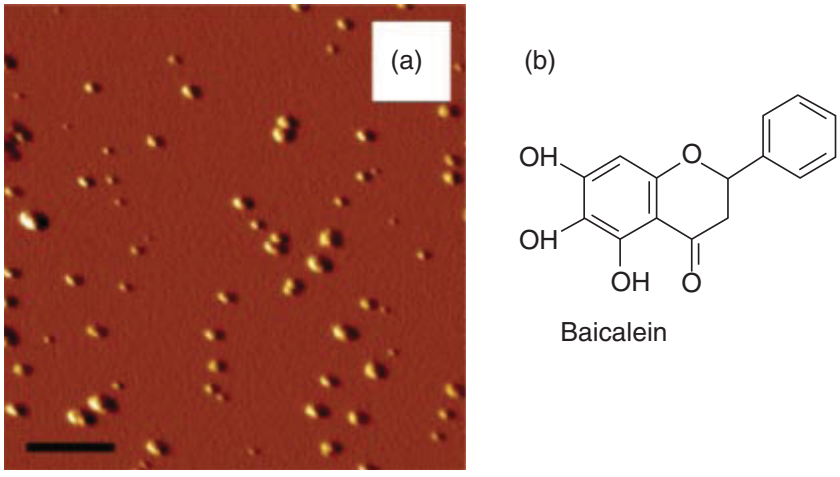

Figure 16.3 (a) AFM images of oligomers of α-synuclein stabilized by baicalein. Length bar represents 200 nm. (b) Structure of baicalein. (Reproduced with permission from (a) Ref. [101] and (b) Ref. [95].)

positive effects in various diseases, including HIV [102], several forms of cancer including leukemia as well as neurodegenerative diseases [103]. Recent studies have demonstrated that EGCG is able to directly influence the amyloidogenesis of various polypeptides, including huntingtin [104], transthyretin (TTR) [105], islet amyloid polypeptide [106], *Plasmodium falciparum* merozoite surface protein 2 [107], κ-casein [108], prion protein [109], the SEVI peptide facilitating HIV viral uptake [102], amyloid-β, and α-synuclein [110]. Thus, it seems to function as a chemical chaperone that can associate with different types of proteins and structures.

Biochemical and biophysical investigations have recently elucidated the mechanism by which EGCG inhibits α-synuclein and amyloid-β fibril formation *in vitro* [110, 111]. An nitro blue tetrazolium (NBT) staining assay showed that EGCG binds directly to both intrinsically disordered and oligomeric α-synuclein molecules [111]. The finding that EGCG can bind to various structurally and functionally distinct proteins indicates that it does not bind to specific amino acid sequences. Supporting this, NMR experiments revealed that equimolar concentrations of EGCG associate with the unstructured C-terminal region of α-synuclein (D119, S129, E130, and D135) [111]. This is consistent with the observations that dopamine preferentially binds ^{125}YEMPS^{129} [96, 97]. When EGCG is in excess, however, the compound unspecifically associates with α-synuclein throughout the whole polypeptide chain [111]. Thus, the currently available structural data suggest that EGCG binds unspecifically to proteins and preferentially associates with highly unstructured regions.

A model for EGCG-mediated inhibition of α-synuclein fibrillogenesis is shown in Figure 16.4. Here EGCG directly binds to unstructured α-synuclein protein molecules and induces the formation of higher molecular weight oligomers that are nontoxic and off-pathway in the fibrillation process [110]. EGCG also forms oligomers with huntingtin and Aβ [104, 110, 112]. The stabilization of higher order structures in a competing pathway is a consequence of EGCG preventing β-sheet formation when bound to α-synuclein [111]. EGCG can disaggregate preformed mature amyloid fibrils into smaller amorphous aggregates [110], making it a potentially useful drug for the treatment of amyloidoses as well. Note that EGCG-α-synuclein oligomers are unable to seed fibril formation, indicating that they are indeed off-pathway structures [111]. However, EGCG-free α-synuclein oligomers are also unable to seed amyloid fibrillation (N.L. and D.O., unpublished), just as other small molecule compounds can inhibit fibrillation without affecting oligomerization [49]. Thus, the question whether α-synuclein indeed forms on-pathway seeding-competent oligomers needs to be further investigated (see below).

As EGCG is not able to cross the BBB [113], it is not a suitable drug for the treatment of neurodegenerative diseases. However, the clear effects of EGCG and other flavonoids on various fibril assembly pathways provide scientists with structural insights that are very useful for the development of new small molecules that directly target amyloidogenic proteins. The general approach seems to be applicable for other compounds: the anti-leprosy drug Rifampicin also disaggregates α-synuclein fibrils in a manner involving oxidation, covalent modifications, and oligomer stabilization [114]. Further progress may be inspired by the observation

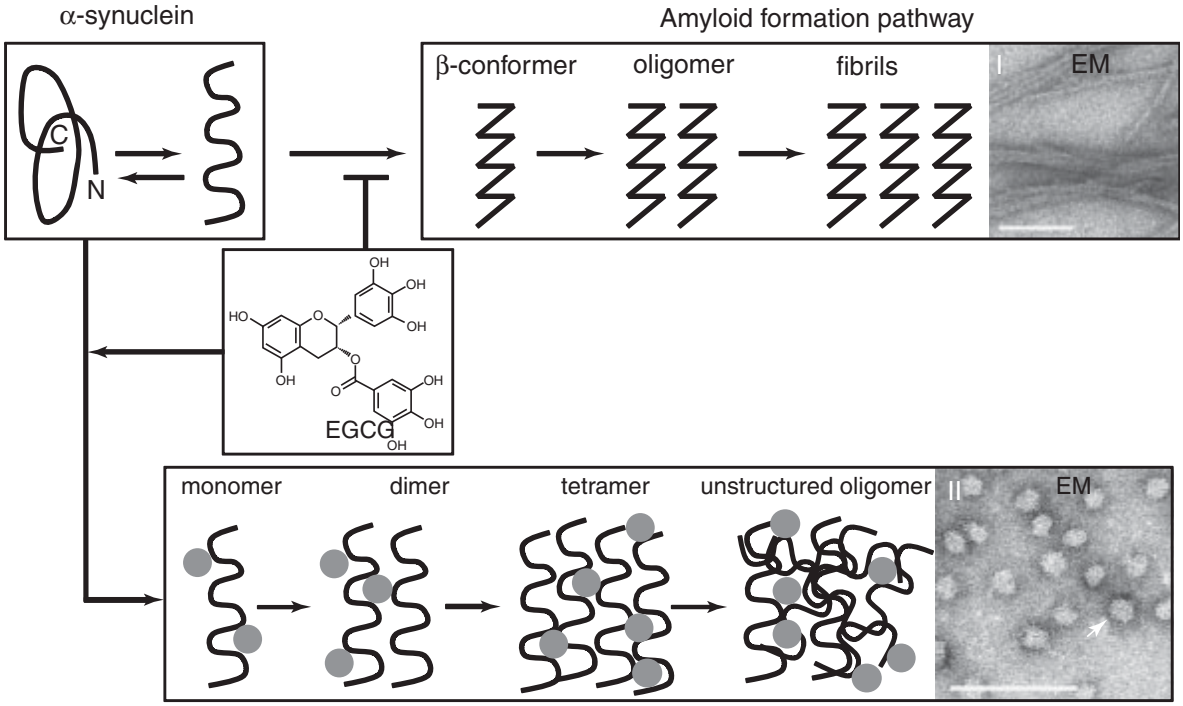

Figure 16.4 Effect of EGCG on the aggregation of α-synuclein. EGCG binds preferentially to unstructured α-synuclein protein molecules and induces the formation of higher molecular weight oligomers that are nontoxic and off-pathway in the fibrillation process. Scale bars represent 100 nm. (Electron micrographs were reproduced with permission from Ref. [95].)

that biflavonoids are much more potent than monoflavonoids in preventing Aβ fibrillation and cytotoxicity and can promote formation of presumably off-pathway aggregates [115]. This is probably an avidity effect due to the covalent linkage of two binding groups.

16.1.3.4 **Promoting Fibrillation to Avoid Toxic Oligomers**

Several lines of evidence indicate that pre-fibrillar assemblies of Aβ polypeptides, such as soluble oligomers or protofibrils, rather than mature, end-stage amyloid fibrils, cause neuronal dysfunction and memory impairment in AD. This suggests that reducing the prevalence of transient intermediates by small-molecule mediated stimulation of amyloid polymerization might decrease toxicity. Calmidazolium chloride (CLC) rapidly converts soluble Aβ peptides into very stable protofibrillar clusters [74]. Methylene Blue also stimulates Aβ fibrillogenesis, both *in vitro* and in cell-free assays, but does not influence oligomerization, suggesting that these processes are not directly linked. However, a recent study suggests that the orcein-related small molecule O4 (2,8-bis-(2,4-dihydroxy-phenyl)-7-hydroxy-phenoxazin-3-one) is a potent enhancer of Aβ42 fibrillogenesis [116]. It binds directly to hydrophobic amino acid residues in Aβ peptides and stabilizes the self-assembly of seeding-competent, β-sheet-rich protofibrils and fibrils. Strikingly, O4-mediated acceleration of amyloid fibril formation efficiently decreased the

concentration of small, toxic Aβ oligomers in complex, heterogeneous aggregation reactions. In addition, O4 treatment suppressed inhibition of long-term potentiation by Aβ oligomers in hippocampal brain slices, supporting the hypothesis that small, diffusible pre-fibrillar amyloid species rather than mature fibrillar aggregates are toxic for mammalian cells.

16.1.4 Peptides and Peptide Mimetics

The repetitive and homopolymeric amyloid structure makes it possible to design peptide ligands based on the primary structure of the amyloid core. In this approach, peptides are designed to bind to the growing ends of fibrils or oligomers in order to prevent fibril elongation [117]. This strategy can even lead to reversal of fibril growth [118]. Targeting the amyloid core in the AD amyloid-β peptide with peptides corresponding to the central fibrillating sequence has proven to be a valid strategy to inhibit fibril formation and to reduce cytotoxicity *in vivo* [119–130]. Similar results were also obtained for other amyloidogenic polypeptides such as α-synuclein [127, 72], PrP, and amylin [131].

Designing ligand peptides can be facilitated by *in silico* methods [132]. When using peptides that resemble the amyloid core, an apparent problem is that these molecules potentially have a high propensity to form amyloid structures and induce toxicity, as shown for α-synuclein by Bodles and coworkers [133]. Different peptide engineering strategies have been employed successfully to reduce the intrinsic amyloid-forming properties and to improve the inhibitory effect of peptides, for example, by introducing proline residues [134], retroinversion [121, 127], N-methylation, or disruptive linkers [123, 124, 126]. The latter two approaches are most widely used and will be discussed briefly.

N-methylation of ligand peptides has been found to be a successful strategy to inhibit aggregation and/or cytotoxicity of various Aβ peptides and α-synuclein [119] though its effect on amylin is more controversial [131, 135]. N-methylation reduces the ability of peptides to form hydrogen bonds, which are a prerequisite for efficient amyloidogenesis. Thus, when an N-methylated peptide binds to the aggregation-prone Aβ peptide, its spontaneous aggregation is potentially inhibited due to destabilization of the hydrogen bond network [118]. Parallel studies by Hughes *et al*. and Gordon *et al*. have clearly demonstrated that the site-specificity of N-methylation is crucial for inhibitory effects of peptides. This is supported by studies indicating that different *N*-methylated versions of the undecamer peptide $A\beta_{25-35}$ have different effects on the aggregation and cytotoxity of Aβ [125]. While N-methylation of Gly33 completely inhibits Aβ amyloid formation and reduces cytotoxicity, N-methylation of Gly25 has a weak effect on aggregation, which corresponds to the wild-type peptide ($A\beta_{25-35}$). In comparison, N-methylation of Leu_{34} changes the fibril morphology and reduces cytotoxicity [122, 125]. A peptide spanning residues 69–72 in α-synuclein blocks oligomer and fibril formation [72]. Accordingly, for the undecamer peptide (α-$synuclein_{68-78}$) a single N-methylation at Gly73 has been demonstrated to inhibit amyloid formation even more efficiently,

and reduce α-synuclein toxicity [119]. An alternative to N-methylation is to include Pro residues due to their inability to participate in hydrogen bonding. Variants of Aβ containing Pro in the core amyloid sequence LVFFAED inhibit amyloid formation and disaggregate existing fibrils [136], while the minimalist peptide LPFFD reduces Aβ plaque formation *in vivo* [129].

Another valid strategy to modify ligand peptides is to link a disruption element to short peptides that recognize aggregation-prone amino acid sequences. The peptide KLVFF ($A\beta_{16-20}$) is a strong recognition element for Aβ peptides and linking it with disruption elements such as, for example, Lys6 has been shown to inhibit cellular toxicity of Aβ aggregates [123, 126]. However, these peptides do not necessarily prevent fibril formation but may rather increase aggregate size and alter aggregate morphology [126]. Linking Lys6 or Glu4 to KLVFF protects Aβ cytotoxicity *in vivo* by promoting aggregation, which is most likely accompanied by a decrease in toxic oligomers [124, 126].

Protein ligands are generally selected due to their specific binding to a defined primary amino acid sequence. However, peptide ligands are not limited to the recognition of primary sequences because they can also recognize higher-order aggregate structures [120, 137, 138]. Reinke *et al.*, for example, have designed a bivalent version of the Aβ ligand KLVFF ($A\beta_{16-20}$) fused to a 19–24 Å long linker, which specifically binds to early oligomeric states of Aβ. In comparison, it only showed a low binding affinity for monomers and mature β-sheet-rich amyloid fibrils [137]. If Aβ monomers indeed are crucial for the survival of neurons, the selective targeting of cytotoxic aggregate species such as oligomers is key to the development of effective therapeutic strategies against AD. The ability of ligand peptides to distinguish between monomers and higher order structures has been utilized by Hoogerhout *et al.* to develop a combined antibody-mediated immunotherapy, which aims to specifically target Aβ aggregate species using a peptide ligand strategy [138]. They designed an undecamer peptide ($A\beta_{22-28}$-YNGK) that recognizes a conformational epitope in Aβ oligomers and fibrils but that does not bind to monomeric Aβ molecules [138]. Using antibodies that bind to the $A\beta_{22-28}$-YNGK peptide reduced the concentration of higher-order Aβ structures in mice by antibody-mediated immunotherapy without depleting potentially non-toxic monomers [138].

16.1.5
Nanoparticles: Untamed Dragons with Fire Power to Heal?

Another promising class of agents are polymeric biocompatible NPs. Fluorinated NPs can efficiently inhibit Aβ fibril formation and reduce the toxicity of aggregate species *in vivo* [139]. NPs have the significant advantage compared to small molecules that they readily cross the BBB, potentially enabling them to be utilized as future drugs for the treatment of neurodegenerative diseases such as AD. Consequently, nanoneurotechnology has emerged as a very promising field because numerous NPs have been discovered in recent years that can efficiently cross the BBB [140, 141]. This has especially been explored with regard to drug delivery where,

for example, nanoliposomes have been applied to transport Aβ-targeting antibodies [142, 143]. Polymeric NPs have also been successfully used for the oral delivery of estradiol to rat brains [144]. Recent studies have demonstrated that NPs have a high potential to bind aggregation-prone Aβ peptides, thereby inhibiting amyloid formation [139, 145–147]. This opens up the possibility to deliver compounds to the brains of transgenic animals and patients that *per se* are unable to cross the BBB. Brezesinski and coworkers have demonstrated that both fluorinated, sulfonated, and sulfated NPs are able to inhibit amyloid formation and disintegrate amyloids of the Aβ peptide [139, 148]. Furthermore, they reduce cytotoxicity *in vivo* of Aβ peptides and oligomers. They conclude that to be effective, NPs must have a highly negative zeta potential and a fine balance between hydrophilic moieties and hydrophobic chains [148, 149].

The application of NPs for the inhibition of amyloid formation is still a very new research field and, to date, only few reports have been published. In the coming years it will be necessary to elucidate whether NPs can be safely applied to treat neurodegenerative disease phenotypes in transgenic mouse model systems [140] and to clarify whether they are applicable as specific ligands.

16.2 Summary

In this chapter we have focused on strategies to intervene against the early-stage aggregates that are believed to play a central role in several neurodegenerative diseases. Despite some setbacks, immunotherapy against toxic Aβ aggregate species remains a promising therapeutic approach for AD, both through active immunization using soluble states of the Aβ peptide and passive immunotherapy directed against both soluble and insoluble states, where it may not be necessary to cross the BBB. Aptamers are probably most promising as diagnostic agents against amyloid deposits. No small-molecule aggregation inhibitors have yet been approved, probably due to difficulties in specifically targeting the toxic aggregate state *in vivo*. However, there are numerous candidates in the pipeline. General features of promising compounds include several aromatic groups separated by linkers; polar groups such as vicinal hydroxy groups and electrostatic interactions may confer additional specificity. A caveat is that many of these compounds self-associate, which may lead to unwanted side-effects *in vivo*. The most promising group of aggregation inhibitors are the flavonoids. Particularly EGCG, which can prevent and reverse fibrillation of many unrelated proteins, probably by forming non-toxic oligomers, might be a very interesting candidate for further development. An alternative approach is to promote fibrillation and thus bypass or reduce oligomer accumulation; here orcein derivatives are particularly promising. Peptide mimetics are obvious candidates since they should be specific for the parent protein sequence, and the most promising strategies include N-methylation and inclusion of β-sheet disruptive linkers. Finally, NPs hold potential due to their combined ability to cross the BBB and to bind aggregation-prone peptides.

References

1. Chiti, F. and Dobson, C.M. (2006) Protein misfolding, functional amyloid, and human disease. *Ann. Rev. Biochem.*, **75**, 333–366.
2. Hirakura, Y. and Kagan, B.L. (2001) Pore formation by beta-2-microglobulin: a mechanism for the pathogenesis of dialysis associated amyloidosis. *Amyloid*, **8**, 94–100.
3. Olzscha, H., Schermann, S.M., Woerner, A.C., Pinkert, S., Hecht, M.H., Tartaglia, G.G., Vendruscolo, M., Hayer-Hartl, M., Hartl, F.U., and Vabulas, R.M. (2011) Amyloid-like aggregates sequester numerous metastable proteins with essential cellular functions. *Cell*, **144**, 67–78.
4. Bodin, K., Ellmerich, S., Kahan, M.C., Tennent, G.A., Loesch, A., Gilbertson, J.A., Hutchinson, W.L., Mangione, P.P., Gallimore, J.R., Millar, D.J., Minogue, S., Dhillon, A.P., Taylor, G.W., Bradwell, A.R., Petrie, A., Gillmore, J.D., Bellotti, V., Botto, M., Hawkins, P.N., and Pepys, M.B. (2010) Antibodies to human serum amyloid P component eliminate visceral amyloid deposits. *Nature*, **468**, 93–97.
5. Botto, M., Hawkins, P.N., Bickerstaff, M.C., Herbert, J., Bygrave, A.E., McBride, A., Hutchinson, W.L., Tennent, G.A., Walport, M.J., and Pepys, M.B. (1997) Amyloid deposition is delayed in mice with targeted deletion of the serum amyloid P component gene. *Nat. Med.*, **3**, 855–859.
6. Bodin, K., S. Ellmerich, M. C. Kahan, G. A. Tennent, A. Loesch, J. A. Gilbertson, W. L. Hutchinson, P. P. Mangione, J. R. Gallimore, D. J. Millar, S. Minogue, A. P. Dhillon, G. W. Taylor, A. R. Bradwell, A. Petrie, J. D. Gillmore, V. Bellotti, M. Botto, P. N. Hawkins, and M. B. Pepys. Antibodies to human serum amyloid P component eliminate visceral amyloid deposits. *Nature* **468**: 93–97.
7. Whitty, A. and Kumaravel, G. (2006) Between a rock and a hard place? *Nat. Chem. Biol.*, **2**, 112–118.
8. Wells, J.A. and McClendon, C.L. (2007) Reaching for high-hanging fruit in drug discovery at protein-protein interfaces. *Nature*, **450**, 1001–1009.
9. Nie, Q., Du, X.G., and Geng, M.Y. (2011) Small molecule inhibitors of amyloid beta peptide aggregation as a potential therapeutic strategy for Alzheimer's disease. *Acta Pharmacol. Sin.*, **32**, 545–551.
10. Pride, M., Seubert, P., Grundman, M., Hagen, M., Eldridge, J., and Black, R.S. (2008) Progress in the active immunotherapeutic approach to Alzheimer's disease: clinical investigations into AN1792-associated meningoencephalitis. *Neurodegener. Dis.*, **5**, 194–196.
11. Boche, D. and Nicoll, J.A. (2008) The role of the immune system in clearance of Abeta from the brain. *Brain Pathol.*, **18**, 267–278.
12. McLaurin, J., Cecal, R., Mierstead, M.E., Tian, X., Phinney, A.L., Manea, M., French, J.E., Lambermon, M.H.L., Darabie, A.A., Brown, M.E., Janus, C., Chishti, M.A., Horne, P., Westaway, D., Fraser, P.E., Mount, H.T.J., Przybylski, M., and St. George-Hyslop, P. (2002) Theraupeutically effective antibodies against amyloid-beta peptide target amyloid-beta residues 4–10 and inhibit cytotoxicity and fibrillogenesis. *Nat. Med.*, **8**, 1263–1269.
13. Serrano-Pozo, A., William, C.M., Ferrer, I., Uro-Coste, E., Delisle, M.B., Maurage, C.A., Hock, C., Nitsch, R.M., Masliah, E., Growdon, J.H., Frosch, M.P., and Hyman, B.T. (2010) Beneficial effect of human anti-amyloid-beta active immunization on neurite morphology and tau pathology. *Brain*, **133**, 1312–1327.
14. Biscaro, B., Lindvall, O., Hock, C., Ekdahl, C.T., and Nitsch, R.M. (2009) Abeta immunotherapy protects morphology and survival of adult-born neurons in doubly transgenic APP/PS1 mice. *J. Neurosci.*, **29**, 14108–14119.
15. Schenk, D., Barbour, R., Dunn, W., Gordon, G., Grajeda, H., Guido, T., Hu, K., Huang, J., Johnson-Wood, K., Khan, K., Kholodenko, D., Lee, M., Liao, Z., Lieberburg, I., Motter, R.,

Mutter, L., Soriano, F., Shopp, G., Vasquez, N., Vandevert, C., Walker, S., Wogulis, M., Yednock, T., Games, D., and Seubert, P. (1999) Immunization with amyloid-beta attenuates Alzheimer-disease-like pathology in the PDAPP mouse. *Nature*, **400**, 173–177.

16. Lee, E.B., Leng, L.Z., Zhang, B., Kwong, L., Trojanowski, J.Q., Abel, T., and Lee, V.M. (2006) Targeting amyloid-beta peptide (Abeta) oligomers by passive immunization with a conformation-selective monoclonal antibody improves learning and memory in Abeta precursor protein (APP) transgenic mice. *J. Biol. Chem.*, **281**, 4292–4299.
17. Moretto, N., Bolchi, A., Rivetti, C., Imbimbo, B.P., Villetti, G., Pietrini, V., Polonelli, L., Del Signore, S., Smith, K.M., Ferrante, R.J., and Ottonello, S. (2007) Conformation-sensitive antibodies against alzheimer amyloid-beta by immunization with a thioredoxin-constrained B-cell epitope peptide. *J. Biol. Chem.*, **282**, 11436–11445.
18. Asuni, A.A., Boutajangout, A., Quartermain, D., and Sigurdsson, E.M. (2007) Immunotherapy targeting pathological tau conformers in a tangle mouse model reduces brain pathology with associated functional improvements. *J. Neurosci.*, **27**, 9115–9129.
19. Fogarty, M.P., McCormack, R.M., Noonan, J., Murphy, D., Gowran, A., and Campbell, V.A. (2010) A role for p53 in the beta-amyloid-mediated regulation of the lysosomal system. *Neurobiol. Aging*, **31**, 1774–1786.
20. Santa-Maria, I., Hernandez, F., Del Rio, J., Moreno, F.J., and Avila, J. (2007) Tramiprosate, a drug of potential interest for the treatment of Alzheimer's disease, promotes an abnormal aggregation of tau. *Mol. Neurodegener.*, **2**, 17.
21. Hawkes, C.A., Deng, L.H., Shaw, J.E., Nitz, M., and McLaurin, J. (2010) Small molecule beta-amyloid inhibitors that stabilize protofibrillar structures *in vitro* improve cognition and pathology in a mouse model of Alzheimer's disease. *Eur. J. Neurosci.*, **31**, 203–213.
22. Bard, F., Cannon, C., Barbour, R., Burke, R.L., Games, D., Grajeda, H., Guido, T., Hu, K., Huang, J., Johnson-Wood, K., Khan, K., Kholodenko, D., Lee, M., Lieberburg, I., Motter, R., Nguyen, M., Soriano, F., Vasquez, N., Weiss, K., Welch, B., Seubert, P., Schenk, D., and Yednock, T. (2000) Peripherally administered antibodies against amyloid beta-peptide enter the central nervous system and reduce pathology in a mouse model of Alzheimer disease. *Nat. Med.*, **6**, 916–919.
23. Solomon, B., Koppel, R., Frankel, D., and Hanan-Aharon, E. (1997) Disaggregation of Alzheimer beta-amyloid by site-directed mAb. *Proc. Natl. Acad. Sci. U.S.A.*, **94**, 4109–4112.
24. Nicoll, J.A., Wilkinson, D., Holmes, C., Steart, P., Markham, H., and Weller, R.O. (2003) Neuropathology of human Alzheimer disease after immunization with amyloid-beta peptide: a case report. *Nat. Med.*, **9**, 448–452.
25. Check, E. (2002) Nerve inflammation halts trial for Alzheimer's drug. *Nature*, **415**, 462.
26. Gilman, S., Koller, M., Black, R.S., Jenkins, L., Griffith, S.G., Fox, N.C., Eisner, L., Kirby, L., Rovira, M.B., Forette, F., and Orgogozo, J.M. (2005) Clinical effects of Abeta immunization (AN1792) in patients with AD in an interrupted trial. *Neurology*, **64**, 1553–1562.
27. Masliah, E., Hansen, L., Adame, A., Crews, L., Bard, F., Lee, C., Seubert, P., Games, D., Kirby, L., and Schenk, D. (2005) Abeta vaccination effects on plaque pathology in the absence of encephalitis in Alzheimer disease. *Neurology*, **64**, 129–131.
28. Janus, C., Pearson, J., McLaurin, J., Mathews, P.M., Jiang, Y., Schmidt, S.D., Chishti, M.A., Horne, P., Heslin, D., French, J., Mount, H.T., Nixon, R.A., Mercken, M., Bergeron, C., Fraser, P.E., St. George-Hyslop, P., and Westaway, D. (2000) A beta peptide immunization reduces behavioural impairment and plaques in a model of Alzheimer's disease. *Nature*, **408**, 979–982.

29. Lemere, C.A. (2009) Developing novel immunogens for a safe and effective Alzheimer's disease vaccine. *Prog. Brain Res.*, **175**, 83–93.
30. Samadi, H. and Sultzer, D. (2011) Solanezumab for Alzheimer's disease. *Expert Opin. Biol. Ther.*, **11**, 787–798.
31. Salloway, S., Sperling, R., Gilman, S., Fox, N.C., Blennow, K., Raskind, M., Sabbagh, M., Honig, L.S., Doody, R., van Dyck, C.H., Mulnard, R., Barakos, J., Gregg, K.M., Liu, E., Lieberburg, I., Schenk, D., Black, R., and Grundman, M. (2009) A phase 2 multiple ascending dose trial of bapineuzumab in mild to moderate Alzheimer disease. *Neurology*, **73**, 2061–2070.
32. Kerchner, G.A. and Boxer, A.L. (2010) Bapineuzumab. *Expert Opin. Biol. Ther.*, **10**, 1121–1130.
33. DeMattos, R.B., Bales, K.R., Cummins, D.J., Dodart, J.C., Paul, S.M., and Holtzman, D.M. (2001) Peripheral anti-A beta antibody alters CNS and plasma A beta clearance and decreases brain A beta burden in a mouse model of Alzheimer's disease. *Proc. Natl. Acad. Sci. U.S.A.*, **98**, 8850–8855.
34. Hoyer, W., Gronwall, C., Jonsson, A., Stahl, S., and Hard, T. (2008) Stabilization of a beta-hairpin in monomeric Alzheimer's amyloid-beta peptide inhibits amyloid formation. *Proc. Natl. Acad. Sci. U.S.A.*, **105**, 5099–5104.
35. Luheshi, L.M., Hoyer, W., de Barros, T.P., van Dijk Hard, I., Brorsson, A.C., Macao, B., Persson, C., Crowther, D.C., Lomas, D.A., Stahl, S., Dobson, C.M., and Hard, T. (2010) Sequestration of the Abeta peptide prevents toxicity and promotes degradation *in vivo*. *PLoS Biol.*, **8**, e1000334.
36. Pardridge, W.M. (2003) Blood–brain barrier drug targeting: the future of brain drug development. *Mol. Interv.*, **3**(90–105), 151.
37. Ghose, A.K., Viswanadhan, V.N., and Wendoloski, J.J. (1999) A knowledge-based approach in designing combinatorial or medicinal chemistry libraries for drug discovery. 1. A qualitative and quantitative characterization of known drug databases. *J. Comb. Chem.*, **1**, 55–68.
38. Thompson, E. J., and G. Keir. 1990. Laboratory investigation of cerebrospinal fluid proteins. *Ann. Clin. Biochem.* **27** (Pt 5):425–435.
39. DeMattos, R.B., Bales, K.R., Cummins, D.J., Paul, S.M., and Holtzman, D.M. (2002) Brain to plasma amyloid-beta efflux: a measure of brain amyloid burden in a mouse model of Alzheimer's disease. *Science*, **295**, 2264–2267.
40. Krewson, C.E., Klarman, M.L., and Saltzman, W.M. (1995) Distribution of nerve growth factor following direct delivery to brain interstitium. *Brain Res.*, **680**, 196–206.
41. Tsukakoshi, K., Harada, R., Sode, K., and Ikebukuro, K. (2010) Screening of DNA aptamer which binds to alpha-synuclein. *Biotechnol. Lett.*, **32**, 643–648.
42. James, W. (2000) in *Encyclopedia of Analytical Chemistry* (ed R.A. Meyers), John Wiley & Sons, Ltd, Chichester, pp. 4848–4871.
43. Rahimi, F., Murakami, K., Summers, J.L., Chen, C.H., and Bitan, G. (2009) RNA aptamers generated against oligomeric Abeta40 recognize common amyloid aptatopes with low specificity but high sensitivity. *PLoS ONE*, **4**, e7694.
44. Bartels, T., Choi, J.G., and Selkoe, D.J. (2011) alpha-Synuclein occurs physiologically as a helically folded tetramer that resists aggregation. *Nature*, **477**, 107–110.
45. Wang, W., Perovic, I., Chittuluru, J., Kagnanovich, A., Nguyen, L.T.T., Liao, J., Auclair, J.R., Johnson, D., Landeru, A., Simorellis, A.K., Ju, S., Cookson, M.R., Asturias, F.J., Agar, J.N., Webb, B.N., Kang, C.H., Ringe, D., Petsko, G.A., Pochapsky, T.C., and Hoang, Q.Q. (2011) A soluble alpha-synuclein construct forms a dynamic tetramer. *Proc. Natl. Acad. Sci. U.S.A.*, **108**, 17797–17802.
46. Chan, P.H., Pardon, E., Menzer, L., De Genst, E., Kumita, J.R., Christodoulou, J., Saerens, D., Brans, A., Bouillenne, F., Archer, D.B., Robinson, C.V., Muyldermans, S., Matagne, A., Redfield, C., Wyns, L., Dobson, C.M., and Dumoulin, M.

(2008) Engineering a camelid antibody fragment that binds to the active site of human lysozyme and inhibits its conversion into amyloid fibrils. *Biochemistry*, **47**, 11041–11054.

47. Ray, S.S., Nowak, R.J., Brown, R.H., and Lansbury, P.T. (2005) Small-molecule-mediated stabilization of familial amyotrophic lateral sclerosis-linked superoxide dismutase mutants against unfolding and aggregation. *Proc. Natl. Acad. Sci. U.S.A.*, **102**, 3639–3644.

48. Dobson, C.M. (2004) Chemical space and biology. *Nature*, **432**, 824–828.

49. Necula, M., Kayed, R., Milton, S., and Glabe, C.G. (2007) Small molecule inhibitors of aggregation indicate that amyloid beta oligomerization and fibrillization pathways are independent and distinct. *J. Biol. Chem.*, **282**, 10311–10324.

50. Wolfe, L.S., Calabrese, M.F., Nath, A., Blaho, D.V., Miranker, A.D., and Xiong, Y. (2010) Protein-induced photophysical changes to the amyloid indicator dye thioflavin T. *Proc. Natl. Acad. Sci. U.S.A.*, **107**, 16863–16868.

51. Li, J., Liu, R., Lam, K.S., Jin, L.W., and Duan, Y. (2011) Alzheimer's disease drug candidates stabilize A-beta protein native structure by interacting with the hydrophobic core. *Biophys. J.*, **100**, 1076–1082.

52. Lorenzo, A. and Yankner, B.A. (1994) Beta-amyloid neurotoxicity requires fibril formation and is inhibited by congo red. *Proc. Natl. Acad. Sci. U.S.A.*, **91**, 12243–12247.

53. Heiser, V., Scherzinger, E., Boeddrich, A., Nordhoff, E., Lurz, R., Schugardt, N., Lehrach, H., and Wanker, E.E. (2000) Inhibition of huntingtin fibrillogenesis by specific antibodies and small molecules: implications for Huntington's disease therapy. *Proc. Natl. Acad. Sci. U.S.A.*, **97**, 6739–6744.

54. Higuchi, M., Iwata, N., Matsuba, Y., Sato, K., Sasamoto, K., and Saido, T.C. (2005) 19F and 1H MRI detection of amyloid beta plaques *in vivo*. *Nat. Neurosci.*, **8**, 527–533.

55. Klunk, W.E., Debnath, M.L., Koros, A.M., and Pettegrew, J.W. (1998) Chrysamine-G, a lipophilic analogue of Congo red, inhibits A beta-induced toxicity in PC12 cells. *Life Sci.*, **63**, 1807–1814.

56. Lee, V.M. (2002) Amyloid binding ligands as Alzheimer's disease therapies. *Neurobiol. Aging*, **23**, 1039–1042.

57. Nakagami, Y., Nishimura, S., Murasugi, T., Kaneko, I., Meguro, M., Marumoto, S., Kogen, H., Koyama, K., and Oda, T. (2002) A novel beta-sheet breaker, RS-0406, reverses amyloid beta-induced cytotoxicity and impairment of long-term potentiation *in vitro*. *Br. J. Pharmacol.*, **137**, 676–682.

58. Yang, F., Lim, G.P., Begum, A.N., Ubeda, O.J., Simmons, M.R., Ambegaokar, S.S., Chen, P., Kayed, R., Glabe, C.G., Frautschy, S.A., and Cole, G.M. (2005) Curcumin inhibits formation of amyloid beta oligomers and fibrils, binds plaques, and reduces amyloid *in vivo*. *J. Biol. Chem.*, **280**, 5892–5901.

59. Schmidt, M.L., Schuck, T., Sheridan, S., Kung, M.P., Kung, H., Zhuang, Z.P., Bergeron, C., Lamarche, J.S., Skovronsky, D., Giasson, B.I., Lee, V.M., and Trojanowski, J.Q. (2001) The fluorescent Congo red derivative, (trans, trans)-1-bromo-2,5-bis-(3-hydroxycarbonyl-4-hydroxy)styrylbenzene (BSB), labels diverse beta-pleated sheet structures in postmortem human neurodegenerative disease brains. *Am. J. Pathol.*, **159**, 937–943.

60. Pickhardt, M., Gazova, Z., von Bergen, M., Khlistunova, I., Wang, Y., Hascher, A., Mandelkow, E.-M., Biernat, J., and Mandelkow, E. (2005) Anthraquinones inhibit tau aggregation and dissolve Alzheimer's paired helical filaments *in vitro* and in cells. *J. Biol. Chem.*, **280**, 3628–3635.

61. Pickhardt, M., Larbig, G., Khlistunova, I., Coksezen, A., Meyer, B., Mandelkow, E.M., Schmidt, B., and Mandelkow, E. (2007) Phenylthiazolylhydrazide and its derivatives are potent inhibitors of tau aggregation and toxicity *in vitro* and in cells. *Biochemistry*, **46**, 10016–10023.

62. Taniguchi, S., Suzuki, N., Masuda, M., Hisanaga, S.-I., Iwatsubo, T., Goedert, M., and Hasegawa, M. (2005) Inhibition of heparin-induced tau filament formation by phenothiazines, polyphenols, and porphyrins. *J. Biol. Chem.*, **280**, 7614–7623.
63. Bulic, B., Pickhardt, M., Schmidt, B., Mandelkow, E.M., Waldmann, H., and Mandelkow, E. (2009) Development of tau aggregation inhibitors for Alzheimer's disease. *Angew. Chem. Int. Ed Engl.*, **48**, 1740–1752.
64. Wischik, C.M., Edwards, P.C., Lai, R.Y., Roth, M., and Harrington, C.R. (1996) Selective inhibition of Alzheimer disease-like tau aggregation by phenothiazines. *Proc. Natl. Acad. Sci. U.S.A.*, **93**, 11213–11218.
65. Levy-Sakin, M., Shreberk, M., Daniel, Y., and Gazit, E. (2009) Targeting insulin amyloid assembly by small aromatic molecules: toward rational design of aggregation inhibitors. *Islets*, **1**, 210–215.
66. Volkova, K.D., Kovalska, V.B., Inshin, D., Slominskii, Y.L., Tolmachev, O.I., and Yarmoluk, S.M. (2011) Novel fluorescent trimethine cyanine dye 7519 for amyloid fibril inhibition assay. *Biotech. Histochem.*, **86**, 188–191.
67. Heiser, V., Engemann, S., Brocker, W., Dunkel, I., Boeddrich, A., Waelter, S., Nordhoff, E., Lurz, R., Schugardt, N., Rautenberg, S., Herhaus, C., Barnickel, G., Bottcher, H., Lehrach, H., and Wanker, E.E. (2002) Identification of benzothiazoles as potential polyglutamine aggregation inhibitors of Huntington's disease by using an automated filter retardation assay. *Proc. Natl. Acad. Sci. U.S.A.*, **99**(Suppl 4), 16400–16406.
68. Zhang, X., Smith, D.L., Meriin, A.B., Engemann, S., Russel, D.E., Roark, M., Washington, S.L., Maxwell, M.M., Marsh, J.L., Thompson, L.M., Wanker, E.E., Young, A.B., Housman, D.E., Bates, G.P., Sherman, M.Y., and Kazantsev, A.G. (2005) A potent small molecule inhibits polyglutamine aggregation in Huntington's disease neurons and suppresses neurodegeneration *in vivo*. *Proc. Natl. Acad. Sci. U.S.A.*, **102**, 892–897.
69. Bertsch, U., Winklhofer, K.F., Hirschberger, T., Bieschke, J., Weber, P., Hartl, F.U., Tavan, P., Tatzelt, J., Kretzschmar, H.A., and Giese, A. (2005) Systematic identification of antiprion drugs by high-throughput screening based on scanning for intensely fluorescent targets. *J. Virol.*, **79**, 7785–7791.
70. Kostka, M., Hogen, T., Danzer, K.M., Levin, J., Habeck, M., Wirth, A., Wagner, R., Glabe, C.G., Finger, S., Heinzelmann, U., Garidel, P., Duan, W., Ross, C.A., Kretzschmar, H., and Giese, A. (2008) Single particle characterization of iron-induced pore-forming alpha-synuclein oligomers. *J. Biol. Chem.*, **283**, 10992–11003.
71. Conway, K.A., Rochet, J.C., Bieganski, R.M., and Lansbury, P.T. Jr., (2001) Kinetic stabilization of the alpha-synuclein protofibril by a dopamine-alpha-synuclein adduct. *Science*, **294**, 1346–1349.
72. El-Agnaf, O.M.A., Paleologou, K.E., Greer, B., Abogrein, A.M., King, J.E., Salem, S.A., Fullwood, N.J., Benson, F.E., Hewitt, R., Ford, K.J., Martin, F.L., Harriott, P., Cookson, M.R., and Allsop, D. (2004) A strategy for designing inhibitors of alpha-synuclein aggregation and toxicity as a novel treatment for Parkinson's disease and related disorders. *FASEB J.*, **18**, 1315–1317.
73. Chen, J., Armstrong, A.H., Koehler, A.N., and Hecht, M.H. (2010) Small molecule microarrays enable the discovery of compounds that bind the Alzheimer's Abeta peptide and reduce its cytotoxicity. *J. Am. Chem. Soc.*, **132**, 17015–17022.
74. Williams, A.D., Sega, M., Chen, M., Kheterpal, I., Geva, M., Berthelier, V., Kaleta, D.T., Cook, K.D., and Wetzel, R. (2005) Structural properties of Abeta protofibrils stabilized by a small molecule. *Proc. Natl. Acad. Sci. U.S.A.*, **102**, 7115–7120.
75. Necula, M., Breydo, L., Milton, S., Kayed, R., van der Veer, W.E., Tone, P., and Glabe, C.G. (2007) Methylene

blue inhibits amyloid Abeta oligomerization by promoting fibrillization. *Biochemistry*, **46**, 8850–8860.

76. Kim, W., Kim, Y., Min, J., Kim, D.J., Chang, Y.-T., and Hecht, M.H. (2007) A high-throughput screen for compounds that inhibit aggregation of the Alzheimer's peptide. *ACS Chem. Biol.*, **1**, 461–469.

77. Lee, L.L., Ha, H., Chang, Y.T., and DeLisa, M.P. (2009) Discovery of amyloid-beta aggregation inhibitors using an engineered assay for intracellular protein folding and solubility. *Protein Sci.*, **18**, 277–286.

78. Blanchard, B.J., Chen, A., Rozeboom, L.M., Stafford, K.A., Weigele, P., and Ingram, V.M. (2004) Efficient reversal of Alzheimer's disease fibril formation and elimination of neurotoxicity by a small molecule. *Proc. Natl. Acad. Sci. U.S.A.*, **101**, 14326–14332.

79. Park, S.K., Pegan, S.D., Mesecar, A.D., Jungbauer, L.M., LaDu, M.J., and Liebman, S.W. (2011) Development and validation of a yeast high-throughput screen for inhibitors of Abeta oligomerization. *Dis. Model. Mech.*, **4**, 822–831.

80. Regazzoni, L., Bertoletti, L., Vistoli, G., Colombo, R., Aldini, G., Serra, M., Carini, M., Caccialanza, G., and De Lorenzi, E. (2010) A combined high-resolution mass spectrometric and in silico approach for the characterisation of small ligands of beta2-microglobulin. *ChemMedChem*, **5**, 1015–1025.

81. Caughey, W.S., Raymond, L.D., Horiuchi, M., and Caughey, B. (1998) Inhibition of protease-resistant prion protein formation by porphyrins and phthalocyanines. *Proc. Natl. Acad. Sci. U.S.A.*, **95**, 12117–12122.

82. Porat, Y., Abramowitz, A., and Gazit, E. (2006) Inhibition of amyloid fibril formation by polyphenols: structural similarity and aromatic interactions as a common inhibition mechanism. *Chem. Biol. Drug Des.*, **67**, 27–37.

83. Zhao, B. (2005) Natural antioxidants for neurodegenerative diseases. *Mol. Neurobiol.*, **31**, 283–294.

84. Lancon, A., Delmas, D., Osman, H., Thenot, J.P., Jannin, B., and Latruffe, N. (2004) Human hepatic cell uptake of resveratrol: involvement of both passive diffusion and carrier-mediated process. *Biochem. Biophys. Res. Commun.*, **316**, 1132–1137.

85. Howlett, D.R., George, A.R., Owen, D.E., Ward, R.V., and Markwell, R.E. (1999) Common structural features determine the effectiveness of carvedilol, daunomycin and rolitetracycline as inhibitors of Alzheimer beta-amyloid fibril formation. *Biochem. J.*, **343**(Pt 2), 419–423.

86. Caruana, M., Hogen, T., Levin, J., Hillmer, A., Giese, A., and Vassallo, N. (2011) Inhibition and disaggregation of alpha-synuclein oligomers by natural polyphenolic compounds. *FEBS Lett.*, **585**, 1113–1120.

87. Convertino, M., Vitalis, A., and Caflisch, A. (2011) Disordered binding of small molecules to Abeta(12–28). *J. Biol. Chem.*, **286**, 41578–41588.

88. Landau, M., Sawaya, M.R., Faull, K.F., Laganowsky, A., Jiang, L., Sievers, S.A., Liu, J., Barrio, J.R., and Eisenberg, D. (2011) Towards a pharmacophore for amyloid. *PLoS Biol.*, **9**, e1001080.

89. Feng, B.Y., Toyama, B.H., Wille, H., Colby, D.W., Collins, S.R., May, B.C.H., Prusiner, S.B., Weissman, J.S., and Shoichet, B.K. (2008) Small-molecule aggregates inhibit amyloid polymerization. *Nat. Chem. Biol.*, **4**, 197–199.

90. Andersen, K.K., Oliveira, C.L.P., Larsen, K.L., Poulsen, F.M., Callisen, T.H., Westh, P., Pedersen, J.S., and Otzen, D.E. (2009) The role of decorated SDS micelles in sub-cmc protein denaturation and association. *J. Mol. Biol.*, **391**, 207–226.

91. McLaurin, J., Golomb, R., Jurewicz, A., Antel, J.P., and Fraser, P.E. (2000) Inositol stereoisomers stabilize an oligomeric aggregate of Alzheimer amyloid beta peptide and inhibit abeta-induced toxicity. *J. Biol. Chem.*, **275**, 18495–18502.

92. Lendel, C., Bolognesi, B., Wahlstrom, A., Dobson, C.M., and Graslund, A. (2010) Detergent-like interaction of

Congo Red with the amyloid beta peptide. *Biochemistry*, **49**, 1358–1360.
93. Lendel, C., Bertoncini, C.W., Cremades, N., Waudby, C.A., Vendruscolo, M., Dobson, C.M., Schenk, D., Christodoulou, J., and Toth, G. (2009) On the mechanism of nonspecific inhibitors of protein aggregation: dissecting the interactions of alpha-synuclein with Congo red and Lacmoid. *Biochemistry*, **48**, 8322–8334.
94. Zhou, W., Gallagher, A., Hong, D.P., Long, C., Fink, A.L., and Uversky, V.N. (2009) At low concentrations, 3,4-dihydroxyphenylacetic acid (DOPAC) binds non-covalently to alpha-synuclein and prevents its fibrillation. *J. Mol. Biol.*, **388**, 597–610.
95. Hong, D.P., Fink, A.L., and Uversky, V.N. (2008) Structural characteristics of alpha-synuclein oligomers stabilized by the flavonoid baicalein. *J. Mol. Biol.*, **383**, 214–223.
96. Herrera, F.E., Chesi, A., Paleologou, K.E., Schmid, A., Munoz, A., Vendruscolo, M., Gustincich, S., Lashuel, H.A., and Carloni, P. (2008) Inhibition of alpha-synuclein fibrillization by dopamine is mediated by interactions with five C-terminal residues and with E83 in the NAC region. *PLoS ONE*, **3**, e3394.
97. Norris, E.H., Giasson, B.I., Hodara, R., Xu, S., Trojanowski, J.Q., Ischiropoulos, H., and Lee, V.M. (2005) Reversible inhibition of alpha-synuclein fibrillization by dopaminochrome-mediated conformational alterations. *J. Biol. Chem.*, **280**, 21212–21219.
98. Li, J., Zhu, M., Manning-Bog, A.B., Di Monte, D.A., and Fink, A.L. (2004) Dopamine and L-dopa disaggregate amyloid fibrils: implications for Parkinson's and Alzheimer's disease. *FASEB J.*, **18**, 962–964.
99. Leong, S.L., Pham, C.L., Galatis, D., Fodero-Tavoletti, M.T., Perez, K., Hill, A.F., Masters, C.L., Ali, F.E., Barnham, K.J., and Cappai, R. (2009) Formation of dopamine-mediated alpha-synuclein-soluble oligomers requires methionine oxidation. *Free Radic. Biol. Med.*, **46**, 1328–1337.
100. Waxman, E.A., Emmer, K.L., and Giasson, B.I. (2010) Residue Glu83 plays a major role in negatively regulating alpha-synuclein amyloid formation. *Biochem. Biophys. Res. Commun.*, **391**, 1415–1420.
101. Zhu, M., Rajamani, S., Kaylor, J., Han, S., Zhou, F., and Fink, A.L. (2004) The flavonoid baicalein inhibits fibrillation of α-synuclein and disaggregates existing fibrils. *J. Biol. Chem.*, **279**, 26846–26857.
102. Hauber, I., Hohenberg, H., Holstermann, B., Hunstein, W., and Hauber, J. (2009) The main green tea polyphenol epigallocatechin-3-gallate counteracts semen-mediated enhancement of HIV infection. *Proc. Natl. Acad. Sci. U.S.A.*, **106**, 9033–9038.
103. Singh, B.N., Shankar, S., and Srivastava, R.K. (2011) Green tea catechin, epigallocatechin-3-gallate (EGCG): mechanisms, perspectives and clinical applications. *Biochem. Pharmacol.*, **82**, 1807–1821.
104. Ehrnhoefer, D.E., Duennwald, M., Markovic, P., Wacker, J.L., Engemann, S., Roark, M., Legleiter, J., Marsh, J.L., Thompson, L.M., Lindquist, S., Muchowski, P.J., and Wanker, E.E. (2006) Green tea (−)-epigallocatechin-gallate modulates early events in huntingtin misfolding and reduces toxicity in Huntington's disease models. *Hum. Mol. Genet.*, **15**, 2743–2751.
105. Ferreira, N., Saraiva, M.J., and Amleida, M.R. (2011) Natural polyphenols inhibit different steps of the process of transthyretin (TTR) amyloid fibril formation. *FEBS Lett.*, **585**, 2424–2430.
106. Meng, F., Abedini, A., Plesner, A., Verchere, C.B., and Raleigh, D.P. (2011) The flavanol (−)-epigallocatechin 3-gallate inhibits amyloid formation by islet amyloid polypeptide, disaggregates amyloid fibrils, and protects cultured cells against IAPP-induced toxicity. *Biochemistry*, **49**, 8127–8133.
107. Chandrashekaran, I.R., Adda, C.G., MacRaild, C.A., Anders, R.F., and Norton, R.S. (2010) Inhibition by flavonoids of amyloid-like fibril formation by Plasmodium falciparum

merozoite surface protein 2. *Biochemistry*, **49**, 5899–5908.

108. Hudson, S.A., Ecroyd, H., Dehle, F.C., Musgrave, I.F., and Carver, J.A. (2009) (−)-epigallocatechin-3-gallate (EGCG) maintains kappa-casein in its pre-fibrillar state without redirecting its aggregation pathway. *J. Mol. Biol.*, **392**, 689–700.

109. Roberts, B.E., Duennwald, M.L., Wang, H., Chung, C., Lopreiato, N.P., Sweeny, E.A., Knight, M.N., and Shorter, J. (2009) A synergistic small-molecule combination directly eradicates diverse prion strain structures. *Nat. Chem. Biol.*, **5**, 936–946.

110. Bieschke, J., Russ, J., Friedrich, R.P., Ehrnhoefer, D.E., Wobst, H., Neugebauer, K., and Wanker, E.E. (2010) EGCG remodels mature alpha-synuclein and amyloid-beta fibrils and reduces cellular toxicity. *Proc. Natl. Acad. Sci. U.S.A.*, **107**, 7710–7715.

111. Ehrnhoefer, D.E., Bieschke, J., Boeddrich, A., Herbst, M., Masino, L., Lurz, R., Engemann, S., Pastore, A., and Wanker, E.E. (2008) EGCG redirects amyloidogenic polypeptides into unstructured, off-pathway oligomers. *Nat. Struct. Mol. Biol.*, **15**, 558–566.

112. Masuda, M., Suzuki, N., Taniguchi, S., Oikawa, T., Nonaka, T., Iwatsubo, T., Hisanaga, S., Goedert, M., and Hasegawa, M. (2006) Small molecule inhibitors of alpha-synuclein filament assembly. *Biochemistry*, **45**, 6085–6094.

113. Zini, A., Del Rio, D., Stewart, A.J., Mandrioli, J., Merelli, E., Sola, P., Nichelli, P., Serafini, M., Brighenti, F., Edwards, C.A., and Crozier, A. (2006) Do flavan-3-ols from green tea reach the human brain? *Nutr. Neurosci.*, **9**, 57–61.

114. Li, J., Zhu, M., Rajamani, S., Uversky, V.N., and Fink, A.L. (2004) Rifampicin inhibits alpha-synuclein fibrillation and disaggregates fibrils. *Chem. Biol.*, **11**, 1513–1521.

115. Thapa, A., Woo, E.R., Chi, E.Y., Sharoar, M.G., Jin, H.G., Shin, S.Y., and Park, I.S. (2011) Biflavonoids are superior to monoflavonoids in inhibiting amyloid-beta toxicity and fibrillogenesis via accumulation of nontoxic oligomer-like structures. *Biochemistry*, **50**, 2445–2455.

116. Bieschke, J., Herbst, M., Wiglenda, T., Friedrich, R.P., Boeddrich, A., Schiele, F., Kleckers, D., Lopez Del Amo, J.M., Gruning, B.A., Wang, Q., Schmidt, M.R., Lurz, R., Anwyl, R., Schnoegl, S., Fandrich, M., Frank, R.F., Reif, B., Gunther, S., Walsh, D.M., and Wanker, E.E. (2011) Small-molecule conversion of toxic oligomers to nontoxic beta-sheet-rich amyloid fibrils. *Nat. Chem. Biol.*, **8**, 93–101.

117. Estrada, L.D. and Soto, C. (2006) Inhibition of protein misfolding and aggregation by small rationally-designed peptides. *Curr. Pharm. Des.*, **12**, 2557–2567.

118. Gordon, D.J., Sciarretta, K.L., and Meredith, S.C. (2001) Inhibition of beta-amyloid(40) fibrillogenesis and disassembly of beta-amyloid(40) fibrils by short beta-amyloid congeners containing N-methyl amino acids at alternate residues. *Biochemistry*, **40**, 8237–8245.

119. Bodles, A.M., El-Agnaf, O.M.A., Greer, B., Guthrie, D.J.S., and Irvine, G.B. (2004) Inhibition of fibril formation and toxicity of a fragment of alpha-synuclein by an N-methylated peptide analogue. *Neurosci. Lett.*, **359**, 89–93.

120. Austen, B.M., Paleologou, K.E., Ali, S.A., Qureshi, M.M., Allsop, D., and El-Agnaf, O.M. (2008) Designing peptide inhibitors for oligomerization and toxicity of Alzheimer's beta-amyloid peptide. *Biochemistry*, **47**, 1984–1992.

121. Matharu, B., El-Agnaf, O., Razvi, A., and Austen, B.M. (2010) Development of retro-inverso peptides as anti-aggregation drugs for beta-amyloid in Alzheimer's disease. *Peptides*, **31**, 1866–1872.

122. Doig, A.J., Hughes, E., Burke, R.M., Su, T.J., Heenan, R.K., and Lu, J. (2002) Inhibition of toxicity and protofibril formation in the amyloid-beta peptide beta(25–35) using N-methylated derivatives. *Biochem. Soc. Trans.*, **30**, 537–542.

123. Pallitto, M.M., Ghanta, J., Heinzelman, P., Kiessling, L.L., and Murphy, R.M. (1999) Recognition sequence design for peptidyl modulators of beta-amyloid

aggregation and toxicity. *Biochemistry*, **38**, 3570–3578.

124. Ghanta, J., Shen, C.L., Kiessling, L.L., and Murphy, R.M. (1996) A strategy for designing inhibitors of beta-amyloid toxicity. *J. Biol. Chem.*, **271**, 29525–29528.

125. Hughes, E., Burke, R.M., and Doig, A.J. (2000) Inhibition of toxicity in the beta-amyloid peptide fragment beta -(25–35) using N-methylated derivatives: a general strategy to prevent amyloid formation. *J. Biol. Chem.*, **275**, 25109–25115.

126. Lowe, T.L., Strzelec, A., Kiessling, L.L., and Murphy, R.M. (2001) Structure-function relationships for inhibitors of beta-amyloid toxicity containing the recognition sequence KLVFF. *Biochemistry*, **40**, 7882–7889.

127. Shaltiel-Karyo, R., M. Frenkel-Pinter, N. Egoz-Matia, A. Frydman-Marom, D. E. Shalev, D. Segal, and E. Gazit. Inhibiting alpha-synuclein oligomerization by stable cell-penetrating beta-synuclein fragments recovers phenotype of Parkinson's disease model flies. *PLoS ONE* **5**:e13863.

128. Frydman-Marom, A., R. Shaltiel-Karyo, S. Moshe, and E. Gazit. The generic amyloid formation inhibition effect of a designed small aromatic beta-breaking peptide. *Amyloid* **18**:119–127.

129. Soto, C., Sigurdsson, E.M., Morelli, L., Kumar, R.A., Castano, E.M., and Frangione, B. (1998) Beta-sheet breaker peptides inhibit fibrillogenesis in a rat brain model of amyloidosis: implications for Alzheimer's therapy. *Nat. Med.*, **4**, 822–826.

130. Frydman-Marom, A., Convertino, M., Pellarin, R., Lampel, A., Shaltiel-Karyo, R., Segal, D., Caflisch, A., Shalev, D.E., and Gazit, E. (2011) Structural basis for inhibiting beta-amyloid oligomerization by a non-coded beta-breaker-substituted endomorphin analogue. *ACS Chem. Biol.*, **6**, 1265–1276.

131. Muthusamy, K., Arvidsson, P.I., Govender, P., Kruger, H.G., Maguire, G.E., and Govender, T. (2010) Design and study of peptide-based inhibitors of amylin cytotoxicity. *Bioorg. Med. Chem. Lett.*, **20**, 1360–1362.

132. Abe, K., Kobayashi, N., Sode, K., and Ikebukuro, K. (2007) Peptide ligand screening of alpha-synuclein aggregation modulators by in silico panning. *BMC Bioinformatics*, **8**, 451.

133. Bodles, A.M., Guthrie, D.J., Greer, B., and Irvine, G.B. (2001) Identification of the region of non-Abeta component (NAC) of Alzheimer's disease amyloid responsible for its aggregation and toxicity. *J. Neurochem.*, **78**, 384–395.

134. Soto, C., Kindy, M.S., Baumann, M., and Frangione, B. (1996) Inhibition of Alzheimer's amyloidosis by peptides that prevent b-sheet conformation. *Biochem. Biophys. Res. Commun.*, **226**, 672–680.

135. Kapurniotu, A., Schmauder, A., and Tenidis, K. (2002) Structure-based design and study of non-amyloidogenic, double N-methylated IAPP amyloid core sequences as inhibitors of IAPP amyloid formation and cytotoxicity. *J. Mol. Biol.*, **315**, 339–350.

136. Wood, S.J., Wetzel, R., Martin, J.D., and Hurle, M.R. (1995) Prolines and amyloidogenicity in fragments of the Alzheimer's peptide beta/A4. *Biochemistry*, **34**, 724–730.

137. Reinke, A.A., Ung, P.M., Quintero, J.J., Carlson, H.A., and Gestwicki, J.E. (2010) Chemical probes that selectively recognize the earliest Abeta oligomers in complex mixtures. *J. Am. Chem. Soc.*, **132**, 17655–17657.

138. Hoogerhout, P., Kamphuis, W., Brugghe, H.F., Sluijs, J.A., Timmermans, H.A., Westdijk, J., Zomer, G., Boog, C.J., Hol, E.M., and van den Dobbelsteen, G.P. (2011) A cyclic undecamer peptide mimics a turn in folded Alzheimer amyloid beta and elicits antibodies against oligomeric and fibrillar amyloid and plaques. *PLoS One*, **6**, e19110.

139. Saraiva, A.M., Cardoso, I., Pereira, M.C., Coelho, M.A., Saraiva, M.J., Mohwald, H., and Brezesinski, G. (2010) Controlling amyloid-beta peptide(1–42) oligomerization and toxicity by fluorinated nanoparticles. *Chembiochem*, **11**, 1905–1913.

140. Brambilla, D., Le Droumaguet, B., Nicolas, J., Hashemi, S.H., Wu,

L.P., Moghimi, S.M., Couvreur, P., and Andrieux, K. (2011) Nanotechnologies for Alzheimer's disease: diagnosis, therapy, and safety issues. *Nanomedicine*, **7**, 521–540.

141. Kanwar, J.R., Sun, X., Punj, V., Sriramoju, B., Mohan, R.R., Zhou, S.F., Chauhan, A., and Kanwar, R. K. (2012) Nanoparticles in the treatment and diagnosis of neurological disorders: untamed dragon with fire power to heal. *Nanomedicine*, **8**, 399–414.

142. Canovi, M., Markoutsa, E., Lazar, A.N., Pampalakis, G., Clemente, C., Re, F., Sesana, S., Masserini, M., Salmona, M., Duyckaerts, C., Flores, O., Gobbi, M., and Antimisiaris, S.G. (2011) The binding affinity of anti-Abeta1-42 MAb-decorated nanoliposomes to Abeta1-42 peptides *in vitro* and to amyloid deposits in post-mortem tissue. *Biomaterials*, **32**, 5489–5497.

143. Jaruszewski, K.M., Ramakrishnan, S., Poduslo, J.F., and Kandimalla, K.K. (2012) Chitosan enhances the stability and targeting of immunonanovehicles to cerebro-vascular deposits of Alzheimer's disease amyloid protein. *Nanomedicine*, **8**, 250–260.

144. Mittal, G., Carswell, H., Brett, R., Currie, S., and Kumar, M.N. (2010) Development and evaluation of polymer nanoparticles for oral delivery of estradiol to rat brain in a model of Alzheimer's pathology. *J. Control. Release*, **150**, 220–228.

145. Cabaleiro-Lago, C., Quinlan-Pluck, F., Lynch, I., Lindman, S., Minogue, A.M., Thulin, E., Walsh, D.M., Dawson, K.A., and Linse, S. (2008) Inhibition of amyloid beta protein fibrillation by polymeric nanoparticles. *J. Am. Chem. Soc.*, **130**, 15437–15443.

146. Skaat, H., Belfort, G., and Margel, S. (2009) Synthesis and characterization of fluorinated magnetic core-shell nanoparticles for inhibition of insulin amyloid fibril formation. *Nanotechnology*, **20**, 225106.

147. Yoo, S.I., Yang, M., Brender, J.R., Subramanian, V., Sun, K., Joo, N.E., Jeong, S.H., Ramamoorthy, A., and Kotov, N.A. (2011) Inhibition of amyloid peptide fibrillation by inorganic nanoparticles: functional similarities with proteins. *Angew. Chem. Int. Ed Engl.*, **50**, 5110–5115.

148. Saraiva, A.M., Cardoso, I., Saraiva, M.J., Tauer, K., Pereira, M.C., Coelho, M.A., Mohwald, H., and Brezesinski, G. (2010) Randomization of amyloid-beta-peptide(1–42) conformation by sulfonated and sulfated nanoparticles reduces aggregation and cytotoxicity. *Macromol. Biosci.*, **10**, 1152–1163.

149. Rocha, S., Thunemann, A.F., Pereira Mdo, C., Coelho, M., Mohwald, H., and Brezesinski, G. (2008) Influence of fluorinated and hydrogenated nanoparticles on the structure and fibrillogenesis of amyloid beta-peptide. *Biophys. Chem.*, **137**, 35–42.

RESEARCH PART

INTRODUCTION TO RESEARCH PART

The research part is divided into two overall sections: (1) amyloid fibrils and (2) oligomers. In the fibril section the focus is on the fibril phenomenon in general, whereas the oligomer section is focused on stable αSN oligomers. Structural characterization of fibrils and particular of oligomers is still limited and the early steps of their assembly process have not been dissected. Held together with the limited knowledge on the role of fibrils and oligomers in the pathogenesis of neurodegenerative disease, it might seem that this research subject is still immature. However, I hope that the introduction and research part will convince the reader that the amyloid field is in a rapid development and approaching detailed descriptions of several subjects.

AMYLOID FIBRILS

Despite the escalating attention on amyloid fibrils, whether related to neurodegenerative diseases, drug formulation or beneficial functionality, the mechanistic description of the assembly process is still not complete (see chapter 3). We have used the ribosomal protein S6 (Fig. 10) as a model system to analyze fibril formation. S6 have worked as a model system for protein folding studies (106) and is able to form fibrils at acidic pH and slightly elevated temperatures (107).

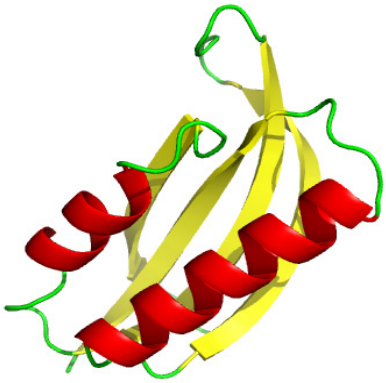

Figure 10. Cartoon drawing of the ribosomal protein S6 (1RIS) with β-sheets in yellow, α-helices in red and loops in green.

In **Article IV** we have used the high reproducibility of seeded fibrillation experiments to generate high quality kinetic data of S6 fibril formation. The concentration of fibril seeds and monomers has been systematically varied and combined with kinetic modeling (97). We have been able to separate secondary pathways from primary nucleation and elongation (see chapter 3). Based on the kinetic modeling we found that the exponential growth phase of S6 fibril formation is catalyzed by secondary processes rather than primary nucleation.

The rate constants of primary nucleation and the extent of fibril formation are generally considered to increase together with protein concentration. In **Article V** we report the atypical concentration dependence of S6 where fibril formation is inhibited at high protein concentrations. Based on pepsin digestion and DLS analysis we speculate that the inhibition stems from the formation of native-like oligomers that are off-pathway to fibril formation and exist in dynamic equilibrium with

the native state. Altogether, this highlights the many competing conformational states in the energy landscape of protein folding and aggregation.

As discussed in chapter 3 the fibril state appear to be thermodynamically more stable than the native state. Then why is fibril formation in the cell a rare exception? One reason is chaperones, as they are key in the proteostasis network where they are responsible of preventing protein misfolding (108). The role of chaperones in neurons and neurodegenerative diseases are not well understood. In **Article VI** we found that the intrinsically disordered protein 7B2 (109) abolished *in vitro* fibril formation of Amloid-β (Aβ) and αSN and rescued cells from Aβ toxicity. Also, 7B2 was found to co-localize with Aβ plaques and Lewy Bodies in human brain material. We established that 7B2 posses post-folding activity *i.e.* it is an anti-aggregation chaperone associated with neurodegenerative diseases. Retarding fibril formation of both Aβ and αSN aggregation suggest that 7B2 is not limited to select proteins but recognize fibril structure in general, supported by a recent report where 7B2 have similar effects on islet amyloid polypeptide (110).

The work in **Articles IV, V, VI, VIII** requires simple and reliable ways to monitor fibril formation. ThT fluorescence is the common probe (see chapter 3), however it has the disadvantage of potential falsh positives e.g. when screening for small molecule inhibitors which might quench fluorescence or compete with ThT binding. In **Article VII** we demonstrate how electrochemical analysis can be used to measure fibril formation due to differences in tyrosine oxidation between the monomeric and fibrillar state. This method is not applicable for online measurements but has the advantage that it does not rely on an extrinsic probe.

OLIGOMERS

αSN oligomers are possibly the culprits in Parkinson's Disease (see **Article II**). Oligomeric species are a tremendous challenge in biophysics as they are often heterogeneous, transient and difficult to obtain in high yields. We focus on a type of stable αSN oligomers which are present during fibril formation (111).

In **Article VIII,** an arsenal of biophysical techniques has been used to obtain an improved oligomer structure. SAXS analysis suggests that oligomers are ellipsoidal; having a structured core and a disordered shell. The dimensions of the oligomers are supported by light scattering techniques and based on FTIR and CD we conclude that the core is build up by β-sheet. This structural characterization was possible due to the relative monodispersity which we have obtained by optimization of oligomer purification. Also, these oligomers are not transient but stable towards dissociation (see **Article XI**). In **Article VIII** we have also addressed the role of these oligomers in fibril formation. Based on kinetic analysis and kinetic modeling we find that the oligomers are unable to seed fibrillation and to become incorporated into fibrils. Consequently, these oligomers are not obligate intermediates in fibril formation. We observe that oligomers moderately inhibit primary nucleation and fibril elongation and based on surface tension analysis we relate the inhibition to competition of monomers and oligomers in the air-water interface, which might be important for fibril formation. The air-water interface could affect these processes by local

concentration of protein or by stabilization of conformational states prone for primary or secondary nucleation.

The oligomers interact strongly with anionic vesicles and permeabilize them (**Articles II, VIII, IX, X, XI**). The N-terminus is highly relevant for the interaction between monomeric αSN and anionic vesicles and N-terminal deletions have dramatic effects on yeast viability (27). Therefore we have systematically analyzed the effect of N-terminal deletions on monomers' and oligomers' interaction with membranes. This is presented in **Article IX** where we find reasonable linearity between monomer folding into the membrane and permeabilization. Also, we conclude that the 12 first residues of the N-terminus are essential for the interaction of monomers and oligomers with anionic vesicles.

Based on these findings the early N-terminal could be a promising epitope for drug development towards Parkinson's Disease. In **Article X** we have analyzed the effect of epigallocatechin gallate (EGCG) on oligomer toxicity. EGCG does not target the N-terminus but associate nonspecifically throughout the polypeptide chain. EGCG completely inhibit the oligomers ability to permeabilize anionic vesicles and rescues rat brain cells from oligomer cytotoxicity. Remarkable, however, EGCG does not induce any major structural changes in the oligomer. Instead EGCG moderately inhibit oligomer-membrane interactions and our inhibition data suggest that oligomers permeabilize membranes by destabilization events rather than by pore formation.

As mentioned initially, the high stability of these oligomers is a prerequisite for the work in **Articles VII, IX, X**. In **Article XI** we find that the oligomers are highly stable towards dissociation by pH, temperature and solvent denaturation (see chapter 2). Also we observe that prolonged incubation times at 37 °C induce self-association of the oligomers into larger non-fibrillar aggregates, again highlighting the multitude of the energy landscape of protein folding and aggregation.

PERSPECTIVES

Interdisciplinary research and continuous method development has really pushed the amyloid field forward, but there are still some black boxes that needs to be uncovered.

(1) The contribution from microscopic processes, such as primary nucleation, elongation and secondary processes, to the overall process of fibril formation is seemingly well-understood and has been described mathematically. However, especially the molecular reaction of primary nucleation is still poorly understood, and it will probably need further instrumental advances, where e.g. microdroplet techniques are promising (112), to uncover this in details.

(2) Whereas we have now provided a low-resolution oligomer structure (**Article VIII)** there is need for high-resolution details on oligomers, before their formation and cytotoxic properties can be fully understood. Currently this seems to be an extremely difficult challenge especially for oligomers of transient nature. However, the recent advances in high-resolution structures of amyloid fibrils (86,89,92) (Chapter 3) provide hope for the future determination of oligomer structures.

(3) The presence of amyloid fibrils and oligomers in neurodegenerative diseases is unambiguous. However it is not established whether amyloid fibrils and oligomers are the primary course of neurodegeneration or a downstream consequence of neurodegeneration. If they are essential in disease it has to be understood why. A vast amount of literature suggests that the interaction of misfolded aggregates with membranes is key in the cytotoxicity (**Articles II, III**). The rise of the oligomers as the potential culprits in neurodegenerative diseases almost ruled out fibrils as cytotoxic entities, however, recently we have witnessed what appear to be the strike back of the fibrils (113,114). Personally I like the idea that everything misfolded in a cell might be toxic due to inappropriate interactions with cellular entities, which would lead to the conclusion that there is no such thing as single culprit but rather a spectrum of toxic species.

REFERENCES

1. Mutch, W. J., Dingwall-Fordyce, I., Downie, A. W., Paterson, J. G., and Roy, S. K. (1986) *Br Med J (Clin Res Ed)* **292**, 534-536
2. Antonelli, F., and Strafella, A. P. (2014) *Parkinsonism Relat Disord* **20 Suppl 1**, S10-12
3. Strecker, K., and Schwarz, J. (2008) *Expert Opin Emerg Drugs* **13**, 573-591
4. Davie, C. A. (2008) *Br Med Bull* **86**, 109-127
5. Masuda-Suzukake, M., Nonaka, T., Hosokawa, M., Oikawa, T., Arai, T., Akiyama, H., Mann, D. M., and Hasegawa, M. (2013) *Brain* **136**, 1128-1138
6. Luk, K. C., Kehm, V., Carroll, J., Zhang, B., O'Brien, P., Trojanowski, J. Q., and Lee, V. M. (2012) *Science* **338**, 949-953
7. Nakajo, S., Shioda, S., Nakai, Y., and Nakaya, K. (1994) *Brain Res Mol Brain Res* **27**, 81-86
8. Spillantini, M. G., Schmidt, M. L., Lee, V. M., Trojanowski, J. Q., Jakes, R., and Goedert, M. (1997) *Nature* **388**, 839-840
9. Spillantini, M. G., Crowther, R. A., Jakes, R., Hasegawa, M., and Goedert, M. (1998) *Proc Natl Acad Sci U S A* **95**, 6469-6473
10. Narhi, L., Wood, S. J., Steavenson, S., Jiang, Y., Wu, G. M., Anafi, D., Kaufman, S. A., Martin, F., Sitney, K., Denis, P., Louis, J. C., Wypych, J., Biere, A. L., and Citron, M. (1999) *J Biol Chem* **274**, 9843-9846
11. Conway, K. A., Harper, J. D., and Lansbury, P. T. (1998) *Nat Med* **4**, 1318-1320
12. Masliah, E., Rockenstein, E., Veinbergs, I., Mallory, M., Hashimoto, M., Takeda, A., Sagara, Y., Sisk, A., and Mucke, L. (2000) *Science* **287**, 1265-1269
13. Feany, M. B., and Bender, W. W. (2000) *Nature* **404**, 394-398
14. Bousset, L., Pieri, L., Ruiz-Arlandis, G., Gath, J., Jensen, P. H., Habenstein, B., Madiona, K., Olieric, V., Bockmann, A., Meier, B. H., and Melki, R. (2013) *Nat Commun* **4**, 2575
15. Polymeropoulos, M. H., Higgins, J. J., Golbe, L. I., Johnson, W. G., Ide, S. E., Di Iorio, G., Sanges, G., Stenroos, E. S., Pho, L. T., Schaffer, A. A., Lazzarini, A. M., Nussbaum, R. L., and Duvoisin, R. C. (1996) *Science* **274**, 1197-1199
16. Polymeropoulos, M. H., Lavedan, C., Leroy, E., Ide, S. E., Dehejia, A., Dutra, A., Pike, B., Root, H., Rubenstein, J., Boyer, R., Stenroos, E. S., Chandrasekharappa, S., Athanassiadou, A., Papapetropoulos, T., Johnson, W. G., Lazzarini, A. M., Duvoisin, R. C., Di Iorio, G., Golbe, L. I., and Nussbaum, R. L. (1997) *Science* **276**, 2045-2047
17. Kruger, R., Kuhn, W., Muller, T., Woitalla, D., Graeber, M., Kosel, S., Przuntek, H., Epplen, J. T., Schols, L., and Riess, O. (1998) *Nat Genet* **18**, 106-108
18. Singleton, A. B., Farrer, M., Johnson, J., Singleton, A., Hague, S., Kachergus, J., Hulihan, M., Peuralinna, T., Dutra, A., Nussbaum, R., Lincoln, S., Crawley, A., Hanson, M., Maraganore, D., Adler, C., Cookson, M. R., Muenter, M., Baptista, M., Miller, D., Blancato, J., Hardy, J., and Gwinn-Hardy, K. (2003) *Science* **302**, 841
19. Fauvet, B., Mbefo, M. K., Fares, M. B., Desobry, C., Michael, S., Ardah, M. T., Tsika, E., Coune, P., Prudent, M., Lion, N., Eliezer, D., Moore, D. J., Schneider, B., Aebischer, P., El-Agnaf, O. M., Masliah, E., and Lashuel, H. A. (2012) *J Biol Chem* **287**, 15345-15364
20. Davidson, W. S., Jonas, A., Clayton, D. F., and George, J. M. (1998) *J Biol Chem* **273**, 9443-9449
21. Jao, C. C., Der-Sarkissian, A., Chen, J., and Langen, R. (2004) *Proc Natl Acad Sci U S A* **101**, 8331-8336
22. Ribeiro, C. S., Carneiro, K., Ross, C. A., Menezes, J. R., and Engelender, S. (2002) *J Biol Chem* **277**, 23927-23933
23. Witt, S. N. (2013) *Mol Neurobiol* **47**, 552-560
24. Chandra, S., Gallardo, G., Fernandez-Chacon, R., Schluter, O. M., and Sudhof, T. C. (2005) *Cell* **123**, 383-396
25. Bonini, N. M., and Giasson, B. I. (2005) *Cell* **123**, 359-361
26. Lee, H. J., Choi, C., and Lee, S. J. (2002) *J Biol Chem* **277**, 671-678

27. Vamvaca, K., Volles, M. J., and Lansbury, P. T., Jr. (2009) *J Mol Biol* **389**, 413-424
28. Robotta, M., Hintze, C., Schildknecht, S., Zijlstra, N., Jungst, C., Karreman, C., Huber, M., Leist, M., Subramaniam, V., and Drescher, M. (2012) *Biochemistry* **51**, 3960-3962
29. Ulmer, T. S., Bax, A., Cole, N. B., and Nussbaum, R. L. (2005) *J Biol Chem* **280**, 9595-9603
30. Ueda, K., Fukushima, H., Masliah, E., Xia, Y., Iwai, A., Yoshimoto, M., Otero, D. A., Kondo, J., Ihara, Y., and Saitoh, T. (1993) *Proc Natl Acad Sci U S A* **90**, 11282-11286
31. Del Mar, C., Greenbaum, E. A., Mayne, L., Englander, S. W., and Woods, V. L., Jr. (2005) *Proc Natl Acad Sci U S A* **102**, 15477-15482
32. Mysling, S., Betzer, C., Jensen, P. H., and Jorgensen, T. J. (2013) *Biochemistry*
33. van Rooijen, B. D., van Leijenhorst-Groener, K. A., Claessens, M. M., and Subramaniam, V. (2009) *J Mol Biol* **394**, 826-833
34. Eliezer, D., Kutluay, E., Bussell, R., Jr., and Browne, G. (2001) *J Mol Biol* **307**, 1061-1073
35. Uversky, V. N., Gillespie, J. R., and Fink, A. L. (2000) *Proteins* **41**, 415-427
36. McCarney, E. R., Kohn, J. E., and Plaxco, K. W. (2005) *Crit Rev Biochem Mol Biol* **40**, 181-189
37. Klein-Seetharaman, J., Oikawa, M., Grimshaw, S. B., Wirmer, J., Duchardt, E., Ueda, T., Imoto, T., Smith, L. J., Dobson, C. M., and Schwalbe, H. (2002) *Science* **295**, 1719-1722
38. Levinthal, C. (1969) *Mossbauer Spectroscopy in Biological Systems: Proceedings of a meeting helt at Allerton House, Monticello Illinois: 22-24*
39. Ramachandran, G. N., Ramakrishnan, C., and Sasisekharan, V. (1963) *J Mol Biol* **7**, 95-99
40. Daggett, V., and Fersht, A. R. (2003) *Trends Biochem Sci* **28**, 18-25
41. Agashe, V. R., Shastry, M. C., and Udgaonkar, J. B. (1995) *Nature* **377**, 754-757
42. Karplus, M., and Weaver, D. L. (1994) *Protein Sci* **3**, 650-668
43. Anfinsen, C. B. (1973) *Science* **181**, 223-230
44. Anfinsen, C. B., Haber, E., Sela, M., and White, F. H., Jr. (1961) *Proc Natl Acad Sci U S A* **47**, 1309-1314
45. Leopold, P. E., Montal, M., and Onuchic, J. N. (1992) *Proc Natl Acad Sci U S A* **89**, 8721-8725
46. Onuchic, J. N., Luthey-Schulten, Z., and Wolynes, P. G. (1997) *Annu Rev Phys Chem* **48**, 545-600
47. Watters, A. L., Deka, P., Corrent, C., Callender, D., Varani, G., Sosnick, T., and Baker, D. (2007) *Cell* **128**, 613-624
48. Dill, K. A., and MacCallum, J. L. (2012) *Science* **338**, 1042-1046
49. Frokjaer, S., and Otzen, D. E. (2005) *Nat. Rev. Drug. Delivery 4*, 298-306
50. Jackson, S. E., and Fersht, A. R. (1991) *Biochemistry* **30**, 10428-10435
51. Finkelstein, A. V., and Pti*t*syn, O. B. (2002) *Protein physics : a course of lectures*, Academic Press, Amsterdam ; Boston
52. Creighton, T. E. (1990) *Biochem J* **270**, 1-16
53. Privalov, P. L. (1979) *Adv Protein Chem* **33**, 167-241
54. Greenfield, N. J. (2006) *Nat Protoc* **1**, 2876-2890
55. Kelly, S. M., Jess, T. J., and Price, N. C. (2005) *Biochim Biophys Acta* **1751**, 119-139
56. Greenfield, N. J. (2006) *Nat Protoc* **1**, 2527-2535
57. Lakowicz, J. R. (2006) *Principles of fluorescence spectroscopy*, 3rd ed., Springer, New York
58. Hawe, A., Sutter, M., and Jiskoot, W. (2008) *Pharm Res* **25**, 1487-1499
59. Nicoli, D. F., and Benedek, G. B. (1976) *Biopolymers* **15**, 2421-2437
60. Kunz, W., Henle, J., and Ninham, B. W. (2004) *Current Opinion in Colloid & Interface Science* **9**, 19-37
61. Bennion, B. J., and Daggett, V. (2003) *Proc Natl Acad Sci U S A* **100**, 5142-5147
62. Myers, J. K., Pace, C. N., and Scholtz, J. M. (1995) *Protein Sci* **4**, 2138-2148
63. Spencer, D. S., Xu, K., Logan, T. M., and Zhou, H. X. (2005) *J Mol Biol* **351**, 219-232
64. Kyle, R. A. (2001) *Br J Haematol* **114**, 529-538
65. Knowles, T. P., Fitzpatrick, A. W., Meehan, S., Mott, H. R., Vendruscolo, M., Dobson, C. M., and Welland, M. E. (2007) *Science* **318**, 1900-1903
66. Pedersen, J. S., Dickov, D., Flink, J. L., Hjuler, H. A., Christensen, G., and Otzen, D. E. (2006) *J. Mol. Biol.* **355**, 501-523

67. Chiti, F., and Dobson, C. M. (2006) *Annu Rev Biochem* **75**, 333-366
68. Oli, M. W., Otoo, H. N., Crowley, P. J., Heim, K. P., Nascimento, M. M., Ramsook, C. B., Lipke, P. N., and Brady, L. J. (2012) *Microbiology* **158**, 2903-2916
69. Zhou, Y., Smith, D., Leong, B. J., Brannstrom, K., Almqvist, F., and Chapman, M. R. (2012) *J Biol Chem* **287**, 35092-35103
70. Ostrowski, A., Mehert, A., Prescott, A., Kiley, T. B., and Stanley-Wall, N. R. (2011) *J Bacteriol* **193**, 4821-4831
71. Dueholm, M. S., Sondergaard, M. T., Nilsson, M., Christiansen, G., Stensballe, A., Overgaard, M. T., Givskov, M., Tolker-Nielsen, T., Otzen, D. E., and Nielsen, P. H. (2013) *Microbiologyopen* **2**, 365-382
72. Maji, S. K., Perrin, M. H., Sawaya, M. R., Jessberger, S., Vadodaria, K., Rissman, R. A., Singru, P. S., Nilsson, K. P. R., Simon, R., Schubert, D., Eisenberg, D., Rivier, J., Sawchenko, P., Vale, W., and Riek, R. (2009) *Science* **325**, 328-332
73. Munch, J., Rucker, E., Standker, L., Adermann, K., Goffinet, C., Schindler, M., Wildum, S., Chinnadurai, R., Rajan, D., Specht, A., Gimenez-Gallego, G., Sanchez, P. C., Fowler, D. M., Koulov, A., Kelly, J. W., Mothes, W., Grivel, J. C., Margolis, L., Keppler, O. T., Forssmann, W. G., and Kirchhoff, F. (2007) *Cell* **131**, 1059-1071
74. Dobson, C. M. (1999) *Trends Biochem Sci* **24**, 329-332
75. Goldschmidt, L., Teng, P. K., Riek, R., and Eisenberg, D. (2010) *Proc Natl Acad Sci U S A* **107**, 3487-3492
76. Jahn, T. R., and Radford, S. E. (2008) *Arch Biochem Biophys* **469**, 100-117
77. Vendruscolo, M., Paci, E., Karplus, M., and Dobson, C. M. (2003) *Proc Natl Acad Sci U S A* **100**, 14817-14821
78. Baldwin, A. J., Knowles, T. P., Tartaglia, G. G., Fitzpatrick, A. W., Devlin, G. L., Shammas, S. L., Waudby, C. A., Mossuto, M. F., Meehan, S., Gras, S. L., Christodoulou, J., Anthony-Cahill, S. J., Barker, P. D., Vendruscolo, M., and Dobson, C. M. (2011) *J Am Chem Soc* **133**, 14160-14163
79. Foguel, D., Suarez, M. C., Ferrao-Gonzales, A. D., Porto, T. C., Palmieri, L., Einsiedler, C. M., Andrade, L. R., Lashuel, H. A., Lansbury, P. T., Kelly, J. W., and Silva, J. L. (2003) *Proc Natl Acad Sci U S A* **100**, 9831-9836
80. Tartaglia, G. G., Pechmann, S., Dobson, C. M., and Vendruscolo, M. (2007) *Trends Biochem Sci* **32**, 204-206
81. Luheshi, L. M., Tartaglia, G. G., Brorsson, A. C., Pawar, A. P., Watson, I. E., Chiti, F., Vendruscolo, M., Lomas, D. A., Dobson, C. M., and Crowther, D. C. (2007) *PLoS Biol* **5**, e290
82. Stefani, M., and Dobson, C. M. (2003) *J Mol Med (Berl)* **81**, 678-699
83. Bonar, L., Cohen, A. S., and Skinner, M. M. (1969) *Proc Soc Exp Biol Med* **131**, 1373-1375
84. Sunde, M., Serpell, L. C., Bartlam, M., Fraser, P. E., Pepys, M. B., and Blake, C. C. (1997) *J Mol Biol* **273**, 729-739
85. Tycko, R. (2004) *Curr. Opin. Struct. Biol.* **14**
86. Sawaya, M. R., Sambashivan, S., Nelson, R., Ivanova, M. I., Sievers, S. A., Apostol, M. I., Thompson, M. J., Balbirnie, M., Wiltzius, J. J., McFarlane, H. T., Madsen, A. O., Riekel, C., and Eisenberg, D. (2007) *Nature* **447**, 453-457
87. Nielsen, J. T., Bjerring, M., Jeppesen, M. D., Pedersen, R. O., Pedersen, J. M., Hein, K. L., Vosegaard, T., Skrydstrup, T., Otzen, D. E., and Nielsen, N. C. (2009) *Angew Chem Int Ed Engl* **48**, 2118-2121
88. Jaroniec, C. P., MacPhee, C. E., Bajaj, V. S., McMahon, M. T., Dobson, C. M., and Griffin, R. G. (2004) *Proc Natl Acad Sci U S A* **101**, 711-716
89. Vilar, M., Chou, H. T., Luhrs, T., Maji, S. K., Riek-Loher, D., Verel, R., Manning, G., Stahlberg, H., and Riek, R. (2008) *Proceedings of the National Academy of Sciences of the United States of America* **105**, 8637-8642
90. Fitzpatrick, A. W., Debelouchina, G. T., Bayro, M. J., Clare, D. K., Caporini, M. A., Bajaj, V. S., Jaroniec, C. P., Wang, L., Ladizhansky, V., Muller, S. A., Macphee, C. E., Waudby, C. A., Mott, H. R., De Simone, A., Knowles, T. P., Saibil, H. R., Vendruscolo, M., Orlova, E. V., Griffin, R. G., and Dobson, C. M. (2013) *Proc Natl Acad Sci U S A* **110**, 5468-5473

91. Nelson, R., Sawaya, M. R., Balbirnie, M., Madsen, A. O., Riekel, C., Grothe, R., and Eisenberg, D. (2005) *Nature* **435**, 773-778
92. Tycko, R., and Wickner, R. B. (2013) *Acc Chem Res*
93. Andersen, C. B., Hicks, M. R., Vetri, V., Vandahl, B., Rahbek-Nielsen, H., Thogersen, H., Thogersen, I. B., Enghild, J. J., Serpell, L. C., Rischel, C., and Otzen, D. E. (2010) *J Mol Biol* **397**, 932-946
94. Jarrett, J. T., and Lansbury, P. T., Jr. (1993) *Cell* **73**, 1055-1058
95. Morris, A. M., Watzky, M. A., and Finke, R. G. (2009) *Biochimica et Biophysica Acta*, 375-397
96. Andersen, C. B., Yagi, H., Manno, M., Martorana, V., Ban, T., Christiansen, G., Otzen, D. E., Goto, Y., and Rischel, C. (2009) *Biophysical Journal* **96**, 1529-1536
97. Knowles, T. P., Waudby, C. A., Devlin, G. L., Cohen, S. I., Aguzzi, A., Vendruscolo, M., Terentjev, E. M., Welland, M. E., and Dobson, C. M. (2009) *Science* **326**, 1533-1537
98. Collins, S. R., Douglass, A., Vale, R. D., and Weissman, J. S. (2004) *Plos Biology* **2**, 1582-1590
99. Marshall, K. E., and Serpell, L. C. (2009) *Biochem Soc Trans* **37**, 671-676
100. Cohen, S. I. A., Vendruscolo, M., Dobson, C. M., and Knowles, T. P. J. (2011) *Journal of Chemical Physics* **135**
101. Cohen, S. I. A., Vendruscolo, M., Dobson, C. M., and Knowles, T. P. J. (2011) *Journal of Chemical Physics* **135**
102. Cohen, S. I. A., Vendruscolo, M., Welland, M. E., Dobson, C. M., Terentjev, E. M., and Knowles, T. P. J. (2011) *Journal of Chemical Physics* **135**
103. Cohen, S. I., Vendruscolo, M., Dobson, C. M., and Knowles, T. P. (2012) *J Mol Biol* **421**, 160-171
104. Lee, J., Culyba, E. K., Powers, E. T., and Kelly, J. W. (2011) *Nat Chem Biol* **7**, 602-609
105. Serio, T. R., Cashikar, A. G., Kowal, A. S., Sawicki, G. J., Moslehi, J. J., Serpell, L., Arnsdorf, M. F., and Lindquist, S. L. (2000) *Science* **289**, 1317-1321
106. Otzen, D. E., and Oliveberg, M. (1999) *Proc Natl Acad Sci U S A* **96**, 11746-11751
107. Pedersen, J. S., Christensen, G., and Otzen, D. E. (2004) *Journal of Molecular Biology* **341**, 575-588
108. Hartl, F. U., Bracher, A., and Hayer-Hartl, M. (2011) *Nature* **475**, 324-332
109. Dasgupta, I., Sanglas, L., Enghild, J. J., and Lindberg, I. (2012) *Biochemistry* **51**, 7456-7464
110. Peinado, J. R., Sami, F., Rajpurohit, N., and Lindberg, I. (2013) *FEBS Lett* **587**, 3406-3411
111. Giehm L, S. D., Otzen DE, Vestergaard B. (2011) *Proc Natl Acad Sci U S A* **108(8)**, 3246-3251
112. Knowles, T. P., White, D. A., Abate, A. R., Agresti, J. J., Cohen, S. I., Sperling, R. A., De Genst, E. J., Dobson, C. M., and Weitz, D. A. (2011) *Proc Natl Acad Sci U S A* **108**, 14746-14751
113. Pieri, L., Madiona, K., Bousset, L., and Melki, R. (2012) *Biophys J* **102**, 2894-2905
114. Milanesi, L., Sheynis, T., Xue, W. F., Orlova, E. V., Hellewell, A. L., Jelinek, R., Hewitt, E. W., Radford, S. E., and Saibil, H. R. (2012) *Proc Natl Acad Sci U S A* **109**, 20455-20460

Article IV

Role of Elongation and Secondary Pathways in S6 Amyloid Fibril Growth

Nikolai Lorenzen,[†‡△] Samuel I. A. Cohen,[§‖△] Søren B. Nielsen,[†‡] Therese W. Herling,[§] Gunna Christiansen,[¶] Christopher M. Dobson,[§] Tuomas P. J. Knowles,[§*] and Daniel Otzen[†‡*]

[†]Interdisciplinary Nanoscience Centre and [‡]Interdisciplinary Nanoscience Center (iNANO), Center for Insoluble Protein Structures (inSPIN), Department of Molecular Biology and Genetics, Aarhus University, Aarhus, Denmark; [§]Department of Chemistry, University of Cambridge, Cambridge, United Kingdom; [¶]Department of Medical Immunology, Aarhus University, Aarhus, Denmark; and [‖]School of Engineering and Applied Sciences, Harvard University, Cambridge, Massachusetts

ABSTRACT The concerted action of a large number of individual molecular level events in the formation and growth of fibrillar protein structures creates a significant challenge for differentiating between the relative contributions of different self-assembly steps to the overall kinetics of this process. The characterization of the individual steps is, however, an important requirement for achieving a quantitative understanding of this general phenomenon which underlies many crucial functional and pathological pathways in living systems. In this study, we have applied a kinetic modeling approach to interpret experimental data obtained for the aggregation of a selection of site-directed mutants of the protein S6 from *Thermus thermophilus*. By studying a range of concentrations of both the seed structures, used to initiate the reaction, and of the soluble monomer, which is consumed during the growth reaction, we are able to separate unambiguously secondary pathways from primary nucleation and fibril elongation. In particular, our results show that the characteristic autocatalytic nature of the growth process originates from secondary processes rather than primary nucleation events, and enables us to derive a scaling law which relates the initial seed concentration to the onset of the growth phase.

INTRODUCTION

The level of interest focused on understanding the assembly and structure of nanoscale protein fibrils has increased significantly in the last decade due to the realization that the formation of amyloid fibrils is intricately associated with a range of neurodegenerative disorders, including Parkinson's (1) and Alzheimer's diseases (2–5), and other medical conditions including type II diabetes. The underlying similarities in the structures and behavior of protein fibrils found in connection with apparently disparate disorders, together with the finding that many proteins, both with and without connection to disease, are able to undergo fibrillar assembly *in vitro*, has led to the idea that the amyloid state represents a generally accessible alternative form of organized protein structure (6,7).

Despite the apparent simplicity associated with the description of amyloid growth as a homomolecular assembly phenomenon, it has become apparent that this process is characterized by a remarkable degree of complexity on the molecular level, and that many different molecular events contribute to the overall assembly pathway. It is widely agreed that fibril formation is initiated by a primary nucleation step (8) wherein soluble proteins come together to form aggregates capable of subsequent growth through incorporation of further species and leading to elongation of the structures when they acquire fibrillar character (9–14). In many cases, it has been shown that this subsequent growth is resulting from the incorporation of monomers rather than oligomers, a conclusion in agreement with the finding that fibril growth can be observed under conditions where no significant oligomer populations can be detected (10,14) and the fact that the elongation of fibrils has been found to be directly proportional to the concentration of soluble protein (10,11).

A crucial characteristic of such fibrillar assembly phenomena is the sigmoidal nature of the reaction profile: the rate of assembly accelerates during the first part of the process, and then slows down to reach an equilibrium endpoint that results from the depletion of available protein in solution. The origin of the acceleration in the reaction rate for early times is, however, still a topic of investigation and discussion. It is important to note that, if the number of fibril ends present in solution remains constant, the rate of the overall conversion of soluble protein into the fibrils will be linear in the monomer concentration because the growth occurs primarily at the ends of the fibrils. A higher than linear concentration dependence requires, therefore, the multiplication of such fibrils in number in order to increase the number of ends where the growth occurs (15–17). This type of proliferation in the number of fibrils in some studies has been attributed to further primary nucleation, where new fibrils emerge from soluble protein in parallel to the growth of existing fibrils, but in others to secondary pathways, where additional growth centers are formed from growing fibrils, e.g., by fibril breakage, surface-catalyzed nucleation, or branching (see (15,18,19) for a more detailed description of secondary pathways).

In the literature, the term "fibril growth" is commonly used to indicate both fibril elongation and multiplication,

Submitted June 7, 2011, and accepted for publication March 14, 2012.

△Nikolai Lorenzen and Samuel I. A. Cohen contributed equally to this work.

*Correspondence: tpjk2@cam.ac.uk or dao@inano.au.dk

Editor: Kathleen B. Hall.

0006-3495/12/05/2167/9 $2.00

doi: 10.1016/j.bpj.2012.03.047

and combinations of such processes; relatively little work has focused on the challenge of identifying the true contribution of the elongation process relative to the contributions of primary and secondary nucleation. Indeed, parameters in empirical sigmoidal functions, such as the logistic function (14), combine both microscopic rates into phenomenological parameters such as the lag-time or the apparent maximal growth rate. A further complication results from the fact that the relative populations of different types of fibrils and their structures can be shifted dramatically upon changes in the environment (20,21). This changing picture of fibril polymorphism can, however, be avoided by seeding with preformed fibrils, thereby templating the subsequent growth of one fibril type without the requirement for primary nucleation.

MATERIALS AND METHODS

General notes

All S6 mutants were expressed recombinantly, purified, and dialyzed against deionized water as described previously in Otzen et al. (22). Protein concentrations were determined by absorption at 280 nm using an ND-1000 spectrophotometer (NanoDrop, ThermoScientific, Wilmington, DE). A theoretical extinction coefficient at 12.700 cm^{-1}, M^{-1} was used. Fibril formation was carried out in 10 mM HCl (pH 2), 0.4 M NaCl at 42°C with agitation (900 rpm during seed formation and 180 rpm in plate reader experiments). All Thioflavin T (ThT) fluorescence measurements were performed in triplicate.

Asymmetric flow field-flow fractionation

Here, we used asymmetric flow field-flow fractionation (AF4). Samples of 100 μM S6 VA88 were harvested from the kinetic plate reader experiments over a period of five days and centrifuged at 13,400 rpm for 15 min in a MiniSpin centrifuge (Eppendorf, Hamburg, Germany). A 100-μL sample was injected onto an AF2000 asymmetrical flow field-flow fractionation system (Postnova, Landsberg, Germany) equipped with an S3240 UV/Vis detector monitoring absorbance at 205 and 280 nm, PN3140 refractive index, and a PN3070 7-angle light scattering detector. The system was equipped with a 5-kDa MWCO ultrafiltration membrane and a 350-μm spacer, and was equilibrated in 10 mM HCl (pH 2), 0.4 M NaCl at room temperature. The sample was separated, injected, and focused for 5 min at 0.2 mL/min with a focus flow of 2.3 mL/min and cross-flow of 2 mL/min. The detector flow was kept constant at 0.5 mL/min throughout the injection, focusing, and separation. After focusing, a cross-flow gradient from 2 to 0.15 mL/min over 20 min followed by a 10-min gradient to 0 mL/min was applied to separate potential S6 species. The system was then washed at 0 mL/min cross-flow for 15 min.

Seed formation

Mature fibrils were prepared in 1.5 mL test tubes containing 100–250 μM of S6 under fibril forming conditions and incubated in a Vortemp 56 evc. Eppendorf shaker (Tehtnica, Zĕlezniki, Slovenia). Fibril formation was followed using ThT fluorescence: samples were diluted 12 times with a ThT solution (40 μM ThT final, 10 mM HCl, pH 2, 10 mM NaCl) and incubated for 10 min in an Eppendorf shaker under conditions identical to those used for fibril growth. Fluorescence measurements were carried out on a LS55 Luminescence spectrometer (Perkin-Elmer, Norwalk, CT) using emission and excitation slit widths of 10 nm, excitation at 450 nm, and emission at 465–555 nm. Seeds were obtained by sonication on ice of mature fibrils using a HD 2070 Bandelin Sonuplus Sonicator (Buch & Holm, Copenhagen, Denmark) for three times,1 min, at 60% power. Seeds were kept at 4°C.

Fibril formation kinetics with platereader

Seeded fibril growth from different mutant variants was monitored using ThT-fluorescence (using excitation at 450 nm and emission at 485 nm) performed every 20 min on a GENios Pro Plate Reader (TECAN, Männedorf, Germany) in 96-well plates. All samples contained 40 μM ThT, 10mM HCl (pH 2), 0.4 M NaCl. The temperature was kept at 42°C, shaking was linear at 180 rpm, and shaking duration was 3 min in every 20-min cycle.

Atomic force microscopy

For analysis by atomic force microscopy (AFM), mature fibrils and seed samples were prepared as described above from a 100 μM S6 monomer solution. 5 μL sample aliquots were deposited on freshly cleaved mica (SPI supplies, West Chester, PA). Samples were imaged by AFM, under ambient conditions at room temperature, using a NanoWizard II (JPK Instruments, Cambridge, UK) and Ultrasharp NSC36 cantilevers (MikroMasch, Tallinn, Estonia) in contact mode at a line rate of 1.5 Hz and a resolution of 512 × 512 pixels. Images were analyzed with the open source software Gwyddion (http://gwyddion.net/).

Fourier transform infrared spectroscopy

Fourier transform infrared spectroscopy (FTIR) spectra of fibrils and monomeric solutions were obtained with a Tensor 27 FT-IR (Bruker Optics, Billerica, MA). Spectra were accumulations of 68 scans, measured with a resolution at 2 cm^{-1} in the range from 1000 to 3998 cm^{-1}. Data processing, consisting of atmospheric compensation, baseline subtraction, and fitting with Lorentzian curves, was performed with the software OPUS ver. 5.5 (http://www.stsci.edu/software/OPUS/kona2.html). For the comparison of seed and second-generation fibrils, spectra were normalized.

Transmission electron microscopy

Transmission electron microscopy (TEM) was carried out as described previously in Pedersen et al. (20). Briefly, a 5-mL aliquot (50–100 mM S6, incubated as above) was placed on a 400-mesh, carbon-coated, glow-discharged grid for 30 s. Grids were washed in two drops of double-distilled water and stained with 1% (w/v) phosphotungstic acid at pH 6.8 and blotted dry on filter paper. Samples were viewed with a model No. 1010 transmission electron microscope (JEOL, Peabody, MA) at 25,000 magnification.

RESULTS AND DISCUSSION

In order to identify the effects of fibril elongation and secondary pathways relative to other processes contributing to the overall fibril growth process, we can analyze systematic variations in the growth kinetics that result from changes in the quantities of preformed aggregates that are added and of monomer. We illustrate this approach in this article by studying members of a library of single and double mutants of the ribosomal protein S6 from *Thermus thermophilus*. The protein S6 has emerged as an outstanding

system for probing protein folding (22–24) and aggregation (20). Under acid-denaturing conditions which promote fibril formation (0.4 M NaCl, 10mM HCl (pH 2), 42°C), the native state of S6 (N) is destabilized and the protein can undergo amyloid assembly. The choice of S6 as the system of study in this work also gives rise to a key advantage, in that the primary nucleation of amyloid structures from S6 monomers is slow under these conditions (Fig. 1), providing a window within which it is possible to study elongation and multiplication of fibrillar species in the knowledge that primary nucleation is not contributing significantly to the evolution of observed fibrillar structures.

By the use of preseeding, hence avoiding the effects of polymorphism, within this window where primary nucleation does not contribute significantly to the fibril population, we reduce the number of variables that need to be defined in the self-assembly reaction. We confirmed directly that no oligomers were present in our preseeded experiments using AF4, AFM, and TEM measurements (see the Supporting Material). We can then use an array of different S6 mutants to span a broad range of fibril formation kinetics to test the validity of our model over an extended parameter range. The fibril kinetics are followed using in situ ThT fluorescence measurements; we have previously shown by electron microscopy that S6 fibrils formed under these conditions lead to high ThT signals (25).

Initial examination of the data describing fibril kinetics reveals that there is a difference between the ThT signal given from pregrown seeds and fibril material that forms in the reaction through addition to the seeds, although the structures of seeds and fibrils grown from seeds are very similar when compared using FTIR and AFM measurements (see the Supporting Material). In other words, the observed ThT signal obeys a dependency of the form

$$\begin{aligned}\text{Signal} &= \rho M_{\text{initial seeds}} + \sigma M_{\text{new material}} \\ &= \rho M(0) + \sigma[M(t) - M(0)]\end{aligned}, \tag{1}$$

where M denotes the concentration of monomer in aggregates, ρ is fixed so that the seed concentration is reported correctly at the beginning of the reaction, and σ is fixed so that the total monomer concentration is defined correctly at the end of the reaction. This effect can be seen in Fig. 1 where the initial seed concentration is 8.3 μM and the initial monomer concentration is 100 μM. The ratio of the final/initial ThT signal is ~24, whereas the ratio of total monomer to monomer initially in seeds is ~13, implying $\sigma \approx 2\rho$.

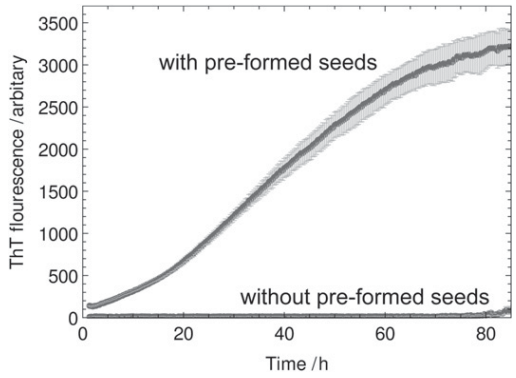

FIGURE 1 Kinetic traces for the fibril formation of S6 protein (LA30) with and without the initial addition of seeds of preformed fibrils. In the absence of such seed material (*lower trace*), no fibrillar material is detected over the time course of 80 h. With the addition of preformed seeds (*upper trace*), however, all monomer is incorporated into aggregates within this time window. Hence, the sigmoidal rate profile that is observed in this case unambiguously reflects the role of secondary pathways. In addition, the preseeded trace demonstrates the different scaling of the ThT fluorescence signal with initial seed material and the new material formed during the reaction, as given by Eq. 1. The system had initial seed concentration 8.3 μM and initial monomer concentration 100 μM. The ratio of the total monomer concentration in the system, 108.3 μM, to the initial seed concentration, 8.3 μM, is ~13, yet the ratio of the final/initial signal reported by ThT is ~24.

Elongation

The time evolution of a population of fibrillar species proliferating through primary nucleation, elongation, and secondary pathways has been studied extensively over the past 40 years (16–18,26–28). Much work has focused on integrated rate laws valid for the early stages of the reaction (10,15,18,29–31), first derived in the pioneering work of Ferrone et al. (18,32) in their studies of sickle hemoglobin gelation; more recently these solutions have been extended, using a self-consistent approach, to give integrated rate laws valid for the entire reaction time course (16,17,33). Solutions valid over the entire reaction will be vital in studying secondary nucleation later in this article, whereas the early time behavior is related to elongation in this section.

The early stages of aggregation in the S6 system can be used to study unambiguously the elongation of fibrillar species. We focused first on the effect of seed concentration on the addition of monomeric protein to fibrillar species in the initial stages of the reaction. For a system where primary nucleation does not contribute significantly to the fibril population, and for which preformed seeds are instead used to initiate the reaction, the fibrillar mass-concentration, $M(t)$, evolves in the initial stages of the reaction according to (17),

$$M(t) = m(0)C_{+}e^{\kappa t} - m(0)C_{-}e^{-\kappa t}, \tag{2}$$

$$\overset{t\to 0}{=} M(0) + 2\tilde{k}_{+}m(0)P(0)t + \mathcal{O}\left(t^2\right), \tag{3}$$

where $P(t)$ denotes the number-concentration of fibrils and $m(t)$ denotes the free monomer concentration. The constants in Eq. 3 are given as

$$\kappa = \sqrt{2\tilde{k}_+ k_2 m(0)^{n_2}}$$
$$C_\pm = \frac{\tilde{k}_+ P(0)}{\kappa} \pm \frac{M(0)}{2m(0)}. \quad (4)$$

The kinetic rate constant for elongation from each end is given as $\tilde{k}_+$ and that for the secondary pathway by k_2. The elongation rate constant in this formulation, $\tilde{k}_+$, may not be independent of the monomer concentration; we discuss this later in this section. The parameter n_2 describes the monomer-dependence of the secondary pathway such that $n_2 = 0$ corresponds to the monomer-independent case of fragmenting filaments (15,16,18,27,34,35); a nonzero value of n_2 represents a monomer-dependent secondary pathway, for example, where the surface of existing filaments is active in catalyzing the formation of new growth nuclei (15,18,33,36). Equation 3 shows that, for early times, the secondary pathway is less important in defining the overall consumption of free monomer $m(t)$ than the direct elongation of fibrils proportional to $2\tilde{k}_+ m(0)$.

Equation 3 shows that for kinetic data describing seeded growth, the intercept is the initial seed concentration $M(0)$ and the initial reaction rate r_0 is given as

$$r_0 = \left.\frac{dM}{dt}\right|_{t\to 0} = 2\tilde{k}_+ m(0) P(0). \quad (5)$$

For systems of fixed initial monomer concentration and varying initial seed concentration, Eq. 5 shows that the initial gradients are expected to be proportional to the initial seed number-concentration, $P(0)$, and the intercept to be proportional to the initial seed mass-concentration, $M(0)$. The mass concentration of seeds added to the system is known for all of our data, and for a given seed preparation used to preseed a series of experiments, the seed number concentration is linked to the seed mass concentration through the average seed length in the preparation, $\langle L(0)\rangle$, so that $P(0) = M(0)/\langle L(0)\rangle$. Therefore, the intercept and initial gradient are both expected to vary linearly with the seed mass-concentration. These predictions are validated in the scaling behavior seen in the data for a range of mutants in Fig. 2.

The separation of fibril elongation from primary nucleation and secondary pathways, as described above, provides an opportunity to investigate the sensitivity of fibril elongation toward single and double mutations. The final (plateau) fluorescence intensities in the experiments, at a given monomer concentration, vary by significantly less than one order of magnitude, showing that the changes in the initial fluorescence intensity reflect principally changes in the intrinsic elongation rates rather than variation in ThT binding affinity or degree of fluorescence enhancement. Under this assumption, the elongation rates for a range of mutant/seed combinations have been evaluated and are shown in Table 1. This assumption is further confirmed by noting that the relative elongation rates when WT and LA30/VA65 seeds are grown with monomeric IA8 (2.8 and 4.5, respectively) and monomeric LA61 (0.2 and 0.4, respectively) result in very similar ratios of the elongation rates of 0.6 (2.8/4.5) and 0.5 (0.2/0.4) (Table 1).

This finding reflects the dominant role of the protein that is converted into its aggregated form rather than the nature of the seed in defining the elongation rate of amyloid fibrils (37,38). In an earlier study, we have reported that single and double mutants of S6 strongly affect the primary nucleation rate (20). Our study clearly demonstrates that the elongation rate is highly affected by single and double mutations, even in the case of conservative mutations. A search performed for correlations between the elongation rates found with WT seed (Table 1) and the corresponding physico-chemical properties of the mutants did not reveal significant trends between the elongation rate and the folding parameters (unfolding rate constant k_u, refolding rate constant k_f, and melting temperature T_m; (20) and data not shown). This finding indicates that factors other than the thermodynamic stability of the folded state relative to unfolding control the

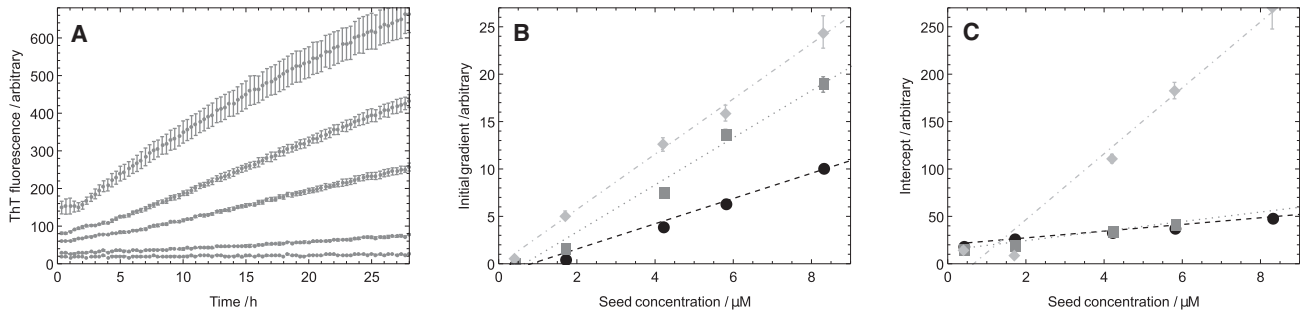

FIGURE 2 Scaling of the intercept and initial gradient with a varying initial seed concentration at a fixed initial monomer concentration as predicted by Eqs. 3 and 5. (*A*) Example of raw data (using VA37) for the early-time evolution of the polymer mass at increasing seed concentration (*bottom* to *top*). (*B*) The slope of the initial linear growth phase shows a linear dependency with the seed concentration. (*C*) The intercepts obtained from linear regression of the initial linear phases also reveal a linear dependency on the seed concentration. The fixed monomer concentration was 100 μM and the data (both seed and monomer) for the variants AG35 (*circle*), IA8 (*square*), and VA37 (*diamond*).

TABLE 1 Data for the linear variation of the initial gradient of fibril growth with seed concentration at a fixed monomer concentration

Seed species	Monomer species	$\partial r_0/\partial M(0)$	Correlation coefficient	Nominal relative elongation rate
WT	YA63	70.7	0.98	1.0
WT	LA75/MA67	154.9	0.97	2.2
WT	LA30	246.9	0.99	3.5
WT	AG35	103.5	0.99	1.5
WT	IA8	194.6	0.98	2.8
WT	VA37	267.6	0.99	3.8
WT	LA61	14.1	0.99	0.2
WT	IA8/LA26	25.1	0.98	0.4
LA30/VA65	IA8	319.8	0.99	4.5
LA30/VA650	LA61	29.7	0.99	0.4

Gradients determined from linear regression analysis, $\partial r_0/\partial M(0)$, equivalent to those of the fitted lines shown in Fig. 2, are tabulated. Data are shown for a range of seed/monomer mutant combinations at fixed monomer concentration (100 μM). The correlation coefficient from the linear fits, R, is given in the table. The final column gives the relative elongation rates that can be extracted as the ratios of the gradients of the linear regressions as discussed in the text.

changes in the elongation rates of the S6 mutant variants. Indeed, mutations can affect parts of the energy landscape that relate to the formation of inter- rather than intramolecular contacts which are involved in amyloid fibril growth but not the unfolding of a single chain.

Considering now the complementary case of systems with a fixed initial seed concentration and varying initial monomer concentration, Eq. 5 shows that, if $\tilde{k}_+$ is independent of the monomer concentration, the theory predicts that the initial gradient will be proportional to the total monomer concentration; indeed, the fibril elongation rate is given as

$$\partial_t^{\text{elongation}} M(t) = 2\tilde{k}_+ m(t) P(t).$$

At high monomer concentrations, however, diffusion of monomers to the fibril ends is no longer rate-limiting; instead, the structural reorganization of the polypeptide chain subsequent to its initial attachment to a fibril end takes over this role. For the overall elongation step, therefore, the rate exhibits a concentration dependence (10,39,40), which is analogous to that of the Michaelis-Menten scheme (41) for enzymatic reactions,

$$r_0 = 2\tilde{k}_+ m(0) P(0) = \frac{2k_+ m(0)}{1 + K_m^{-1} m(0)} P(0), \qquad (6)$$

where k_+ is a true elongation rate constant that is independent of the monomer concentration, and K_m is the crossover concentration above which elongation is rearrangement-limited. This form emerges naturally from the landscape model of protein folding (39), without the requirement to assume two discrete steps in the overall conversion process. It is interesting to note that the elongation rate constant k_+, which is partially determined by the probability of success of a given encounter between a monomer and a fibril end, is expected to be highly dependent on changes in reaction conditions, point mutations, etc.; the crossover concentration, K_m, may be less effected by such changes (39). Differences in r_0 between S6 mutants could be expected to reflect, therefore, primarily changes in the elongation rate constant k_+. For lower monomer concentrations such that ${K_m}^{-1} m(0) \ll 1$, Eq. 6 reduces $\tilde{k}_+ = k_+$ and the reaction rate increases linearly with the total monomer concentration. However, for very high monomer concentrations such that ${K_m}^{-1} m(0) \gg 1$, Eq. 6 shows that the initial rate of incorporation of monomers into fibrils saturates and no longer possesses a concentration dependence. The data shown in Fig. 3 show that the elongation rate increases with the concentration of monomer for lower concentrations before becoming saturated at higher monomer concentrations, as predicted by the theory.

Secondary pathways

We now turn to the analysis of the lag-phase in order to identify the role of secondary pathways in the fibrillation reaction. The existence of a lag-phase in a system where primary nucleation does not make a significant contribution to the increase in the number of fibrils or their mass over the time course of the experiment is direct evidence for the presence of a fibril-dependent secondary pathway responsible for the proliferation of fibrils, and has previously provided support for the role of filament fragmentation in prion propagation (42) and lateral growth in the aggregation of glucagon (43). Indeed, for seeded growth in the absence of a secondary pathway, it is not possible to observe a lag-phase (17,44). In systems which exhibit a significant contribution from primary nucleation, the identification of

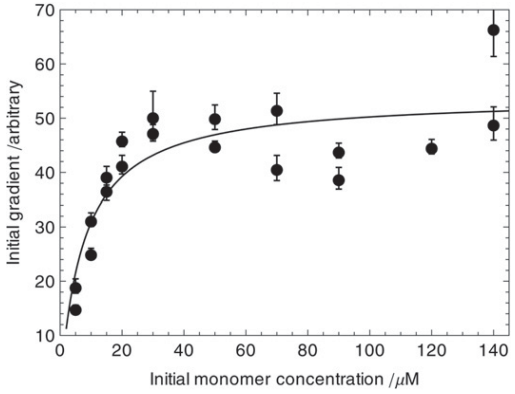

FIGURE 3 Saturation of the initial gradient of fibril growth at high monomer concentration as prediction by Eq. 6. By varying the initial monomer concentration at a fixed initial seed concentration, we identify clearly the predicted saturation in the initial gradient corresponding to the transition from diffusion to conformational-rearrangement limited fibril elongation discussed in the text, in Eq. 6; the line is a fit to this predicted form. The seed concentration is 8.3 μM. The data shown are for IA8 seed and monomer.

secondary pathways is more complicated. Indeed, it is in general difficult to establish under such conditions what fraction of the bulk kinetic behavior can be attributed to secondary pathways, and what fraction may originate instead from potentially very complex, and possibly incompletely understood, primary nucleation pathways. This problem does not exist with the system studied in this work and the results represent a striking example of a system where secondary pathways alone lead to a very clear sigmoidal rate profile.

We see in Fig. 1 that in the S6 system, primary nucleation does not generate a significant fibril population over the timecourse shown. However, upon addition of initial seed material, we are able to observe fibril formation within this window, and moreover the reaction follows a sigmoidal rate profile. The measurement of this rate profile, where without the influence of primary nucleation the reaction rate nevertheless initially accelerates even as the monomer is depleted, provides an unambiguous and striking identification of the role of secondary pathways in S6 aggregation.

We can analyze our data further within the standard framework of filamentous growth through elongation and secondary pathways (16–18,26,27,34). In a previous analysis (16), closed-form analytical solutions to the rate equations for filament assembly that are valid for the entire reaction time course were derived using a self-consistent approach to extend the validity of the well-known linearized solution (15,18,29); see Eq. 2. Interestingly, within this theoretical framework it has been shown (16) that for a constant initial monomer concentration and varying initial seed concentration, the time for the reaction to reach half-completion, $\tau_{50\%}$, varies logarithmically with the initial seed concentration, $M(0)$:

$$\tau_{50\%} \propto \text{const} - \log(M(0)). \quad (7)$$

This result was derived (16) in the regime where the elongation rate is proportional to the monomer concentration, $\tilde{k}_+ = k_+$; the self-consistent solution (16,17) is required to derive Eq. 7 in this case because the previously known linearized form, Eq. 2, is no longer valid at the half-time (Fig. 4 *A*). It is interesting to note that in the opposite regime, where the elongation rate is saturated and no longer depends on the monomer concentration, $m(0) \ll K_m$, the nonlinearity of the rate laws (17,18,29) is reduced significantly, resulting in the linearized solution (Eq. 2), having extended validity. For the low values of $n_2 \leq 4$ typically observed for amyloid formation (10,16,36), the linearized solution has validity, in the case where the elongation rate is saturated, that extends to the time to half-completion (Fig. 4 *B*). In this case, inversion of the linearized rate law (Eq. 2) predicts also a scaling relationship (15,18,42) for the half-time identical to Eq. 7. Therefore, the scaling law Eq. 7 has general validity independent of whether the elongation rate is saturated or not, as verified in Fig. 4 *C*.

This scaling from Eq. 7 is observed clearly in our data in Fig. 5. The decrease in lag-time with increasing initial seed concentration can be explained by noting that with a higher seed concentration the incorporation of monomers through elongation is accelerated, and also that concordantly the number of bonds and the surface area of fibrillar species in the system increases faster, resulting in secondary pathways being active at an earlier time.

An additional feature characteristic of the aggregation of S6 is the pronounced transition from the early phase linear growth into the late stage sigmoidal growth at a finite time after the beginning of the reaction. In order to gain insight

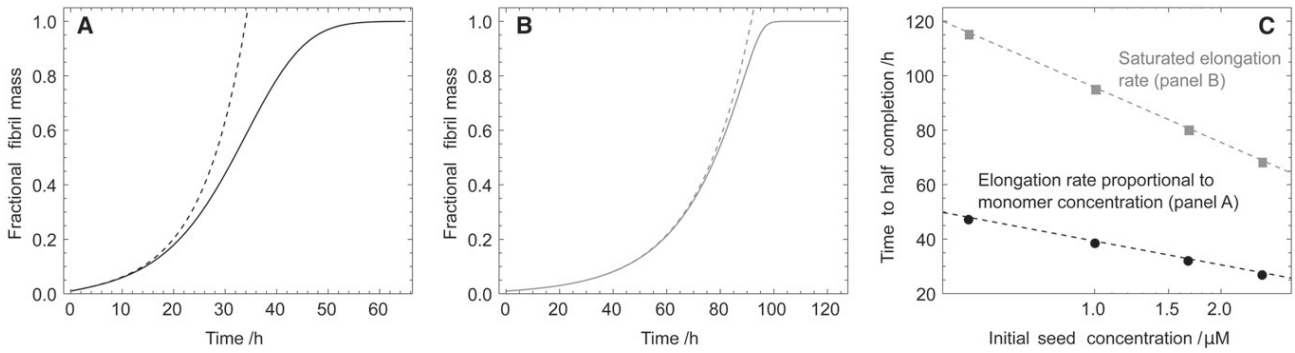

FIGURE 4 Effect of the saturation of the elongation rate on the time course of the reaction, and comparison with the well-known linearized solution to the rate equations (29,18,15). (*A*) Time course computed numerically (17) (*solid line*) for the aggregation reaction for the case where the elongation rate depends linearly on the monomer concentration (16). In this case, the linearized solution (*dotted line*), from Eq. 2, is only accurate for the early part of the reaction time course. A self-consistent solution has been derived previously that is accurate for the full time-course in this case (16). (*B*) Time-course computed numerically (17) (*solid line*) for the case where the elongation rate is saturated (39) and does not depend on the monomer concentration. In this case, the nonlinearity in the rate equations (17) is reduced, increasing the range of validity of the linearized solution (*dotted line*), from Eq. 2. (*C*) Scaling of the half-time with the seed concentration calculated numerically for the cases shown in panels *A* (*solid*) and *B* (*shaded*). In both cases a logarithmic scaling, from Eq. 7, is found. In panel *A*, $\tilde{k}_+ = k_+$ with $k_+ = 5 \cdot 10^3\ k_+ = 1\ \text{M}^{-1}\ \text{s}^{-1}$; in panel *B*, $\tilde{k}_+ = k_+/[1 + m(0)/K_m]$ with $K_m = m(0)/10$ and $k_+ = 1 \cdot 10^4\ k_+ = 1\ \text{M}^{-1}\ \text{s}^{-1}$. For panels *A* and *B*, the other parameters are: $m(0) = 50\ \mu\text{M}$, $k_- = 2 \cdot 10^{-9}\ \text{s}^{-1}$, $k_n = 0$, $n_2 = 0$, $M(0) = m(0)/100$, and $P(0) = M(0)/5000$. Panel *C* has parameters from panel *A* (*shaded*) and panel *B* (*solid*), respectively, except for the varying seed (mass) concentrations shown.

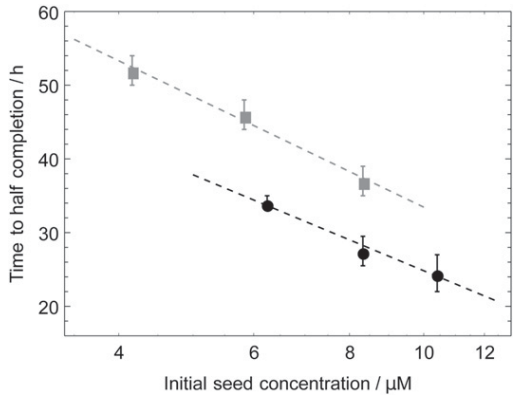

FIGURE 5 Logarithmic scaling of the time to half-completion of the fibril formation reaction with the initial seed concentration as predicted by Eq. 7; the data are extracted from the traces shown in Fig. 4. (*Solid circles*) Monomer LA75/MA67 in solution and added seed from LA30/VA65, with a fixed initial monomer concentration 80 μM. (*Shaded squares*) Monomeric LA30 and WT seed, with a fixed initial monomer concentration of 100 μM.

into this behavior, we first consider the case where the elongation rate is linear in the concentration of monomeric peptide, $\tilde{k}_+ = k_+$. It is possible to derive the expected dependency of this characteristic time to onset on the initial seed concentration, because the initial gradient and the maximum gradient are known (17). By solving for the intercept of these two straight lines $M_{\mathrm{early}}(t)$ and $M_{\mathrm{growth}}(t)$ (Fig. 6 *a*), we find the time to onset, τ_{on}, given from the condition $M_{\mathrm{early}}(\tau_{\mathrm{on}}) = M_{\mathrm{growth}}(\tau_{\mathrm{on}})$, where

$$M_{\mathrm{early}}(t) \;=\; M(0) + 2k_+m(0)P(0)t, \tag{8}$$

$$M_{\mathrm{growth}}(t) \;=\; \frac{m(0)\kappa}{e}t - \frac{\log\left(C_+^{-1}\right)+1}{e} + 1, \tag{9}$$

yielding

$$\tau_{\mathrm{on}} \;=\; \frac{e\,M(0) + m(0)\,\left[1 - e + \log\left(C_+^{-1}\right)\right]}{\left[\kappa - 2eP(0)k_+\right]\,m(0)}. \tag{10}$$

The condition for the existence of a lag-phase is $\kappa \gg 2eP(0)k_+m(0)$ (17), and so for low seed concentrations, $M(0) \ll m(0)$, the result reduces in this limit to an equivalent logarithmic relation to that found for the time to half-completion:

$$\tau_{\mathrm{on}} \propto \mathrm{const} - \log(M(0)). \tag{11}$$

This result has been derived for the case where the elongation rate depends linearly on the monomer concentration (16,17); an identical result emerges in the case where the elongation rate is saturated, through the use of the linearized solution (Eq. 2), as discussed for Fig. 4. The scaling result, Eq. 11, is applied to our measurements in Fig. 6 where the predicted scaling is observed. It is interesting to note that in the other limiting situation where no lag-phase exists, $\kappa \ll 2eP(0)k_+m(0)$, the full relationship Eq. 10 returns the scaling law $t \sim 1/P(0)$, a finding consistent with the solution $M(t) \sim e^{-2k_+P(0)t}$ in this limit.

Interestingly, the effects of mutations in the sequence of S6 on the fibril elongation rate also imply changes in the time to the onset of the growth phase. Indeed, Eq. 10 shows that this time is, to first-order, inversely proportional to the parameter κ which contains a dependency on the elongation rate $\kappa \sim {k_+}^{1/2}$. In agreement with this deduction, WT seed with monomeric mutant YA63, which has a low relative elongation rate (1.0; Table 1), was found not to reach the growth phase during the time course of 100 h, whereas substituting mutant LA75/MA67 as monomer (relative elongation rate 2.2; Table 1) resulted in a shorter time to the growth phase, and substituting mutant LA30 as monomer (relative elongation rate 3.5; Table 1) resulted in a still further decrease in the observed time to onset.

CONCLUSIONS

In conclusion, the analysis of the aggregation behavior of a selection of site-directed mutants of the model protein S6 from *Thermus thermophilus* has enabled us to separate unambiguously the action of secondary pathways from

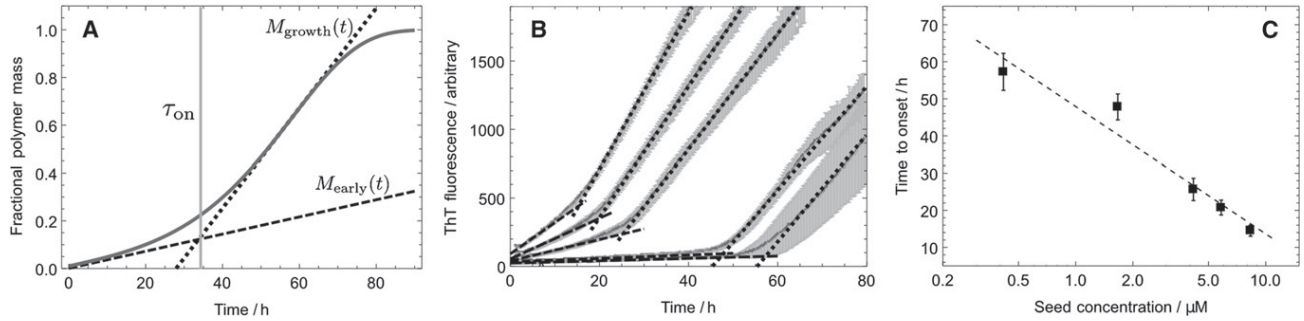

FIGURE 6 Logarithmic scaling of the time to onset of the growth phase with the initial seed concentration as predicted by Eq. 11. (*A*) The time to onset of the growth phase is defined as the time at the intercept of the straight lines $M_{\mathrm{early}}(t)$ and $M_{\mathrm{growth}}(t)$ shown. (*B*) Extraction of the characteristic time defined in this way. The data are for monomer LA30 with WT seed with a fixed monomer concentration 100 μM. (*C*) The predicted logarithmic scaling with a line of best fit to the predicted form, from Eq. 11.

that of primary nucleation and that of fibril elongation. Because multiple processes contribute to the rate of the overall growth reaction, we employed an approach whereby a given system parameter, here the seed concentration, was varied systematically while keeping the others constant. Furthermore, our results show that the generation of new fibrils in this system originates from secondary pathways rather than primary nucleation events, and that a lag phase can originate even in the absence of primary nucleation.

SUPPORTING MATERIAL

Additional methods and seven figures are available at http://www.biophysj.org/biophysj/supplemental/S0006-3495(12)00388-8.

Nikolai Lorenzen, Søren B. Nielsen, and Daniel E. Otzen are supported by the Michael J. Fox Foundation, the Danish Research Council, and the Center for Insoluble Protein Structures. Samuel I. A. Cohen is supported by the Schiff Foundation and the Kennedy Memorial Trust.

REFERENCES

1. Spillantini, M. G., M. L. Schmidt, …, M. Goedert. 1997. Alpha-synuclein in Lewy bodies. *Nature.* 388:839–840.
2. Dobson, C. M. 2003. Protein folding and misfolding. *Nature.* 426: 884–890.
3. Haass, C., and D. J. Selkoe. 2007. Soluble protein oligomers in neurodegeneration: lessons from the Alzheimer's amyloid β-peptide. *Nat. Rev. Mol. Cell Biol.* 8:101–112.
4. Hardy, J., and D. J. Selkoe. 2002. The amyloid hypothesis of Alzheimer's disease: progress and problems on the road to therapeutics. *Science.* 297:353–356.
5. Selkoe, D. J. 2003. Folding proteins in fatal ways. *Nature.* 426: 900–904.
6. Chiti, F., and C. M. Dobson. 2006. Protein misfolding, functional amyloid, and human disease. *Annu. Rev. Biochem.* 75:333–366.
7. Dobson, C. M. 1999. Protein misfolding, evolution and disease. *Trends Biochem. Sci.* 24:329–332.
8. Jarrett, J. T., and P. T. Lansbury, Jr. 1993. Seeding "one-dimensional crystallization" of amyloid: a pathogenic mechanism in Alzheimer's disease and scrapie? *Cell.* 73:1055–1058.
9. Tanaka, M., and J. S. Weissman. 2006. An efficient protein transformation protocol for introducing prions into yeast. *Methods Enzymol.* 412:185–200.
10. Collins, S. R., A. Douglass, …, J. S. Weissman. 2004. Mechanism of prion propagation: amyloid growth occurs by monomer addition. *PLoS Biol.* 2:e321.
11. Knowles, T. P., A. W. Fitzpatrick, …, M. E. Welland. 2007. Role of intermolecular forces in defining material properties of protein nanofibrils. *Science.* 318:1900–1903.
12. Kardos, J., K. Yamamoto, …, Y. Goto. 2004. Direct measurement of the thermodynamic parameters of amyloid formation by isothermal titration calorimetry. *J. Biol. Chem.* 279:55308–55314.
13. Kim, H. J., E. Chatani, …, S. R. Paik. 2007. Seed-dependent accelerated fibrillation of α-synuclein induced by periodic ultrasonication treatment. *J. Microbiol. Biotechnol.* 17:2027–2032.
14. Morris, A. M., M. A. Watzky, and R. G. Finke. 2009. Protein aggregation kinetics, mechanism, and curve-fitting: a review of the literature. *Biochim. Biophys. Acta.* 1794:375–397.
15. Ferrone, F. 1999. Analysis of protein aggregation kinetics. *Methods Enzymol.* 309:256–274.
16. Knowles, T. P. J., C. A. Waudby, …, C. M. Dobson. 2009. An analytical solution to the kinetics of breakable filament assembly. *Science.* 326:1533–1537.
17. Cohen, S. I. A., M. Vendruscolo, …, T. P. Knowles. 2011. Nucleated polymerization with secondary pathways. I. Time evolution of the principal moments. *J. Chem. Phys.* 135:065105.
18. Ferrone, F. A., J. Hofrichter, and W. A. Eaton. 1985. Kinetics of sickle hemoglobin polymerization. II. A double nucleation mechanism. *J. Mol. Biol.* 183:611–631.
19. Andersen, C. B., D. Otzen, …, C. Rischel. 2007. Glucagon amyloid-like fibril morphology is selected via morphology-dependent growth inhibition. *Biochemistry.* 46:7314–7324.
20. Pedersen, J. S., G. Christensen, and D. E. Otzen. 2004. Modulation of S6 fibrillation by unfolding rates and gatekeeper residues. *J. Mol. Biol.* 341:575–588.
21. Pedersen, J. S., D. Dikov, …, D. E. Otzen. 2006. The changing face of glucagon fibrillation: structural polymorphism and conformational imprinting. *J. Mol. Biol.* 355:501–523.
22. Otzen, D. E., O. Kristensen, …, M. Oliveberg. 1999. Structural changes in the transition state of protein folding: alternative interpretations of curved chevron plots. *Biochemistry.* 38:6499–6511.
23. Otzen, D. E., and M. Oliveberg. 2002. Conformational plasticity in folding of the split β-α-β protein S6: evidence for burst-phase disruption of the native state. *J. Mol. Biol.* 317:613–627.
24. Otzen, D. 2005. Antagonism, non-native interactions and non-two-state folding in S6 revealed by double-mutant cycle analysis. *Protein Eng. Des. Sel.* 18:547–557.
25. Zandomeneghi, G., M. R. H. Krebs, …, M. Fändrich. 2004. FTIR reveals structural differences between native β-sheet proteins and amyloid fibrils. *Protein Sci.* 13:3314–3321.
26. Oosawa, F., and S. Asakura. 1975. Thermodynamics of the Polymerization of Protein. Academic Press, New York.
27. Wegner, A. 1982. Spontaneous fragmentation of actin filaments in physiological conditions. *Nature.* 296:266–267.
28. Cohen, S. I. A., M. Vendruscolo, …, T. P. Knowles. 2011. Nucleated polymerization with secondary pathways. III. Equilibrium behavior and oligomer populations. *J. Chem. Phys.* 135:065107.
29. Bishop, M. F., and F. A. Ferrone. 1984. Kinetics of nucleation-controlled polymerization. A perturbation treatment for use with a secondary pathway. *Biophys. J.* 46:631–644.
30. Chen, S., F. A. Ferrone, and R. Wetzel. 2002. Huntington's disease age-of-onset linked to polyglutamine aggregation nucleation. *Proc. Natl. Acad. Sci. USA.* 99:11884–11889.
31. Vitalis, A., and R. V. Pappu. 2011. Assessing the contribution of heterogeneous distributions of oligomers to aggregation mechanisms of polyglutamine peptides. *Biophys. Chem.* 159:14–23.
32. Ferrone, F. A., J. Hofrichter, …, W. A. Eaton. 1980. Kinetic studies on photolysis-induced gelation of sickle cell hemoglobin suggest a new mechanism. *Biophys. J.* 32:361–380.
33. Cohen, S. I. A., M. Vendruscolo, …, T. P. Knowles. 2011. Nucleated polymerization with secondary pathways. II. Determination of self-consistent solutions to growth processes described by non-linear master equations. *J. Chem. Phys.* 135:065106.
34. Masel, J., V. A. Jansen, and M. A. Nowak. 1999. Quantifying the kinetic parameters of prion replication. *Biophys. Chem.* 77:139–152.
35. Tanaka, M., S. R. Collins, …, J. S. Weissman. 2006. The physical basis of how prion conformations determine strain phenotypes. *Nature.* 442:585–589.
36. Ruschak, A. M., and A. D. Miranker. 2007. Fiber-dependent amyloid formation as catalysis of an existing reaction pathway. *Proc. Natl. Acad. Sci. USA.* 104:12341–12346.
37. Wang, Y.-Q., A. K. Buell, …, S. Perrett. 2011. Relationship between prion propensity and the rates of individual molecular steps of fibril assembly. *J. Biol. Chem.* 286:12101–12107.

38. Buell, A. K., G. G. Tartaglia, …, T. P. Knowles. 2009. Position-dependent electrostatic protection against protein aggregation. *ChemBioChem.* 10:1309–1312.

39. Buell, A. K., J. R. Blundell, …, T. P. Knowles. 2010. Frequency factors in a landscape model of filamentous protein aggregation. *Phys. Rev. Lett.* 104:228101.

40. Scheibel, T., J. Bloom, and S. L. Lindquist. 2004. The elongation of yeast prion fibers involves separable steps of association and conversion. *Proc. Natl. Acad. Sci. USA.* 101:2287–2292.

41. Fersht, A. 1999. Structure and Mechanism in Protein Science. W.H. Freeman, New York.

42. Stöhr, J., N. Weinmann, …, D. Riesner. 2008. Mechanisms of prion protein assembly into amyloid. *Proc. Natl. Acad. Sci. USA.* 105:2409–2414.

43. Andersen, C. B., H. Yagi, …, C. Rischel. 2009. Branching in amyloid fibril growth. *Biophys. J.* 96:1529–1536.

44. Cohen, S. I. A., M. Vendruscolo, …, T. P. Knowles. 2011. Nucleated polymerization in the presence of pre-formed seed filaments. *Int. J. Mol. Sci.* 12:5844–5852.

Role of Elongation and Secondary Pathways in S6 Amyloid Fibril Growth

SUPPORTING MATERIAL

April 16, 2012

1 AF4

1.1 AF4 detection limit

The asymmetrical flow field-flow fractionation (AF4) system is used to separate S6 species according to size. To test this systems ability to detect potential oligomeric S6 structures, we analysed the sensitivity of our AF4 absorbance and multi-angle light scattering (MALS) detectors.

1.1.1 Analysis of absorbance intensity using standard protein

We prepared a dilution series of 1mg/ml Ribonuclease A (RibA) (13.7kDa, theoretical $\epsilon_{280\text{nm}}^{\text{RibA}} = 8640\text{cm}^{-1}\text{M}^{-1}$). RibA is similar in size to S6 (11 kDa), but its extinction coefficient is slightly lower ($\epsilon_{280\text{nm}}^{\text{S6}} = 12700\text{cm}^{-1}\text{M}^{-1}$). 100$\mu$l of RibA sample was injected onto a 5ml Hitrap desalting column, using 5mM Tris-Cl, 150mM NaCl pH 7.4 at 1ml/min as eluent. We probed the sensitivity of the AF4 instrument using absorbance at 205nm, where proteins show relatively little variability in their extinction coefficients due to amino acid composition[1]. For comparison, the detection limit using absorbance at 280nm was also evaluated. A total RibA protein load of $\sim$410ng gave rise to a peak slightly above the baseline. Injection of 1.2μg RibA showed a clear increase in absorbance at 205nm and increasing amounts continued to show larger peaks (Fig. S1 A). Thus, it is safe to assume that the detection limit of 205nm absorbance is between 0.41μg and 1.2μg which is $\leq$1% of the injected S6 protein (120μg) in AF4 analysis. We also evaluated the sensitivity

using absorbance at 280nm. Injection of ∼410ng RibA did not give rise to a noticeable peak. However, clear peaks were observed on injection of 1.2μg RibA and higher concentration indicating that the detection lies around this level (Fig. S1 B). Note that the S6 $\epsilon_{280\text{nm}}$ is approximately 50% larger than the RibA $\epsilon_{280\text{nm}}$, suggesting that the sensitivity to S6 species will be higher than for RibA species.

1.1.2 Analysis of light scattering intensity using polystyrene beads

The light scattering (LS) intensity at a 90 degree scattering angle was used to evaluate the sensitivity of the MALS detector using 19nm polystyrene (PS) standards (Postnova Analytics, Z-PS-POS-001-0.02) separated on the desalting column using 1ml/min 2% SDS solution to avoid particle aggregation. While the lowest concentration assayed (45.2ng) showed 90° LS intensities comparable to the blank injection (2% SDS), the injection of ∼136ng of PS particles showed an increase in intensity and the LS intensity continued to increase at increasing particle concentrations (Fig. S2). We emphasize here that the maximum intensity recorded after injection of a 1.2μg PS particle suspension is approaching approximately 50% of detector saturation. Thus, oligomeric S6 species of similar size and amount (corresponding to 1% of the total protein) would easily be captured by the MALS detector even though they are close to the threshold value for absorbance detection.

1.2 AF4 measurements

Having demonstrated the sensitivity of our AF4 measurements, we performed AF4 measurements in order to confirm directly whether oligomeric species were present over the time-course of our pre-seeded experiments. We detected no soluble S6 oligomeric species by absorbance or light scattering within 5 days of incubation, as shown in Fig. S3.

We also confirmed that during this time period all of the monomeric S6 protein had aggregated into insoluble fibrils as shown by a decrease in absorbance at 280nm of the S6 monomer peak, a large rise in ThT fluorescence intensity and the presence of a maximum at 1630cm^{-1} in the FTIR spectrum.

2 TEM

We performed TEM measurements to investigate the (2nd generation) fibrillar material grown from pre-formed seeds in our experiments. Firstly, no fibril branching was observed for any of the mutants; for example, images of

3 mutants are displayed in Fig. S4. This implies that the secondary pathway identified in the main text is either filament fragmentation, or a surface catalysed nucleation reaction that does not result in branching. These observations corresponds well with earlier observations for S6 fibrils where branching was not observed[2].

In addition, no oligomeric structures were observed in the second generation samples, with only fibrillar material seen over many images (around 20 pictures).

Interestingly, we observed some bundling of 2nd generation fibrils, Fig. S4, after time scales much longer than that for monomer depletion in the kinetic experiments in the main text. Bundling was not observed for the initial seed solutions, likely due to the disruptive force of sonication with subsequent storage at 4°C.

3 AFM

Images of S6 fibril seeds and mature fibrils grown from seeds were obtained by AFM, Fig. S5, of fibrils grown from seeds. We observed only fibrillar species, and did not detect small oligomers. In addition, we were unable to identify any differences in structure between AFM images of the initial seeds and the final fibrils grown from them, apart from the bundling seen after long time scales for the 2nd generation fibrils already observed in the TEM images.

4 FTIR

Seeds and the fibrils formed from elongation of the seeds (2nd generation fibrils) are expected to give the same fibril structure since they are grown under the same conditions. AFM analysis of seed structures indicate that seeds are a uniform population so polymorphism is not expected. Nevertheless we confirmed directly using FTIR spectras that seeds have similar structure to their corresponding 2nd generation fibrils, Fig. S6.

In addition, we note that S6 monomer and fibril are readily distinguishable by FTIR, Fig. S7. S6 display a small but significant spectral shift in the amide I region. S6 monomers have a spectral maximum at 1638 cm^{-1} whereas S6 fibrils have a spectral maximum at 1630 cm^{-1} corresponding well with other observations for fibril systems[3]. In addition to the spectral shift, the spectra also reveal an additional shoulder at 1700-1750 cm^{-1} and the Lorentzian fitting clearly show that they are different. All S6 mutants

showed a similar fingerprint as LA30/VA65.

References

[1] R. K. Scopes, *Measurement of protein by spectrophotometry at 205 nm.*, Anal Biochem **59**, 277 (1974).

[2] J. S. Pedersen, G. Christensen, D. E. Otzen, *Modulation of S6 fibrillation by unfolding rates and gatekeeper residues.*, J Mol Biol **341**, 575 (2004).

[3] G. Zandomeneghi, M. R. H. Krebs, M. G. McCammon, M. Fndrich, *FTIR reveals structural differences between native beta-sheet proteins and amyloid fibrils.*, Protein Sci **13**, 3314 (2004).

Figure captions

Fig S1. Calibration of the sensitivity of the AF4 absorbance unit using 0.41-33.3μg Ribonuclease A. A: absorbance at 205nm. B: absorbance at 280nm.

Fig S2. Light scattering intensity of 0-1.22μg polystyrene standards recorded by MALS detector.

Fig S3. Absorbance at 205nm from AF4 measurements, showing that no oligomers are detected within 5 days of incubation. Absorbance at 280nm and light scattering measurements gave identical results.

Fig S4. TEM of S6 fibrils grown from monomer and pre-formed seed of (A) LA30/VA65, (B) IA8, and (C) LA30. Dimensions are 1000 nm x 780 nm.

Fig S5. Representative AFM image of S6 fibrils grown from LA75/MA67 monomeric peptide with LA30/VA65 pre-formed seeds. Small oligomeric species were not observed.

Fig S6. Comparison of normalized FTIR spectra of LA30/VA65 seed (crosses) and 2nd generation fibrils (open circles), showing no significant differences.

Fig S7. Spectra of LA30/VA65 monomers (A) and fibrils (B). Experimental data are displayed as open circles (50% of datapoints shown), components of a Lorentzian fit are displayed as small filled circles and the sum of the components is a continuous line, overlapping the experimental data.

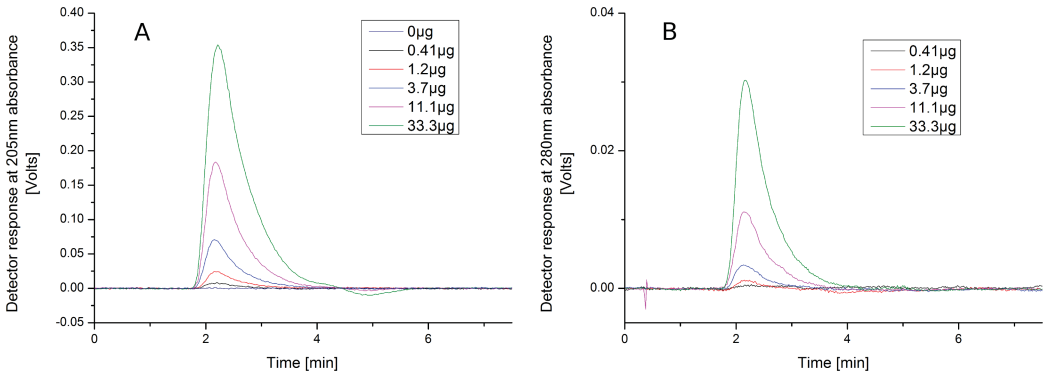
A
0µg
0.41µg
1.2µg
3.7µg
11.1µg
33.3µg
Detector response at 205nm absorbance [Volts]
Time [min]
B
0.41µg
1.2µg
3.7µg
11.1µg
33.3µg
Detector response at 280nm absorbance [Volts]
Time [min]

Figure S1:

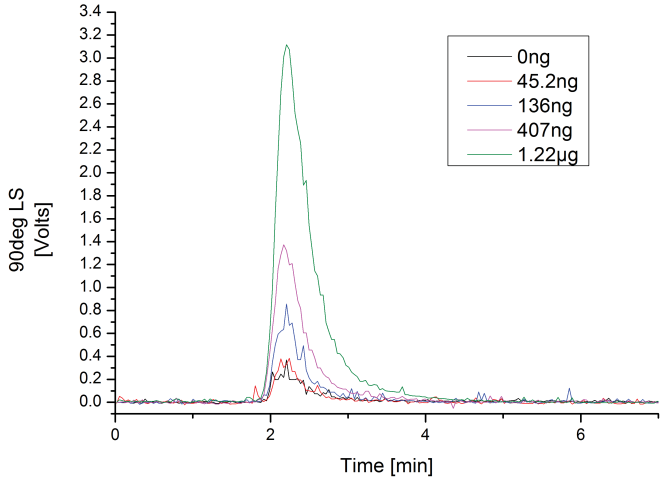

Figure S2:

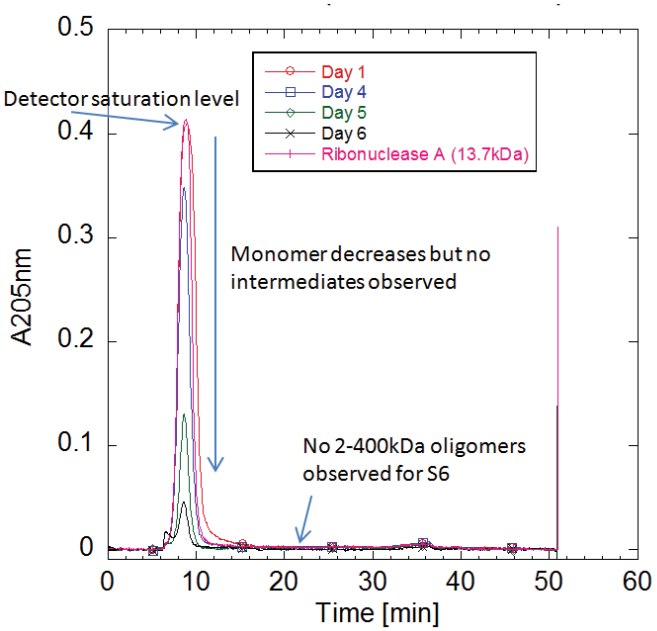
Detector saturation level
Day 1
Day 4
Day 5
Day 6
Ribonuclease A (13.7kDa)
Monomer decreases but no intermediates observed
No 2-400kDa oligomers observed for S6
A205nm
Time [min]
0.5
0.4
0.3
0.2
0.1
0
0
10
20
30
40
50
60

Figure S3:

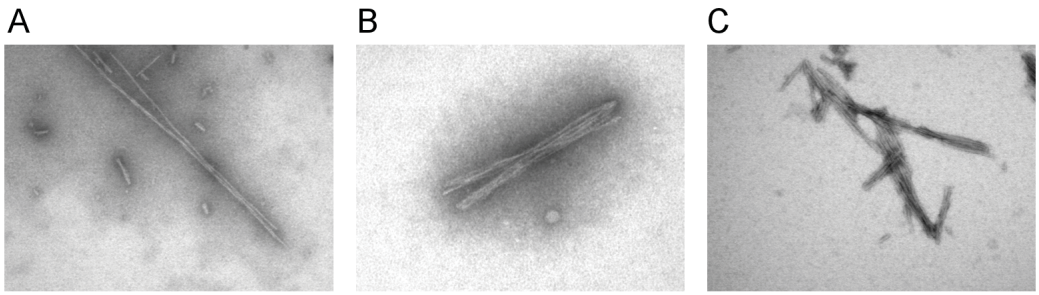

Figure S4:

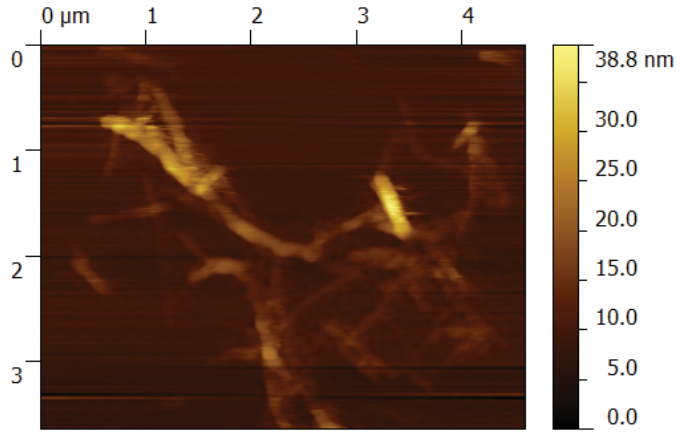

Figure S5:

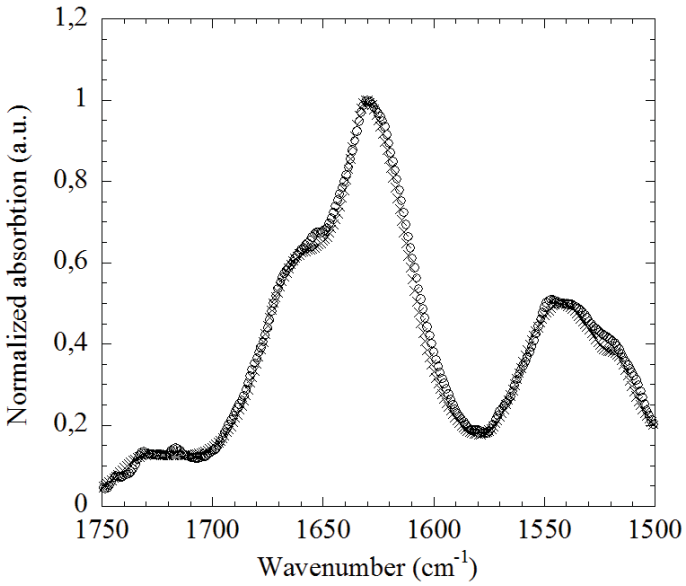
1,2
1
0,8
0,6
0,4
0,2
0
Normalized absorbtion (a.u.)
1750
1700
1650
1600
1550
1500
Wavenumber (cm-1)

Figure S6:

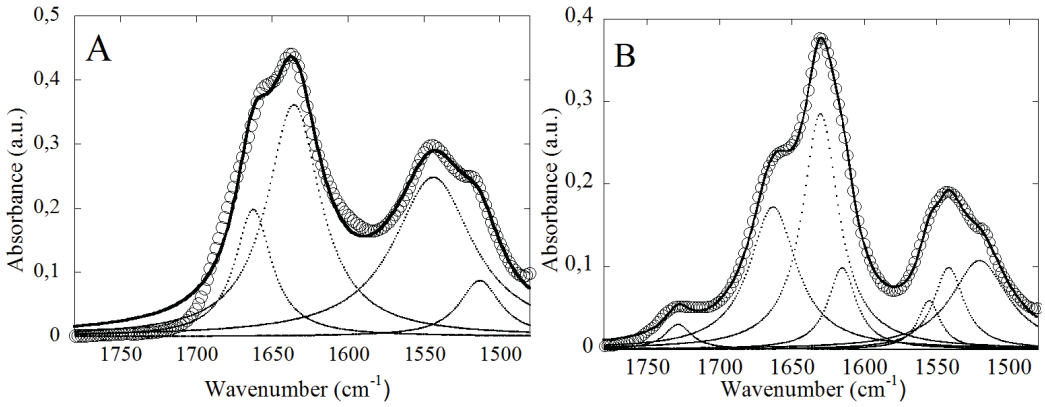
A
B
Absorbance (a.u.)
Wavenumber (cm-1)
0,5
0,4
0,3
0,2
0,1
0
1750
1700
1650
1600
1550
1500

Figure S7:

Article V

Biochimica et Biophysica Acta 1834 (2013) 677–687

Contents lists available at SciVerse ScienceDirect

Biochimica et Biophysica Acta

journal homepage: www.elsevier.com/locate/bbapap

Off-pathway aggregation can inhibit fibrillation at high protein concentrations

Taru Deva *, Nikolai Lorenzen, Brian S. Vad, Steen V. Petersen, Ida Thørgersen, Jan J. Enghild, Torsten Kristensen, Daniel E. Otzen **

Center for Insoluble Protein Structures (inSPIN), Interdisciplinary Nanoscience Center (iNANO), Department of Molecular Biology and Genetics, University of Aarhus, Gustav Wieds Vej 14, DK-8000 Aarhus C, Denmark

ARTICLE INFO

Article history:
Received 8 September 2012
Received in revised form 11 December 2012
Accepted 28 December 2012
Available online 8 January 2013

Keywords:
Amyloid formation
S6
Soluble oligomers
Proteolysis
Fibril morphology
Acid cleavage

ABSTRACT

Ribosomal protein S6 fibrillates readily at slightly elevated temperatures and acidic pH. We find that S6 fibrillation is retarded rather than favored when the protein concentration is increased above a threshold concentration of around 3.5 mg/mL. We name this threshold concentration C_{FR}, the concentration at which fibrillation is retarded. Our data are consistent with a model in which this inhibition is due to the formation of an off-pathway oligomeric species with native-like secondary structure. The oligomeric species dominates at high protein concentrations but exists in dynamic equilibrium with the monomer so that seeding with fibrils can overrule oligomer formation and favors fibrillation under C_{FR} conditions. Thus, fibrillation competes with formation of off-pathway oligomers, probably due to a monomeric conversion step that is required to commit the protein to the fibrillation pathway. The S6 oligomer is resistant to pepsin digestion. We also report that S6 forms different types of fibrils dependent on protein concentration. Our observations highlight the multitude of conformational states available to proteins under destabilizing conditions.

1. Introduction

Amyloid diseases such as Alzheimer's disease, type II diabetes and prion diseases are characterized by the accumulation of fibrillar deposits. It has been shown that these types of deposits can be formed by essentially all soluble proteins under appropriate environmental conditions [1]. The deposits show fibrillar morphology, bind specific dyes such as Congo red and Thioflavin T (ThT) and give rise to a characteristic cross-β x-ray diffraction pattern [2]. Fibrillar assemblies were initially described in disease-associated amyloid deposits, followed by the discovery of naturally occurring fibrils as part of spider and silk moth silk [3], bacterial biofilms [4,5], aerial hyphae of *Streptomyces* [6], and more recently also as functional amyloids in humans [7]. Fibrils also occur in processed foods [8] and bacterial inclusion bodies [9]. Thus, the conversion of soluble proteins to fibrillar structures is a very widespread process in nature and is important both in terms of biological function and disease pathology.

Although much research has been conducted on protein fibrillation, the mechanistic basis of this process is not yet completely understood. Major factors that drive the conversion of globular proteins to fibrillar forms are: a) reduced thermodynamic stability of globular proteins and consequent access to partially unfolded states, b) stabilization of natively unfolded proteins in certain conformations due to chemical changes or binding to specific cellular components such as heparan sulfate [10] and c) high concentrations of proteins. Several proteins have also been demonstrated to require a minimal critical aggregation concentration (CAC) for fibrillation to occur. Above this threshold concentration they are able to assemble into higher-order structures which will subsequently form fibrils [11,12].

The ribosomal protein S6 from *Thermus thermophilus* is a 101 amino acid residue protein with α/β secondary structure elements and βαββαβ topology. S6 is an attractive fibrillation model due to its lack of co-factors and cysteine residues. Folding and stability of this protein are well characterized and it has been shown to fold directly from the denatured to the native state without intermediates [13] although an off-pathway intermediate can accumulate under certain conditions [14,15]. S6 can fibrillate at low pH and high ionic strength and fibrillation is favored by different mutations [16]. A quadruple-mutant of S6 engineered to achieve 60% sequence identity to the Aβ peptide in a 15 amino acid residue segment has been demonstrated to undergo complex reversible aggregation in the refolding process and form soluble aggregates in the folded state [17].

Here we describe a new and unexpected aspect of protein aggregation, namely the retardation of S6 fibrillation at elevated protein

Abbreviations: AFM, atomic force microscopy; ATR-FTIR, attenuated total reflectance-Fourier transform infrared spectroscopy; CAC, critical aggregation concentration; CD, circular dichroism; C_{FR}, concentration at which fibrillation is retarded; DLS, dynamic light scattering; IPTG, isopropyl β-D-thiogalactopyranoside; PAGE, polyacrylamide gel electrophoresis; PCR, polymerase chain reaction; PVDF, polyvinylidene fluoride; SDS, sodium dodecyl sulfate; SCC, super-critical concentration; ThT, thioflavin T; Tris, tris(hydroxymethyl)aminomethane

* Corresponding author.
** Corresponding author. Tel.: +45 20 72 52 38; fax: +45 86 12 31 78.
E-mail addresses: taru.deva@gmail.com (T. Deva), dao@inano.au.dk (D.E. Otzen).

1570-9639/$ – see front matter © 2013 Elsevier B.V. All rights reserved.
http://dx.doi.org/10.1016/j.bbapap.2012.12.020

concentrations (>3.5 mg/mL). Fibrillation is retarded by the formation of a soluble, protease-resistant oligomer with native-like structure. Simple kinetic modeling suggests that such an oligomer can only arise at high concentrations if oligomer formation competes with monomeric conversion of S6 to a state that is committed to the fibrillar pathway. Although S6 fibrillation and oligomerization occur at low pH and elevated temperature (42 °C), we propose that other proteins may be able to undergo similar fibril-inhibiting oligomerization under physiological conditions.

2. Experimental procedures

2.1. Preparation of mutant S6-D55A

This was done using QuikChange as described [13] with the modification that the enzyme used for PCR was Herculase Enhanced DNA polymerase (Stratagene, CA). The D55A mutation was confirmed by sequencing selected clones. S6-WT and S6-D55A were expressed after transformation in BL21(DE3) and induction with 1 mM IPTG or with autoinduction [18].

2.2. S6 purification and fibrillation

S6-WT was purified as described [13], except for the change that the clarified cell lysate was loaded directly on a CM sepharose equilibrated in 50 mM Tris, pH 7.5 (GE Healthcare Life Sciences) and precipitation with ammonium sulfate was not carried out. Due to a significantly higher p*I* value of the S6-D55A mutant, S6-D55A bound to CM-Sepharose column and was subsequently eluted by a linear gradient of NaCl in 50 mM Tris (pH 7.5) at ~0.6 M NaCl. The fractions containing S6-D55A were pooled and dialyzed against 50 mM ethanolamine (pH 9.5) and the cleared dialysate subsequently applied onto a 1 mL HiTrap Q Sepharose Fast Flow column (GE Healthcare Life Sciences). Bound proteins were eluted by a linear gradient of NaCl in ethanolamine (pH 9.5). Purified S6-WT and S6-D55A were dialyzed against Milli-Q water, lyophilized and stored at −20 °C. For fibrillation assays, black, clear-bottomed microtiter plates (Nalgene Nunc) were used. As it is generally difficult to obtain reproducible data for S6 fibrillation (probably because of the long incubation times needed for fibrillation), experiments were conducted with and without the addition of 1 glass beads (dia.: 3 mm) per plate-well to check for improved reproducibility of S6 fibrillation. Appropriate amounts of lyophilized protein were then weighed out and dissolved in deionized water. The solution was filtered through 20 μM filter. Protein concentration was determined using absorbance at 280 nm using a theoretical extinction coefficient. Appropriate buffer stock solutions were used to obtain the desired pH and NaCl concentrations. Standard fibrillating conditions were 10 mM HCl and 0.4 M NaCl (pH 2). To the protein (100 μL), 40 μM ThT (2 μL of 2 mM filtered stock) was added and 150 μL of the solution was transferred to an empty or glass bead containing wells of the microtiter

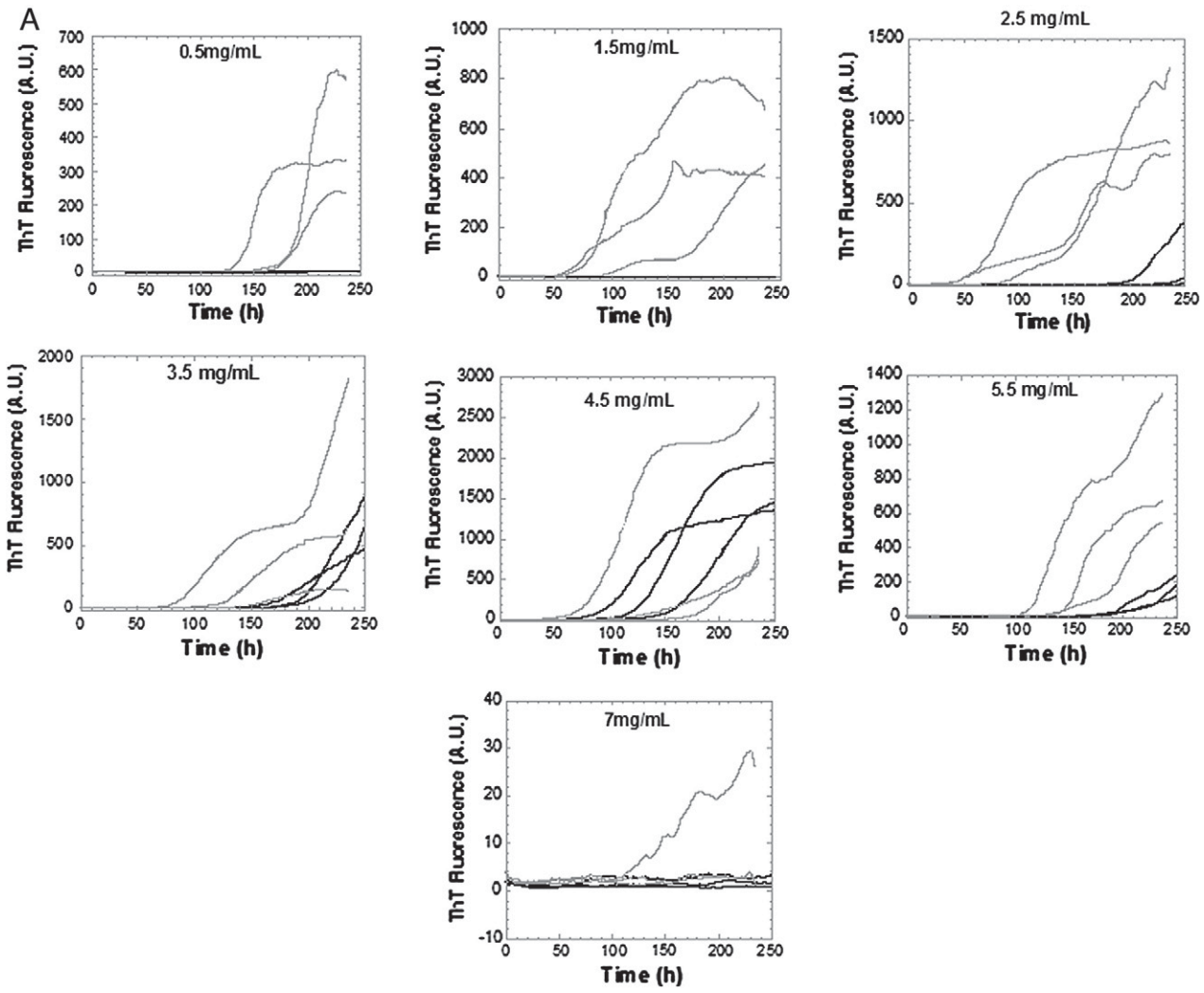

Fig. 1. Fibrillation profiles A) without glass beads and B) with glass beads for S6-WT at different protein concentrations. Data from 6 samples (2 experimental repeats) at each concentration. Plate 1 — black lines, plate 2 — gray lines. C) Average lag-times for S6-WT fibrillation without and with glass beads.

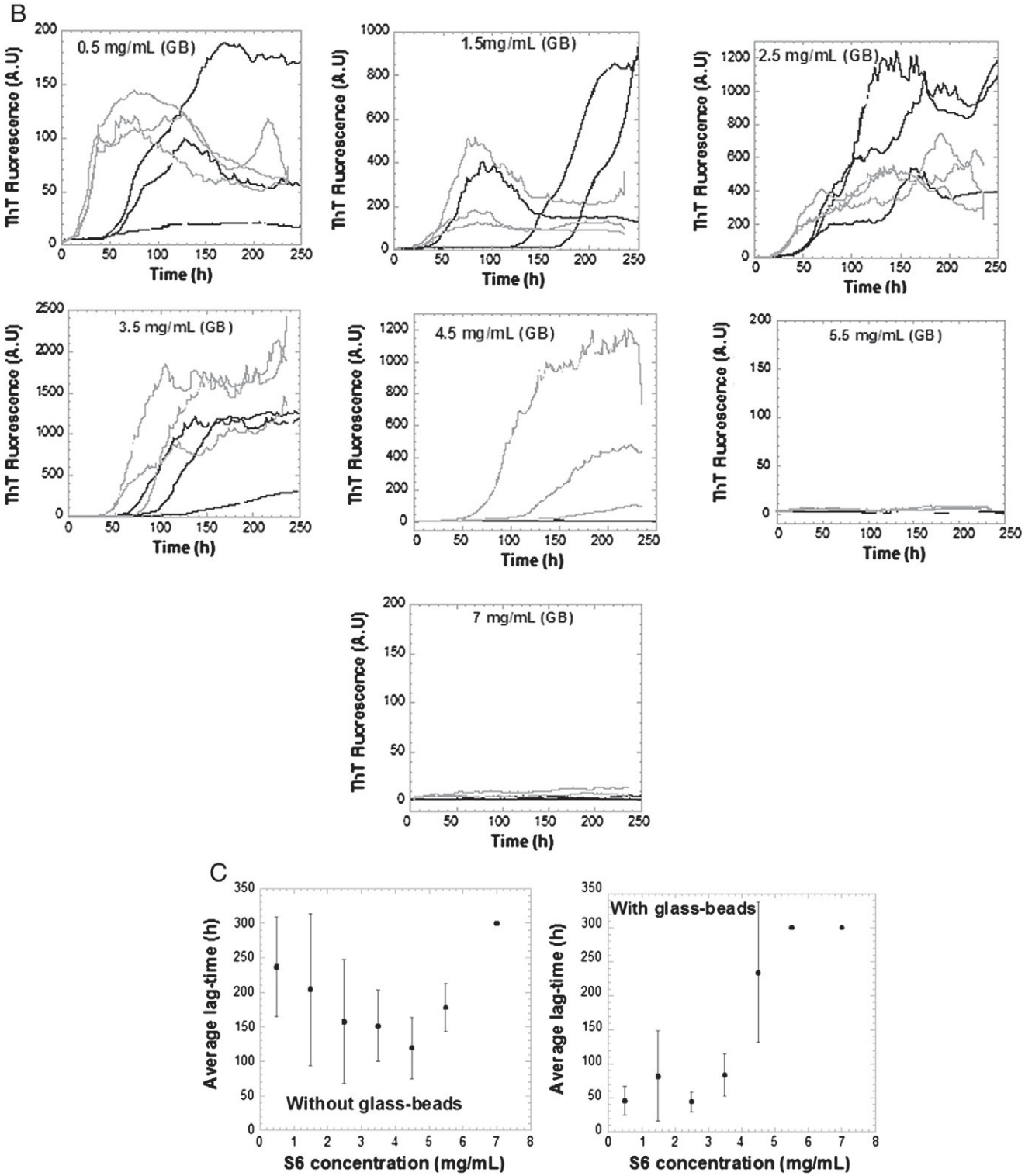

Fig. 1 (*continued*).

plate. The solution was incubated in the plate after sealing immediately with plate sealing tape (Nalgene Nunc). Fibrillation was monitored by concomitantly measuring ThT fluorescence using a Tecan Genios Pro microplate reader. Each protein condition was measured in 2 experimental replicates (conducted at different times) with a total of 6 replicates per sample. Measurements were made at 42 °C at 20 min intervals with 3 min shaking (99 rpm) between readings.

2.3. Fibril self- and cross-seeding

A seed stock of fibrils was prepared by suspending fibrils obtained at 2.5 mg/mL into fresh fibrillation buffer (10 mM HCl and 0.4 M NaCl) followed by sonication. Freshly dissolved protein at 3.5 or 7.0 mg S6/mL was seeded with 1% (w/v) of the seed stock prepared from sample fibrillated at 3.5 mg/mL. Likewise, the 7 mg/mL sample, having passed through fibrillating conditions, was sonicated to any

resuspend precipitated material and used at 1% (w/v) to seed S6 samples at 3.5 mg/mL or 7 mg/mL monomer concentration. The samples were incubated as described in the previous section.

2.4. Far-UV Circular Dichroism (CD)

Far-UV CD spectra were recorded on a Jasco J-810 spectropolarimeter (Jasco Spectroscopic Co. Ltd.). Ellipticity was measured at 25 °C and five accumulations were averaged to yield the final spectrum. A 1.0 or 0.2 mm path length cuvette was used for 0.5 mg S6/mL and a 0.2 mm path length cuvette for higher protein concentrations. The contribution to the ellipticity by the buffer used was subtracted as blank. The mean residue ellipticity (MRE) was expressed as deg cm^2 $dmol^{-1}$ $residue^{-1}$. For comparison, data at different protein concentrations were normalized to the lowest MRE.

2.5. Atomic force microscopy (AFM)

Fibril samples were diluted to 0.01–0.001 mg/mL and 10 μL of sample was deposited on freshly cleaved mica (SPI supplies, West Chester, PA). After drying, the sample was washed once with deionized water to remove salt residues. The samples were then dried for AFM analysis. The images were acquired at room temperature (25 °C) with an Agilent 5100 AFM (Agilent Technologies, Santa Clara, CA) in acoustic AC mode, equipped with a Tap190-G cantilever, frequency 190 kHz, force constant 48 N/m (Innovative Solutions Bulgaria Ltd., Sofia, Bulgaria). The ratio of the set point amplitude to the free amplitude (A/A_0) wαSN maintained at 0.9. The scanning speed wαSN set to 0.5 lines/second with an image resolution of 1024×1024. The AFM Images were analyzed using the open source software Gwyddion [48].

2.6. ATR-FTIR spectroscopy

Spectra were recorded on a Bruker Tensor 27 infrared spectrometer (Bruker Optik GmbH) with a Specac Golden Gate single-reflection ATR unit (Specac Ltd.). Protein was dried under a gentle stream of nitrogen prior to data acquisitions. Data were processed with atmospheric compensation and baseline subtraction. For comparison, data recorded at different protein concentrations were normalized to the largest absorption peak.

2.7. Dynamic light scattering (DLS)

DLS experiments were carried out at 20 °C using a PDDLS Batch/Coolbatch Dynamic Light Scattering Instrument (Precision Detectors Inc.).

2.8. Calculation of the amount of non-fibrillated/non-aggregated protein

These experiments were carried out for plates both with and without glass beads. Two wells at each concentration were used as duplicate samples. One hundred microliters of samples were withdrawn from each well. Samples were centrifuged at 13400 rpm for 10 min. in a microcentrifuge. The supernatant was measured (each reading taken twice) for absorbance at 280 nm and protein concentration calculated using the theoretical extinction coefficient for S6-WT.

2.9. Pepsin digestion

Pepsin digestion was carried out at different concentrations of S6 at pH 2 with 0.4 M NaCl prior to fibrillation. Samples were incubated with 5% w/w pepsin at 37 °C. Incubation was carried out for 3 h and the samples were subsequently electrophoresed on a 15% SDS–PAGE gel.

2.10. N-terminal sequencing

The digested samples were mixed with sample buffer and heated to 95 °C, separated by Tris-Tricine gel electrophoresis [19] and electroblotted to a PVDF membrane using Towbin buffer (25 mM Tris, 192 mM glycine, 20% methanol, pH 8.3) containing 0.01% SDS. Bands were visualized by Coomassie Brilliant Blue staining, excised and analyzed by automated Edman degradation using a Procise 494HT amino acid sequencer (Applied Biosystems) with on-line phenylthiohydantoin analysis.

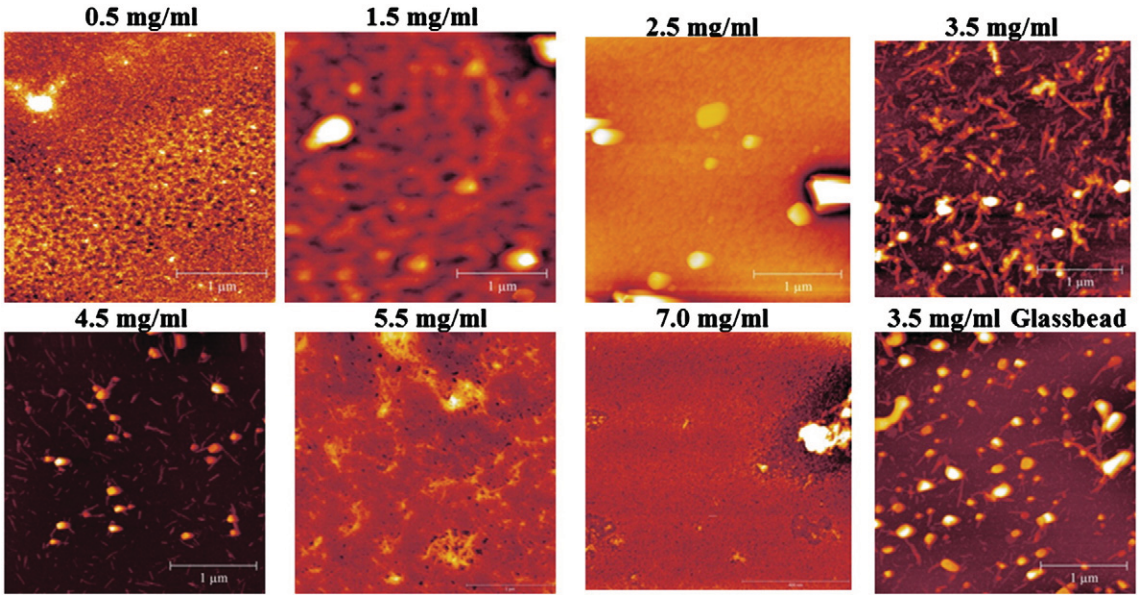

Fig. 2. Atomic force microscopy of S6-WT at different concentrations after 250 hrs exposure to fibrillation conditions. a) 0.5 mg/mL, b) 1.5 mg/mL, c) 2.5 mg/mL, d) 3.5 mg/mL, e) 4.5 mg/mL, f) 7 mg/mL.

Table 1
Statistics of fibrils formed at different concentrations of S6 protein as measured by AFM.

S6 concentration (mg/mL)	Fibrils	Fibril thickness (nm)	Fibril length (nm)	Fibril height (nm)
0.5	−	N.A.	N.A.	N.A.
1.5	−	N.A.	N.A.	N.A.
2.5	−	N.A.	N.A.	N.A.
3.5	+	40–80	200–500	7–20
4.5	+	30–40	50–300	5–8
5.5	+	40–50	1000+	8–10
7.0	−	N.A.	N.A.	N.A.
3.5 (GB)[a]	+	30–40	150–500	8–16

[a] With glass beads.

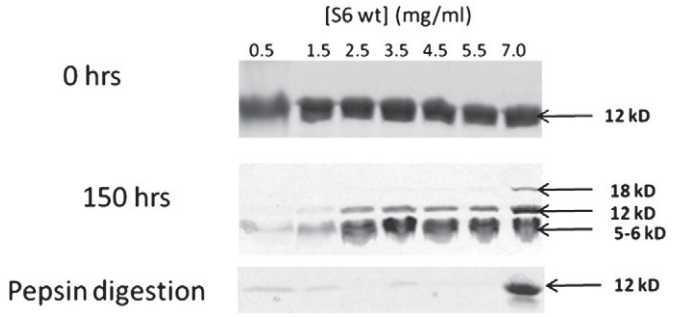

Fig. 3. SDS–PAGE of S6-WT just prior to incubation under fibrillation conditions (top panel), after 150 h incubation under fibrillation conditions (middle panel), and after 3 h of incubation with 5% w/w pepsin at 37 °C (bottom panel). The same amount of S6 was loaded in each lane.

3. Results

3.1. Wild type S6 fibrillation is inhibited above 5 mg/mL

Our previous work focused on the fibrillation at 0.5–1 mg/mL protein [16], but did not investigate the impact of protein concentration on the fibrillation process. Concentrations of S6 ranging from 0.5 to 7 mg/mL (0.5, 1.5, 2.5, 3.5, 4.5, 5.5, 7 mg/mL) were therefore checked for the tendency to fibrillate as monitored by measuring ThT fluorescence. Fig. 1A and B show the fibrillation curves obtained in the two experimental setups, with and without glass beads. Firstly, it can be observed that there is a greater difference between the two experimental repeats (plates 1 and 2) without glass beads. This difference is reduced to a large extent by addition of glass-beads to the plate-wells. Plots of average lag-times against S6 concentration without and with glass beads (Fig. 1C) also show the impact of glass-beads on reproducibility of fibrillation lag-times. Secondly, from 0.5 mg/mL to 3.5 mg/mL S6, as expected, there was an increase in fibrillation as indicated by a general increase in the fluorescence intensity (Fig. 1A, B). Unexpectedly, at 4.5 mg/mL, replicates from one plate and at 5.5 mg/mL and 7 mg/mL the replicates from both plates did not fibrillate at all in the 250 h period. A plot of the average lag-times of fibrillation against S6 concentration (Fig. 1C) also shows that as the concentration increases above 3.5 mg/mL, there is an increase in average lag-time. We have chosen 300 h as the arbitrary lag-time for the samples that failed to fibrillate within 250 h. In the experiment with glass beads, one sample that did not fibrillate at 0.5 mg/mL until 250 h was rejected as it failed Dixon's Q test at 99% confidence level. These observations intrigued us and prompted further investigations.

We will use the term C_{FR} to denote the concentration at which fibrillation is inhibited or retarded (here, 3.5 mg/mL for S6-WT).

AFM imaging of S6 samples from plate 1 without glass beads allowed to fibrillate for 250 h (Fig. 2) followed the ThT fluorescence pattern of the plate (Fig. 1A-black lines). The samples at 0.5–2.5 mg/mL did not show any presence of fibrils, samples at 3.5–5.5 mg/mL had fibrils, while the sample at 7 mg/mL showed only few large amorphous aggregates. Slightly thinner fibrils were formed at 4.5 and 5.5 mg/mL as compared to 3.5 mg/mL, and were appreciably longer at 5.5 mg/mL (Table 1).

3.2. S6 undergoes acid cleavage but this is not essential for fibrillation

Fibrillation of S6 occurs at low pH and elevated temperatures which could affect the covalent integrity of S6. We investigated this using SDS–PAGE. Although samples were electrophoresed immediately after the solubilization of protein at different concentrations, all samples showed a very faint lower molecular weight band (Fig. 3). However, the majority of protein material was initially uncleaved (Fig. 3 top panel). After 150 h of incubation, a large proportion of the intact protein was converted into two lower molecular weight bands (Fig. 3 middle panel). The 101 amino acid residue S6 contains an Asp–Pro bond (residues 55–56), which is known to be particularly sensitive to acid hydrolysis. The sizes of the two predicted fragments (~5 and ~6 kDa) agree well with the observed bands. N-terminal sequencing confirms this, identifying Met1 and Pro56 as the N-terminal residues of the 6 and 5 kDa bands, respectively. A high molecular weight band (~18 kDa) is also observed at most concentrations, particularly for the 7 mg/mL sample which, in this set of experiments, did not show any fibrillation or visible aggregate formation up to 150 h. N-terminal sequencing of the 18 kDa band proved it to be S6 with the N-terminal residues being MRRYEVN just as for intact S6. The 18 kDa band could thus either be an alternate conformation of the full length S6 or a trimer of cleaved fragments.

It would seem reasonable to assume that acid hydrolysis and formation of two flexible fragments of the original intact protein could promote fibrillation. However, we have two different lines of evidence to suggest that fibrillation is not linked to acid hydrolysis. Firstly, not all acid-cleaved S6 fibrillates. Although S6 is cleaved at pH 2.6 (Suppl. Fig. 1A), it shows a reduced tendency to form fibrils at this pH (Suppl. Fig. 1B). Secondly, hydrolysis-resistant S6 can fibrillate. This was demonstrated by constructing the mutant S6-D55A which is resistant to acid hydrolysis as demonstrated by SDS–PAGE (Fig. 4). While S6-D55A fibrillated better and with progressively shorter lag times at 2.5, 4.5 and 7 mg/mL (unlike S6 WT), it showed significantly retarded fibrillation at 14 mg/mL (Fig. 5A,B). The morphology of S6 D55A fibrils formed at 2.5–4.5 mg/mL was also very similar to that of S6 WT (data not shown).

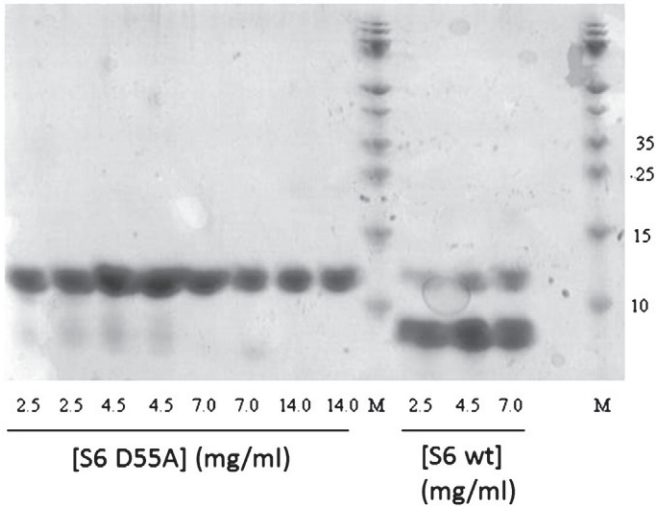

Fig. 4. SDS–PAGE of cleavage-mutant S6-D55A and native S6-WT at different protein concentrations after 150 h incubation.

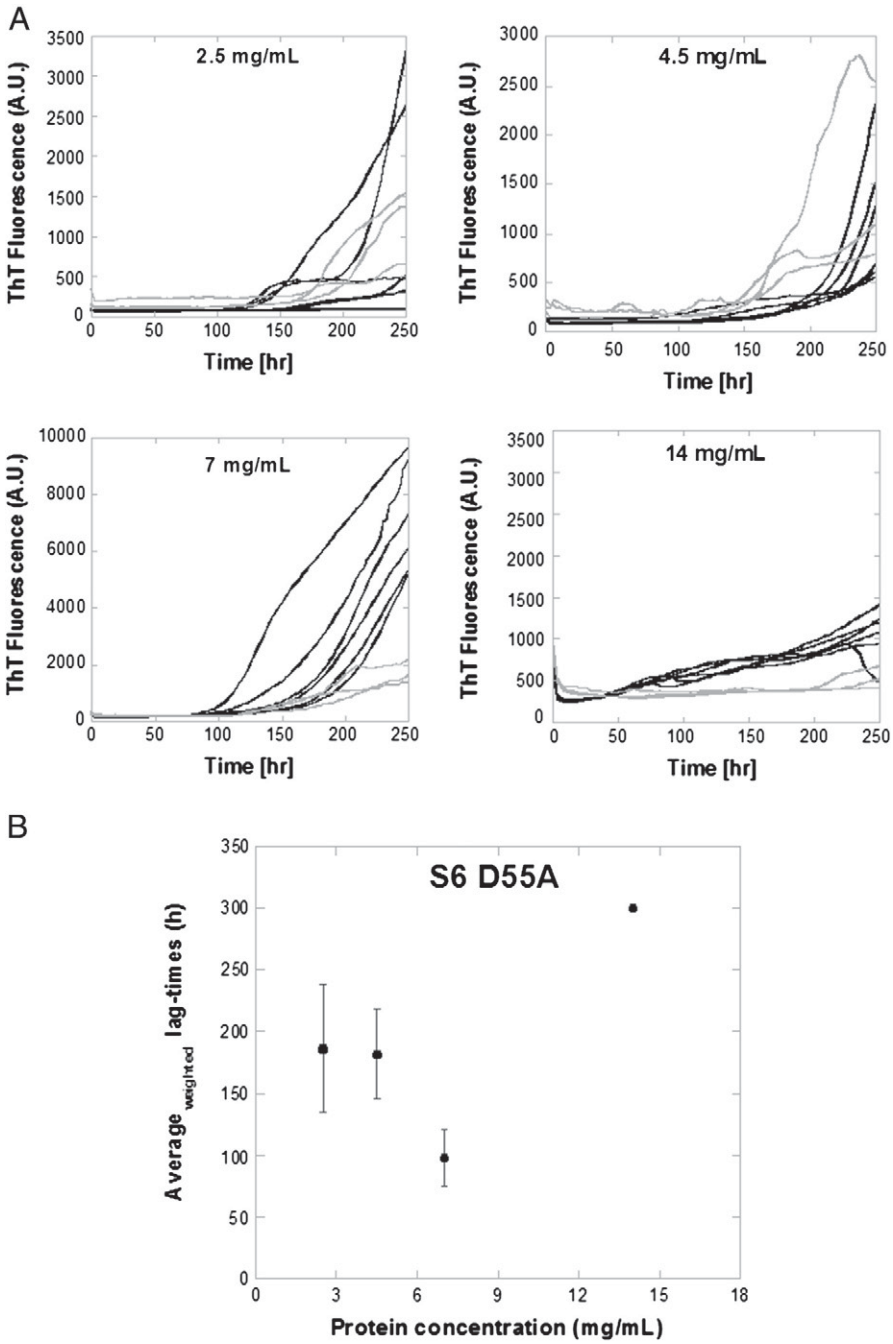

Fig. 5. A) Fibrillation profiles for S6-D55A at different protein concentrations. Data from 9–12 samples (2 experimental repeats) at each concentration. Plate 1 — black lines, plate 2 — gray lines. B) Average lag-times of S6-D55A fibrillation at different protein concentrations.

3.3. Pre-fibrillar S6 does not undergo concentration-dependent changes in secondary structure but forms large protease-resistant aggregates at higher concentrations

To check whether the inhibition of fibrillation at high concentrations could be related to changes in secondary structure, far-UV CD and FTIR spectra were recorded immediately after the protein was solubilized at conditions for fibrillation. The far-UV CD spectra were representative of non-fibrillated protein and there was no major change in the secondary structural profiles with change in protein concentration (Fig. 6A), although the spectra at 5.5–7 mg/mL S6 showed a 10–15% decrease in ellipticity (as was observed in data before normalization — Suppl. Fig. 2). The simplest explanation for this decline in signal is light scattering. This could indicate that soluble or suspended aggregates are present right from the start at higher protein concentrations. Likewise, FTIR spectra presented profiles representative of non-fibrillated protein and with no major changes in the secondary structure dependent on protein concentration (Fig. 7A). To see if there were changes in secondary structure after the samples passed through fibrillation conditions, a typical sample at each concentration (and a fibrillated sample at 7 mg/mL) was subjected to CD and FTIR. The spectra showed change in secondary structure profile more representative of β-sheet rich fibrillated/aggregated protein, involving a minimum around 218 nm in far-UV CD spectra (Fig. 6B) and a peak around 1628 cm^{-1} in FTIR (Fig. 7B), which is typical of amyloid structures [20].

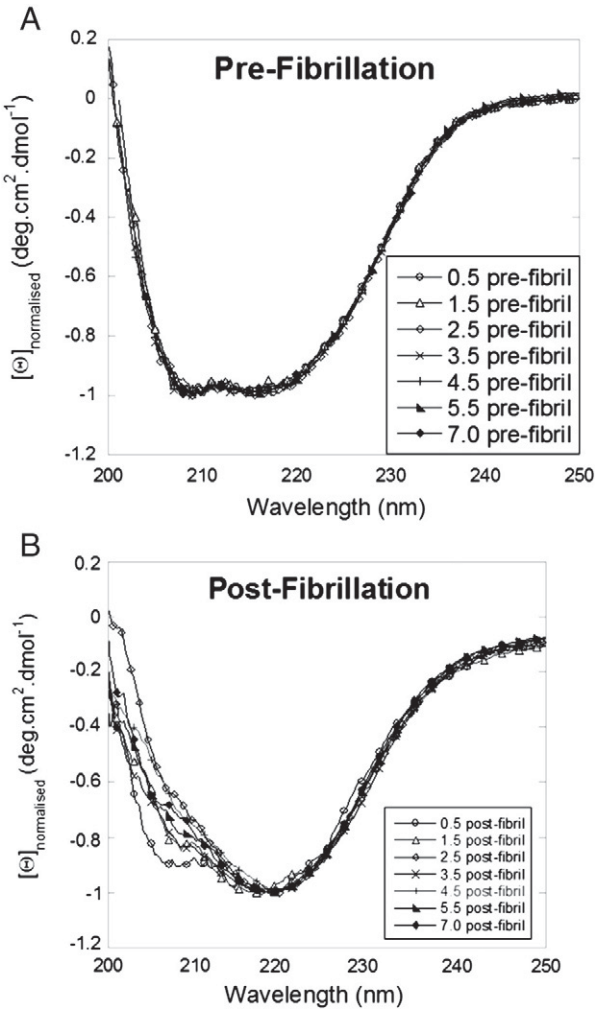

Fig. 6. Normalized CD spectra of S6-WT at different concentrations A) before fibrillation and B) after fibrillation. Open circles — 0.5 mg/mL, open triangles — 1.5 mg/mL, open diamonds — 2.5 mg/mL, cross — 3.5 mg/mL, plus — 4.5 mg/mL, filled triangles — 5.5 mg/mL, filled diamonds — 7 mg/mL.

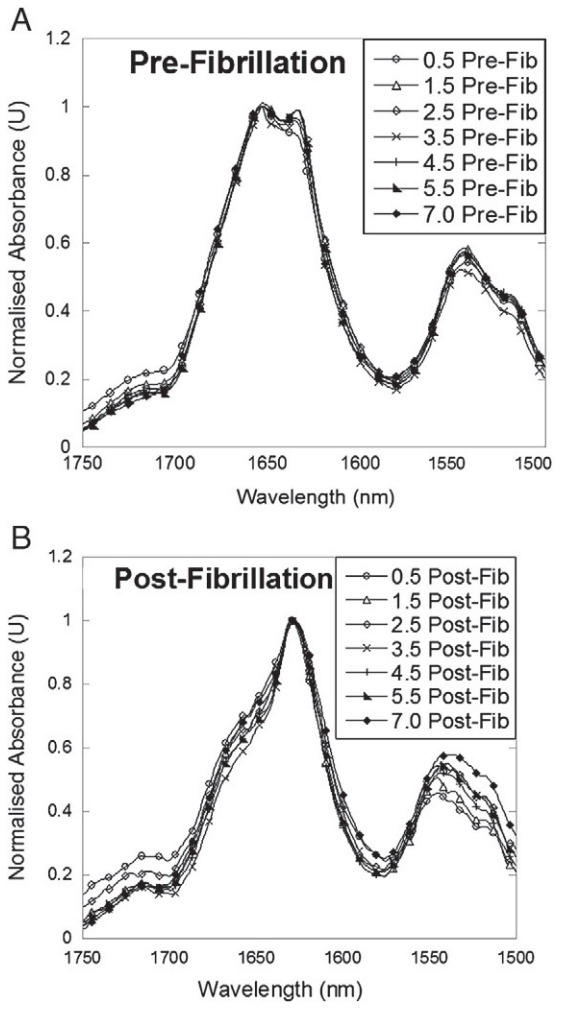

Fig. 7. Normalized ATR-FTIR spectra of S6-WT at different concentrations A) before fibrillation and B) after fibrillation. Open circles — 0.5 mg/mL, open triangles — 1.5 mg/mL, open diamonds — 2.5 mg/mL, cross — 3.5 mg/mL, plus — 4.5 mg/mL, filled triangles — 5.5 mg/mL, filled diamonds — 7 mg/mL.

S6 oligomer formation could not be detected by gel filtration, most likely because dilution to low concentrations (which is unavoidable during gel filtration) leads to the dissociation of the oligomeric species. Instead, we turned to dynamic light scattering to investigate formation of larger size aggregates at higher concentrations of S6 (Table 2). Up to 2.5 mg/mL, S6 was mainly present as monomer and larger molecular sizes were almost negligible in these samples. As the concentration of the protein increased, the percentage of larger size species increased. At concentrations of 7 mg/mL, DLS could not be carried out due to bad correlation values. Nevertheless, in the experiments at 7 mg/mL concentrations where no fibrillation occurred even after 200 h incubation under conditions for fibrillation, no visible aggregation was observed. Thus, the aggregates formed at C_{FR} are large but soluble.

We also calculated the amount of non-fibrillated/non-aggregated sample remaining after the samples were put through fibrillating conditions. There were very low amounts of non-fibrillated/non-aggregated protein in the ThT positive wells while there was much more of such protein in ThT negative wells (Fig. 8). This also confirms the soluble nature of aggregates formed at higher protein concentration.

Sensitivity to proteolysis using a non-specific protease such as pepsin can be a useful way to test the dynamics of a protein conformation. Significantly, S6 is completely degraded by the aspartic protease pepsin at S6 concentrations below 7 mg/mL but is remarkably resistant at 7 mg/mL (Fig. 3, lower panel). This suggests that the oligomeric species which forms at the high S6 concentrations organizes itself into structures that are significantly less dynamic than the monomers that dominate at lower concentrations.

3.4. Slow-fibrillating S6 at C_{FR} undergoes fibrillation on seeding

Another way to investigate the relationships between aggregates formed at different concentrations of S6 is to test their ability to affect each other's aggregation. On seeding fresh S6 samples at 3.5 mg/mL with seed stock from fibrils formed at 3.5 mg/mL, the lag time of fibrillation drastically decreased and start of fibrillation was almost instantaneous (Fig. 9A). On cross-seeding fresh 7 mg/mL samples

Table 2
Dynamic light scattering data for S6 WT at different concentrations at pH 2.0, 0.4 M NaCl immediately after solubilization in fibrillation solution (pH 2.0, 0.4 M NaCl).

Protein conc. (mg/mL)	R_h^{major} (nm)[a]	% with size >4 nm
1.5	2.13	0.004
2.5	2.5	1
3.5	2.9	8.2
4.5	2.8	13
5.5	3.01	17
7.0	_[b]	_[b]

[a] Hydrodynamic radius of the majority species in solution.
[b] Could not be determined due to bad correlation values.

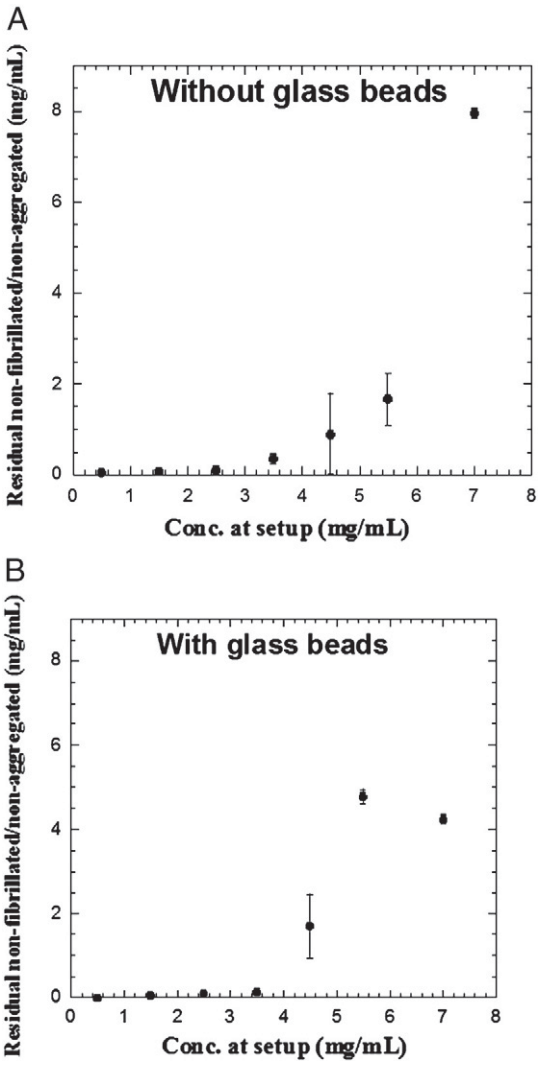

Fig. 8. Residual protein that has not fibrillated or formed insoluble aggregates at different protein concentrations after exposure to fibrillating conditions. Average residual protein concentration is plotted against protein concentration prior to exposure to fibrillating conditions.

with seeds from 3.5 mg/mL there was a marked acceleration in fibrillation (Fig. 9B). In contrast, cross seeding of 3.5 mg/mL monomer with of 7 mg/mL aggregate stock actually ended up retarding fibrillation (Fig. 9C). When fresh samples at 7 mg/mL were self-seeded with 7 mg/mL seed stock, there was no effect and there was no fibrillation observed in the 250 h time-period (Fig. 9D).

4. Discussion

4.1. An unusual case of fibril inhibition at high concentrations

Protein concentration is an important parameter in protein aggregation. Increasing protein concentration generally leads to an increased rate of fibrillation along with a reduction in the length of the lag phase [21,22]. Often self assembling oligopeptides need to exceed a critical aggregation concentration (CAC) to polymerize and form fibrils [11]. Above the CAC, peptides and proteins can form micellar structures that are on-pathway to fibril formation and act as monomer reservoirs. CAC is distinct from the phenomenon of supercritical concentration (SCC), above which it becomes thermodynamically favorable for the protein to form structural nuclei that seed the fibrillation reaction [23]. Concentrations above the SCC of the peptide/protein result in no further reduction in the lag time of fibril formation [24].

The present study on the fibrillation of the model protein S6 reveals an unexpected inhibitory effect of concentrations above ca. 3.5 mg/mL (0.29 mM) on the fibrillation of S6. We report this effect in terms of the lag-times of fibrillation. Formation of fibrillation nuclei is energetically unfavorable and is suggested to be a stochastic process [25,26]. High variance in lag times in fibrillation studies is attributed to a dependence on a small number of nuclei forming events [25,26]. Hence, the large variations in the lag-times as observed in our data of fibrillation are not surprising — especially considering the fact that these data are from experimental repeats carried out at different time. We have been able to reduce this variability to a certain extent by addition of glass beads to the plate-wells.

An inverse relationship between protein concentration and rate of fibrillation has previously been demonstrated in the case of immunoglobulin light chain (LEN) [27], though in this case there is a monotonic decrease in fibrillation propensity with an increase in protein concentration which is related to dimer formation in the native state. In contrast to this, we observed for S6 that up to ~3.5 mg/mL the kinetics and extent of fibrillation increase with protein concentration; however, above this concentration there is an inverse relationship. Inverse relationship between protein concentration and agitation induced aggregation has been reported previously [28], where the authors propose the air–water interface to be the factor responsible for this effect. However, as for LEN, an increase in concentration leads to a monotonic decrease in aggregation. In contrast, although a reduction in fibril formation was apparent, light scattering results revealed that S6 existed at higher concentrations as soluble larger molecular weight oligomers. Although no significant conformational change was observed in the pre-fibrillar stages, the higher molecular weight species formed at high protein concentrations were much less sensitive to proteolysis compared to S6 at lower protein concentrations.

4.2. Acid cleavage is not important for fibrillation

We also observed that the S6-WT protein underwent peptide bond cleavage at pH 2 to form two similarly sized peptides. Gratifyingly, this cleavage did not affect fibrillation in the low-concentration range as shown by non-hydrolyzable S6-D55A, and thus does not affect our previous comprehensive protein engineering study of S6 fibrillation [16]. Interestingly, S6-D55A fibrillation was only significantly retarded at twice the concentration where this occurs for S6-WT. The difference in C_{FR} could be due to subtle changes wrought by the substitution. Our previous protein engineering work on S6 show that fibrillation lag times can be heavily affected by hydrophobic truncation mutations [16]. The Asp-to-Ala substitution could have an effect for steric reasons. It remains to be elucidated whether this effect is caused by the exposure of hydrophobic residues in the pH cleaved form of S6, leading to easier formation of the off-pathway aggregates, or by other factors.

Protein assembly and aggregation can be influenced by factors such as macromolecular crowding caused, for example, by the presence of long-chain polymers, which generally encourage association due to excluded volume effects [29–31]. At very high concentrations (typically above 10 weight percent) the consequent increase in viscosity can have a negative effect [29]. However, the concentrations of S6 used in our studies are in all cases well below 1 weight percent. Solution viscosity increases linearly up to 10 weight percent protein [32], so that 7 mg/mL protein increases viscosity only roughly 50% compared to the pure buffer. Also, a simple viscosity effect cannot explain the rescuing effect of addition of seeds to the 7 mg/mL solution with a dilution of only 0.2–2% attributed to the addition of seeds. Finally, from the fibrillation profiles of S6-D55A, it can be seen that this mutant undergoes fibrillation even at 7 mg/mL concentration and the inhibitory effect is observed only at 14 mg/mL, thus providing further evidence that viscosity effects are not responsible for the inhibition of fibrillation at these concentrations.

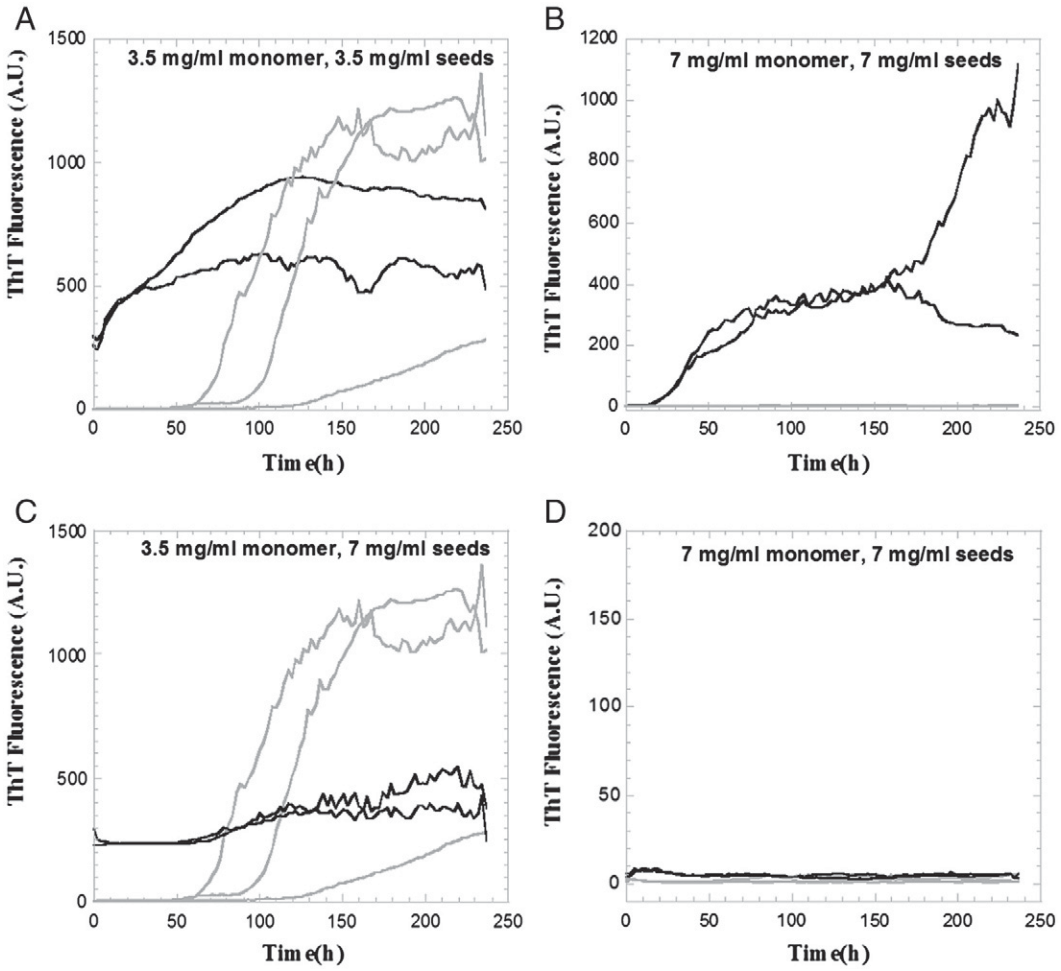

Fig. 9. Self- and cross-seeding of S6 samples at 2.5 mg/mL and 7 mg/mL concentrations. A) S6-WT monomer at 3.5 mg/mL unseeded (gray lines), or seeded with 1% (w/v) seed stock derived from fibrillated sample at 3.5 mg/mL (black lines). B) S6-WT monomer at 7 mg/mL, unseeded (gray lines), or seeded with 1% (w/v) seed stock derived from fibrillated sample at 3.5 mg/mL (black lines). C) S6-WT monomer at 3.5 mg/mL unseeded (gray lines), or seeded with 1% (w/v) seed stock derived from fibrillated sample at 7 mg/mL. D) S6-WT monomer at 7 mg/mL, unseeded (gray lines), or seeded with 1% seed stock derived from fibrillated sample at 7 mg/mL (black lines).

4.3. A model for C_{FR}: a bifurcating aggregation pathway with a monomeric conversion step

A model to explain our data, which includes competition between formation of finite-sized oligomers and fibrils of infinite length, has to include the observation that the off-pathway oligomer, only dominates at high protein concentrations. Using simulation software provided by KinTek [33] we find that this can be attained in model that involves a bifurcation between the two aggregation pathways, provided there is a pre-aggregation monomer conversion step in the fibrillation part of the pathway (scheme illustrated in Fig. 10). Such a monomer conversion step will not be favored by increasing protein concentration, in contrast to the competing oligomerization step. We assume this conversion step, for which we do not have direct experimental evidence, occurs on prolonged exposure to pH 2 and high ionic strength. The transformed monomer feeds into the structured nucleus which upon incorporation of additional transformed monomers grows into bona fide fibrils. In our model, this transformation step is not required for the formation of the off-pathway oligomer. Thus, at sufficiently high concentrations of S6, the monomers will be siphoned off to the off-pathway oligomer to an extent that reduces the concentration of transformed monomers so much that nucleation and fibril growth will be very slow and can easily exceed the experimental observation time.

We also observe that S6 at C_{FR} can undergo more rapid fibrillation upon seeding with seeds of fibrils formed below C_{FR} (Fig. 9A,B). This can be explained by considering that the addition of seeds (and thus of preformed nuclei) can shift the equilibrium away from the off-pathway oligomer towards the monomer, simply by incorporating transformed monomers into the pre-made fibrils and thus pulling the equilibrium towards the transformed monomer. The result is fibrillation of the protein accompanied with a reduction of lag time. This assumes that the fibril dissociation rates are less rapid than oligomer dissociation, which appears reasonable due to the higher stability of fibrils and their lower rates of dissociation.

On the other hand, addition of oligomer seeds obtained from samples incubated above C_{FR} tended to retard fibrillation of samples below C_{FR} (Fig. 9C,D), indicating that oligomers can also directly interfere with the fibrillation process, perhaps by sequestering monomers and preventing their transformation.

Powers and Powers [34] have provided an elegant mathematical model for nucleated polymerization (fibril formation) and competing off-pathway aggregation. They propose that off-pathway aggregates will tend to retard fibril formation and can cause the fibril formation to have reverse concentration dependence. Our data on S6 fibril formation agree with and provide experimental evidence for the model. Viewed in this light, we conclude that the C_{FR} for LEN [27] is much lower than that of S6 due to the formation of stable dimers, and thus the formation of off-pathway aggregates takes place at much lower

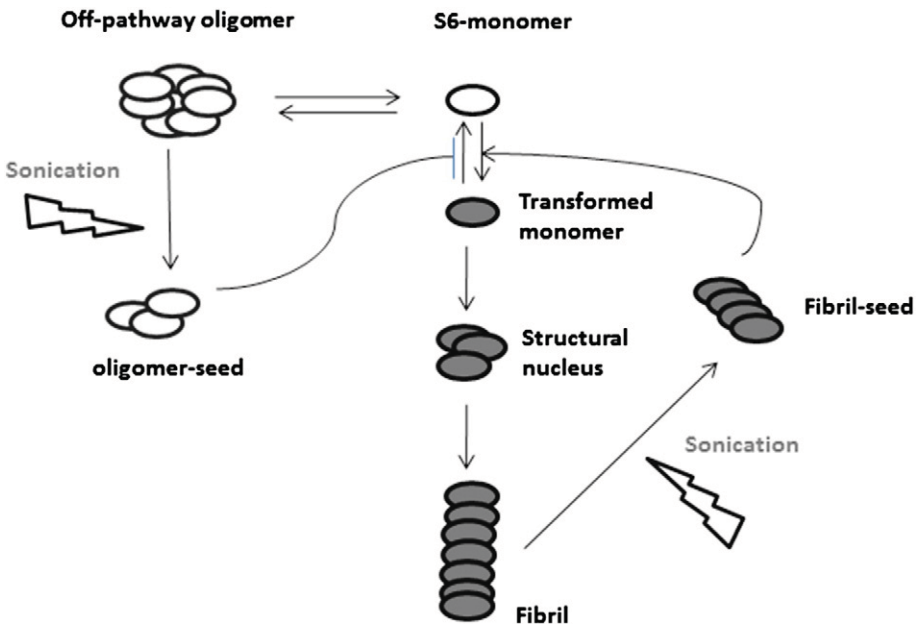

Fig. 10. Model for formation of off-pathway oligomers at high S6 concentration which inhibits fibrillation. There is a bifurcation between off-pathway oligomers and the fibrillation pathway which we suggest to be delimited by a monomer conversion step.

concentrations for LEN than those that are required for S6. It would be interesting to find out the minimum concentration limits for LEN fibril formation.

4.4. C_{FR} as an example of aggregate polymorphism

AFM studies showed that the fibrils formed by S6 at different protein concentrations were morphologically different. Fibrils formed at 3.5 mg/mL were thicker and shorter than those at 4.5 or 5.5 mg/mL, whereas the fibrils formed at 5.5 mg/mL were thinner and longer. This illustrates that there is aggregate polymorphism at several levels, not only in terms of competition between off-pathway oligomers and fibrils, but also between different types of fibrils, which could arise from different types of aggregates. We [35] and others [36–38] have reported numerous instances of such fibrillar polymorphism. The phenomenon probably arises from the lack of biological optimization of these types of protein–protein interactions [39] as well as polymer-like plasticity in the formation of different hydrogen-bonding registers [40].

4.5. Biological implications of C_{FR}

It will be interesting to see how other disease causing proteins behave at much higher concentrations than have been used experimentally to date to study the fibrillation process. Furthermore, C_{FR} may occur at physiologically accessible concentrations if cellular conditions promote the formation of these slow-fibrillating species. It is also important to note that C_{FR} leads to an absence of the easily detectable Thioflavin T fluorescence and will therefore not normally be detected in fibrillation studies, but will only be revealed if the studies are conducted over a broad range of concentrations. The obvious question is whether the oligomers formed at C_{FR} have physiological impact. Non-fibrillar oligomers rather than mature fibrils are generally believed to represent the cytotoxic species [41,42]. On the other hand, a given protein can form both toxic and benign oligomers, depending on the conditions. For α-synuclein, oligomers stabilized by e.g. dequalinium [43] or C-terminal cleavage [44] appear to be toxic whereas oligomers stabilized by baicalein [45] or catechins [46] are not, and similar conclusions may be made for HypF-N [47]. We have not been able to carry out membrane-permeabilizing studies with S6 using e.g., calcein-release assays due to the low pH and the high concentrations of protein required which induce non-specific membrane-disruption (data not shown). Nevertheless, although it is difficult to extrapolate from the S6 fibrillation environment to physiological conditions, it is noteworthy that the oligomer appears resistant to proteolysis. Oligomers formed by other proteins might similarly be proteolysis-resistant and thus resist the normal clearance mechanisms. Thus any cytotoxicity that such oligomers might possess could have significant consequences.

Supplementary data to this article can be found online at http://dx.doi.org/10.1016/j.bbapap.2012.12.020.

Acknowledgments

We are grateful to Hanne Krone Nielsen for S6 WT protein purification and thank Dr. Rajiv Vaid Basaiawmoit and Professor Niels Chr. Nielsen for useful discussions. We are grateful to the Danish National Research Foundation and the inSPIN Center for funding.

References

[1] C.M. Dobson, Protein misfolding, evolution and disease, Trends Biochem. Sci. 24 (1999) 329–332.
[2] L.C. Serpell, Alzheimer's amyloid fibrils: structure and assembly, Biochim. Biophys. Acta 1502 (2000) 16–30.
[3] J.M. Kenney, D. Knight, M.J. Wise, F. Vollrath, Amyloidogenic nature of spider silk, Eur. J. Biochem. 269 (2002) 4159–4163.
[4] M.R. Chapman, L.S. Robinson, J.S. Pinkner, R. Roth, J. Heuser, M. Hammar, S. Normark, S.J. Hultgren, Role of *Escherichia coli* curli operons in directing amyloid fiber formation, Science 295 (2002) 851–855.
[5] P. Larsen, M. Dueholm, G. Christiansen, J.L. Nielsen, D.E. Otzen, P.H. Nielsen, Amyloid adhesins are abundant in natural biofilms, Environ. Microbiol. 9 (2007) 3077–3090.
[6] D. Claessen, R. Rink, W. de Jong, J. Siebring, P. de Vreugd, F.G. Boersma, L. Dijkhuizen, H.A. Wosten, A novel class of secreted hydrophobic proteins is involved in aerial hyphae formation in Streptomyces coelicolor by forming amyloid-like fibrils, Genes Dev. 17 (2003) 1714–1726.
[7] S.K. Maji, M.H. Perrin, M.R. Sawaya, S. Jessberger, K. Vadodaria, R.A. Rissman, P.S. Singru, K.P. Nilsson, R. Simon, D. Schubert, D. Eisenberg, J. Rivier, P. Sawchenko, W. Vale, R. Riek, Functional amyloids as natural storage of peptide hormones in pituitary secretory granules, Science 325 (2009) 328–332.
[8] F.G. Pearce, S.H. Mackintosh, J.A. Gerrard, Formation of amyloid-like fibrils by ovalbumin and related proteins under conditions relevant to food processing, J. Agric. Food Chem. 55 (2007) 318–322.
[9] M. Carrio, N. Gonzalez-Montalban, A. Vera, A. Villaverde, S. Ventura, Amyloid-like properties of bacterial inclusion bodies, J. Mol. Biol. 347 (2005) 1025–1037.
[10] N. Motamedi-Shad, T. Garfagnini, A. Penco, A. Relini, F. Fogolari, A. Corazza, G. Esposito, F. Bemporad, F. Chiti, Rapid oligomer formation of human muscle

acylphosphatase induced by heparan sulfate, Nat. Struct. Mol. Biol. 19 (2012) 547–554, S541-542.
[11] S.Y. Fung, C. Keyes, J. Duhamel, P. Chen, Concentration effect on the aggregation of a self-assembling oligopeptide, Biophys. J. 85 (2003) 537–548.
[12] P. Hortscansky, T. Christopeit, V. Schroeckh, M. Fändrich, Thermodynamic analysis of the aggregation propensity of oxidized Alzheimer's beta-amyloid variants, Protein Sci. 14 (2005) 2915–2918.
[13] D.E. Otzen, O. Kristensen, M. Proctor, M. Oliveberg, Structural changes in the transition state of protein folding: alternative interpretations of curved chevron plots, Biochemistry 38 (1999) 6499–6511.
[14] D.E. Otzen, M. Oliveberg, Salt-induced detour through compact regions of the protein folding landscape, Proc. Natl. Acad. Sci. U. S. A. 96 (1999) 11746–11751.
[15] D.E. Otzen, Expansion during folding of a collapsed state, Biochim. Biophys. Acta 1750 (2005) 146–153.
[16] J.S. Pedersen, G. Christensen, D.E. Otzen, Modulation of S6 fibrillation by unfolding rates and gatekeeper residues, J. Mol. Biol. 341 (2004) 575–588.
[17] D.E. Otzen, O. Kristensen, M. Oliveberg, Designed protein tetramer zipped together with a hydrophobic Alzheimer homology: a structural clue to amyloid assembly, Proc. Natl. Acad. Sci. U. S. A. 97 (2000) 9907–9912.
[18] F.W. Studier, Protein production by auto-induction in high density shaking cultures, Protein Expr. Purif. 41 (2005) 207–234.
[19] H. Schägger, G. von Jagow, Tricine-sodium dodecyl sulfate-polyacrylamide gel electrophoresis for the separation of proteins in the range from 1 to 100 kDa, Anal. Biochem. 166 (1987) 368–379.
[20] G. Zandomeneghi, M.R. Krebs, M.G. McCammon, M. Fandrich, FTIR reveals structural differences between native beta-sheet proteins and amyloid fibrils, Protein Sci. 13 (2004) 3314–3321.
[21] V.N. Uversky, J. Li, A.L. Fink, Evidence for a partially folded intermediate in alpha-synuclein fibril formation, J. Biol. Chem. 276 (2001) 10737–10744.
[22] L. Nielsen, R. Khurana, A. Coats, S. Frokjaer, J. Brange, S. Vyas, V.N. Uversky, A.L. Fink, Effect of environmental factors on the kinetics of insulin fibril formation: elucidation of the molecular mechanism, Biochemistry 40 (2001) 6036–6046.
[23] E.T. Powers, D.L. Powers, The kinetics of nucleated polymerizations at high concentrations: amyloid fibril formation near and above the "supercritical concentration", Biophys. J. 91 (2006) 122–132.
[24] R. Sabate, J. Estelrich, Evidence of the existence of micelles in the fibrillogenesis of beta-amyloid peptide, J. Phys. Chem. 109 (2005) 11027–11032.
[25] J. Hofrichter, Kinetics of sickle hemoglobin polymerization. III. Nucleation rates determined from stochastic fluctuations in polymerization progress curves, J. Mol. Biol. 189 (1986) 553–571.
[26] V. Fodera, F. Librizzi, M. Groenning, M. van de Weert, M. Leone, Secondary nucleation and accessible surface in insulin amyloid fibril formation, J. Phys. Chem. 112 (2008) 3853–3858.
[27] P.O. Souillac, V.N. Uversky, I.S. Millett, R. Khurana, S. Doniach, A.L. Fink, Elucidation of the molecular mechanism during the early events in immunoglobulin light chain amyloid fibrillation. Evidence for an off-pathway oligomer at acidic pH, J. Biol. Chem. 277 (2002) 12666–12679.
[28] M.J. Treuheit, A.A. Kosky, D.N. Brems, Inverse relationship of protein concentration and aggregation, Pharm. Res. 19 (2002) 511–516.
[29] L.A. Munishkina, E.M. Cooper, V.N. Uversky, A.L. Fink, The effect of macromolecular crowding on protein aggregation and amyloid fibril formation, J. Mol. Recognit. 17 (2004) 456–464.
[30] M. Hayer-Hartl, A.P. Minton, A simple semiempirical model for the effect of molecular confinement upon the rate of protein folding, Biochemistry 45 (2006) 13356–13360.
[31] M.D. Shtilerman, T.T. Ding, P.T. Lansbury, Molecular crowding accelerates fibrillization of alpha-synuclein: could an increase in the cytoplasmic protein concentration induce Parkinson's Disease, Biochemistry 41 (2002) 3855–3860.
[32] P. Pradipasena, C. Rha, Effect of concentration on apparent viscosity of a globular protein solution, Polym. Eng. Sci. 17 (2004) 861–864.
[33] K.A. Johnson, Z.B. Simpson, T. Blom, Global Kinetic Explorer: a new computer program for dynamic simulation and fitting of kinetic data, Anal. Biochem. 387 (2009) 20–29.
[34] E.T. Powers, D.L. Powers, Mechanisms of protein fibril formation: nucleated polymerization with competing off-pathway aggregation, Biophys. J. 94 (2008) 379–391.
[35] J.S. Pedersen, D. Dikov, J.L. Flink, H.A. Hjuler, G. Christiansen, D.E. Otzen, The changing face of glucagon fibrillation: structural polymorphism and conformational imprinting, J. Mol. Biol. 355 (2006) 501–523.
[36] A.T. Petkova, R.D. Leapman, Z. Guo, W.-M. Yau, M.P. Mattson, R. Tycko, Self-propagating, molecular-level polymorphism in Alzheimer's β-amyloid fibrils, Science 307 (2005) 262–265.
[37] C. Goldsbury, P. Frey, V. Olivieri, U. Aebi, S.A. Müller, Multiple assembly pathways underlie amyloid-β fibril polymorphisms, J. Mol. Biol. 352 (2005) 282–298.
[38] H. Heise, W. Hoyer, S. Becker, O.C. Andronesi, D. Riedel, M. Baldus, Molecular-level secondary structure, polymorphism, and dynamics of full-length alpha-synuclein fibrils studied by solid-state NMR, Proc. Natl. Acad. Sci. U. S. A. 102 (2005) 15871–15876.
[39] J.S. Pedersen, D.E. Otzen, Amyloid—a state in many guises: survival of the fittest fibril fold, Protein Sci. 17 (2008) 1–9.
[40] R. Kodali, R. Wetzel, Polymorphism in the intermediates and products of amyloid assembly, Curr. Opin. Struct. Biol. 17 (2007) 48–57.
[41] P.T. Lansbury, H.A. Lashuel, A century-old debate on protein aggregation and neurodegeneration enters the clinic, Nature 443 (2006) 774–779.
[42] F. Chiti, C.M. Dobson, Protein misfolding, functional amyloid, and human disease, Annu. Rev. Biochem. 75 (2006) 333–366.
[43] C.-H. Lee, H.J. Kim, J.-H. Lee, H.-J. Cho, J. Kim, K.C. Chung, S. Jung, S.R. Paik, Dequalinium-induced protofibril formation of alpha-synuclein, J. Biol. Chem. 281 (2006) 3463–3472.
[44] C.-W. Liu, B.I. Giasson, K.A. Lewis, V.M. Lee, G.N. DeMartino, P.J. Thomas, A precipitating role for truncated alpha-synuclein and the proteasome in alpha-synuclein aggregation: implications for pathogenesis of Parkinson's Disease, J. Biol. Chem. 280 (2005) 22670–22678.
[45] D.-P. Hong, A.L. Fink, V.N. Uversky, Structural characteristics of alpha-synuclein oligomers stabilized by the flavonoid baicalein, J. Mol. Biol. 383 (2008) 214–223.
[46] D.E. Ehrnhoefer, J. Bieschke, A. Boeddrich, M. Herbst, L. Masino, R. Lurz, S. Engemann, A. Pastore, E.E. Wanker, EGCG redirects amyloidogenic polypeptides into unstructured, off-pathway oligomers, Nature Struct. Mol. Biol. 15 (2008) 558–566.
[47] S. Campioni, B. Mannini, M. Zampagni, A. Pensalfini, C. Parrini, E. Evangelisti, A. Relini, M. Stefani, C.M. Dobson, C. Cecchi, F. Chiti, A causative link between the structure of aberrant protein oligomers and their toxicity, Nat. Chem. Biol. 6 (2010) 140–147.
[48] N.D. Neas, P. Klapetek, Gwyddion: an open-source software for SPM data analysis, Cent. Eur. J. Phys. 10 (2012) 181–188.

Article VI

⌘ *Author's Choice*

THE JOURNAL OF BIOLOGICAL CHEMISTRY VOL. 288, NO. 2, pp. 1114–1124, January 11, 2013

The Neuroendocrine Protein 7B2 Suppresses the Aggregation of Neurodegenerative Disease-related Proteins*

Received for publication, September 7, 2012, and in revised form, November 11, 2012 Published, JBC Papers in Press, November 21, 2012, DOI 10.1074/jbc.M112.417071

Michael Helwig[‡], Akina Hoshino[‡], Casey Berridge[§], Sang-Nam Lee[¶], Nikolai Lorenzen[‖], Daniel E. Otzen[‖], Jason L. Eriksen[§], and Iris Lindberg[‡1]

From the [‡]Department of Anatomy and Neurobiology, University of Maryland School of Medicine, Baltimore, Maryland 21201, the [§]Department of Pharmacological and Pharmaceutical Sciences, College of Pharmacy, University of Houston, Houston, Texas 77204, the [¶]Research Center for Natural Human Defense System, Yonsei University College of Medicine, Seoul 120-752, Korea, and the [‖]Department of Molecular Biology and Genetics, Interdisciplinary Nanoscience Centre, Aarhus University, 8000 Aarhus C, Denmark

Background: The neuroendocrine protein 7B2 blocks the aggregation of certain secreted proteins.
Results: 7B2 co-localizes with protein aggregates in Parkinson and Alzheimer disease brains; blocks the fibrillation of $A\beta_{1-40}$, $A\beta_{1-42}$, and α-synuclein; and blocks $A\beta_{1-42}$-induced Neuro-2A cell death.
Conclusion: 7B2 inhibits the cytotoxicity of $A\beta_{1-42}$ by modulation of oligomer formation.
Significance: 7B2 is a novel anti-aggregation secretory chaperone associated with neurodegenerative disease.

Neurodegenerative diseases such as Alzheimer (AD) and Parkinson (PD) are characterized by abnormal aggregation of misfolded β-sheet-rich proteins, including amyloid-β (Aβ)-derived peptides and tau in AD and α-synuclein in PD. Correct folding and assembly of these proteins are controlled by ubiquitously expressed molecular chaperones; however, our understanding of neuron-specific chaperones and their involvement in the pathogenesis of neurodegenerative diseases is limited. We here describe novel chaperone-like functions for the secretory protein 7B2, which is widely expressed in neuronal and endocrine tissues. In *in vitro* experiments, 7B2 efficiently prevented fibrillation and formation of $A\beta_{1-42}$, $A\beta_{1-40}$, and α-synuclein aggregates at a molar ratio of 1:10. In cell culture experiments, inclusion of recombinant 7B2, either in the medium of Neuro-2A cells or intracellularly via adenoviral 7B2 overexpression, blocked the neurocytotoxic effect of $A\beta_{1-42}$ and significantly increased cell viability. Conversely, knockdown of 7B2 by RNAi increased $A\beta_{1-42}$-induced cytotoxicity. In the brains of APP/PSEN1 mice, a model of AD amyloidosis, immunoreactive 7B2 co-localized with aggregation-prone proteins and their respective aggregates. Furthermore, in the hippocampus and substantia nigra of human AD- and PD-affected brains, 7B2 was highly co-localized with Aβ plaques and α-synuclein deposits, strongly suggesting physiological association. Our data provide insight into novel functions of 7B2 and establish this neural protein as an anti-aggregation chaperone associated with neurodegenerative disease.

Excessive aggregation of misfolded proteins is a common feature in the pathophysiology of many neurodegenerative disorders such as Alzheimer disease (AD),[2] Parkinson disease (PD), and amyotrophic lateral sclerosis (1). AD, for example, is neuroanatomically characterized by extracellular plaques composed of amyloid precursor protein (APP)-derived amyloid-β (Aβ) peptides (2) and intracellular neurofibrillary tangles made up of hyperphosphorylated tau (3). Similarly, Lewy bodies, the hallmark of PD, are large cytosolic inclusion bodies composed of aggregated α-synuclein protein within dopaminergic neurons of the substantia nigra (4). Although the exact pathogenic role of these various aggregates is incompletely understood, it has been hypothesized that aggregation of Aβ peptides into oligomers and plaques results in a neurotoxic environment, disrupting cell function and leading to the loss of specific neuronal populations (5).

In the search for the underlying molecular mechanisms for these toxic effects, chaperone proteins have been implicated as important modulators of abnormal protein folding and aggregation in various neurodegenerative diseases (6). For example, several ubiquitously expressed molecular chaperones within the heat shock (*e.g.* HSP90, HSP70, and HSP27) and α-crystallin protein families have been shown to be associated with protein-misfolding diseases (7–10). The secreted chaperone clusterin has also been implicated in neurodegenerative disease (reviewed in Refs. 11 and 12). However, our understanding of the role of chaperone-mediated quality control machinery in neurodegenerative disease is still limited, and the question of whether chaperones other than heat shock proteins, crystallins, and clusterin might contribute to plaque pathogenesis or clearance remains open.

The secretory protein 7B2, known best for its role as a prohormone convertase 2 (proPC2)-binding protein (13, 14), is universally expressed in endocrine, neural, and neuroendocrine

* This work was supported, in whole or in part, by National Institutes of Health Grants 1R01DK49703 (to I. L.) and 1R15AG039008 (to J. L. E.). This work was also supported by Alzheimer's Association Grant NIRG-08-92033 (to J. L. E.), the Michael J. Fox Foundation for Parkinson's Research (to N. L. and D. E. O.), and German Academy of Sciences Leopoldina Foundation Postdoctoral Grant LPDS 2009-33 (to M. H.).
⌘ *Author's Choice*—Final version full access.
[1] To whom correspondence should be addressed: Dept. of Anatomy and Neurobiology, University of Maryland School of Medicine, HSF II, Rm. S251, 20 Penn St., Baltimore, MD 21201. Tel.: 410-706-4778; Fax: 410-706-2512; E-mail: ilind001@umaryland.edu.

[2] The abbreviations used are: AD, Alzheimer disease; PD, Parkinson disease; APP, amyloid precursor protein; Aβ, amyloid-β; ThT, thioflavin T.

cells, which all possess a regulated secretory pathway (15, 16). Because expression of 7B2 in the brain is not confined to convertase-containing neurons (15), it seems likely that 7B2 must possess physiological functions exceeding its involvement in neuropeptide synthesis. Early reports indicated that 7B2 could be distantly related to a subclass of molecular chaperones called chaperonins (17). 7B2 blocks the formation of proPC2 oligomers and aggregates (18) as well as IGF-1 aggregates (19), demonstrating that 7B2 functions as a post-folding and post-secretion chaperone. Moreover, independent discovery studies searching for biomarkers of early-onset AD, PD, and amyotrophic lateral sclerosis have identified 7B2 as a potential candidate protein (20–23).

On the basis of findings showing association of 7B2 with neurodegenerative disease and the known role of 7B2 in blocking proPC2 aggregation, we investigated the hypothesis that neuronal 7B2 could function to block neurodegenerative disease-related protein aggregation. We tested the action of 7B2-derived proteins on the cytotoxicity and fibrillation of the $A\beta_{1-42}$ and $A\beta_{1-40}$ peptides and α-synuclein. Our experiments using animal, cellular, and *in vitro* approaches provide collective support for the idea that 7B2 represents a novel neuroprotective chaperone.

EXPERIMENTAL PROCEDURES

Animal Models—All studies were conducted following University of Houston-approved Institutional Animal Care and Use Committee protocols. B6C6-Tg(APPswe,PSEN1dE9)85Dbo/J (APP/PSEN1; The Jackson Laboratory) mice (12 months old) were used in this study. APP/PSEN1 double transgenic mice express a chimeric mouse/human APP (Mo/HuAPP695swe) and a mutant human presenilin-1 (PS1-dE9) protein, both directed to CNS neurons; these familial mutations are strongly associated with early-onset AD. The mice were killed, and the brains were fixed with Accustain (Sigma) and subjected to paraffin processing. Brains were sectioned using a Leica microtome at 10-μm intervals.

Immunohistochemistry of Mouse Brain Tissue—Coronal sections (10 μm) of formalin-fixed tissue were deparaffinized and subjected to an antigen retrieval protocol using Aqua DePar and Reveal antigen retrieval solutions in a Decloaking Chamber system (Biocare Medical). Following antigen retrieval, some sections were briefly stained with methoxy-X04 (1 μM), followed by extensive washing to visualize dense core amyloid pathology. Other sections were treated with an avidin/biotin blocking kit (Vector Laboratories, Burlingame, CA), followed by treatment with 5% normal goat serum in Tris-buffered saline containing 0.5% Tween 20 (TBST) for 20 min. Sections were incubated with polyclonal rabbit anti-7B2 antiserum (LSU13BF; 1:200) for 1 h and washed with TBST. Sections were incubated with biotinylated goat anti-rabbit antibody (Vector Laboratories) for 30 min, washed with TBST, and then incubated with Texas Red-labeled avidin DCS (Vector Laboratories) for 10 min. Sections were then washed with TBST. For co-localization, tissue was reblocked using the avidin/biotin blocking kit, subjected to a second round of blocking, and incubated with a second round of antibodies (anti-$A\beta_{1-42}$; 12F4; 1:250; Covance), followed by washing and incubation with fluorescein-avidin (Vector Laboratories) for 10 min. The sections were then washed extensively with Tris-HCl, mounted using VECTASHIELD medium, and viewed under an Olympus IX61 DSU confocal microscope. Images were processed with Neurolucida (MicroBrightField, Inc., Williston, VT).

Human Brain Tissues—An AD-affected human brain sample (73-year-old female donor) and a control sample (72-year-old male donor, naturally deceased) containing the hippocampus and a PD-affected human midbrain sample containing the substantia nigra of a 89-year-old male donor were obtained from the NICHD Brain and Tissue Bank for Developmental Disorders of the University of Maryland, Baltimore. Formalin-fixed brain samples at either the level of the cortex or mesencephalon, respectively, were cryoprotected in 30% sucrose, deep-frozen in isopentane over dry ice (1 min), and stored at −80 °C until required.

Immunohistochemistry of Human Brain Tissue—Coronal sections (16 μm) containing the hippocampus (AD and control samples) and the substantia nigra (PD sample) were processed using a Leica cryostat, collected on Superfrost Plus object slides (Fisher Scientific, Hampton, NH), and treated with blocking solution containing 3% BSA in 0.5% Triton X-100 in PBS (0.5% PBST) for 1 h to block nonspecific reactions. Sections were then incubated with polyclonal rabbit anti-7B2 antiserum (LSU13BF; 1:250) and monoclonal mouse anti-α-synuclein antiserum (1:150; BD Biosciences) (24) in blocking solution overnight at 4 °C. Sections were rinsed briefly with 0.25% PBST and PBS and incubated with Cy3-conjugated (Ex_{max} = 550 nm and Em_{max} = 570 nm) goat anti-rabbit (A10520; 1:200; Invitrogen) and Cy2-conjugated (Ex_{max} = 492 nm and Em_{max} = 510 nm) donkey anti-mouse (AP124J; 1:250; Millipore) secondary antibodies in blocking solution containing H33342 (Ex_{max} = 350 nm and Em_{max} = 461 nm) nuclear/DNA staining reagent (1:10,000; ALX-620-050, Axxora LLC, San Diego, CA) for 2 h at room temperature. Sections were rinsed with PBS and coverslipped with Fluoromount G (Electron Microscopy Sciences, Hatfield, PA). Immunofluorescence was visualized using an Olympus BX61 confocal microscope and a Nikon Eclipse TE2000-E epifluorescence microscope. Images of immunoreactivity were merged by color channel overlay using microscope-specific image processing software (Olympus FluoView and Nikon MetaView). Anatomical localization of immunoreactivity within the brain was annotated according to the Allen Human Brain Atlas Data Portal and *Gray's Anatomy of the Human Body* (54).

$A\beta_{1-42}$ Oligomer Preparation—$A\beta_{1-42}$ peptide films were resuspended in Me_2SO at a concentration of 5 mM, and the peptide solutions were sonicated in a water bath sonicator for 10 min at room temperature. The solutions were then diluted to a final concentration of 100 μM with Ham's F-12 medium (phenol red-free; BIOSOURCE) and incubated at 4 °C for 24 h to form $A\beta_{1-42}$ oligomers (25). In some experiments, $A\beta_{1-42}$ oligomers were added to the medium of Neuro-2A cells in the presence of vehicle (Ham's F-12), recombinant 7B2 (see below), α-crystallin (Sigma), or α-lactalbumin (14.2 kDa; L4385, Sigma).

Cell Proliferation and Viability Assay—Neuro-2A cells were seeded at 5×10^3/well in 96-well plates and left to attach at

37 °C overnight. Subsequently, cells were treated with 10 μM $A\beta_{1-42}$ oligomers in the presence or absence of 2–4 μM 7B2, α-lactalbumin as a negative control, or vehicle (Ham's F-12) for 48 h. Cell survival was measured at the indicated times by adding 10 μl of a 1:3 (v/v) diluted WST-1 cell proliferation reagent stock solution (Roche Applied Science). Samples were incubated for 60–240 min, and absorbance at 450 nm was measured with a SpectraMax M2 fluorometer (Molecular Devices, Sunnyvale, CA) using a 690-nm reference filter. After subtraction of the background absorbance, the mean values of the untreated control cells were set as 100%. In addition, cell viability was assessed by labeling cells with calcein AM (2 μM; Ex_{max} = 485 nm and Em_{max} = 530 nm; L3224, Invitrogen), and fluorescence was measured using the SpectraMax M2 fluorometer. Representative photomicrographs were taken using the Nikon Eclipse TE2000-E epifluorescence microscope.

Adenoviral Infection of Neuro-2A Cells—To infect Neuro-2A cells with 7B2-encoding adenovirus (26), cells were seeded at 5×10^3/well into 96-well plates. Replicate wells were trypsinized and counted again the following day for calculation of adenoviral multiplicity of infection. Cells were washed twice with PBS, and 7B2 or control (β-galactosidase-encoding) adenovirus was diluted to achieve a multiplicity of infection of 1 in PBS in a final volume of 50 μl/well. The diluted adenovirus solution was added directly to cells in growth medium, and the plates were swirled to mix well and incubated for 30 min to permit adenoviral infection. Fifty μl of high glucose DMEM containing 2% fetal bovine serum were then added to each well. Adenovirus-infected cells were incubated for 36 h at 37 °C in a CO_2 incubator. The medium was then changed to DMEM containing 10 μM $A\beta_{1-42}$ for 48 h. Cell viability was assessed at this time using the WST-1 cell proliferation assay as described above.

7B2 RNAi Experiments—Three different specific sequences of Stealth siRNA (Invitrogen) were designed for the murine 7B2 mRNA sequence (MSS237887, MSS237888, and MSS237889). Following assessment of individual knockdown efficiencies, the most effective siRNA, MSS237887, was deployed. A control scrambled sequence was designed to have the same GC content (46-2000, Invitrogen). Neuro-2A cells grown in 96-well plates were transfected sequentially with the respective siRNA at 100 nM on the first day and 200 nM on the second day using 5 μl/well Lipofectamine 2000 (Invitrogen). The medium was then changed overnight to DMEM containing 4 μM $A\beta_{1-42}$ for 48 h. Transfection efficiency in Neuro-2A cells was monitored using a scrambled siRNA sequence conjugated to fluorescein (N2100S, New England Biolabs). The total cell number was determined by counterstaining with 5 μg/ml Hoechst 33342 (Invitrogen) for 45 min and subsequent examination by fluorescence microscopy. Cell viability was assessed using the WST-1 cell proliferation assay as described above.

Cellular Uptake of 7B2 and $A\beta_{1-42}$ into Neuro-2A Cells—Neuro-2A cells were grown overnight in 24-well plates on coverslips in DMEM supplemented with 10% (v/v) fetal bovine serum. On the next day, 250 nM Alexa Fluor 647-labeled $A\beta_{1-42}$ (64161, AnaSpec, Fremont, CA) and recombinant 7B2 were added to the medium, and cells were incubated at 37 °C in 5% CO_2 for 24 h. Neuro-2A cells were then treated with 4% paraformaldehyde for 20 min and incubated with blocking solution containing 3% BSA in 0.5% PBST for 1 h to block nonspecific reactions. Exogenous 7B2 was then visualized using Alexa Fluor 488-labeled anti-His tag antibody (16-254, Millipore). Cells were rinsed briefly with 0.25% PBST and PBS containing DAPI (Ex_{max} = 358 nm and Em_{max} = 461 nm) nuclear/DNA staining reagent (1:10,000; D1306, Invitrogen) for 2 h at room temperature. Cells were then rinsed with PBS and mounted on object slides with Fluoromount G. Immunofluorescence was visualized using the Olympus BX61 confocal microscope and the Nikon Eclipse TE2000-E epifluorescence microscope.

Peptide Synthesis and Purification of Recombinant 7B2-derived Peptides—An automated bench-top simultaneous multiple solid-phase peptide synthesizer (PSSM-8 system, Shimadzu) was used for the synthesis of 7B2 peptide 86–121 by the *N*-(9-fluorenyl)methoxycarbonyl (Fmoc) procedure in NovaSyn TGR resin (Novabiochem, San Diego, CA) as described previously (27). The molecular mass and purity of the synthetic peptide were verified by reverse-phase HPLC and matrix-assisted laser desorption/ionization time-of-flight mass spectrometry (TofSpec E, Micromass). Recombinant His-tagged 27- and 21-kDa 7B2 and 7B2 peptides 30–150 and 68–150 were prepared using the QIAexpress system (Qiagen). Primers were designed as described previously (27). PCR fragments were cloned into pQE30, and sequences were verified by DNA sequencing. Proteins were expressed in *Escherichia coli* XL1-Blue (Stratagene) and purified with the guanidine HCl/refolding method as described previously (28).

Thioflavin T Assay—Fibrillation of amylogenic peptides ($A\beta_{1-42}$, $A\beta_{1-40}$, and α-synuclein) in the presence and absence of 7B2 was measured by thioflavin T (ThT) fluorescence assays in 96-well plates (29). Recombinant $A\beta_{1-42}$ and $A\beta_{1-40}$ were purchased from Biopeptide Co. (San Diego, CA), and α-synuclein was expressed and purified as described (30). $A\beta_{1-40}$ and $A\beta_{1-42}$ were diluted in 0.5% Me_2SO and 0.5 M Tris-HCl buffer (pH 7.4; 1 mg/ml) and then diluted into 40 μM ThT solutions (in quadruplicate) containing or lacking the various forms of 7B2 in a total volume of 100 μl. α-Synuclein fibrillation assays were performed in PBS (pH 7.4) and included one 3/32-inch diameter polytetrafluoroethylene bead (McMaster-Carr, Santa Fe Springs, CA) per well. The final concentrations of fibrillogenic peptides were 20 μM for $A\beta_{1-40}$ and $A\beta_{1-42}$ and 44 μM for α-synuclein. Plates were incubated at 37 °C with agitation on a microtiter plate shaker (Glas-Col, Terre Haute, IN), with the speed set to 30 for the time periods indicated. Controls for the fibrillation reactions included carbonic anhydrase (molecular mass of ~29 kDa; C5024, Sigma), a protein chosen because of its comparable weight to 7B2. The development of fibrillation was monitored by measuring the fluorescence of ThT using the SpectraMax M2 fluorometer at 485 nm emission (444 nm excitation).

Dot Blot Analysis—Fibrillated $A\beta_{1-42}$ samples were centrifuged, transferred to a nitrocellulose membrane, and subjected to anti-Aβ Western blot analysis. $A\beta_{1-42}$ fibrillation assays were performed as described above. At 48 h, samples of $A\beta_{1-42}$ control reactions and of reactions incubated with 27- or 21-kDa 7B2 were removed. One-third of each reaction was used as a reference for the total reaction, whereas the remaining material

was centrifuged for 30 min at 20,000 × g (4 °C) to separate soluble material containing mono- and oligomeric $A\beta_{1-42}$ and pelletable material containing heavy fibrils. An appropriate volume of PBS was added to the total, supernatant, and pellet samples to make the volume up to 100 μl. Ten μl of these reactions were transferred to a 0.2-μm nitrocellulose membrane (Bio-Rad) and air-dried, and the membrane was then blocked with 0.5% BSA and 0.2% goat serum in Tris-buffered saline containing 0.3% Triton X-100. The blot was incubated with monoclonal anti-Aβ antiserum (6E10; 1:1000; Covance) in blocking buffer overnight at 4 °C. On the following day, the blots were washed three times with TBS containing 0.05% Tween 20, followed by incubation at room temperature for 1.5 h using horseradish peroxidase conjugate as the secondary antibody. Blots were incubated with SuperSignal West Pico chemiluminescent substrate (Pierce) for 1 min, and chemiluminescent bands were visualized using HyBlot CL autoradiography film (Denville Scientific Inc.). Dot intensities were analyzed using NIH ImageJ densitometric analysis software and displayed as mean intensity ($n = 3$/group), and the ratios between the supernatant and pellet samples were calculated.

Transmission Electron Microscopy—Specimens (incubated for 72 h) were adsorbed onto 400-mesh Formvar-coated copper grids and negatively stained with 2% phosphotungstic acid (pH 7). After wicking off excess solution, grids were air-dried and examined in a Tecnai T12 transmission electron microscope (FEI) operated at 80 kV. Digital images were acquired using an AMT bottom-mount CCD camera and AMT600 software.

Luciferase Refolding Assay—A possible ATP-dependent, chaperone-like protein-refolding function of 7B2 was tested by incubating unfolded firefly luciferase with recombinant 21- and 27-kDa 7B2, followed by measurement of regained luciferase activity. A 10 μM solution of *Photinus pyralis* luciferase (Roche Applied Science) was resuspended in 0.5 M Tris acetate buffer (pH 7.5), followed by denaturation in 6 M guanidine hydrochloride and 5 mM DTT for 30 min at room temperature. The guanidine hydrochloride solution was dialyzed against PBS overnight at 4 °C. Refolding reactions were performed by diluting denatured luciferase 1:100 in refolding buffer (25 mM HEPES (pH 7.4), 5 mM $MgCl_2$, 50 mM KCl, 5 mM DTT, and 3 mM ATP) in the presence or absence of recombinant 21- or 27-kDa 7B2 (4 μM) using BSA as a negative control and human recombinant HSP70 (Enzo Life Sciences, Farmingdale, NY) as a positive control. The incubation with 7B2 was performed for 3 h at room temperature, followed by 1:10 dilution of reactions into luciferase assay buffer (Promega). Luciferase activity was determined by measurement of luciferin bioluminescence using a FlexStation 3 microplate reader (Molecular Devices). Protein refolding was defined as recovery of luciferase activity expressed as a percent of the activity of native luciferase measured at the same concentration.

Statistical Analysis—Data were analyzed with one- or two-way analysis of variance, followed by the Student-Newman-Keuls multiple comparison test, as appropriate, using a statistical software package (SigmaStat, Systat Software, Inc., San Jose, CA). Data not meeting a normal distribution were analyzed using one-way analysis of variance, followed by the Newman-Keuls multiple comparison test. $p < 0.05$ was considered statistically significant.

RESULTS

7B2 Co-localizes with $A\beta_{1-42}$ Amyloid Plaque Pathology in APP/PSEN1 Mice—To assess a possibly physiologically relevant relationship between 7B2 and proteins involved in amyloid plaque pathology, we performed an immunohistochemical co-localization study using brains from 12-month-old APP mutant mice. Immunoreactive 7B2 was observed in association with $A\beta_{1-42}$ immunoreactivity throughout the brain. Within the hippocampus, 7B2 immunoreactivity strongly overlapped with staining for $A\beta_{1-42}$ (Fig. 1*A*). Furthermore, within the hippocampus, 7B2 immunoreactivity strongly co-localized with staining for $A\beta_{1-42}$ dense core plaque pathology, as demonstrated by its apparent overlap with methoxy-X04-positive $A\beta_{1-42}$ aggregates (Fig. 1*B*).

7B2 Co-localizes with $A\beta_{1-42}$ Deposits in Human AD Hippocampus and with α-Synuclein-rich Lewy Bodies within the Substantia Nigra of a PD Patient—7B2 immunoreactivity was detected throughout the extent of the human brain, including somata and dendritic and axonal branches in neurons of the cortex and mesencephalon (data not shown). Within the hippocampus of a human AD brain, 7B2 strongly co-localized with extracellular $A\beta_{1-42}$ deposits (Fig. 2*A*). 7B2 strongly co-localized with α-synuclein-positive cytoplasmic inclusions (Lewy bodies) in neurons within the substantia nigra of a PD brain (Fig. 2*B*). Although >80% of the observed 7B2 co-localized with α-synuclein immunoreactivity, scattered α-synuclein immunoreactivity could be observed that was not 7B2-immunoreactive (*arrowhead* with *asterisk*). In a similar hippocampus sample from a healthy human control, 7B2 staining was found near cell nuclei, indicating intracellular localization, whereas no significant staining for $A\beta_{1-42}$ could be observed, demonstrating no plaque pathology (Fig. 2*C*).

7B2 Counteracts the Neurocytotoxic Effect of $A\beta_{1-42}$ and Increases Cell Viability—To investigate whether 7B2 is neuroprotective, we performed cell toxicity assays using Neuro-2A cells. A 48-h treatment of Neuro-2A cells with $A\beta_{1-42}$ produced an ~50% decrease in the number of living cells as revealed by quantification of viable cells using both WST-1 assays (Fig. 3*A*, *left panel*) and calcein AM staining (*right panels*). Inclusion of 27- and 21-kDa 7B2 in the medium of Neuro-2A cells during Aβ treatment significantly diminished Aβ-induced cell death. This effect was more pronounced when the 27-kDa form of 7B2 was added and was dose-dependent. $A\beta_{1-42}$-induced cell death was completely prevented when 27-kDa 7B2 was added to the medium together with $A\beta_{1-42}$. Neither of the negative controls, carbonic anhydrase (a similarly sized cytosolic protein) or α-lactalbumin (an irrelevant secreted protein), reduced Aβ neurotoxicity; however, α-crystallin, a known chaperone for Aβ (31, 32), was also able to block toxicity (data not shown).

To determine whether endogenously expressed 7B2 can also prevent Aβ neurotoxicity, we overexpressed 7B2 via adenoviral infection of Neuro-2A cells. A neuroprotective effect was observed when 7B2 was overexpressed by 3-fold (Fig. 3*B*), resulting in a significant increase in living cells, which reached

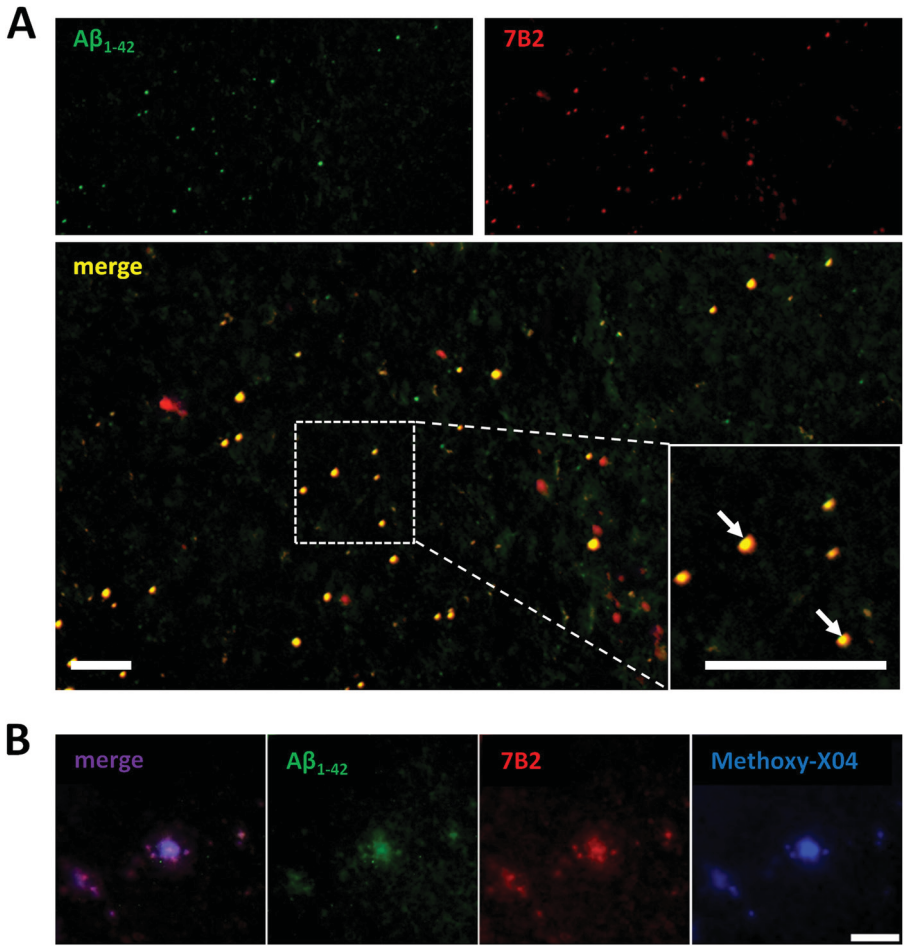

FIGURE 1. **7B2 co-localizes with amyloid plaque pathology.** *A*, the hippocampus of a 12-month-old mutant APP/PSEN1 mouse strongly stained for $A\beta_{1-42}$ immunoreactivity. A composite image shows significant overlap between $A\beta_{1-42}$ (*green*)and 7B2 (*red*) immunoreactivity, resulting in a *yellow* color in the merged image (*arrows*). *Scale bars* = 100 μm. *B*, staining showing significant co-localization (overlap resulting in *purple* hue) of 7B2 (*red*) with $A\beta_{1-42}$ (*green*) and genuine extracellular plaques (*blue*) in the cortices of APP/PSEN1 mice. Plaques were visualized by staining with the *in vivo* amyloid-imaging fluorophore methoxy-X04.

~85% of untreated controls; these results indicate that endogenously expressed 7B2 can rescue cells from $A\beta_{1-42}$-induced neurotoxicity (Fig. 3*C*). In a parallel experiment, we decreased intracellular 7B2 levels using 7B2-specific siRNA. The siRNA-induced decrease in 7B2 was accompanied by a similar decrease in the number of viable Neuro-2A cells; control oligonucleotides showed no such deleterious effect. We observed some co-localization of exogenously added recombinant His-tagged 7B2 with Alexa Fluor-labeled $A\beta_{1-42}$ within Neuro-2A cells (Fig. 3*D*), indicating cellular uptake of both proteins into the cytosol of Neuro-2A cells.

7B2 Inhibits the Fibrillation of $A\beta_{1-42}$, $A\beta_{1-40}$, and α-Synuclein in Vitro—To elucidate the molecular mode of action by which 7B2 inhibits the formation of cytotoxic Aβ species and to obtain structure-function information, we performed *in vitro* fibrillation assays. The addition of full-length 27-kDa 7B2 (structure shown in Fig. 4*A*) inhibited the fibrillation of $A\beta_{1-42}$ at 7B2:$A\beta_{1-42}$ molar ratios of 1:10. Structure-function analysis using truncated forms of 7B2 revealed that this anti-aggregation effect was greatest when the protein was full-length (Fig. 4*B*) and moreover was dose-dependent (Fig. 4*C*). In agreement with these findings, the majority of $A\beta_{1-42}$ became insoluble during the course of the fibrillation assay, as shown by dot blot analysis of centrifugally separated $A\beta_{1-42}$ fibrillation reaction samples, which indicated greater formation of aggregates following 48 h of incubation (Fig. 4*D*). However, the ratio of soluble/lighter $A\beta_{1-42}$ to insoluble/heavier $A\beta_{1-42}$ oligomers (supernatant:pellet) shifted to favor soluble $A\beta_{1-42}$ species when reactions were co-incubated with either 21- or 27-kDa 7B2, suggesting inhibition of the generation of larger fibrils by these proteins. Blockade of fibril formation was independently substantiated by quantification of transmission electron microscope images of $A\beta_{1-42}$ fibrils and oligomers (Fig. 4*E*) incubated at 37 °C for 48 h, which demonstrated a substantial decrease in fibril length when 27-kDa 7B2 was added to the reaction. Although fibrils in the untreated $A\beta_{1-42}$ samples reached an average length of 575 ± 302 nm (mean ± S.D., n = 10) following incubation, fibril length decreased by ~80% when 7B2 was included in the reaction (to 124 ± 233 nm). In these samples, we also observed an increase in the number of smaller spherical $A\beta_{1-42}$ aggregates with an average diameter of 10 ± 4 nm.

The addition of 7B2 to preincubated $A\beta_{1-42}$ samples (at the time point indicated by an arrow) did not result in the disintegration of preformed $A\beta_{1-42}$ fibrils (Fig. 5*A*), indicating that 7B2 does not function as a disaggregase. However, consistent

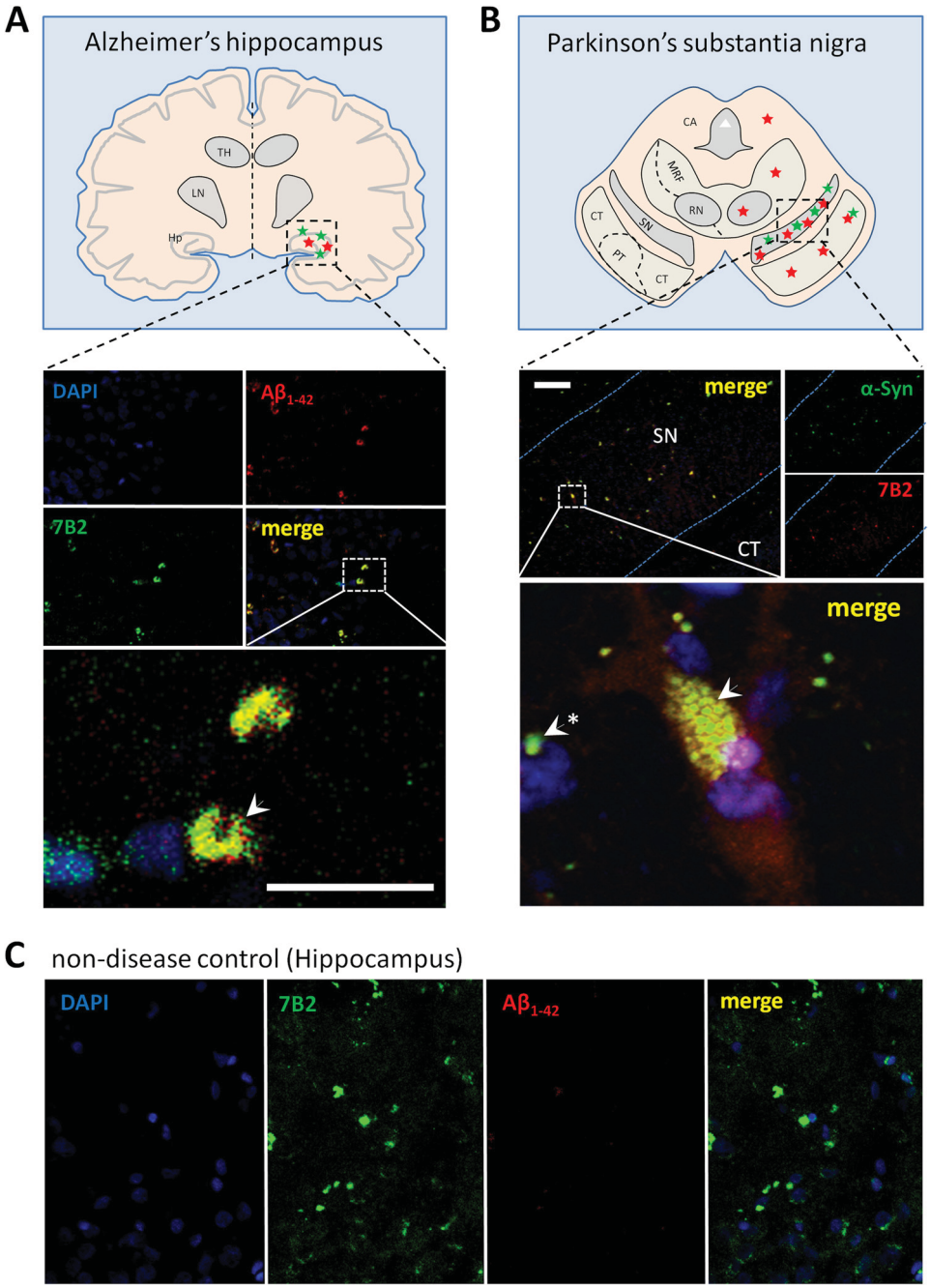

FIGURE 2. **Co-localization of 7B2 with extra- and intracellular protein aggregates in AD hippocampus and PD Lewy bodies.** *A*, AD brain: schematic representation of 7B2 immunoreactivity (*red stars*) and Aβ-positive plaques (*green stars*) as detected throughout the extent of the human brain sample at the level of the hippocampus. *Upper panels*, low magnification images provide an overview of the areas of Aβ-immunoreactive deposits (*red*) and 7B2 expression (*green*) within in the hippocampus. *Lower panel*, high magnification image of representative amyloid plaques within the hippocampus confirms a high degree of co-localization (*arrowhead*) of 7B2 immunoreactivity with Aβ immunoreactivity. *B*, PD brain: 7B2 immunoreactivity (*red stars*) was found throughout the mesencephalon, whereas Lewy bodies were confined to the substantia nigra (*green stars*). *Upper panels*, low magnification images provide an overview of the areas of α-synuclein-immunoreactive deposits in Lewy bodies (*green*) and 7B2 expression (*red*) within the substantia nigra. *Lower panel*, high magnification image of representative Lewy bodies within the substantia nigra confirms a high degree of co-localization (*arrowhead*) of 7B2 immunoreactivity with α-synuclein immunoreactivity. The majority of 7B2 immunoreactivity was confined to areas near the nucleus, suggesting intracellular localization. *C*, 7B2 immunoreactivity was detected in a human control brain sample. Shown are representative images of the hippocampus in a non-diseased control brain. Although only limited Aβ immunoreactivity (*red*) and no plaque burden were detected, we observed significant 7B2 immunoreactivity (*green*) that was confined to areas near cell nuclei, suggesting intracellular localization. *CA*, cerebral aqueduct; *CT*, corticopontine tract; *Hp*, hippocampus; *LN*, lentiform nucleus; *MRF*, mesencephalic reticular formation; *PT*, pyramidal tract; *RN*, red nucleus; *SN*, substantia nigra; *TH*; thalamus. *Scale bars* = 10 μm.

with its effects on $A\beta_{1-42}$ fibrillation, 7B2 also inhibited the formation of $A\beta_{1-40}$ (Fig. 5*B*) and α-synuclein fibrils (Fig. 5*C*). A dose-dependent relationship was observed for blockade of α-synuclein fibrillation by 27-kDa 7B2 (Fig. 5*D*).

We next aimed to determine whether 7B2 exhibits ATP-dependent chaperone-like refolding properties similar to those of larger chaperones such as members of the HSP70 and HSP90 families. Although denatured luciferase was efficiently refolded

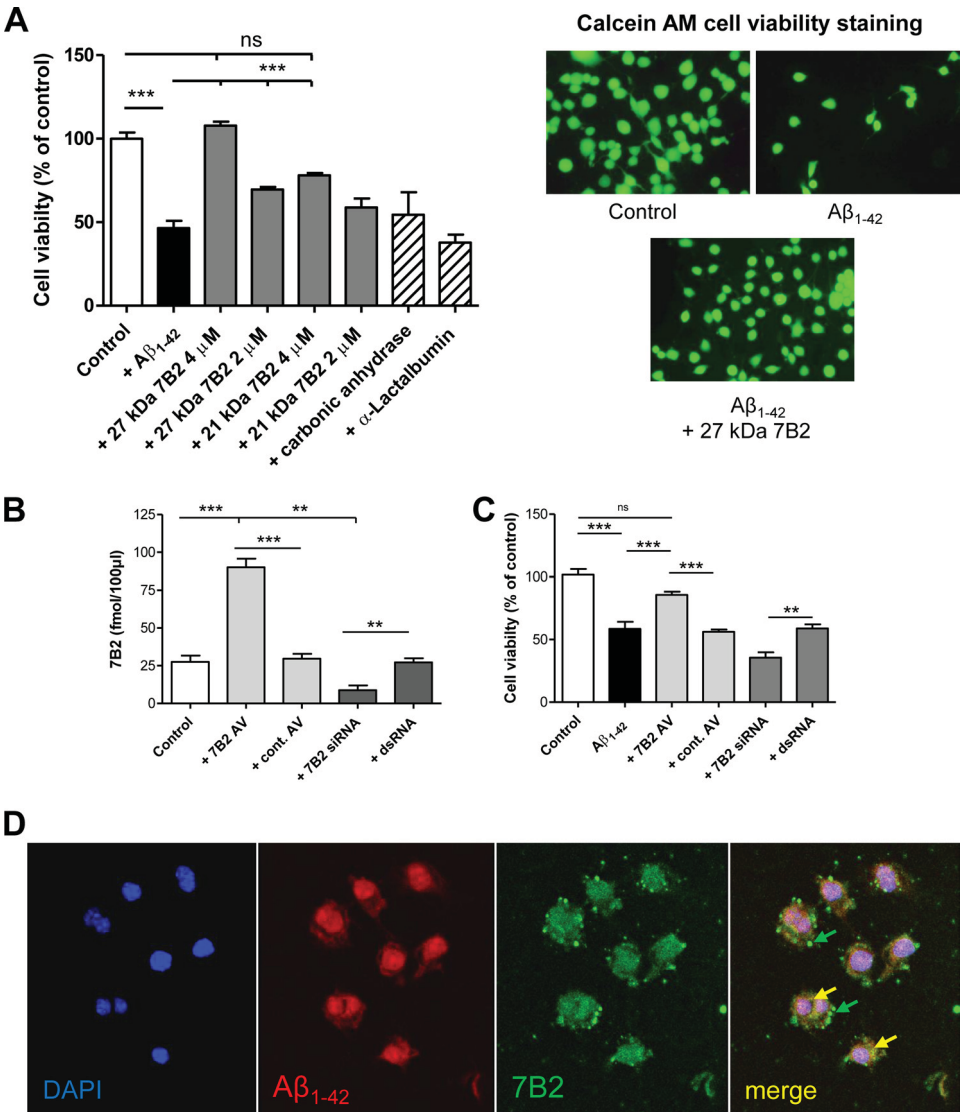

FIGURE 3. **7B2 decreases Aβ-induced cell death in Neuro-2A cells.** *A*, Neuro-2A cells were treated with 10 μM $A\beta_{1-42}$ for 48 h to induce cell death in the presence or absence of 7B2. *Left panel*, quantification of Aβ-induced cell death by the WST-1 cell viability assay. *Right panels*, representative photomicrographs showing viable calcein AM-stained Neuro-2A cells following treatment with $A\beta_{1-42}$ with or without 7B2. *ns*, not significant. *B*, quantification of endogenous 7B2 levels in Neuro-2A cells by radioimmunoassay following either adenoviral (*AV*) overexpression or RNAi-mediated knockdown. *cont.*, control. *C*, $A\beta_{1-42}$-induced cell death following manipulation of intracellular 7B2 levels was monitored using the WST-1 cell viability assay. *D*, exogenously added recombinant His-tagged 7B2 (*green arrows*) was internalized and co-localized with Alexa Fluor-labeled $A\beta_{1-42}$ (*red*) in Neuro-2A cells, indicating co-uptake into the cytosol of Neuro-2A cells (*yellow arrows*). Anti-His tag antiserum was used for the experiment in *D*.

by HSP70, restoring about half of its enzymatic function, 7B2 displayed no significant refolding activity (Fig. 6).

The small molecular mass of 7B2 potentially qualifies this protein to be classified as a small heat shock protein; these chaperone proteins possess masses between 15 and 40 kDa and share the conserved sequence known as the α-crystallin domain (33). However, multisequence alignment using 3D/T-Coffee Web server tools revealed no significant sequence identity to either α-crystallin itself or the comparably sized heat shock protein sHSP27 (data not shown).

DISCUSSION

Neurodegenerative diseases such as AD and PD have been established as "protein-folding disorders," the etiology of which involves the aggregation of non-native protein conformations, resulting in extracellular and intracellular protein aggregates (34). The abundance of these protein aggregates in neurodegenerative disease is, however, difficult to explain and appears to represent an essential failure of neuronal chaperone systems to sustain native protein conformation. The particular toxicity of protein aggregates in the nervous system implies that neurons may require special mechanisms to maintain continuous chaperone control of protein aggregation during secretory pathway transit, granule residence, and even following secretion and reuptake, yet few specifically neuronal secretory chaperone mechanisms have been described.

Although 7B2 has long been recognized as an excellent neuroendocrine marker involved in PC2-mediated peptide synthesis (13, 14), its widespread neuronal distribution within the brain, and also in areas lacking prohormone convertases (15), strongly suggests non-convertase-related functions. Our immunohistochemical data show clear co-localization of 7B2

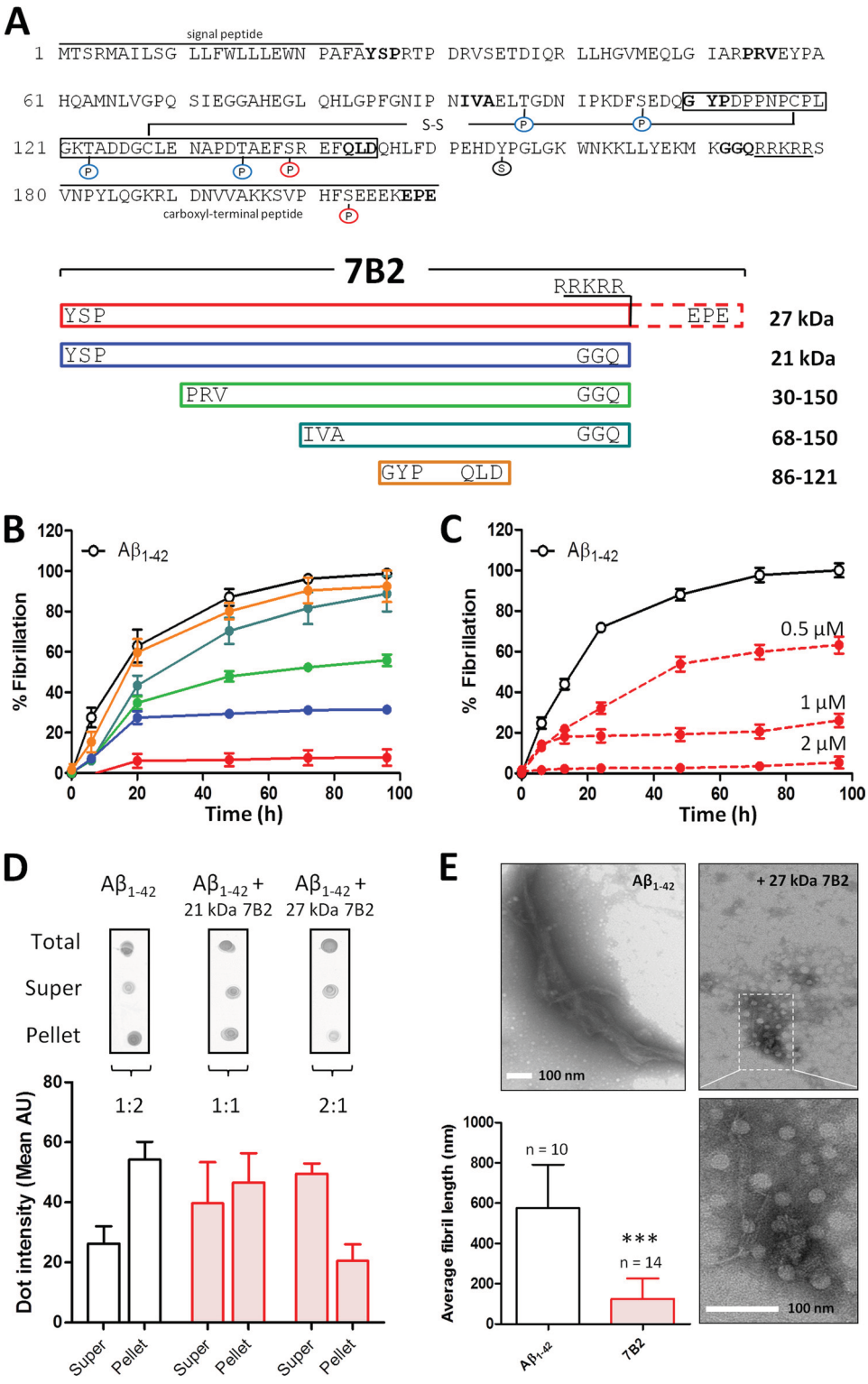

FIGURE 4. **Structure-function analysis of 7B2 proteins in suppressing Aβ fibrillation.** *A*, *upper*, amino acid sequence of rat 7B2 including the N-terminal signal peptide and the C-terminal inhibitory peptide domain. Putative post-translational modification sites are marked (*red P*, known phosphorylation site; *blue P*, hypothetical phosphorylation site; *black S*, sulfation; *S-S*, disulfide bond); the C-terminal cleavage site is *underlined*; and the minimal amino acid sequence required for PC2 activation is *boxed*. The first and last three amino acids of the 7B2 fragments used in this study are indicated in *boldface*. *Lower*, domain structure of 7B2 and schematic representation of the N-terminal deletions and peptides used in this study. *B*, $A\beta_{1-42}$ (20 μM) was incubated with either full-length 7B2 (27 kDa; *red*) or truncated proteins and peptides (2 μM). Protein fibrillation was monitored using a ThT fibrillation assay. *C*, the inhibition of $A\beta_{1-42}$ aggregation in the presence of 27-kDa 7B2 was dose-dependent and was most effective at a 7B2:$A\beta_{1-42}$ molar ratio of 1:10. *D*, quantification of supernatant (soluble $A\beta_{1-42}$) *versus* pellet (insoluble $A\beta_{1-42}$) dot intensities revealed a ratio shift (supernatant:pellet) toward the soluble $A\beta_{1-42}$ species following the addition of 7B2. *AU*, absorbance units. *E*, quantification of $A\beta_{1-42}$ fibril formation observed after 72 h of incubation in reactions with or without 7B2 by transmission electron microscopy. ***, $p < 0.001$.

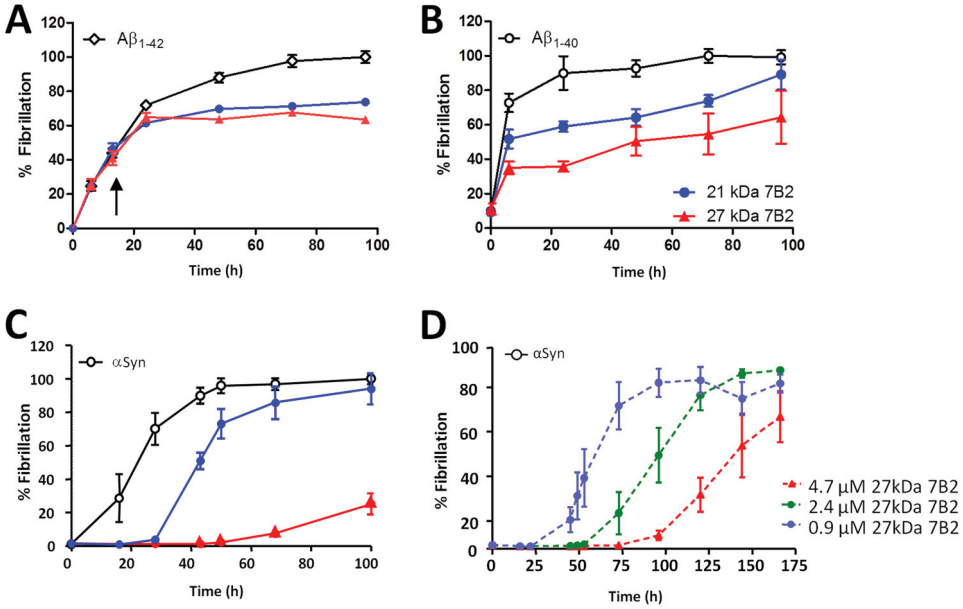

FIGURE 5. **7B2 does not disintegrate preformed mature Aβ_{1-42} fibrils but suppresses Aβ_{1-40} and α-synuclein fibrillation.** *A*, Aβ_{1-42} (20 μM) was incubated at 37 °C, followed by the addition of 2 μM 27- or 21-kDa 7B2 at the time point indicated by the *arrow*. Protein aggregation was monitored with the ThT fibrillation assay. Further Aβ_{1-42} aggregation was inhibited once 7B2 was added; however, preformed mature fibrils were not affected (n = 3/group). Aβ_{1-40} (20 μM) (*B*) and α-synuclein (*αSyn*; 44 μM) (*C*) were incubated with full-length 7B2 (27 kDa; *red*) or 21-kDa 7B2 (*blue*), respectively, and fibrillation was monitored by the ThT assay. *D*, dose dependence relationship for inhibition of α-synuclein fibrillation by 27-kDa 7B2.

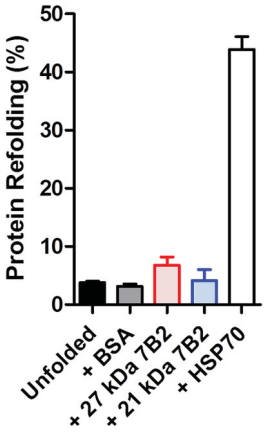

FIGURE 6. **7B2 does not possess chaperone-like refolding activity.** Unfolded and inactive firefly luciferase (40 μM) was incubated with either 21- or 27-kDa 7B2 (4 μM), followed by measurement of regained (refolded) luciferase enzyme activity, determined by luciferin bioluminescence assay.

with aggregated proteins in neurodegenerative disease, indicating a potential functional relationship. A similar accumulation of chaperones within amyloid-like plaques in the brains of AD and PD patients has been reported for α-crystallin, HSP47, and clusterin (8, 35, 36). Interestingly, the distribution of immunoreactive 7B2 in diseased brain indicates that this protein may possess a higher affinity for non-aggregated Aβ_{1-40}, Aβ_{1-42}, and Aβ_{1-40} and a lesser affinity for fully mature dense core plaques. This suggests an anti-aggregation effect of 7B2 that is temporally organized, occurring prior to compaction of Aβ deposits, as would be expected from a chaperone-mediated defense response to Aβ plaque maturation. A general association of 7B2 with neurodegenerative protein aggregation is further substantiated by the pronounced intracellular co-localization of 7B2 with α-synuclein-rich Lewy bodies within the substantia nigra of a PD patient.

7B2 is found together with intracellular and extracellular protein aggregates, implying that it could act at both locations. We speculate that 7B2 may block inappropriate protein-protein interactions initially during intracellular protein trafficking through the secretory pathway, extracellularly following secretion of 7B2 and Aβ, and possibly even following reuptake. Interestingly, cellular reuptake of Aβ into endosomes and lysosomes has been reported to facilitate its aggregation (37). Here, we have shown that Neuro-2A cells are capable of taking up added Aβ simultaneously with added exogenous 7B2, raising the idea that these compartments serve as sites for 7B2 interaction with Aβ under physiological conditions. The cytoplasmic protein α-synuclein has been reported to be secreted and to be localized intravesicularly in a similar fashion (38); an analogous mechanism could be operative for α-synuclein/7B2. However, whether extracellular association of these proteins occurs prior to uptake or whether both species are nonspecifically endocytosed together is not yet clear.

We have further demonstrated here that added 7B2 can block the cytotoxic effects of Aβ peptides. Neuro-2A cells exposed to toxic Aβ oligomers died rapidly; inclusion of either 7B2 or α-crystallin, but not the control proteins carbonic anhydrase and α-lactalbumin, blocked the cytotoxic effects of these oligomers. It is unlikely that fibril formation is involved in Aβ neurotoxicity because the concentration of Aβ used was low (10 μM) and because Aβ oligomers appear to be much more toxic than fibrils (39). Thus, 7B2 may function to block protein-protein association at the oligomer level; this idea is in line with the known ability of 7B2 to block both the oligomerization and the aggregation of the convertase proPC2 (18).

Of great physiological importance is our observation that modulation of intracellular 7B2 expression directly correlates with the cytotoxicity of exogenously administered Aβ_{1-42}. In a

similar approach, Magrané *et al.* (40) have shown that viral overexpression of HSP70 successfully rescues neurons from the toxic effects of intracellular Aβ accumulation. Moreover, another study demonstrated that drug-induced chaperone overexpression of HSP70 and HSP90 maintains tau protein in a soluble and functional conformation, preventing it from aggregating (10). In line with these studies, our data indicate that a certain level of endogenous 7B2 may be sufficient to prevent the formation of harmful Aβ_{1-42} species and support the idea that loss of neuronal 7B2 might facilitate Aβ_{1-42}-induced neurotoxicity. The location of 7B2 action in blocking Aβ_{1-42}-induced neurotoxicity requires further investigation; it is possible that 7B2 acts both extracellularly to block oligomer formation and intracellularly following reuptake.

In addition to these *in vivo* and cellular data linking 7B2 with the toxic effects of Aβ, we have directly demonstrated that 7B2 suppresses the fibrillation of aggregation-prone proteins *in vitro*. The ability of 7B2 to act at low stoichiometric ratios with respect to client proteins is remarkable and further supports the idea of 7B2 involvement in Aβ-related plaque formation.

Most protein chaperones described to date function intracellularly. Only four secreted chaperones that act extracellularly have been identified thus far: (i) the ubiquitously expressed glycoprotein clusterin/ApoJ, which in the brain appears to be of glial origin (11); (ii) the heat shock-related lens protein α-crystallin (41); (iii) the presumed Aβ chaperone prostaglandin D synthase/β-trace (42); and the receptor-associated protein RAP (43). Of these, the chaperone with by far the greatest genetic association with AD is clusterin (reviewed in Refs. 11 and 12). A key feature that distinguishes 7B2 from clusterin is that clusterin is expressed in nearly all mammalian tissues, whereas 7B2 expression is limited to cells containing a regulated secretory pathway: the central and peripheral nervous systems and endocrine/neuroendocrine systems. Interestingly, a recent study investigating the interaction of clusterin and Aβ using biophysical approaches reported that clusterin binds to and stabilizes Aβ oligomers of all sizes, thereby influencing the equilibrium of Aβ oligomers, aggregates, and fibrils (44). It is possible that 7B2 acts via similar molecular mechanisms to decrease Aβ protein oligomerization, fibrillation, and cytotoxicity. The appearance of the disc-shaped structures observed by electron microscopy in this study seems to represent an increase in spherical Aβ_{1-42} oligomers, potentially indicating that 7B2 promotes the formation of nontoxic stable off-pathway Aβ species, similar to what has been reported following treatment with inositol (45).

Biophysical characterization of recombinant 7B2 has shown that it is an intrinsically disordered protein capable of oligomerization (46). These properties are similar to those of certain small anti-aggregant cytosolic heat shock proteins (reviewed in Refs. 47 and 48), and we speculate that 7B2 may block the formation of protein aggregates using similar mechanisms. Although weak homology to chaperonin-related sequences has been reported (17), 7B2 exhibits no significant sequence homology to clusterin, crystallins, or small heat shock proteins. Thus, 7B2 appears to have novel anti-aggregation domains. The role of the known post-translational modifications of this protein, sulfation (49) and phosphorylation (50, 51) (see Fig. 4*A*), in anti-aggregation remains to be established.

In summary, our data provide new insight into the function of neuronal 7B2 and establish this protein as a novel anti-aggregation chaperone strongly associated with neurodegenerative disease. Interestingly, recent proteomics studies also point to an association of 7B2 with various neurodegeneration-related protein-misfolding diseases, including AD, PD, and amyotrophic lateral sclerosis (20–23). These observations are supported by data showing that 7B2 is significantly up-regulated in brain tissues of AD patients (52) and by a fifth proteomics study in which 7B2 was found to be elevated in the cerebrospinal fluid of amyotrophic lateral sclerosis patients (53), indicating possible up-regulation of 7B2 as a response to increased protein aggregation and misfolding. Taken together with the work presented here, these studies provide support for the idea that 7B2 plays a role in the etiology of aggregate formation in neurodegenerative disease.

Acknowledgments—We acknowledge the technical support of the Core Imaging Facility, the UMB Biopolymer Core Lab for Peptide Synthesis, and the NICHD Brain and Tissue Bank for Developmental Disorders of the University of Maryland, Baltimore.

REFERENCES

1. Ross, C. A., and Poirier, M. A. (2004) Protein aggregation and neurodegenerative disease. *Nat. Med.* **10,** S10–S17
2. Glenner, G. G., and Wong, C. W. (1984) Alzheimer's disease: initial report of the purification and characterization of a novel cerebrovascular amyloid protein. *Biochem. Biophys. Res. Commun.* **120,** 885–890
3. Kosik, K. S., Joachim, C. L., and Selkoe, D. J. (1986) Microtubule-associated protein tau (tau) is a major antigenic component of paired helical filaments in Alzheimer disease. *Proc. Natl. Acad. Sci. U.S.A.* **83,** 4044–4048
4. Spillantini, M. G., Schmidt, M. L., Lee, V. M., Trojanowski, J. Q., Jakes, R., and Goedert, M. (1997) α-Synuclein in Lewy bodies. *Nature* **388,** 839–840
5. Pike, C. J., Walencewicz, A. J., Glabe, C. G., and Cotman, C. W. (1991) *In vitro* aging of β-amyloid protein causes peptide aggregation and neurotoxicity. *Brain Res.* **563,** 311–314
6. Muchowski, P. J., and Wacker, J. L. (2005) Modulation of neurodegeneration by molecular chaperones. *Nat. Rev. Neurosci.* **6,** 11–22
7. Nemes, Z., Devreese, B., Steinert, P. M., Van Beeumen, J., and Fésüs, L. (2004) Cross-linking of ubiquitin, HSP27, parkin, and α-synuclein by γ-glutamyl–ϵ-lysine bonds in Alzheimer's neurofibrillary tangles. *FASEB J.* **18,** 1135–1137
8. Renkawek, K., Bosman, G. J., and de Jong, W. W. (1994) Expression of small heat-shock protein hsp 27 in reactive gliosis in Alzheimer disease and other types of dementia. *Acta Neuropathol.* **87,** 511–519
9. McLean, P. J., Kawamata, H., Shariff, S., Hewett, J., Sharma, N., Ueda, K., Breakefield, X. O., and Hyman, B. T. (2002) TorsinA and heat shock proteins act as molecular chaperones: suppression of α-synuclein aggregation. *J. Neurochem.* **83,** 846–854
10. Dou, F., Netzer, W. J., Tanemura, K., Li, F., Hartl, F. U., Takashima, A., Gouras, G. K., Greengard, P., and Xu, H. (2003) Chaperones increase association of tau protein with microtubules. *Proc. Natl. Acad. Sci. U.S.A.* **100,** 721–726
11. Jones, S. E., and Jomary, C. (2002) Clusterin. *Int. J. Biochem. Cell Biol.* **34,** 427–431
12. Wu, Z. C., Yu, J. T., Li, Y., and Tan, L. (2012) Clusterin in Alzheimer's disease. *Adv. Clin. Chem.* **56,** 155–173
13. Mbikay, M., Seidah, N. G., and Chrétien, M. (2001) Neuroendocrine secretory protein 7B2: structure, expression and functions. *Biochem. J.* **357,** 329–342
14. Muller, L., and Lindberg, I. (1999) The cell biology of the prohormone convertases PC1 and PC2. *Prog. Nucleic Acid Res. Mol. Biol.* **63,** 69–108
15. Seidel, B., Dong, W., Savaria, D., Zheng, M., Pintar, J. E., and Day, R. (1998)

Neuroendocrine protein 7B2 is essential for proteolytic conversion and activation of proprotein convertase 2 *in vivo*. *DNA Cell Biol.* **17,** 1017–1029
16. Iguchi, H., Chan, J. S. D., Seidah, N. G., and Chrétien, M. (1984) Tissue distribution and molecular forms of a novel pituitary protein in the rat. *Neuroendocrinology* **39,** 453–458
17. Braks, J. A. M., and Martens, G. J. M. (1994) 7B2 is a neuroendocrine chaperone that transiently interacts with prohormone convertase PC2 in the secretory pathway. *Cell* **78,** 263–273
18. Lee, S.-N., and Lindberg, I. (2008) 7B2 prevents unfolding and aggregation of prohormone convertase 2. *Endocrinology* **149,** 4116–4127
19. Chaudhuri, B., Stephan, C., Huijbregts, R. P., and Martens, G. J. (1995) The neuroendocrine protein 7B2 acts as a molecular chaperone in the *in vitro* folding of human insulin-like growth factor-1 secreted from yeast. *Biochem. Biophys. Res. Commun.* **211,** 417–425
20. Jahn, H., Wittke, S., Zürbig, P., Raedler, T. J., Arlt, S., Kellmann, M., Mullen, W., Eichenlaub, M., Mischak, H., and Wiedemann, K. (2011) Peptide fingerprinting of Alzheimer's disease in cerebrospinal fluid: identification and prospective evaluation of new synaptic biomarkers. *PLoS ONE* **6,** e26540
21. Pasinetti, G. M., Ungar, L. H., Lange, D. J., Yemul, S., Deng, H., Yuan, X., Brown, R. H., Cudkowicz, M. E., Newhall, K., Peskind, E., Marcus, S., and Ho, L. (2006) Identification of potential CSF biomarkers in ALS. *Neurology* **66,** 1218–1222
22. Finehout, E. J., Franck, Z., Choe, L. H., Relkin, N., and Lee, K. H. (2007) Cerebrospinal fluid proteomic biomarkers for Alzheimer's disease. *Ann. Neurol.* **61,** 120–129
23. Bayés, A., and Grant, S. G. (2009) Neuroproteomics: understanding the molecular organization and complexity of the brain. *Nat. Rev. Neurosci.* **10,** 635–646
24. Croisier, E., MRes, D. E., Deprez, M., Goldring, K., Dexter, D. T., Pearce, R. K., Graeber, M. B., and Roncaroli, F. (2006) Comparative study of commercially available anti-α-synuclein antibodies. *Neuropathol. Appl. Neurobiol.* **32,** 351–356
25. Stine, W. B., Jungbauer, L., Yu, C., and LaDu, M. J. (2011) Preparing synthetic Aβ in different aggregation states. *Methods Mol. Biol.* **670,** 13–32
26. Helwig, M., Lee, S.-N., Hwang, J. R., Ozawa, A., Medrano, J. F., and Lindberg, I. (2011) Dynamic modulation of PC2-mediated precursor processing by 7B2. Preferential effect on glucagon synthesis. *J. Biol. Chem.* **286,** 42504–42513
27. Muller, L., Zhu, P., Juliano, M. A., Juliano, L., and Lindberg, I. (1999) A 36-residue peptide contains all of the information required for 7B2-mediated activation of prohormone convertase 2. *J. Biol. Chem.* **274,** 21471–21477
28. Zhu, X., Lamango, N. S., and Lindberg, I. (1996) Involvement of a polyproline helix-like structure in the interaction of 7B2 with prohormone convertase 2. *J. Biol. Chem.* **271,** 23582–23587
29. Giasson, B. I., Forman, M. S., Higuchi, M., Golbe, L. I., Graves, C. L., Kotzbauer, P. T., Trojanowski, J. Q., and Lee, V. M. (2003) Initiation and synergistic fibrillization of tau and α-synuclein. *Science* **300,** 636–640
30. Kjaer, A., Knigge, U., Bach, F. W., and Warberg, J. (1995) Stress-induced secretion of pro-opiomelanocortin-derived peptides in rats: relative importance of the anterior and intermediate pituitary lobes. *Neuroendocrinology* **61,** 167–172
31. Raman, B., Ban, T., Sakai, M., Pasta, S. Y., Ramakrishna, T., Naiki, H., Goto, Y., and Rao, Ch. M. (2005) αB-crystallin, a small heat-shock protein, prevents the amyloid fibril growth of an amyloid β-peptide and β_2-microglobulin. *Biochem. J.* **392,** 573–581
32. Tanaka, N., Tanaka, R., Tokuhara, M., Kunugi, S., Lee, Y. F., and Hamada, D. (2008) Amyloid fibril formation and chaperone-like activity of peptides from αA-crystallin. *Biochemistry* **47,** 2961–2967
33. Kim, K. K., Kim, R., and Kim, S. H. (1998) Crystal structure of a small heat-shock protein. *Nature* **394,** 595–599
34. Kopito, R. R., and Ron, D. (2000) Conformational disease. *Nat. Cell Biol.* **2,** E207–E209
35. Bianchi, F. T., Camera, P., Ala, U., Imperiale, D., Migheli, A., Boda, E., Tempia, F., Berto, G., Bosio, Y., Oddo, S., LaFerla, F. M., Taraglio, S., Dotti, C. G., and Di Cunto, F. (2011) The collagen chaperone HSP47 is a new interactor of APP that affects the levels of extracellular β-amyloid peptides. *PLoS ONE* **6,** e22370
36. Sasaki, K., Satomi, Y., Takao, T., and Minamino, N. (2009) Snapshot peptidomics of the regulated secretory pathway. *Mol. Cell. Proteomics* **8,** 1638–1647
37. Hu, X., Crick, S. L., Bu, G., Frieden, C., Pappu, R. V., and Lee, J. M. (2009) Amyloid seeds formed by cellular uptake, concentration, and aggregation of the amyloid-β peptide. *Proc. Natl. Acad. Sci. U.S.A.* **106,** 20324–20329
38. Lee, H. J., Patel, S., and Lee, S. J. (2005) Intravesicular localization and exocytosis of α-synuclein and its aggregates. *J. Neurosci.* **25,** 6016–6024
39. Bieschke, J., Herbst, M., Wiglenda, T., Friedrich, R. P., Boeddrich, A., Schiele, F., Kleckers, D., Lopez del Amo, J. M., Grüning, B. A., Wang, Q., Schmidt, M. R., Lurz, R., Anwyl, R., Schnoegl, S., Fändrich, M., Frank, R. F., Reif, B., Günther, S., Walsh, D. M., and Wanker, E. E. (2012) Small-molecule conversion of toxic oligomers to nontoxic β-sheet-rich amyloid fibrils. *Nat. Chem. Biol.* **8,** 93–101
40. Magrané, J., Smith, R. C., Walsh, K., and Querfurth, H. W. (2004) Heat shock protein 70 participates in the neuroprotective response to intracellularly expressed β-amyloid in neurons. *J. Neurosci.* **24,** 1700–1706
41. Andley, U. P. (2007) Crystallins in the eye: function and pathology. *Prog. Retin. Eye Res.* **26,** 78–98
42. Kanekiyo, T., Ban, T., Aritake, K., Huang, Z. L., Qu, W. M., Okazaki, I., Mohri, I., Murayama, S., Ozono, K., Taniike, M., Goto, Y., and Urade, Y. (2007) Lipocalin-type prostaglandin D synthase/β-trace is a major amyloid β-chaperone in human cerebrospinal fluid. *Proc. Natl. Acad. Sci. U.S.A.* **104,** 6412–6417
43. Kanekiyo, T., and Bu, G. (2009) Receptor-associated protein interacts with amyloid-β peptide and promotes its cellular uptake. *J. Biol. Chem.* **284,** 33352–33359
44. Narayan, P., Orte, A., Clarke, R. W., Bolognesi, B., Hook, S., Ganzinger, K. A., Meehan, S., Wilson, M. R., Dobson, C. M., and Klenerman, D. (2012) The extracellular chaperone clusterin sequesters oligomeric forms of the amyloid-β(1–40) peptide. *Nat. Struct. Mol. Biol.* **19,** 79–83
45. McLaurin, J., Golomb, R., Jurewicz, A., Antel, J. P., and Fraser, P. E. (2000) Inositol stereoisomers stabilize an oligomeric aggregate of Alzheimer amyloid β peptide and inhibit Aβ-induced toxicity. *J. Biol. Chem.* **275,** 18495–18502
46. Dasgupta, I., Sanglas, L., Enghild, J. J., and Lindberg, I. (2012) The neuroendocrine protein 7B2 is intrinsically disordered. *Biochemistry* **51,** 7456–7464
47. Jakob, U., Gaestel, M., Engel, K., and Buchner, J. (1993) Small heat shock proteins are molecular chaperones. *J. Biol. Chem.* **268,** 1517–1520
48. McHaourab, H. S., Godar, J. A., and Stewart, P. L. (2009) Structure and mechanism of protein stability sensors: chaperone activity of small heat shock proteins. *Biochemistry* **48,** 3828–3837
49. Paquet, L., Bergeron, F., Boudreault, A., Seidah, N. G., Chrétien, M., Mbikay, M., and Lazure, C. (1994) The neuroendocrine precursor 7B2 is a sulfated protein proteolytically processed by a ubiquitous furin-like convertase. *J. Biol. Chem.* **269,** 19279–19285
50. Lee, S.-N., Hwang, J. R., and Lindberg, I. (2006) Neuroendocrine protein 7B2 can be inactivated by phosphorylation within the secretory pathway. *J. Biol. Chem.* **281,** 3312–3320
51. Sigafoos, J., Chestnut, W. G., Merrill, B. M., Taylor, L. C. E., Diliberto, E. J., Jr., and Viveros, O. H. (1993) Identification of a 7B2-derived tridecapeptide from bovine adrenal medulla chromaffin vesicles. *Cell. Mol. Neurobiol.* **13,** 271–278
52. Winsky-Sommerer, R., Grouselle, D., Rougeot, C., Laurent, V., David, J. P., Delacourte, A., Dournaud, P., Seidah, N. G., Lindberg, I., Trottier, S., and Epelbaum, J. (2003) The proprotein convertase PC2 is involved in the maturation of prosomatostatin to somatostatin-14 but not in the somatostatin deficit in Alzheimer's disease. *Neuroscience* **122,** 437–447
53. Ranganathan, S., Williams, E., Ganchev, P., Gopalakrishnan, V., Lacomis, D., Urbinelli, L., Newhall, K., Cudkowicz, M. E., Brown, R. H., Jr., and Bowser, R. (2005) Proteomic profiling of cerebrospinal fluid identifies biomarkers for amyotrophic lateral sclerosis. *J. Neurochem.* **95,** 1461–1471
54. Clemente, C. D. (1985) *Gray's Anatomy of the Human Body*, 30th Ed., Lea & Febiger, Philadelphia

Article VII

Analyst

Dynamic Article Links ▶
View Article Online
DOI: 10.1039/C3AN01616A

Cite this: DOI: 10.1039/c0xx00000x

www.rsc.org/xxxxxx

ARTICLE TYPE

Electrochemical Analysis of the Fibrilation of Parkinson's Disease α-Synuclein

Paula Lopes,[a] Hans Dyrnesli,[a] Nikolai Lorenzen,[a,b] Daniel Otzen[a,b] and Elena E. Ferapontova*[a]

Received (in XXX, XXX) Xth XXXXXXXXX 20XX, Accepted Xth XXXXXXXXX 20XX

DOI: 10.1039/b000000x

Amyloid formation of proteins and peptides is an important biomedical and biotechnological problem, intensively studied and yet not fully understood. In this context, the development of fast and reliable methods for real-time monitoring of protein misfolding is of particular importance for unambiguous establishment of disease-, drug- and environmentally induced mechanisms of protein aggregation. Here we show that the extent of aggregation of α-synuclein (αSN), involved in Parkinson's disease and other neurodegenerative disorders, can be electrochemically monitored by oxidizing tyrosine (Tyr) residues surface-exposed in monomeric αSN and buried in fibrillated αSN adsorbed onto graphite electrodes. Adsorption of αSN, analyzed through the Tyr electrochemistry, followed the Langmuir adsorption isotherm. A degree of electrooxidation of Tyr in αSN decreased upon protein fibrillation and correlated with the extent of αSN aggregation determined by the spectroscopic analysis of the fibrillation process. Minor changes in the adsorption state of αSN were followed through the shift of the Tyr oxidation potential, consistent with the compact and less-compact/unfolded conformation of αSN. Our results allow reliable electroanalysis of the extent of αSN fibrillation *in vitro* and offer an efficient tool for future *in vivo* monitoring of the protein conformational state.

Introduction

Over 30 human diseases are now associated with amyloidogenesis, the formation of aggregated *β*-sheet polypeptide structures that appear as water-insoluble pathological deposits of amyloid fibrils. [1, 2] Among these diseases are such neurodegenerative disorders as Parkinson's disease (PD),[3] dementia with Lewy bodies,[4] multiple system atrophy,[5] and some cases of Alzheimer's disease.[6] All of them are related to aggregation and formation of insoluble fibrillar deposits of α-synuclein (αSN), a 14 kDa (140 amino acid residues) protein involved in neurotransmitter release and neuronal plasticity, stabilization of cellular membranes and protein interaction networks in brain.[7, 8] The primary structure of αSN is composed of three regions: the α-helical N-terminal region, which is crucial for the protein-membrane interactions, the hydrophobic 61-95 residues area (originally labeled as NAC, also shown to constitute the insoluble fibril core of senile plaques in Alzheimer's disease), and the C-terminal acidic region (Figure 1A).

In its native state αSN was shown to possess a highly unfolded and flexible random coil structure[9] that can exists as an equilibrium mixture of unstructured *α*-helix and *β*-sheet-rich conformers.[10] Under various conditions, αSN spontaneously forms amyloid fibrils through a nucleation mechanism; in this process pre-fibrillar oligomeric intermediates are also formed.[7, 11] The aggregation mechanism of αSN is still not completely clear. It was suggested that αSN first aggregates into soluble low molecular weight oligomeric species stabilized with a *β*-sheet structure interactions and then into insoluble higher molecular weight ordered fibrils.[11, 12] Aggregation of αSN into pathological structures is a late-stage event that occurs in some neurons.[11] αSN mutations and environmental conditions (*in vitro*: buffer or pH conditions; *in vivo*: phosphorylation, enzymatic truncation, chemical modifications via reactions with reactive nitrogen species produced in inflammation) promote pathogenic aggregation of αSN, also by shifting the equilibrium towards formation of the *β*-sheet conformers and their further aggregation.[10, 11] For example, truncation of the C-terminal region (last 20 amino acid residues) lead to the enhanced fibrillation of the protein as compared to native αSN.[13]

Unsurprisingly, factors influencing protein aggregation attract much attention in the context of neuropathological implications and mechanisms of disorders onset and prevention. Studies of protein misfolding and aggregation employ such physical-chemical methods such as circular dichroism spectroscopy (CD), [14] and small angle X-ray scattering, [15] fluorescence detection,[16] Fourier-transform infrared spectroscopy,[17] quartz crystal microbalance,[18] and electron microscopy and atomic force microscopy (EM and AFM) [19-21]. In particular, the detection of protein aggregation and visualization of plaques using thioflavin T (ThT) and its derivatives has become a reference method [22]. ThT, a cationic benzothiazole fluorescent dye, binds stoichiometrically to the *β*-sheet structure of amyloid fibrils in such a specific manner that their long axes are parallel, [23] leading to a change in the optical signal from the dye and enhanced

View Article Online
DOI: 10.1039/C3AN01616A

fluorescence.[24] Upon binding to β-sheets the peak of the emission spectrum for ThT shifts characteristically from ~450nm to ~490nm,[25] making quantification of binding possible. Formation of the protein amyloid structures can be also electrochemically assessed through oxidation of ThT and some other benzothiazole dyes specifically bound to the formed fibrils.[26] Electrochemical methods have also been successfully used for down to pM electroanalysis of proteins and their conformational changes.[27-31] With non-redox active proteins, electrochemical oxidation of tyrosine (Tyr), tryptophan (Trp), and cysteine residues of proteins has been used for sensitive nM-pM protein and peptide electroanalysis.[27, 28, 30-34] Electroanalysis of αSN at the hanging mercury drop electrode (HMDE) performed via monitoring of a so-called H peak (resulting from the protein catalyzed hydrogen evolution reaction) was shown to be particularly useful for analysis of the overall changes in the αSN structure, including its nucleation and aggregation. [35, 36]

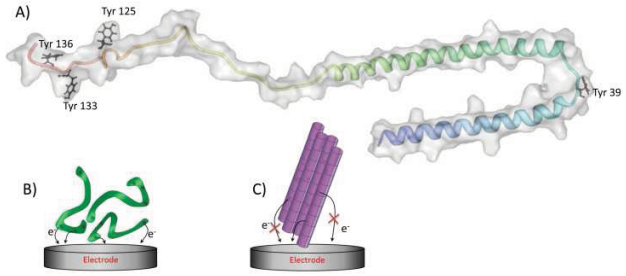

Fig. 1. Schematic representation of (A) the molecular structure of human αSN (PDB files ID:1xq8) and (B, C) the electrochemical assay for analysis of the protein aggregation based on electrooxidation of Tyr residues of αSN.

αSN possesses four redox active Tyr residues at positions 39, 125, 133 and 136 of the polypeptide chain, and any changes in the protein conformation due to nucleation and subsequent fibril formation are expected to affect the electrochemical accessibility of these Tyr residues. We anticipated that electrochemical monitoring of the aggregation process (as shown for Aβ–peptide fibrillation [28, 37]) will provide fast and reliable information on the conformational transitions (and thus extent of misfolding) in αSN (Figure 1B,C). In the present work we show that αSN amyloid formation can be followed and evaluated accurately by electrochemical analysis of the amyloid fibril structure of αSN adsorbed at the electrodes, by oxidizing the Tyr residues that are surface exposed in monomeric αSN and largely buried inside the protein after formation of the oligomeric structures.

Experimental

Materials

L-tyrosine (Tyr), tryptophan (Trp), Thioflavin T and components of buffer solutions were from Sigma-Aldrich (Germany). All reagents were of analytical grade or of ultra-high purity and used as received. All solutions were prepared with de-ionized Biocell Milli-Q water (18.2 MΩ, Millipore, Bedford, MA, USA). αSN was produced in competent *E. coli* BL21(DE3) cells with a plasmid vector pET11-D using auto-induction as described in ref. [38] To obtain high purity αSN the purification protocol described in refs. [39, 40] was used, modified with an additional acid precipitation step prior to ion exchange, where pH was lowered to pH 3.5 by a drop-wise addition of 1M HCl. A soluble protein was collected by centrifugation at 9.000 g, 4 °C, for 20 min. The pH of the supernatant was immediately adjusted to pH 7.5 with 1 M NaOH. Freshly dissolved αSN was filtered (0.2 µm filter) and its concentration was determined with a NanoDrop UV-VIS spectrophotometer (ND-1000, Thermo Scientific) using a theoretical extinction coefficient of 0.412 (mg $ml^{-1})^{-1}$ cm^{-1}. [41] All fibrillation experiments were conducted in a phosphate buffer saline buffer (20 mM phosphate, 0.15 M NaCl, PBS), pH 7.4, at 37 °C, and then the aliquots of the αSN solution in PBS, pH 7.4, were used for the electrode modification.

Methods

Electrode preparation. Rods of solid spectroscopic graphite (Gr, SGL Carbon AG, Werk Ringsdorff, Bonn, Germany, type RW001, 3.05 mm diameter) were cut; their disk surface was polished on emery paper (Tufbak Durite, P600), fitted into Teflon holders and used in electrochemical experiments. For protein film formation, 3 µl of the αSN aqueous solution in PBS, pH 7.4, (0, 1, 10, and 100 ng ml^{-1}, 1, 10, 25, 50, 100, and 500 µg ml^{-1}, 1 and 2 mg ml^{-1} (1.7 mg ml^{-1} for fibrils)) were placed onto the electrode surface and dried in a flow of N_2. Then the αSN-modified electrodes were thoroughly washed with a 20 mM phosphate buffer solution, containing 0.15 M NaCl (PBS), pH 7.0, and mounted in the cell.

Instrumentation and procedure. Cyclic voltammetry (CV) and differential pulse voltammetry (DPV) were performed at 22±1°C in a standard three-electrode cell connected to the potentiostat AUTOLAB PGSTAT 30 (Eco Chemie B. V., Utrecht, Netherlands) equipped with a GPES 4.9.007 software. An Ag/AgCl (3M KCl) electrode was the reference and a Pt plate was the auxiliary electrode. In DPV the effective scan rate was 20 mV s^{-1} (modulation amplitude was 50 mV, and modulation time was 50 ms). All measurements were performed in PBS, pH 7, as corresponding to the physiological conditions (brain media). The reproducibility of the data was verified by measurements with at least four equivalently prepared electrodes. Data fitting was performed with a Sigma-Plot Dynamic Fit Wizard program module.

Fibril formation and Thioflavin T fluorescence. A highly reproducible ThT-based fibrillation assay in a 96-well plate reader setup was used as described by Giehm et al. [42] Briefly, 150 µL of 70 µM αSN (in PBS, pH 7.4, with 40 µM ThT) were loaded to each well in a clear bottom 96-well-plate (Nunc, Thermo Fisher Scientific, Denmark). Glass beads of 3-4 mm in diameter (Glaswarenfabrik Karl Hecht GmbH & Co KG, Germany) were added to each well and the plates were sealed with Crystal clear sealing tape (Hampton Research, America). The plate was loaded to a Genios Pro plate reader (Tecan, Switzerland) and incubated at 37° C for approximately 100 h. The plate was shaken with orbital agitation at 300 rpm for approximately 50 min h^{-1}. ThT fluorescence was measured every 20^{th} min with excitation at 450 nm and emission at 485 nm. During the αSN fibrillation process, triplicates were extracted from the plate every 3^{rd} hour and 20 µL from each triplicate were frozen in liquid nitrogen and subsequently stored at -20 °C prior to electrochemical measurements. In parallel, 100 µL of the assay

View Article Online
DOI: 10.1039/C3AN01616A

solution of each triplicate were centrifuged to remove fibrils and the concentration of a soluble protein in the supernatant was measured.

Results and discussion

Electrochemical oxidation of tyrosine at graphite electrodes

As can be followed from the CVs recorded in 10 μM solution of Tyr, at Gr electrodes Tyr is irreversibly oxidized at around 0.6 V (Figure 2). The CV peak potential corresponding to electrochemical oxidation of Tyr was 625±3 mV, while DPV gave a characteristic oxidation potential of 574±7 mV (Figure 2, inset). Oxidation of Tyr at spectroscopic graphite seems to be facilitated compared to the commonly used hydrophobic glassy carbon electrode material (0.87 V, at pH 7, solution chemistry [43] and 0.7 V, at pH 6, surface electrochemistry [44]).

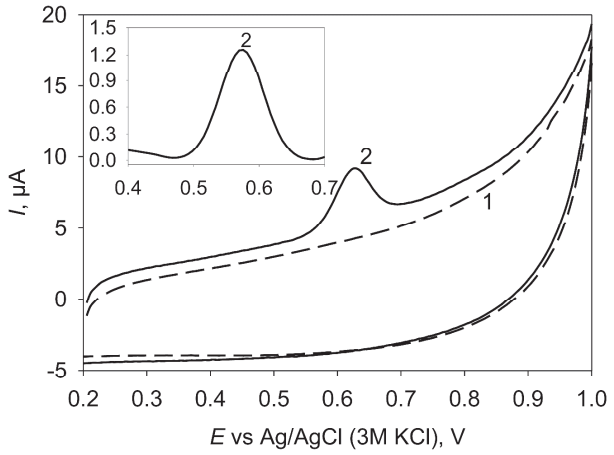

Fig. 2. Representative CV recorded with graphite electrodes (1) in the absence of Tyr and (2) in 10 μM solution of Tyr in PBS, pH 7. Potential scan rate is 50 mV s^{-1}. Inset: Representative DPV, the apparent scan rate is 20 mV s^{-1}.

The reported mechanisms of Tyr oxidation depend on the electrode materials and experimental conditions used (solution pH, oxidation potential, electrode material, composition of buffer solutions and solvent used); both $2e^-$ and $1e^-$ oxidations of Tyr have been discussed. [43-47] Likewise, the mechanism of Tyr oxidation in proteins and peptides is also expected to vary and depends on the experimental and environmental conditions,[44, 46, 48] under moderate oxidation conditions proceeding, in neutral and basic media, via $1e^-$ oxidation pathway. For the present studies, we note that the most important readout is the relative change of the electrooxidation signal, i.e. the relationship between the signals from native monomer and fibrillated αSN. This should provide the ratio between the surface exposed Tyr and Tyr buried inside the protein amyloid structure in the course of protein aggregation. In the context of the relative signal change, the reaction mechanism and absolute number of electrons involved in this reaction become less important, assuming that it is the same for different forms of αSN, namely the monomer and fibrillated protein forms.

Electrochemical analysis of αSN oxidation: potentials of Tyr oxidation.

Changes in the peptide conformation, due to nucleation and later aggregation, might affect the electrochemical signal from the Tyr residues in the peptide, as shown by Vestergaard et al.[28] by electroanalysis of the conformational state of Aβ-peptide in solution, thus enabling detection of the complete aggregation of the peptide. Here, the conformational state of the adsorbed αSN was interrogated at Gr electrodes through electrochemistry of its four Tyr residues as naturally existing electrochemical tags. The aim was to find out both the conditions enabling unambiguous monitoring of the protein aggregation (the native unfolded monomer state versus fibrillated).

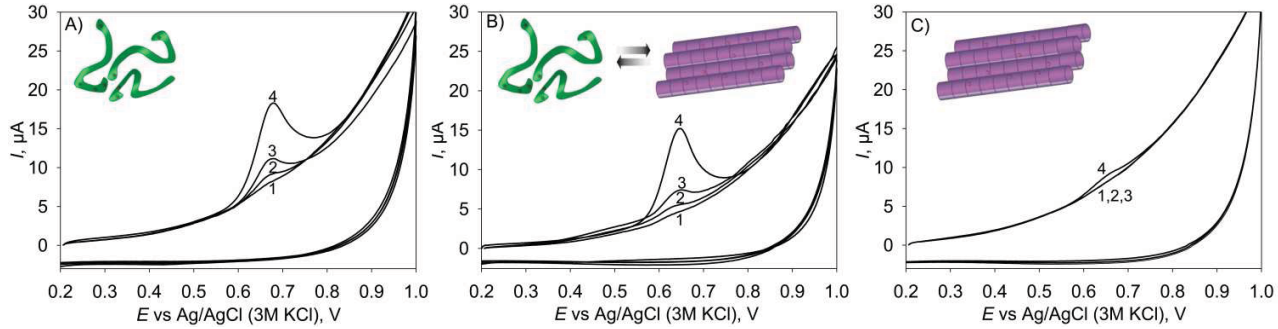

Fig. 3. Representative CVs of (A) native, (B) fibrillated mixture and (C) pure fibrils of αSN recorded at different concentrations, (1) 0.6 (2) 1.2 (3) 2.3 and (4) 11.5 μM, in PBS, pH 7. Potential scan rate is 50 mV s^{-1}.

A fibrillation mixture was prepared by allowing αSN fibrillation to run to completion according to the ThT fluorescence assay (PBS, pH 7.4, at 37°C for at least 50 hours). This led to a mixture of ca. 60% of αSN monomers transformed into fibrils, ca. 35-38% monomers left and negligible amounts of αSN oligomer.[15] In addition, we prepared a monomer-free solution by centrifuging the fibrillation mixture, after which the pellet, including the fibrils, was dissolved in buffer solution. The two different fibril preparations as well as non-aggregated αSN monomer were adsorbed onto the Gr electrodes, and electrochemical oxidation of Tyr residues of adsorbed αSN was followed. As can be seen in Figure 3, for monomeric αSN and the fibrillation mixture, Tyr oxidation proceeds with different efficiency (signal intensities for similar concentrations of the protein are different) and at slightly different potentials, 679±6 mV and 649±1 mV (Table 1). The signal from the sample containing solely fibrils was much smaller and may be attributed to the presence of residual monomeric αSN with surface exposed

View Article Online
DOI: 10.1039/C3AN01616A

Tyr residues, which form rapidly after dissolution of fibrils[49]. The potential of oxidation of native monomeric protein was 54 mV higher than that of free Tyr (625 mV, Figure 2) and 30 mV higher than that of Tyr in αSN samples containing both monomers and fibrils (Figure 4).

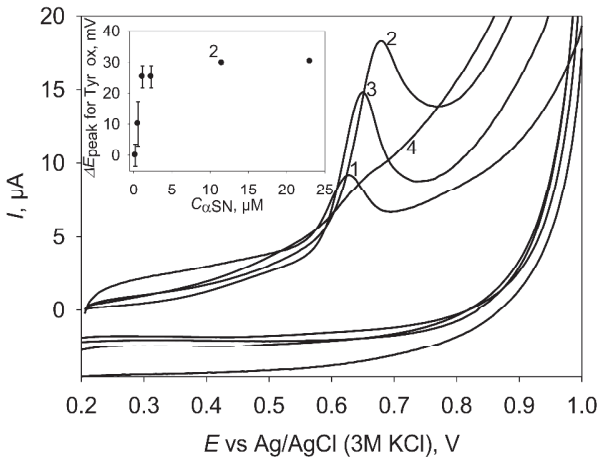

Fig. 4. Representative cyclic voltammograms of (1) 10 μM solution of Tyr and (2) monomer, (3) fibrillated mixture of αSN and (4) pure fibrils of αSN (11.5 μM) adsorbed on the electrode surface, recorded in PBS, pH 7. Potential scan rate is 50 mV s^{-1}. Inset: the shift in the oxidation potential of Tyr in monomer αSN plotted versus the concentration of αSN, evaluated from the DPV recorded under the same conditions as in the main figure, the apparent scan rate is 20 mV s^{-1}.

In general, redox properties of Tyr within the monomer polypeptide chain should be more similar to those of free Tyr, since all Tyr residues of the monomer protein are expected to be exposed to the Gr surface, while in fibrillated samples, providing generally less polar environment for Tyr electrooxidation, the shift of the oxidation potential towards more positive potentials may be expected, as previously observed with ferrocene redox species embedded in organic and thus less polar environment. [50, 51] It has previously been shown that monomeric αSN is more compact than a random coil, and it has been suggested that the Tyr-rich C-terminal tail (residue 120-140) shields the most hydrophobic part of αSN, the NAC region composed of residue 61-95 and directly involved in the amyloid fibril formation (Figure 1A), thereby inhibiting the aggregation of αSN.[52] Such long-range interactions, providing more intimate contact between tyrosines of the C-terminal region and the most hydrophobic/non-polar part of αSN, might correspondingly affect the kinetics of the Tyr oxidation reactions and result in a shift of the oxidation potential to more positive values. Fibrillation of αSN implies the presence of monomers in the fibrillated samples, though a different conformational state of monomer αSN can be expected. For such monomers C-terminal tyrosines may be no longer intimately interacting with the NAC region, which is commonly considered as a prerequisite/first step of oligomerization. Thus monomeric αSN in the presence of fibrils may be less compact and allow oxidation of its surface exposed Tyr, but at less positive Tyr oxidation potentials, as observed in Figure 4.

Two major conclusions may be drawn based on the results obtained. First, complete fibrillation of αSN makes all Tyr residues unavailable for electrooxidation at electrodes (only a residual signal representing less than 6% compared to that observed with monomers could be detected) Secondly, in the equilibrated fibrillated samples, the signal from Tyr oxidation is most likely to stem from monomers that are no longer in the compact C-terminal-NAC interaction state (the population of lower-weight oligomers is negligible under these conditions [15]). The potential shift thus observed for monomer αSN's Tyr and fibrillated αSN's samples can designate different extents of the protein conformational changes.

Table 1. Some experimental parameters characteristic of electrochemical oxidation of αSN at graphite evaluated for its saturating monolayer adsorption

αSN samples	Oxidation potential of Tyr residues, E_{ox}, V	CV peak currents, I_{lim}, μA, at 20 mV s^{-1}	Surface amount of αSN, pmoles	Limiting surface coverage, $\Gamma_{\alpha SN}$, pmol cm^{-2}
free Tyr	0.625±0.003	-	-	-
monomers	0.679±0.006	6.10± 1.13	81.2±14.3	111.2±19.59
fibrillated sample[a]	0.649±0.001	4.61±0.32	61.4±3.80	84.1±5.21
pure fibrils	0.665±0.090[b]	0.27±0.21	3.6±0.75	4.9±1.02

[a] sample at the end of the fibrillation time course, which contains a mixture of ca. 35-38% monomers, < 2%oligomers and ca. 60% fibrils
[b] the peak was too broad to more precisely determine the peak potential

Another important observation is the shift of the Tyr oxidation potential to more positive values with increasing αSN concentration (Figure 4, inset). Multiple interactions between the protein and the electrode surface may produce essential conformational changes,[53, 54] including protein unfolding as well. Such changes, expected to be most pronounced at lower concentrations of αSN (Figure 5B-a), may detrimentally affect the interactions between the C-terminus and the NAC region of αSN, thus shifting Tyr oxidation potential to less positive values, closer to the values characteristic of free Tyr and very similar to the values observed for fibrillated samples. At higher concentrations of αSN, providing conditions for the compact monolayer adsorption of the protein with minimized protein-Gr surface interactions, the probability of the protein adsorption in its most compact conformational state increases. A Tyr oxidation signal consistent with this conformation state is then observed (Figure 5B-d).

Electrochemical analysis of αSN oxidation: Adsorption behavior

With the increasing concentration of the monomer protein, the Tyr oxidation signal consistently increased, being directly proportional to the amount of αSN at up to 0.5 mg ml^{-1} (11.5 μM) αSN. It is important to mention, that all Tyr residues were completely oxidized in the first scan (no Tyr signal could be observed in the consecutive scans), so in the following we only discuss 1st scan data. The dependence of the Tyr oxidation

View Article Online
DOI: 10.1039/C3AN01616A

current, I, on the concentration of αSN, $C_{\alpha SN}$, to a first approximation followed a simple Langmuir isotherm (Figure 5):

$$I = I_{max} \times K \times C_{\alpha SN} / (1 + K \times C_{\alpha SN}) \quad (1)$$

with a maximal current I_{max} of 6.9±0.3 μA corresponding to a saturated protein monolayer consistent with 90.9±3.8 pmoles of the electroactive protein adsorbed (assuming one-electron electrooxidation of four Tyr residues per protein molecule). Here, K is the equilibrium parameter[55] that reflects the strength of adsorbate binding, namely the relationship between the adsorption-desorption constants, and equals 0.17±0.03 for the monomer αSN adsorbate (fitting of the experimental data to Eq. 1, solid line 1 in Figure 5A).

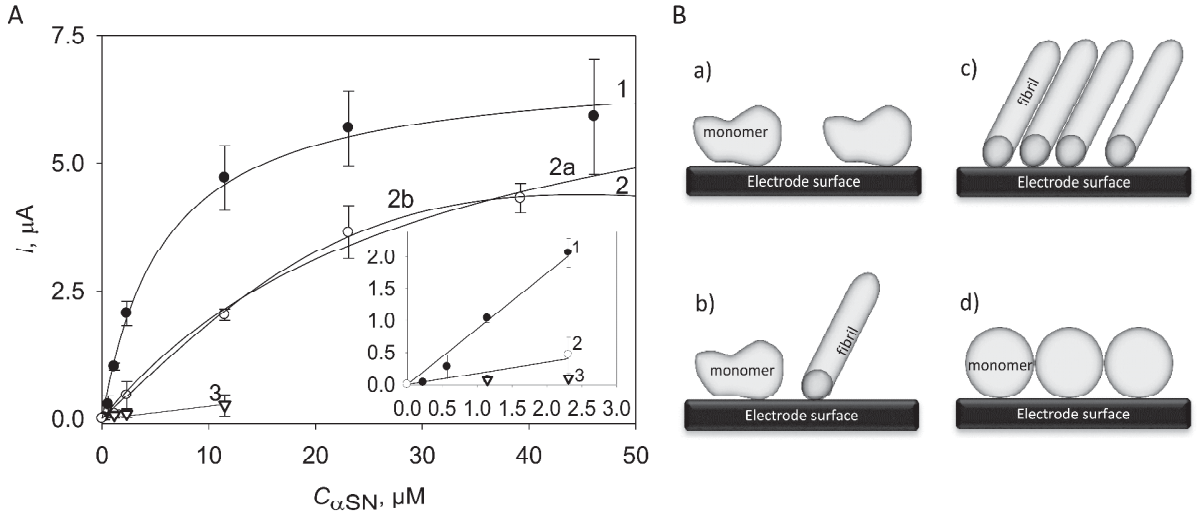

Fig. 5. Dependence of the Tyr oxidation signals (peak current, I), derived from CVs (A), plotted against the αSN concentration, monomer (1), fibrillated mixture of monomers and fibrils (2) and fibrils (3), in PBS pH 7. Potential scan rate was 20 mV s^{-1}. Solid lines 1 and 2a are non-linear curve fitting with Eq. 1, and 2b - with Eq. (2), see the text for more details. Inset: the linear response range for lower concentrations of αSN. (B) Schematic representation of adsorption of different states of αSN at the electrode surface. (a) monomer at low concentrations, (b) monomer and fibrils at low concentrations (c) fibrils at high concentrations and (d) monomers at high concentrations of αSN.

The experimentally measured maximum surface amount of αSN was 81.2 pmoles (Figure 5). It was of a particular interest to correlate this value with the actual surface coverage of the protein. The emery-paper polished surface of the spectroscopic graphite is highly microstructured, with a reported roughness factor of at least 5, [56] and thus is problematic for precise determination of the available for protein adsorption area [57, 58] Estimations of the electrochemically active surface area of the Gr surface polished to a mirror luster on Discovery office paper, Portucel S.A., Portugal, (additional polishing with office paper decreased the surface roughness) using the Cottrell equation, [55] with ferricyanide as a redox probe,[59] give a roughness factor of 2.1, while double-layer capacitance measurements indicated up to 4.5-fold increase in the electrode surface area for the emery-paper polished Gr used here as compared to the mirror luster polished Gr. Then, considering a Gr surface roughness of at least 10 and a resulting electrode surface coverage with the monomer protein (Table 1), the footprint of the αSN molecule on Gr will be around 1.51 nm^2 for experimentally observed currents and 1.33 nm^2 for a limiting monolayer conditions. While for totally unfolded αSN an average hydrodynamic radius was estimated to vary between 3.3-3.7 nm, compact αSN may have a radius as small as 0.7 nm,[52] approaching the protein minimal dimensions of around 0.5 nm^2. The latter value fits well our data and implies sufficiently tight packing of the compactly folded protein at the Gr electrode surface. This conclusion is also valid for the experimentally determined hydrodynamic radius of partially folded αSN of 2.7 nm (a one dimensional parameter)[52, 60] forming an ellipsoid with another dimension of around 0.6 nm.

At the microscopic level, αSN adsorption is definitely more complex process than the one following the Langmuir isotherm, to the energetically non-uniform micro-porous electrode surface and envisioned interactions between the adsorbed protein molecules. Nevertheless, data for native αSN fit well the simple Langmuir adsorption isotherm, Eq. 1. In the case of co-adsorption of monomer and fibrillated αSN, the Langmuir isotherm is not expected to properly describe the protein adsorption behavior (Figure 5A, 2). The dependence of the I on the $C_{\alpha SN}$ becomes less steep and the maximal current becomes less as well, which may be connected either with a competitive adsorption of fibrils or a lower amount of monomers in the monomer/fibril mixture with the same total amount of αSN. If the data in Figure 5A, 2, are fitted to the simplest case of the Langmuir isotherm (Eq. 1) for the $C_{\alpha SN}^{fibrillated} = 0.4 \times C_{\alpha SN}$, reflecting the corresponding decrease in the monomer concentration, a maximal current I_{max} of 7.9±0.7 μA and a K of 0.08±0.02 are obtained (solid line 2a in Figure 5A). Those values are inconsistent with the parameters extracted from the data in Figure 5A, curve 1 (adsorption of monomer αSN, the I_{max} of 6.9 μA and the K of 0.17) and they do imply that the observed effects are not related to the lower concentration of monomers, but to co-adsorption of fibrils.

On the other hand, fitting the data to a model involving competitive adsorption (curve 2b),[55] with the adjustment parameter for competitive co-adsorption m of -2, -1, -0.5, 0.5, 1

View Article Online
DOI: 10.1039/C3AN01616A

and 2 and $0.06 \leq x \leq 0.6$ (since the concentration of fibrils should be less than $0.6 \times C_{\alpha SN}$, as a result of the 2-15-mer and higher monomer aggregation[49]):

$$I = I_{max} \times K \times 0.4\ C_{\alpha SN}/(1 + 0.4K \times C_{\alpha SN} + (xK_1 \times C_{\alpha SN})^m), \qquad (2)$$

did not provide any physically relevant values for the I_{max} (becomes several amperes in magnitude) and K (dramatically decreases down to 10^{-12} values).

As can be seen in Figure 5A, Tyr electrooxidation signals in fibrillated αSN samples adsorbed onto Gr are lower than those from the monomer protein, which is consistent with the assumption that a smaller number of Tyr residues is now available for electrooxidation at the electrode surface, Tyr becoming hidden inside the protein structure upon the monomers alignment in β-sheets during fibrillation (Figure 3B,C). However, when the Tyr oxidation signals were calibrated versus the concentration of αSN, the signal variation for the protein concentrations higher than 20 μM αSN (conditions close to saturation) was not as high as might be expected from the composition of the fibrillated solution, which contains 35-40% of monomers. For saturation conditions, the signal decrease was 25%, correlating with at least 75% of the electrode surface occupied by the monomers and the rest of the surface by fibrils. Mature fibrils of 9.8 nm in diameter and 100-150 nm in length[21] may be composed of up to 150 monomer units[52], and then their theoretical surface coverage (for 25% of the electrode surface area left and 100 nm length of fibrils) may be estimated as 0.17 pmol cm^{-2}. This corresponds to approximately 26 pmol cm^{-2} of αSN monomers forming the fibrils. The rest of the electrode surface is occupied by co-adsorbed αSN monomers, which surface concentration is around 84 pmol cm^{-2} (the saturation adsorption conditions, Table 1). The ratio between fibrillated and monomer αSN adsorbed at the electrode surface (26:84, correspondingly) does not reflect accurately the composition of the fibrillated samples (60:40, maximum 40% of protein present in its monomer state) and thus the extent of αSN fibrillation.

At αSN concentrations lower than 3 μM, the difference in the Tyr oxidation signals for monomer and fibrillated samples becomes larger, providing conditions where no signal has been observed for fibrillated αSN samples, whilst an essential oxidation signal was detected for the monomer αSN samples (Figure 5A, inset). Formally, under these conditions no signal (or a very low signal) designates a maximal possible fibrillation of the protein (60% of αSN initially present in the sample), and the most pronounced differential variation of the Tyr oxidation signal upon fibrillation may be detected, which should allow better discrimination of the extent of the protein fibrillation in samples. Further electroanalysis of the effect of fibrillation on the electrochemical activity of αSN's tyrosines was studied under conditions of unsaturated monolayers that fall within the concentration range in the Figure 5A, inset.

Electrochemical monitoring of αSN fibrillation and correlation with the ThT fluorescence assay

Structural changes of αSN during the fibrillation process were followed by ThT fluorescence analysis and, in parallel, electrochemically, by electroanalysis of the Tyr oxidation signals. The oxidation potential of ThT is close to 0.9 V under the experimental conditions used and thus ThT oxidation does not interfere with the electrochemical oxidation of Tyr. The obtained fluorescence data were correlated with the electrochemically obtained ones to find out if the electrochemical method gives reliable information on protein fibrillation process and the extent of fibril formation.

The development of αSN fibrillation in time was followed by measurements of ThT fluorescence with 20 min time increments; the final level of ThT fluorescence corresponded to approximately 60% of αSN forming fibrils. In parallel, at each time step of fibrillation, aliquots of the protein solution were taken every three hours from the reaction mixture and analyzed electrochemically. Tyr oxidation currents (triplicate measurements) and ThT fluorescence were plotted within the same time scale to directly correlate the data on the extent of αSN aggregation (Figure 6).

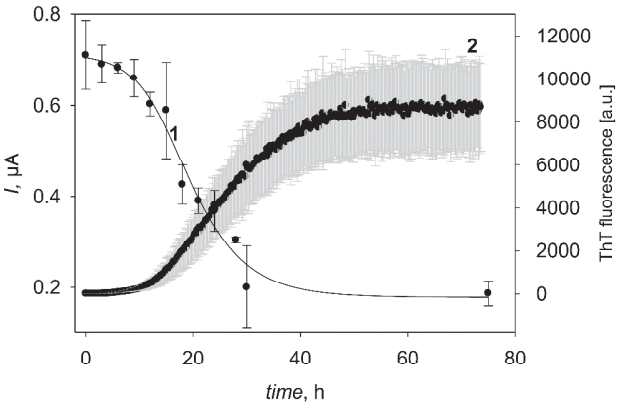

Fig. 6. Dependence of (1) the Tyr oxidation signals (peak current, I), derived from CVs, and (2) ThT fluorescence as a function of fibrillation time. Electrochemical measurements were performed with 1.15 μM αSN, in PBS, pH 7, and the potential scan rate of 20 mV s^{-1}.

Two extreme areas corresponding to monomer (zero time) and fibrillated αSN states (40-80 h of fibrillation) may be seen in Figure 6. The current, I, measured at t=0 correlates with electrooxidation of all available Tyr residues of αSN, while only background fluorescence can be followed under the same conditions. Both techniques reveal a 5-10 h lag-period time in the fibrillation process, after which, within the next 20 h, fibrillation is completed.

As expected, fibrillation results in the decreasing intensity of the Tyr oxidation signals and the increasing intensity of ThT fluorescence, reflecting the decrease of the apparent number of Tyr residues exposed to the electrode surface, due to the alignment of αSN monomers into β-sheet amyloid fibrils. The shape of the electrochemically obtained sigmoidal curve corresponds the different phases of the αSN fibrillation process, in good agreement with the inverted dependence of ThT fluorescence on time. The half-time of fibrillation shows only minor changes for the two techniques (21 h versus 24 h, for electrochemical and fluorescence analysis, respectively). That might be ascribed to the formation of αSN prefibrilar intermediates (protofibrils) and oligomeric forms with Tyr residues less accessible for electrochemical oxidation, which are not detectable by fluorescence analysis. The αSN oligomer formation, after 6 h of protein incubation, was earlier shown with

View Article Online
DOI: 10.1039/C3AN01616A

HMDE and supported by DLS measurements. [36] In the case of the Tyr-oxidation approach, taking into account a low population of oligomers present in solution (only a few percent of the total mass) and their relative instability, it is difficult to conclude if we are monitoring the oligomer growth, and we should ascribe our data to the fibrillation process. Thus, the proposed electroanalytical approach allows simple and fast analysis of the extent of αSN fibrillation in solutions of a low protein concentration, providing conditions for unsaturated protein monolayer formation.

Conclusions

We have shown that the extent of αSN amyloid fibril formation and the possible surface state of the protein can be followed and evaluated accurately by electrochemical analysis of αSN adsorbed at the electrodes, by oxidizing the Tyr residues that are surface exposed in monomer αSN and hidden inside the protein after formation of fibrillar structures. The Tyr residues of αSN adsorbed onto the surface of spectroscopic graphite electrodes are surface exposed and oxidized at potentials 54 mV higher than those of free Tyr. Minor conformational changes of monomer αSN were followed through a shift of the Tyr oxidation potential, becoming 30 mV less positive when the compact conformation consistent with the intimate interaction between the Try-rich C-terminus and the hydrophobic NAC region of αSN changed to the less compact/unfolded one. The extent of αSN aggregation into fibrils was followed via Tyr oxidation signal intensity, measured for the αSN concentrations down to 3 μM (1.15 μM) and confirmed by fluorescence studies of ThT binding to fibrillated protein. These results demonstrate that electroanalysis of αSN fibrillation provides reliable tools for the protein *in vitro* characterization and may be considered to be relevant for future *in vivo* research.

Acknowledgments

The work was supported by the Aarhus University starting grant to EF, the Danish Council for Independent Research, Natural Sciences (FNU), project number 11-107176 (EF), NL and DEO are supported by the Michael J. Fox Foundation and the Danish Research Foundation (inSPIN).

Notes and references

[a] *Interdisciplinary Nanoscience Center (iNANO), Science and Technology, Aarhus University, Gustav Wieds Vej 1590-14, DK-8000 Aarhus C, Denmark Fax: +45 8715 4041 ; Tel: +45 8715 6703; E-mail: Elena.Ferapontova@inano.au.dk*
[b] *Department of Molecular Biology and Genetics, Aarhus University, Gustav Wieds Vej 10C, DK-8000 Aarhus C, Denmark*

† Electronic Supplementary Information (ESI) available: [details of any supplementary information available should be included here]. See DOI: 10.1039/b000000x/

1. M. Stefani and C. M. Dobson, *J. Mol. Med.*, 2003, **81**, 678-699.
2. F. Chiti and C. M. Dobson, *Ann. Rev. Biochem.* , 2006, **75**, 333-366.
3. R. S. Harrison, P. C. Sharpe, Y. Singh and D. P. Fairlie, *Rev. Physiol. Biochem. Pharmacol.*, 2007, **159**, 1-77.
4. Arima K, Uéda K, Sunohara N, Hirai S, Izumiyama Y, Tonozuka-Uehara H and K. M, *Brain Res.* , 1998, **808**, 93-100.
5. Arima K, Uéda K, Sunohara N, Arakawa K, Hirai S, Nakamura M, Tonozuka-Uehara H and K. M, *Acta Neuropathol.* , 1998, **96**, 439–444.
6. O. Yokota, S. Terada, H. Ishizu, H. Ujike, T. Ishihara, H. Nakashima, M. Yasuda, Y. Kitamura, K. Uéda, F. Checler and S. Kuroda, *Acta Neuropathol.*, 2002, **104**, 637-648.
7. E. A. Waxman and B. I. Giasson, *Biochim. Biophys. Acta* 2009, **1792**, 616-624.
8. A. D. Gitler, A. Chesi, M. L. Geddie, K. E. Strathearn, S. Hamamichi, K. J. Hill, K. A. Caldwell, G. A. Caldwell, A. A. Cooper, J.-C. Rochet and S. Lindquist, *Nat. Genet.* , 2009, **41**, 308-315.
9. T. D. Kim, S. R. Paik and C.-H. Yang, *Biochemsitry*, 2002, **41**, 13782-13790.
10. M. Sandal , F. Valle, I. Tessari, S. Mammi, E. Bergantino, F. Musiani, M. Brucale, L. Bubacco and B. Samorì, *PLoS Biol.* , 2008, **6 (1)**, e6.
11. M. R. Cookson, *Mol. Neurodegener.* , 2009, **4**, 9 (1-14).
12. H. Y. Kim, H. Heise, C. O. Fernandez, M. Baldus and M. Zweckstetter, *ChemBioChem 8 (14):* , 2007, **8**, 1671–1674.
13. R. A. Crowther, R. Jakes, M. G. Spillantini and M. Goedert, *FEBS Lett.*, 1998, **436**, 309-312.
14. S. Ghodke, S. B. Nielsen, G. Christiansen, H. A. Hjuler, J. Flink and D. Otzen, *FEBS J.* , 2012, **279**, 752-765.
15. L. Giehm, D. I. Svergun, D. E. Otzen and B. Vestergaard, *Proc. Natl. Acad. Sci. U S A*, 2011, **108**, 3246-3251.
16. E. E. Nesterov, J. Skoch, B. T. Hyman, W. E. Klunk, B. J. Bacskai and T. M. Swager, *Angew. Chem. Int. Ed.*, 2005, **44**, 5452 –5456.
17. G. Zandomeneghi, M. R. Krebs, M. G. McCammon and M. Fändrich, *Protein Sci.* , 2004, **13**, 3314-3321.
18. T. P. J. Knowles, W. Shu, G. L. Devlin, S. Meehan, S. Auer, C. M. Dobson and M. E. Welland, *Proc. Natl. Acad. Sci. U S A*, 2007, **104**, 10016–10021.
19. A. L. Fink, *Acc. Chem. Res.*, 2006, **39**, 628-634.
20. H. A. Lashuel, B. M. Petre, J. Wall, M. Simon, R. J. Nowak, T. Walz and P. T. Lansbury J., *J. Mol. Biol.*, 2002, **322**, 1089-1102.
21. R. Khurana, C. Ionescu-Zanetti, M. Pope, J. Li, L. Nielson, M. Ramírez-Alvarado, L. Regan, A. L. Fink and S. A. Carter, *Biophys. J.*, 2003, **85**, 1135-1144.
22. W. E. Klunk, Y. Wang, G. Huang, M. L. Debnath, D. P. Holt, L. Shao, R. L. Hamilton, M. D. Ikonomovic, S. T. DeKosky and C. A. Mathis, *J. Neurosci.*, 2003, **23**, 2086 –2092
23. M. R. H. Krebs, E. C. H. Bromley and A. M. Donald, *J. Struct. Biol.*, 2005, **149**, 30-37.
24. R. Khurana, C. Coleman, C. Ionescu-Zanetti, S. A. Carter, V. Krishna, R. K. Grover, R. Roy and S. Singh, *J. Struct. Biol.*, 2005, **151**, 229-238.
25. H. Levine, *Protein Sci.*, 1993, **2**, 404-410.
26. A. J. Veloso, V. W. S. Hung, G. Sindhu, A. Constantinof and K. Kerman, *Anal. Chem.*, 2009, **81**, 9410-9415.
27. R. Kizek, L. Trnková and E. Palecek, *Anal. Chem.*, 2001, **73**, 4801–4807.
28. M. d. Vestergaard, K. Kerman, M. Saito, N. Nagatani, Y. Takamura and E. Tamiya, *J Am Chem Soc*, 2005, **127**, 11892-11893.
29. A. V. Kartashov, G. Serafini, M. Dong, S. Shipovskov, I. Gazaryan, F. Besenbacher and E. E. Ferapontova, *Phys. Chem. Chem. Phys.*, 2010, **12**, 10098-10107.
30. V. Ostatná, H. Cernocká and E. Palecek, *J. Am. Chem. Soc.*, 2010, **132**, 9408-9413.
31. E. Palecek, V. Ostatná, H. Cernocká, A. C. Joerger and A. R. Fersht, *J. Am. Chem. Soc.*, 2011, **133**, 7190-7196.
32. V. Brabec and I. Schindlerova, *Bioelectrochem. Bioenerg.*, 1981, **8**, 451-458.
33. J. A. Reynaud, B. Malfoy and A. Bere, *J. Electroanal. Chem.*, 1980, **116**, 595-606.
34. X. Cai, G. Rivas, P. A. M. Farias, H. Shiraishi, J. Wang and E. Palecek, *Anal. Chim. Acta*, 1996, **332**, 49-57.
35. M. Masařík, A. Stobiecka, R. Kizek, F. Jelen, Z. Pechan, W. Hoyer, T. M. Jovin, V. Subramaniam and E. Paleček, *Electronanalysis*, 2004, **16**, 1172-.
36. E. Palecek, V. Ostatna, M. Masarik, C. W. Bertoncini and T. M. Jovin, *Analyst*, 2008, **133**, 76-84.

View Article Online
DOI: 10.1039/C3AN01616A

37. K. Kerman, M. d. Vestergaard, M. Chikae, S. Yamamura and E. Tamiya, *Electrochem. Commun.*, 2007, **9**, 976-980.
38. F. W. Studier, *Protein. Expr. Purif.*, 2005, **41**, 207-234.
39. C. Huang, G. Ren, H. Zhou and C. C. Wang, *Protein. Expr. Purif.*, 2005, **42**, 173-177.
40. L. Giehm, N. Lorenzen and D. E. Otzen, *Methods*, 2011, **53**, 295-305.
41. E. Gasteiger, A. Gattiker, C. Hoogland, I. Ivanyi, R. D. Appel and A. Bairoch, *Nucleic Acids Res.*, 2003, **31**, 3784-3788.
42. L. Giehm and D. E. Otzen, *Anal. Biochem.*, 2010, **400**, 270-281.
43. G.-P. Jin and X.-Q. Lin, *Electrochem. Commun.*, 2004, **6**, 454-460.
44. A. Lokszteijn, W. Dzwolak and P. Krysinski, *Bioelectrochem.*, 2008, **72**, 34-40.
45. V. Brabec and V. Mornstein, *Biophys. Chem.*, 1980, **12**, 159-165.
46. S. M. MacDonald and S. G. Roscoe, *Electrochim. Acta*, 1997, **42**, 1189-1200.
47. C. J. Fecenko, T. J. Meyer and H. H. Thorp, *J. Am. Chem. Soc.*, 2006, **128**, 11020-11021.
48. J. Roeser, H. P. Permentier, A. P. Bruins and R. Bischoff, *Anal. Chem.*, 2010, **82**, 7556-7565.
49. N. Cremades, S. I. A. Cohen, E. Deas, A. Y. Abramov, A. Y. Chen, A. Orte, M. Sandal, R. W. Clarke, P. Dunne, F. A. Aprile, C. W. Bertoncini, N. W. Wood, T. P. J. Knowles, C. M. Dobson and D. Klenerman, *Cell*, 2012, **149**, 1048-1059.
50. S. E. Creager and G. K. Rowe, *J. Electroanal. Chem.*, 1997, **420**, 291-299.
51. S. Shipovskov, A. M. Saunders, J. S. Nielsen, M. N. Hansen, Gothelf K.V. and F. E.E., *Biosens. Bioelectron.*, 2012, **37**, 99-106.
52. M. M. Dedmon, K. Lindorff-Larsen, J. Christodoulou, M. Vendruscolo and D. C.M., *J. Am. Chem. Soc.*, 2005, **127**, 476-477.
53. T. Arai and W. Norde, *Coll. Surf.*, 1990, **51**, 1-15.
54. P. Roach, D. Farrar and C. C. Perry, *J. Am. Chem. Soc.*, 2005, **127**, 8168-8173.
55. A. J. Bard and L. R. Faulkner, *Electrochemical Methods - Fundamental and Applications*, 2nd edn., Wiley, New York, 2001.
56. H. Jaegfeldt, T. Kuwana and G. Johansson, *J. Am. Chem. Soc.* , 1983, **105**, 1805-1814.
57. M. Sosna, Bonamore A., Gorton L., Boffi A. and E. E. Ferapontova, *Biosens. Bioelectron.*, 2013, **42**, 219-224.
58. B. Royo, M. Sosna, A. C. Asensio, J. F. Moran and E. E. Ferapontova, *J. Electroanal. Chem.*, 2013, **704**, 67-74.
59. E. Ferapontova and E. Puganova, *J. Electroanal. Chem.*, 2002, **518**, 20-26.
60. A. S. Morar, A. Olteanu, G. B. Young and G. J. Pielak, *Protein Sci.*, 2001, **10**, 2195-2199.

View Article Online
DOI: 10.1039/C3AN01616A

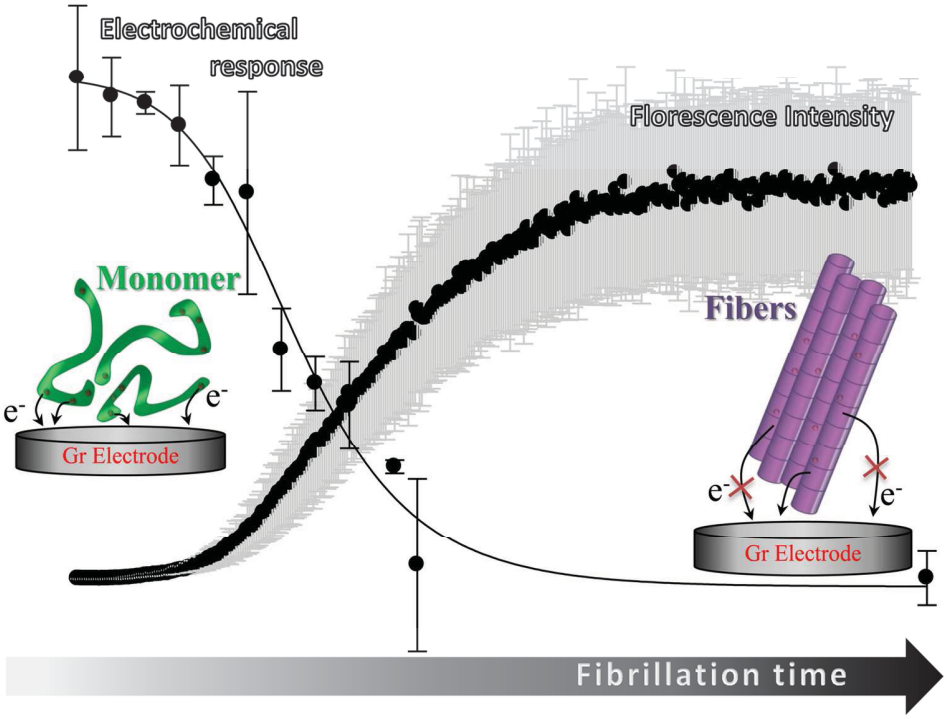

136x103mm (300 x 300 DPI)

Article VIII

The role of stable α-synuclein oligomers in the molecular events underlying amyloid formation

Nikolai Lorenzen[¶], Søren Bang Nielsen[¶], Alexander K. Buell[#], Jørn Døvling Kaspersen[§], Paolo Arosio[#], Brian Stougaard Vad[¶], Gunna Christiansen [‡], Zuzana Valnickova-Hansen[¶], Maria Andreasen[¶], Wojciech Paslawski[¶], Jan J. Enghild[¶], Jan Skov Pedersen[§], Christopher M. Dobson[#], Tuomas P. J. Knowles[#], and Daniel Erik Otzen[¶,*]

[¶]Interdisciplinary Nanoscience Center (iNANO), Department of Molecular Biology, Center for Insoluble Protein Structures (inSPIN), Aarhus University, Gustav Wieds Vej 14, 8000 Aarhus C, Denmark

[#] Department of Chemistry, University of Cambridge, Lensfield Road, CB2 1EW, Cambridge UK.

[§]Department of Chemistry and Interdisciplinary Nanoscience Center (iNANO), Aarhus University, Gustav Wieds Vej 14, 8000 Aarhus C, Denmark

[‡] Department of Biomedicine-Medical Microbiology and Immunology, Aarhus University, 8000 Aarhus C, Denmark

* To whom correspondence should be addressed at dao@inano.au.dk (D.E.O.)

Keywords: synuclein, aggregation, amyloid fibril, elongation, growth

ABSTRACT: Studies of protein amyloid formation have revealed that potentially cytotoxic oligomers frequently accumulate during fibril formation. An important question in the context of mechanistic studies of this process is whether or not oligomers are intermediates in the process of amyloid fibril formation, either as precursors of fibrils or as species involved in the fibril elongation process or instead if they are associated with an aggregation process that is distinct from that generating mature fibrils. Here we describe and characterize in detail two well-defined oligomeric species formed by the protein α-synuclein (αSN), whose aggregation is strongly implicated in the development of Parkinson's disease (PD). The two types of oligomers are both formed under conditions where amyloid fibril formation is observed but differ in molecular weight by an order of magnitude. Both possess a degree of β-sheet structure that is intermediate between that of the disordered monomer and the fully structured amyloid fibrils, and both have the capacity to permeabilize vesicles *in vitro*. The smaller oligomers, estimated to contain ~30 monomers, are more numerous under the conditions used here than the larger ones and small-angle x-ray scattering (SAXS) data suggest that they are ellipsoidal with a high degree of flexibility at the interface with solvent. This oligomer population is unable to elongate fibrils, and indeed results in an inhibition of the kinetics of amyloid formation in a concentration-dependent manner.

Introduction

It is increasingly well accepted that soluble oligomers of proteins associated with amyloid formation are the most important toxic species in a range of neurodegenerative disorders such as Parkinson's disease (PD) [1-4] and Alzheimer's disease (AD) [5-10]. There is good evidence that these oligomers possess, amongst other properties, the ability to disrupt membrane functions and thereby have the ability to induce neuronal damage [2,11,12]. Oligomers are often observed in co-existence with amyloid fibrils [13] but many aspects of the relationship between oligomers and the mechanism of amyloid fibril assembly are not yet understood. In some cases, oligomers appear to be direct building blocks of amyloid fibrils [14,15] but there are also examples of fibril systems where no significant quantities of oligomers are observed [16-21]; in other cases, the oligomeric species under study have been shown not to be direct precursors of fibrils [22-26]. There are also examples of different assembly processes in given protein systems leading to different types of fibril morphology and structure [27-29].

Recent advances in modern structural techniques have led to significant increases in our knowledge of the structures of amyloid fibrils, although such information is still limited. Thus, a range of techniques, notably X-ray diffraction of microcrystals [30] solid-state nuclear magnetic resonance spectroscopy (NMR), and cryo-electron microscopy have provided structural information at different levels of resolution of a series of amyloidogenic peptides and proteins [31-35]. Structural data on oligomers is, however, even sparser due to the transient nature and inherent polydispersity of such species [36,37] although such problems have been addressed by methods such as photochemical cross-linking [38] and protein engineering [39].

It is of great importance to understand the role of αSN oligomers in the aggregation process, not least because αSN is a highly validated drug discovery target for PD [40-43]. Here we analyze the role of well-defined αSN oligomers which accumulate under conditions where amyloid fibrils are formed, and which can be isolated. We have analyzed the structure and size distribution of these oligomers using size-exclusion chromatography coupled with online multi-angle laser light scattering (SEC-MALLS) and dynamic light scattering (SEC-DLS), native gel electrophoresis, transmission electron microscopy (TEM), atomic force microscopy (AFM) small-angle X-ray scattering (SAXS), Fourier transform infrared (FTIR) and circular dichroism (CD) spectroscopy. We identify two different oligomer populations which differ significantly in size but are structurally similar. Both oligomer populations are significantly more potent in membrane permeabilization than the monomers and fibrils. The small oligomers, which are most highly populated, on average consists of ca. 30 monomers. These appear to form an ellipsoidal structure with a compact core and a less highly structured corona, each making up 50 % of the total mass. Using an optimized thioflavin T (ThT) aggregation assay [44,45], we show that the oligomers inhibit fibril formation in a concentration dependent manner. The ThT time profiles can be fitted by a kinetic model in which the oligomers inhibit both the initial nucleation and the subsequent elongation steps. We also use a quartz crystal microbalance with dissipation monitoring (QCM-D), previously shown to be an excellent method to monitor fibril growth accurately [46-48], and confirm that isolated oligomers, unlike αSN monomers, are not able to elongate preformed fibrils significantly.

Materials and methods

Protein production and handling: Freshly dissolved αSN was filtered (0.2µm) prior to use and the concentration determined by absorption measurements with a NanoDrop instrument (ND-1000, Thermo Scientific) using a theoretical extinction coefficient of 0.412 $(mg/ml)^{-1}cm^{-1}$. (give units in $M^{-1}cm^{-1}$) All experiments were conducted in phosphate saline buffer (PBS) (20 mM phosphate, 150 mM NaCl, pH

7.4). Details of protein purification, oligomer purification, QCM, SEC-MALLS, SEC-DLS and SAXS are provided in Supporting information.

Plate reader fibril formation assays: ThT fluorescence was monitored using a 96-well plate reader setup as described previously[45].

Pore limit gel electrophoresis: The oligomers were analysed by pore limit gel electrophoresis in the presence of Tris, boric acid and EDTA system, as described previously [49]. In short, the samples were prepared under non-denaturing conditions (the addition of SDS and dithiothreitol was omitted) and separated by non-denaturing PAGE for 17 h at 100 V, using 4-20% gradient gels (10x10x0.15 cm^3). Oligomers were visualized by Coomassie Blue staining.

Circular dichroism spectroscopy: Far-UV wavelength spectra of αSN monomers, oligomers and fibrils with protein concentrations of 0.2 mg/ml (14 μM) in a 1 mm cuvette were obtained at 25 °C with a Jasco J-810 spectrophotometer (Jasco Spectroscopic Co. Ltd., Japan). Prior to CD analysis, fibril solutions were sonicated 3x 10 sec on ice with an HD 2070 Bandelin Sonuplus Sonicator (Buch and Holm, place of company).

ATR-FTIR spectroscopy: FTIR measurements were carried out with a Tensor 27 FTIR (Bruker Optics, Billerica, MA). 2 μL samples were loaded onto the crystal and carefully dried with nitrogen gas. Spectra were accumulations of 68 scans, measured with a resolution of 2 cm^{-1} in the range from 1000 to 3998 cm^{-1}. Data processing, consisting of atmospheric compensation, baseline subtraction, deconvolution with Lorentzian curves and second derivative analysis, was performed with the software OPUS version 5.5 (http://www.stsci.edu/software/OPUS/kona2.html). For comparison all absorbance spectra were normalized.

Transmission electron microscopy: 5 μL aliquots of 0.2-0.4 mg/ml αSN in PBS buffer were transferred to 400-mesh carbon-coated, glow-discharged grids for 30 sec. The grids were washed using two drops of doubly distilled water, stained with 1% phosphotungstic acid (pH 6.8) and blotted dry on filter paper. The samples were viewed in a microscope (JEM-1010; JEOL, Tokyo, Japan) operating at 60 kV. Images were obtained using an Olympus KeenViewG2 camera.

Dye leakage measurements: Dioleoyl-phosphatidylglycerol (DOPG) vesicles with a diameter of 100 nm containing 70 mM calcein were prepared by extrusion as described previously [50]. αSN monomers, oligomers and fibrils were each mixed in appropriate concentrations and loaded in a 96-well plate (Nunc, Thermo Fischer Scientific, Roskilde, Denmark) in triplicates. Calcein release was measured (excitation 485 nm; emission 520 nm) over 2 hrs in a Genios Pro fluorescence plate reader (Tecan, Mänerdorf, Switzerland) at 37 °C with 2 sec shaking every 2 min. Finally, Triton X-100 (0.1% (w/v)) was added to obtain 100 % calcein release. The saturated calcein levels after 2 hrs were corrected for background fluorescence and the % calcein release calculated.

Kinetic model: We consider an aggregation mechanism which includes primary nucleation, and fibril elongation and de-polymerization events characterized by reaction rate constants k_N, k_+ and k_{off}, respectively. In addition, since aggregation is induced under shaking conditions we expect that secondary nucleation events related to fibril fragmentation will also be important and are characterized by a rate constant k_2. The kinetic equation governing the formation of fibril mass during time, $M(t)$, is given by [51,52]:

$$\frac{M(t)}{M(\infty)} = 1 - \exp\left(-C_+ e^{kt} + C_- e^{-kt} + D\right) \quad (1)$$

where $M(\infty)$ is the fibril mass in the long-time limit and the constants are given as:

$$k = \sqrt{2\left(m_0 k_+ - k_{off}\right)k_2} \approx \sqrt{2m_0^{n_2+1}k_+ k_2} \quad (2)$$

$$\lambda = \sqrt{2k_+ k_n m_0^{n_C}} \quad (3)$$

$$C_\pm = \frac{\lambda^2}{2k^2} \pm \frac{k_+ P_0}{k} \pm \frac{k_+ M_0}{2(m_0 k_+ - k_{off})} \approx \frac{\lambda^2}{2k^2} \pm \frac{k_+ M_0}{k\bar{L}} \pm \frac{M_0}{2m_0} \quad (4)$$

$$D = \frac{\lambda^2}{k^2} - \frac{M_0}{M(\infty)} + \frac{k_+ M_0}{(m_0 k_+ - k_{off})} \approx \frac{\lambda^2}{2k^2} - \frac{M_0}{M(\infty)} + \frac{M_0}{m_0} \qquad (5)$$

where m_0, M_0 and P_0 are, respectively, the monomer concentration, the seed mass concentration and the seed number concentration at time zero. The seed mass and number concentrations are connected via the average fibril length, $\bar{L} = \frac{M_0}{P_0}$.

Surface tension measurements: The effects of monomers and oligomers on the surface tension were analyzed with the pendant drop method using a KSV CAM 101 surface tension meter (KSV Instruments Ltd.). For every protein concentration, three different drops were measured and 20 pictures were obtained from each drop. The surface tension was determined by fitting the drop shape with the CAM software (KSV Instruments Ltd.).

Results

Both types of αSN oligomers have a distribution of sizes: In accordance with our previous approach to optimizing αSN oligomer formation [1], oligomers were prepared by incubation of monomeric αSN at 12 mg/ml for 5 hrs. The Superose 6 matrix was able to separate monomers from two distinct oligomer populations eluting around ~14.8 and ~19.4 min (Fig. 1A). In the following discussion, we refer to these two populations as the large oligomers and the small oligomers, respectively. Typically, the small and large oligomers formed, respectively, 2-5 % and < 1 % of the total αSN population. Based on the elution times of known globular proteins, we estimated the M_r to be 1812±60 kDa for the small oligomers and 67±11 kDa (n=3) for the monomers (since monomeric αSN is natively unfolded, its size will be overestimated by all methods which rely on hydrodynamic volume). We were not able to estimate the M_r of the large oligomers, which elute at, or close to, the exclusion limit (~$4x10^4$ kDa) of the SEC matrix (Fig. 1ACD). Superdex 120 and Superdex 200 (exclusion limits at ~100 kDa and ~1.300 kDa, respectively) matrices were found to separate monomers from oligomers but were unable to separate the small and large oligomers which both eluted in the exclusion limits [1].

The two oligomer populations also could not be separated by conventional gel electrophoresis techniques and pore limit gel-electrophoresis (PLGE), which are optimized for separation of large proteins. However, SEC followed by non-denaturing PLGE (Fig. 1B) revealed a smear of sizes ≥ ~670 kDa for the small oligomers. The large oligomers migrated as a much narrower band, an effect likely to be caused by the limited pore size of the gel.

To determine the sizes of the two types of oligomers independently of their hydrodynamic radius, we combined SEC with multi-angle laser light scattering (MALLS) (Fig. 1C). Consistent with the Superose 6 matrix exclusion limit of ~$4x10^4$ kDa for globular proteins, size species exceeding 10^4 kDa occur in the void volume with a weight-averaged Mw of (5.8±3.3)$x10^3$ kDa (n=6) and thus in the upper range of the optimal separation range of the separation medium (5 kDa-$5x10^3$ kDa). Mw estimates of the smaller oligomer population ranged from ~310±90 to 770±210 kDa with a weight-averaged value of 430±88 kDa (n=7) across the peak, corresponding to 30±6 aSN monomers in each oligomer.

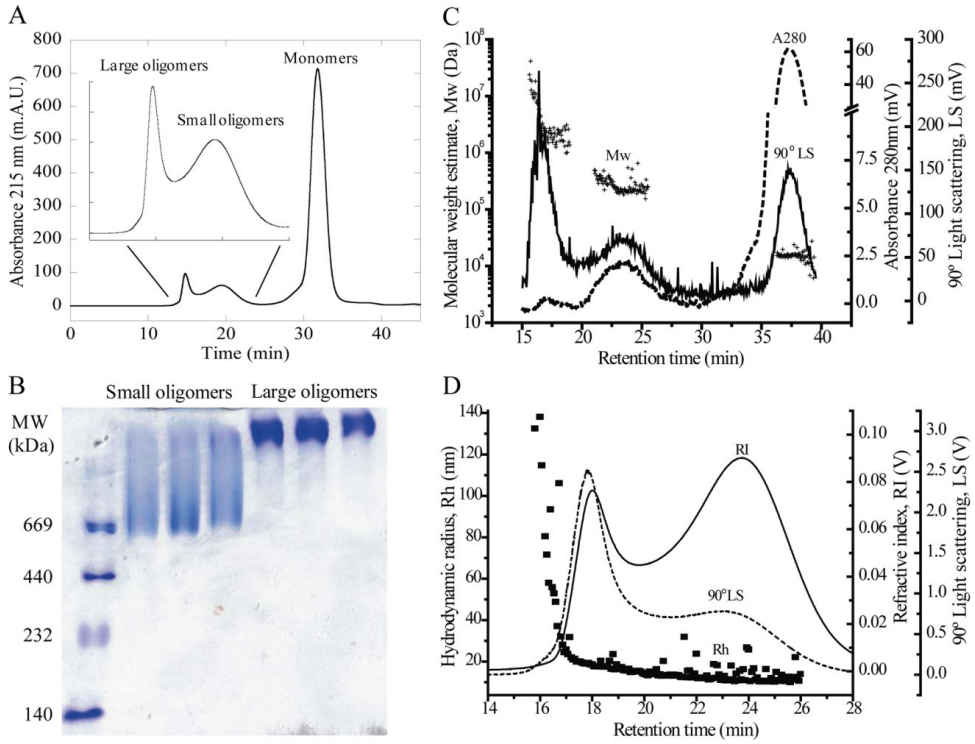

Figure 1. Analysis of the size distribution, molecular weights and hydrodynamic radii of the oligomer populations. A: SEC separation of monomers, small oligomers and large oligomers. An expanded region of the oligomer populations is included. B: Pore-limit native gel-electrophoresis of fractionated small and large oligomers. C: SEC-MALLS analysis of the oligomer populations measured with 90º light scattering and 280 nm absorbance. The Mw of large oligomers, small oligomers and monomers estimated with MALLS is shown. D: Hydrodynamic radii estimated with SEC-DLS are shown together with refractive index and 90º light scattering.

SEC-DLS was used to estimate the hydrodynamic radius (R_h) of eluting oligomer species (Fig. 1D). Aggregate sizes >100 nm in hydrodynamic radius (well in excess of the Superose 6 pore size of ~40 nm) were observed in the void volume, quickly declining to ~30 nm. R_h values of ~19 nm and ~11 nm were obtained from the peak maxima for the large and small oligomers, respectively (Fig. 1D).

TEM pictures of isolated small oligomers as well as large oligomers show that the small oligomers are generally spherical (Fig. 2A), while the large oligomers are distinctly elongated and co-exist with occasional short fibrils of length ~150-300 nm (Fig. 2B). AFM analysis of the small oligomers revealed a disc shape structure with an average height of 1-2 nm (Fig. 2C). Protein aggregates with a loose structure are expected to collapse when they are dried on mica, so the apparent small height is probably caused by drying artifacts.

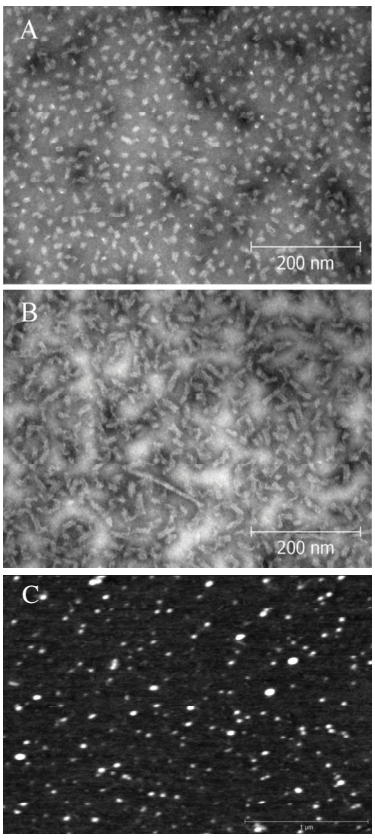

Figure 2. Structure analysis of the small oligomers. TEM images of (A) small oligomers and (B) large oligomers (C) AFM images of the small oligomers (C).

Small and large oligomers have a similar secondary structure content that differs from those of both monomers and fibrils: The secondary structures of the small and large oligomers are identical when analyzed by FTIR and CD (Fig. S1). This similarity is remarkable, given their substantial size difference. , The monomer has an absorption maximum in the amide I region of the FTIR spectrum at 1657 cm^{-1} (Fig. 3A) as determined by second derivative analysis (data not shown); this wavelength corresponds to disordered structure [53-55]. Reference spectra of well-defined random coil proteins in H_2O have a band at 1660-1642 cm^{-1} with a maximum at 1654 cm^{-1} [55]. α-helices also absorb within this region (1660-1648 cm^{-1}), but H/D exchange band shift analysis has previously shown that the band for αSN monomers in this region can be assigned to disordered structure [55]. Previous FTIR analysis demonstrates that the oligomers are likely to consist of anti-parallel β-sheets and fibrils of parallel β-sheets [54]. Our oligomer and fibril FTIR spectra (Figs. 3A, S1) are in good agreement with similar data reported by Raussens and co-workers, who use comparable methods to prepare oligomers [12,54,56,57]. The oligomer spectrum shows a maximum at 1655 cm^{-1}, indicative of a significant degree of disordered structure [53,55], while the peak maximum at 1623 cm^{-1} and a weak but significant contribution at 1695 cm^{-1} (Fig. 3A) both suggest anti-parallel β-sheet structure [54]. Thus FTIR spectra support the combination of compact and extended structure predicted by our SAXS data, see later.

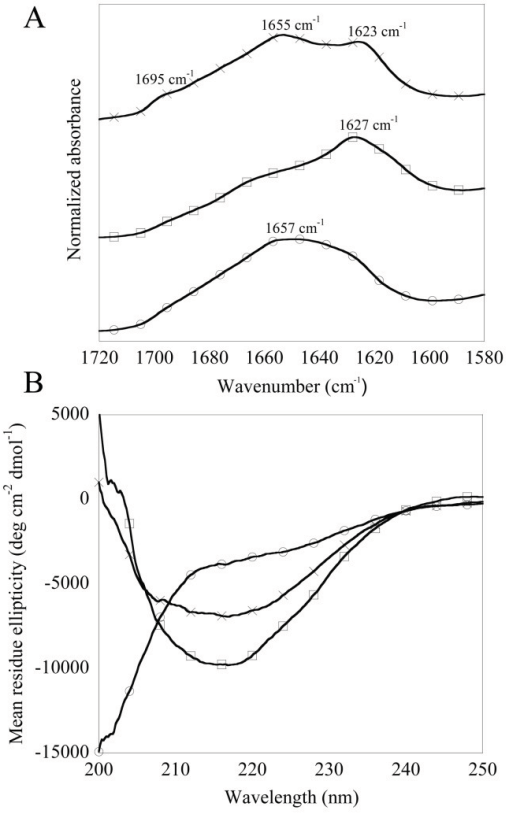

Figure 3. Analysis using FTIR (A) and CD (B) of monomers (circles), fibrils (squares) and small oligomers (crosses). In the FTIR spectra the peak maximum, determined with secondary derivative analysis, is indicated and the spectra are displaced for better comparison.

Far-UV CD analysis also reveals that the spectra of the two oligomers differ from those of both monomers and fibrils (Fig. 3B). That of the monomers resembles the classical spectrum of an unstructured protein. The oligomer and fibril spectra differ clearly in the intensity of different wavelengths, although both have a minimum at 217 nm, which, in conjunction with the absence of minima at 208 and 222 nm, indicates the presence of β-sheet rather than α-helical structure. The secondary structure composition of the oligomers could not be estimated using conventional fitting programs. Nor could the oligomer spectra be reconstructed by linear combinations of the monomer and fibril spectra (deviations were particularly pronounced around 200-210 nm), indicating that the oligomers exist as distinct species.

Both oligomers bind ANS: The fluorophore 1-anilinonapthalene-8-sulfonate (ANS) has been found to show binding specificity towards a variety of amyloid oligomers [58]. In the present study, both fibrils and oligomers were found to increase ANS fluorescence emission intensity and to generate a blueshift significantly larger than that of monomer (although the shift in λ_{max} of fibrils and oligomers is less pronounced than previously observed [58]). Fibrils lead to higher ANS intensity, but to a smaller ANS blueshift (Fig. S4), indicating that the nature of the ANS binding sites are different in the oligomers and the fibrils. As with the FTIR and CD data, ANS fluorescence intensity and λ_{max} in the presence of the small and large oligomers is identical (Fig. S4).

Both oligomers permeabilize vesicles: Both small and large oligomers are significantly more potent in inducing the loss of calcein from inside vesicles than the monomers (Fig. 4). We estimate that the stoichiometric potency of the small oligomers to disrupt vesicles is ~500, *i.e.* one oligomer is as potent in inducing calcein release as ~500 monomers (Table 1). The fibrils are significantly less potent than the oligomers, see Fig. S5 and Table 1. The high reproducibilities of both the dye leakage experiments and the oligomer preparations are revealed by the small standard deviation of the potency values, based on two separate experimental series (Table 1).

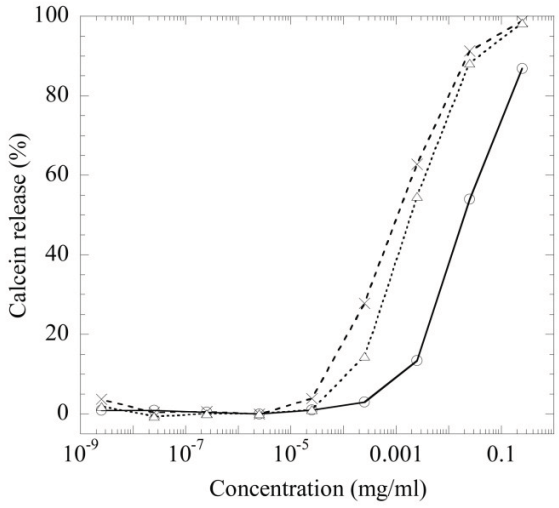

Figure 4. Calcein release by small oligomers (crosses), large oligomers (hollow triangles), and monomers (hollow circles).

Table 1. Ability of different αSN species to release calcein from vesicles[a]

Species	$C_{50\%}$ (mg/ml)[b]	$C_{50\%}$ (μM, monomer)	Relative potency (concentration)[c]	Relative potency (stoichiometric)[d]
Monomer	0.019	1.31	1	1
Small oligomers	0.001	0.08	17	~500
Large oligomers	0.002	0.14	9	N/A
Fibrils	N/A	N/A	3	N/A

Notes:

[a] We estimate ~10% deviation on the relative potency when comparing distinct experimental series.

[b] Concentration needed for 50 % calcein release. Estimated by fitting data in Fig. 4 to a sigmoidal function.

[c] Defined as $C_{50\%}$(species)/$C_{50\%}$(monomer) (columns 2 and 3).

[d] As b, but based on the molar concentration of oligomer.

SAXS data of the small oligomers indicate an ellipsoid with a rim of flexible protein molecules: More detailed data on oligomer structure and size estimates were obtained from

SAXS. Our analysis has been limited to the small oligomers, since it is not possible to purify the large oligomers to sufficiently high concentrations for these experiments. SAXS data for αSN monomers and the small oligomers are presented in Fig. 5A together with the best fits of the models described as a function of the modulus of the scattering vector, given by $q = 4\sin(\theta)/\lambda$ where 2θ is the scattering angle and $\lambda = 1.54$ Å is the wavelength of the X-ray radiation. A first indication of the shape is provided by the model-independent $p(r)$ functions of the two data sets (Fig. 5B), which reflect the distribution of internal distances in the particles [59].

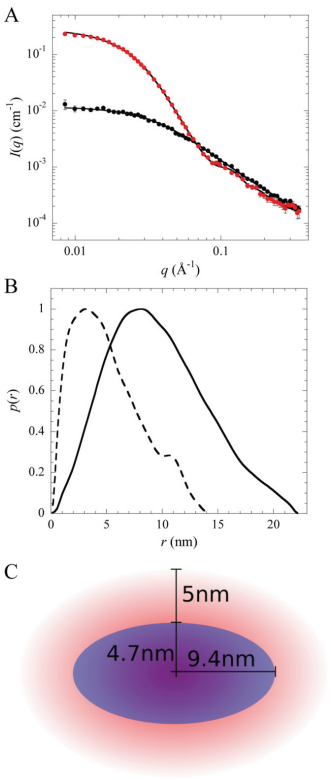

Figure 5. SAXS analysis of the small oligomers. A: SAXS data of monomers (filled squares) and oligomers (filled circles) with the best fit to data of the models described in the text. The data are normalized to a concentration of 1 mg/ml. B: p(r) functions of the monomer (dashed line) and oligomer (continuous line) data, normalized so the maximum value is equal to unity. C: Schematic representation of the oligomer model predicted from SAXS data.

The monomer data are those expected for a random coil with a maximum around R_g and a tail at larger distances. The R_g value of 4.23±0.11 nm is in good agreement with previously published values [60,61]. Independent fitting of the monomer data to a random coil model [62] gives an R_G of 4.2±0.05 nm. The correspondence of R_G values between these two approaches emphasizes that αSN is an intrinsically disordered protein, consistent with the literature [63].

While the symmetric bell-shape of the $p(r)$ function for the oligomers suggests some non-random structure, it also shows a rather long tail, indicative of a random coil. Indeed, the linear appearance of the spectrum at high-q values in a double logarithmic plot (seen for the oligomer at $q > 0.08$ Å^{-1}, Fig. 5A) typically originates from the scattering from disordered structure (q^{-2}). Combining these two types of structures, we find that the best model to fit the oligomer data consists of a core in the shape of a prolate ellipsoid (ellipse rotated around its major axis, dimensions R, R, εR, where ε is the width:height aspect ratio) with a rim of flexible protein molecules [64], as presented schematically in Fig. 5C.

We expect the number of polypeptide chains in the model of the SAXS data (q-dependence) to correspond to the experimentally determined number of molecules in the oligomer. This number has been determined from the forward scattering intensity, which provides the Mwt of the complexes if the concentration is known. From the forward scattering, we estimate the Mw of the oligomers to be ca. 420 kDa, which corresponds to ca. 29 monomers per oligomer, in excellent agreement with the SEC-MALLS estimation of 30±6 monomers. The results of the fit of the prolate ellipsoidal model fit to the oligomer data give $R = 4.72\pm0.17$ nm and $\varepsilon = 1.99\pm0.19$, while the radius of gyration of the attached coils is $R_g = 2.48\pm0.19$ nm. From the fit, the number of chains in the model is 21.1±3.3 nm, which is broadly similar to the number expected from the forward scattering (30±6.). The fraction of scattering length in the chains (which in this model corresponds to the volume or mass fraction of protein) is

0.46±0.02, indicating that around half of the protein is present in the flexible regions of the shell.

The presence of the oligomers alters the aggregation kinetics: To explore the role of the oligomers studied here in the process of amyloid fibril formation, we have analyzed their effects on the kinetics of fibril formation and of fibril elongation. To obtain as high a concentration of oligomers as possible, we purified the oligomers after incubating them under fibril forming conditions (12 mg/ml αSN for 5 hrs) and analyzed their effects in aggregation assays at 1 mg/ml. We obtained a similar fraction of oligomers at 1, 5 and 12 mg/ml (Fig. S5A). Moreover, fibrils formed at 1 and 12 mg/ml have the same FTIR and CD spectra (Fig. S2) and the same vesicle permeabilization potency (Fig. S5). To elucidate the roles of the oligomers in the aggregation pathway of αSN, we investigated the influence of the oligomers on the aggregation kinetics. We were unable to purify sufficient quantities of the large oligomer for these experiments, and confine ourselves to using a mixture of small and large oligomers (similar effects are seen for the small oligomers alone, implying that the two oligomers have essentially the same effect).

Seeding has been widely used to bypass the primary nucleation step of amyloid fibril formation[16]. When adding sonicated pre-formed αSN

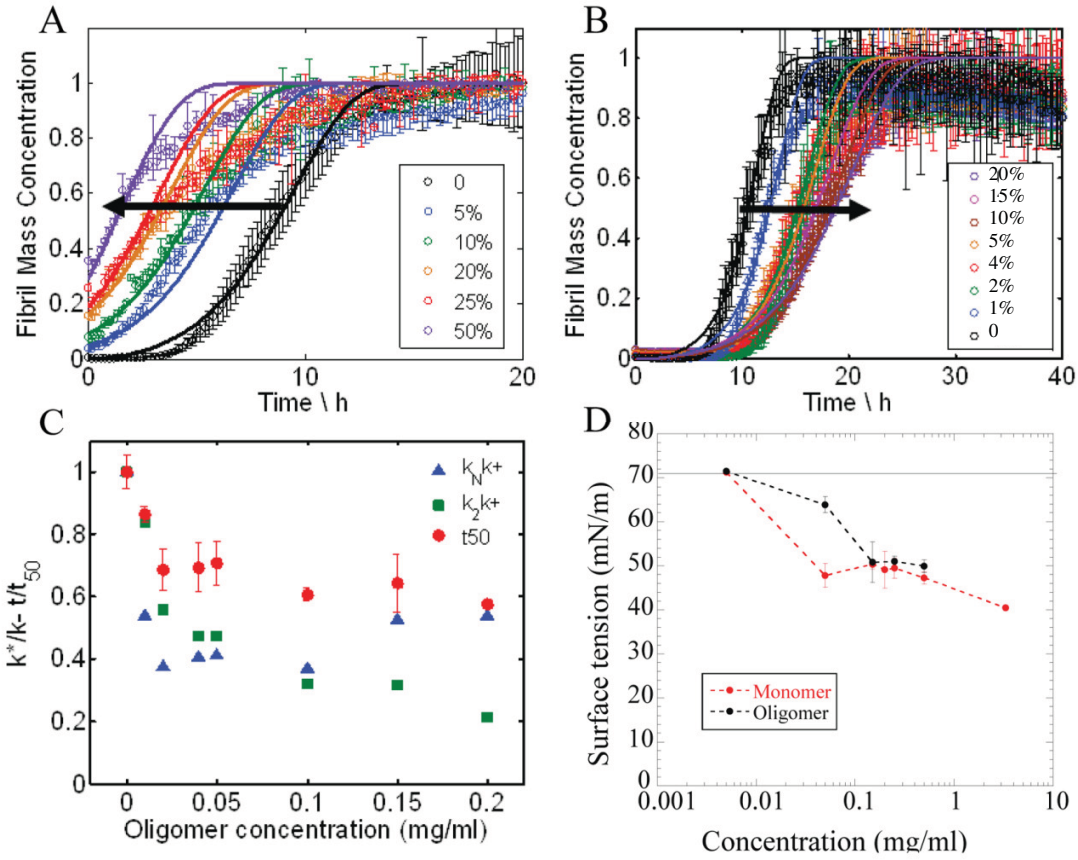

Figure 6. Kinetic analysis of the ability of different αSN species to inhibit the process of fibril formation. A: Seeding experiment with 1.2 mg/ml monomer and increasing amounts of pre-formed fibrils as seeds (5; 10; 20; 25; 50 % of monomer concentration). The continuous lines represent simulations to a model that includes fibril growth and fragmentation. B: Kinetic traces of 1 mg/ml monomer with increasing oligomer concentrations. The arrow indicates the increasing concentration of oligomers: (1; 2; 4; 5; 10; 15; 20 % of monomer concentration). Fibril mass have been normalized with respect to the final quantity of fibrils. The continuous lines represent simulations to

a model that includes primary nucleation and growth of fibrils (see SI). C: The microscopic rate constants corresponding to the simulations in B as well as the experimental half-times are plotted as a function of the oligomer concentration. The inhibitory effect of the oligomers reaches saturation at a critical oligomer concentration of about 0.05 mg/ml. D: Surface tension values as a function of monomer and oligomer concentrations. The decrease in surface tension shown in D and the inhibition effect shown in C reach saturation at a comparable critical concentration of oligomers.

fibrils (seeds) to monomers, aggregation is rapid (Fig. 6A). We can describe quantitatively the effects of the variation in seed concentration on the aggregation kinetics by applying theoretical analysis [51,52,65,66]. Since aggregation occurs under conditions of strong shaking, we included secondary nucleation induced by breakage together with primary nucleation and elongation as microscopic processes. The global fit of the data to such a model shows that it is able to explain the data quantitatively (Fig. 6A) [16].

To test whether the oligomers are able to accelerate the aggregation process in a fashion similar to the seed fibrils, we added different concentrations of oligomers to solutions of the monomeric protein. Remarkably, the oligomers do not shorten or eliminate the lag phase, as is the case for seed fibrils; rather, the oligomers lead to longer lag phases in a concentration-dependent manner (Fig. 6B). To rationalize this finding, we have fitted this data set to a model that allows for inhibition of the individual molecular steps, through semi-empirical rate constants which do not specifically include the oligomer but provide values for the rate constants associated with the individual molecular steps at different oligomer concentrations. The global fit together with the experimental data are shown in Fig. 6B and the corresponding microscopic kinetic rate constants are reported in Fig. 6C together with the experimental half-times. This analysis suggests that the oligomers may reduce both the primary nucleation and the elongation rate to an extent which reaches saturation at a critical oligomer concentration of about 0.05 mg/ml. Interestingly, this concentration is close to the concentration (0.1 mg/ml) beyond which surface tension does not decrease further (Fig. 6D). Increasing the oligomer concentration above the critical value does not further affect the aggregation kinetics.

To ensure that the inhibitory effect of the oligomers is not simply the effect of a decrease in the monomer concentration due to its sequestration by oligomers, we performed a simple binding assay (Fig. S6). We incubated monomers and oligomers for 1 hr under fibril forming conditions and compared the levels of the monomers and the oligomers before and after this procedure. Incubation with oligomers did not lead to any significant change in the monomer or oligomer concentrations, nor to any differences in the area of the oligomer peak (Table S1; Fig. S6), indicating that any sequestration was insignificant.

αSN oligomers do not elongate fibrils: We used the ThT fluorescence assay to determine whether or not the oligomers are able to elongate fibril seeds. When pre-formed seed fibrils were incubated with oligomers, hardly any increase in fluorescence was observed, whereas monomers at the same mass/volume concentration yielded the expected increase in fluorescence (Fig. 7A). This result suggests that the oligomers do not incorporate into fibrils to a significant extent.

To rule out that ThT-negative aggregates were formed upon interaction between oligomers and seed fibrils, we attached αSN fibril seeds on a sensor surface [67] and used QCM to monitor fibril growth directly, based on changes in the resonant frequency (Δf) of the sensor crystal [46,47,68]. To a first approximation, Δf is proportional to the change in the mass deposited on the crystal. First, all four channels were subjected to two injections of 20 μM freshly prepared monomer solution separated by a washing step. This procedure consistently led to essentially linear decreases in the resonant frequency (Fig. 7B), suggesting addition of

monomers to the growing end(s) of fibrils attached to the sensor surface. The same fibril-loaded sensors were then either incubated again with a solution of 20 µM (0.28 mg/ml) monomer or with one containing the same mass concentration (0.28 mg/ml) of oligomers to examine the possible interaction of oligomers with attached fibrils.

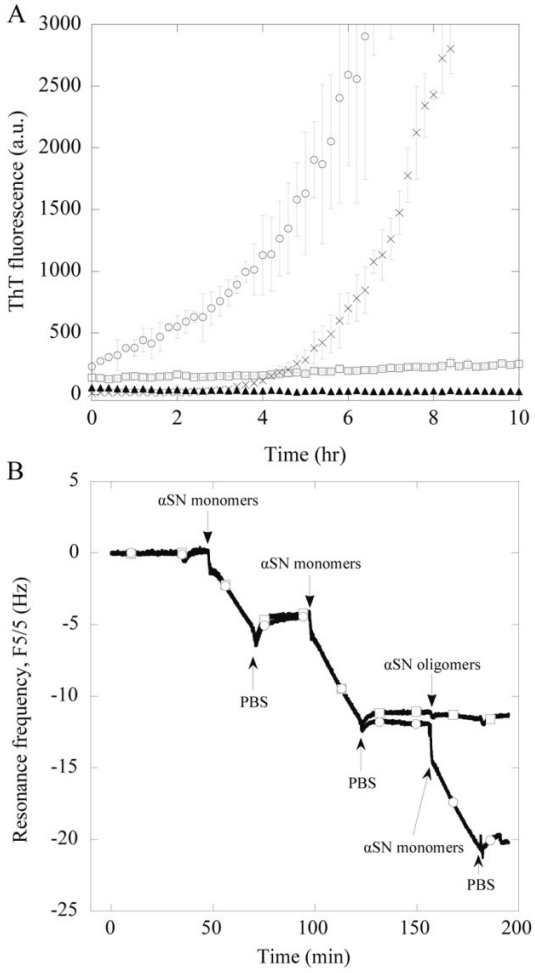

Figure 7**.** Kinetic analysis of the ability of oligomers to elongate seeds. A: Kinetic traces of fibril formation followed by observing ThT fluorescence of the following: 0.7 µM seeds (filled triangles); 0.7 µM seeds and 35 µM oligomers (squares), 0.7 µM seeds and 35 µM monomers (circles), and 35µM monomers (crosses). All datapoints are averaged triplicates and the standard deviations are shown. B: Direct monitoring of fibril growth by QCM with dissipation upon injection of 2x 20µM αSN monomers and either 20µM AS monomers (squares) or 20µM αSN oligomers (circles) separated by PBS washes. The experiment was repeated three times with qualitatively similar results.

While monomers efficiently elongated the attached fibrils, we consistently observed at most very small changes in resonant frequency when the sensors were incubated with oligomers; indeed the small Δf (as well as the small rise in ThT fluorescence in Fig. 7A) may be attributed to a small quantity of monomer in equilibrium with the oligomer preparation, as identified by analytical SEC of prepurified oligomers (Fig. S6).

Discussion

The small αSN oligomers consist of ca. 30 molecules and contain significant amounts of unstructured regions: SEC, gel electrophoresis and TEM show that αSN forms two distinct oligomer populations, and AFM confirm the spherical shape of the small oligomers observed with TEM. FTIR and CD measurements reveal that the small and large oligomers have similar secondary structure, distinct from both monomers and fibrils. Furthermore, both oligomer populations induce more vesicle permeabilization than monomers and fibrils (Table. 1), and give a similar response to the fluorophore ANS (Fig. S3).

Mw values of unstructured proteins are overestimated by methods relying on hydrodynamic volume, such as SEC, in the case of the 14.5 kDa αSN this effect leads to a 4-fold overestimate (67±11 kDa). However, when SEC is combined with MALLS, a reliable estimate (15±3 kDa) can be obtained which also agrees well with SAXS data (17.9 kDa). In the case of the small oligomers, the high quality of the SAXS fit (based on the assumption of a single species) indicates that there is limited polydispersity in our samples, consistent with the relatively narrow SEC peak for the small oligomer. SEC-MALLS and SAXS give estimates of the size of the small oligomers as 430±88 kDa and 420 kDa, respectively, corresponding to ca. 30 monomers per oligomer. This result is in good agreement with a single-molecule photobleaching

study by Subramaniam and co-workers in which the number of monomers in stable and well-defined αSN oligomers was determined to be 31 [69]. The higher estimates of the Mwt of the small oligomers from SEC and gel electrophoresis (1812±60 and 670 kDa, respectively) suggest the presence of a degree of extended structure; this conclusion is consistent with our SAXS based model, where a compact ellipsoidal core (50% of the mass) is surrounded by an outer rim of flexible regions of polypeptide chains (also 50% of the mass). The dimensions of the SAXS based model, a width of 15 nm and a height of 10 nm (Fig. 5C), are in good agreement with SEC-DLS data where the average R_h is determined to be 11 nm. Both CD and FTIR show a strong β-sheet signal, which FTIR suggests is organized in anti-parallel β-sheets. The FTIR data also suggest a significant contribution from disordered polypeptide structure, consistent with the flexible outer rim discussed above.

Comparisons with previous investigations of oligomer structure: We have previously followed the process of fibril formation of αSN by SAXS, in which we obtained spectra of the complete mixture of species present during aggregation[1]. We were able to decompose these spectra to obtain contributions from monomers/dimers, oligomers and fibrils, and to propose an ellipsoidal model for the oligomeric species. That model lacked a flexible outer layer, but its width:height dimensions (4.5:9.0 nm) are similar to the dimensions of the core of the oligomer structure determined in the present study (4.7:9.4 nm). The absence of an outer layer in the previous model most likely reflects the challenges of extracting data for individual species from mixtures; in contrast, the present study is based on purified species. We consider it unlikely that the process of purifying the oligomers should lead to structural changes such as the formation of an unstructured outer layer. Consistent with this conclusion, we do not observe from CD spectra any structural rearrangements in the oligomers during concentration of the sample (data not shown) and both concentrated and non-concentrated oligomers have a similar inhibitory effect on amyloid formation. In addition, concentrated small oligomers have the same Mw, as determined by SAXS as non-concentrated small oligomers analyzed by SEC-MALLS.

Oligomers induce greater perturbation in membranes than monomer. The ability of the N-terminus of the αSN monomer to fold into a helical conformation upon interaction with anionic vesicles is well described in the literature [70-72]. The N-terminal part of αSN (residues 1-60) is highly basic with a pI of 9.5, and electrostatic interactions with this part of the protein are believed to drive interaction with anionic vesicles. In the dye leakage experiment (Fig. 4 & S4) we found that ~500 monomers are needed to cause the same degree of calcein release as a single small oligomer (consisting of ca. 30 monomers). We suggest two possible mutually reinforcing reasons for oligomer potency. First, the initial 10-20 residues in the N-terminus could be disordered in the oligomers and located primarily in the outer rim. The N-terminus has previously been shown to be important for the interactions of oligomers with membranes [73] and we have demonstrated the importance of the initial 11 residues on the oligomers ability to interact with and permeabilize membranes (N. L. et al. FEBS letter. In revision). The simultaneous binding of several proximal N-termini to a vesicle would be expected to induce a high degree of disruption. In contrast, the monomers will be widely distributed in the membrane due to diffusion and electrostatic repulsion and are likely to bind more weakly, requiring higher concentrations to cause the same extent of release as oligomers. Secondly, the hydrophobic core of the oligomers which binds ANS (Fig. S3) might be included in the vesicle interactions and could lead to a stronger interaction and increased permeability. The lowered potency of fibrils may reflect that it is mainly the ends of the fibrils that interact with membranes [74,75] and in addition that much of the polypeptide chain is buried in the highly ordered structure. Nevertheless, fibrils are not completely inert, and at the stoichiometric level (but not in terms of mass units), one fibril might be more toxic than one oligomer, as proposed recently [76 77].

Oligomers are not able to elongate seed fibrils and they do not act as seeds: Our data analysis demonstrates that whereas sonicated fibrils (seeds) initiate the aggregation process efficiently through recruitment of monomers to the growth-competent ends, oligomers have an inhibitory effect, prolonging the lag time in a concentration dependent manner. There is no significant sequestration of monomers by oligomers, *i.e.* the oligomers do not prolong lag times by decreasing (or increasing) the effective monomer concentration, and QCM fails to detect direct interactions between oligomers and fibrils. The inhibitory effect on fibril formation reaches saturation at a critical oligomer concentration, which corresponds to the onset of the saturation in the decrease of surface tension with increasing oligomer concentration. This observation, together with evidence in the literature on the effect of air-water interfaces on αSN aggregation [78,79] , suggests that the critical oligomer concentration represents the point at which the interface is saturated with oligomers. The monomers and the oligomers therefore compete for the air-water interface, where primary nucleation of the aggregation process is likely to occur. Furthermore, we find that the oligomers are not able to elongate seed fibrils detectably.

We can refine our modelling even further: In a recent single molecule study, the characteristic time scale of rearrangment of one type of αSN oligomer into another type was determined to be of the order of $5x10^{-5}$ s^{-1} [80]. If we assume that the oligomers in the present study have to rearrange with a rate constant of this order of magnitude after attachment to a fibril end in order to create a template for further attachment, we find that fibril growth by oligomer addition is 2-3 orders of magnitude less efficient than growth by monomer addition (A.K.B. et al. in revision; see Fig. S7 and SI for details on the calculation).

Our previous SAXS study showed that oligomers of the type investigated here are mainly observed during the growth phase of fibril formation at a protein concentration of 12 mg/ml and disappear at the completion of the aggregation process [1], leading to our earlier suggestion that oligomers are the elongating species in the aggregation process. The present data, however, suggests instead that the disappearance of the small oligomers at the end of an aggregation reaction is due to their self-aggregation into much larger aggregates, as seen upon prolonged incubation (data not shown), or by dissociation into monomers as the concentration of the latter becomes depleted. The fact that we do not observe any other well-defined species between the monomers and the oligomers containing ca. 30 αSN molecules by means of SEC, SEC-MALLS or gel electrophoresis (data not shown) is consistent with monomers being the species which elongate αSN fibrils, as shown previously by analysis of the kinetics of aggregation (A.K.B. et al. in revision).

In summary, we have characterized the form of the αSN oligomer that is most prevalent under conditions where amyloid fibril formation is observed. The oligomers consist of an average of ~30 monomers and have an ellipsoidal structure, consistent with our previous SAXS study [1]. We find that the compact core is organized in β-sheet structure and that ca. 50 % of the polypeptide chains are unstructured and located in an outer rim. These oligomers are unable to elongate fibrils to a significant extent and also do not act as seeds for fibril growth.

AUTHOR INFORMATION

Corresponding authors

*Correspondence should be addressed to dao@inano.au.dk (D.E.O.).

Present addresses

Søren Bang Nielsen: Arla Foods Ingredients, R&D Nr. Vium, Sønderupvej 26, DK - 6920 Videbæk.

ACKNOWLEDGEMENT

N.L., S.B.N., B.S.V., M.A. and D.E.O are supported by the Michael J. Fox Foundation, the Danish Research Council (Industrial Post-doc and The Danish Council for Independent Research | Natural Sciences) and the Danish Research

Foundation (inSPIN). J.D.K. acknowledges LUNDBECKFONDEN for financial support. A.K.B. thanks EMBO, Magdalene College, Cambridge and the Leverhulme trust for support. C.M.D and T.P.J.K. thank the Wellcome trust and the BBSRC for funding.

References

(1) Giehm L, S. D., Otzen DE, Vestergaard B. *Proc Natl Acad Sci U S A* **2011**, *108(8)*, 3246-51.
(2) Lashuel, H. A.; Hartley, D.; Petre, B. M.; Walz, T.; Lansbury, P. T., Jr. *Nature* **2002**, *418*, 291.
(3) Conway, K. A.; Lee, S. J.; Rochet, J. C.; Ding, T. T.; Williamson, R. E.; Lansbury, P. T., Jr. *Proc Natl Acad Sci U S A* **2000**, *97*, 571-6.
(4) Beate Winner, T. J., Samir K. Maji, Paula A. Desplats, Leah Boyer, Stefan Aigner, Claudia Hetzer, Thomas Loher, Marcal Vilar, Silvia Campioni, Cristos Tzitzilonis, Alice Soragni, Sebastian Jessberger, Helena Mira, Antonello Consiglio, Emiley Pham, Eliezer Masliah, Fred H. Gage, Roland Riek *PNAS* **2010**.
(5) Walsh, D. M.; Selkoe, D. J. *J Neurochem* **2007**, *101*, 1172-84.
(6) Luheshi, L. M.; Tartaglia, G. G.; Brorsson, A. C.; Pawar, A. P.; Watson, I. E.; Chiti, F.; Vendruscolo, M.; Lomas, D. A.; Dobson, C. M.; Crowther, D. C. *PLoS Biol* **2007**, *5*, e290.
(7) Dobson, C. M. *Nature* **2003**, *426*, 884-90.
(8) Lesne, S.; Koh, M. T.; Kotilinek, L.; Kayed, R.; Glabe, C. G.; Yang, A.; Gallagher, M.; Ashe, K. H. *Nature* **2006**, *440*, 352-7.
(9) Nilsberth, C.; Westlind-Danielsson, A.; Eckman, C. B.; Condron, M. M.; Axelman, K.; Forsell, C.; Stenh, C.; Luthman, J.; Teplow, D. B.; Younkin, S. G.; Naslund, J.; Lannfelt, L. *Nat Neurosci* **2001**, *4*, 887-93.
(10) Bernstein, S. L.; Dupuis, N. F.; Lazo, N. D.; Wyttenbach, T.; Condron, M. M.; Bitan, G.; Teplow, D. B.; Shea, J. E.; Ruotolo, B. T.; Robinson, C. V.; Bowers, M. T. *Nat Chem* **2009**, *1*, 326-31.
(11) Bucciantini, M.; Giannoni, E.; Chiti, F.; Baroni, F.; Formigli, L.; Zurdo, J.; Taddei, N.; Ramponi, G.; Dobson, C. M.; Stefani, M. *Nature* **2002**, *416*, 507-11.
(12) Volles, M. J.; Lee, S. J.; Rochet, J. C.; Shtilerman, M. D.; Ding, T. T.; Kessler, J. C.; Lansbury, P. T., Jr. *Biochemistry* **2001**, *40*, 7812-9.
(13) Chiti, F.; Dobson, C. M. *Annu Rev Biochem* **2006**, *75*, 333-66.
(14) Hill, S. E.; Robinson, J.; Matthews, G.; Muschol, M. *Biophys J* **2009**, *96*, 3781-90.
(15) Vestergaard, B.; Groenning, M.; Roessle, M.; Kastrup, J. S.; van de Weert, M.; Flink, J. M.; Frokjaer, S.; Gajhede, M.; Svergun, D. I. *PLoS Biol* **2007**, *5*, e134.
(16) Lorenzen, N.; Cohen, S. I. A.; Nielsen, S. B.; Herling, T. W.; Christiansen, G.; Dobson, C. M.; Knowles, T. P. J.; Otzen, D. *Biophysical Journal* **2012**, *102*, 2167-2175.
(17) Kardos, J.; Yamamoto, K.; Hasegawa, K.; Naiki, H.; Goto, Y. *Journal of Biological Chemistry* **2004**, *279*, 55308-55314.
(18) Kim, H. J.; Chatani, E.; Goto, Y.; Paik, S. R. *Jounal of Microbiology and Biotechnology* **2007**, *17*, 2027-2032.
(19) Morris, A. M.; Watzky, M. A.; Finke, R. G. *Biochimica et Biophysica Acta* **2009**, 375-397.
(20) Knowles, T. P.; Fitzpatrick, A. W.; Meehan, S.; Mott, H. R.; Vendruscolo, M.; Dobson, C. M.; Welland, M. E. *Science* **2007**, *318*, 1900-3.
(21) Collins, S. R.; Douglass, A.; Vale, R. D.; Weissman, J. S. *Plos Biology* **2004**, *2*, 1582-1590.
(22) Jain, S.; Udgaonkar, J. B. *Biochemistry*, *50*, 1153-61.
(23) Necula, M.; Kayed, R.; Milton, S.; Glabe, C. G. *J Biol Chem* **2007**, *282*, 10311-24.
(24) Souillac, P. O.; Uversky, V. N.; Millett, I. S.; Khurana, R.; Doniach, S.; Fink, A. L. *J Biol Chem* **2002**, *277*, 12666-79.
(25) Gellermann, G. P.; Byrnes, H.; Striebinger, A.; Ullrich, K.; Mueller, R.; Hillen, H.; Barghorn, S. *Neurobiol Dis* **2008**, *30*, 212-20.
(26) Hong, D. P.; Han, S.; Fink, A. L.; Uversky, V. N. *Protein Pept Lett* **2011**, *18*, 230-40.
(27) Pedersen, J. S.; Dickov, D.; Flink, J. L.; Hjuler, H. A.; Christensen, G.; Otzen, D. E. *J. Mol. Biol.* **2006**, *355*, 501-523.
(28) Andersen, C. B.; Hicks, M. R.; Vetri, V.; Vandahl, B.; Rahbek-Nielsen, H.; Thogersen, H.; Thogersen, I. B.; Enghild, J. J.; Serpell, L. C.; Rischel, C.; Otzen, D. E. *J Mol Biol* **2010**, *397*, 932-46.
(29) Ghodke, S.; Nielsen, S. B.; Christiansen, G.; Hjuler, H. A.; Flink, J.; Otzen, D. *FEBS Journal* **2011**.
(30) Sawaya, M. R.; Sambashivan, S.; Nelson, R.; Ivanova, M. I.; Sievers, S. A.; Apostol, M. I.; Thompson, M. J.; Balbirnie, M.; Wiltzius, J. J.; McFarlane, H. T.; Madsen, A. O.; Riekel, C.; Eisenberg, D. *Nature* **2007**, *447*, 453-7.
(31) Tycko, R. *Curr. Opin. Struct. Biol.* **2004**, *14*.

(32) Nielsen, J. T.; Bjerring, M.; Jeppesen, M. D.; Pedersen, R. O.; Pedersen, J. M.; Hein, K. L.; Vosegaard, T.; Skrydstrup, T.; Otzen, D. E.; Nielsen, N. C. *Angew Chem Int Ed Engl* **2009**, *48*, 2118-21.
(33) Jaroniec, C. P.; MacPhee, C. E.; Bajaj, V. S.; McMahon, M. T.; Dobson, C. M.; Griffin, R. G. *Proc Natl Acad Sci U S A* **2004**, *101*, 711-6.
(34) Vilar, M.; Chou, H. T.; Luhrs, T.; Maji, S. K.; Riek-Loher, D.; Verel, R.; Manning, G.; Stahlberg, H.; Riek, R. *Proceedings of the National Academy of Sciences of the United States of America* **2008**, *105*, 8637-8642.
(35) Fitzpatrick, A. W.; Debelouchina, G. T.; Bayro, M. J.; Clare, D. K.; Caporini, M. A.; Bajaj, V. S.; Jaroniec, C. P.; Wang, L.; Ladizhansky, V.; Muller, S. A.; Macphee, C. E.; Waudby, C. A.; Mott, H. R.; De Simone, A.; Knowles, T. P.; Saibil, H. R.; Vendruscolo, M.; Orlova, E. V.; Griffin, R. G.; Dobson, C. M. *Proc Natl Acad Sci U S A* **2013**, *110*, 5468-73.
(36) Uversky, V. N. *FEBS J* **2010**, *277*, 2940-53.
(37) Fandrich, M. *J Mol Biol* **2012**.
(38) Rosensweig, C.; Ono, K.; Murakami, K.; Lowenstein, D. K.; Bitan, G.; Teplow, D. B. *Methods Mol Biol* **2012**, *849*, 23-31.
(39) Sandberg, A.; Luheshi, L. M.; Sollvander, S.; Pereira de Barros, T.; Macao, B.; Knowles, T. P.; Biverstal, H.; Lendel, C.; Ekholm-Petterson, F.; Dubnovitsky, A.; Lannfelt, L.; Dobson, C. M.; Hard, T. *Proc Natl Acad Sci U S A* **2010**, *107*, 15595-600.
(40) Polymeropoulos, M. H.; Higgins, J. J.; Golbe, L. I.; Johnson, W. G.; Ide, S. E.; Di Iorio, G.; Sanges, G.; Stenroos, E. S.; Pho, L. T.; Schaffer, A. A.; Lazzarini, A. M.; Nussbaum, R. L.; Duvoisin, R. C. *Science* **1996**, *274*, 1197-9.
(41) Spillantini, M. G.; Schmidt, M. L.; Lee, V. M.; Trojanowski, J. Q.; Jakes, R.; Goedert, M. *Nature* **1997**, *388*, 839-40.
(42) Spillantini, M. G.; Crowther, R. A.; Jakes, R.; Hasegawa, M.; Goedert, M. *Proc Natl Acad Sci U S A* **1998**, *95*, 6469-73.
(43) Polymeropoulos, M. H.; Lavedan, C.; Leroy, E.; Ide, S. E.; Dehejia, A.; Dutra, A.; Pike, B.; Root, H.; Rubenstein, J.; Boyer, R.; Stenroos, E. S.; Chandrasekharappa, S.; Athanassiadou, A.; Papapetropoulos, T.; Johnson, W. G.; Lazzarini, A. M.; Duvoisin, R. C.; Di Iorio, G.; Golbe, L. I.; Nussbaum, R. L. *Science* **1997**, *276*, 2045-7.
(44) Levine, H. *Protein Science* **1993**, 404-410.
(45) Giehm, L.; Otzen, D. E. *Anal Biochem* **2010**, *400*, 270-81.
(46) Buell, A. K.; Dobson, C. M.; Welland, M. E. *Methods Mol Biol* **2012**, *849*, 101-19.
(47) Buell, A. K.; Dhulesia, A.; White, D. A.; Knowles, T. P.; Dobson, C. M.; Welland, M. E. *Angew Chem Int Ed Engl* **2012**.
(48) Hovgaard, M. B.; Dong, M.; Otzen, D. E.; Besenbacher, F. *Biophys. J.* **2007**, *93*, 2162-9.
(49) Manwell, C. *Biochem J* **1977**, *165*, 487-95.
(50) Nesgaard, L.; Vad, B.; Christiansen, G.; Otzen, D. *Biochim Biophys Acta* **2009**, *1794*, 84-93.
(51) Cohen, S. I. A.; Vendruscolo, M.; Welland, M. E.; Dobson, C. M.; Terentjev, E. M.; Knowles, T. P. J. *Journal of Chemical Physics* **2011**, *135*.
(52) Cohen, S. I. A.; Vendruscolo, M.; Dobson, C. M.; Knowles, T. P. J. *Journal of Chemical Physics* **2011**, *135*.
(53) Kong, J.; Yu, S. *Acta Biochim Biophys Sin (Shanghai)* **2007**, *39*, 549-59.
(54) Celej, M. S.; Sarroukh, R.; Goormaghtigh, E.; Fidelio, G. D.; Ruysschaert, J. M.; Raussens, V. *Biochem J* **2012**, *443*, 719-26.
(55) Natalello, A.; Ami, D.; Doglia, S. M. *Intrinsically Disordered Protein Analysis: Volume 1, Methods and Experimental Tools, Methods in Molecular Biology* **2012**, *895*, 229-244.
(56) van Rooijen, B. D.; Claessens, M. M.; Subramaniam, V. *Biochim Biophys Acta* **2009**, *1788*, 1271-8.
(57) Apetri, M. M.; Maiti, N. C.; Zagorski, M. G.; Carey, P. R.; Anderson, V. E. *J Mol Biol* **2006**, *355*, 63-71.
(58) Bolognesi, B.; Kumita, J. R.; Barros, T. P.; Esbjorner, E. K.; Luheshi, L. M.; Crowther, D. C.; Wilson, M. R.; Dobson, C. M.; Favrin, G.; Yerbury, J. J. *ACS Chem Biol* **2010**, *5*, 735-40.
(59) Glatter, O. *J. Appl. Cryst.* **1977**, *10*, 415-421.
(60) Li, J.; Uversky, V. N.; Fink, A. L. *Neurotoxicology* **2002**, *23*, 553-67.
(61) Binolfi, A.; Rasia, R. M.; Bertoncini, C. W.; Ceolin, M.; Zweckstetter, M.; Griesinger, C.; Jovin, T. M.; Fernandez, C. O. *J Am Chem Soc* **2006**, *128*, 9893-901.
(62) Debye, P. *J Phys Colloid Chem* **1947**, *51*, 18-32.
(63) Fauvet, B.; Mbefo, M. K.; Fares, M. B.; Desobry, C.; Michael, S.; Ardah, M. T.; Tsika, E.; Coune, P.; Prudent, M.; Lion, N.; Eliezer, D.; Moore, D. J.; Schneider, B.; Aebischer, P.; El-Agnaf, O. M.; Masliah, E.; Lashuel, H. A. *J Biol Chem* **2012**, *287*, 15345-64.
(64) Pedersen, J. S. *Journal of Applied Crystallography* **2000**, *33*, 637-640.
(65) Cohen, S. I. A.; Vendruscolo, M.; Dobson, C. M.; Knowles, T. P. J. *Journal of Chemical Physics* **2011**, *135*.
(66) Knowles, T. P.; Waudby, C. A.; Devlin, G. L.; Cohen, S. I.; Aguzzi, A.; Vendruscolo, M.; Terentjev, E. M.; Welland, M. E.; Dobson, C. M. *Science* **2009**, *326*, 1533-7.

(67) Buell, A. K.; White, D. A.; Meier, C.; Welland, M. E.; Knowles, T. P.; Dobson, C. M. *The journal of physical chemistry. B* **2010**, *114*, 10925-38.
(68) White, D. A.; Buell, A. K.; Dobson, C. M.; Welland, M. E.; Knowles, T. P. J. *FEBS letters* **2009**, *583*, 2587-2592.
(69) Zijlstra, N.; Blum, C.; Segers-Nolten, I. M.; Claessens, M. M.; Subramaniam, V. *Angew Chem Int Ed Engl* **2012**, *51*, 8821-4.
(70) Davidson, W. S.; Jonas, A.; Clayton, D. F.; George, J. M. *J Biol Chem* **1998**, *273*, 9443-9.
(71) Eliezer, D.; Kutluay, E.; Bussell, R., Jr.; Browne, G. *J Mol Biol* **2001**, *307*, 1061-73.
(72) Ulmer, T. S.; Bax, A.; Cole, N. B.; Nussbaum, R. L. *J Biol Chem* **2005**, *280*, 9595-603.
(73) van Rooijen, B. D.; van Leijenhorst-Groener, K. A.; Claessens, M. M.; Subramaniam, V. *J Mol Biol* **2009**, *394*, 826-33.
(74) Milanesi, L.; Sheynis, T.; Xue, W. F.; Orlova, E. V.; Hellewell, A. L.; Jelinek, R.; Hewitt, E. W.; Radford, S. E.; Saibil, H. R. *Proc Natl Acad Sci U S A* **2012**, *109*, 20455-60.
(75) Xue, W. F.; Hellewell, A. L.; Gosal, W. S.; Homans, S. W.; Hewitt, E. W.; Radford, S. E. *J Biol Chem* **2009**, *284*, 34272-82.
(76) Pieri, L.; Madiona, K.; Bousset, L.; Melki, R. *Biophys J* **2012**, *102*, 2894-905.
(77) Stefani, M.; Dobson, C. M. *J Mol Med (Berl)* **2003**, *81*, 678-99.
(78) Fink, A. L. *Factors affecting the fibrillation of a-synuclein, a natively unfolded protein*; Springer: New York, 2007.
(79) Sluzky, V.; Tamada, J. A.; Klibanov, A. M.; Langer, R. *Proc Natl Acad Sci U S A* **1991**, *88*, 9377-81.
(80) Cremades, N.; Cohen, S. I.; Deas, E.; Abramov, A. Y.; Chen, A. Y.; Orte, A.; Sandal, M.; Clarke, R. W.; Dunne, P.; Aprile, F. A.; Bertoncini, C. W.; Wood, N. W.; Knowles, T. P.; Dobson, C. M.; Klenerman, D. *Cell* **2012**, *149*, 1048-59.

SUPPORTING INFORMATION

The role of stable α-synuclein oligomers in the molecular events underlying amyloid formation

Nikolai Lorenzen, Søren Bang Nielsen, Alexander K. Buell, Jørn Døvling Kaspersen, Paolo Arosio, Brian Stougaard Vad, Gunna Christiansen, Zuzana Valnickova-Hansen, Maria Andreasen, Wojciech Paslawski, Jan J. Enghild, Jan Skov Pedersen, Christopher M. Dobson, Tuomas P. J. Knowles, and Daniel Erik Otzen

Contents:

Materials and methods

Purification of αSN: αSN was produced in *E. coli* BL21(DE3) cells with a plasmid vector pET11-D using auto-induction as described in [1]. To obtain high purity αSN, we used the purification protocol described in [2,3] modified with an additional step. Briefly, cells were harvested by centrifugation at 3.500rpm, 4 °C for 20 min and quickly resuspended in 10% volume osmotic shock buffer (30mM Tris HCl, 40 % sucrose, 2mM EDTA, pH 7.2), incubated for 10 min at room temperature and centrifuged at 9.000g, 20 °C for 30 min. The pellet was quickly resuspended in ice-cold deionised water, with subsequent addition of 40 µL saturated $MgCl_2$ and incubation on ice for 3 min. Supernatant containing the periplasmic preparation was collected by centrifugation at 9.000 g, 4 °C in 20 min. The periplasmic preparation was acid precipitated with drop wise addition of 1 M HCl to a final pH 3.5, 5 min incubation and collection of soluble protein by centrifugation at 9.000g, 4 °C for 20 min. Supernatant pH was immediately adjusted to pH 7.5 with 1 M NaOH. The solution was filtered (0.45 µm) and loaded on a Q-sepharose column (Hitrap DEAE FF Q-HP) with a 20mM Tris HCl

pH 7.5 running buffer and elution of αSN with a NaCl gradient from 0-0.5 M. Subsequent SDS-PAGE analysis identified fractions containing αSN. Finally, high molecular weight proteins at very low concentrations (only observable upon concentration of αSN to 12 mg/ml) were removed by filtration through a 30 kDa (Amicon stirred cell, Millipore). The filtrate was collected, analyzed with SDS-PAGE to ensure protein purity, dialyzed exhaustively with deionised water, lyophilized and stored at -20 °C.

Preparation of oligomers: αSN oligomers were purified as described in [4] with the modification that the incubation time was reduced from 6 hrs to 5 hrs. Briefly, αSN was dissolved to 12 mg/ml and incubated in an eppendorf shaker at 37°C, 900 rpm for 5 hrs. Insoluble material was removed by centrifugation at RT, 13.400 rpm in 10 min. The supernatant were loaded on either a Superdex 120, superdex 200 or superpose 6 column in PBS buffer at a flow-rates of 2, 0.5 and 0.5 ml/min respectively. Oligomer fractions were collected, concentrated with a 2H2 U-Tube concentrator with a cutoff at 2 kDa (Novagen) and stored at 4 °C.

Atomic force microscopy: Oligomer samples were diluted to 0.01-0.001 mg/ml and spread on freshly cleaved mica (SPI supplies, West Chester, PA). The samples were then dried for AFM analysis. The images were acquired at room temperature (25 °C) with an Agilent 5100 AFM (Agilent Technologies, Santa Clara, CA) in acoustic AC mode, equipped with a Tap190-G cantilever, frequency 190 kHz, force constant 48 N/m (Innovative Solutions Bulgaria Ltd., Sofia, Bulgaria). The ratio of the set point amplitude to the free amplitude (A/A_0) was maintained at 0.9. The scanning speed was set to 0.5 lines/second with an image resolution of 1024 × 1024. The AFM Images were analyzed using the open source software Gwyddion [5].

Quartz crystal microbalance assays: Quartz crystal microbalance with dissipation monitoring (QCM-D) was used to monitor the elongation rate of preformed fibrils in presence of monomers or purified oligomers. QSX 301 gold coated sensor crystals (Q-Sense AB, Västre Frölunda, Sweden) were heated for 3 h at 80 °C in 7 M NaOH, rinsed with water and dried in a stream of nitrogen gas. Sensors were further cleaned by UV/Ozone treatment for approximately 15 min in a Bioforce nanoscience zone cleaner (USA). 12 mg/ml αSN was fibrillated by overnight incubation at 37 °C and 900 rpm shaking in a Biosan TS-100 Thermo shaker and diluted to 100 µM (~1.43 mg/ml) in PBS. 3-400 µl 100 µM sample was sonicated for several minutes on ice to induce fibril fragmentation and increase the number of possible growing ends. 0.5 mg Trauts reagent was added and the sample incubated for 5 minutes to introduce reactive thiol groups to primary amines of αSN [6]. 100 µl suspension was transferred to the QCM sensor surface and kept in a humidity chamber for 1 h to avoid sample dehydration. Sensors were rinsed with deionised water and incubated for 30 min in 100 ml 1vol-% PEG thiol (Polypure AS, Sweden) in PBS to block remaining accessible surface area and reduce non-specific binding. The modified QCM sensors were dried in nitrogen gas and mounted in a Q-sense E4 QCM-D system (Q-Sense AB, Västre Frölunda, Sweden) at RT for overnight equilibration in PBS buffer. The temperature was then raised to 37 °C and allowed to equilibrate for approximately 2 h. After ~10 min of baseline, 350 µl 0.29 mg/ml (20 µM monomer) monomer in the same buffer was injected at 100 µl/min onto each of the 4 channels and the rate of elongation was monitored by the linear decrease in resonance frequency (Δf) and increase in energy dissipation (ΔD) over time. Sensors were then washed with 500 µl PBS at 100 µl/min until the baseline had stabilized before another aliquot of 0.29 mg/ml αSN was injected as described above. 0.29 mg/ml αSN monomer, oligomer or PBS were injected to compare the rate of elongation between monomers and oligomers. The QCM experiment was repeated three times showing qualitatively similar results.

Size-exclusion chromatography (SEC) and asymmetrical flow field-flow fractionation (aFFF) with dynamic and multi angle laser light scattering (SEC-DLS/MALLS): SEC-DLS/MALLS was used to separate and estimate the size of oligomer species using a Postnova AF2000 field-flow fractionation system (Postnova Analytics GmbH, Germany) operating in SEC mode and equipped with UV/Vis, Brookhaven BI-MwA (S3240) molecular weight analyzer (measuring scattering intensity at 30, 50, 75, 90, 105, 130 and 145° angles), PN 3000 DLS and PN3140 refractive index detectors (listed in flow order). 20 µl (MALLS) or 100µl (DLS) of 12 mg/ml αSN sample incubated for 5 hrs was injected a ~24 ml superose 6 10/30 GL size exclusion chromatography column at a flow rate of 0.5 ml/min. The absorbance at 280nm was used to quantify eluting species and dynamic and static light scattering detectors for the determination of hydrodynamic radius (Rh) and molecular weight (Mw), respectively.

The hydrodynamic radius was recorded using the Precision Acquire32 v.0.99.017 software supplied by the manufacturer (Precision detectors Inc.) and the hydrodynamic radius (*Rh*) at peak maximum was estimated using the Discovery32 light scattering software v.1.039 supplied by the manufacturer (Precision detectors Inc.).

The molecular weight of αSN species was determined from MALLS data using the Zimm model built into the Postnova AF2000 control software v. 1.1.027. In brief, MALLS and A280nm data were baseline corrected and the Zimm model was applied to estimate molecular mass of protein species by extrapolating scattering data to zero scattering angle and zero concentration for each data point (~1 sec intervals) within eluting peaks. The molecular weight was represented as the weight-average molar mass across each of the eluting peaks:

$$M_W = \frac{\sum c_i M_i}{\sum c_i}$$

where the quantities M_i and c_i are the molar mass and concentration at the *i*th elution volume slice.

The AF2000 system was further employed to evaluate the distribution between monomer and oligomers at different protein concentrations (1-5-12 mg/mL, respectively) thus exploiting the unique ability of asymmetric flow field-flow aFFF to focus the sample in a narrow band prior to sample elution. Samples each containing 240 µg total protein load independent of aSN concentration was focused for 8 min with an injection tip flow of 0.2 mL/min and crossflow cross flow of 2 mL/min followed by isocratic elution at 2 mL/min cross flow for 5 minutes during which aSN monomers elute from the channel. A linear cross flow gradient from 2 ml/min to 0.1 mL/min over 20 min was then applied to elute aSN followed by a linear cross flow gradient to 0 mL/min over 5 minutes. Finally, the channel was flushed at 0 ml/min cross flow (no separation force). A constant detector flow of 0.5ml/min was maintained throughout the separation. The oligomer amount was further evalutated using freshly dissolved aSN and aSN fibrillated at 1 mg/ml.The A280 nm and MALLS detectors were calibrated using BSA (66 kDa) and 67 kDa polystyrene sulfonate standards as described by the manufacturer. The calibration was validated by separation of 20 µl 0.5 mg/ml BSA and 20 µl 2 mg/ml thyroglobulin in PBS buffer using a Superdex 200 column at 0.5 ml/min, yielding molecular weight estimates of 63.3 kDa (66.3 kDa theoretically) and 660 kDa (669 kDa theoretically), respectively.

Small-angle x-ray scattering: Monomeric αSN at a concentration of 12 mg/ml and purified oligomers at 1.82 mg/ml were measured on a flux- and background optimized NanoSTAR SAXS instrument from Bruker [7]. The acquisition time was 30 minutes for the monomers and 60 minutes for the oligomers, and in both cases the buffer background was measured for the same time period. Background subtraction and conversion to absolute scale was done with the SUPERSAXS program package (Oliveira, C.L.P. and Pedersen. J.S., unpublished), and water was used as a calibration standard. The intensity is displayed as a function of the modulus of the scattering vector $q = \frac{4\pi \sin\theta}{\lambda}$, where $\lambda = 1.54$ Å is the wavelength and 2θ is the scattering angle. Model-independent information has been extracted from the data using the IFT procedure [8] implemented in the program WIFT [9,10]. This procedure provides the pair distance distribution function $p(r)$ function, which can be understood as a histogram of internal distances weighted by the excess scattering length density at the endpoints. It thus gives information about the particles size and shape in real space, and the model presented in the following was consistent with the $p(r)$ function.

The scattering of particles in solution can be described by $I(q) = nV^2\Delta\rho^2 P(q)S(q)$, where n is the particle number density, V is the volume of the particle, and $\Delta\rho$ is excess scattering length density, $\Delta\rho = \rho_{particle} - \rho_{solvent}$, which is proportional to the excess electron density. $P(q)$ is the form factor of the particle, which is related to the shape of the particle, while $S(q)$ is the structure factor, which describes interactions between the particles in the solution. At low concentrations, the interaction potential $S(q)$ is negligible and can be fixed at unity. In the model presented here a structure factor is not needed to describe interparticle interactions.

The monomer data were fitted by a random coil model obeying Gaussian statistics for which the form factor has been calculated by Debye [11] as:

$P_G(q) = \frac{2\cdot(\exp(-u)+u-1)}{u^2}$.

Here $u = \langle R_g^2 \rangle q^2$, and $\langle R_g^2 \rangle$ is the ensemble average of the squared radius of gyration.

For the oligomer we propose a model where part of the protein is in a rather compact ellipsoidal core while another projects randomly into the solution. Such a model with an ellipsoidal core and random coil chains on the surface has been calculated by Pedersen and Gerstenberg [12]:

$$P_{ec}(q) = \frac{1}{(N(\rho_c+\rho_e))^2}\Big(N^2{\rho_e}^2 P_{ell}(q,R,\epsilon) + N{\rho_c}^2 P_G\big(q,R_g\big) + N\,(N-1){\rho_c}^2 S_{cc}(q) + 2N\rho_e\rho_c S_{ec}(q)\Big)\,,$$

where ρ_e is the total excess scattering length of the part of the protein that is in the ellipsoidal core, while ρ_c is the total excess scattering length of the part of the protein that is in the Gaussian chain conformation. Since a scale factor is applied in the fitting procedure, the absolute value of the total scattering length is not exploited and we can therefore set $\rho_e + \rho_c = 1$. Since the excess scattering length density is assumed to be constant throughout the protein, the values of ρ_c and ρ_e will provide a measure of how much of the protein is in the random coil conformation and how much is in the ellipsoidal core, respectively. Setting $\rho_e + \rho_c = 1$, the form factor for the model can be rewritten as

$$P_{ec}(q) = (1-\rho_c)^2 P_{ell}(q,R,\epsilon) + \frac{{\rho_c}^2}{N} P_G\big(q,R_g\big) + \Big(1-\frac{1}{N}\Big){\rho_c}^2 S_{cc}(q) + 2(1-\rho_c)\rho_c S_{ec}(q)\,,$$

which includes the ellipsoid form factor:

$$P_{ell}(q,r) = \int_0^{\pi/2}\Big(\frac{3(\sin(qr)-qr\cos(qr))}{(qr)^3}\Big)^2 \sin\alpha\, d\alpha\,,$$

the cross correlation between the core and the chains:

$$S_{ec}\big(q,r,R_g\big) = \Psi\big(q,R_g\big)\int_0^{\pi/2}\frac{3(\sin(qr)-qr\cos(qr))}{(qr)^3}\frac{\sin\big(q(r+dR_g)\big)}{q(r+dR_g)}\sin\alpha\, d\alpha\,,$$

and the cross correlation between the different chains:

$$S_{cc}\big(q,r,R_g\big) = \Psi\big(\mathrm{q},\mathrm{R_g}\big)^2\int_0^{\pi/2}\left(\frac{\sin\big(q(r+dR_g)\big)}{q(r+dR_g)}\right)^2\sin\alpha\, d\alpha\,.$$

In these expressions $r = R(\sin^2\alpha + \epsilon^2\cos^2\alpha)^{1/2}$, R is the radius of the compact core, ϵ is the aspect ratio, N is the number of random coils on the ellipsoid which should correspond to the number of monomers in the oligomer, d is the distance from the random coil center of mass to the surface of the ellipsoid, and

$$\Psi\big(q,R_g\big) = \frac{1-\exp(-u)}{u}$$

with $u = \langle R_g^2 \rangle q^2$ as specified above. The distance d is fixed at unity to place the coils at the surface so they do not penetrate the core significantly [12].

ANS fluorescence: 10 µM of αSN monomer, small oligomer, large oligomer and fibril was mixed with 10 µM 1-anilinonapthalene-8-sulfonate (ANS) in PBS buffer and the fluorescence emission was measured from 400-600 nm with excitation at 365 nm, slit widths of 10 nm and a scan speed of 200 nm/min on an LS55 luminescence spectrophotometer (Perkin Elmer Instruments). Three spectra were accumulated and averaged for each sample. Fibrils were separated from soluble protein by 10 min centrifugation at 13.400 rpm at RT. The protein concentration of the supernatant were determined and the amount of fibrils in the pellet were estimated.

1. Comparison of secondary and tertiary structure of small oligomers and large oligomers

Separated small oligomers and large oligomers show similar secondary structure fingerprints with both CD (Fig S1A) and FTIR (Fig S1B). This indicates that the secondary (CD, FTIR) and the tertiary (FTIR) structure elements of the two populations are identical.

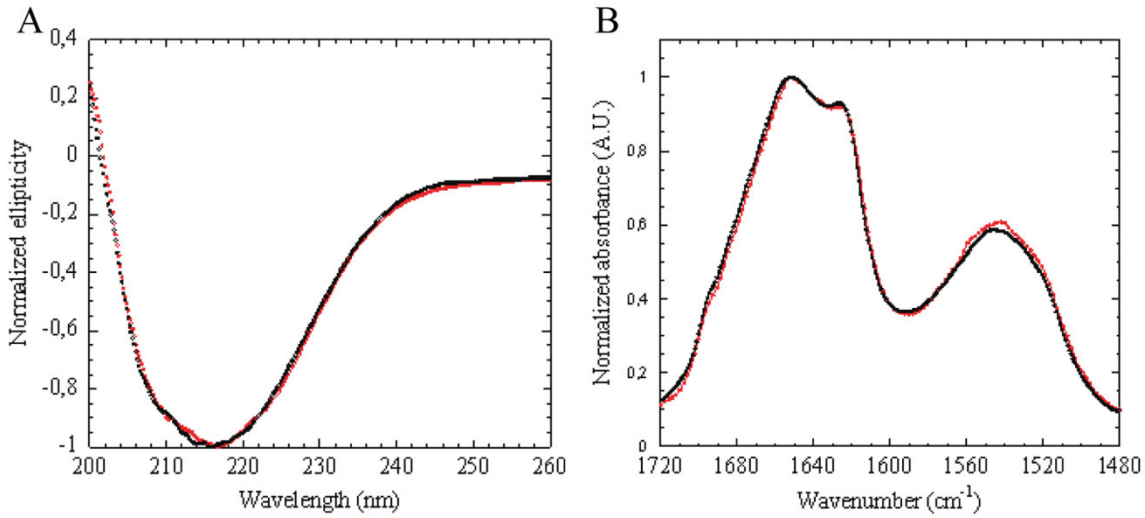

Figure S1. Structural comparison of small oligomers (red) and large oligomers (black). A: Far-UV CD spectra with normalized ellipticity. B: FTIR analysis of the amide I and amide II regions, absorbance is normalized.

2. Structural comparison of fibrils formed at 1 and 12 mg/ml

To obtain high amounts of oligomers to be used in fibrillation experiments and SAXS analysis it is necessary to use elevated protein concentrations at 12 mg/ml. Thus, we use oligomers purified at 12 mg/ml in fibrillation assays with concentrations of 1 mg/ml. To ensure that there are no changes in fibrils prepared at 1 and 12 mg/ml, we have compared their secondary structure by CD (Fig. S2A) and FTIR (Fig. S2B). We obtain similar spectra and therefore conclude that oligomers extracted from protein concentrations at 12 mg/ml co-exist with the same type of fibrils that are formed at 1 mg/ml. Thus, we can use oligomers purified at high concentrations and analyze their effect in assays at low concentrations. Furthermore, fibrils extracted from 12 mg/ml and 1 mg/ml show the same quantitative ability to permeabilize membranes as analyzed with calcein release experiments (Fig. S5).

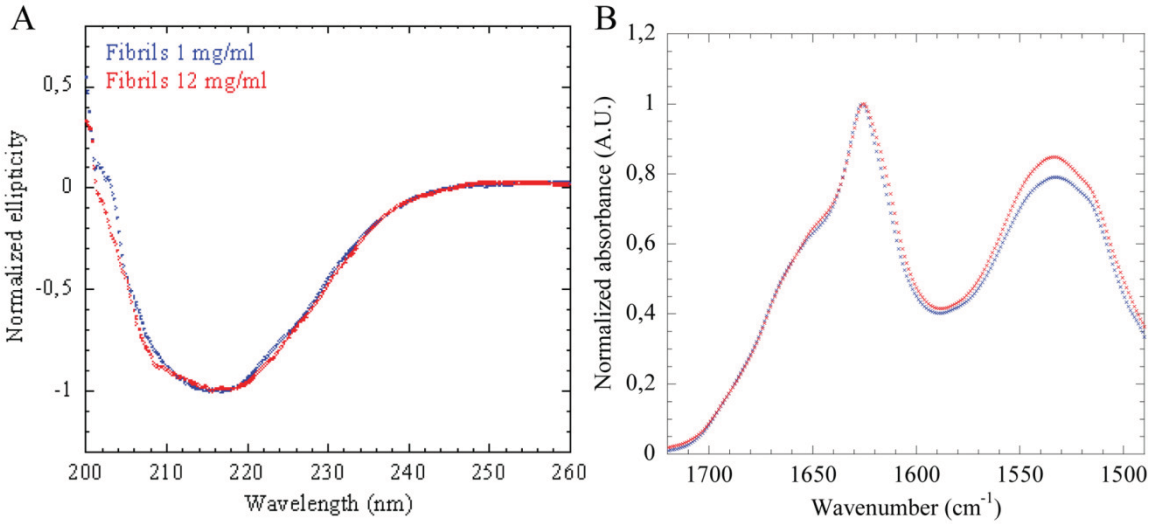

Figure S2. Structural comparison of fibrils formed at 1 mg/ml (blue) and 12 mg/ml (red). A: Far-UV CD spectra with normalized ellipticity. B: FTIR analysis of the amide I and II regions. Absorbance is normalized.

Another concern is whether the oligomers are formed to the same relative extent at 1 and 12 mg/ml. With conventional SEC it would be difficult to analyze the oligomer yield of a 1 mg/ml sample from the baseline. Instead we have used asymmetrical flow field-flow fractionation (aFFF) where samples are focused in a

cross flow upon separation. This allowed us to load different concentrations of protein at different volumes to obtain the same amount of protein to be separated. Separation of fibril-oligomer samples at 1, 5 and 12 mg/ml (all incubated for 5 hrs), revealed that at these concentrations the same fraction of oligomer is formed relative to monomers (Fig. S5A). Thus, the oligomers are present at the same ratios under fibrillation at 1 and 12 mg/ml, making it plausible to harvest oligomers from 12 mg/ml and use them in 1 mg/ml fibrillation assays. We have previously described how the oligomers accumulate in the early phase of fibrillation at 12 mg/ml and disappear when fibrillation saturates [4]. With aFFF we were able to show the same tendency for the oligomers at 1 mg/ml (Fig. S5B). We observed significant less oligomer in the sample that were readily dissolved and subsequently loaded, *i.e.* as close as we could approach a zero sample, compared with the sample that have been incubated for 5 hrs (Fig. S5B). Analysis of the soluble protein at the end of fibrillation revealed no residual oligomers and only a low amount of monomer (Fig. S5B). When samples are focused on the aFFF they are briefly concentrated, however, since our zero sample contain significantly less oligomers (Fig. S5B), we do not attribute this focusing step to have any effect on oligomer formation.

3. The oligomers bind ANS

The small and large oligomers show the same ANS fluorescence intensity and λ_{max} (475 nm) (Fig. S3). Fibrils have a higher ANS fluorescence intensity but the ANS spectrum is slightly less blue shifted than with oligomers (477 nm) (Fig. S3). No ANS fluorescence is observed from monomer (Fig. S3), indicating that hydrophobic patches have been formed in the oligomer and fibril structure.

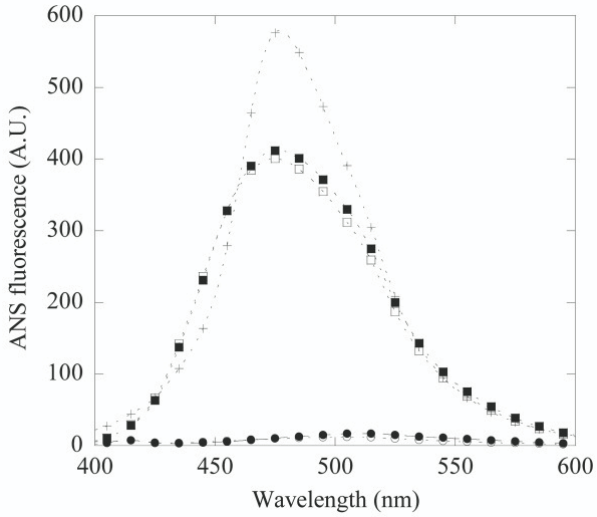

Figure S3. Wavelength spectra of ANS fluorescence of buffer (●), monomer (○), large oligomers (❑), small oligomers (■), and fibrils (+). Every 20th datapoint is shown.

4. Oligomers are more potent in permabilizing membranes than fibrils and monomers

Small oligomers and large oligomers are more potent than fibrils and monomers in permeabilizing vesicles. The effect of large oligomers can be seen in Fig. 5 in the main text. The concentrations needed for 50 % release are given in Table 1.

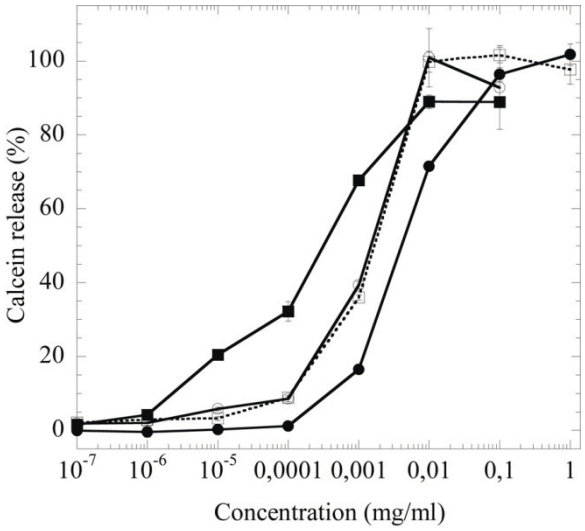

Figure S4. Calcein release percentage of monomer (●), fibrils extracted from 1 mg/ml (○) and 12 mg/ml (❑), and small oligomers (■). Standard deviation (n=3) is given.

5. Oligomer formation at different concentrations and varying times

Different volumes of varying concentration were loaded on an aFFF system after 5 hrs incubation under fibrillation conditions. The same fraction of oligomers relative to monomers is formed at 1, 5 and 12 mg/ml protein (Fig. S5A). Thus, the oligomers are present at the same ratios under fibrillation at 1 and 12 mg/ml, making it plausible to harvest oligomers from 12 mg/ml and use them in 1 mg/ml fibrillation assays. Oligomers do not accumulate during purification of αSN; there is significant less oligomer present in a freshly dissolved sample than in a sample incubated for 5 hrs (Fig. S5B). Analysis of the soluble protein after fibrillation has reached a plateau in ThT fluorescence reveals that there are no oligomers left, only a small amount of monomer (Fig. S5B).

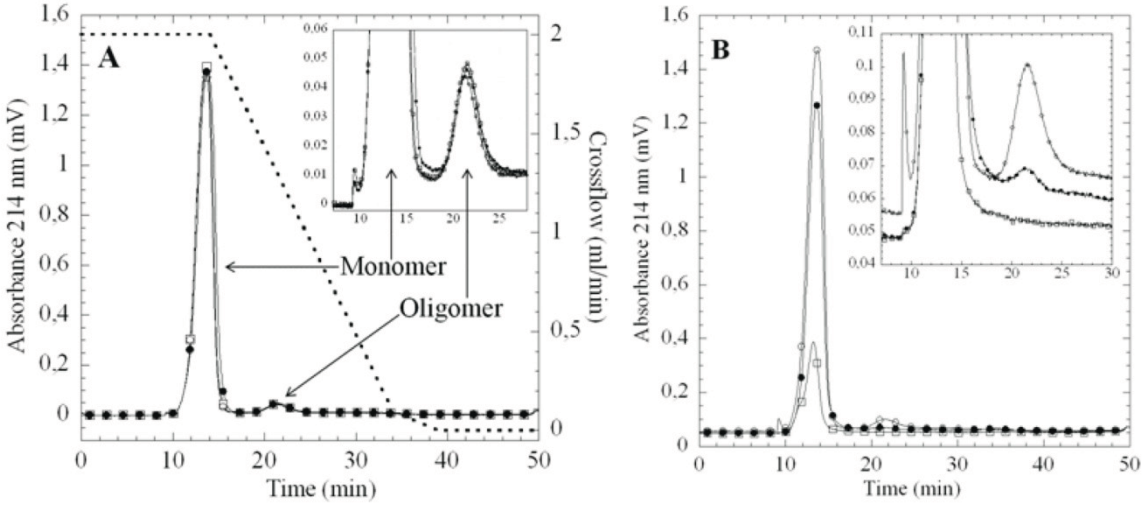

Figure S5. aFFF analysis of oligomer formation at different protein concentrations and at different times measured with absorbance at 214 nm. A: oligomer formation after 5 hrs incubation under varying concentrations: 1 (●), 5 (○), and 12 mg/ml (❑). The cross flow gradient is depicted with the dotted line and the scale is on the second y-axis. Zoom of the oligomer peak is shown in insert. B: oligomer formation of 1 mg/ml readily after the protein is dissolved (●), after 5 hrs (○) and post-fibrillation (❑). Zoom of oligomers

is included in the upper right corner. Same cross flow gradient is used as on A and B. 2 % of data points are shown on figures, and on inserts 10 % are shown.

6. Oligomers do not sequester monomers

Addition of oligomers to monomers prolongs the fibrillation lag time (Fig. 6B). Increasing the protein concentration normally leads to a decrease of the fibrillation lag time. To investigate whether the oligomers inhibition of fibrillation is the result of a decrease in the actual monomer concentration caused by complexation with oligomers, we have incubated monomers and oligomers for 1 hr under fibrillation conditions and consequently separated them with SEC. We do not observe any significant decrease in monomer concentration upon incubation with oligomers (Fig S6, Table S1). We conclude that monomers are not able to elongate oligomers within the time range of this experimental setup.

6.1. Small oligomers do not self associate into large oligomers

To test whether small oligomers are able to self-associate or transform into either large oligomers or other ThT-negative higher order aggregates, we incubated small oligomers at fibrillation conditions for 5 hrs. This is the same incubation time used for oligomer purification where large oligomers are normally observed in co-existence with small oligomers. Upon incubation of small oligomers, we did not observe any formation of large oligomers (Fig. S6).

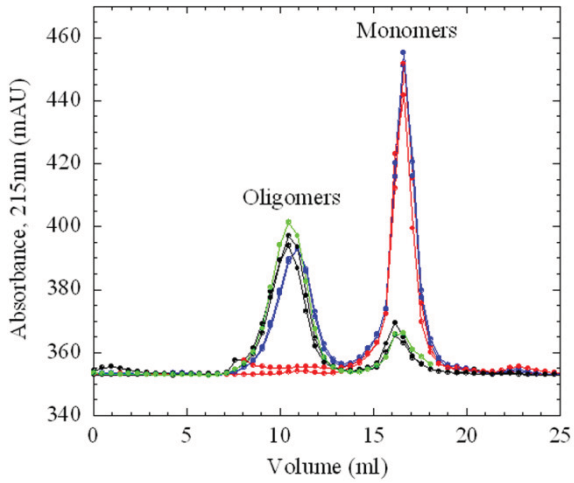

Figure S6. SEC runs of pre-incubated oligomers and monomers (blue) compared with controls of monomers (red) and oligomers (black) separately. SEC run of small oligomers incubated for 5 hrs under fibril forming conditions is also shown (yellow).

Specie	Oligomer (mAU×mL)	Monomer (mAU×mL)
Monomer	-	135±1
Oligomer	98±4	23±4
Monomer Oligomer	91±1	151±2

Table S1. Comparison of peak areas of chromatograms from (Fig. S3) with standard deviation (n=2). Same concentration of monomer and oligomer is added in all experimental series.

7. Estimate of the fibril elongating capacity of oligomers

We base the following estimates and calculations on the rate constant for rearrangement of one type of oligomers of α-synuclein (”type A”) into another type (”type B”), reported by some of us (T.P.K. and

C.M.D.) in a previous single-molecule study [13] to be $5x10^{-6}$ s^{-1}. We are not sure whether the small oligomers in the present study are related to the type A oligomers, but for the lack of other reported data on oligomer rearrangment kinetics, we decided to use this value. The oligomers observed previously [13] are smaller than the ones we study here (ca. 30 vs. <10) and therefore the rearrangement rate reported is likely to be an upper bound for the rearrangement of the oligomers in our present study (assuming that the rearrangement rate decreases with increasing size, which is plausible).

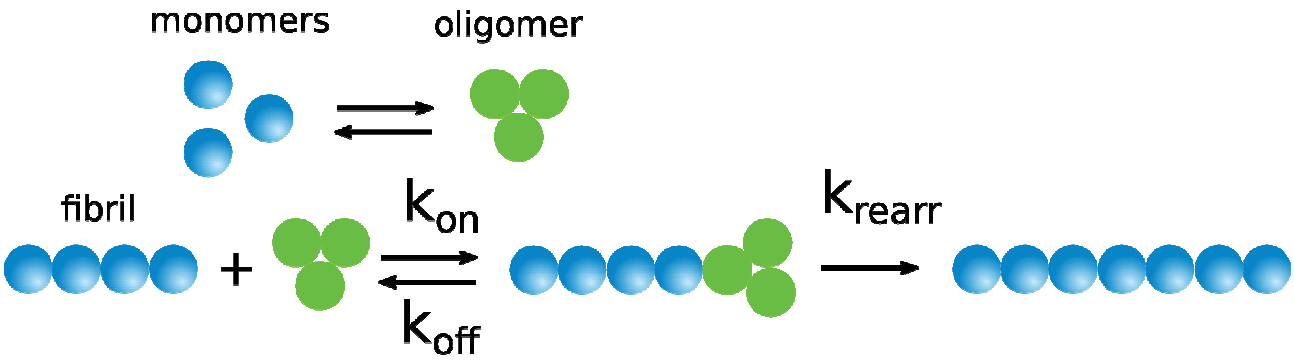

Figure S7. Model of the elongation of fibril seeds by oligomers.

We model the elongation of fibril seeds by oligomers as a two step reaction: diffusional arrival of the entire oligomer at the fibril end, followed by rearrangement (see Figure S7). The (barrier-less) diffusional arrival rate can be computed by the simple Smoluchowski expression: k_{on} = DcR, where D is the diffusion coefficient and c the concentration of the oligomers and R is the linear dimension of a reaction volume into which the oligomer has to diffuse. We will assume that R corresponds roughly to the size of the oligomer, which has an effective radius of ca. 10 nm, leading to D = $2x10^{-11}$ m^2/s . At a total protein concentration of 30 µM protein, we have c = 1 µM, leading finally to k_{on} ~ 130 s^{-1} . If there is a free energy barrier for attachment, this rate can be much slower.

We do not have an estimate for the oligomer detachment rate, as it depends on the attractive potential between the fibril end and the oligomer. Therefore, we will give an upper bound for the elongation rate, calculated under the assumption that at any given time, all the fibril ends are occupied by oligomers and therefore the elongation rate is given by the rate of rearrangement. This is a very generous estimate and unlikely to be the case, as this would lead to a drastic decrease in the rate of fibril elongation by monomer in the presence of oligomers, which is not observed.

If the elongation rate is purely the rearrangement rate, we obtain an initial rate of fibril growth at the beginning of the experiment (30 µM oligomers by mass, 3µM seed fibrils, 1000 molecules per fibril) of $4.5x10^{-13}$ M^{-1} s^{-1}, whereas the initial elongation rate by monomer is given by (using k_+ = $2x10^{-3}$ M^{-1} s^{-1}, from A.K.B. et al., submitted to Proc. Natl. Acad. Sci. U.S.A., under revision) $1.8x10^{-10}$ M^{-1} s^{-1}. Therefore, an upper bound for the elongation of fibrils by oligomers is 2-3 orders of magnitude lower than for elongation by monomer.

References

(1) Studier, F. W. *Protein Expr Purif* **2005**, *41*, 207.
(2) Huang, C.; Ren, G.; Zhou, H.; Wang, C. C. *Protein Expr Purif* **2005**, *42*, 173.
(3) Giehm, L.; Lorenzen, N.; Otzen, D. E. *Methods* **2011**, *53*, 295.

(4) Giehm L, S. D., Otzen DE, Vestergaard B. *Proc Natl Acad Sci U S A* **2011**, *108(8)*, 3246.
(5) Necas, D.; Klapetek, P. *Central European Journal of Physics* **2012**, *10*, 181.
(6) Buell, A. K.; White, D. A.; Meier, C.; Welland, M. E.; Knowles, T. P.; Dobson, C. M. *J Phys Chem B* **2010**, *114*, 10925.
(7) Pedersen, J. S. *journal of applied crystallography* **2004**, *37*, 368.
(8) Glatter, O. *Journal of Applied Crystallography* **1977**, *10*, 415.
(9) Oliveira, C. L. P.; Behrens, M. A.; Pedersen, J. S.; Erlacher, K.; Otzen, D.; Pedersen, J. S. *Journal of Molecular Biology* **2009**, *387*, 147.
(10) Pedersen, J. S.; Hansen, S.; Bauer, R. *Eur Biophys J* **1994**, *22*, 379.
(11) Debye, P. *J Phys Colloid Chem* **1947**, *51*, 18.
(12) Pedersen, J. S.; Gerstenberg, M. C. *Macromolecules* **1996**, *29*, 1363.
(13) Cremades, N.; Cohen, S. I.; Deas, E.; Abramov, A. Y.; Chen, A. Y.; Orte, A.; Sandal, M.; Clarke, R. W.; Dunne, P.; Aprile, F. A.; Bertoncini, C. W.; Wood, N. W.; Knowles, T. J.; Dobson, C. M.; Klenerman, D. *Cell* **2012**, 1048.

Article IX

The N-terminus of α-synuclein is essential for both monomeric and oligomeric interactions with membranes

Nikolai Lorenzen, Lasse Lemminger[1], Jannik Nedergaard Pedersen, Søren Bang Nielsen[2] and Daniel Erik Otzen*

Interdisciplinary Nanoscience Center (iNANO), Department of Molecular Biology and Genetics, Center for Insoluble Protein Structures (inSPIN), Aarhus University, Gustav Wieds Vej 14, DK – 8000 Aarhus C, Denmark

[1] Present address: Biogen Idec (Denmark) Manufacturing ApS, Biogen Idec Allé 1, DK-3400 Hillerød, Denmark

[2] Present address: Arla Foods, Sønderupvej 26, DK - 6920 Videbæk, Denmark

*To whom correspondence should be addressed. Tel. +45 20725238; E-mail: dao@inano.au.dk

Abstract

The intrinsically disordered protein α-synuclein (αSN) is linked to Parkinson's Disease and forms both oligomeric species and amyloid fibrils. The N-terminal part of monomeric αSN interacts strongly with membranes and αSN cytotoxicity has been attributed to oligomers' ability to interact and perturb membranes. We show that membrane folding of monomeric wt αSN and N-terminally truncated variants correlates with membrane permeabilization. Further, the first 11 N-terminal residues are crucial for monomers' and oligomers' interactions with and permeabilization of membranes. We attribute oligomer permeabilization both to cooperative electrostatic interactions through the N-terminus and interactions mediated by hydrophobic regions in the oligomer.

Keywords: oligomer; toxicity; membrane interactions; membrane folding; permeabilization

Abbreviations: 1-anilinonapthalene-8-sulfonate (ANS), Asymmetrical flow-field flow fractionation (a4F), α-synuclein (αSN), circular dichroism (CD), dynamic light scattering (DLS), multi-angle laser light scattering (MALLS), Parkinson's Disease (PD), sodium dodecyl sulfate (SDS), Size Exclusion chromatography (SEC), thioflavin T (ThT)

Highlights

- We have analyzed the membrane interactions of α-synuclein monomers and oligomers.
- Different N-terminal deletion mutants have been compared.
- The first 11 N-terminal residues are essential for this membrane interaction.
- Membrane folding correlates with membrane permeabilization and toxicity.
- Oligomers bind to membranes by electrostatic and hydrophobic interactions.

Introduction

Though intrinsically disordered (*1*), the presynaptic protein α-synuclein (αSN) can fold into membranes *in vivo (2)* and *in vitro (3, 4)*. Association of αSN with membranes has been linked to its physiological role (*5*) and its part in the pathogenesis of Parkinson's disease (PD). αSN is the main component of PD-associated intracellular deposits known as Lewy Bodies (*6*), and αSN mutations lead to early onset PD (*7*). αSN also forms aggregates both *in vitro* and *in vivo*, including oligomers and amyloid fibrils which also interact with membranes (*8-10*).

The αSN primary sequence forms three regions (Fig. 1A). The N-terminal region is important for membrane binding (*11-13*) while the NAC (non-amyloid-β component) region nucleates amyloid fibril formation (*14*) and the C-terminal region is typical for an intrinsically disordered region (*15*). In sodium dodecyl sulfate (SDS) micelles, αSN forms two helices, helix-N (residues 3-37) and helix-C (residues 45-92) connected by an ordered extended linker in an anti-parallel arrangement. Another extended region (residues 93-97) is followed by an unstructured C-terminus (residues 98-140) (*16*). Consistently, residues 1-100 interact with membranes (*3, 17*). Binding may be a two-step process initiated by residues 3-25 which anchor αSN to the membrane, after which residues 25-100 undergo a coil→helix transition (*18, 19*). Deletion of the first N-terminal residues reduces toxicity towards yeast; toxicity is completely reduced by deleting residues 2-11 (*20*). Yeast toxicity correlates with the different deletion mutants' membrane binding (*20*), indicating a direct link between αSN toxicity and membrane binding. The importance of residues 2-11 on membrane interaction has been underlined in another study, where the quantitative binding of αSN to isolated mitochondria was abolished when residues 2-11 were deleted (*21*).

Although neurodegenerative diseases such as PD and Alzheimer's disease were initially mainly associated with amyloid deposits, there is growing consensus that non- or pre-fibrillar oligomeric species are the cytotoxic species (*22-28*). This may be linked to their structure and ability to interact with membranes. Though inherent polydispersity and low oligomer yields have precluded detailed molecular analysis of membrane interactions, single tryptophan mutants reveal that αSN oligomers selectively binds to anionic lipids, preferentially in liquid disordered regions (*12, 29*). Hydrophobic interactions are likely important for oligomer-membrane interactions, given that the binding is strongest when the bilayer is loosely packed, making the hydrophobic membrane interior more accessible (*29*).

Here we report that N-terminal truncation mutants of αSN affect folding into, binding and permeabilization of anionic large unilamellar vesicles (LUVs). Monomer ability to permeabilize

membranes correlates with their degree of folding in membranes. Monomeric and oligomeric membrane permeabilization can be abolished by deleting residue 2-11 in the N-terminal, highlighting the N-terminal's critical role in both species' membrane interaction. We suggest that the pronounced ability of αSN oligomers to permeabilize vesicles stems from a combination of N-terminal electrostatic interactions and the formation of hydrophobic patches in the oligomer structure.

Materials and Methods

Materials: Lipids were from Avanti Polar Lipids (Alabaster, AL); unless otherwise stated, all other chemicals were from Sigma Aldrich (St. Louis, MO). PBS buffer (20 mM phosphate, 150 mM NaCl, pH 7.4) was used throughout. Plasmids containing N-terminal deletion mutants (Fig. 1A) were a generous gift from P. Lansbury.

Protein handling: Mutants were expressed and purified as decribed in (*30*) and Supplementary Information (SI). Prior to all experiments, lyophilized αSN were freshly dissolved with PBS buffer and filtered (0.2 μm). Protein concentration was determined by absorbance measurements with a NanoDrop^{TM} 1000 spectrophotometer (Thermo Scientific) using a theoretical extinction coefficient of 5900 M^{-1} cm^{-1}.

Vesicle preparation: Large unilamellar vesicles (LUVs) of pure 1,2-dimyristoyl-sn-3-phosphatidylglycerol (DMPG) or 1,2-dioleoyl-sn-3-phosphatidylglycerol (DOPG) were prepared by 10 freeze-thaw cycles followed by 21 extrusions to the desired diameter (*31*).

Oligomer purification: Oligomers were purified as described in (*8, 32*). Briefly, αSN was prepared at 840 μM at 900 rpm, 37 ºC at 5-6 hrs. Soluble oligomers were purified from insoluble material by centrifugation at 13.400 rpm, RT, in 10 min. The supernatant was loaded on a Superdex 200 (10/300G L) and oligomers collected, baseline separated from monomers. Oligomers were concentrated using a 2H2 U-Tube centrifugation concentrator with a cutoff of 2kDa (Novagen) and stored at 4 ºC. Oligomers were generally used readily after purification.

Dynamic light scattering (DLS): We used a ZS Zetasizer Nano ZS (Malvern Instruments) to measure oligomeric hydrodynamic radius (R_H) at 25 °C at 21-42 μM oligomer. Oligomer samples were analyzed readily after purification with SEC. All samples were measured five times using 15-40 accumulated scans to give number-percentage averaged R_H.

ANS fluorescence: 10 μM of αSN monomer or oligomer was mixed with 10 μM 1-anilinonapthalene-8-sulfonate (ANS) in PBS buffer. ANS fluorescence was measured on a LS55 luminescence spectrophotometer (Perkin Elmer Instruments) using excitation at 365 nm and 400-

600 nm emission, 10 nm slit widths of 10 nm and 150 nm/min scan speed. Five spectra were averaged for each sample.

Note: Details of protein purification, fibrillation assay, asymmetrical flow-field flow fractionation (a4F), calcein release assay and folding assay are provided in SI.

Results

Formation and analysis of amyloid fibrils and oligomers

To evaluate the importance of the first 11 N-terminal residues of αSN in different membrane binding assays, we have studied deletion mutants Del2, Del2-5 and Del2-11 (Fig. 1A). All mutants formed amyloid fibrils *in vitro* both in an SDS-induced and a shaking-induced fibrillation assay (Fig. S1). While Del2-11 showed significantly longer lag times than the other αSN constructs and followed an erratic aggregation profile, Del2 fibrillated with the shortest lag times in both assays (Fig. S1). All deletion mutants formed oligomers of the same size as wildtype (wt), eluting close to the exclusion limit (M_r = $1.3 \cdot 10^6$ Da) of the Superdex 200 size-exclusion chromatography (SEC) column. Therefore we used dynamic light scattering (DLS) and found that all mutants had comparable hydrodynamic radii (R_h) of 9.9-11.7 nm (Fig. 1B & Table 1). The number distribution shows reasonable oligomer monodispersity (Fig. 1B).

To identify hydrophobic patches on oligomers, we used the dye ANS, whose fluorescence increases and blue shifts upon binding to hydrophobic regions (*33*). ANS fluorescence was not affected by monomers, but oligomers induced both a blue shift and an intensity increase (Fig. 1C). The monomer averaged emission fluorescence maximum $<\lambda_{max}^{monomer}>$ = 510 nm while $<\lambda_{max}^{oligomer}>$ = 474 nm, indicating formation of hydrophobic patches on the oligomers. $\lambda_{max}^{oligomer}$ varies little (472.5- 477.5 nm, Table 1), indicating small variations in hydrophobicity.

Monomer membrane interactions correlate with degree of folding

We have measured αSN membrane binding, folding in membranes and membrane permeabilization, respectively. As a simple measure of binding, we used asymmetrical flow field-flow fractionation (a4F), in which a cross-flow gradient baseline separates monomers, oligomers and vesicles, to quantitatively evaluate the association of monomers and oligomers to DOPG vesicles. a4F is a unique method with its broad separation range and we have previously used this method to separate and analyze monomer and oligomeric populations during the fibril formation of the protein TGFIBp (*34*) and to show that no significant oligomeric species are formed during fibril formation of the

protein S6 (*35*). Furthermore, aF4 is also capable of separating LUVs (*36*), and we have designed a cross-flow gradient (See SI) which enables baseline separation of monomers, oligomer and DOPG vesicles (Fig. 2AB, 3B, SI2). Degree of binding was estimated by comparing peak area (214 nm absorbance) of monomers incubated ± DOPG vesicles, at a mole ratio of 1:100 (protein:lipid) (Fig. 2AB). For wt, Del2 and Del2-5, > 70 % of the monomers were membrane-associated, whereas < 10 % of Del2-11 was membrane-associated (Fig. 2AB, Table 1).

Monitored by circular dichroism (CD), binding and folding of wt αSN monomers in vesicles is a coil→helix transition which requires the lipids to be in the liquid disordered phase (*31*). We analyze the folding (degree of helix formation) of the different deletion mutants in DMPG vesicles with a mole ratio of 1:21 (protein:lipid) between 5 and 100^{o}C. 215 nm was chosen as it lies between the two minima of 222 and 209 nm observed for membrane bound monomer (*31*). Both the transition broadness and amplitude (minimum) as observed by the CD scans (Fig. 2C) revealed clear differences between the deletion mutants and wt. Del2-11 undergoes very little folding, Del2-5 folds only slightly less than wt and Del2 folds to an even greater extent than wt (Fig. 2C). The dye leakage experiment revealed the same trend: Del2 was more potent than wt, Del2-5 less potent than wt and Del2-11 did not induce any significant release (Fig. 2D). To correlate the ability of the monomers to permeabilize membranes with membrane folding, we plot the protein concentration needed for 50 % dye leakage with the temperature range of folding (the temperature range where a coil→helix transition is observed) (Fig. 2D insert). The reasonable linearity predicts Del2-11 to have a 5.5 times higher concentration for 50 % dye leakage than wt.

Oligomer membrane interactions follow the same pattern as the monomers, but the ranking in the permeabilization assay differ slightly

Wt, Del2 and Del2-5 oligomers led to similar membrane affinities as monomers according to a4F measurements, > 70 % associated with membranes (Fig. 3A, Table 1.). We were unable to analyzed Del2-11 oligomers in the a4F experiment due to the low oligomer yields obtained this mutant (Table 1). However, in dye leakage experiments, the wt oligomer was the most potent and there was no significant difference between Del2 and Del2-5 oligomers (Fig. 3B). Del2-11 induced up to 40 % dye leakage, which is better than the near-complete lack of effect of Del2-11 monomers. At μM level, wt and Del2-5 oligomers were 31 and 23 times more potent in dye leakage, respectively, than the corresponding monomer, while the Del2 oligomer is only 7 times more potent than the Del2 monomer (Table 1).

Discussion

Formation of amyloid fibrils and oligomers

Despite the slow and somewhat stochastic fibrillation kinetics of Del2-11, deletions within the first 11 N-terminal residues did not remove the ability of αSN to form amyloid fibrils, consistent with reports that truncated variants of αSN (residues 30-110 and 11-140) forms amyloid fibrils indistinguishable from wt (*37*). All mutants were able to form oligomers, wt, Del2 and Del2-5 at comparable levels whereas we obtained a significant lower yield of Del2-11 oligomers. The R_H of the oligomers, as determined by DLS, are comparable. Thus, deletions in the first 11 residues of the N-terminal affect neither oligomer nor fibril gross structure.

Monomer: membrane permeabilization correlates with folding in the membrane

The degree of membrane binding of Del2 and Del2-5 monomers was similar to wt monomers, whereas Del2-11 has a severely lowered affinity (Table 1). This correlates with monomer folding in DMPG vesicles, where Del2-11 has a radical decrease in structure formation relative to the others. This is reasonable, since less binding should lead to less folding. Deletion of Asp2 (Del2) decreases electrostatic repulsion between αSN and the negative charges at the membrane interface, possibly leading to a more energetically favorable binding interaction which could explain the increase in folding of the Del2 monomers relative to wt (Fig. 2C). Del2-5 reduces folding relative to Del2 and wt. Here the positive contribution of removing Asp2 to the folding is cancelled by the deletion of residues 3-5 which is part of the first helix (residues 3-37). In Del2-11, interactions with both DOPG and DMPG are almost completely eliminated, since deleting residues 3-11 of the helix removes three positively charged residues, weakening electrostatic monomer-lipid attractions and eliminating dye leakage potency. The linear correlation in Fig. 2C (insert) predicts a 50% dye leakage concentration for Del2-11 to be considerably higher than the other 3 αSN constructs. Since we demonstrate that there is a high degree of binding between the αSN monomer and DOPG and DMPG vesicles, it is not surprising that it leads to membrane permeabilization since general protein adsorption to anionic vesicles can induce vesicle leakage (*38*). Moreover, previous studies suggest that the αSN monomers can lead to membrane permeability by bilayer deformation (*39, 40*).

The N-terminal is essential for oligomer membrane interaction

Our a4F oligomer-DOPG vesicle binding assay establishes that wt, Del2 and Del2-5 oligomers interact strongly with vesicles, just as the monomers of αSN. The observation that αSN oligomers binds to DOPG vesicles is in agreement with dynamic light scattering (DLS) data where we have observed an increase in the r_H from 109 nm of pure DOPG vesicles to 140 nm when oligomers are

present (Lorenzen, Nielsen & Otzen unpublished). The DLS experiment is carried out at a mole ratio of 1:60 (protein:lipid) comparable with the a4F experiment, and indirectly confirm the validity of the a4F experiments. Together with the calcein release assay, we observe a clear trend for both monomers and oligomers, where wt, Del2 and Del2-5 showed a high degree of binding and membrane permeabilization whereas Del2-11 oligomers only induced little membrane-permeabilizing. Although trends in the dye leakage experiment for the oligomers and monomers were similar, they were not identical:

Monomers: Del2 > wt >> Del2-5 >> Del2-11

Oligomers: wt > Del2 ≈ Del2-5 >> Del2-11

We expected oligomers to permeabilize vesicles much more strongly than monomers because a large number of N-terminals in close proximity in the oligomer structure would stress and perturb vesicles. In contrast, for monomers the N-terminals would be widely distributed in the membrane due to electrostatic repulsion and diffusion, leading to less disorder in the membrane. The fact that Del2-11 distorts the membrane interaction of both monomers and oligomers clearly indicates that the N-terminal is important, given that the different constructs have the same overall size and hydrophobicity according to DLS and ANS. However, the discrepancy in the ranking of the dye release assays indicates that the interaction of oligomers is not driven solely by the N-termini. We speculate that the formation of a hydrophobic core and/or solvent exposed hydrophobic patches in the oligomer structure, as indicated by ANS binding (Fig. 1C), is important for oligomer–membrane interaction. The importance of hydrophobic interactions in the membrane binding of αSN oligomers has previously been demonstrated by Rooijen *et al*. (*41*) where an increase in accessibility of the hydrocarbon core of the lipid bilayer increases bilayer disruption by αSN oligomers. We propose that the hydrophobic patches together with N-termini in close proximity in the oligomers could explain the extraordinary toxicity of oligomers relative to monomers. However, the differences between the dye release ranking of monomers and oligomers could also be the consequence of structural changes amongst wt, Del2, Del2-5 and Del2-11 oligomers in the positioning of the N-termini or the arrangement of hydrophobic regions.

Vamvaca *et al. (20)* showed that N-terminal deletions in αSN dramatically reduced toxicity towards yeast. While the yeast maximum specific growth rates of Del2, Del2-5 and Del2-11 do not correlate with the membrane interaction, folding and permeabilization of the monomer form, we note that wt αSN, which in the oligomeric form shows the highest degree of vesicle disruption, also shows the greatest toxicity towards yeast.

Building on the observation that the N-terminus is important for oligomer-membrane interaction (*12*) we have identified the first 11 N-terminal residues to be critical for the interaction of both the monomer and oligomer forms. We suggest that the increased ability of αSN oligomers to permeabilize membranes compared to monomers stems from a combination of juxtaposed N-terminal binding domains and contiguous regions of hydrophobic surface area resulting from oligomerization.

Acknowledgements

We are grateful to Catherine Vamvaca and Peter Lansbury for providing plasmids for αSN mutants. We thank Jørgen Kjems for the use of Zetasizer Nano ZS.

TABLES

Table 1. Overview of determined parameters for wt αSN and deletion mutants

Mutant	CR50 % Monomer [a]	CR50 % Oligomer [b]	CR50 % monomer : CR50 % oligomer[c]	Monomer membrane folding range (°C) [d]	Monomer vesicle interaction[e]	Oligomer vesicle interaction[f]	R_H of oligomers (nm)[g]	λmax, ANS (nm)[h]	Oligomer yield [i]	μ(yeast) (hr^{-1}) [j]
Wt	2.8	0.09	31	54	+	+	11.7 ± 3.2	473.5	1.5	0.04
Del2	1.8	0.26	7	61	+	+	9.9 ± 2.5	474.0	1.5	0.14
Del2-5	6.4	0.26	23	46	+	+	10.9 ± 2.6	477.5	1.2	0.19
Del2-11	15.5[k]	N/A[l]	N/A[l]	16	-	N/A[l]	10.5 ± 2.6	472.5	0.2	0.22

Notes:

[a,b] Protein concentration leading to 50 % vesicle permeabilization (μM)

[c] Ratio of [a] and [b]

[d] Temperature interval in which the monomer is folded in DMPG vesicles.

[e,,f] interaction of monomer/oligomer with DOPG vesicles. "-": < 10 % and "+": > 70 % bound.

[g] Hydrodynamic radius, given as the number mean of oligomers, determined with DLS. In all cases, the peak integral of the oligomers is 100 %.

[h] λ_{max} of ANS fluorescence of oligomers.

[i] Percentage oligomer eluting from the SEC column relative to total αSN. These vary significantly between different purifications with standard deviations of 60-80 %.

[j] Yeast specific maximum growth rate *(20)*.

[k] Extrapolated from Fig. 2D insert.

[l] Not available.

References

1. Fauvet, B., Mbefo, M. K., Fares, M. B., Desobry, C., Michael, S., Ardah, M. T., Tsika, E., Coune, P., Prudent, M., Lion, N., Eliezer, D., Moore, D. J., Schneider, B., Aebischer, P., El-Agnaf, O. M., Masliah, E., and Lashuel, H. A. (2012) alpha-Synuclein in central nervous system and from erythrocytes, mammalian cells, and Escherichia coli exists predominantly as disordered monomer, *J Biol Chem 287*, 15345-15364.
2. McLean, P. J., Kawamata, H., Ribich, S., and Hyman, B. T. (2000) Membrane association and protein conformation of alpha-synuclein in intact neurons. Effect of Parkinson's disease-linked mutations, *J Biol Chem 275*, 8812-8816.
3. Davidson, W. S., Jonas, A., Clayton, D. F., and George, J. M. (1998) Stabilization of alpha-synuclein secondary structure upon binding to synthetic membranes, *J Biol Chem 273*, 9443-9449.
4. Perrin, R. J., Woods, W. S., Clayton, D. F., and George, J. M. (2000) Interaction of human alpha-Synuclein and Parkinson's disease variants with phospholipids. Structural analysis using site-directed mutagenesis, *J Biol Chem 275*, 34393-34398.
5. Bonini, N. M., and Giasson, B. I. (2005) Snaring the function of alpha-synuclein, *Cell 123*, 359-361.
6. Spillantini, M. G., Schmidt, M. L., Lee, V. M., Trojanowski, J. Q., Jakes, R., and Goedert, M. (1997) Alpha-synuclein in Lewy bodies, *Nature 388*, 839-840.
7. Polymeropoulos, M. H., Lavedan, C., Leroy, E., Ide, S. E., Dehejia, A., Dutra, A., Pike, B., Root, H., Rubenstein, J., Boyer, R., Stenroos, E. S., Chandrasekharappa, S., Athanassiadou, A., Papapetropoulos, T., Johnson, W. G., Lazzarini, A. M., Duvoisin, R. C., Di Iorio, G., Golbe, L. I., and Nussbaum, R. L. (1997) Mutation in the alpha-synuclein gene identified in families with Parkinson's disease, *Science 276*, 2045-2047.
8. Volles, M. J., Lee, S. J., Rochet, J. C., Shtilerman, M. D., Ding, T. T., Kessler, J. C., and Lansbury, P. T., Jr. (2001) Vesicle permeabilization by protofibrillar alpha-synuclein: implications for the pathogenesis and treatment of Parkinson's disease, *Biochemistry 40*, 7812-7819.
9. Grey, M., Linse, S., Nilsson, H., Brundin, P., and Sparr, E. (2011) Membrane Interaction of alpha-Synuclein in Different Aggregation States, *Journal of Parkinsons Disease 1*, 359-371.
10. Stockl, M. T., Zijlstra, N., and Subramaniam, V. (2013) Alpha-synuclein oligomers: an amyloid pore? Insights into mechanisms of alpha-synuclein oligomer-lipid interactions, *Mol Neurobiol 47*, 613-621.
11. Drescher, M., Godschalk, F., Veldhuis, G., van Rooijen, B. D., Subramaniam, V., and Huber, M. (2008) Spin-label EPR on alpha-synuclein reveals differences in the membrane binding affinity of the two antiparallel helices, *Chembiochem 9*, 2411-2416.
12. van Rooijen, B. D., van Leijenhorst-Groener, K. A., Claessens, M. M., and Subramaniam, V. (2009) Tryptophan fluorescence reveals structural features of alpha-synuclein oligomers, *J Mol Biol 394*, 826-833.
13. Maltsev, A. S., Chen, J., Levine, R. L., and Bax, A. (2013) Site-specific interaction between alpha-synuclein and membranes probed by NMR-observed methionine oxidation rates, *J Am Chem Soc 135*, 2943-2946.
14. Han, H., Weinreb, P. H., and Lansbury, P. T., Jr. (1995) The core Alzheimer's peptide NAC forms amyloid fibrils which seed and are seeded by beta-amyloid: is NAC a common trigger or target in neurodegenerative disease?, *Chem Biol 2*, 163-169.
15. Garner, E., Cannon, P., Romero, P., Obradovic, Z., and Dunker, A. K. (1998) Predicting Disordered Regions from Amino Acid Sequence: Common Themes Despite Differing Structural Characterization, *Genome Inform Ser Workshop Genome Inform 9*, 201-213.
16. Ulmer, T. S., Bax, A., Cole, N. B., and Nussbaum, R. L. (2005) Structure and dynamics of micelle-bound human alpha-synuclein, *J Biol Chem 280*, 9595-9603.
17. Eliezer, D., Kutluay, E., Bussell, R., Jr., and Browne, G. (2001) Conformational properties of alpha-synuclein in its free and lipid-associated states, *J Mol Biol 307*, 1061-1073.

18. Bodner, C. R., Maltsev, A. S., Dobson, C. M., and Bax, A. (2010) Differential phospholipid binding of alpha-synuclein variants implicated in Parkinson's disease revealed by solution NMR spectroscopy, *Biochemistry 49*, 862-871.
19. Bartels, T., Ahlstrom, L. S., Leftin, A., Kamp, F., Haass, C., Brown, M. F., and Beyer, K. (2010) The N-terminus of the intrinsically disordered protein alpha-synuclein triggers membrane binding and helix folding, *Biophys J 99*, 2116-2124.
20. Vamvaca, K., Volles, M. J., and Lansbury, P. T., Jr. (2009) The first N-terminal amino acids of alpha-synuclein are essential for alpha-helical structure formation in vitro and membrane binding in yeast, *J Mol Biol 389*, 413-424.
21. Robotta, M., Hintze, C., Schildknecht, S., Zijlstra, N., Jungst, C., Karreman, C., Huber, M., Leist, M., Subramaniam, V., and Drescher, M. (2012) Locally resolved membrane binding affinity of the N-terminus of alpha-synuclein, *Biochemistry 51*, 3960-3962.
22. Conway, K. A., Lee, S. J., Rochet, J. C., Ding, T. T., Williamson, R. E., and Lansbury, P. T., Jr. (2000) Acceleration of oligomerization, not fibrillization, is a shared property of both alpha-synuclein mutations linked to early-onset Parkinson's disease: implications for pathogenesis and therapy, *Proc Natl Acad Sci U S A 97*, 571-576.
23. Lashuel, H. A., Hartley, D., Petre, B. M., Walz, T., and Lansbury, P. T., Jr. (2002) Neurodegenerative disease: amyloid pores from pathogenic mutations, *Nature 418*, 291.
24. Beate Winner, T. J., Samir K. Maji, Paula A. Desplats, Leah Boyer, Stefan Aigner, Claudia Hetzer, Thomas Loher, Marcal Vilar, Silvia Campioni, Cristos Tzitzilonis, Alice Soragni, Sebastian Jessberger, Helena Mira, Antonello Consiglio, Emiley Pham, Eliezer Masliah, Fred H. Gage, Roland Riek. (2010) In vivo demonstration that alpha-synculein oligomers are toxic, *PNAS*.
25. Ono, K., Condron, M. M., and Teplow, D. B. (2009) Structure-neurotoxicity relationships of amyloid beta-protein oligomers, *Proc Natl Acad Sci U S A 106*, 14745-14750.
26. Bernstein, S. L., Dupuis, N. F., Lazo, N. D., Wyttenbach, T., Condron, M. M., Bitan, G., Teplow, D. B., Shea, J. E., Ruotolo, B. T., Robinson, C. V., and Bowers, M. T. (2009) Amyloid-beta protein oligomerization and the importance of tetramers and dodecamers in the aetiology of Alzheimer's disease, *Nat Chem 1*, 326-331.
27. Walsh, D. M., Lomakin, A., Benedek, G. B., Condron, M. M., and Teplow, D. B. (1997) Amyloid beta-protein fibrillogenesis. Detection of a protofibrillar intermediate, *J Biol Chem 272*, 22364-22372.
28. Lesne, S., Koh, M. T., Kotilinek, L., Kayed, R., Glabe, C. G., Yang, A., Gallagher, M., and Ashe, K. H. (2006) A specific amyloid-beta protein assembly in the brain impairs memory, *Nature 440*, 352-357.
29. van Rooijen, B. D., Claessens, M. M., and Subramaniam, V. (2008) Membrane binding of oligomeric alpha-synuclein depends on bilayer charge and packing, *FEBS Lett 582*, 3788-3792.
30. Giehm, L., Lorenzen, N., and Otzen, D. E. (2011) Assays for alpha-synuclein aggregation, *Methods 53*, 295-305.
31. Kjaer, L., Giehm, L., Heimburg, T., and Otzen, D. (2009) The influence of vesicle size and composition on alpha-synuclein structure and stability, *Biophys J 96*, 2857-2870.
32. Giehm L, S. D., Otzen DE, Vestergaard B. (2011) Low-resolution structure of a vesicle disrupting α-synuclein oligomer that accumulates during fibrillation., *Proc Natl Acad Sci U S A 108(8)*, 3246-3251.
33. Bolognesi, B., Kumita, J. R., Barros, T. P., Esbjorner, E. K., Luheshi, L. M., Crowther, D. C., Wilson, M. R., Dobson, C. M., Favrin, G., and Yerbury, J. J. (2010) ANS binding reveals common features of cytotoxic amyloid species, *ACS Chem Biol 5*, 735-740.
34. Andreasen, M., Nielsen, S. B., Runager, K., Christiansen, G., Nielsen, N. C., Enghild, J. J., and Otzen, D. E. (2012) Polymorphic fibrillation of the destabilized fourth fasciclin-1 domain mutant A546T of the Transforming growth factor-beta-induced protein (TGFBIp) occurs through multiple pathways with different oligomeric intermediates, *J Biol Chem 287*, 34730-34742.

35. Lorenzen, N., Cohen, S. I. A., Nielsen, S. B., Herling, T. W., Christiansen, G., Dobson, C. M., Knowles, T. P. J., and Otzen, D. (2012) Role of Elongation and Secondary Pathways in S6 Amyloid Fibril Growth, *Biophysical Journal 102*, 2167-2175.
36. Hupfeld, S., Ausbacher, D., and Brandl, M. (2009) Asymmetric flow field-flow fractionation of liposomes: optimization of fractionation variables, *Journal of Separation Science 32*, 1465-1470.
37. Vilar, M., Chou, H. T., Luhrs, T., Maji, S. K., Riek-Loher, D., Verel, R., Manning, G., Stahlberg, H., and Riek, R. (2008) The fold of alpha-synuclein fibrils, *Proceedings of the National Academy of Sciences of the United States of America 105*, 8637-8642.
38. van Rooijen BD, C. M., Subramaniam V. (2010) Membrane Permeabilization by Oligomeric α-Synuclein: In Search of the Mechanism., *PLoS One 5*.
39. Ouberai, M. M., Wang, J., Swann, M. J., Galvagnion, C., Guilliams, T., Dobson, C. M., and Welland, M. E. (2013) alpha-Synuclein senses lipid packing defects and induces lateral expansion of lipids leading to membrane remodeling, *J Biol Chem 288*, 20883-20895.
40. Varkey, J., Isas, J. M., Mizuno, N., Jensen, M. B., Bhatia, V. K., Jao, C. C., Petrlova, J., Voss, J. C., Stamou, D. G., Steven, A. C., and Langen, R. (2010) Membrane curvature induction and tubulation are common features of synucleins and apolipoproteins, *J Biol Chem 285*, 32486-32493.
41. van Rooijen, B. D., Claessens, M. M., and Subramaniam, V. (2009) Lipid bilayer disruption by oligomeric alpha-synuclein depends on bilayer charge and accessibility of the hydrophobic core, *Biochim Biophys Acta 1788*, 1271-1278.

FIGURE LEGENDS

Figure 1. Oligomer structure and hydrophobicity. A. Schematic representation of αSN including deletions at the N-terminus. B: Oligomer radii determined by DLS. C: ANS fluorescence of monomers and oligomers. Legends as in Fig. 1B including ANS control (x). Insert: Zoom of monomer spectra.

Figure 2. Monomer-membrane interactions. A: Monomer-vesicle interaction analyzed with aF4. Del2 alone (black) and Del2 mixed with vesicles (grey). B: Degree of monomer folding as a function of temperature using CD. Dashed line shows the temperature range of Del2-11 coil→helix folding. C: Dye leakage induced by monomers. All data points are averaged triplicates with standard deviation. Insert: Correlation between temperature range of folding and efficacy of membrane permeabilization (see text for details).

Figure 3. Oligomer-membrane interactions. A: Oligomer binding analyzed with aF4. Del2 oligomers alone (black) and mixed with vesicles (grey). B: Dye leakage of the four aSN oligomers.

Figures 1-3

Click here to download Figure: Lorenzen Lemminger Figures Revised SUBMITTED.pptx

Figure 1 Lorenzen *et al.*

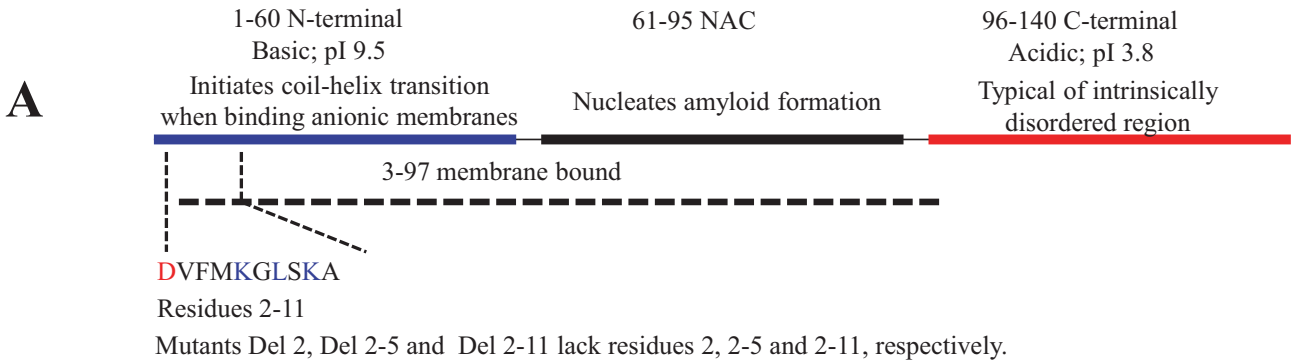

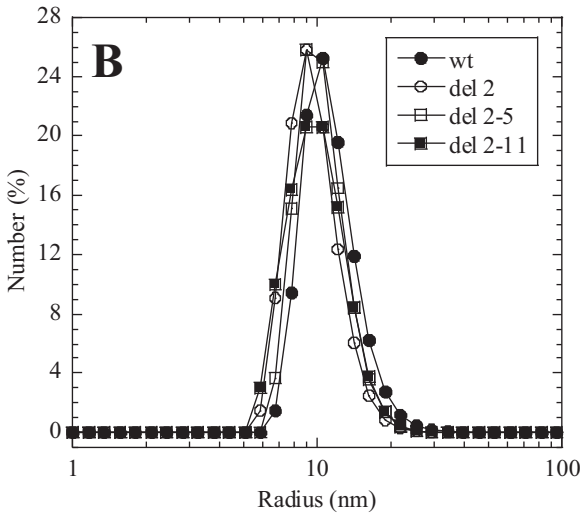

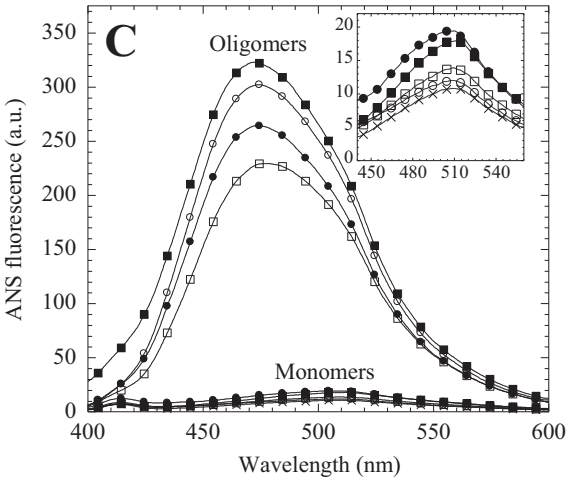

Figure 2 Lorenzen *et al.*

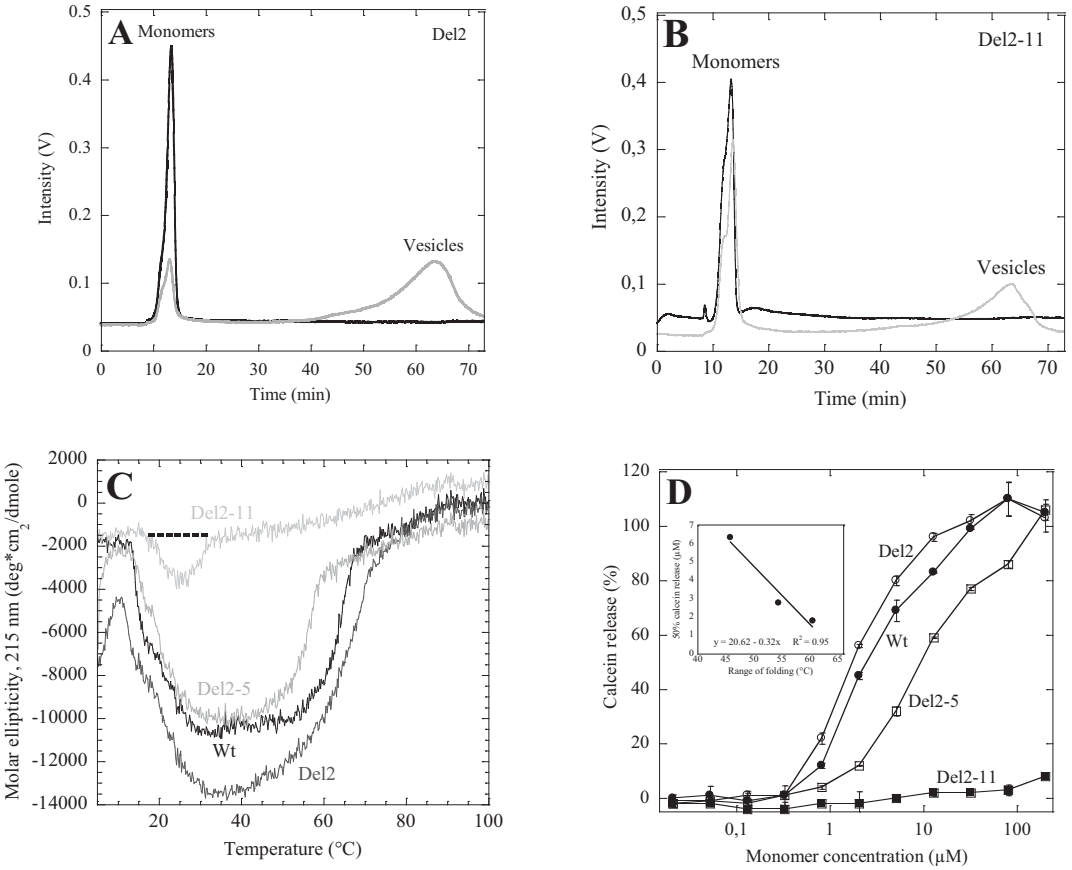

Figure 3 Lorenzen *et al.*

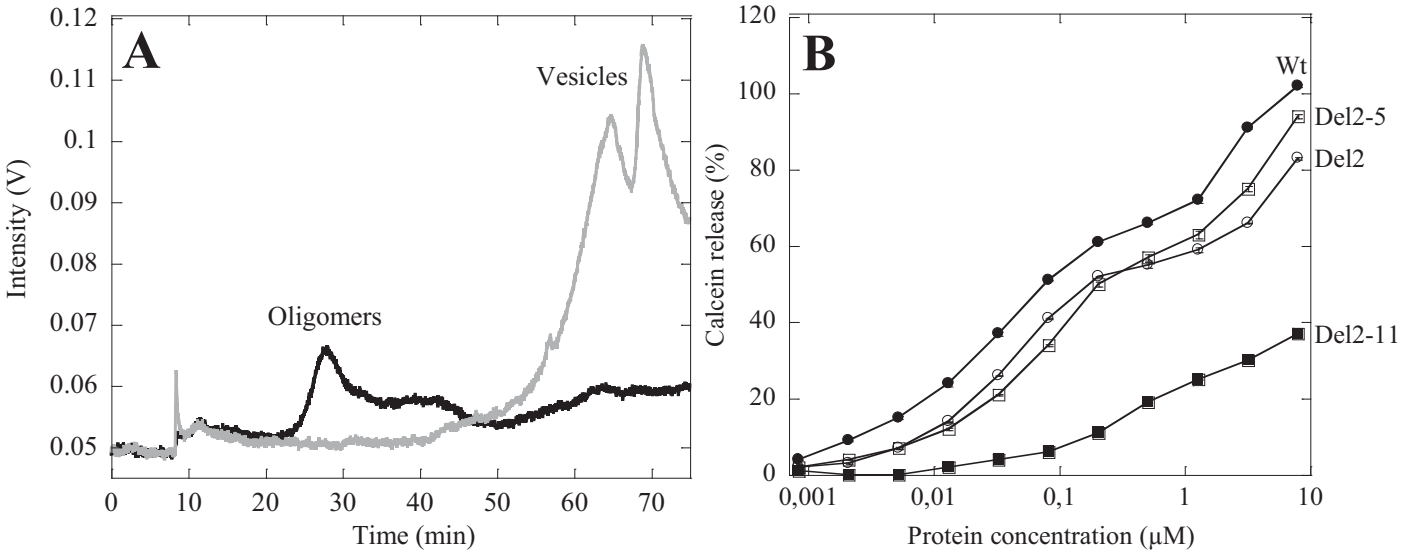

The N-terminus of α-synuclein is essential for both monomeric and oligomeric interactions with membranes

Nikolai Lorenzen, Lasse Lemminger, Jannik Nedergaard Pedersen,
Søren Bang Nielsen & Daniel Erik Otzen*

Supplementary information

Experimental procedures

Protein production and purification: αSN was produced in *E. coli* BL21(DE3) cells with a plasmid vector pET11-D using auto-induction as described (*1*). High purity αSN was obtained by the purification protocol described in *(2,3)* modified with an additional step. Briefly, cells were harvested by centrifugation at 3500 rpm, 4 °C for 20 min. Harvested cells were subjected to osmotic shock by resuspension of cells from 1 L culture in 100 mL osmotic shock buffer (30 mM Tris-HCl, 40 % sucrose, 2mM EDTA, pH 7.2), incubation for 10 min at RT followed by centrifugation at 9000 g, 20 °C for 30 min. The pellet was resuspended in 90 mL ice-cold deionised water and 40 µL of saturated $MgCl_2$ was added. The pellet was incubated on ice for 3 min. The supernatant, containing the periplasmic preparation, was collected by centrifugation at 9000 g, 4 °C in 20 min. The periplasmic preparation was subjected to acid precipitation with drop-wise addition of 1 M HCl to a final pH level of 3.5 and then incubated for 5 min. The supernatant was collected by centrifugation at 9000 g, 4 °C for 20 min. Supernatant pH was immediately adjusted to pH 7.5 with drop-wise addition of 1 M NaOH. The solution was filtered (0.45 µm) and loaded on a Q-Sepharose column (HiTrap Q HP) pre-equilibrated with 20 mM Tris-HCl pH 7.5. The column was washed with three column volumes of 0.1 M NaCl in buffer followed by elution of αSN with a NaCl gradient from 0.1-0.5 M. SDS-PAGE analysis was used to identify fractions with αSN and ensure protein purity. Finally the αSN was dialyzed exhaustively against deionised water, lyophilized and stored at -20 °C.

Asymmetrical flow field-flow fractionation (A4F): Binding of monomers and oligomers to vesicles (100 nm diameter) of DOPG was analyzed by size separation of monomers and oligomers alone and in the presence of vesicles. A decrease in the amount of free protein in the presence of

vesicles indicates membrane binding. Separation was carried out with an AF2000 field-flow fractionation system (Postnova Analytics GmbH, Germany) equipped with a UV/Vis (S3240) detector (A_{214nm}) operating in AF4 mode. 21 µM αSN (monomer equivalents) and 2.1 mM DOPG vesicles (mole ratio 1:100) were mixed and incubated at 37 °C for 1 hr prior to separation using the following steps: (1) 100 µL sample was injected and focused for 7 min at 0.2 mL/min and a cross-flow (CF) of 2 mL/min followed by elution via (2) 2 mL/min CF for 10 min, (3) a CF gradient to 0.35 mL/min over 25 min and (4) a CF gradient to 0 mL/min for 25 min after which field release (no CF) took place for 10 min to flush remaining species out of the channel. The detector flow was maintained at 0.5 mL/min through injection, focusing and elution steps and a 1 min crossover time was used between focusing/injection and elution steps (steps 1-2). The absorbance at 214 nm was recorded throughout the separation using Postnova AF2000 Control v.1.1.0.27. The monomer signal originating from monomers co-eluting with vesicles could not be accurately determined due to light scattering by DOPG vesicles.

Dye leakage assay: We used the fluorophore calcein entrapped in DOPG vesicles (100 nm diameter) at self-quenching concentrations. Vesicles were prepared in the presence of 70 mM calcein and separated from free calcein with a PD-10 desalting column (GE Healthcare). As a consequence of vesicle permeabilization, calcein leaks out and gives rise to an increased fluorescence signal due to dilution. Different concentrations of monomers or oligomers were mixed with vesicles to a final concentration of ~42 µM lipid. The lipid concentration is based on an estimated two-fold dilution of the vesicles in the desalting step. Calcein fluorescence was monitored by excitation at 485 nm and emission at 520 nm for at least 1.5 hrs in a Genios Pro fluorescence plate reader (Tecan, Mänerdorf, Switzerland) at 37 °C with 2 sec shaking every 2nd min. Finally, Triton X-100 (0.1% (w/V)) was added to measure the fluorescence associated with 100% calcein release. Background fluorescence was subtracted.

Folding assay: The folding of monomeric αSN in DMPG vesicles (200 nm diameter) was analyzed as described (*4*). Briefly, 291 µM DMPG vesicles were mixed with 14 µM αSN, transferred to a 1 mm quartz cuvette and subjected to thermal scans in a Jasco J-810 circular dichroism spectrophotometer (Jasco Spectroscopic Co. Ltd., Japan) from 5 to 95 °C with a scan speed of 90 °C/hr in steps of 0.2 nm at a fixed wavelength of 215 nm.

Note that we use DMPG for the folding assay to evaluate the degree of folding of αSN around the lipid phase transition. In both the binding assay and the dye leakage experiment we have used DOPG to ensure that the lipid system is in the liquid disordered phase throughout the experiments

which are carried out at RT, close to the lipid phase transition of DMPG (23°C). In practice it is very difficult to obtain consistent calcein leakage data with DMPG, possibly because phase transitions, which are difficult to avoid when handling DMPG around RT, adversely affect the leakage measurements. Since both DOPG and DMPG are anionic and we compare data where the lipids are in the liquid disordered phase, we consider it reasonable to compare these assays.

For practical reasons we have used different protein:lipid mole ratios in the different assays. Our CD-based folding assay uses a molar ratio of 1:21 (protein:lipid) to obtain robust and reproducible CD signals as described *(4)*. For our A4F binding experiments we use a mole ratio of 1:100 (protein:lipid) *i.e.* more lipid relative to protein compared to the CD experiment. A mole ratio similar to the CD experiments (1:21) led to more baseline noise in the A4F experiment (while qualitatively leading to the same binding distributions as the 1:100 ratios), possibly due to a low degree of membrane disruption, while 1:100 ratios leads to solid baselines. The calcein release assays are carried out over a range of concentrations that spans the protein:lipid ratios used in CD and AF4 experiments. 50% release is achieved at molar protein:lipid ratios of ~1:470 (oligomeric αSN) and ~1:15 (monomeric αSN).

SDS induced fibrillation assay: Fibrillation experiments were carried out as previously described *(5,6)*. Briefly, assay conditions were 20 μM αSN, PBS buffer (20 mM phosphate, 150 mM NaCl, pH 7.4), 0.5 mM SDS and 40 μM ThT. Samples were loaded into a 96-well plate (nunc, Thermo Fischer Scientific, Roskilde, Denmark) with 150 μL assay solution in each well. Plates were sealed with Crystal clear sealing tape (Hampton Research, Aliso Viejo, CA) and loaded into a Genios Pro fluorescence plate reader (Tecan, Mänerdorf, Switzerland). Plates were incubated at 28 °C without shaking for 2-4 days. ThT fluorescence intensity was measured with 12 min intervals with excitation at 448 nm and emission at 485 nm.

Shaking induced fibrillation assay: Fibrillation experiments were carried out as previously described (*5*). Briefly, assay conditions were 70 μM αSN, PBS buffer (20 mM phosphate, 150 mM NaCl, pH 7.4), 40 μM ThT and addition of a 3 mm diameter glass bead in each well. Assay solutions were loaded into a 96-well-plate (nunc, Thermo Fischer Scientific, Roskilde, Denmark) with 150 μL assay solution in each well. Plates were sealed with Crystal clear sealing tape (Hampton Research, Aliso Viejo, CA). The plates were transferred to a Genios Pro fluorescence plate reader (Tecan, Mänerdorf, Switzerland) and incubated at 37 °C with continuously shaking over 10 out of 12 min at 300 rpm in 3-4 days. ThT fluorescence intensity was measured with 12 min intervals with excitation at 448 nm and emission at 485 nm.

All αSN N-terminal truncation mutants are able to form amyloid fibrils

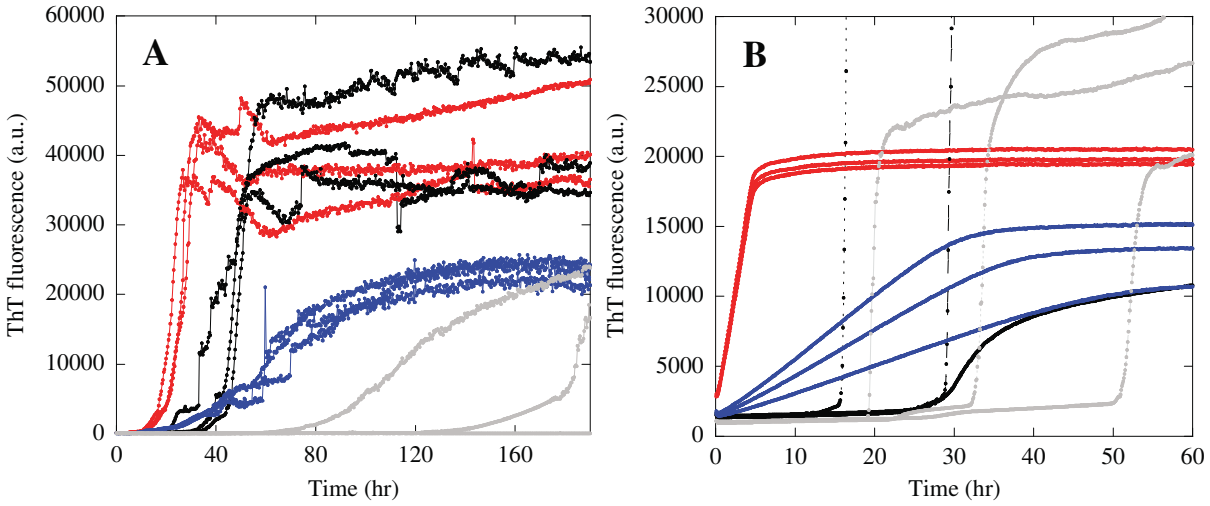

Figure S1. Kinetic traces of ThT fluorescence of the different mutants in (A) shaking induced and (B) SDS induced fibrillation assays. The mutants are depicted in triplicates as follows: wt (blue), Del2 (red), Del2-5 (black) and Del2-11 (grey).

Negative control for quantitative analysis of monomer and oligomer interactions with vesicles using AF4

There is no difference of the BSA elution profile with and without DOPG LUVs (Fig. S2). This is due to insignificant association of BSA and vesicles.

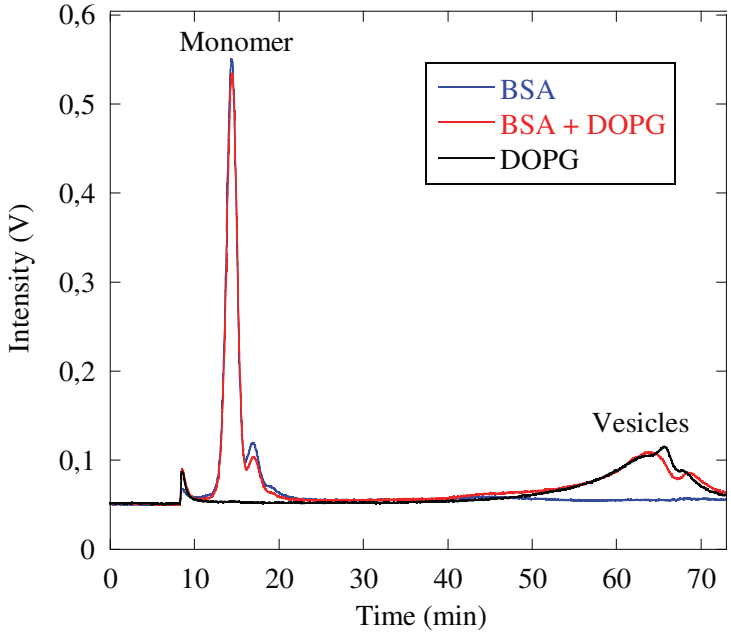

Figure S2. Comparison of BSA elution when pre-incubated with and without DOPG vesicles. DOPG vesicle control sample is shown.

References

1. Studier, F. W. (2005) *Protein Expr Purif* **41**, 207-234
2. Huang, C., Ren, G., Zhou, H., and Wang, C. C. (2005) *Protein Expr Purif* **42**, 173-177
3. Giehm, L., Lorenzen, N., and Otzen, D. E. (2011) *Methods* **53**, 295-305
4. Kjaer, L., Giehm, L., Heimburg, T., and Otzen, D. (2009) *Biophys J* **96**, 2857-2870
5. Giehm, L., and Otzen, D. E. (2010) *Anal Biochem* **400**, 270-281
6. Giehm, L., Oliveira, C. L., Christiansen, G., Pedersen, J. S., and Otzen, D. E. (2010) *J Mol Biol* **401**, 115-133

Article X

EGCG inhibits the toxicity of α-synuclein oligomers

Nikolai Lorenzen[1,2], Søren B. Nielsen[1,2,5], Cristine Betzer[3], Yuichi Yoshimura[1,2], Brian S. Vad[1,2], Jørn D. Kaspersen[1], Gunna Christiansen[4], Jan S. Pedersen[1], Poul Henning Jensen[3], Frans A. Mulder[1,2] and Daniel E. Otzen[1,2]*

[1] Interdisciplinary Nanoscience Center (iNANO), Aarhus University, Gustav Wieds Vej 14 8000 Aarhus C Denmark.

[2] Center for Insoluble Protein Structures, Interdisciplinary Nanoscience Center, University of Aarhus, Langelandsgade 140, 8000 Aarhus C, Denmark.

[3] Department of Biomedicine - Medical Biochemistry, Ole Worms Allé 3, building 1171, 8000 Aarhus C, Denmark

[4] Department of Biomedicine - Medical Immunology, Aarhus University, Aarhus, Denmark

[5] Present address: Arla Foods, Sønderupvej 26, DK - 6920 Videbæk, Denmark

* To whom correspondence should be addressed dao@inano.au.dk (D.E.O).

Keywords: α-synuclein, EGCG, membrane, oligomer, toxicity

Abstract

Oligomeric species of various proteins are linked to the pathogenesis of different neurodegenerative disorders. Consequently, there is intense focus on the discovery of novel inhibitors, *e.g.* small molecules and antibodies, to inhibit the formation and toxicity of oligomers. In Parkinson's Disease the protein α-synuclein (αSN) forms cytotoxic oligomers. The flavonoid epigallocatechin gallate (EGCG) has previously been shown to redirect the aggregation of αSN monomers and remodel αSN amyloid fibrils into disordered oligomers. Here we dissect EGCG's mechanism of action. Although EGCG inhibits preformed oligomer's ability to permeabilize vesicles and induce cytoxicity in a rat brain cell line. EGCG does not affect oligomer size-distribution or secondary structure. Rather, EGCG immobilizes the C-terminal region and moderately reduces the degree of binding of oligomers to membranes. We interpret our data to mean that the oligomer acts by destabilizing the membrane rather than by direct pore formation. This suggests that reduction (but not complete abolition) of oligomers' membrane affinity is sufficient to avoid cytotoxicity.

The intrinsically disordered protein α-synuclein (αSN) has been linked to Parkinson's Disease (PD) since 1997. The focus on αSN stems from αSN's accumulation in intracellular amyloid-rich Lewy bodies (LB) (1,2), which accumulate in the brain of PD patients. Also, certain mutations in the αSN gene have been linked with familial PD (3) where a few of these mutations have been reported to increase the propensity of the αSN monomer to form amyloid material *in vitro (4,5)*. Recently, we have come to view soluble non- or prefibrillar oligomers as the toxic species that leads to neuronal damage in PD (6,7). This is further supported by reports on elevated concentrations of αSN oligomers in post-mortem brain extracts from patients with Lewy Body Dementia (8) and in CSF from PD patients(9). A current challenge in the field of protein misfolding and neurodegeneration is to understand the molecular mechanism behind oligomer toxicity. One of the most widespread hypotheses is that oligomers can interact with and perturb membranes, thereby leading to cell death (6,7,10-12).

There is an enormous interest in finding molecules that inhibit the formation of αSN oligomers with the ultimate aim of developing drugs towards PD. With the need to develop molecules that are both specific towards αSN and able to cross the blood-brain barrier, the focus has been on small molecules. One remarkably efficient and well-studied example is the small molecule epigallocatechin gallate (EGCG). EGCG is reported to reduce toxicity by (1) redirecting the aggregation pathway of monomeric αSN into unstructured non-toxic oligomers (13), as is the case for the two structurally related compounds, baicalein (14) and dopamine (15) and by (2) reducing the toxicity of αSN fibrils by remodeling them into non-toxic aggregates (16). EGCG is a potent antioxidant found in green tea and appears to counteract several diseases, including cancer (17). EGCG's benzene rings with vicinal dihydroxy groups (Fig. 1A) are also found in numerous other fibril inhibitors (14,15,18-20). EGCG is not specific towards αSN and has been shown to inhibit the fibrillation process of a range of proteins (21-27). At equimolar concentrations, EGCG preferentially binds the C-terminus of αSN (D119, S129, E130 and D135) (13), consistent with the observation that dopamine predominantly targets the $Y_{125}EMPS_{129}$ region (28,29). At higher EGCG:αSN mole ratios, EGCG binds nonspecifically throughout the whole amino acid sequence (13).

Drugs that directly target and stabilize the αSN monomer, thereby keeping it in a soluble conformation, may compromise the physiological role of αSN. Instead of preventing oligomer formation we have focused on inhibiting the toxicity of pre-formed toxic oligomers formed during the process of fibril formation (30). These oligomers have not been chemically modified and on average consist of ~30 monomers (Lorenzen, Nielsen *et al*. submitted)(31), forming a compact β-sheet core with a disordered outer shell (Lorenzen, Nielsen *et al.* submitted). αSN oligomers interact with and perturb membranes by a combination of electrostatic interactions between the N-terminus of αSN and lipid head groups combined with hydrophobic interactions (32-36) (Lorenzen, Lemminger *et al.* in revision).

Here we use *in vitro* assays to analyze the inhibitory effects of the small molecule EGCG on αSN oligomer' toxicity. EGCG potently inhibits αSN oligomers' ability to permeabilize membranes, probed by a calcein release assay and fluorescence confocal microscopy. EGCG's inhibition of oligomer activity is confirmed by its ability to rescue rat neuronal cells from oligomer toxicity. Gratifyingly, inhibition occurs at similar EGCG concentrations in the membrane permeabilization assay and the extracellular toxicity assay. Liquid-state NMR confirms that the N-terminus and NAC region build up the oligomer core whereas the C-terminal remain disordered in the oligomer state; we show that the flexibility of the C-terminus decreases upon EGCG binding. Importantly, EGCG binds to the oligomers without changing the oligomer structure and size distribution. Thus inhibition of membrane permeabilization and extracellular toxicity is not due to dissociation or aggregation of the oligomers. Rather, EGCG inhibits the toxicity of αSN oligomers by decreasing their interaction with membranes, highlighting reduction of oligomers' membrane interactions as a viable therapeutic approach against Parkinson's Disease.

Experimental Procedures

αSN production and handling: αSN was produced and purified according to (Lorenzen, Lemminger et al. in revsion). ^{15}N labeled αSN was produced and purified with the exception that *E.coli* was grown in M9 minimal media with $^{15}NH_4CL$ as the only nitrogen source. A 100 ml preculture was inoculated with a transformed colony and grown overnight at 37 ºC. The preculture was subsequently split into growth media and incubated at 37 ºC until an OD_{600}~0.6 was reached. Protein expression was induced by addition of IPTG to a final concentration of 0.1 mM followed by 4 hrs incubation prior to harvest. Freshly dissolved αSN was filtered (0.2 µm) prior to use and protein concentration determined by absorption measurements with a NanoDrop UV-VIS spectrophotometer (ND-1000, Thermo Scientific) using a theoretical extinction coefficient of 0.412

$(mg/ml)^{-1}cm^{-1}$. All experiments were carried out in phosphate buffer saline (PBS) (20 mM phosphate, 150 mM NaCl, pH 7.4). Details of SAXS, SEC and AF4 are provided in Supporting information.

Oligomer production: Monomeric αSN was incubated at 840 µM in PBS buffer for 5 hrs at 37 °C and 900 rpm shaking in a Biosan TS-100 Thermo shaker. Soluble material was separated from insoluble material by centrifugation at 13.400 rpm RT and loaded on a ~24 ml superose 6 10/30 GL SEC column at 0.5 ml/min in PBS buffer. Small oligomers were separated from larger aggregates and monomers. The concentration of oligomers was estimated the same way as described above for monomers. When necessary, oligomers were concentrated using 0.5 and 15 mL Amicon Ultracentrifugal filters (Merck Millipore, Darmstadt, Germany).

Preparation of large unilamellar vesicles (LUVs): LUVs of pure 1,2-dimyristoyl-sn-3-phosphatidylglycerol (DMPG) or 1,2-dioleoyl-sn-3-phosphatidylglycerol (DOPG) were dissolved at 5 mg/ml in PBS. The samples were subjected to 10 freeze-thaw cycles between liquid N_2 and a 50 ºC water bath, followed by 21 extrusions to a diameter of 100 or 200 nm. During extrusion of DMPG vesicles, the extruder was kept at 50 ºC to keep the lipid in the liquid disordered phase. DOPG vesicles for calcein release were prepared in the presence of 70 mM calcein. After extrusion, vesicles were separated from free calcein with a PD-10 desalting column (GE Healthcare).

Calcein release assay: The fluorophor calcein was entrapped at self-quenching concentrations (70 mM) inside DOPG vesicles. Upon membrane permeabilization, calcein is released from the vesicles and diluted, leading to a fluorescence increase. Oligomers were mixed with varying concentrations of EGCG and 1 % DMSO and loaded in triplicates of 148 µL assay solution onto 96-well-plate (nunc, Thermo Fischer Scientific, Roskilde, Denmark). The plates were sealed with Crystal clear sealing tape (Hampton Research, Aliso Viejo, CA) and incubated in a Genios Pro fluorescence platereader (Tecan, Männerdorf, Switzerland) for 1 hr at 37 °C and 2 sec autoshake. Subsequently, DOPG vesicles with calcein were added to a final lipid concentration of ~42 µM and a final volume of 150 µL assay solution. Calcein release was monitored with excitation at 485 nm and emission at 520 nm for at least 1 hr under the same conditions used for incubation. Titration of EGCG to vesicles did not lead to any changes in fluorescence signal, nor did EGCG affect the fluorescence signal of free calcein (data not shown).

Cell line and culture conditions (CB&PHJ): The cell line used was OLN-93, an immortalized oligodendroglial cell line derived from primary Wistar rat brain glial cultures (37). Cells were kept at 37 °C under 5 % CO_2 and grown in Dulbecco's modified Eagle's medium (Lonza) supplemented with 10 % fetal calf serum, 50 units/ml penicillin, and 50 µg/ml streptomycin.

Measurement of cell viability by MTT assay and trypan staining: In short, 5000 cells/well were seeded into poly-L-lysine coated 96 well plates with growth medium and allowed to attach for 24 h. αSN monomer or oligomer was added (final concentration 5µM) to the cells with or without various concentrations of EGCG or αSN specific antibody (ASY-1) and incubated for additional 24h. Cells were washed in RPMI 1640 medium (Sigma, R7509), after which 50 µl MTT (5 mg/ml in RPMI medium) was added. After 3 hrs, cells and the formed formazan crystals were dissolved in lysis buffer (1 % Triton-100, 40 mM HCl diluted in isopropanol) and incubated on shaker overnight shielded from light. The absorbance at 570 nm was measured and background (650nm) was subtracted in a VERSA max microplate reader (Molecular Devices). 5000 cells/well were seeded into poly-L-lysine coated 96-well plates with growth medium and allowed to attach for 24 h. αSN monomer or oligomer was added (final concentration 5 µM) to the cells with or without various concentrations of EGCG or αSN specific antibody (ASY-1) and incubated for additional 24h. Cells were washed in RPMI 1640 medium (Sigma, R7509) and 0.02 % Trypan blue in RPMI medium subsequently added. Cells were visualized on an Olympus inverted microscope CKX41 connected to a camera, 100 x magnifications and cell fraction with blue stained nuclei were quantified.

Preparation of giant unilamellar vesicles (GUVs): GUVs were prepared by the electroformation method originally described by Angelova and Dimitrov (38). The GUVs were made using a home-built electroformation chamber partly built on the specifications published by Bagatolli and Gratton (39). GUVs were prepared from chloroform stocks containing 10 g/L. The chloroform lipid stocks were spread on platinum electrodes with approximately 10µl on each and the solvent was allowed to evaporate. The chamber was filled with a solution of 200 mM sucrose containing Alexa488. The platinum wires were connected to a function generator (Digimess FG 100, Grundig Instruments, Nürnberg, Germany) and a low-frequency alternating field sinusoidal function with a frequency of 10 Hz and amplitude of 1.5 V was applied for 90 min followed by 30 min at 1 Hz and amplitude of 3 V. To remove free fluorophor, the GUVs were run over a PD10 column pre-equilibrated with 200 mM glucose. The eluent from the column was collected and transferred to an eight-well microscopy chamber (Lab-Tek Brand Products, Naperville, IL). GUVs were left overnight at 4 °C to allow them to sediment at the bottom of the viewing chamber prior to analysis.

Fluoerescence labeling of αSN oligomers: A single cysteine mutant of αSN (Ala 140 Cys) was produced and purified as described above. Labeling of Alexa Fluor® 633 Maleimide was carried out according to the

procedures provided by the manufacture (Invitrogen). Labelled αSN were mixed with unlabeled monomer at a ratio of 1:10 and oligomers were produced as described above.

Laser Scanning Confocal Microscopy (LSCM) measurements: GUV´s were equilibrated to room temperature in the microscopy wells for 15-20 min before measuring. 5 µl of $Alexa_{633}$ labeled αSN oligomer solution was injected into the microscope and images were recorded every 6 s. GUVs were analyzed with a LSM 510 scanning confocal microscope (Zeiss GmbH, Jena, Germany). Excitation of Alexa488 and $Alexa_{633}$ was done at 488 and 588 nm and Fluorescence emission was measured at 505-548 and 612-750 nm for Alexa488 and $Alexa_{633}$, respectively.

Nuclear magnetic resonance spectroscopy (NMR): The NMR samples contained 200 µM protein in (monomer equivalents) PBS buffer, with about 6% (v/v) D_2O and 0.1 mM sodium 4,4-dimethyl-4-silapentane-1-sulfonate (DSS) as an internal chemical shift reference. ^{1}H-^{15}N heteronuclear single-quantum coherence (HSQC) spectra were recorded on a Bruker Avance NMR spectrometer at 500 MHz ^{1}H frequency at 1 ºC. The spectra were processed using NMRPipe and analyzed with Sparky (T. D. Goddard and D. G. Kneller, SPARKY 3, University of California, San Francisco) (40). Spectral assignment is taken from BMRB entry ID 18857.

Transmission electron microscopy (TEM): 5 µL aliquots of 28 µM oligomer (monomer equivalents) with varying mole ratio of EGCG (1:0, 1:1 and 1:5 (αSN:EGCG) in PBS buffer were transferred to 400-mesh carbon-coated, glow-discharged grids for 30 sec. The grids were washed using two drops of doubly distilled water, stained with 1% phosphotungstic acid (pH 6.8) and blotted dry on filter paper. The samples were viewed in a microscope (JEM-1010; JEOL, Tokyo, Japan) operating at 60 kV. Images were obtained using an Olympus KeenViewG2 camera.

Far-UV circular dichroism (CD): Far-UV CD spectra were recorded on a Jasco J-810 spectropolarimeter (Jasco Spectroscopic Co. Ltd.). Ellipticity was measured at 25 °C and five accumulations were averaged to yield the final spectrum. A 1.0 mm path length cuvette was used for 14 µM oligomer (monomer equivalents). The contribution from PBS buffer was subtracted and the CD signal given as mean residue ellipticity (MRE) expressed as deg $cm^2dmol^{-1}residue^{-1}$.

Dynamic light scattering (DLS): We have used a ZS Zetasizer Nano ZS (Malvern Instruments) to measure the hydrodynamic radius (R_h) of oligomer and vesicles at 25 °C, 21 µM oligomer (monomer equivalent) and 1.26 mM of DOPG vesicles (mole ratio 1:60) prepared with 100 nm diameter as described above. All samples were measured five times using 15-40 accumulated scans. We have given the Z-average with standard deviation of the five accumulation scans

Differential scanning calorimetry (DSC): DSC experiments were carried out on a VP-DSC Microcalorimeter (MicroCal, Inc.), with a cell volume of ~0.5 ml. The sample cell was carefully cleaned, emptied, reloaded with 1.45 mM (1 mg/ml) DMPG vesicles with a diameter of 200 nm ± 70 µM EGCG *i.e.* mole ratio 1:20.8 (EGCG:lipid). The samples were equilibrated for 30 min at the scan starting temperature of 10 ºC and the thermograms were recorded on heating with a 90 °C/hr scan rate.

Results

We produce αSN oligomers by incubating monomeric αSN at high concentrations at 37ºC under shaking for several hours in the absence of chemically modifying agents. Oligomers are purified as a single well-defined peak on a gel filtration column with a size estimated to ~30 monomers according to multi-angle light scattering and Small-Angle X-ray Scattering (Lorenzen, Nielsen *et al*. submitted).

Inhibition of membrane permeabilization and extracellular toxicity

Extracellular toxicity: To evaluate whether the oligomers are cytotoxic, we have analyzed the effect of the oligomers on viability of a rat oligodendroglial cell line using the MTT assay that quantifies functional mitochondrial activity. Oligomers decreased viability by about 15% compared to controls (monomer and buffer) (Fig. 1B). However, pre-incubation of oligomers with EGCG led to complete rescue of OLN-93 cells as measured both by MTT assay (Fig. 1 BC) and Trypan blue staining of nuclei in death cells permeable cell membranes (Fig. 1C). EGCG is able to suppress oligomers' viability reduction to half (*i.e.* to 7.5% reduction) at a molar ratio of 0.36:1 (EGCG: $\alpha SN_{monomer}$) (Fig. 1BC, Table 1) *i.e.* ~11 EGCG molecules per one oligomer.

Membrane permeabilization: We use a simple *in vitro* assay to investigate EGCG inhibition of membrane permeabilization by these αSN oligomers where we monitor release of the fluorescent dye calcein from DOPG large unilamellar vesicles (LUVs). Similar assays have previously been used to analyze membrane permeabilization of anionic LUVs in-

duced by αSN oligomers (10,33,35). Pre-incubation of αSN oligomers with EGCG (1 hr, 37 °C) leads to inhibition in a dose-response fashion, reaching complete inhibition around 1 μM (Fig. 1A), with 50 % inhibition ($MI_{50\%}$) at an EGCG:$\alpha SN_{monomer}$ mole ratio of 0.23:1 (Table 1). Given that the oligomer consists of ~30 monomers (Lorenzen, Nielsen *et al*., submitted) (31), ~7 EGCG molecules are needed per oligomer to reach 50 % inhibition (Table 1). EGCG has no effect on the fluorescence spectra of calcein, ruling out that fluorescence quenching affects the assay (data not shown).

Gratifyingly, the $MI_{50\%}$ values based on the extracellular toxicity assay and the calcein release assay are essentially identical within error (Table 1).

Table 1. EGCG:αSN molar ratios needed for 50 % inhibition of oligomer membrane permeabilization and cytotoxicity.

Assays	$MI_{50\%}$, EGCG:Oligomer (EGCG:monomer)[b]
Calcein release	~7(±2):1 (0.23:1)
OLN-93 toxicity	~11(±2):1 (0.36:1)

[a,b] *$MI_{50\%}$: Mole ratio of EGCG needed for 50 % inhibition of calcein release and for 50% reduction in the decrease in cell viability caused by oligomer (i.e. from 15% to 7.5%). Ratios are given in units of oligomer concentration (monomer equivalents in brackets based on an average of 30 monomers per oligomer). Data from fits to Fig. 1A and Fig. 1C.*

Oligomer interactions with GUVs: We also probed the membrane permeabilizing properties of the αSN oligomers with fluorescence confocal microscopy where we entrapped the fluorophor Alexa488 inside giant unilamellar vesicles (GUVs) of either pure DOPG or DOPC. For the neutrally charged lipid DOPC, we observed no vesicle permeabilization (data not shown). With the anionic lipid DOPG oligomers permeabilized the membrane by vesicle lysis (Fig. 2ABCD, SI video). To address whether oligomers pre-incubated with EGCG were able to bind membranes without inducing membrane permeabilization, we introduced the fluorophor Alexa633 at the C-terminus using the single cysteine mutant Ala→Cys140. The C-terminus is not involved in oligomer-membrane interaction (34). We labeled every 10th αSN molecule prior to oligomerization to ensure ~3 labelled monomers per oligomer. When pre-incubated with EGCG at a mole ratio of 1:1 (EGCG:$\alpha SN_{monomer}$), the oligomers colocalized with the GUV vesicle but did not cause rupture, and membrane permeabilization was only rarely observed (Fig. 2EFG). Our confocal fluorescence microscopy data do not allow a quantitative estimate of the ratio of membrane-associated and free oligomers. This is measured by AF4 (see below).

Liquid state NMR shows that EGCG reduces the flexibility of the C-terminus

Liquid state NMR does not readily provide structural information on large protein complexes such as αSN oligomers (ca. 420 kDa). Instead, we exploit this size limitation to detect signals from unstructured (and therefore highly mobile) regions which remain visible by NMR. We compare spectra of monomeric and oligomeric αSN to determine which parts of the αSN sequence become structured in the oligomer (and hence invisible), and which parts remain flexible. Due to the presence of a significant fraction of monomeric protein in the oligomer sample, the contribution from monomer needs first to be subtracted from the oligomer spectra. We estimated the monomer contribution by assuming that residues 1-86 give no signal in the oligomer structure based on the spectra. We observed that essentially the whole N-terminus and NAC-region become structured upon oligomerization (residue 1-95) whereas the C-terminus remains disordered (residue 96-140 (Fig. 3AB)). We then recorded the same experiment for monomeric αSN, and subtracted that spectrum from the mixed monomer/oligomer spectrum in such a way that no peaks were visible for the NAC region anymore. This procedure resulted in signal loss also for the N-terminal region, indicating that this part of αSN is also

immobile in the oligomer (Fig 3B; black line). Only residues 86 and onwards are flexible in the oligomers described here.

Titration of EGCG to the oligomers led to a pronounced decrease in the ^{1}H-^{15}N HSQC signal in the C-terminal, where ~50 % signal was lost at a mole ratio of 1:1 (EGCG:$\alpha SN_{monomer}$) (Fig. 3B). We attribute this loss of flexibility to structure formation in the C-terminus upon binding of EGCG. No aggregation was observed as analyzed with DLS before and after EGCG titration (data not shown).

EGCG does not change the size-distribution and secondary structure of oligomers

We have employed a wide range of techniques to investigate whether EGCG affected the size, shape and molecular structure of the αSN oligomer. Free oligomers are compared with oligomers pre-incubated with EGCG for 1 hr and 37 ºC at 1:1 mole ratio (EGCG:$\alpha SN_{monomer}$), conditions which lead to near complete inhibition of membrane permeabilization and cell toxicity (Fig. 1ABC). According to TEM, there was no sign of aggregation of oligomers incubated with 0:1 (Fig. 4A), 1:1 (data not shown) and 5:1 (Fig. 4B) (EGCG:$\alpha SN_{monomer}$) (Fig. 4AB).

TEM sample preparation can affect oligomer size and shape, and we have therefore used other biophysical techniques to evaluate the effect of EGCG. Batch-mode DLS reveals no significant changes in the size of oligomers upon incubation with EGCG and R_h is determined to ~22±6 nm (Table 1). This is confirmed by SEC coupled with refractive index meter (SEC-RI) analysis where similar traces of oligomers incubated with and without EGCG are obtained, suggesting similar size-distributions (Fig. 5A). Superose 6 10/30 GL with an exclusion limit of ~$4x10^7$ Da is used as SEC matrix. The oligomers elute within this separation range, consistent with our previous work (Lorenzen, Nielsen *et al*. in revision).

We next used SAXS to evaluate whether EGCG affects the form and size-distribution of the oligomers. SAXS spectra of the oligomers with and without EGCG were highly similar (Fig. 5B). We have previously been able to fit data for the isolated oligomer to a model with a slightly elongated core of folded protein with almost half of the protein protruding as random coils into the solution (Lorenzen, Nielsen *et al.* submitted). The EGCG-oligomer complex can be fitted very well to this model, allowing us to disregard the structural contribution of EGCG, and the presence of EGCG does not change these parameters (Table 2). The number of monomers per oligomer is also similar for the pure oligomer and oligomer incubated with EGCG determined from the forward scattering to 29 and 28, respectively. Thus EGCG has no significant effect on the overall size and shape of the oligomers.

Table 2. Fitting results from the SAXS analysis.

Sample	Radius (Å) [a]	Aspect ratio [b]	R_g of chains (Å) [c]	Number of monomers [d]	Coil fraction [e]
Oligomer	47±2	2.0±0.2	25±2	29	0.46±0.02
Oligomer +EGCG	47±1	1.7±0.5	27±4	28	0.45±0.08

[a] *Short radius of the core prolate ellipsoid of revolution*
[b] *Ratio between long and short radius of ellipsoidal core*
[c] *Radius of gyration of the random coil scattering in the oligomer shell*
[d] *Number of monomers in the oligomer*
[e] *Fraction of the protein that is in random coil configuration in the oligomers*

Far-UV CD measures the average content of secondary structure. Whereas monomers show a spectrum typical of disordered structure, the oligomer spectrum indicates a signif-

icant increase in β-sheet structure (Fig. 5C), which is consistent with Fourier transform infrared spectroscopy (Lorenzen, Nielsen *et al* submitted). There were no significant changes in the secondary structure of oligomers pre-incubated with EGCG at a mole ratio of 1:1 (EGCG:$\alpha SN_{monomer}$). The oligomer is highly stable and does not undergo conformational changes at 5-90 °C as measured with Far-UV CD thermal scans; this is not affected by the presence of EGCG (data not shown).

EGCG inhibits oligomer-membrane interactions

The effect of oligomers in the calcein release assay and confocal microscopy analysis makes it evident that the oligomers interact with DOPG vesicles. We have used AF4 and DLS as two additional assays to probe the interaction of oligomers and vesicles, and to test whether EGCG inhibits this interaction.

We utilize the broad separation range of the AF4 method to obtain near-baseline separation of monomers (R_h=2.7 nm (41), oligomers (R_h=21±6 nm) and LUVs (R_h=104±32) (Table 1). As shown in Fig. 6A, the oligomer sample includes a monomeric αSN component eluting between the 13.7 kDa and 45 kDa globular standards (data not shown) in agreement with αSN being an intrinsically disordered protein. The αSN oligomer elutes as a broad peak from 23-39 min. When αSN oligomers are incubated with 100 nm DOPG vesicles, at a mole ratio of 100:1 (lipid:$\alpha SN_{monomer}$) for 1 hr at 37 °C, the monomer peak height decreases to ~20 % of the initial sample, indicating an interaction of αSN monomers with the vesicles (Fig. 6A). Further, the oligomer peak essentially disappears (~5-10 % of original size). We note that the vesicle signal, starting at a retention time of 60 min, represents a combination of signals arising from αSN bound to vesicles and from light scattering by the vesicles, and can therefore not be used as a direct measure of the degree of binding. When the oligomer is pre-incubated with EGCG at a mole ratio of 1:1 (EGCG:$\alpha SN_{monomer}$) and mixed with DOPG vesicles, the monomer peak height is decreased to ~20% (Fig. 6B) similarly to Fig. 6A. Based on this experiment, it is not possible to conclude whether the monomer binds to vesicles or forms oligomers induced by EGCG. The oligomer peak decreases to ~40 %. This suggests that EGCG reduces but does not completely abolish oligomer interactions with the membrane.

DLS measures the R_h of the DOPG vesicles to 104±32 nm, consistent with vesicles extruded with a 100 nm filter. When DOPG vesicles were mixed with oligomers, the R_h increased to 142±56 nm, suggesting that oligomers associate to the surface of the vesicles and possibly expand or distort the vesicles. When vesicles were mixed with oligomers pre-incubated with EGCG, the R_h was comparable with DOPG vesicles without oligomers, suggesting little, if any, oligomer-membrane interaction. Monomer addition to DOPG vesicles did not lead to any significant increase in the R_h (Table 3). All DLS analyses of vesicles with and without oligomer or monomer led to only one peak in the volume and intensity size-distribution.

Altogether, both the AF4 and DLS assay strongly indicate that EGCG reduces oligomer-membrane interactions.

Table 3. R_h determined with DLS as the volume mean.

Sample	R_h (nm)
Oligomer	21±6
EGCG Oligomer (1:1)	23±6
EGCG Oligomer (5:1)	21±7
DOPG	104±32
DOPG EGCG	105±29
DOPG Oligomer	142±56
DOPG EGCG Oligomer (1:1)	109±38
DOPG EGCG Oligomer (5:1)	103±36
DOPG Monomer	101±33

Inhibition of oligomer-membrane interactions could in principle be caused by EGCG-

membrane interactions, *e.g.* due to screening of charges at the bilayer interphase by EGCG. However, isothermal titration calorimetry revealed no endo- or exothermic signals when EGCG was titrated into DOPG vesicles (data not shown). Finally, we used DSC to analyze the transition of DMPG vesicles from gel-phase to the liquid disordered phase. The melting temperature is highly sensitive towards ligand interactions with the bilayer surface and hydrophobic core. However, we saw no significant effect from EGCG (Fig. 6C). Further, DLS measurements reveal no change in vesicle size upon adding EGCG (Table 3). This confirms that free EGCG has no significant interaction with vesicles.

Discussion

EGCG is an effective inhibitor of αSN oligomers' extracellular toxicity toward OLN-93 cells (Fig. 1BC). The mole ratio of EGCG:$\alpha SN_{oligomer}$ needed for 50 % inhibition (~11:1) is within the range (and fit error) of the one needed in our *in vitro* calcein release assay (~7:1) (Table 1), which we use as a simple measure of toxicity (Fig. 1A). The enormous difference in complexity between a cell membrane and a vesicle membrane makes it inappropriate to equate conclusions from the two assays. However, the similar effect of EGCG in these assays provides a direct link between oligomer membrane permeabilization and toxicity. Furthermore, this suggests that simple membrane permeablization assays might be useful as a first-round screen to evaluate inhibition of oligomer toxicity.

Wanker and co-workers found EGCG to have a dramatic effect both on αSN monomers which formed disordered oligomers (13), and on mature αSN fibrils which were remodeled by EGCG (16). Our study differs from that of Wanker in that we focus on how EGCG affects oligomers. We find it remarkable that no pronounced structural changes are induced in the oligomer structure by EGCG. At a mole ratio of 1:1 (EGCG:$\alpha SN_{monomer}$) where near complete inhibition is reached in the extracellular toxicity and membrane permeabilization assay, we see no changes in the oligomer structure according to TEM, SEC-RI, SAXS, CD and DLS. We do detect a difference in the degree of disorder according to NMR, whose spectra demonstrate that the otherwise highly mobile C-terminus loses flexibility. Nevertheless, the loss of mobility does not imply that the oligomer collapses to a more compact state, since SAXS data do not detect any significant decrease in the size of the disordered shell. At the higher mole ratios used (10:1, Fig. 3B), EGCG can likely associate with all residues that are exposed at the oligomer surface (13).

To complement the permeabilization assays, we used AF4 and DLS as oligomer-membrane binding assays. The AF4 assay demonstrated that nearly all oligomer associated with DOPG vesicles (Fig. 6A). This was supported by DLS measurements where a ~40 % increase in the R_h of vesicles was observed when oligomers were bound (Table 1). Oligomers pre-incubated with EGCG at 1:1 mole ratio (EGCG:$\alpha SN_{monomer}$), completely inhibited membrane permeabilization and cell toxicity (Fig. 6B), even though ~60% of oligomers remain membrane associated. Confocal fluorescence microscopy also shows that oligomers, pre-incubated with EGCG, are bound to vesicle without inducing membrane permeabilization (Fig. 2EFG).

EGCG could in principle be acting by different mechanisms: (1) The oligomer acts as a pore, as suggested in the literature, and EGCG directly blocks the pore. (2) A critical concentration of oligomer in the membrane is required to permeabilize the membrane as suggested by Subramaniam and co-workers (35), and EGCG reduces the concentration of membrane-bound oligomers. Thus EGCG simply shifts the equilibrium away from the bound state, and we would expect lysis or permeabilization to occur (albeit at lower frequency) at sufficiently high oligomer concentrations. Direct evidence for pore formation generally comes in the form of AFM and TEM images, showing oligomers as ring-

shaped structures with hollow interiors. It is not clear to what extent binding to a solid surface will compromise these structures. SAXS measures oligomer structures in solution, reducing the risk of artifacts, and does not provide any direct evidence of pores (30). An indirect support of the critical-concentration-destabilization model is that it will likely distort membranes to a greater extent than pore-formation, and indeed we see a significant expansion of vesicle size upon addition of oligomers, but not when EGCG is added together with the oligomers.

AF4, SEC and NMR identified a significant amount of monomer in the oligomer batches (10-20%) (Fig. 2AB, 3A, 6A). However, the monomers are considerably less potent in the vesicle permeabilization assay and cell toxicity assay. Furthermore, we observe no changes in the oligomer and monomer populations as a result of EGCG or incubation time (Fig. 5A). Therefore, we do not attribute any effect from monomers in our assays. Also, we do not observe pronounced interaction, between vesicles and EGCG, and do not believe that this could lead to the observed inhibition (Fig. 6B, Table 3).

In conclusion, our data suggest that an *in vitro* membrane permeabilization assay can be used as a simple model of the highly more complex extracellular toxicity assay, since EGCG potently inhibits oligomer activity in both assays at similar concentrations. Contrary to our initial expectations, EGCG has no major effects on the oligomer structure. From our oligomer-membrane binding assays, moderately inhibition is observed by EGCG on oligomer-membrane interactions. However, the inhibition is only partial and we therefore speculate, that membrane permeabilization by αSN oligomers is caused by membrane destabilization events rather than pore formation. Our inhibition model is summarized in Fig. 7.

Acknowledgements

N.L. is supported by the Michael J. Fox Foundation. S.B.N., is supported by The Danish Council for Independent Research | Natural Sciences. B.S.V. and D.E.O. are supported by the Danish Research Foundation (inSPIN). J.D.K. and S.B.N. gratefully acknowledge LUNDBECKFONDEN for financial support. Y.Y., is supported by an EMBO Long-Term Fellowship (ALTF 687-2013). We are grateful to Professor Luis Bagatolli from Southern University of Denmark and Ph.D. Nelson Ferreira from University of Porto for valuable discussions. We also thank Jørgen Kjems for the use of his laboratory's Zetasizer Nano ZS.

Figure legends

Figure 1. EGCG inhibits oligomer toxicity. A: inhibition of oligomers' ability to permeabilize membranes at 0.2 μM oligomer (measured in monomer equivalents). Data fitted to simple binding isotherm. B: OLN-93 cells were exposed to 5 μM αSN oligomer or monomer and EGCG in concentrations from 0 to 5 μM for 24 h. Viability of the cells was measured with MTT-assay and trypan nuclei staining. C: Dose-response inhibition of MTT and Trypan staining. Both assays are given as triplicates with ± S.D. Data fitted to simple binding isotherm.

Figure 2. Fluorescence confocal microscopy of vesicles before (A and C) and after (B and D) disruption by oligomers. EFG: Montage of images double-stained with Alexa633-labeled oligomers pre-incubated with equimolar amounts of EGCG (green) and subsequently added to vesicles containing encapsulated Alexa488 (red). Bar in panels EFG is 200 μm.

Figure 3. (A) ^{1}H-^{15}N HSQC spectrum of the αSN oligomer sample before (black) and after (red) subtracting the signal contribution from monomeric αSN. (B) Loss of the NMR signals derived from the αSN oligomer.

Figure 4. Electron microscopy pictures of (A) free oligomers and (B) oligomers incubated with an EGCG:$\alpha SN_{monomer}$ mole ratio of 5:1.

Figure 5. EGCG does not induce any major structural changes in the oligomer. A: SEC-RI analysis of oligomers incubated alone (black) and with EGCG (red). B: SAXS data of oligomers (black) and oligomers pre-incubated with EGCG (red) with the best fit to data of the models described in the text. For visual comparison, the EGCG data and fit have been displaced down by a factor of 10. C: FAR-UV CD spectra of monomer ( ), oligomer (X) and oligomer and EGCG in mole ratio 1:1 (and grey line).

Figure 6. Inhibition of oligomer-membrane interactions. A: AF4-UV size separation of monomer and oligomer from an oligomer preparation incubated without (black) and with (red) DOPG vesicles. B: As panel A, but here oligomers have been pre-incubated with EGCG. C: DSC analysis of the phase transition of DMPG vesicles with ( ) and without (X) EGCG. Data is baseline corrected for better comparison but not normalized.

Figure 7. Schematic representation of EGCG inhibition of oligomer toxicity.

References

1. **Spillantini, M. G., Schmidt, M. L., Lee, V. M., Trojanowski, J. Q., Jakes, R., and Goedert, M. (1997) *Nature* 388, 839-840**
2. **Spillantini, M. G., Crowther, R. A., Jakes, R., Hasegawa, M., and Goedert, M. (1998) *Proc Natl Acad Sci U S A* 95, 6469-6473**
3. **Polymeropoulos, M. H., Lavedan, C., Leroy, E., Ide, S. E., Dehejia, A., Dutra, A., Pike, B., Root, H., Rubenstein, J., Boyer, R., Stenroos, E. S., Chandrasekharappa, S., Athanassiadou, A., Papapetropoulos, T., Johnson, W. G., Lazzarini, A. M., Duvoisin, R. C., Di Iorio, G., Golbe, L. I., and Nussbaum, R. L. (1997) *Science* 276, 2045-2047**
4. **Conway, K. A., Harper, J. D., and Lansbury, P. T. (1998) *Nat Med* 4, 1318-1320**
5. **Narhi, L., Wood, S. J., Steavenson, S., Jiang, Y., Wu, G. M., Anafi, D., Kaufman, S. A., Martin, F., Sitney, K., Denis, P., Louis, J. C., Wypych, J., Biere, A. L., and Citron, M. (1999) *J Biol Chem* 274, 9843-9846**
6. **Beate Winner, T. J., Samir K. Maji, Paula A. Desplats, Leah Boyer, Stefan Aigner, Claudia Hetzer, Thomas Loher, Marcal Vilar, Silvia Campioni, Cristos Tzitzilonis, Alice Soragni, Sebastian Jessberger, Helena Mira, Antonello Consiglio, Emiley Pham, Eliezer Masliah, Fred H. Gage, Roland Riek. (2010) *PNAS***
7. **Lashuel, H. A., Hartley, D., Petre, B. M., Walz, T., and Lansbury, P. T., Jr. (2002) *Nature* 418, 291**
8. **Paleologou, K. E., Kragh, C. L., Mann, D. M., Salem, S. A., Al-Shami, R., Allsop, D., Hassan, A. H., Jensen, P. H., and El-Agnaf, O. M. (2009) *Brain* 132, 1093-1101**
9. **Tokuda, T., Qureshi, M. M., Ardah, M. T., Varghese, S., Shehab, S. A., Kasai, T., Ishigami, N., Tamaoka, A., Nakagawa, M., and El-Agnaf, O. M. (2010) *Neurology* 75, 1766-1772**
10. **Volles, M. J., Lee, S. J., Rochet, J. C., Shtilerman, M. D., Ding, T. T., Kessler, J. C., and Lansbury, P. T., Jr. (2001) *Biochemistry* 40, 7812-7819**
11. **Quist, A., Doudevski, I., Lin, H., Azimova, R., Ng, D., Frangione, B., Kagan, B., Ghiso, J., and Lal, R. (2005) *Proc Natl Acad Sci U S A* 102, 10427-10432**

12. Kayed, R., Head, E., Thompson, J. L., McIntire, T. M., Milton, S. C., Cotman, C. W., and Glabe, C. G. (2003) *Science* 300, 486-489
13. Ehrnhoefer, D. E., Bieschke, J., Boeddrich, A., Herbst, M., Masino, L., Lurz, R., Engemann, S., Pastore, A., and Wanker, E. E. (2008) *Nat Struct Mol Biol* 15, 558-566
14. Hong, D. P., Fink, A. L., and Uversky, V. N. (2008) *J Mol Biol* 383, 214-223
15. Conway, K. A., Rochet, J. C., Bieganski, R. M., and Lansbury, P. T., Jr. (2001) *Science* 294, 1346-1349
16. Bieschke J, R. J., Friedrich RP, Ehrnhoefer DE, Wobst H, Neugebauer K, Wanker EE. (2010) *Proc Natl Acad Sci U S A.* 107
17. Singh, B. N., Shankar, S., and Srivastava, R. K. (2011) *Biochem Pharmacol* 82, 1807-1821
18. Zhu, M., Rajamani, S., Kaylor, J., Han, S., Zhou, F., and Fink, A. L. (2004) *J Biol Chem* 279, 26846-26857
19. Li, J., Zhu, M., Manning-Bog, A. B., Di Monte, D. A., and Fink, A. L. (2004) *FASEB J* 18, 962-964
20. Meng, X., Munishkina, L. A., Fink, A. L., and Uversky, V. N. (2010) *Parkinsons Dis* 2010, 650794
21. Ehrnhoefer, D. E., Duennwald, M., Markovic, P., Wacker, J. L., Engemann, S., Roark, M., Legleiter, J., Marsh, J. L., Thompson, L. M., Lindquist, S., Muchowski, P. J., and Wanker, E. E. (2006) *Hum Mol Genet* 15, 2743-2751
22. Ferreira N, S. M., Amleida MR. (2011) *FEBS Lett*
23. Meng, F., Abedini, A., Plesner, A., Verchere, C. B., and Raleigh, D. P. (2011) *Biochemistry* 49, 8127-8133
24. Chandrashekaran, I. R., Adda, C. G., MacRaild, C. A., Anders, R. F., and Norton, R. S. (2010) *Biochemistry* 49, 5899-5908
25. Hudson, S. A., Ecroyd, H., Dehle, F. C., Musgrave, I. F., and Carver, J. A. (2009) *J Mol Biol* 392, 689-700
26. Roberts, B. E., Duennwald, M. L., Wang, H., Chung, C., Lopreiato, N. P., Sweeny, E. A., Knight, M. N., and Shorter, J. (2009) *Nat Chem Biol* 5, 936-946
27. Palhano, F. L., Lee, J., Grimster, N. P., and Kelly, J. W. (2013) *J Am Chem Soc* 135, 7503-7510
28. Herrera, F. E., Chesi, A., Paleologou, K. E., Schmid, A., Munoz, A., Vendruscolo, M., Gustincich, S., Lashuel, H. A., and Carloni, P. (2008) *PLoS One* 3, e3394
29. Norris, E. H., Giasson, B. I., Hodara, R., Xu, S., Trojanowski, J. Q., Ischiropoulos, H., and Lee, V. M. (2005) *J Biol Chem* 280, 21212-21219
30. Giehm L, S. D., Otzen DE, Vestergaard B. (2011) *Proc Natl Acad Sci U S A* 108(8), 3246-3251
31. Zijlstra, N., Blum, C., Segers-Nolten, I. M., Claessens, M. M., and Subramaniam, V. (2012) *Angew Chem Int Ed Engl* 51, 8821-8824
32. van Rooijen, B. D., Claessens, M. M., and Subramaniam, V. (2008) *FEBS Lett* 582, 3788-3792
33. van Rooijen, B. D., Claessens, M. M., and Subramaniam, V. (2009) *Biochim Biophys Acta* 1788, 1271-1278
34. van Rooijen, B. D., van Leijenhorst-Groener, K. A., Claessens, M. M., and Subramaniam, V. (2009) *J Mol Biol* 394, 826-833
35. van Rooijen BD, C. M., Subramaniam V. (2010) *PLoS One* 5
36. Stockl, M. T., Zijlstra, N., and Subramaniam, V. (2013) *Mol Neurobiol* 47, 613-621
37. Richter-Landsberg, C., and Heinrich, M. (1996) *J Neurosci Res* 45, 161-173
38. Angelova, M. I., and Dimitrov, D. S. (1986) *Faraday Discussions* 81, 303-+
39. Bagatolli, L. A., and Gratton, E. (1999) *Biophys J* 77, 2090-2101
40. Delaglio, F., Grzesiek, S., Vuister, G. W., Zhu, G., Pfeifer, J., and Bax, A. (1995) *J Biomol NMR* 6, 277-293
41. Morar, A. S., Olteanu, A., Young, G. B., and Pielak, G. J. (2001) *Protein Sci* 10, 2195-2199

Figure 1 Lorenzen et al.

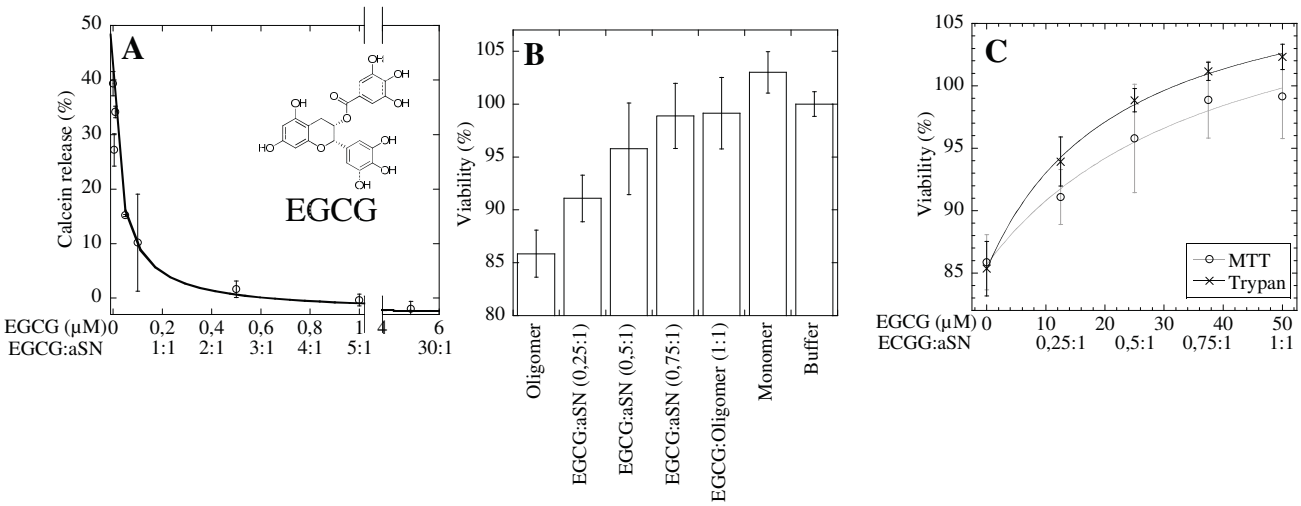

Figure 2 Lorenzen et al.

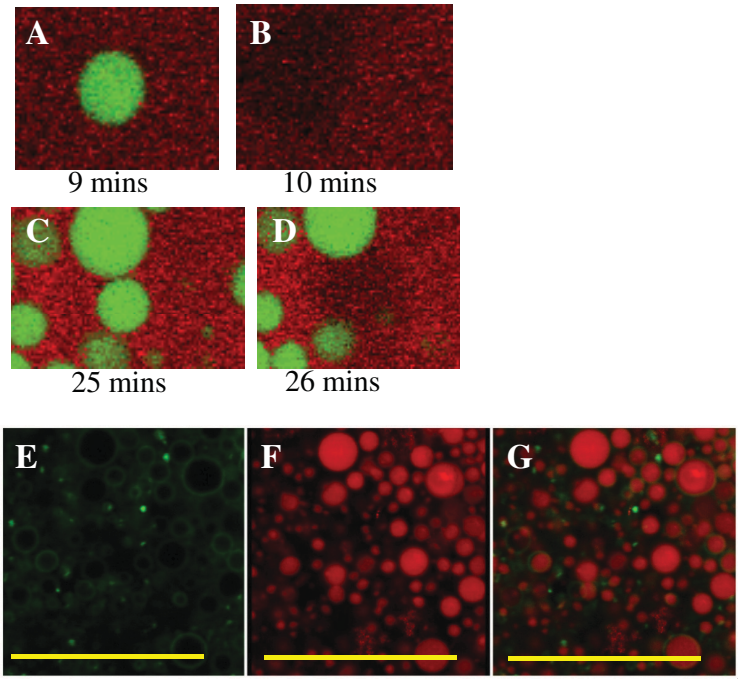

Figure 3 Lorenzen et al.

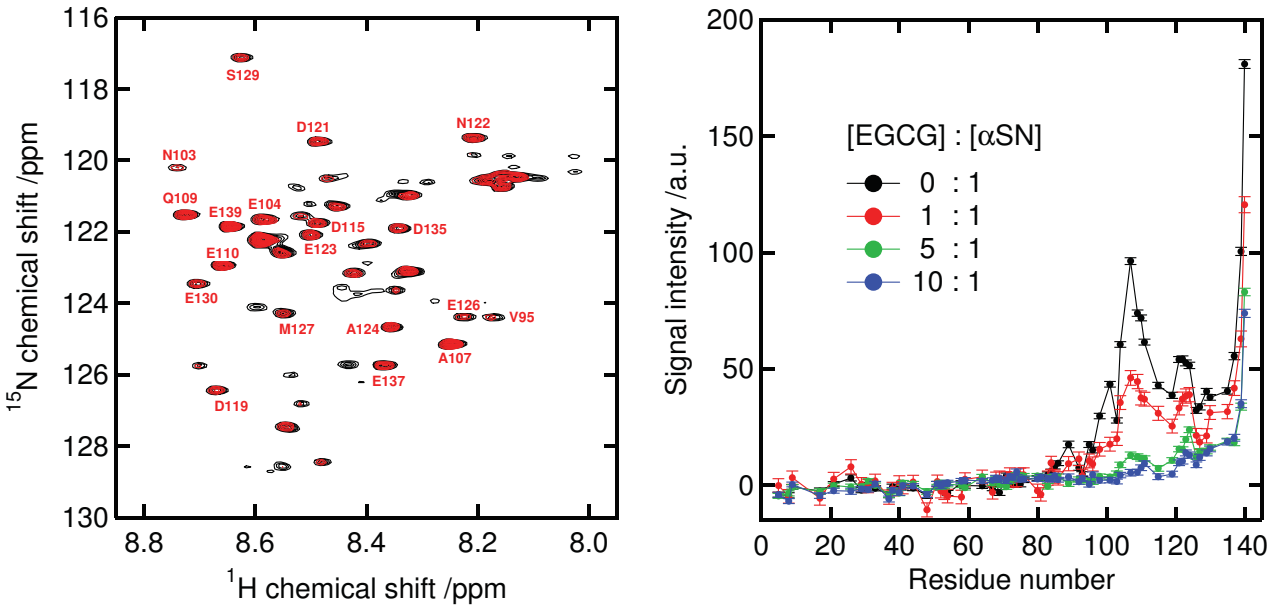

Figure 4 Lorenzen et al.

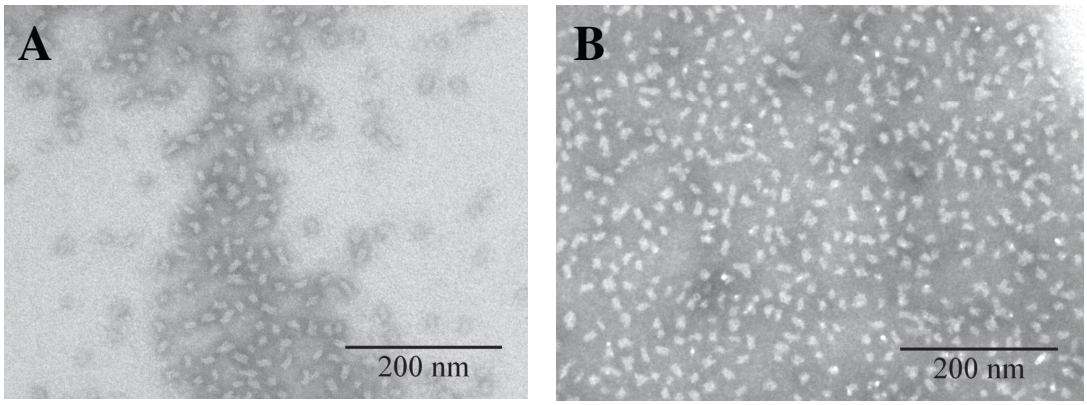

Figure 5 Lorenzen et al.

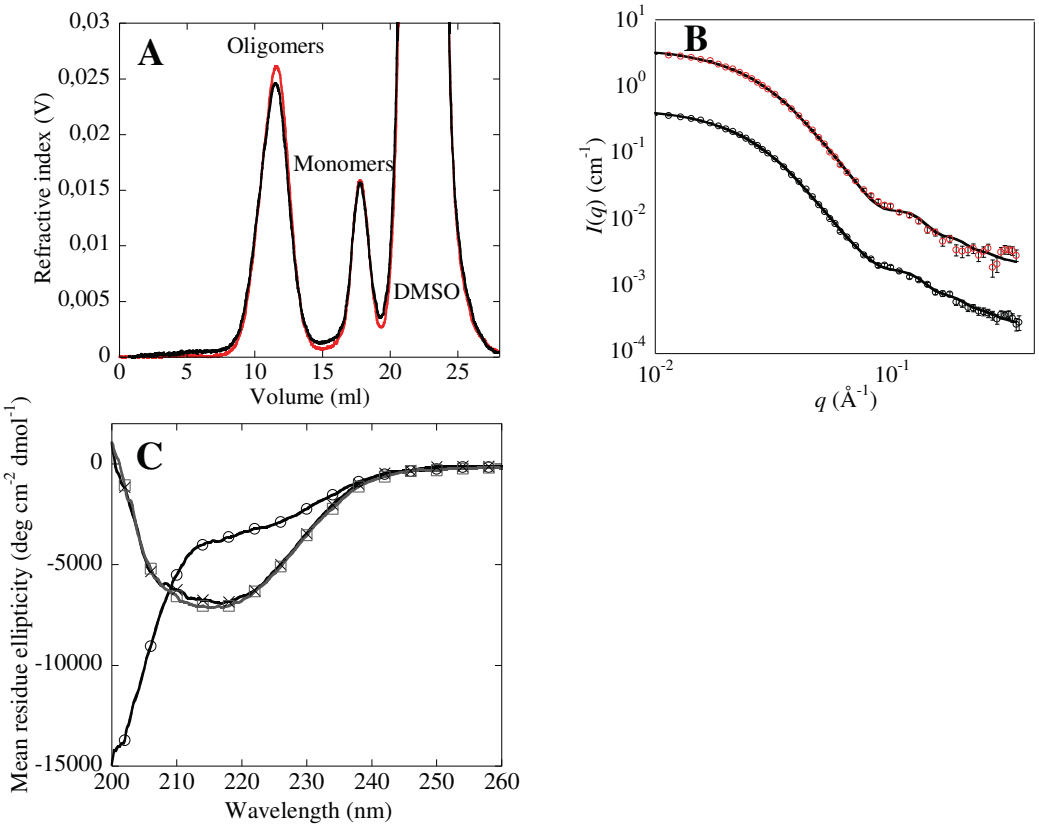

Figure 6 Lorenzen et al.

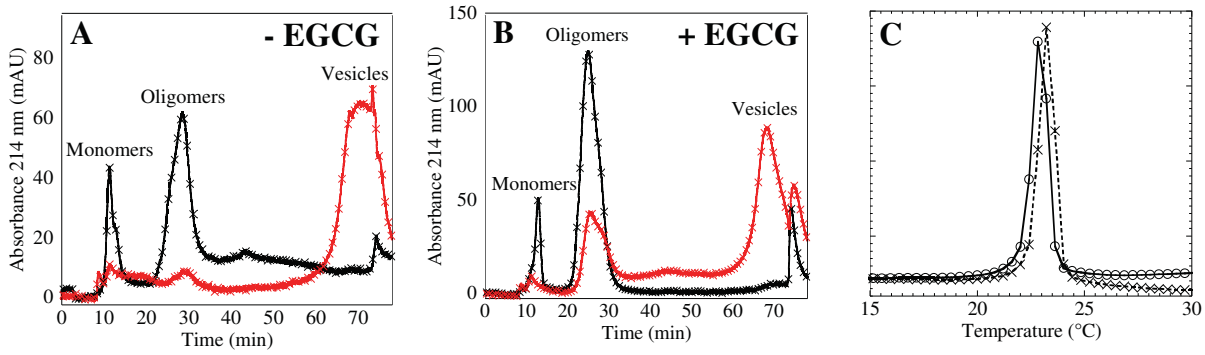

Figure 7 Lorenzen et al.

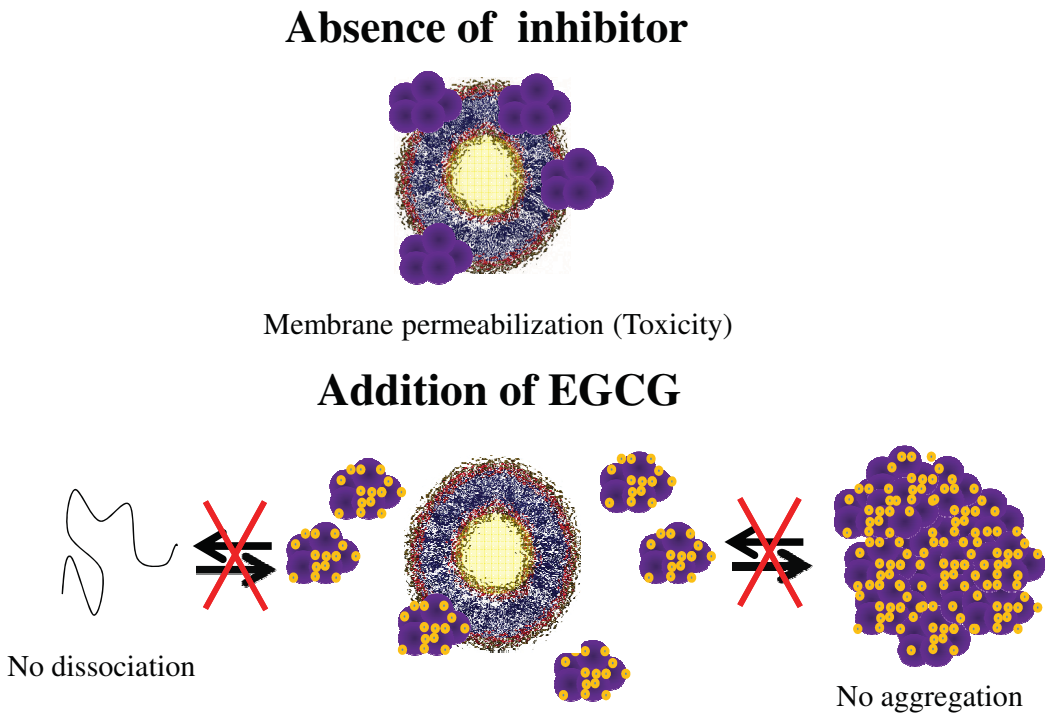

Supplementary information

EGCG inhibits the toxicity of alpha-synuclein oligomers

Nikolai Lorenzen[1,2], Søren B. Nielsen[1,2,5], Cristine Betzer[3], Yuichi Yoshimura[1,2], Brian S. Vad[1,2], Jørn D. Kaspersen[1], Gunna Christiansen[4], Jan S. Pedersen[1], Poul Henning Jensen[3], Frans A. Mulder[1,2] and Daniel E. Otzen[1,2]*

Experimemtal procedures

Small angle X-ray scattering: Data were recorded on an in-house instrument at Aarhus University(*1*). The acquisition time was one hour for both sample and buffer solution. Background subtraction and conversion to absolute scale was performed with home-written software (CLP Oliveira and JS Pedersen, unpublished). The data are expressed as the intensity versus the modulus of the scattering vector, $q = \frac{4\pi}{\lambda}\sin\theta$, where λ is the X-ray wavelength (1.54 Å) and 2θ is the scattering angle.
For dilute solutions with no interactions between the individual particles the scattering can be expressed as $I(q) = nV^2\Delta\rho^2P(q)$. Here n is the particle number density, V is the volume of the particle, and $\Delta\rho$ is the difference in scattering length density of the particle and solvent. $P(q)$ is the particle form factor which depends on its shape and is normalized to 1 at $P(q{=}0)$. Therefore, knowing the concentration and the scattering length density of a protein, the forward scattering can be used to estimate the MW of the particles in the solution and thereby the oligomer aggregation number.
In the presents study we have used form factor developed and described in detail earlier (Lorenzen, Nielsen *et al*., submitted), based on the work of Pedersen and Gerstenberg (*2*). In short, the particles are described as a compact ellipsoid of revolution with flexible protein chains on the surface, giving the expression

$$P_{ec}(q) = (1-\rho_c)^2P_{ell}(q,r) + \frac{{\rho_c}^2}{N}P_G\left(q,R_g\right) + \left(1-\frac{1}{N}\right){\rho_c}^2S_{cc}(q) + 2(1-\rho_c)\rho_cS_{ec}(q)\ .$$

This expression includes the form factor of the ellipsoidal core (*3*):

$$P_{ell}(q,r) = \int_0^{\pi/2}\left(\frac{3(\sin(qr)-qr\cos(qr))}{(qr)^3}\right)^2\sin\alpha\ \mathrm{d}\alpha,$$

the form factor of a random coil (*4*):

$$P_G(q) = \frac{2\cdot(\exp(-u)+u-1)}{u^2},$$

the cross correlation between the core and the chains:

$$S_{ec}\left(q,r,R_g\right) = \frac{1-\exp\left(-u\right)}{u}\int_0^{\pi/2}\frac{3(\sin(qr)-qr\cos(qr)\,)}{(qr)^3}\frac{\sin\left(q\left(r+R_g\right)\right)}{q\left(r+R_g\right)}\sin\alpha\ \mathrm{d}\alpha\ ,$$

and the cross correlation between different chains:

$$S_{cc}\left(q,r,R_g\right) = \left(\frac{1-\exp(-u)}{u}\right)^2\int_0^{\pi/2}\left(\frac{\sin\left(q\left(r+R_g\right)\right)}{q\left(r+R_g\right)}\right)^2\sin\alpha\ \mathrm{d}\alpha\ .$$

In the above equations $r = R(\sin^2\alpha + \epsilon^2\cos^2\alpha)^{½}$, R is the short radius of the core, ϵ is the aspect ratio of the short and long radii, N is the number of random coils on the ellipsoid surface, $u = \langle R_g^2\rangle q^2$, R_g is the random coil radius of gyration, and ρ_c is the fraction of the protein that is situated in the random coil configuration. The centers of mass of the random coils are placed at a distance of R_g from the surface of the core.

Size exclusion chromatography (SEC) and asymmetrical flow field-flow fractionation (AF4): SEC and AF4 was carried out using a Postnova AF2000 field-flow fractionation system (Postnova

Analytics GmbH, Germany) operating in SEC or AF4 mode and equipped with UV/Vis (S3240) detector (A_{214}nm) and a PN3140 refractive index detector (listed in flow order).
Analysis of αSN oligomer samples and the effect of EGCG were done in SEC mode using a Superose 6 10/300 GL SEC column with PBS as the mobile phase. 100 µl 0.5 mg/ml sample mixed with or without equimolar amounts of EGCG was for 1 hr at 37 °C prior to injection and separation at a flow rate of 0.75 ml/min. Eluting species was detected by the RI detector.
Analysis of the interaction of αSN oligomers with 100 nm diameter DOPG vesicles was carried out in AF4 mode using a 10 kDa membrane (Reg. Cellulose) and a flow program similar to (Lorenzen, Lemminger *et al.,* in revision) was used to allow separation of monomers, oligomers and vesicles within the same run. αSN and vesicles were mixed at a mole ratio of 1:100 (21 mM αSN and 2.1 mM DOPG) and incubated for 1 hr at 37 ºC prior to injection. The sample was focused for 7 min with an injection tip flow of 0.2 ml/min and cross-flow (CF) of 2 ml/min followed by isocratic elution at 2 ml/min CF for 10 min during which αSN monomers elute from the channel. A linear CF gradient from 2 ml/min to 0.35 ml/min over 25 min was then applied to elute oligomers followed by a linear CF gradient to 0 ml/min over 25 min where vesicles eluted. Finally, the channel was flushed at 0 ml/min CF for 5 min (no separation force) and further purged for 5 min at 2 ml/min focus and tip flows. A constant detector flow of 0.5 ml/min was maintained throughout the separation.
A relative calibration was achieved by injection of 100 µl 1-2 mg/ml of Ribonuclease A (13.7 kDa), Ovalbumin (45 kDa), BSA (66 kDa) and thyroglobulin (669 kDa).

References

1. Pedersen, J. S. (2004) *journal of applied crystallography* **37**, 368-380
2. Pedersen, J. S., and Gerstenberg, M. C. (1996) *Macromolecules* **29**, 1363-1365
3. Guinier, A. (1939) *Ann Phys (Paris)* **12**, 161-237
4. Debye, P. (1947) *J Phys Colloid Chem* **51**, 18-32

Article XI

Cytotoxic α-synuclein oligomers are remarkably stable against dissociation

Wojciech Paslawski[a,b], Maria Andreasen[a,b], Søren Bang Nielsen[a,b], Nikolai Lorenzen[a,b], Karen Thomsen[a], Jørn Døvling Kaspersen[a,c], Jan Skov Pedersen[a,c] and Daniel E. Otzen[a,b]*

[a] Interdisciplinary Nanoscience Center (iNANO), Aarhus University, Gustav Wieds Vej 14, DK – 8000 Aarhus C, Denmark

[b] Department of Molecular Biology and Genetics, Aarhus University, Gustav Wieds Vej 10C, DK – 8000 Aarhus C, Denmark

[c] Department of Chemistry, Aarhus University, Langelandsgade 140, DK – 8000 Aarhus C, Denmark

* Correspondence to: Daniel E. Otzen: Tel. + 45 20 72 52 38, e-mail: dao@inano.au.dk

ABSTRACT

Many neurodegenerative diseases are linked with formation of amyloid aggregates. It is increasingly accepted that not the fibrils but rather oligomeric species are responsible for degeneration of neuronal cells. Strong evidence suggests that in Parkinson's disease (PD) the formation of cytotoxic α-synuclein (αSN) oligomers is key to pathogenicity. Nevertheless insight into oligomers' molecular properties remains scarce. Here we show that αSN oligomers, despite a large amount of disordered structure, are remarkably stable against extreme pH, temperature and even molar amounts of chemical denaturants, though they undergo cooperative unfolding at higher denaturant concentrations. Isolated oligomers do not revert to monomers, but form larger aggregates consisting of stacked oligomers, suggesting that they are off-pathway relative to the process of fibril formation. We also demonstrate that the small molecule 4-(dicyanovinyl)julolidine (DCVJ) can be used as a specific probe for detection of αSN oligomers.

Key words: α-synuclein, oligomers, stability, aggregation, amyloid fibril

Abbreviations: β-amyloid (Aβ), α-synuclein (αSN), Coomassie Brilliant Blue (CBB), circular dichroism (CD), 4-(dicyanovinyl)julolidine (DCVJ), dynamic light scattering (DLS), Ethylenediaminetetraacetic acid (EDTA), fourier-transform infrared (FTIR), human islet amyloid polypeptide (hIAPP), non-amyloid-beta peptide component (NAC), nuclear magnetic resonance (NMR), polyacrylamide gel electrophoresis (PAGE), Phosphate buffered saline (PBS), Parkinson's disease (PD), size exclusion chromatography (SEC), sodium dodecyl sulphate (SDS), transmission electron microscopy (TEM), thioflavin T (ThT), wild type (wt).

INTRODUCTION

Neurodegenerative diseases (NDs) are often connected with formation of amyloid fibrils[1]. However, cytotoxic oligomeric species are increasingly seen as the main culprits in NDs like Parkinson's disease (PD)[2-5], Alzheimer's disease (AD)[6-9] and tauopathies[10]. These soluble oligomers disrupt membranes and thereby introduce neuronal damage[3,11]. Their role in the fibrillation process is complex. In some cases they seem to be directly engaged in assembly of fibrils, either as direct

building blocks [12,13] or as nuclei which can be further elongated by monomeric species[14-19]. But they can also act as a off-pathway species not directly involved in fibril formation[20-24].

PD is one of the most widespread neurodegenerative disorders. The main component of PD-associated oligomers is α-synuclein (αSN), a pre-synaptic protein which plays a central role in disease[25]. The αSN point mutations A30P, E46K and A53T, together with the duplication/triplication of the gene coding for αSN[26-30], are responsible for familial forms of PD. αSN has been proposed to facilitate the exocytosis and regulation of the synaptic vesicles trafficking[31] or take part in neurite outgrowth and adhesion of brain cells[32,33], however its true role in the neuronal cells remains unknown. Despite recent controversy[34-39], it is still generally accepted that αSN has no persistent structure in the monomeric state under physiological conditions[40]. αSN can also self-associate into oligomeric species[2-5] and amyloid fibrils[41,42]. The well-documented cytotoxicity of oligomeric species of αSN[5,43-48] probably derive from formation of a pore-like structure which disrupt the neuronal membrane, causing cell death[2,11,46,49-51]. Strong evidence that these oligomers are key players in PD makes them promising targets for therapies against disease[41,52-54]. Recent advances in structural studies techniques made it possible to resolve the structures of fibrillar forms of β-amyloid (Aβ) [55,56], human islet amyloid polypeptide (hIAPP)[57], transthyretin (TTR)[58] and α-synuclein (αSN) fibrils[59]. However, oligomers' transient nature and intrinsic structural polydispersity are a challenge to structural studies [60,61]. Here we analyze αSN oligomers formed under fibrillation conditions [2]. We have analyzed their structure, stability and appearance in the fibrillation process using size-exclusion chromatography (SEC), dynamic light scattering (DLS), sodium dodecyl sulphate polyacrylamide gel electrophoresis (SDS-PAGE), transmission electron microscopy (TEM), small-angle X-ray scattering (SAXS), circular dichroism (CD) and fluorescence spectroscopy. We report that 4-(dicyanovinyl)-julolidine (DCVJ), previously used for detection of prefibrillar aggregates of TTR[62], is able to bind αSN oligomers with significantly higher affinity than monomers and fibrils. The formed oligomers are very stable and resist both extreme temperature and extreme pH; only high urea concentrations dissociate them to monomers. Prolonged incubation of oligomers leads to an increase in their size and formation of larger non-fibrillar aggregates.

MATERIALS AND METHODS

Materials: Unless stated otherwise, all chemicals were from Sigma Chemical Co. (St. Louis, MO) and were of analytical grade. All solutions were prepared using deionized water (Millipore, Milli-Q).

Preparation of αSN*:* αSN was expressed recombinantly in *E. coli* and purified as described [63,64]. For all experiments, fresh samples were prepared by dissolving lyophilized αSN in phosphate saline buffer (PBS) (20 mM phosphate, 150 mM NaCl, pH 7.4) and filtered (0.2μm) prior to use. The concentration was determined using a NanoDrop (ND-1000, Thermo Scientific, USA) using the theoretical extinction coefficient of 0.412 $(mg/ml)^{-1}cm^{-1}$.

Plate-reader fibrillation of αSN: αSN wt, A30P, E46K and A53T was fibrillated at a final concentration of 12 mg/mL with 40 μM Thioflavin T (ThT) or 10 μM 4-(dicyanovinyl)-julolidine (DCVJ) in a Tecan Infinite Pro (Tecan Nordic AB) plate-reader at 37 °C with 10 min shaking every 12 min as described in [65]. Both ThT and DCVJ fluorescence was monitored with excitation at 448 nm and emission at 485 nm.

Purification of oligomer: αSN oligomers were prepared as described[2]. Briefly, αSN was dissolved at 12 mg/ml in PBS buffer (20 mM phosphate, 150 mM NaCl, pH 7.4) and incubated in a Thermo–Shaker (TS-100, BioSan, Latvia) at 37°C, 900 rpm for 5 hrs. Insoluble material was removed by centrifugation for 10 min at 12000 g. Soluble fractions were loaded on a Superose 6 gel filtration column connected to an ÄKTA Basic system (GE Healthcare, USA) resin and eluted with PBS buffer at 2 ml/min. Oligomer fractions were collected and stored at 4°C.

4-(dicyanovinyl)julolidine (DCVJ) fluorescence: 10 μM DVCJ was mixed with 10 μM αSN monomer, oligomer or fibril and the DCVJ fluorescence emission spectra was measured from 480-650 nm with excitation at 470 nm, 10 nm slit widths and a scan speed of 200 nm/min on a LS55 luminescence spectrophotometer (Perkin Elmer Instruments). Three spectra were accumulated and averaged for each sample.

Fourier Transform Infra-Red (FTIR) spectroscopy: FTIR spectroscopy was performed using a Tensor27 FTIR spectrometer (Bruker) equipped with Attenuated Total Reflection accessory with a continuous flow of N_2 gas. All samples were dried with N_2 gas. 64 interferograms were accumulated at a spectral resolution of 2 cm^{-1} in the range from 1000 to 3998 cm^{-1}. Peak positions were assigned where the second order derivative had local minima and the intensity was modeled by Gaussian curve fitting using the OPUS 5.5 software. For comparison all absorbance spectra are normalized.

Size-exclusion chromatography (SEC): The αSN oligomer was analyzed using SEC by using a Postnova AF2000 field-flow fractionation system (Postnova Analytics GmbH, Germany) operating in SEC mode and equipped with a UV/Vis (S3240) detector, Brookhaven BI-MwA molecular weight analyzer (measuring scattering intensity at 30, 50, 75, 90, 105, 130 and 145° angles) and PN3140 refractive index detectors (listed in flow order). The analysis was carried out using a Superose 6 10/30 GL size exclusion chromatography column at a flow rate of 0.5 ml/min.

The appearance of the oligomer was monitored by loading 20 μl 12 mg/ml αSN sample incubated for various amounts of time at 37 °C in an eppendorf shaker at 900 rpm. To remove fibrillar species, the sample was centrifuged for 10 min at 13,000 rpm prior to analysis and only the supernatant was loaded on the column.

The stability of the αSN oligomer was monitored by loading 100 μL 0.2 mg/mL αSN oligomer sample at various incubation times at 37°C using the autosampler.

Far-UV circular dichroism (CD) spectroscopy: Far-UV wavelength spectra from 250 to 190 nm of 0.2 mg/mL αSN oligomers before and after heating to 120 °C using a 2 mm quartz cuvette were recorded with a Jasco J-810 spectrophotometer (Jasco Spectroscopic Co. Ltd., Japan). Scans were conducted at 20 °C with a step size of 0.2 nm, bandwidth 2 nm and a scan speed of 50 nm/min. Five spectra were averaged for each sample and the buffer spectra was subtracted. To examine the thermal stability, αSN monomers, oligomers and fibrils at a concentration of 0.3 mg/ml (21 μM) were used in a 1 mm cuvette. Scans were conducted at 25 °C. Thermal scans were performed from 20 °C to 95 °C with 2 °C step increase and the signal recorded at 218 nm. Fibril solutions were sonicated 3x 10sec at 50 % power on ice with an HD 2070 Bandelin Sonuplus Sonicator (Buch and Holm).

Membrane permeabilization assay*:* αSN oligomers at varying concentrations were mixed with dioleoylphosphatidylglycerol (DOPG) large unilamellar vesicles (LUV's) with a diameter of ~100 nm, prepared as previously described[66]. The fluorophore calcein was entrapped at self-quenching concentrations (70 mM) inside the vesicles; upon membrane permeabilization, calcein leaks from the vesicles and gives a fluorescence response upon dilution. Calcein release was measured in a 96-well-plate (Nunc, Thermo Fischer Scientific, Roskilde, Denmark) in duplicates. Calcein release was measured (excitation 485 nm; emission 520 nm) for 1 hr in a Genios Pro fluorescence plate reader (Tecan, Männerdorf, Switzerland) at 37 °C with 2 sec shaking every 2nd min. The calcein release percentage was calculated based on background fluorescence and 100 % calcein release (addition of 0.2% (w/V) Triton X-100).

SDS-PAGE: The protein sample was mixed with reducing 6x sample buffer (375 mM Tris-HCl pH 6.8, 6% SDS, 50% glycerol, 9% β-mercaptoethanol, and 0.03% bromophenol blue) at a ratio of 5:1. The mixture was vortexed and then boiled at 100ºC for 5 minutes. The samples were loaded onto a bis-tris acrylamide gel (5%/15% - stacking/running gel). Electrophoresis was performed using a vertical electrophoresis gel apparatus at a constant voltage of 140 volts. The run was stopped when the dye front reached the bottom edge of the gel. The gel was stained using CBB R-250 solution (0.1% CBB R-250/ 40% methanol/ 10% glacial acetic acid) and destained using 4%/4% glacial acetic acid/ethanol solution. SDS-PAGE gels were scanned using standard table-top scanner or Typhoon Scanner (9400, GE Healthcare, USA). The intensity of protein bands was analysed using ImageJ[67].

Urea dissociation of αSN oligomers: Concentrated urea solutions in water were prepared and then adjusted to desired concentrations with water and 10x concentrated PBS buffer (200 mM phosphate, 1500 mM NaCl, pH 7.4). Protein samples (84 μM) were diluted into urea solutions of known concentrations and incubated for 1h. Subsequently samples were mixed with reducing gel loading buffer and analysed using SDS-PAGE.

Urea dissociation of αSN oligomers monitored using DCVJ fluorescence: DVCJ was mixed with αSN oligomer to final concentrations of 10 μM DCVJ and 84 μM αSN, diluted into urea solutions of known concentrations and incubated for 1h. The fluorescence emission spectra were measured from 480-650 nm with excitation at 470 nm, 10 nm slit widths and a scan speed of 200 nm/min on a LS55 luminescence spectrophotometer (Perkin Elmer Instruments). Three spectra were accumulated and averaged for each sample. Concentrated urea solutions in water were prepared and then adjusted to desired concentrations with water and 10x concentrated PBS buffer (200 mM phosphate, 1500 mM NaCl, pH 7.4).

Fitting of Dissociation Curves: SDS-PAGE band intensity was normalized within each gel. Fluorescence spectra were parameterized by calculating an average emission wavelength [68], defined as:

$$< \lambda >= \frac{\sum(\lambda_i F_i)}{\sum(F_i)} \qquad (1)$$

λ_i and F_i are the emission wavelength and the corresponding fluorescence intensity at the i^{th} measuring point. The dissociation curves were fitted to a two-state model using Kaleidagraph 4.0:

$$Signal = \frac{S_M + S_O 10^{\left(m_{O-M}\left(-[den]^{50\%}+[urea]\right)\right)}}{1+10^{\left(m_{O-M}\left(-[den]^{50\%}+[urea]\right)\right)}} \qquad (2)$$

Here S_M and S_O are the average signals of the monomeric and oligomeric states, $[den]^{50\%}$ is the denaturant concentration for which the fractions of folded and unfolded states are equal. The equations assumes a linear relationship between the logarithm of the equilibrium constant and the denaturant concentration:

$$logK_{O-M}^{denaturant} = logK_{O-M}^{dwater} + m_{O-M}[urea] \qquad (3)$$

Consequently, the equilibrium constant and free energy in the absence of denaturant can be calculated using the following equations:

$$logK_D^{water} = -m_{O-M}[urea] \qquad (4)$$

$$\Delta G_{D,app}^{water} = 1.36 logK_D^{water} \qquad (5)$$

We emphasize that $\Delta G_{D,app}^{water}$ values are apparent values, since they assume slow conversion between monomer and oligomer (which are separated during SDS-PAGE). SDS present in the running buffer appears not to destabilize oligomers significantly, since the same monomer-oligomer distribution was obtained independent of SDS up to 3% SDS (see Results).

pH stability: The αSN oligomers were diluted into buffer with pre-adjusted pH to obtain a final protein concentration of 28 μM. The samples were incubated at room temperature for 24 hours and then analyzed using SDS-PAGE. For pH 3-6. phosphate-citrate buffer was used (citric acid, dibasic sodium phosphate). For pH 9-11, glycine-NaOH buffer was used, while PBS buffer was used for pH 6-9.

Transmission Electron Microscopy (TEM): 10 µL of 0.5 mg/ml (35 µM) αSN in PBS buffer were transferred to a 400-mesh carbon-coated, glow-discharged grid for 30 sec. The grids were washed twice with a drop of doubly distilled water, stained with 1% uranyl acetate and blotted dry on filter paper. The samples were imaged on a transmission electron microscope (Philips CM100 Bio, Philips/FEI Corporation, Eindhoven, The Netherlands) operating at 80 kV.

Dynamic Light Scattering (DLS): DLS measurements were performed on a Zetasizer NANO ZS (Malvern Instruments Ltd, Worcestershire, UK) instrument. The oligomers were scanned in disposable, solvent resistant micro cuvettes (Malvern Instruments Ltd, Worcestershire, UK) at 28 µM (αSN monomer equivalents). For each sample 5 repeats were acquired.

Small-angle x-ray scattering (SAXS): Data were collected and analyzed as described (Lorenzen et al., submitted).

RESULTS

The αSN oligomer is present from the beginning of the fibrillation process

We have previously by Small Angle X-ray Scattering (SAXS) shown that an oligomer is present in freshly dissolved αSN and has disappeared as a separate soluble species by the time fibrillation is complete[2]. In principle this may be caused by either transformation to monomers, fibrils or higher aggregates coexisting with amyloid fibrils. Here we examine the appearance of the αSN oligomer in more detail by SEC analysis. The oligomer population is rather steady and remains relatively constant over time. However the process is accompanied by a shift in the oligomers' retention peak centroid from 23 min at 1 h incubation to 22.5 min at 4 h incubation (Fig. 1A). After 4 h incubation the retention time of the oligomer peak no longer shifts. This indicates that the oligomer grows slightly in size with increasing incubation times up to 4 h. The fraction of larger aggregates, eluting in the void volume of the column, also increases with incubation time (Fig. 1A insert).

The observed oligomer possesses a "doughnut"-shaped structure

The αSN oligomer, examined in the present work, resembles the annular shaped oligomer observed in a previous study[2]. The obtained TEM of αSN wt oligomers reveals a characteristic doughnut shape (Fig. 1B), with a diameter of 13.9 ± 1.6 nm. The morphology of the oligomer is not changed by the concentration step in the purification of the oligomer (Fig. 2).

Table 1. SAXS analysis of dimensions and flexibility of wt, A30P, E46K and A53T αSN oligomers.

αSN variant	Dimensions (nm)						Flexible fraction	
	A		B		C			
wt	10.34	±0.30	3.83	±0.30	4.26	±0.14	0.61	±0.05
E46K	10.99	±0.06	4.07	±0.06	4.20	±0.16	0.53	±0.02
A30P	11.85	±0.12	4.39	±0.12	5.04	±0.44	0.51	±0.03
A53T	12.05	±0.12	4.82	±0.12	5.06	±0.36	0.45	±0.02

We also investigate the structure of A30P, E46K and A53T αSN oligomers in comparison to wt oligomers using SAXS (Fig. 1C, Table 1). Although the dimensions of the mutants are similar to that of wt αSN, all mutants are significantly larger than wt, in the overall order E46K < A30P < A53T. At the same time, the fraction of flexible structure increases. Given that we have fixed the number of monomer chains per oligomer in the αSN mutant models, the C dimension of the

oligomer (Fig. 3) is linked to the fraction of flexible structure, rendering the two parameters inherently difficult to determine. However, the A and B dimensions are independent of the number of chains and clearly highlight the differences in sizes of the three αSN mutant oligomers (Fig. 1C, Table 1).

DCVJ can be used as a probe for αSN oligomers

The oligomer identified in the early hours of the fibrillation process has previously been shown to bind the dye 1-anilinonaphthalel-8-sulphonate (ANS), indicating an exposure of hydrophobic surface in the oligomer[69,70]. However this dye is not oligomer specific as it also binds to αSN fibrils. The dye 4-(dicyanovinyl)julolidine (DCVJ) has previously been used to detect prefibrillar oligomers of transthyretin with great success[71]. We here use DCVJ as a dye to detect prefibrillar oligomers of αSN. The increase in the fluorescence signal of DCVJ coincides with the occurrence of oligomer, detected by SEC, during lag-phase and the exponential growth phase of αSN fibrillation (Fig. 4A). While fibrillation reaction reaches a plateau, the DCVJ fluorescence signal disappears. This indicates that DCVJ binds to an intermediate αSN species which appears during the lag-phase and either disappears or rearranges during the fibrillation process. To further confirm the specificity of DCVJ probe toward αSN oligomers, the fluorescence emission spectra of DCVJ in the presence of various αSN species was recorded. The strongest signal was recorded in the presence of αSN oligomers and verifies that DCVJ is specific for αSN oligomers (Fig. 4B). Moreover the DCVJ binding does not alter the secondary structure of the resulting fibril (Fig. 4C). DCVJ can also be used as an oligomer specific probe for oligomers of αSN mutants A30P, E46K, and A53T (data not shown).

Even significant change in pH and temperature do not alter αSN oligomer structure

We further investigate the stability of αSN oligomers (wt as well as mutants) over pH 2.5-11. Remarkably, the oligomer remains equally stable to dissociation over this entire pH range, indicating that titratable electrostatic interactions are not critical for oligomer stability (Fig. 5).

The thermal stability of the oligomer was tested using CD spectroscopy. Wavelength scans at 2 °C intervals from 4 to 95 °C reveal no major rearrangement in the secondary structure of the αSN oligomer (Fig. 6A). This indicates that the oligomer is thermally stable up to at least 95 °C. Thermal scans of A30P, E46K and A53T αSN oligomers show identical thermal robustness (Fig. 6B). Even differential scanning calorimetry, which allows us to scan up to up to 120 °C, shows no transitions with ~0.4 mg/ml aSN oligomer (data not shown) . These data indicate that the αSN oligomer is thermally stable up to 120 °C. Moreover the secondary structure of oligomer cooled down to 20 ºC, after heating to 100 ºC, is the same as before temperature treatment (Fig. 6C), indicating that no irreversible conformational changes occur.

αSN oligomers are highly resistant to dissociation by common denaturants

The thermodynamic stability of the αSN oligomer was tested using urea denaturation followed by SDS-PAGE (Fig. 7A). The wt αSN oligomer have a dissociation mid-point of 5.2 ± 0.1 M urea yielding an apparent $\Delta G_{D,app}^{water}$ of 2.5 ± 0.1 kcal/mol (Tab. 2). The A30P and E46K mutants of αSN present similar stability, while A53T variant is slightly more protected against urea treatment (Fig. 7B, Tab. 2).

To ensure that the denaturation of the oligomer is not caused by the presence of SDS during gel electrophoresis the stability of the oligomer against SDS was tested. Even in the presence of 3 %

SDS the oligomer is still stable (Fig. 8). Furthermore the urea denaturation of the oligomer was tested using DCVJ as a reporter probe. The obtained midpoint of denaturation (5.3 ± 0.3 M urea) and the $\Delta G_{D,app}^{water}$ of 2.8 ± 0.3 kcal/mol (Fig. 7C, Tab. 2) is consistent with the values obtained from the SDS-PAGE analysis.

Table 2. αSN oligomer's stability determined by urea denaturation using SDS-PAGE and (for wt) DCVJ fluorescence.

	Wt [a]		A30P [a]		E46K [a]		A53T [a]		wt (DCVJ) [b]	
$m_{O\text{-}M}$ [c]	-0.352	±0.019	-0.451	±0.028	0.384	±0.061	-0.354	±0.030	-0.507	±0.033
$den_{50\%}$ (M) [c]	5.226	±0.073	4.150	±0.068	5.268	±0.201	5.321	±0.113	4.472	±0.063
$logK_{O\text{-}M}$ [c]	1.837	±0.076	1.871	±0.073	2.023	±0.210	1.883	±0.116	2.268	±0.071
$\Delta G_{D,app}^{water}$	2.499	±0.103	2.545	±0.099	2.752	±0.285	2.562	±0.158	3.084	±0.096

αSN oligomers do not revert to monomers over several days of incubation

To investigate how the oligomers are altered over time we have investigated their stability over time. Overnight incubation at 4 °C show no reduction in the high membrane permeation potential of oligomers (Fig. 9A). This indicates that the potential to interact with lipid vesicles did not change by overnight incubation and that no dissociation occurs at such low temperature. We observe similar results for sample incubated at increasing temperature (37 °C). According to SEC-based quantification, the amount of αSN oligomer remains constant over 9 hours (Fig. 9B). This indicates that over this period of time no significant dissociation of the αSN oligomer occurs. Furthermore the prolonged incubation of αSN oligomers in presence of oligomer specific DCVJ shows no changes in signal over almost 5 days, and therefore no dissociation to monomers is occurring (Fig. 9C). The SAXS data also indicate no dissociation of oligomers; rather, the oligomers increase in all dimensions; the major A dimension increases more slowly than the other two, but they all increase by ca. 50% over 1½ days (Fig. 9D, Table 3). Furthermore, the increase in intensity for low q values (data not shown) indicates that aggregation occur.

αSN oligomer aggregates to larger structures with prolonged incubation

To verify that the oligomer indeed are still present in the sample after prolonged incubation at 37 °C, the morphology of the species present in the samples at various time points was examined by TEM (Fig. 10). In the fresh sample, mostly round shaped species are observed with small amounts of larger aggregates. After 3 days of incubation the oligomers start to associate, forming two types of larger aggregates. The first type is highly populated and consists of worm-like structures, consisting of agglomerated round-shaped oligomers (Fig. 11). The second type is made up of a small amount of straight short fibrils. After 5 days, only few individual oligomers are seen in the samples, and after this point only larger aggregates are observed. Interestingly, after one week of incubation at 4 °C, no significant aggregation can be seen in the oligomer sample. Moreover the aggregates after 5 days of incubation show the secondary structure to be identical to the one observed for oligomers (Fig. 12). To further verify the self-association of the oligomer over time, the size distribution of the species present in the oligomer sample was examined using DLS (Fig. 13). 3 major species are observed in the different samples, namely: small (diameter < 50 nm), medium (diameter 50 nm – 500 nm) and large aggregates (diameter > 500 nm). Significantly, the

diameter of the three different species does not change significantly, supporting our theory that the oligomer does not dissociate but rather joins together to form larger aggregates, instead of the larger aggregates being formed from monomers dissociated from the oligomers. Inspection of the volume fraction of the individual species in the samples over time reveals that after 4 days of incubation the small aggregates have disappeared. This is consistent with the results obtained using TEM imaging. The medium aggregates are a transient species occurring in the samples at 2 to 4 days, peaking at 4 days of incubation after which the large aggregates dominate in the samples. Furthermore, DLS data confirm that αSN oligomers incubated at 4 °C do not aggregate into larger aggregates but rather remain oligomeric (Fig. 12C).

Table 3. SAXS analysis of the radius and flexibility of the wt oligomer during 34 hours of incubation at 37 ºC.

Incubation time (h)	Dimensions (nm)						Flexible fraction	
	A		B		C			
1	10.34	±0.30	3.83	±0.30	4.26	±0.14	0.61	±0.05
3	11.27	±0.19	4.90	±0.19	5.06	±0.28	0.45	±0.03
5	11.75	±0.19	4.70	±0.19	5.12	±0.20	0.51	±0.03
7	12.05	±0.20	5.02	±0.20	5.48	±0.28	0.48	±0.03
9	12.19	±0.20	5.30	±0.20	5.92	±0.36	0.46	±0.02
11	13.13	±0.17	5.25	±0.17	5.78	±0.26	0.46	±0.02
13	13.28	±0.15	5.31	±0.15	6.04	±0.26	0.46	±0.02
15	13.78	±0.19	5.30	±0.19	5.90	±0.26	0.47	±0.02
17	13.93	±0.17	5.16	±0.17	5.78	±0.20	0.49	±0.02
19	14.31	±0.15	5.30	±0.15	6.02	±0.20	0.47	±0.02
21	14.82	±0.15	5.11	±0.15	5.76	±0.14	0.50	±0.02
23	14.31	±0.19	5.11	±0.19	5.80	±0.18	0.51	±0.03
25	14.36	±0.18	5.32	±0.18	6.10	±0.22	0.48	±0.02
27	15.06	±0.16	5.38	±0.16	6.04	±0.20	0.47	±0.02
29	14.59	±0.16	5.21	±0.16	6.00	±0.18	0.50	±0.02
31	14.95	±0.18	5.34	±0.18	6.14	±0.22	0.48	±0.02
33	15.57	±0.16	5.56	±0.16	6.22	±0.22	0.45	±0.02

DISCUSSION

αSN oligomers can be detected by DCVJ fluorescence

There are few known florescent probes that can be used to detect αSN fibrils in addition to the common ThT[72]. ANS has been used both to detect fibrils[73,74] and oligomers[69,70]. Fluorescence polarization, when combined with a suitable amyloid dye, allows monitoring of fibrillization process and detection of oligomeric species[75]. Conformational specific antibodies may also be used[76] but remain impractical for real-time measurements. However we have found that DCVJ fluorophore, which was previously used for detection of TTR aggregates[62], can be used as probe for detecting αSN oligomers. DCVJ is a molecular rotor containing a fluorescent julolidine and

intrinsic di-cyano group responsible for self-quenching. This type of quenching makes it sensitive to intrinsic rotational relaxation, which is decreased upon binding to aggregated species. DCVJ has higher specificity against αSN oligomers than fibrils and shows little flouresecens with αSN monomers. This phenomenon may be caused by intercalation of DCVJ molecule into the oligomer cavity, leading to a greater decrease in intrinsic rotational relaxation than upon binding to fibrils. Importantly, DCVJ does not appear to alter the secondary structure or stability of oligomeric αSN species upon binding, making it a valid probe for future studies.

The oligomer appears during lag phase in the fibrillation process

TEM images and SAXS studies reveal a αSN with the same round shape as the previously described doughnut shaped oligomers[2]. SEC and DCVJ fluorescence indicate that the oligomer is present in the fibrillating sample during the lag phase and exponential growth phase. We are not able to detect the oligomers after the fibrillation process has reached a plateau, which might suggest that they are intermediate species in fibril formation. However, further aggregation steps will affect both SEC (due to limits in aggregate size that can enter the filtration resin) and DCVJ fluorescence (due to depletion of binding sides). Therefore the drop in the signal might also occur due to the assembly of larger species or formation of amorphous aggregates. Interestingly, DCVJ fluorescence peaks at 5 h, possibly because it does not bind to the initial oligomeric species, but rather to the form that exhibits shifted retention time as observed using SEC analysis during fibrillation process.

αSN oligomers assembly into larger aggregates and do not revert to monomers

To further investigate the disappearance of oligomer during fibrillation process, we have investigated their behavior after isolation. The short incubation for up to 24 hours, both at 4 °C and 37 °C, does not change the membrane permeabilization properties of oligomers or dissociate them into monomers as shown by SEC and DCVJ fluorescence. Nor do we observe a decrease in DCVJ signal upon incubation of oligomers at 37 °C for 5 days. However, DLS and TEM reveal that larger aggregates are formed during incubation in 37 °C. Initially only round-shaped oligomers are observed. After around 3 days we see the appearance of worm-like structures which appear to be linearly associated oligomers. A small amount of straight short fibrils is also present, suggesting the existence of other type of oligomers which gives rise to fibrils. After 5 days of incubation only large clusters of described worm-like aggregates joined with small amount of fibrils are observed. Interestingly, when oligomers are incubated in 4 °C for 7 days no aggregation was observed, suggesting that the process is highly dependent on temperature. Additionally the SAXS analysis revealed that during incubation at 37 °C, the oligomer dimensions increase with subsequent decrease of flexible fragment. This behavior is probably caused by either aggregation of oligomers or some internal rearrangements which are enhanced by increased temperature and therefore not observable at 4 °C. Taken together the data suggest that once the oligomers are formed they do not dissociate into monomers and form bigger aggregates.

αSN oligomers are very stable structure and are not easily altered by changes in environment

Our data demonstrate that αSN oligomers are far more stable than one would expect for partially folded aggregated states with extensive amounts of denatured structure. Neither heating to extreme temperatures nor significant change in pH were able to dissociate the oligomers back to monomers or even modify their structure as oligomers. They are not affected by reducing conditions used during SDS-PAGE and even pre-incubation in up to 3 % SDS was not able to dissolve or alter the

structure of αSN oligomers. Furthermore, the oligomers are also quite resistant to urea; concentrations in excess of 5 M are needed to reach the midpoint of dissociation to monomers, while the $\Delta G_{D,app}^{water}$ of 2.5 kcal/mol is around half of the average unfolding free energy observed for single domain proteins[77] and a third of elongation free energy observed for αSN fibrils[78]. Oligomers' neuronal toxicity[5,43-46] make them an extremely important target for treatment of PD. The very high stability of αSN oligomers indicates that drug development should be aimed at surface passivation or inhibition of their formation rather than simple structure disruption, as is confirmed by previously reported inhibition of αSN oligomers' toxicity by compounds like curcumin[79], geldanamycin (and its derivatives)[80-82] and EGCG[83,84].

ACKOWLEDGMENTS

W.P., M.A., N.L., S.B.N. and D.E.O. are supported by the Michael J. Fox Foundation, the Danish Research Council (Industrial Post-doc and The Danish Council for Independent Research | Natural Sciences) and the Danish Research Foundation (inSPIN). J.D.K. acknowledges LUNDBECKFONDEN for financial support.

Figures and tables descriptions

Figure 1. Appearance and shape of αSN oligomers. (A) Appearance of oligomer during the first few hours of fibrillation process analyzed by SEC. (B) Quantitation of observed aggregates. Initially only oligomers and small amount of larger aggregates are observed, while after around 6 hours quantity of larger aggregates start to increase. (C) TEM image of αSN oligomers, showing doughnut-shaped structures with diameter around 13 nm. (D) SAXS spectra of wild type, A30P, E46K and A53T αSN oligomers show no significant difference in structure of oligomers formed by different variants of αSN.

Figure 2. SEC-MALS analysis of the concentration step on αSN oligomers . (A) Absorbance at 214 nm. (B) Backscattering signal at 90º.

Figure 3. SAXS based model of αSN oligomer. A and B are the dimensions of the rigid oligomer's core, while C represents the thickness of flexible outer region of structure.

Figure 4. DCVJ binding to αSN species. (A) αSN fibrillation followed by ThT and DCVJ, showing the binding of DCVJ to intermediate αSN species. (B) Analysis of DCVJ fluorescence signal intensity upon binding to αSN monomers, oligomers and fibrils. (C) FTIR analysis of αSN fibrils prepared with ThT and DCVJ.

Figure 5. Stability of wt, A30P, E46K and A53T αSN oligomers between pH 2.5 and 11. Data are presented as a ratio of oligomer quantity in analyzed pH to oligomer amount in pH 7.5. For each data column, an average of triplicates is shown with standard deviation on error bars.

Figure 6. Thermal stability of αSN oligomers. (A) CD wavelength scans from 4 ºC to 96 ºC taken every 2 ºC. No significant change in spectra suggest no disruption of oligomer's secondary structure. (B) CD thermal scans form 20 ºC to 95 ºC of wt (black), A30P (blue), E46K (red) and A53T (green) αSN oligomers. Normalized signal at 218 nm is shown. For each variant of αSN the average of triplicates is shown with standard deviation on error bars. (C) CD wavelength scans of

wt αSN oligomers before heating to 100 ºC (black), at 100 ºC (red) and after cooling back to 20 ºC (blue).

Figure 7. Dissociation of αSN oligomer using urea. (A) Example of an SDS-PAGE gel image showing decreaseing oligomer band intensity with increasing urea concentration. (B) Oligomer band intensity (left Y axis) and lambda value, obtained from DCVJ fluorescence scans (right Y axis), plotted versus urea concentration (points) and fitting to two-state dissociation model (lines) for wt, A30P, E46K and A53T αSN oligomer.

Figure 8. Stability of wt αSN oligomer with increasing SDS concentration. For each data column the average of triplicates is shown with standard deviation on error bars.

Figure 9. Stability of wt αSN oligomers over time. (A) Calcein release from phospholipid vesicles by oligomers at time zero after preparation (circle) and after 24 hours of incubation (crosses). (B) SEC analysis of oligomer sample during 8 hours of incubation presented as intensity of oligomer peak on chromatogram. (C) DCVJ fluorescence analysis of oligomers incubated in 37 ºC for 5 days. (D) Oligomer dimensions obtained from SAXS analysis of oligomers incubated at 37 ºC for 34 hours.

Figure 10. TEM imaging of wt αSN oligomers incubated at 37 ºC for one week. Samples were imaged every 24 hours. In addition the sample incubated for one week in 4 ºC is presented.

Figure 11. Magnification of worm-like aggregates formed by doughnut-shaped αSN oligomers.

Figure 12. Comparison of secondary structure of oligomers and aggregates formed by oligomers using (A) CD and (B) FTIR.

Figure 13. DLS size distribution of wt αSN oligomers incubated at 37 ºC for one week. Samples were analyzed every 24 hours. In addition the sample incubated for one week in 4 ºC is presented. Observed aggregates are divided into three sections: small (diameter < 50 nm), medium (diameter 50 nm – 500 nm) and large aggregates (diameter > 500 nm). In addition on a pie charts the fractions of each type of aggregate are presented.

REFERENCES

(1) Chiti, F.; Dobson, C. M. *Annual review of biochemistry* **2006**, *75*, 333.

(2) Giehm, L.; Svergun, D. I.; Otzen, D. E.; Vestergaard, B. *Proceedings of the National Academy of Sciences of the United States of America* **2011**, *108*, 3246.

(3) Lashuel, H. A.; Hartley, D.; Petre, B. M.; Walz, T.; Lansbury, P. T., Jr. *Nature* **2002**, *418*, 291.

(4) Conway, K. A.; Lee, S. J.; Rochet, J. C.; Ding, T. T.; Williamson, R. E.; Lansbury, P. T., Jr. *Proceedings of the National Academy of Sciences of the United States of America* **2000**, *97*, 571.

(5) Winner, B.; Jappelli, R.; Maji, S. K.; Desplats, P. A.; Boyer, L.; Aigner, S.; Hetzer, C.; Loher, T.; Vilar, M.; Campioni, S.; Tzitzilonis, C.; Soragni, A.; Jessberger, S.; Mira, H.; Consiglio, A.; Pham, E.; Masliah, E.; Gage, F. H.; Riek, R. *Proceedings of the National Academy of Sciences of the United States of America* **2011**, *108*, 4194.

(6) Walsh, D. M.; Selkoe, D. J. *Journal of neurochemistry* **2007**, *101*, 1172.

(7) Lesne, S.; Koh, M. T.; Kotilinek, L.; Kayed, R.; Glabe, C. G.; Yang, A.; Gallagher, M.; Ashe, K. H. *Nature* **2006**, *440*, 352.

(8) Nilsberth, C.; Westlind-Danielsson, A.; Eckman, C. B.; Condron, M. M.; Axelman, K.; Forsell, C.; Stenh, C.; Luthman, J.; Teplow, D. B.; Younkin, S. G.; Naslund, J.; Lannfelt, L. *Nature neuroscience* **2001**, *4*, 887.

(9) Bernstein, S. L.; Dupuis, N. F.; Lazo, N. D.; Wyttenbach, T.; Condron, M. M.; Bitan, G.; Teplow, D. B.; Shea, J. E.; Ruotolo, B. T.; Robinson, C. V.; Bowers, M. T. *Nat Chem* **2009**, *1*, 326.

(10) Ward, S. M.; Himmelstein, D. S.; Lancia, J. K.; Binder, L. I. *Biochemical Society transactions* **2012**, *40*, 667.
(11) Volles, M. J.; Lee, S. J.; Rochet, J. C.; Shtilerman, M. D.; Ding, T. T.; Kessler, J. C.; Lansbury, P. T., Jr. *Biochemistry* **2001**, *40*, 7812.
(12) Hill, S. E.; Robinson, J.; Matthews, G.; Muschol, M. *Biophysical journal* **2009**, *96*, 3781.
(13) Vestergaard, B.; Groenning, M.; Roessle, M.; Kastrup, J. S.; van de Weert, M.; Flink, J. M.; Frokjaer, S.; Gajhede, M.; Svergun, D. I. *PLoS Biol* **2007**, *5*, e134.
(14) Lorenzen, N.; Cohen, S. I. A.; Nielsen, S. B.; Herling, T. W.; Christiansen, G.; Dobson, C. M.; Knowles, T. P. J.; Otzen, D. *Biophysical Journal* **2012**, *102*, 2167.
(15) Kardos, J.; Yamamoto, K.; Hasegawa, K.; Naiki, H.; Goto, Y. *The Journal of biological chemistry* **2004**, *279*, 55308.
(16) Kim, H. J.; Chatani, E.; Goto, Y.; Paik, S. R. *Journal of microbiology and biotechnology* **2007**, *17*, 2027.
(17) Morris, A. M.; Watzky, M. A.; Finke, R. G. *Biochimica et biophysica acta* **2009**, *1794*, 375.
(18) Knowles, T. P.; Fitzpatrick, A. W.; Meehan, S.; Mott, H. R.; Vendruscolo, M.; Dobson, C. M.; Welland, M. E. *Science* **2007**, *318*, 1900.
(19) Collins, S. R.; Douglass, A.; Vale, R. D.; Weissman, J. S. *PLoS Biol* **2004**, *2*, e321.
(20) Jain, S.; Udgaonkar, J. B. *Biochemistry* **2011**, *50*, 1153.
(21) Necula, M.; Kayed, R.; Milton, S.; Glabe, C. G. *The Journal of biological chemistry* **2007**, *282*, 10311.
(22) Souillac, P. O.; Uversky, V. N.; Millett, I. S.; Khurana, R.; Doniach, S.; Fink, A. L. *The Journal of biological chemistry* **2002**, *277*, 12666.
(23) Gellermann, G. P.; Byrnes, H.; Striebinger, A.; Ullrich, K.; Mueller, R.; Hillen, H.; Barghorn, S. *Neurobiol Dis* **2008**, *30*, 212.
(24) Hong, D. P.; Han, S.; Fink, A. L.; Uversky, V. N. *Protein Pept Lett* **2011**, *18*, 230.
(25) Stefanis, L. *Cold Spring Harbor perspectives in medicine* **2012**, *2*, a009399.
(26) Kruger, R.; Kuhn, W.; Muller, T.; Woitalla, D.; Graeber, M.; Kosel, S.; Przuntek, H.; Epplen, J. T.; Schols, L.; Riess, O. *Nature genetics* **1998**, *18*, 106.
(27) Zarranz, J. J.; Alegre, J.; Gomez-Esteban, J. C.; Lezcano, E.; Ros, R.; Ampuero, I.; Vidal, L.; Hoenicka, J.; Rodriguez, O.; Atares, B.; Llorens, V.; Gomez Tortosa, E.; del Ser, T.; Munoz, D. G.; de Yebenes, J. G. *Annals of neurology* **2004**, *55*, 164.
(28) Hamilton, B. A. *Genomics* **2004**, *83*, 739.
(29) Chartier-Harlin, M. C.; Kachergus, J.; Roumier, C.; Mouroux, V.; Douay, X.; Lincoln, S.; Levecque, C.; Larvor, L.; Andrieux, J.; Hulihan, M.; Waucquier, N.; Defebvre, L.; Amouyel, P.; Farrer, M.; Destee, A. *Lancet* **2004**, *364*, 1167.
(30) Singleton, A. B.; Farrer, M.; Johnson, J.; Singleton, A.; Hague, S.; Kachergus, J.; Hulihan, M.; Peuralinna, T.; Dutra, A.; Nussbaum, R.; Lincoln, S.; Crawley, A.; Hanson, M.; Maraganore, D.; Adler, C.; Cookson, M. R.; Muenter, M.; Baptista, M.; Miller, D.; Blancato, J.; Hardy, J.; Gwinn-Hardy, K. *Science* **2003**, *302*, 841.
(31) Chandra, S.; Gallardo, G.; Fernandez-Chacon, R.; Schluter, O. M.; Sudhof, T. C. *Cell* **2005**, *123*, 383.
(32) Takenouchi, T.; Hashimoto, M.; Hsu, L. J.; Mackowski, B.; Rockenstein, E.; Mallory, M.; Masliah, E. *Molecular and cellular neurosciences* **2001**, *17*, 141.
(33) Tsuboi, K.; Grzesiak, J. J.; Bouvet, M.; Hashimoto, M.; Masliah, E.; Shults, C. W. *Molecular and cellular neurosciences* **2005**, *29*, 259.
(34) Bartels, T.; Choi, J. G.; Selkoe, D. J. *Nature* **2011**, *477*, 107.
(35) Fauvet, B.; Mbefo, M. K.; Fares, M. B.; Desobry, C.; Michael, S.; Ardah, M. T.; Tsika, E.; Coune, P.; Prudent, M.; Lion, N.; Eliezer, D.; Moore, D. J.; Schneider, B.; Aebischer, P.; El-Agnaf, O. M.; Masliah, E.; Lashuel, H. A. *The Journal of biological chemistry* **2012**, *287*, 15345.
(36) Wang, W.; Perovic, I.; Chittuluru, J.; Kaganovich, A.; Nguyen, L. T.; Liao, J.; Auclair, J. R.; Johnson, D.; Landeru, A.; Simorellis, A. K.; Ju, S.; Cookson, M. R.; Asturias, F. J.; Agar, J. N.; Webb, B. N.; Kang, C.; Ringe, D.; Petsko, G. A.; Pochapsky, T. C.; Hoang, Q. Q. *Proceedings of the National Academy of Sciences of the United States of America* **2011**, *108*, 17797.
(37) Dettmer, U.; Newman, A. J.; Luth, E. S.; Bartels, T.; Selkoe, D. *The Journal of biological chemistry* **2013**, *288*, 6371.
(38) Binolfi, A.; Theillet, F. X.; Selenko, P. *Biochemical Society transactions* **2012**, *40*, 950.

(39) Coelho-Cerqueira, E.; Carmo-Goncalves, P.; Sa Pinheiro, A.; Cortines, J.; Follmer, C. *Febs J* **2013**, *280*, 4915.
(40) Weinreb, P. H.; Zhen, W.; Poon, A. W.; Conway, K. A.; Lansbury, P. T., Jr. *Biochemistry* **1996**, *35*, 13709.
(41) Spillantini, M. G.; Crowther, R. A.; Jakes, R.; Hasegawa, M.; Goedert, M. *Proceedings of the National Academy of Sciences of the United States of America* **1998**, *95*, 6469.
(42) Fink, A. L. *Folding & design* **1998**, *3*, R9.
(43) Celej, M. S.; Sarroukh, R.; Goormaghtigh, E.; Fidelio, G. D.; Ruysschaert, J. M.; Raussens, V. *The Biochemical journal* **2012**, *443*, 719.
(44) Cremades, N.; Cohen, S. I.; Deas, E.; Abramov, A. Y.; Chen, A. Y.; Orte, A.; Sandal, M.; Clarke, R. W.; Dunne, P.; Aprile, F. A.; Bertoncini, C. W.; Wood, N. W.; Knowles, T. P.; Dobson, C. M.; Klenerman, D. *Cell* **2012**, *149*, 1048.
(45) Outeiro, T. F.; Putcha, P.; Tetzlaff, J. E.; Spoelgen, R.; Koker, M.; Carvalho, F.; Hyman, B. T.; McLean, P. J. *PloS one* **2008**, *3*, e1867.
(46) Stockl, M. T.; Zijlstra, N.; Subramaniam, V. *Mol Neurobiol* **2013**, *47*, 613.
(47) Lashuel, H. A.; Overk, C. R.; Oueslati, A.; Masliah, E. *Nature reviews. Neuroscience* **2013**, *14*, 38.
(48) Kalia, L. V.; Kalia, S. K.; McLean, P. J.; Lozano, A. M.; Lang, A. E. *Annals of neurology* **2013**, *73*, 155.
(49) Tsigelny, I. F.; Sharikov, Y.; Wrasidlo, W.; Gonzalez, T.; Desplats, P. A.; Crews, L.; Spencer, B.; Masliah, E. *Febs J* **2012**, *279*, 1000.
(50) van Rooijen, B. D.; Claessens, M. M.; Subramaniam, V. *PloS one* **2010**, *5*, e14292.
(51) van Rooijen, B. D.; Claessens, M. M.; Subramaniam, V. *Biochimica et biophysica acta* **2009**, *1788*, 1271.
(52) Polymeropoulos, M. H.; Higgins, J. J.; Golbe, L. I.; Johnson, W. G.; Ide, S. E.; Di Iorio, G.; Sanges, G.; Stenroos, E. S.; Pho, L. T.; Schaffer, A. A.; Lazzarini, A. M.; Nussbaum, R. L.; Duvoisin, R. C. *Science* **1996**, *274*, 1197.
(53) Spillantini, M. G.; Schmidt, M. L.; Lee, V. M.; Trojanowski, J. Q.; Jakes, R.; Goedert, M. *Nature* **1997**, *388*, 839.
(54) Polymeropoulos, M. H.; Lavedan, C.; Leroy, E.; Ide, S. E.; Dehejia, A.; Dutra, A.; Pike, B.; Root, H.; Rubenstein, J.; Boyer, R.; Stenroos, E. S.; Chandrasekharappa, S.; Athanassiadou, A.; Papapetropoulos, T.; Johnson, W. G.; Lazzarini, A. M.; Duvoisin, R. C.; Di Iorio, G.; Golbe, L. I.; Nussbaum, R. L. *Science* **1997**, *276*, 2045.
(55) Tycko, R. *Curr. Opin. Struct. Biol.* **2004**, *14*.
(56) Fitzpatrick, A. W.; Debelouchina, G. T.; Bayro, M. J.; Clare, D. K.; Caporini, M. A.; Bajaj, V. S.; Jaroniec, C. P.; Wang, L.; Ladizhansky, V.; Muller, S. A.; MacPhee, C. E.; Waudby, C. A.; Mott, H. R.; De Simone, A.; Knowles, T. P.; Saibil, H. R.; Vendruscolo, M.; Orlova, E. V.; Griffin, R. G.; Dobson, C. M. *Proceedings of the National Academy of Sciences of the United States of America* **2013**, *110*, 5468.
(57) Nielsen, J. T.; Bjerring, M.; Jeppesen, M. D.; Pedersen, R. O.; Pedersen, J. M.; Hein, K. L.; Vosegaard, T.; Skrydstrup, T.; Otzen, D. E.; Nielsen, N. C. *Angew Chem Int Ed Engl* **2009**, *48*, 2118.
(58) Jaroniec, C. P.; MacPhee, C. E.; Bajaj, V. S.; McMahon, M. T.; Dobson, C. M.; Griffin, R. G. *Proceedings of the National Academy of Sciences of the United States of America* **2004**, *101*, 711.
(59) Vilar, M.; Chou, H. T.; Luhrs, T.; Maji, S. K.; Riek-Loher, D.; Verel, R.; Manning, G.; Stahlberg, H.; Riek, R. *Proceedings of the National Academy of Sciences of the United States of America* **2008**, *105*, 8637.
(60) Uversky, V. N. *Febs J* **2010**, *277*, 2940.
(61) Fandrich, M. *J Mol Biol* **2012**, *421*, 427.
(62) Lindgren, M.; Sorgjerd, K.; Hammarstrom, P. *Biophysical journal* **2005**, *88*, 4200.
(63) Huang, C.; Ren, G.; Zhou, H.; Wang, C. C. *Protein expression and purification* **2005**, *42*, 173.
(64) Giehm, L.; Lorenzen, N.; Otzen, D. E. *Methods* **2011**, *53*, 295.
(65) Giehm, L.; Otzen, D. E. *Analytical biochemistry* **2010**, *400*, 270.
(66) Nesgaard, L.; Vad, B.; Christiansen, G.; Otzen, D. *Biochimica et biophysica acta* **2009**, *1794*, 84.
(67) Abramoff, M. D.; Magelhaes, P. J.; Ram, S. J. *Biophotonics International* **2004**, *11*, 36.
(68) Royer, C. A.; Mann, C. J.; Matthews, C. R. *Protein science : a publication of the Protein Society* **1993**, *2*, 1844.
(69) Celej, M. S.; Jares-Erijman, E. A.; Jovin, T. M. *Biophysical journal* **2008**, *94*, 4867.

(70) Bolognesi, B.; Kumita, J. R.; Barros, T. P.; Esbjorner, E. K.; Luheshi, L. M.; Crowther, D. C.; Wilson, M. R.; Dobson, C. M.; Favrin, G.; Yerbury, J. J. *ACS chemical biology* **2010**, *5*, 735.
(71) Lindgren, M.; SÃ¶rgjerd, K.; HammarstrÃ¶m, P. *Biophysical Journal* **2005**, *88*, 4200.
(72) Ban, T.; Hamada, D.; Hasegawa, K.; Naiki, H.; Goto, Y. *The Journal of biological chemistry* **2003**, *278*, 16462.
(73) Dusa, A.; Kaylor, J.; Edridge, S.; Bodner, N.; Hong, D. P.; Fink, A. L. *Biochemistry* **2006**, *45*, 2752.
(74) Munishkina, L. A.; Phelan, C.; Uversky, V. N.; Fink, A. L. *Biochemistry* **2003**, *42*, 2720.
(75) Luk, K. C.; Hyde, E. G.; Trojanowski, J. Q.; Lee, V. M. *Biochemistry* **2007**, *46*, 12522.
(76) Kayed, R.; Head, E.; Thompson, J. L.; McIntire, T. M.; Milton, S. C.; Cotman, C. W.; Glabe, C. G. *Science* **2003**, *300*, 486.
(77) Jackson, S. E. *Folding and Design* **1998**, *3*, R81.
(78) Baldwin, A. J.; Knowles, T. P.; Tartaglia, G. G.; Fitzpatrick, A. W.; Devlin, G. L.; Shammas, S. L.; Waudby, C. A.; Mossuto, M. F.; Meehan, S.; Gras, S. L.; Christodoulou, J.; Anthony-Cahill, S. J.; Barker, P. D.; Vendruscolo, M.; Dobson, C. M. *Journal of the American Chemical Society* **2011**, *133*, 14160.
(79) Singh, P. K.; Kotia, V.; Ghosh, D.; Mohite, G. M.; Kumar, A.; Maji, S. K. *ACS chemical neuroscience* **2013**, *4*, 393.
(80) Putcha, P.; Danzer, K. M.; Kranich, L. R.; Scott, A.; Silinski, M.; Mabbett, S.; Hicks, C. D.; Veal, J. M.; Steed, P. M.; Hyman, B. T.; McLean, P. J. *The Journal of pharmacology and experimental therapeutics* **2010**, *332*, 849.
(81) McLean, P. J.; Klucken, J.; Shin, Y.; Hyman, B. T. *Biochemical and biophysical research communications* **2004**, *321*, 665.
(82) Riedel, M.; Goldbaum, O.; Schwarz, L.; Schmitt, S.; Richter-Landsberg, C. *PloS one* **2010**, *5*, e8753.
(83) Ehrnhoefer, D. E.; Bieschke, J.; Boeddrich, A.; Herbst, M.; Masino, L.; Lurz, R.; Engemann, S.; Pastore, A.; Wanker, E. E. *Nature structural & molecular biology* **2008**, *15*, 558.
(84) Grelle, G.; Otto, A.; Lorenz, M.; Frank, R. F.; Wanker, E. E.; Bieschke, J. *Biochemistry* **2011**, *50*, 10624.

Figure 1

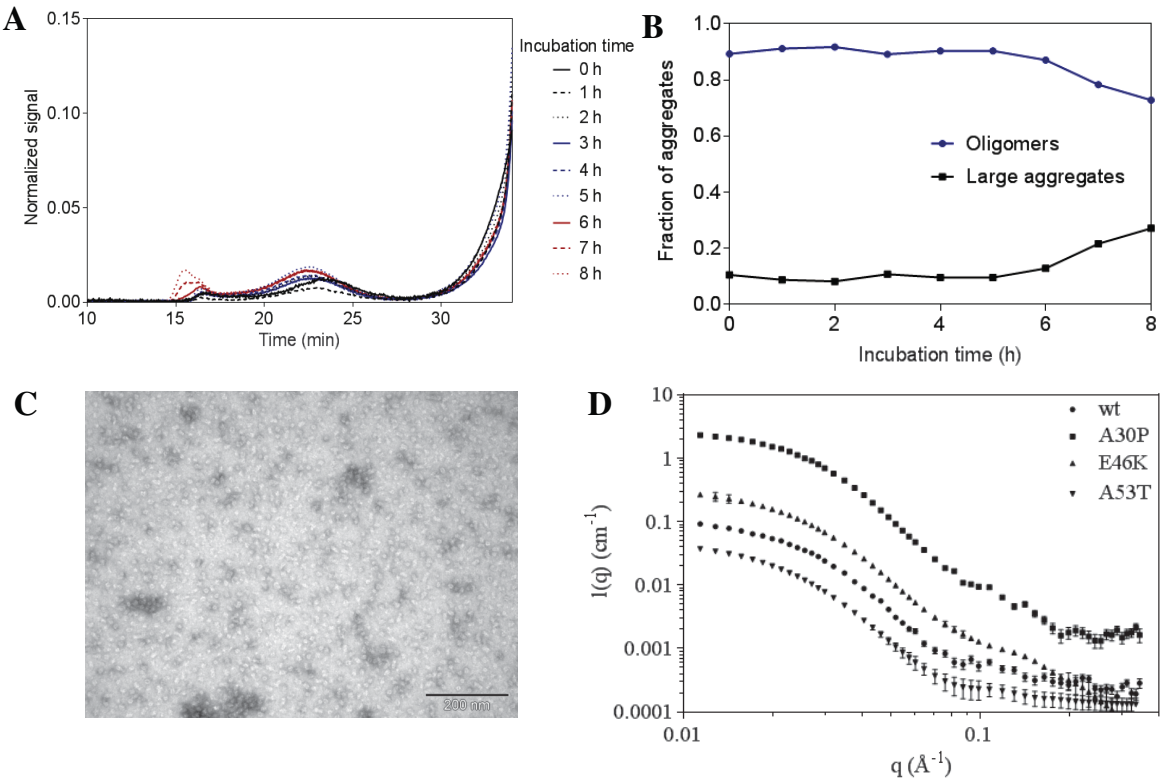
A
Normalized signal
Time (min)
Incubation time
0 h
1 h
2 h
3 h
4 h
5 h
6 h
7 h
8 h
B
Fraction of aggregates
Incubation time (h)
Oligomers
Large aggregates
C
200 nm
D
I(q) (cm-1)
q (Å-1)
wt
A30P
E46K
A53T

Figure 2

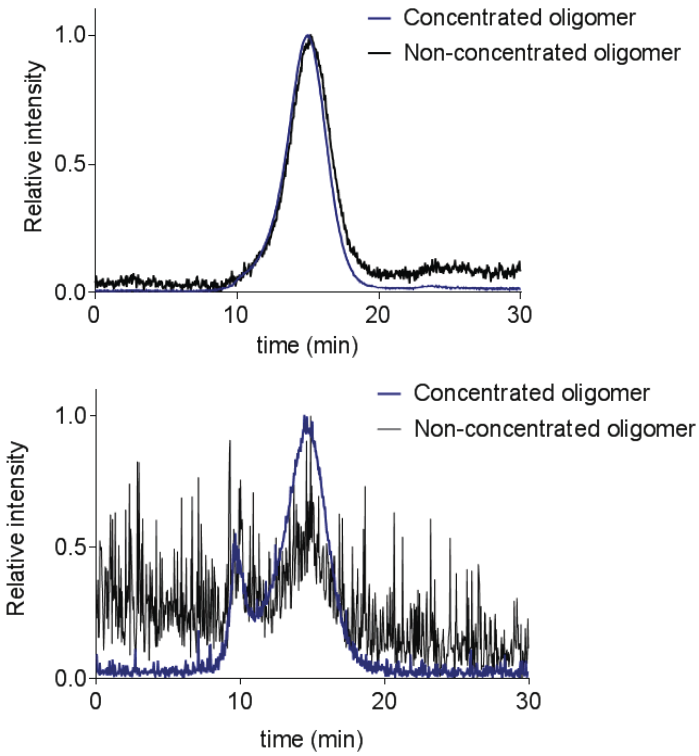
Concentrated oligomer
Non-concentrated oligomer
Relative intensity
1.0
0.5
0.0
0
10
20
30
time (min)
Concentrated oligomer
Non-concentrated oligomer
Relative intensity
1.0
0.5
0.0
0
10
20
30
time (min)

Figure 3

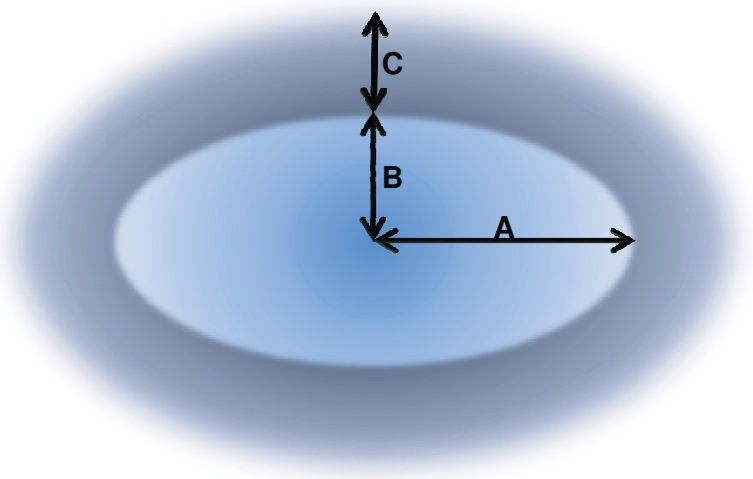

Figure 4

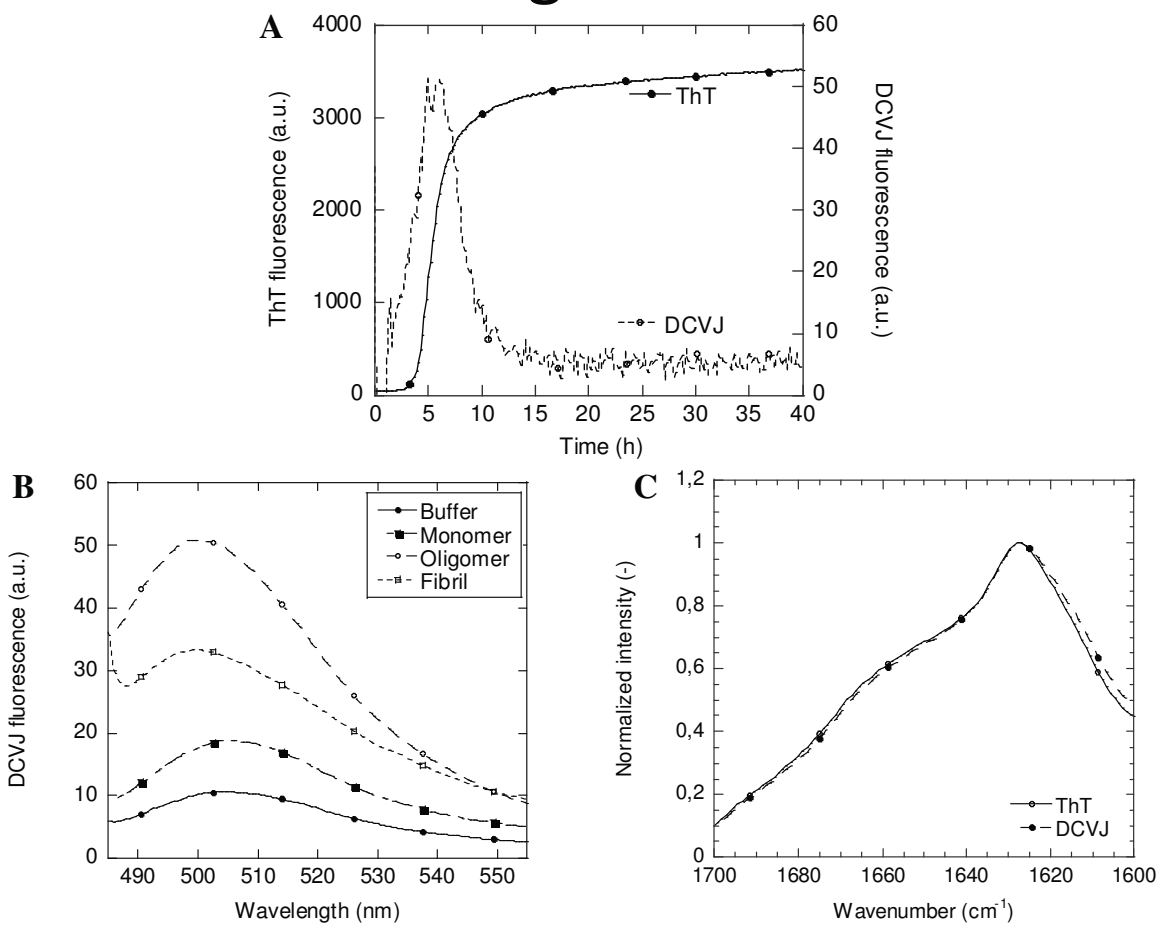
A
ThT fluorescence (a.u.)
DCVJ fluorescence (a.u.)
Time (h)
ThT
DCVJ
B
DCVJ fluorescence (a.u.)
Wavelength (nm)
Buffer
Monomer
Oligomer
Fibril
C
Normalized intensity (-)
Wavenumber (cm-1)
ThT
DCVJ

Figure 5

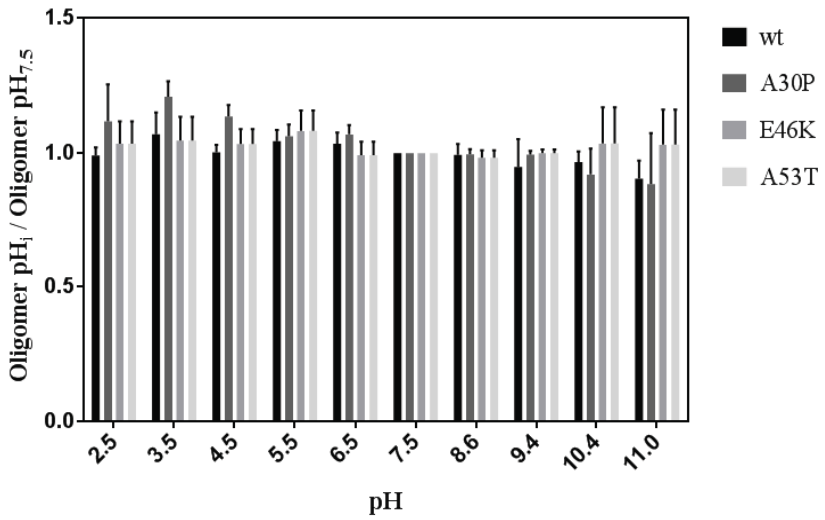
1.5
1.0
0.5
0.0
Oligomer pH$_i$ / Oligomer pH$_{7.5}$
2.5
3.5
4.5
5.5
6.5
7.5
8.6
9.4
10.4
11.0
pH
wt
A30P
E46K
A53T

Figure 6

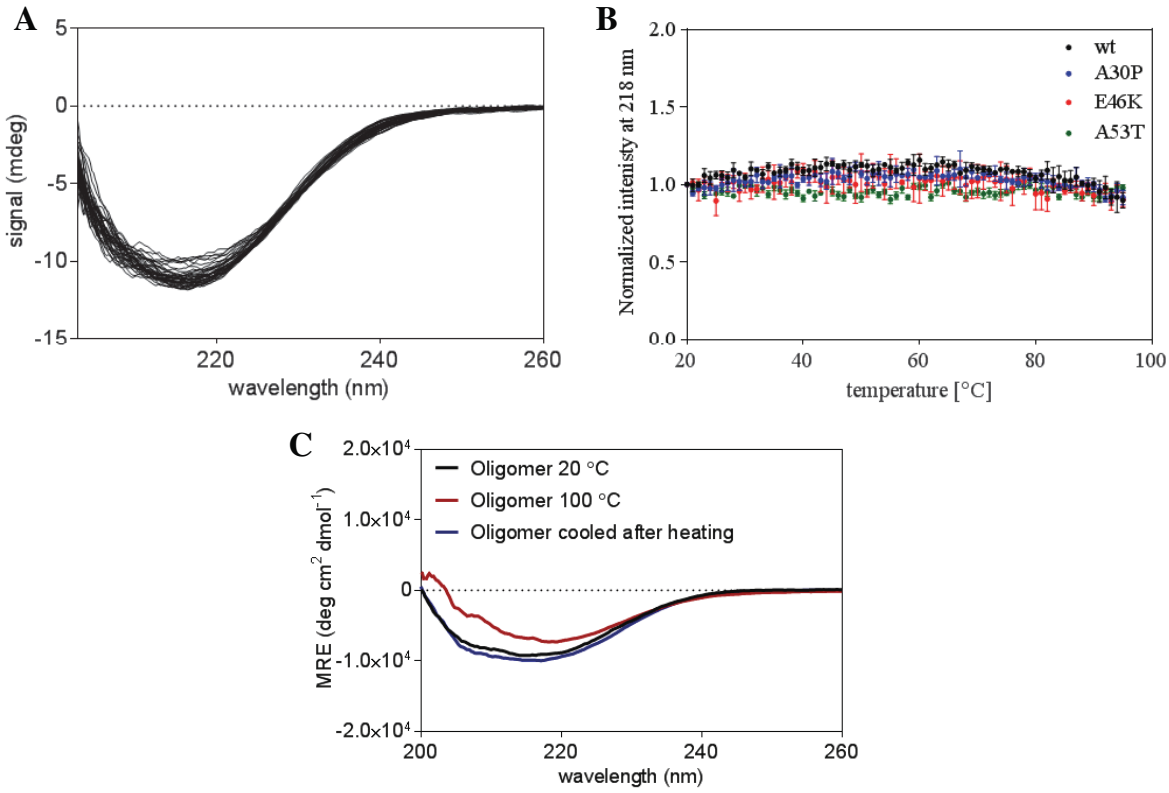
A
signal (mdeg)
wavelength (nm)
B
Normalized intenisty at 218 nm
temperature [°C]
wt
A30P
E46K
A53T
C
MRE (deg cm2 dmol-1)
wavelength (nm)
Oligomer 20 °C
Oligomer 100 °C
Oligomer cooled after heating

Figure 7

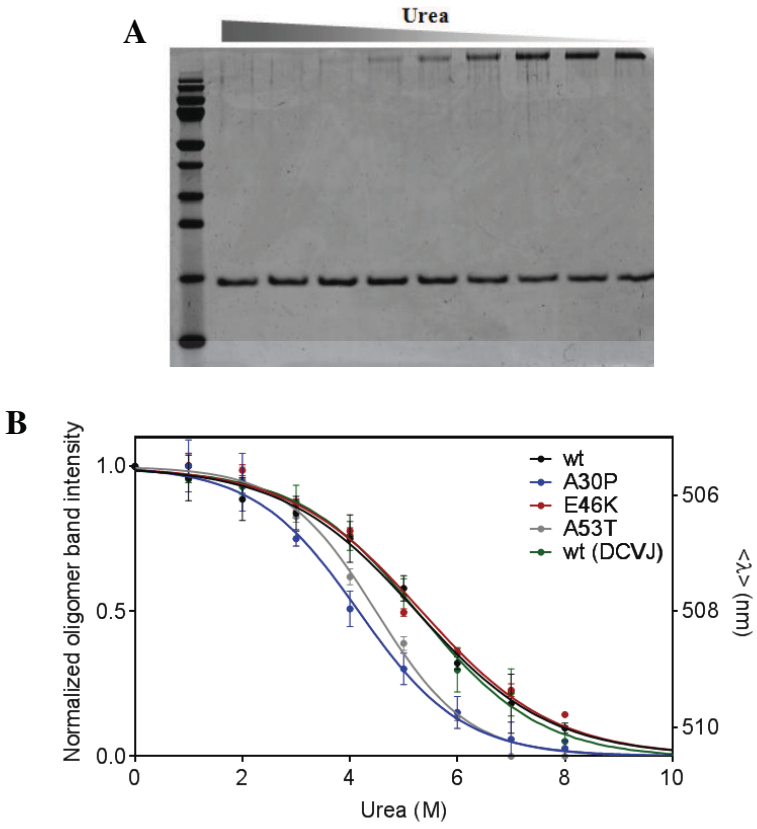
A
Urea
B
Normalized oligomer band intensity
1.0
0.5
0.0
0
2
4
6
8
10
Urea (M)
wt
A30P
E46K
A53T
wt (DCVJ)
506
508
510
<λ> (nm)

Figure 8

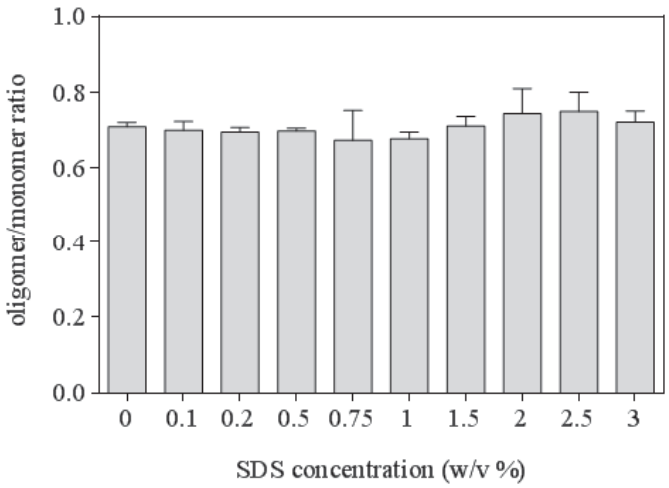
oligomer/monomer ratio
1.0
0.8
0.6
0.4
0.2
0.0
0
0.1
0.2
0.5
0.75
1
1.5
2
2.5
3
SDS concentration (w/v %)

Figure 9

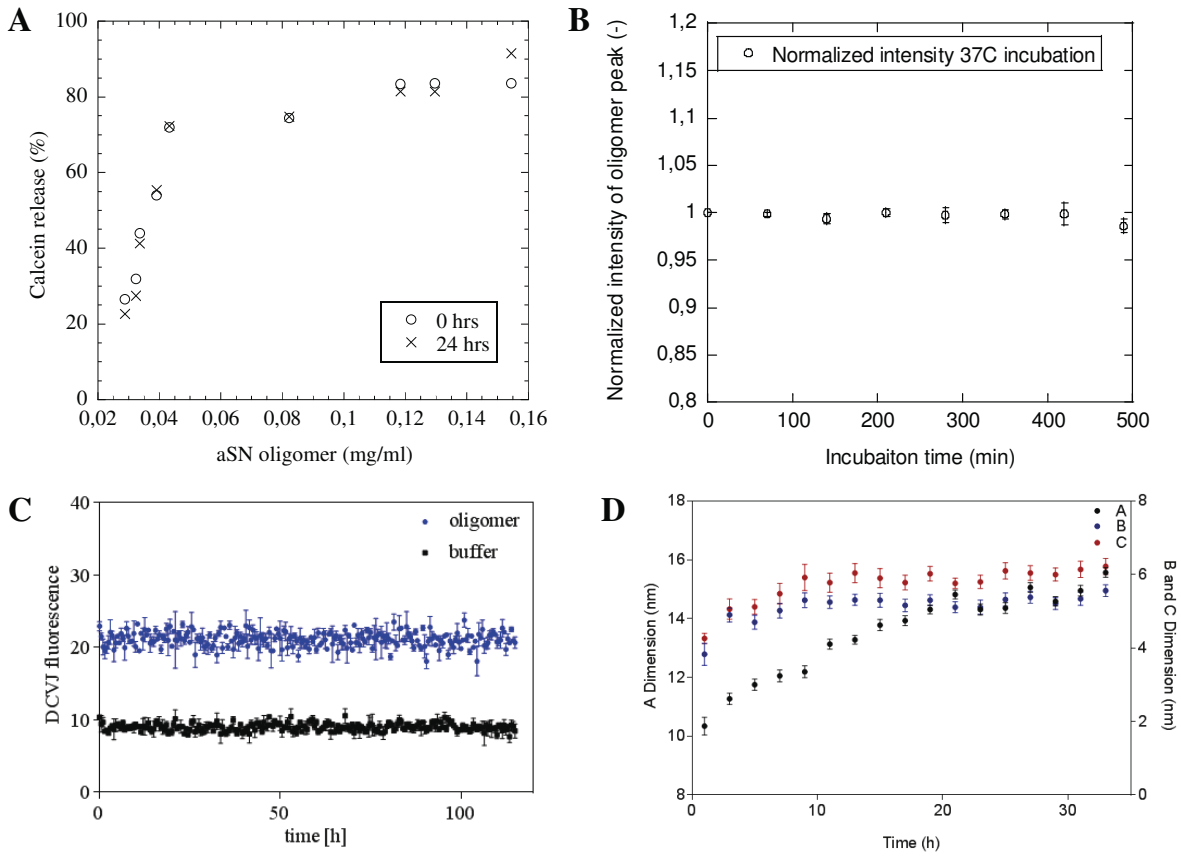
A
Calcein release (%)
aSN oligomer (mg/ml)
0 hrs
24 hrs
B
Normalized intensity of oligomer peak (-)
Normalized intensity 37C incubation
Incubaiton time (min)
C
DCVJ fluorescence
oligomer
buffer
time [h]
D
A Dimension (nm)
B and C Dimension (nm)
A
B
C
Time (h)

Figure 10

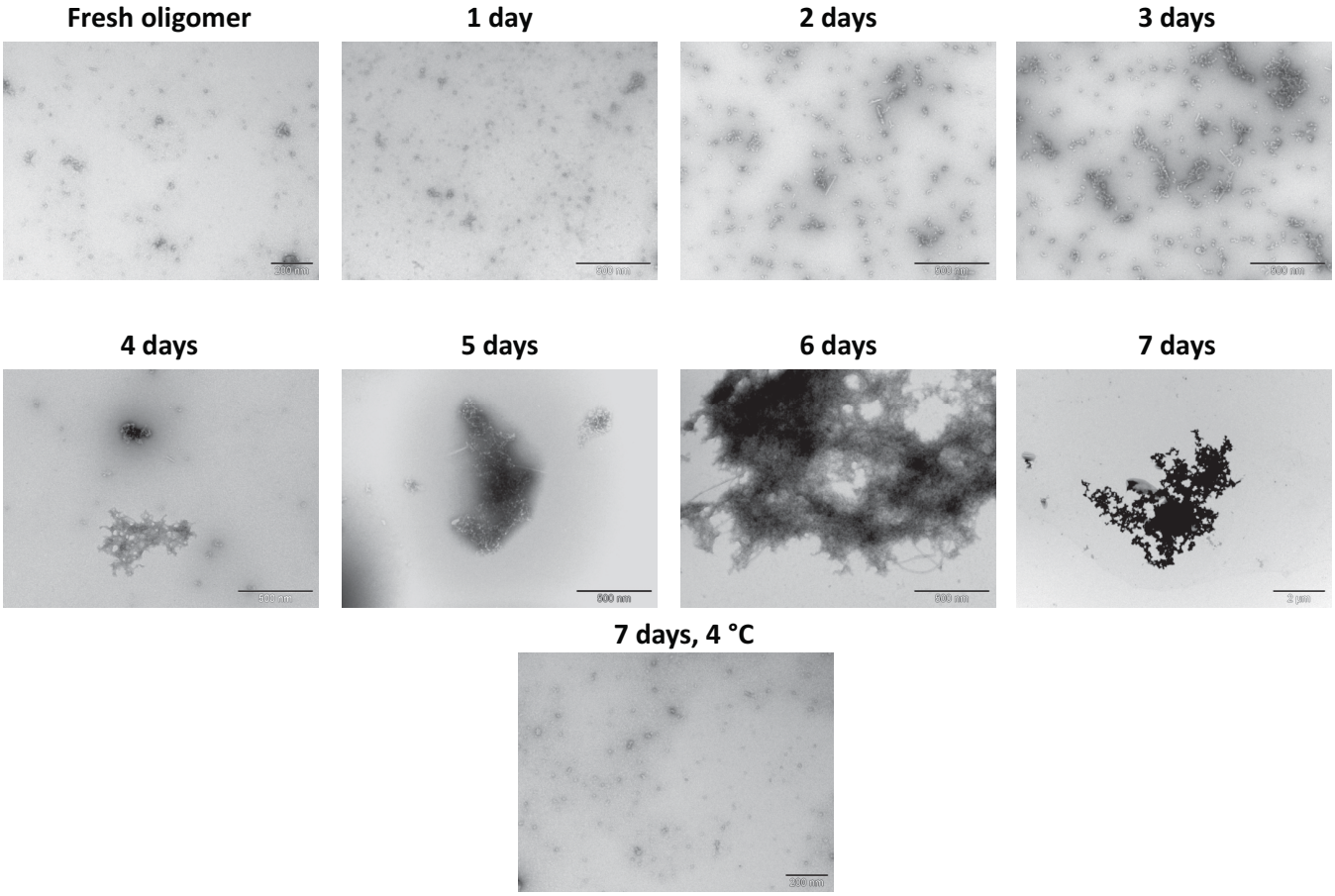
Fresh oligomer
1 day
2 days
3 days
4 days
5 days
6 days
7 days
7 days, 4 °C

Figure 11

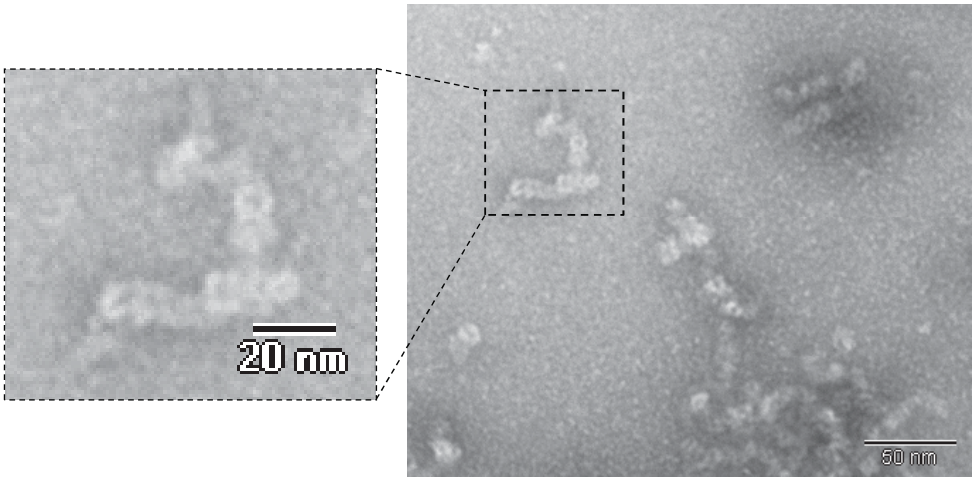

Figure 12

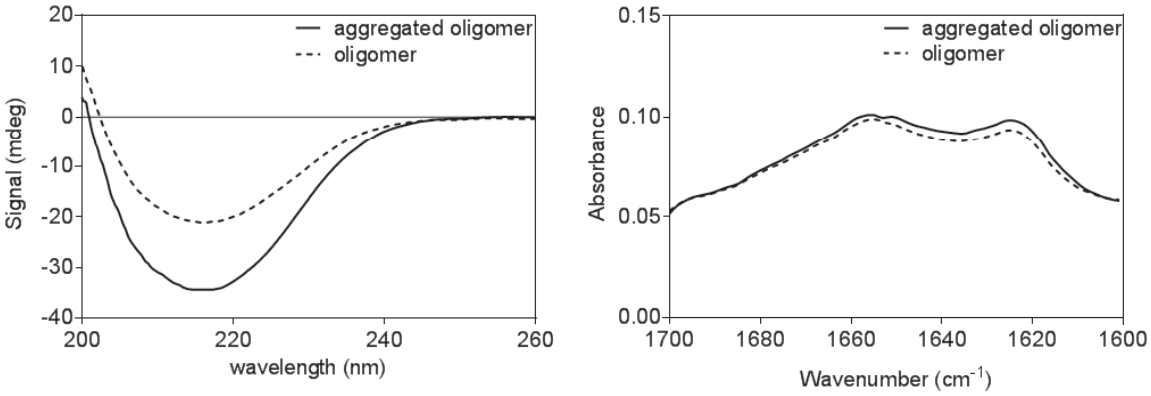
aggregated oligomer
oligomer
Signal (mdeg)
20
10
0
-10
-20
-30
-40
200
220
240
260
wavelength (nm)
aggregated oligomer
oligomer
Absorbance
0.15
0.10
0.05
0.00
1700
1680
1660
1640
1620
1600
Wavenumber (cm-1)

Figure 13

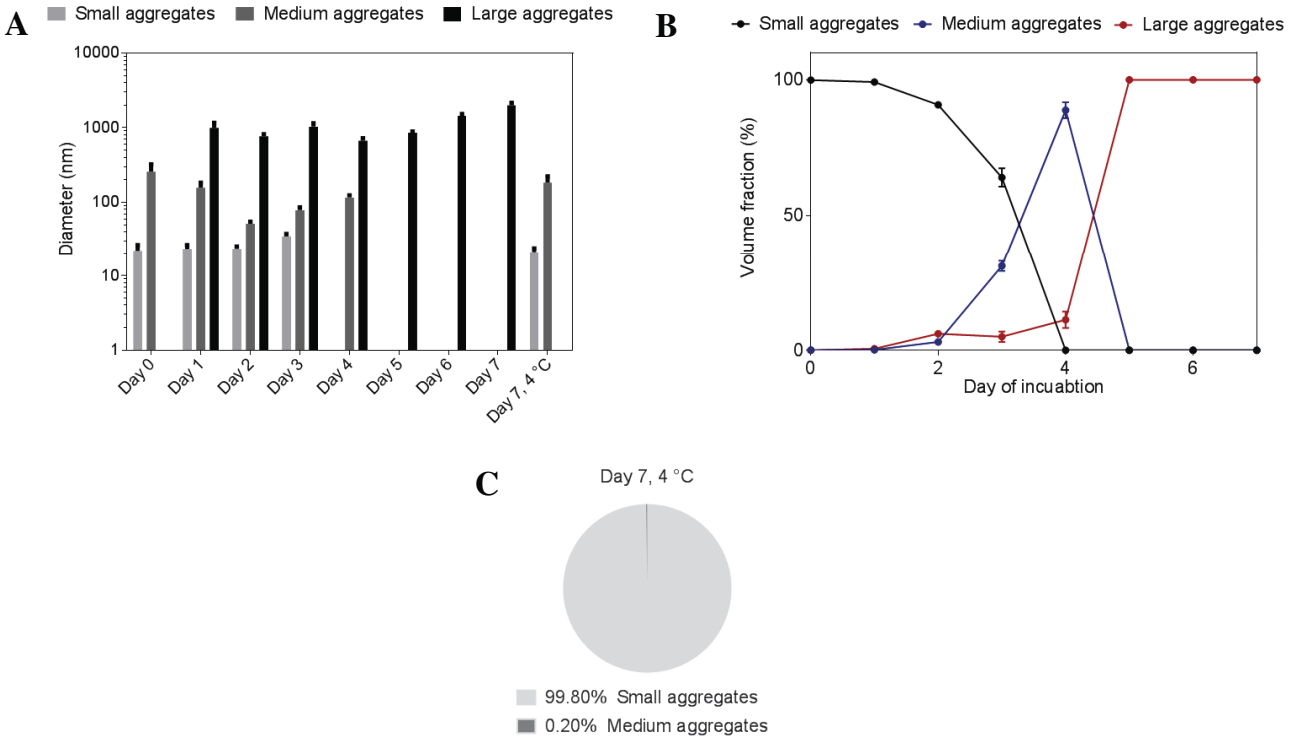
A
Small aggregates
Medium aggregates
Large aggregates
Diameter (nm)
10000
1000
100
10
1
Day 0
Day 1
Day 2
Day 3
Day 4
Day 5
Day 6
Day 7
Day 7, 4 °C
B
Small aggregates
Medium aggregates
Large aggregates
Volume fraction (%)
100
50
0
0
2
4
6
Day of incuabtion
C
Day 7, 4 °C
99.80% Small aggregates
0.20% Medium aggregates